AD NUMBER
ADB063654
NEW LIMITATION CHANGE

TO
Approved for public release, distribution unlimited

FROM
Distribution authorized to U.S. Gov't. agencies only; Test and Evaluation; Feb 1981. Other requests shall be referred to the Air Force Armament Laboratory, Attn: DLJC, Eglin AFB, FL 32542.

AUTHORITY
AFAL Notice, 18 Aug 1982

AFATL-TR-81-19

Aerodynamics Of Supersonic Lifting Bodies

AD B063654

M C Jischke
M L Rasmussen

UNIVERSITY OF OKLAHOMA
SCHOOL OF AEROSPACE
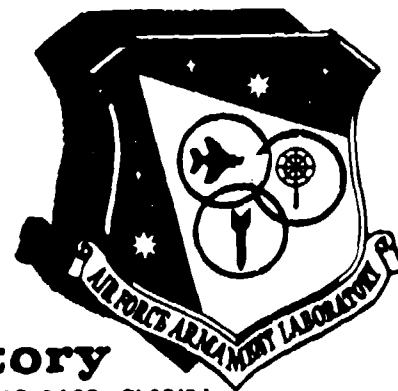MECHANICAL AND ENGINEERING
NORMAN, OKLAHOMA 73019

FEBRUARY 1981

FINAL REPORT FOR PERIOD OCTOBER 1977-SEPTEMBER 1980

DTIC
APR 0 9 1982
E

DTIC FILE COPY

Air Force Armament Laboratory
AIR FORCE SYSTEMS COMMAND ★ UNITED STATES AIR FORCE ★ EGLIN AIR FORCE BASE, FLORIDA

82   04   09   027

NOTICE

Please do not request copies of this report from the Air Force Armament Laboratory.
Additional copies may be obtained from:

Defense Technical Information Center
Cameron Station
Alexandria, Virginia 22314

REPORT DOCUMENTATION PAGE	READ INSTRUCTIONS BEFORE COMPLETING FORM	
1. REPORT NUMBER AFATL-TR-81-19	2. GOVT ACCESSION NO. AD-B063 654	3. RECIPIENT'S CATALOG NUMBER
4. TITLE (and Subtitle) Aerodynamics of Supersonic Lifting Bodies	5. TYPE OF REPORT & PERIOD COVERED Final Report October 1977 to September 1980	
	6. PERFORMING ORG. REPORT NUMBER	
7. AUTHOR(s) M. C. Jischke M. L. Rasmussen	8. CONTRACT OR GRANT NUMBER(s) AFOSR-77-3468 F08635-79-C-0017	
9. PERFORMING ORGANIZATION NAME AND ADDRESS University of Oklahoma School of Aerospace, Mechanical and Nuclear Engineering Norman, Oklahoma 73019	10. PROGRAM ELEMENT, PROJECT, TASK AREA & WORK UNIT NUMBERS PE: 61102F JON: 2307E105	
11. CONTROLLING OFFICE NAME AND ADDRESS Air Force Armament Laboratory Armament Division Eglin Air Force Base, Florida 32542	12. REPORT DATE February 1981	
	13. NUMBER OF PAGES 409	
14. MONITORING AGENCY NAME & ADDRESS(if different from Controlling Office)	15. SECURITY CLASS. (of this report) UNCLASSIFIED	
	15a. DECLASSIFICATION/DOWNGRADING SCHEDULE	

16. DISTRIBUTION STATEMENT (of this Report)

Distribution limited to U.S. Government agencies only; this report documents test and evaluation; distribution limitation applied February 1981. Other requests for this document must be referred to the Air Force Armament Laboratory (DLJC), Eglin Air Force Base, Florida 32542.

17. DISTRIBUTION STATEMENT (of the abstract entered in Block 20, if different from Report)

18. SUPPLEMENTARY NOTES

SUBJECT TO EXPORT CONTROL LAWS.

Availability of this report is specified on verso of front cover.

19. KEY WORDS (Continue on reverse side if necessary and identify by block number)
Theoretical Aerodynamics
Lifting Bodies
Wind Tunnel Tests
Boundary Layer Analysis

20. ABSTRACT (Continue on reverse side if necessary and identify by block number)
This report describes a combined theoretical and experimental program of research in the aerodynamics of supersonic lifting bodies. Analytical perturbation techniques are used to study the supersonic flow past slightly elliptical cones, cones whose cross-sections deviate slightly but arbitrarily from that of a right circular cone, cones of small longitudinal curvature, and right circular cones undergoing small harmonic pitching and/ or plunging motions. These studies all involve perturbations of the well-known
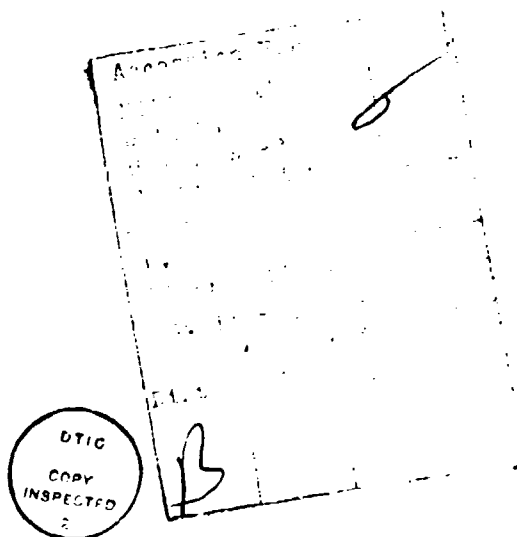(continued on reverse)

20. Continued

solution for supersonic flow past a right circular cone. Closed-form
analytical results are achieved through the use of an approximation
that accurately predicts results over the entire range of the hypersonic
similarity parameter. These results give hypersonic limiting solutions that
agree well with other independent analyses and, at the same time, agree
exactly with linearized theory in the linear theory limit. Comparisons with
experiment, where possible, also show good agreement.

SUMMARY

This report describes a combined theoretical and experimental program of research in the aerodynamics of supersonic lifting bodies. Perturbation techniques are used to study the supersonic flow past slightly elliptical cones, cones whose cross-section deviates slightly but arbitrarily from that of a right circular cone, cones of small longitudinal curvature, and right circular cones undergoing small harmonic pitching and/or plunging motions. These studies all involve perturbations of the well-known solution for supersonic flow past a right circular cone. Closed-form analytical results are achieved through the use of an approximation that accurately predicts results over the entire range of the hypersonic similarity parameter. These results give hypersonic limiting solutions that agree well with other independent analyses and, at the same time, agree exactly with linearized theory in the linear theory limit. Comparisons with experiment, where possible, also show good agreement.

An inverse method is used to study the hypersonic flow past slender lifting bodies with slightly blunted noses. Again, the body cross-section is assumed to deviate slightly from a circle and a perturbation technique is used to develop explicit closed-form solutions that demonstrate the effects of nose bluntness on the aerodynamic characteristics of the lifting body. Explicit results are obtained for power-law shock waves.

The perturbed right circular cone solutions are then used to develop a new class of supersonic lifting bodies known as waveriders. Making use of the principle that any streamsurface of an inviscid flow can be taken to be a boundary of the flow, the approximate streamsurfaces for supersonic flow past a circular cone at angle of attack and a slightly elliptical cone at angle of attack are used to generate a family of new waveriders. The well-known caret waverider solution, developed from the supersonic wedge flow solution, is then

used to fashion vertical stabilizer-like control surfaces.

Wind tunnel studies of two such waveriders, one generated from the circular cone at angle of attack solution and the other from the elliptical cone at angle of attack solution, and an elliptic cone with 1.87 major-minor axis ratio were conducted in the Mach number range 3 to 5 and unit Reynolds number range 1 to 2 million per foot. Six-component force and moment data are presented over the angle of attack and sideslip range of $\pm 20°$. Schlieren data for the waverider shock wave positions are also presented along with results of surface oil flow data. Maximum lift-to-drag ratios of the waveriders are found to be 2.5 times greater than that for the elliptic cone. Normal-force and rolling-moment coefficients, along with the lift-to-drag ratios, are found to decrease for the waveriders as M_∞ increases. Complementary surface pressure measurements were also conducted. Comparisons of the surface pressure measurements with theory for the on-design condition showed good agreement.

The various sections of this report have been written so as to be essentially independent of each other. Thus, individuals interested in only one portion of the work can proceed directly to the section of interest.

This document contains information for manufacturing or using munitions of war. Export of the information contained herein, or release to foreign nationals within the United States, without first obtaining an export license, is a violation of the International Traffic in Arms Regulations. Such violation is subject to a penalty of up to 2 years imprisonment and a fine of $100,000 under 22 U.S.C. 2778. Include this notice with any reproduced portion of this document.

This technical report has been reviewed and is approved for publication.

FOR THE COMMANDER

CARL A. FORBRICH, JR., Lt Col, USAF
Chief, Munitions Division

TABLE OF CONTENTS

LIST OF FIGURES

LIST OF SYMBOLS

Symbol	Definition
a	sound speed, semi-minor axis of elliptic cone, constant of integration
A	perturbation sound speed, constant of integration
b	semi-major axis of elliptic cone
C_A	axial-force coefficient
C_N	normal-force coefficient
C_y	side-force coefficient
C_ℓ	rolling-moment coefficient
C_m	pitching-moment coefficient
C_n	yawing-moment coefficient
C_D	drag-force coefficient
C_L	lift-force coefficient
C_M	moment coefficient
C_p	pressure coefficient, specific heat at constant pressure
C_v	specific heat at constant volume
D	drag force, constant of integration
E	constant of integration
e	internal energy, eccentricity parameter
$\hat{e}$	unit vector
$\vec{F}$	force
F	constant proportional to entropy perturbation, function (see Equation (335))
f(r)	longitudinal curvature function
f	constant (see Equation (233)), function (see Equation (346))
G_m	perturbation shock wave parameter, function (see Equation (559))
G_n	perturbation shock wave parameter

Symbol	Definition
$g(r)$	shock wave shape function
h	enthalpy, vertical displacement
I	integrating factor (see Equation (60))
I_n	modified Bessel function of the first kind and nth order, bluntness constant (see Equation (535))
J_n	function (see Equation 367f)), constant (see Equation (556))
K_n	modified Bessel function of the second kind and nth order
K_θ	hypersonic similarity variable, $M_\infty \sin \theta$
K_β	hypersonic similarity parameter, $M_\infty \sin \beta$
K_δ	hypersonic similarity parameter, $M_\infty \sin \delta$
k_n	constants (see Equations (591, 623, 635))
L	lift force, length, function (see Equations (278))
M	Mach number, moment
N	constant (see Equation (99))
$\hat{n}$	unit normal vector
P	perturbation pressure function
P_n	Legendre function of the first kind and order n
p	pressure
Q_n	Legendre function of the second kind and order n
$Q_n{}^m$	Associated Legendre function of the second kind of order n and degree m
q	angular velocity about Y-axis
R	perturbation density function, thickness
r, θ, ϕ	spherical polar coordinates
r, ϕ, z	cylindrical polar coordinates
S	perturbation entropy function, area

Symbol	Definition
T_n	function (see Equation (397))
t	time
u, v, w	velocity components
U, V, W	perturbation velocity components
$\vec{V}$	velocity vector
V	volume
x, y, z	body fixed rectangular coordinates
X, Y, Z	inertial rectangular coordinates
z	θ/δ
α	angle of attack
β	shock angle, sideslip angle
γ	ratio of specific heats
ε	small parameter
δ	circular cone half angle
Δ	deflection angle
ζ	angle (see Equation (164)), constant (see Equation (573g))
η	thickness of high density layer near shock wave
θ'	$(\theta-\delta)/(\beta-\delta)$
κ	constant
	dihedral angle
λ	$(\theta-\theta_c(\phi))/(\theta_s(\phi) - \theta_c(\phi))$, lip angle
μ	$\cos\theta, \cos\phi$
ξ	density ratio across shock
ρ	density
σ	β/δ

LIST OF SYMBOLS (Concluded)

Symbol	Definition
ϕ_n	phase angle
ψ	angle (see Equation (325)), fin angle (see Figure 118)
$\vec{\Omega}$	vorticity
Ω	phase angle
ω	frequency

Subscripts

b	body-fixed coordinates
c	cone surface
f	fin
i	initial value
n	nth term in expansion
o	zeroth order, contribution due to pitching
p	contribution due to plunging
s	shock wave
w	wedge
z	contribution due to pitching about $z_0 \neq 0$
∞	free stream

Superscripts

(c)	correction
p_1	plunging contribution
$-$	normalized quantity
$\cdot$	derivative with respect to time
$*$	initial value (see Equation (618))

INTRODUCTION

Increasingly demanding air vehicle maneuverability requirements in the high supersonic, low hypersonic Mach number range have focused attention on the need for aerodynamic prediction capabilities for vehicle geometries of practical interest. Of particular importance in this regard is the identification of high-lift configurations with low drag and good control effectiveness. The likely range of Mach numbers (1.2 to 5+) and angles of attack (0 to 70 degrees) require vehicle configurations that efficiently integrate the volumetric storage, lifting, and propulsive components of the vehicle in order to minimize adverse heating effects and maximize the lift-to-drag ratio.

Traditional linear aerodynamic theories are not adequate to the task of analyzing flows past such vehicles. Finite strength shock waves and large changes in the thermodynamic state of the medium require a nonlinear flowfield description. Typical vehicle configurations being considered for this high supersonic, low hypersonic Mach number range also exhibit considerable geometrical complexity. Existing methods for analyzing flows past complex lifting shapes -- which are based either on linearized aerodynamics and use the superposition principle or on elaborate, expensive computer codes which do not easily accommodate realistic geometries -- cannot be relied upon for design purposes. Analytical results are generally not available to describe the flow past most lifting body shapes of interest.

The nonlinear nature of high supersonic, low hypersonic Mach number flows has made the few known exact solutions for flows past elementary geometries extremely important. The solutions for the supersonic flows past a two-dimensional wedge and a right circular cone have been particularly

valuable not only as models of wing leading edges and vehicle noses, but also as the building blocks for flows past more complex geometries. The wedge solution has been used by Nonweiler (Reference 1), Kuchemann (Reference 2), Kuchemann and Weber (Reference 3), and others to describe supersonic flows past caret-shaped lifting bodies. In a similar fashion, Jones (Reference 4) and others have used the right circular cone solution to describe exactly the flow past a delta wing with a half-cone underbody. These so-called waverider configurations all derive from the general principle that any streamsurface of an inviscid flow can be viewed as part of a solid boundary of the flow. The variety of waverider configurations available is, therefore, limited by the number of flowfield solutions for which the streamline geometry can be determined. Until recently (Reference 5), the two-dimensional wedge and right circular cone flows were the only flowfields for which this waverider notion had been pursued.

The otherwise uniform supersonic flow past a two-dimensional wedge or right circular cone are examples of conical flows--flowfields which are independent of distance along a ray emanating from a vertex. Conical bodies are defined as shapes generated by a semi-infinite line, one end of which is fixed at a point called the vertex of the body. A conical body is generated by moving any point in the line through a closed curve. Provided the bow shock wave is attached, the flowfield generated by a uniform supersonic flow past a conical body is also conical. The analysis of conical flows is somewhat easier than that for more general shapes, and the results have been extremely valuable as building blocks for more complex situations and as guides to the nature of supersonic flow.

With few exceptions, the analysis of supersonic flows past conical shapes has been done numerically. The numerical methods used include the theory of

2

characteristics (Reference 6), iterative finite difference schemes (References 7 and 8), the method of lines (Reference 9), the method of integral relations (Reference 10), and others. Numerical solutions, while providing accuracy and a certain generality, do not as readily lend themselves to understanding and easy use as do explicit analytical results. Explicit analytical answers, on the other hand, inevitably employ approximations which can reduce the accuracy and/or generality of the results. Van Dyke's analysis of supersonic flow past elliptic cones (Reference 11) uses linearized theory (through second order) and gives surprisingly useful results over a wide range of conditions. Van Dyke's results, however, are not valid in the nonlinear hypersonic limit and thus do not possess the generality that might be desired. Chapkis (Reference 12), using a perturbation scheme orginally suggested by Ferri, Ness, and Kaplita (Reference 13), studied supersonic flow past conical bodies whose cross-sections deviate slightly from that of a right circular cone. To proceed analytically, Chapkis, influenced by Lees (Reference 14), employed an approximate result for the hypersonic flow past a right circular cone at zero angle of attack, a result that incorrectly assumes the solution can be expanded in a Taylor series about the cone surface conditions. In addition, the expressions obtained by Chapkis do not reduce to the linearized theory results in the linear theory limit.

The present work concerns itself with the development of analytical methods that describe the flow past bodies that deviate slightly from that of steady supersonic flow past a right circular cone at zero angle of attack. The deviations can result from angle of attack, cross-sectional elliptic eccentricity, longitudinal curvature, pitching and plunging motions, and nose bluntness. The methods employed are more accurate than those used by Chapkis and, in addition, reduce exactly to the linearized flow theory results in the appropriate limit.

3

This analytical work is the basis upon which a novel class of supersonic lifting bodies is developed. These lifting bodies, called waveriders, give configurations with attractive aerodynamic performance characteristics that efficiently integrate the lifting, propulsive, and volumetric requirements for highly maneuverable, supersonic vehicles.

A series of wind tunnel tests have been conducted to both guide and verify this analytical work. Six component force and moment measurements were made. Schlieren and surface oil-flow visual data were recorded along with surface pressure measurements. These experimental results confirm the basic theoretical work on waveriders and provide data over a variety of off-design conditions.

The report ends with a summary of conclusions and suggestions for future research directions.

CONE PERTURBATION STUDIES

This section deals with analytical studies of supersonic and hypersonic flow past bodies which deviate slightly from a right circular cone. In this way can be studied the effects of elliptical eccentricity and other cross-sectional deviations from a circle, angle of attack, longitudinal curvature, pitching and plunging motions, and the effects of nose bluntness.

1. ELLIPTICAL CONE

For supersonic flows past bodies without axial symmetry, the elliptical cone is a basic body shape. Its counterpart, the circular cone, is a basic axisymmetric body shape with flowfield properties that are extensively tabulated. Even the supersonic flow past a circular cone at small angle of attack is extensively tabulated and fairly well understood. On the other hand, the properties of the supersonic flowfield past an elliptic cone are not extensively tabulated, at least in comparison with the circular cone of attack. Although numerous papers have been directed toward supersonic flows past elliptic cones, their goals have been specific, and no general or comprehensive flowfield calculations have been set forth. The purpose of this work is to partially remedy this situation and to present an approximate analytic solution that illustrates the general flowfield features of hypersonic flow past a slender elliptic cone with small eccentricity.

Supersonic flow past slender cones with arbitrary cross sections can be treated with some generality by means of linearized theory (Reference 15), and linearized theory can be extended to second order (Reference 11) to account somewhat for weak nonlinear effects. These results, however, are frequently

not appropriate for the hypersonic Mach numbers and flow deflections of practical concern.

Another approach to the problem deals with flows that deviate slightly from the basic axisymmetric flow past a circular cone. The so-called scheme of linearized characteristics was applied (Reference 13) to several conical bodies with non-axisymmetric cross sections. This method is subject to a number of criticisms for cross-section areas that deviate significantly from circles (Reference 16), and thus a modification of the linearized characteristics method was applied to elliptic cones at angle of attack by Martellucci (Reference 17). In the above use of the linearized characteristics method, the perturbation equations were solved numerically. Chapkis (Reference 12), applying the linearized characteristics method, used hypersonic approximations for the basic cone flow to obtain relatively simple specific results for an elliptic cone.

Besides the above methods of computation, there are numerical schemes for integrating the complete governing gas dynamic equations. Two notable schemes applied to elliptic cones are those of Stocker and Mauger (Reference 18) and Babenko, et. al. (Reference 7). There are also semi-empirical methods for dealing with certain features of supersonic flows past elliptic cones, such as tangent-cone methods, equivalent circular-cone methods, and the method of Kaattari (Reference 19). Whichever method has been utilized to date, the general features of the supersonic flowfield past an elliptic cone, showing effects of Mach number, cone angle, and ellipse eccentricity on the shock shape, the shock-layer structure, and the surface conditions, have not been delineated.

This undertaking starts with the small-perturbation equations for perturbed flow past a basic circular cone at zero angle of attack and takes

the approach of Chapkis (Reference 12) for the elliptic cone. Improved

approximations shall be used for the basic cone flow (References 20 and 21)

and approximate analytical solutions for the perturbation equations shall be

obtained. The analysis is analogous to that of Doty (Reference 22) and Doty

and Rasmussen (Reference 23) for obtaining approximations for hypersonic flow

past circular cones at small angles of attack, wl ch was shown to be very

accurate. The analysis is cast in the form of hypersonic similarity theory,

and the results are presented in appropriate similarity form.

The perturbation expansions involve a small parameter for the angle of

attack and for the measure of the eccentricity of the ellipse cross section.

These expansions are not uniformly valid in a thin vortical layer adjacent to

the cone surface. It can be shown (References 24 and 25), however, that at

least the pressure and azimuthal velocity component are valid across the

vortical layer. Since these two variables are of most importance, further

consideration of the vortical layer will not be undertaken.

a.   Unyawed Elliptic Cone Body and Shock Geometry

In rectangular Cartesian coordinates, as shown in Figure 1, the unyawed

elliptic cone body is represented by

$$\frac{x^2}{a^2 z^2} + \frac{y^2}{b^2 z^2} = 1 \quad , \tag{1}$$

where $a \equiv \tan \vartheta_a$ and $b \equiv \tan \vartheta_b$ are the tangents of the semivertex angles of

the semiminor and semimajor axes of the elliptic cone. In terms of spherical

polar coordinates, also shown in Figure 1, Equation (1) can be rewritten as

$$\tan \vartheta = \frac{\tan \vartheta_m}{\sqrt{1 + e \cos 2\varphi}} \quad , \tag{2}$$
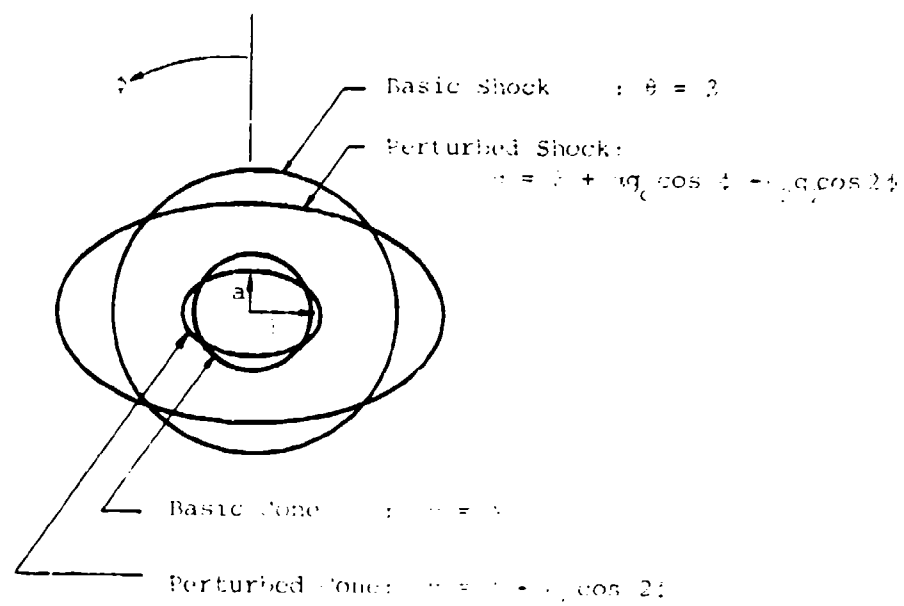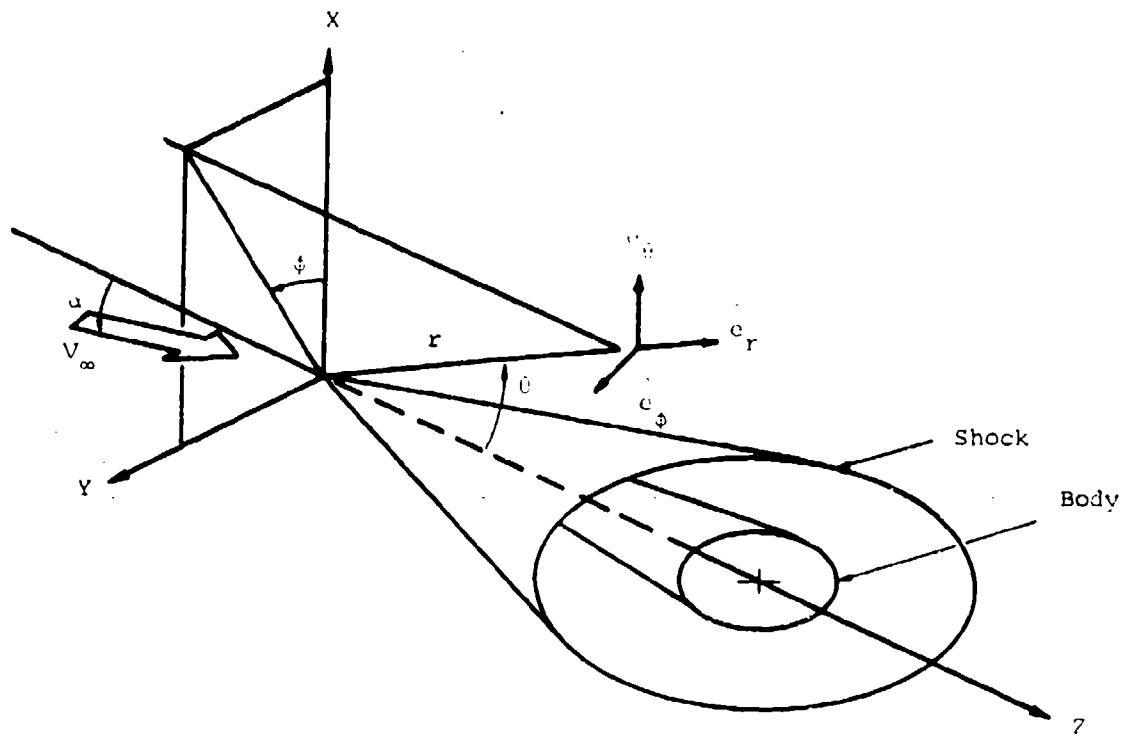
Figure 1. Cone Coordinates and Geometry

where

$$\tan \theta_m \equiv \frac{\sqrt{2}\ ab}{\sqrt{a^2 + b^2}} = b\sqrt{1-e} = a\sqrt{1+e} \qquad (3a)$$

$$= \sqrt{ab}\ (1-e^2)^{1/4}$$

$$e \equiv \frac{b^2 - a^2}{b^2 + a^2} \qquad (3b)$$

The parameter e is a measure of the eccentricity of the elliptic cone.

The first three terms of the Fourier-series representation of Equation (2) are given by

$$\tan \theta = \tan \theta_m\ [A_0 + A_2 \cos 2\phi + A_4 \cos 4\phi + \ldots] \quad , \qquad (4)$$

where

$$A_0 \equiv \frac{2}{\pi}\ \frac{K(k)}{\sqrt{1+e}} \qquad (5a)$$

$$A_2 \equiv -\frac{4}{\pi k^2\ \sqrt{1+e}}\ [(2-k^2)\ K(k) - 2E(k)] \qquad (5b)$$

$$A_4 \equiv -\frac{2}{3}\ A_0 - \frac{4}{3e}\ A_2 \qquad (5c)$$

$$k^2 \equiv \frac{2e}{1+e} \qquad (5d)$$

and

$$E(k) \equiv \int_0^{\pi/2} \sqrt{1 - k^2 \sin^2 u}\ \ du \qquad (5e)$$

$$K(k) \equiv \int_0^{\pi/2} \frac{du}{\sqrt{1 - k^2 \sin^2 u}} \qquad (5f)$$

are the complete elliptic integrals of the first and second kinds. For small values of the eccentricity, e, the Fourier coefficients can be expanded as

$$A_0 = 1 + \frac{3}{16} e^2 + O(e^4) \tag{6a}$$

$$A_2 = -\frac{e}{2} \left[1 + \frac{15}{32} e^2 + O(e^4)\right] \tag{6b}$$

$$A_4 = \frac{3}{16} e^2 \left[1 + \frac{35}{48} e^2 + O(e^4)\right] \tag{6c}$$

When the eccentricity, e, is small the successive Fourier coefficients become smaller and smaller. For sufficiently small e, the Fourier coefficients for the higher harmonics can be neglected.

Equation (4) can be expanded for θ in a Fourier expansion and give for small eccentricities

$$\theta = \delta - \varepsilon_2 \cos 2\phi + O(\varepsilon_2^2) \tag{7}$$

where

$$\delta \equiv \tan^{-1}(A_0 \tan \theta_m) - \frac{A_0 A_2^2}{4} \sin 2\theta_m + O(e^4)$$

$$\equiv \theta_m + \frac{e^2}{32} [3 - 2 \sin^2\theta_m] \sin 2\theta_m + O(e^4) \tag{8a}$$

$$\varepsilon_2 \equiv -\frac{A_2 \tan \theta_m}{1+A_0^2\tan^2\theta_m} \left[1-(\frac{A_2^2}{4} + A_4) \sin^2\theta_m + \frac{A_2^2}{4} (1+3A_0^2) \sin^4\theta_m + O(e^4)\right]$$

$$\equiv \frac{e}{4} \left[1 + e^2 \left(\frac{15}{32} - \frac{5}{8} \sin^2\theta_m + \frac{1}{4} \sin^4\theta_m\right) + O(e^4)\right] \sin 2\theta_m \tag{8b}$$

The parameter ε_2 is a new measure of the eccentricity and is the appropriate parameter to be used in the subsequent analysis. The subscript 2 on ε is introduced here for later convenience. The parameter δ specifies the semivertex angle of the basic circular cone about which a perturbation analysis is to be performed.

Comparison of the two-term approximation Equation (7), with the exact Equation (2) for the elliptic cone is shown in Figure 2. When a = 0.2555 and

a= 0.2555
b= 0.3562
e= 0.320
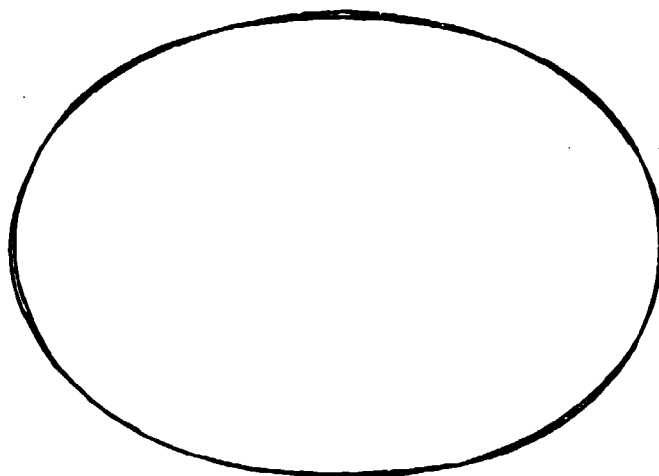
a= 0.2256
b= 0.4034
e= 0.523
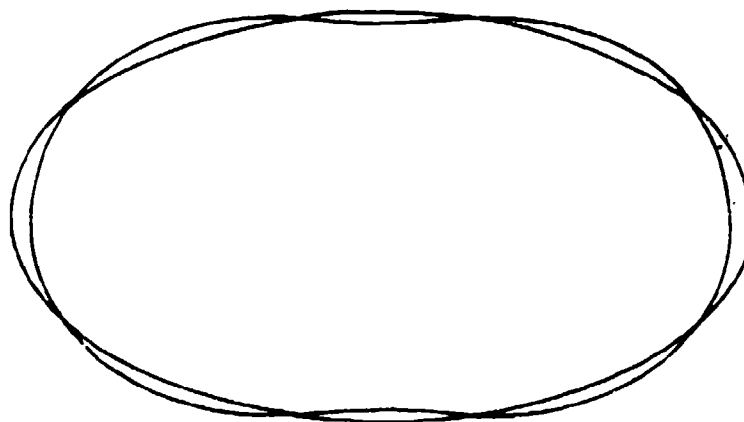
Figure ... Fourier Series ... ...tion of the Ellipse

$b = 0.3562$, such that $e = 0.320$ and $\theta_m = 16.30$ degrees, the two-term approximation gives a good representation of the actual ellipse. When $a = 0.2256$ and $b = 0.4034$, such that $e = 0.523$ and $\theta_m = 15.56$ degrees, the representation is not as good but is still a reasonable approximation when precise accuracy is not paramount.

The conical shock wave attached to the elliptic cone is assumed to have the form (for $\alpha = 0$)

$$\theta_s = \beta - \epsilon_2 g_2 \cos 2\phi + 0(\epsilon^2) \quad , \tag{9}$$

which is analogous to Equation (7) for the body shape. Here β is the semivertex angle of the basic circular shock corresponding to the basic body with semivertex angle δ. The factor g_2 is to be determined from the perturbation analysis. It, in effect, represents the deviation of the shock eccentricity from the body eccentricity.

By means of vector analysis, the outward unit normal on the shock is given by

$$\hat{n}_s = \hat{e}_\theta - 2\epsilon_2 g_2 \frac{\sin 2\phi}{\sin \beta} \hat{e}_\phi + 0(\epsilon_2^2) \tag{10}$$

This result is needed to establish the shock jump conditions.

b. Boundary Conditions

Let the velocity vector for conical flow be represented in spherical coordinates by

$$\vec{V} = u(\theta,\phi)\hat{e}_r + v(\theta,\phi)\hat{e}_\theta + w(\theta,\phi)\hat{e}_\phi \quad . \tag{11}$$

The Fourier representation for the body and shock shapes suggest that the velocity components, pressure, and density can be expanded in the following forms, valid outside the vortical layer adjacent to the body surface (for $\alpha = 0$):

$$u(\theta,\phi) = u_0(\theta) + \varepsilon_2 U_2(\theta) \cos 2\phi + 0(\varepsilon_2{}^2) \qquad (12a)$$

$$v(\theta,\phi) = v_0(\theta) + \varepsilon_2 V_2(\theta) \cos 2\phi + 0(\varepsilon_2{}^2) \qquad (12b)$$

$$w(\theta,\phi) = \varepsilon_2 W_2(\theta) \sin 2\phi + 0(\varepsilon_2{}^2) \qquad (12c)$$

$$p(\theta,\phi) = p_0(\theta) + \varepsilon_2 P_2(\theta) \cos 2\phi + 0(\varepsilon_2{}^2) \qquad (12d)$$

$$\rho(\theta,\phi) = \rho_0(\theta) + \varepsilon_2 R_2(\theta) \cos 2\phi + 0(\varepsilon_2{}^2) \qquad (12e)$$

The lowest-order terms, with the subscript naught, pertain to the basic circular-cone solution, which is presumed known.

The free stream velocity in spherical coordinates is given by

$$\vec{V}_\infty = V_\infty \{\cos\theta \; \hat{e}_r - \sin\theta \; \hat{e}_\theta\} \qquad (13)$$

At the shock, $\theta = \theta_s \equiv \beta - \varepsilon_2 g_2 \cos 2\phi$, it is necessary to first order from $\cos(\varepsilon_2 g_2 \cos 2\phi) = 1$, $\sin(\varepsilon_2 g_2 \cos 2\phi) = \varepsilon_2 g_2 \cos 2\phi$

$$\vec{V}_\infty = V_\infty \{ \{\cos\beta + \varepsilon_2 g_2 \sin\beta \cos 2\phi\} \; \hat{e}_r$$
$$- \{\sin\beta - \varepsilon_2 g_2 \cos\beta \cos 2\phi\} \; \hat{e}_\theta + 0(\varepsilon_2{}^2)\} \qquad (14)$$

Using Equation (10), the normal velocity at the shock is found to be, to first order,

$$\vec{V}_\infty \cdot \hat{n}_s = -V_\infty \sin\beta + \varepsilon_2 g_2 V_\infty \cos\beta \cos 2\phi + 0(\varepsilon_2{}^2) \qquad (15)$$

The shock jump conditions give for the pressure ratio across the shock

$$\frac{p_s}{p_\infty} = 1 + \frac{2\gamma}{\gamma+1}(M_n{}^2 - 1) \qquad (16)$$

for a thermally and calorically perfect gas. Here γ is the ratio of specific heats, $\gamma \equiv c_p/c_v$, and M_n is the normal component of the free stream Mach number. Substituting (15) into (16) yields

$$\frac{p_s}{p_\infty} = 1 + \frac{2\gamma}{\gamma+1}(K_\beta{}^2 - 1) - \varepsilon_2 \frac{4\gamma}{\gamma+1} K_\beta{}^2 g_2 \cot\beta \cos 2\phi + 0(\varepsilon^2) \qquad (17)$$

where $K_\beta \equiv M_\infty \sin\beta$.

13

Equation (12d) for the pressure evaluated at the shock reads

$$p(\theta_s, \phi) = p_0(\theta_s) + \epsilon_2 P_2(\theta_s) \cos 2\phi + 0(\epsilon^2) \qquad (18)$$

Transferring this value to the basic unperturbed shock by means of a Taylor expansion yields, to first order,

$$p(\theta_s, \phi) = p_0(\beta) + \epsilon_2 \left[- \left(\frac{dp_0}{d\theta}\right)_\beta g_2 + P_2(\beta) \right] \cos 2\phi + 0(\epsilon_2^2) \qquad (19)$$

Identifying the first-order perturbation terms in (7) and (9) leads to the shock boundary conditions for the perturbation pressure

$$\frac{P_2(\beta)}{p_\infty} = - \frac{4\gamma}{\gamma+1} g_2 K_\beta^2 \cot \beta + \frac{g_2}{p_\infty} \left(\frac{dp_0}{d\theta}\right)_\beta \qquad (20)$$

For the undisturbed conical flow, the pressure gradient can be evaluated in terms of the velocity gradient. Hence,

$$\left(\frac{dp_0}{d\theta}\right)_\beta = \rho_\infty V_\infty \sin \beta \left[V_\infty \cos \beta + \left(\frac{dv_0}{d\theta}\right)_\beta \right] \qquad (21)$$

Thus, alternatively, the pressure boundary condition can be written

$$P_2(\beta) = \rho_\infty g_2 V_\infty^2 \sin \beta \cos \beta \left[\frac{\gamma-3}{\gamma+1} + \left\{ \left(\frac{dv_0}{d\theta}\right)_\beta / V_\infty \cos \beta \right\} \right] \qquad (22)$$

The derivative $(dv_0/d\theta)_\beta$ can be evaluated in terms of the density ratio across the shock, as shown below.

The density ratio across the shock is given by

$$\frac{\rho_\infty}{\rho_s} = \frac{(\gamma-1) M_n^2 + 2}{(\gamma+1) M_n^2} \cdot \qquad (23)$$

Expanding this expression analogously to that for the pressure, the shock density, to first order, is obtained:

$$\frac{\rho_\infty}{\rho_s} = \zeta_0 + \epsilon_2 \zeta_2 \cos 2\phi + 0(\epsilon^2) \quad , \qquad (24a)$$

14

where

$$\zeta_0 \equiv \frac{\rho_\infty}{\rho_0(\beta)} = \frac{(\gamma-1)K_\beta^2 + 2}{(\gamma+1)K_\beta^2} \qquad (24b)$$

$$\xi_2 \equiv 2g_2 \cot \beta \left[\zeta_0 - \frac{\gamma-1}{\gamma+1}\right] \qquad (24c)$$

An explicit expression for $R_2(\beta)$ is not needed. It can be shown from the basic cone solution that

$$\left(\frac{dv_0}{d\theta}\right)_\beta = -V_\infty \cos \beta \left[2 - \frac{\gamma-1}{\gamma+1} \zeta_0\right] \qquad (25)$$

The velocity components immediately downstream of the shock are obtained from the governing conditions on the normal and tangential components. The normal components of the velocity are governed by the mass conservation equation:

$$(\vec{V}\cdot\hat{n})_s = \frac{\rho_\infty}{\rho s} (\vec{V}_\infty\cdot\hat{n})_s \qquad (26)$$

The right side is determined to first order by means of (15) and (24):

$$(\vec{V}_\infty\cdot\hat{n})_s = -\zeta_0 V_\infty \sin \beta + \epsilon_2 V_\infty (\zeta_0 g_2 \cos \beta - \xi_2 \sin \beta) \cos 2\phi + 0(\epsilon_2^2) \qquad (27)$$

The left side of Equation (26) is determined to first order from (10), (11) and (12) as:

$$(\vec{V}\cdot\hat{n})_s = v_0(\theta_s) + \epsilon_2 v_2(\theta_s) \cos 2\phi + 0(\epsilon_2^2) \qquad (28)$$

Transferring this value to the unperturbed shock yields

$$(\vec{V}\cdot\hat{n})_s = v_0(\beta) + \epsilon_2 [v_2(\beta) - g_2 \left(\frac{dv_0}{d\theta}\right)_\beta] \cos 2\phi + 0(\epsilon_2^2) \qquad (29)$$

Comparing Equations (27) and (29) leads to the following results:

$$v_0(\beta) = -\zeta_0 V_\infty \sin \beta \qquad (30)$$

$$v_2(\beta) = -\xi_2 V_\infty \sin \beta + g_2 [\zeta_0 V_\infty \cos \beta + \left(\frac{dv_0}{d\theta}\right)_\beta] \qquad (31a)$$

15

Utilizing (24c) for ξ_2 now gives

$$V_2(\beta) = g_2\{[\frac{2(\gamma-1)}{\gamma+1} - \zeta_0] V_\infty \cos \beta + (\frac{dv_0}{d\vartheta})_\beta \} \tag{31b}$$

The other two velocity components at the shock are determined from conservation of the tangential components:

$$\vec{V}_\infty \times \hat{n}_s = \vec{V}_s \times \hat{n}_s \tag{32}$$

Substitution of the first-order expansions and transfer of the conditions to the basic unperturbed shock yields

$$u_0(\beta) = V_\infty \cos \beta \tag{33}$$

$$U_2(\beta) = g_2 V_\infty \sin \beta (1-\zeta_0) \tag{34}$$

$$W_2(\beta) = -2g_2 V_\infty (1-\zeta_0) \tag{35}$$

The needed boundary conditions at the shock have now been specified.

At the body surface, $\theta = \theta_c \equiv \delta - \varepsilon_2 \cos 2\phi$, the normal velocity must vanish:

$$(\vec{V} \cdot \hat{n})_c = 0 \tag{36}$$

By means of vector analysis, the unit outward normal vector on the elliptic cone surface is found to be, to first order,

$$\hat{n}_c = \hat{e}_\theta - 2\varepsilon_2 \frac{\sin 2\phi}{\sin \delta} \hat{e}_\phi + 0(\varepsilon^2) \tag{37}$$

Substituting this expression and the velocity expansions into (3.25) and transferring the boundary conditions to the basic circular cone surface leads to the surface boundary conditions

$$v_0(\delta) = 0 \tag{38}$$

$$V_2(\delta) = (\frac{dv_0}{d\vartheta})_\delta \tag{39}$$

Equation (38), of course, is the tangency condition for the basic cone

problem, and Equation (39) is the surface boundary condition for the
first-order perturbation. Rigorously, Equation (39) should have been obtained
by matching the outer expansion with an inner expansion for the vortical layer
adjacent to the cone surface. Such an analysis shows that Equation (39) is
indeed proper (References 24 and 25).

c.   Perturbation Equations

The pressure, density, and velocity are governed by the equations of
change for mass, momentum, and energy, plus appropriate equations of state.
Here the assumption is that the flow is inviscid, nonconducting, steady, and
behaves as a thermally and calorically perfect gas. The task is first to
obtain expressions for the pressure and density perturbations in terms of the
velocities, and then finally to obtain a single equation for only one of the
perturbation velocity components.

For steady flow, the energy equation can be expressed in terms of the
entropy, s, as

$$\vec{V} \cdot grad \ s = 0 \tag{40}$$

Thus the flow on either side of the shock is isentropic, that is, the entropy
along a streamline is a constant. Of course, the uniform flow upstream of the
shock is homentropic since the entropy is the same on every streamline before
it passes through the shock. If the entropy is expanded in the form

$$s(\theta,\phi) = s_0(\theta) + \varepsilon_2 s_2(\theta) \cos 2\phi + 0(\varepsilon^2) \tag{41}$$

then expansion of Equation (40) leads to the result that s_0 is a constant and
that S_2 is also a constant. Thus the zeroth-order flow past the basic cone is
homentropic downstream of the shock. Since S_2 is a constant, the first-order
entropy perturbation depends only on the azimuthal angle ϕ. This result is
not valid on the body surface because the body surface is a stream surface

17

that has a constant entropy, since grad s is a vector that is perpendicular to the surface $s(\theta,\phi)$ = constant and is also perpendicular to the velocity, which itself is tangent to the body surface. Thus expansion (41) is not valid in a thin layer, called the vortical layer, adjacent to the body surface. Only the pressure and azimuthal velocity are uniformly valid across the vortical layer.

From the thermodynamic state relation for a perfect gas

$$\frac{ds}{c_v} = \frac{dp}{p} - \gamma \frac{d\rho}{\rho} \quad , \tag{42}$$

it is deduced that the first-order pressure and density perturbation satisfy the relation

$$\frac{P_2(\theta)}{p_0(\theta)} - \gamma \frac{R_2(\theta)}{\rho_0(\theta)} = \frac{S_2}{c_v} = \text{constant} \tag{43}$$

Another relation between the pressure and density perturbation can be found from energy considerations. Since the uniform flow upstream of the shock is homenergic (constant total enthalpy) and homenergic across the shock, it is also homenergic downstream of the shock. Thus for a perfect gas,

$$\frac{\gamma}{\gamma-1} \frac{p}{\rho} + \frac{V^2}{2} = \frac{\gamma}{\gamma-1} \frac{p_\infty}{\rho_\infty} + \frac{V_\infty^2}{2} = \text{constant} \tag{44}$$

Substituting the perturbation forms (12) into this equation and extracting the first-order perturbation yields

$$\frac{P_2(\theta)}{p_0(\theta)} - \frac{R_2(\theta)}{\rho_0(\theta)} = -\frac{\gamma-1}{\gamma} \frac{\rho_0}{p_0} (u_0 u_2 + v_0 v_2) \tag{45}$$

This is a relation between the pressure and density perturbations in terms of the velocity perturbation.

Equations (43) and (45) can be solved separately for the pressure and density perturbations.

$$R_2(\theta) = -\frac{\rho_0(u_0 u_2 + v_0 v_2)}{a_0^2} + \rho_0 F_2 \tag{46}$$

$$P_2(\theta) = - \rho_0(a_0^2\rho_2 + v_0 V_2) + \rho_0 F_2 \tag{47}$$

where $a_0^2(\theta) \equiv \gamma p_0/\rho_0$ is the speed of sound squared in the basic unperturbed flow, and

$$F_2 \equiv - \frac{S_2}{(\gamma-1)c_v} = \text{constant} \tag{48}$$

The pressure and density perturbations are thus determined in terms of the velocity perturbations. The constant F_2 can be obtained from the shock boundary conditions

$$F_2 = \frac{P_2(\beta)}{\rho_0(\beta)} + \frac{\rho_0(\beta)}{\rho_0(\beta)} [u_0(\beta) U_2(\beta) + v_0(\beta) V_2(\beta)]$$

$$= \gamma q_2 V_\infty^2 \sin \beta \cos \beta \, (1-\xi_0)^2/a_0^2(\beta) \tag{49}$$

The momentum equation for inviscid steady flow is

$$\rho[\nabla(\frac{V^2}{2}) - \vec{V} \times \vec{\Omega}] = -\nabla p \tag{50}$$

where

$$\vec{\Omega} = \text{curl } \vec{V}$$

is the vorticity vector. For the vector quantities let

$$\vec{V} = \vec{v}_0 + \varepsilon_2 \vec{V}_2 + \theta(\varepsilon_2^2) \tag{51a}$$

$$\vec{\Omega} = \varepsilon_2 \vec{\Omega}_2 + \theta(\varepsilon^2) \tag{51b}$$

When the perturbation expansions are substituted into Equation (50), the first-order perturbation equation can be extracted, and it is

$$(\rho_2 \cos 2\phi) \nabla (\frac{u_0^2 + v_0^2}{2}) + \rho_0(\vec{V}_0 \cdot \vec{V}_2) - \rho_0 \vec{V}_0 \times \vec{\Omega}_2 = -\nabla(P_2 \cos 2\phi) \tag{52}$$

The first-order vorticity perturbation has the components

$$\Omega_{2r} = \frac{\sin 2\phi}{r \sin \theta} \left[\frac{d}{d\theta} (V_2 \sin \theta) + 2V_2 \right] \tag{53a}$$

$$\Omega_{2\theta} = - \frac{\sin 2\phi}{r \sin \theta} \left[2U_2 + W_2 \sin \theta \right] \tag{53b}$$

$$\Omega_{2\phi} = \frac{\cos 2\phi}{r} \left[V_2 - \frac{dU_2}{d\theta} \right] \tag{53c}$$

In addition,

$$\vec{V}_0 \times \vec{\Omega}_2 = \hat{e}_r (v_0 \Omega_{2\phi}) - \hat{e}_\theta (u_0 \Omega_{2\phi}) + \hat{e}_\phi (u_0 \Omega_{2\theta} - v_0 \Omega_{2r}) \tag{54}$$

From Equation (52) it can be determined that

$$(\vec{V}_0 \times \vec{\Omega}_2) \cdot \hat{e}_r = 0 \tag{55}$$

It follows from (54) that $\Omega_{2\phi} = 0$, and hence that

$$V_2 = \frac{dU_2}{d\theta} \tag{56}$$

Thus Equation (54) reduces to

$$\vec{V}_0 \times \vec{\Omega}_2 = \hat{e}_\phi (u_0 \Omega_{2\theta} - v_0 \Omega_{2r})$$

The ϕ-component of Equation (52) can be written as

$$u_0 \Omega_{2\theta} - v_0 \Omega_{2r} = -2 \left[\frac{P_2}{\rho_0} + u_0 U_2 + v_0 V_2 \right] \frac{\sin 2\phi}{r \sin \theta} \tag{57}$$

The pressure perturbation P_2 can be eliminated by means of Equation (47), and results in

$$u_0 \Omega_{2\theta} - v_0 \Omega_{2r} = \frac{-2a_0^2 F_2}{\gamma} \frac{\sin 2\phi}{r \sin \theta} \tag{58}$$

20

where $a_0^2(\theta) \equiv \gamma p_0/\rho_0$ and F_2 is a constant given by (49). By means of

(53 a,b) Equation (58) can be further rewritten as

$$v_0 \frac{d}{d\theta} [2U_2 + W_2 \sin \theta] + u_0[2U_2 + W_2 \sin \theta] = \frac{2F_2}{\gamma} a_0^2(\theta) \qquad (59)$$

Introducing the integration factor

$$I(\theta) \equiv \exp \left[\int_\beta^\theta \left(\frac{u_0}{v_0}\right) d\theta \right] , \qquad (60)$$

allows integration of Equation (59) and provides

$$2U_2 + W_2 \sin \theta = \frac{2F_2}{\gamma} \frac{1}{I} \int_\beta^\theta \frac{a_0^2 I}{v_0} d\theta \qquad (61)$$

The constant of integration vanishes by virtue of the shock boundary

conditions (34) and (35). Equations (56) and (61) give V_2 and W_2 in terms of

U_2. It remains to find a single equation for U_2.

Mass conservation is described by the continuity equation

$$\text{div}(\rho \vec{V}) = 0 \qquad (62)$$

When the perturbation expansions are substituted into this equation and the

first-order perturbation extracted, the result is

$$\text{div} (R_2 \cos 2\phi \ \vec{v}_0 + \rho)\vec{V}_2) = 0 \qquad (63)$$

With the basic mass conservation equation accounted for, this equation can be

rearranged to read

$$\text{div} \vec{V}_2 = -\vec{v}_0 \cdot \nabla \left(\frac{R_2 \cos 2\phi}{\rho_0}\right) - \frac{\vec{V}_2}{\rho_0} \cdot \nabla \rho_0 \qquad (64)$$

If it were assumed that the density varies so slowly that it is approximately

a constant, then the right side of Equation (64) can be set equal to zero as

21

an approximation, and a relatively simple equation for V_2 ensues. Note that the right side does, in fact, vanish at the body surface, $\theta = \delta$. This so-called constant-density approximation leads to remarkably accurate results for the basic-flow solution and for the flow past a circular cone at angle of attack (References 22, 23). These constant-density approximations were justified a posteriori by comparison with extensive numerical tabulated results. Such comparisons are not so available for the elliptic-cone problem of present interest, and hence more attention must be devoted to the terms on the right side of Equation (64).

Now eliminate $R_2(\theta)$ in Equation (64) by means of Equation (46) and utilize the following basic-flow results:

$$\frac{a_0^2}{\rho_0} \frac{d\rho_0}{d\theta} = \frac{1}{\rho_0} \frac{dp_0}{d\theta} = \frac{1}{\gamma-1} \frac{da_0^2}{d\theta} = - \frac{d}{d\theta} \frac{(u_0^2 + v_0^2)}{2} \qquad (65)$$

Equation (64) can now be expanded and written in the form

$$[1-A] \frac{dV_2}{d\theta} + \cot\theta [1-B]V_2 + (2 - \frac{4}{\sin^2\theta} - C)U_2 = - \frac{2(2U_2 + W_2 \sin\theta)}{\sin^2\theta} \qquad (66)$$

where

$$A(\theta) \equiv \frac{v_0^2}{a_0^2} \qquad (67a)$$

$$B(\theta) \equiv \tan\theta \frac{v_0}{a_0^2} (u_0 + \frac{dv_0}{d\theta}) \{2 + (\gamma-1) \frac{v_0^2}{a_0^2}\} \qquad (67b)$$

$$C(\theta) \equiv \frac{v_0^2}{a_0^2} \{1 + (\gamma-1) \frac{u_0}{a_0^2} (u_0 + \frac{dv_0}{d\theta})\} \qquad (67c)$$

The factors A, B, and C in Equation (66) are variable coefficients, and they stem from the right side of Equation (64). At the cone surface $\theta = \delta$, the factors A, B, and C all vanish since $v_0(\delta) = 0$. At the shock surface $\theta = \beta$, the factors A, B, and C take the values

$$A(\beta) = \frac{2\xi_0}{(\gamma+1) - \xi_0(\gamma-1)} \qquad , \qquad (68a)$$

$$B(\beta) = \frac{4}{(\gamma+1) - \xi_0(\gamma-1)} \qquad , \qquad (68b)$$

$$C(\beta) = \frac{\xi_0 - 2(\gamma-1/\gamma+1) \cot^2\beta}{(\gamma+1) - \xi_0(\gamma-1)} \qquad , \qquad (68c)$$

where the undisturbed shock density ratio, ξ_0, is given by (24b). In the hypersonic limit, $K_\beta = \infty$ and $A(\beta)$ takes the value $(\gamma-1)/2\gamma$. Thus for $\gamma = 7/5$, $A(\beta) = 1/7$ for $K_\beta = \infty$. For hypersonic flow it is thus safe to neglect $A(\theta)$ compared to unity. Since $A(\delta) = 0$, it is thus reasonable to neglect $A(\theta)$ always except perhaps very near sonic conditions, for which $A(\beta) = 1$ when $K_\beta = 1$. Likewise $C(\beta)$ is small compared to $(2 - 4 \csc^2 \beta)$ in the coefficient of U_2 for all values of K_β. Thus $C(\theta)$ should be negligible in general since it also vanishes at $\theta = \delta$. The factor $B(\beta)$ varies between $(\gamma+1)/\gamma$ for $K_\beta = \infty$ and 2 for $K_\beta = 1$, and thus apparently should not be neglected compared to unity. Moreover, the factor $(1-B)$ changes sign between the shock and the body. On the other hand, if A, B, and C are all neglected, the resulting differential equation still behaves properly at the body surface since A, B, and C vanish there anyway. In addition, the resulting second-order differential equation must satisfy the two boundary conditions for $U_2(\beta)$ and $V_2(\beta)$ at the shock. Thus, even though A, B, and C be neglected, the resulting solution should behave properly at both sides of the shock layer, and presumably also in between. As mentioned earlier, neglecting A, B, and C yields good results for the circular cone at angle of attack.

Even though it is intended eventually to obtain an approximate solution by neglecting A, B, and C, the results can be justified still further by recasting the differential equation as an integral equation. Replacing V_2 by (56) and W_2 by (61), Equation (66) can be rewritten as

23

$$U_2'' + \cot\theta\, U_2' + (2 - 4\csc^2\theta)U_2 = -\frac{4F_2}{\gamma}\frac{H_0(\theta)}{\sin^2\theta} + H_2(\theta) \qquad (69)$$

where

$$H_0(\theta) \equiv \frac{1}{I}\int_\beta^\theta \frac{a_0^2\, I}{v_0}\, d\theta \qquad (70a)$$

$$H_2(\theta) \equiv AU_2'' + B\cot\theta\, U_2' + CU_2 \qquad (70b)$$

When H_0 and H_2 vanish, a solution to equation (69) is $U_2 = \csc^2\theta$. This suggests the substitution

$$U_2 = X(\theta)\csc^2\theta \qquad (71)$$

Equation (69) can now be written

$$\left(\frac{X'}{\sin^3\theta}\right)' = -\frac{4F_2}{\gamma}\frac{H_0(\theta)}{\sin^3\theta} + \frac{H_2(\theta)}{\sin\theta} \qquad (72)$$

Two integrations yield

$$X(\theta) = X(\beta) + \frac{X'(\beta)}{\sin^3\beta}\int_\beta^\theta \sin^3\theta\, d\theta \qquad (73)$$

$$- \frac{4F_2}{\gamma}\int_\beta^\theta\left[\sin^3\theta\int_\beta^\theta \frac{H_0(\theta)}{\sin^3\theta}\, d\theta\right]d\theta + \int_\beta^\theta\left[\sin^3\theta\int_\beta^\theta \frac{H_2(\theta)}{\sin\theta}\, d\theta\right]d\theta$$

where

$$X(\beta) = U_2(\beta)\sin^2\beta$$

$$= q_2 V_\infty \sin^3\beta\,(1 - \xi_0) \qquad (74a)$$

$$X'(\beta) = q_2\sin^2\beta\left[\frac{(4\gamma - 3\xi_0)}{\gamma+1}V_\infty\cos\beta + \left(\frac{dv_0}{d\theta}\right)_\beta\right] \qquad (74b)$$

When $X(\theta)$ is known, the veloci'   onents are determined by

$$U_2(\theta) = \qquad \qquad {}^2\theta \qquad (75a)$$

$$V_2(\theta) \qquad \qquad X(\theta)\cot\theta/\sin^2\theta \qquad (75b)$$

$$W_2(\theta) = [-2U_2(\theta) + \frac{2F_1}{\gamma} H_0(\theta)]/\sin \theta \qquad (75c)$$

The shock eccentricity factor g_2 is determined by satisfying the surface boundary condition (39) and then solving for g_2. Equation (73) is an integral equation because the unknown function $X(\theta)$ also appears in the function $H_2(\theta)$.

d. Approximate Solution for Hypersonic Flow

For hypersonic flow in the limit $M_\infty \to \infty$ and $\sin \theta \to 0$ such that the combination $K \equiv M_\infty \sin \theta$ remains finite, the basic cone flow can be approximated accurately by (References 20 and 21)

$$\frac{u_0(\theta)}{V_\infty} = 1 - \sin^2 \delta [\sin^2 \theta/\sin^2 \delta + 2\ell n \ ((\sin \beta/\sin \theta))]/2 \qquad (76a)$$

$$\frac{v_0(\theta)}{V_\infty} = - \sin \theta \ [1 - \frac{\sin^2 \delta}{\sin^2 \theta}] \qquad (76b)$$

and the relation between the shock and body angles is given by

$$\frac{\sin \beta}{\sin \delta} = \sqrt{\frac{\gamma+1}{2} + \frac{1}{(M_\infty \sin \delta)^2}} \qquad (76c)$$

Now restrict computations to small angles such that $\sin \theta = \theta$ and neglect second-order terms in (76). The results are

$$\frac{u_0}{V_\infty} \approx 1 \qquad (77a)$$

$$\frac{v_0}{V_\infty} \approx -\theta \ (1 - \frac{\delta^2}{\theta^2}) \qquad (77b)$$

$$\frac{\beta}{\delta} = \sqrt{\frac{\gamma+1}{2} + \frac{1}{K_\delta^2}} \qquad (77c)$$

where $K_\delta \equiv K_\infty \delta$ is the hypersonic similarity parameter.

With the approximations (77a,b), the integrating factor I becomes

$$I = ((\beta^2 - \delta^2)/(\theta_2 - \delta^2))^{1/2} \tag{78}$$

In the evaluation of the function $H_0(\theta)$ given by (70a), the speed of sound squared $a_0^2(\theta)$ varies only by a few percent across the shock layer. Replace it by $a_0^2(\beta)$, and the function $H_0(\theta)$ becomes

$$H_0(\theta) = \frac{a_0^2(\beta)}{V_\infty} \left\{ 1 - \sqrt{\frac{\theta^2 - \delta^2}{\beta^2 - \delta^2}} \right\} \tag{79}$$

Thus are attained

$$\int_\beta^\theta \frac{H_0(\theta)}{\theta^3} d\theta = \frac{a_0^2(\beta)}{2V_\infty} \left[\frac{1}{\theta^2} \left\{ \sqrt{\frac{\theta^2 - \delta^2}{\beta^2 - \delta^2}} - 1 \right\} + \frac{1}{\delta\sqrt{\beta^2 - \delta^2}} \left(\cos^{-1}\frac{\delta}{\beta} - \cos^{-1}\frac{\delta}{\theta} \right) \right]$$

$$\tag{80}$$

$$\int_\beta^\theta [\theta^3 \int_\beta^\theta \frac{H_0(\theta)}{\theta^3} d\theta] = \frac{a_0^2(\beta)}{4V_\infty} \left\{ \sqrt{\frac{\theta^2 - \delta^2}{\beta^2 - \delta^2}} \left(\frac{5}{6}\theta^2 - \frac{\delta^2}{3} \right) \right.$$

$$\tag{81}$$

$$\left. + \frac{\theta^4}{2\delta\sqrt{\beta^2 - \delta^2}} \left(\cos^{-1}\frac{\delta}{\beta} - \cos^{-1}\frac{\delta}{\theta} \right) + \frac{\beta^2}{6} + \frac{\delta^2}{3} - \theta^2 \right\}$$

The first approximation solution for the integral equation (4.35) is obtained by neglecting the integral involving $H_2(\theta)$, which is the same as omitting the factors A, B, and C in the original differential equation. The results are

$$U_2(\theta) = \frac{X(\beta)}{\theta^2} + \frac{X'(\beta)}{4\beta^3\theta^2} (\theta^4 - \beta^4) + \frac{f_2}{2} \left\{ \sqrt{\frac{\theta^2 - \delta^2}{\beta^2 - \delta^2}} \left(\frac{5}{6} - \frac{\delta^2}{3\theta^2} \right) \right.$$

$$\left. + \frac{\theta^2}{2\delta\sqrt{\beta^2 - \delta^2}} \left(\cos^{-1}\frac{\delta}{\beta} - \cos^{-1}\frac{\delta}{\theta} \right) + \frac{\beta^2}{6\theta^2} + \frac{\delta^2}{3\theta^2} - 1 \right] \tag{82}$$

$$V_2(\theta) = -\frac{2X(\beta)}{\theta^3} + \frac{X'(\beta)}{2}\left(\frac{\theta}{\beta^3} + \frac{\beta}{\theta^3}\right) + f_2\left[\frac{1}{\theta}\sqrt{\frac{\theta^2 - \delta^2}{\beta^2 - \delta^2}}\left(\frac{1}{6} + \frac{\delta^2}{3\theta^2}\right)\right.$$

$$+ \frac{\theta}{2\delta\sqrt{\beta^2 - \delta^2}}\left(\cos^{-1}\frac{\delta}{\beta} - \cos^{-1}\frac{\delta}{\theta}\right) - \frac{\beta^2}{6\theta^3} - \frac{\delta^2}{3\theta^3}\left.\right] \tag{83}$$

$$W_2(\theta) = -\frac{2X(\beta)}{\theta^3} - \frac{X'(\beta)}{2\beta^3\theta^3}(\theta^4 - \beta^4) - f_2\left[\frac{1}{\theta}\sqrt{\frac{\theta^2 - \delta^2}{\beta^2 - \delta^2}}\left(-\frac{1}{6} - \frac{\delta^2}{3\theta^2}\right)\right.$$

$$+ \frac{\theta}{2\delta\sqrt{\beta^2 - \delta^2}}\left(\cos^{-1}\frac{\delta}{\beta} - \cos^{-1}\frac{\delta}{\theta}\right) + \frac{\beta^2}{6\theta^3} + \frac{\delta^2}{3\theta^3}\left.\right] \tag{84}$$

where

$$f_2 \equiv -\frac{2F_2 a_0{}^2(\beta)}{\gamma V_\infty} = -2q_2 V_\infty \sin\beta \cos\beta(1 - \xi_0)^2$$

$$\approx -2q_2 V_\infty \beta(1 - \xi_0)^2 \tag{85}$$

$$X(\beta) \approx q_2 V_\infty \beta^3(1 - \zeta_0) \tag{86a}$$

$$X'(\beta) \approx q_2\beta^2\left[\left(\frac{4\gamma}{\gamma+1} - 3\xi_0\right)V_\infty + \left(\frac{dv_0}{d\theta}\right)_\beta\right] \tag{86b}$$

$$\approx \frac{2}{\gamma+1}q_2 V_\infty \beta^2\left[(\gamma-1) - \xi_0(\gamma+1)\right] \tag{86c}$$

Expression (86c) is the approximation consistent with the velocity approximation (77b), that is,

$$\left(\frac{dv_0}{d\theta}\right)_\beta \approx -V_\infty\left(1 + \frac{\delta^2}{\beta^2}\right) \tag{87a}$$

$$\approx -V_\infty(2 - \zeta_0) \tag{87b}$$

since

$$\zeta_0 \approx 1 - \frac{\delta^2}{\beta^2} \tag{87c}$$

The shock eccentricity factor, q_2, can now be determined from the boundary condition

$$V_2(\delta) = \left(\frac{dv_0}{d\theta}\right)_\delta = -2V_\infty \tag{88}$$

Solving for q_2 from Equation (83) yields

$$\frac{1}{q_2} = (1 - \xi_0)^2 \left\{ \frac{\beta \cos^{-1}(\delta/\beta)}{2\sqrt{\beta^2 - \delta^2}} - \frac{\beta^3}{6\delta^3} - \frac{\beta}{3\delta} \right\} + (1 - \xi_0)\frac{\beta^3}{\delta^3}$$

$$+ \frac{1}{2}\left\{\xi_0 - \frac{\gamma-1}{\gamma+1}\right\}\left(\frac{\delta}{\beta} + \frac{\beta^3}{\delta^3}\right) \tag{89}$$

Denoting the basic-cone shock-body ratio by

$$\sigma \equiv \frac{\beta}{\delta} = \sqrt{\frac{\gamma+1}{2} + \frac{1}{K_\delta^2}} \quad , \tag{90}$$

one obtains

$$\frac{1}{q_2} = \frac{1}{6\sigma^3}\left[\frac{3\cos^{-1}(1/\sigma)}{\sqrt{\sigma^2 - 1}} + \frac{6}{\gamma+1}(\sigma^6 + \sigma^2) + 3\sigma^4 - \sigma^2 - 5\right] \tag{91}$$

The shock eccentricity factor, q_2, is plotted in Figure 3 as a function of K_δ for $\gamma = 7/5$. For $K_\delta \to 0$, which corresponds to the limit of linearized theory, the eccentricity factor tends to zero, $q_2 \to 0$; that is, the shock tends to a circular Mach cone. For the limiting hypersonic flow, $K_\delta \to \infty$, q_2 approaches the asymptote $q_2 = 0.955$, and the shock tends to embrace the elliptic cone body. The shock, however, is always less eccentric than the body. When $K_\delta \to \infty$ and $\gamma \to 1$, then $\beta \to \delta$ and $q_2 \to 1$, and the shock embraces the body, in agreement with hypersonic Newtonian theory. The angle-of-attack shock eccentricity factor, q_0, obtained later, is also shown in Figure 3 for comparison.

The first approximation for the velocity U_2, given by Equation (82), is plotted in Figure 4. The hypersonic similarity form gives $U_2/V_\infty\delta$ as a

29

$\Delta_0 = |2 + w_0^2 \cos \zeta + \frac{1}{2} w_0^2 \cos 2\zeta \cdots$
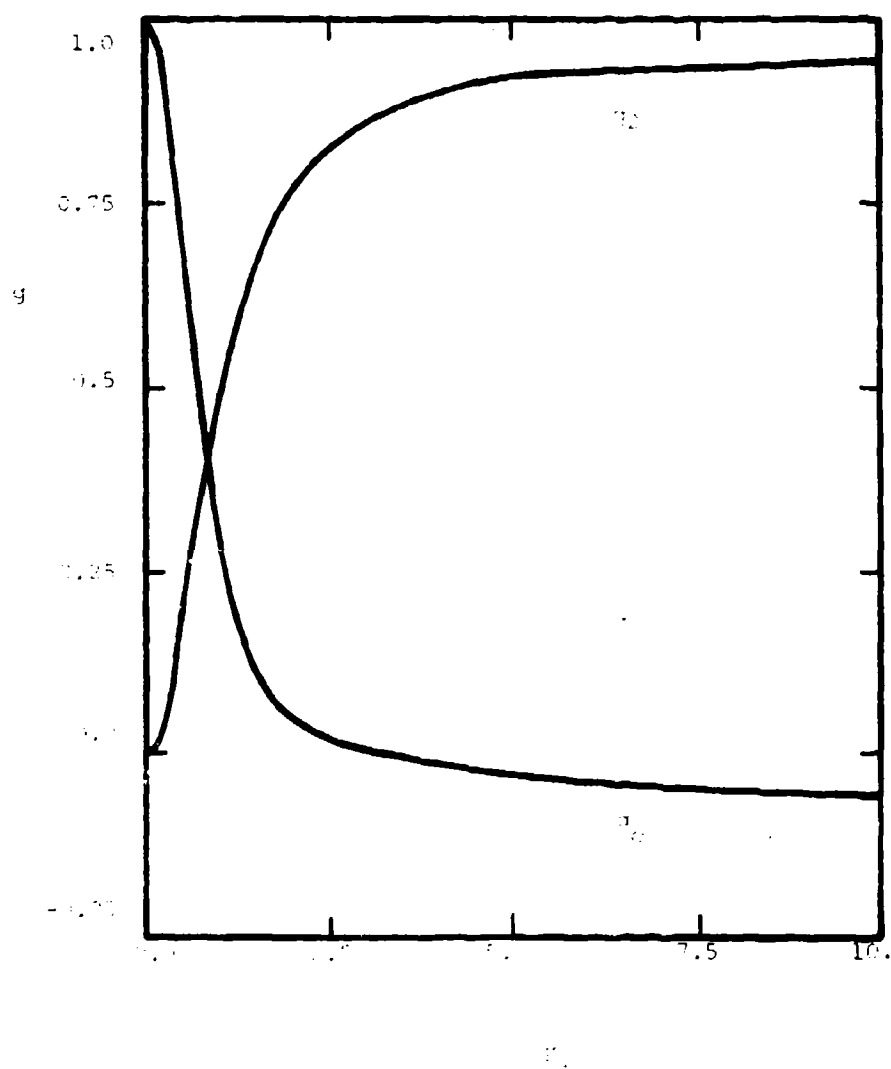
function of θ/δ, K_δ, and γ. Because the thickness of the shock layer varies as a function of K_δ, the shock layer is normalized by means of the variable

$$\theta' = \frac{\theta - \delta}{\beta - \delta} \quad . \tag{92}$$

The body surface corresponds to $\theta' = 0$ and the shock surface to $\theta' = 1$. At the body surface $U_2/V_\infty\delta$ is insensitive to variations in K_δ, having approximately the value unity. At the shock surface, $U_2/V_\infty\delta$ is quite sensitive to variations in K_δ. In the hypersonic limit $K_\delta = \infty$, $U_2/V_\infty\delta$ increases only slightly from the shock to the body.

The velocity perturbation V_2/V_∞ is shown in Figure 5 as a function of θ', $\gamma = 1.4$, and various values of K_δ. The variation of V_2/V_∞ across the shock layer is analogous to the variation of $U_2/V_\infty\delta$, except that V_2/V_∞ is equal to -2 at $\theta' = 0$ as imposed by the boundary condition, Equation (88).

The azimuthal velocity perturbation W_2/V_∞ is shown in Figure 6 as a function of θ', $\gamma = 1.4$, and various values of K_δ. At the shock surface, W_2/V_∞ increases as K_δ increases. For $K_\delta = 2$, the variation of W_2/V_∞ across the shock layer is very slight. At the body surface, W_2/V_∞ decreases as K_δ increases. This is shown also in Figure 7. When $K_\delta \to 0$, $W_2(\delta)/V_\infty \to -2$ which is in agreement with linearized theory. In the hypersonic limit $K_\delta \to \infty$, $W_2(\delta)/V_\infty$ becomes asymptotic to the value 0.659 for $\gamma = 1.4$. The corresponding angle-of-attack contribution, $W_0(\delta)/V_\infty$, discussed in Section 2, is shown in Figure 7 for comparison.

e. Evaluation of the Approximate Analysis

Let the first approximation for the integral Equation (73) be denoted by $U_2^{(0)}$, which is given by Equation (82). Then the integral Equation (73) can be written, for small angles, as

Figure 5. Radial Variation of Velocity, γ = 1.4
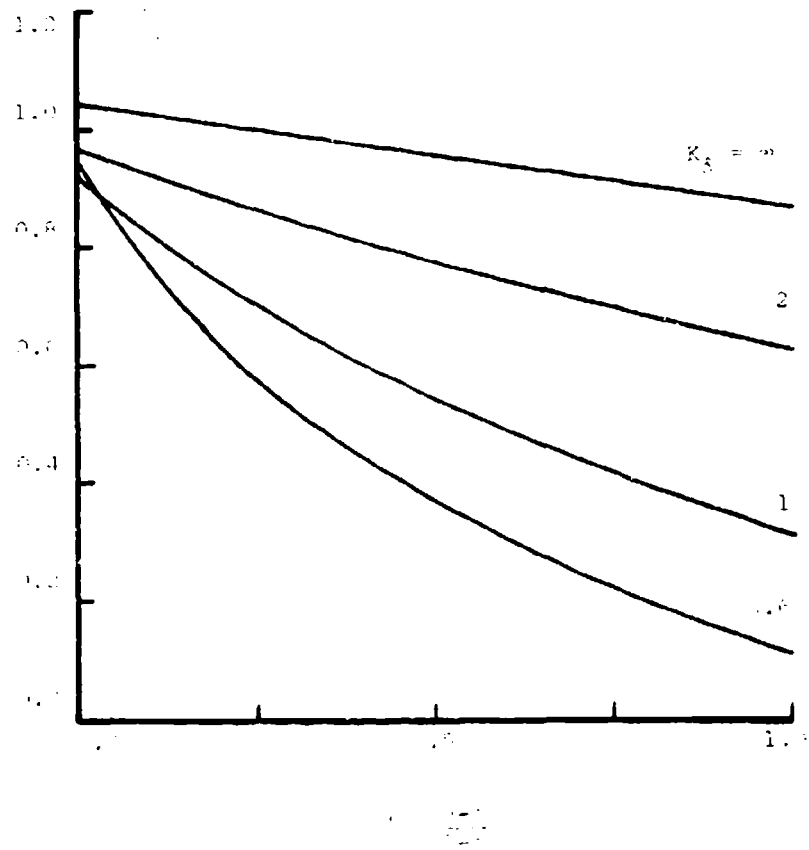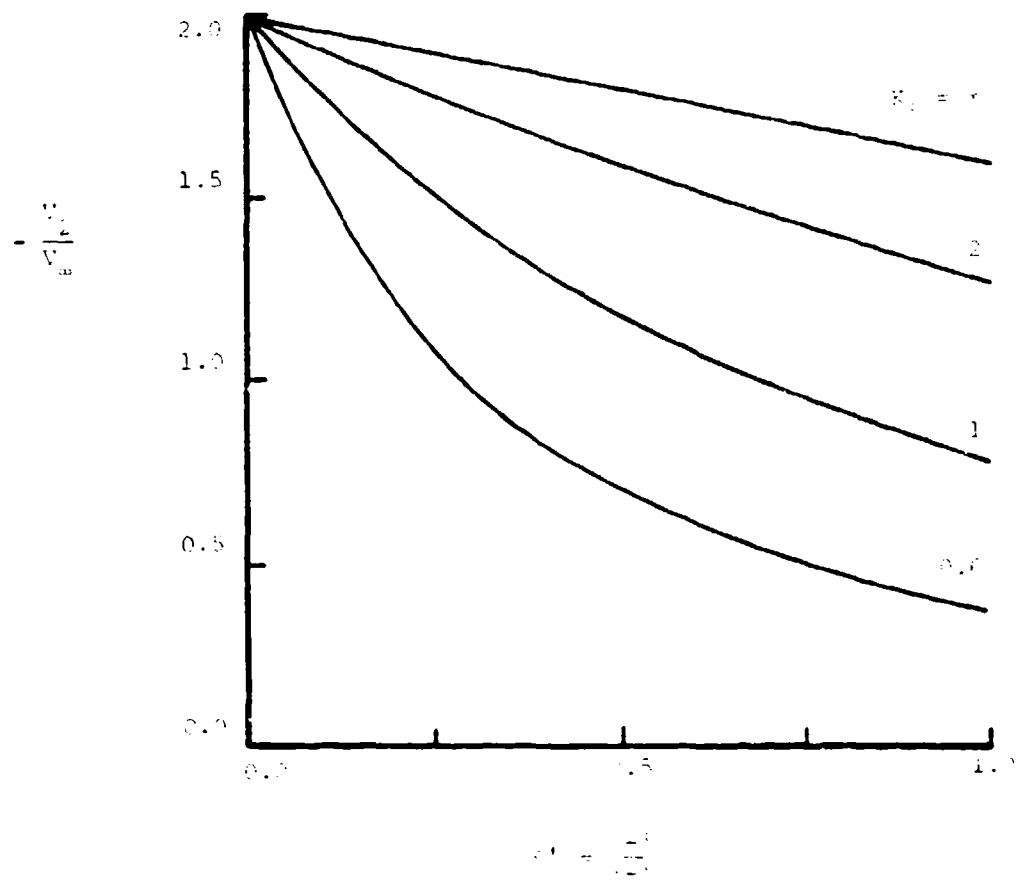
Figure 8. Polar Perturbation Velocity Component, $\gamma = 1.4$

Figure ... Non-dimensional ... Bending ... ... moment, ...
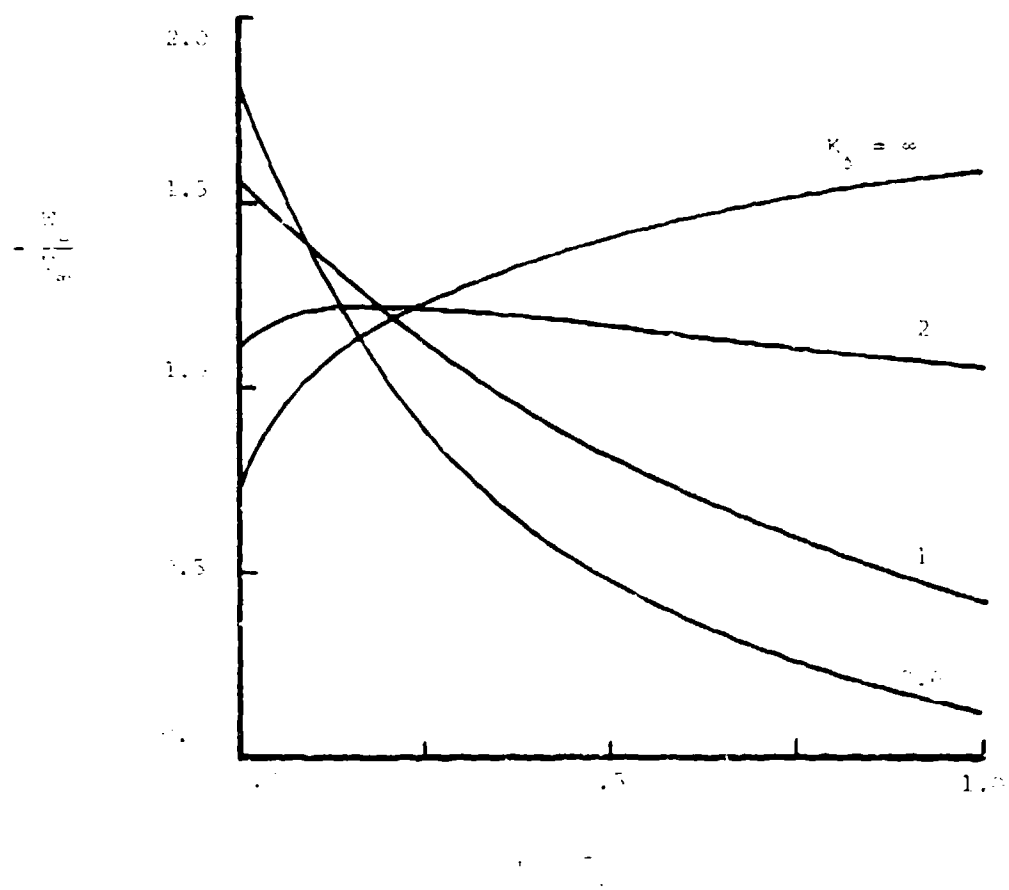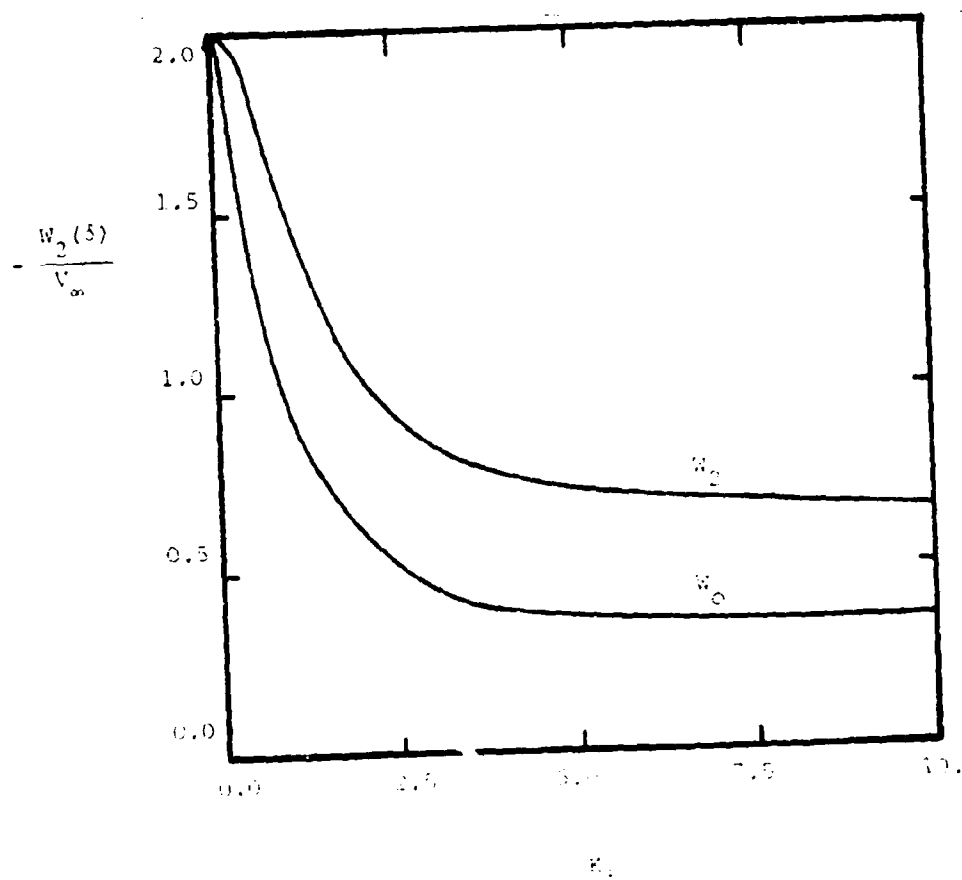
Figure 7. Azimuthal Velocity at the Body Surface, $\gamma = 1.4$

$$U_2 = U_2{}^{(0)} + U_2{}^{(c)} \, , \tag{93}$$

where

$$U_2{}^{(c)}(\theta) \equiv \frac{1}{\sin^2\theta} \int_\beta^\theta \sin^3\theta \left(\int_\beta^\theta \frac{H_2(\theta)}{\sin\theta} \, d\theta \right) d\theta \tag{94a}$$

$$= \frac{1}{\theta^2} \int_\beta^\theta \theta^3 \left(\int_\beta^\theta \frac{H_2(\theta)}{\theta} \, d\theta \right) d\theta \tag{94b}$$

$$H_2(\theta) = A U_2'' + B \cot\theta \, U_2' + c U_2 \tag{95}$$

Consider now an approximate evaluation of the correction function $U_2{}^{(c)}$. Towards this end we utilize the well-known convergent iteration procedure for Voltera-type integral equations. The first step is to substitute the first approximation $U_2{}^{(0)}$ into $H_2(\theta)$ and then evaluate $U_2{}^{(c)}$. Expression (82) for $U_2{}^{(0)}$ is fairly complicated and does not lend itself to a simple analytical evaluation of $U_2{}^{(c)}$. Figure 4 shows, however, that $U_2{}^{(0)}(\theta)$ can be approximated by the simple formula

$$\frac{U_2{}^{(0)}}{V_\infty \delta} = \left(\frac{\delta}{\theta}\right)^2 G(\theta, K_\delta) \tag{96a}$$

where $G(\theta, K_\delta)$ is a slowly varying function of θ and K_δ, being approximately unity. It now follows approximately that

$$\frac{U_2'{}^{(0)}}{V_\infty} = \frac{V_2{}^{(0)}}{V_\infty} = -2 \left(\frac{\delta}{\theta}\right)^3 G \tag{96b}$$

$$\frac{U_2''{}^{(0)}}{V_\infty} = 6 \frac{\delta^3}{\theta^4} G \tag{96c}$$

since G is nearly a constant. Again it may be verified that expression (96b) gives a reasonable approximation to Figure 5.

Substitution of expression (96) into (95) and then (94b) yields

$$U_2^{(c)}(\theta) \simeq U_2^{(0)}(\theta) \int_\beta^\theta \theta^3 \left(\int_\beta^\theta \left[\frac{6A}{\theta^5} - \frac{2B}{\theta^5} + \frac{C}{\theta^3} \right] d\theta \right) d\theta \qquad (97)$$

In the evaluation of A, B, and C, given by Equation (67), set $a_0^2(\theta) \simeq a_0^2(\delta)$ since $a_0^2(\theta)$ varies by only a few percent over the shock layer. With the approximations (77a,b) the result, for small angles and with $z \equiv \theta/\delta$, is

$$A \simeq Nz^2 \left(1 - \frac{1}{z^2}\right)^2 \qquad (98a)$$

$$B \simeq N \left(1 - \frac{1}{z^2}\right) \left[2 + (\gamma-1) Nz^2 \left(1 - \frac{1}{z^2}\right)^2\right] \qquad (98b)$$

$$C \simeq - (\gamma-1) N^2 \frac{z^2}{\theta^2} \left(1 - \frac{1}{z^2}\right)^2 \qquad (98c)$$

where

$$N \equiv \frac{V_\infty^2 \delta^2}{a_0^2(\beta)} \frac{2\sigma^2}{(\sigma^2-1)(2\sigma^2+\gamma-1)} \qquad (99)$$

where $\sigma \equiv \beta/\delta$, given by (90). With the formulas (98), the integral in (97) can be evaluated, and the following expressions result. -

$$\frac{U_2^{(c)}(\theta)}{NU_2^{(0)}(\theta)} \simeq -4 \ln \left(\frac{\sigma}{z}\right) + \frac{(\sigma^2-z^2)}{2} \left(3 + \frac{5}{3\sigma^2 z^2}\right)$$

$$+ (\sigma^4-z^4) \left(- \frac{3}{4\sigma^2} + \frac{1}{\sigma^4} - \frac{5}{12\sigma^6}\right)$$

$$+ (\gamma-1)N \left[2 \ln \left(\frac{\sigma}{z}\right) - \frac{(\sigma^2-z^2)}{4} \left(3 + \frac{7}{3\sigma^2 z^2}\right)\right.$$

$$\left. + (\sigma^4-z^4) \left(\frac{3}{8\sigma^2} - \frac{1}{2\sigma^4} + \frac{7}{24\sigma^6} - \frac{1}{16\sigma^8} + \frac{1}{16\sigma^4 z^4}\right)\right] \qquad (100)$$

At the shock, $z = \sigma$, the correction vanishes, $U_2^{(c)}(\beta) = 0$. The largest correction occurs at the body surface, $z = 1$, so that

$$\frac{U_2^{(c)}(\delta)}{NU_2^{(0)}(\delta)} \simeq -4 \ln \sigma + \frac{(\sigma^2-1)}{4} \left(3 + \frac{13}{3\sigma^2} + \frac{7}{3\sigma^4} - \frac{5}{3\sigma^6}\right)$$

$$+ (\gamma-1) N \left[2 \ln - \frac{(\sigma^2-1)}{8} \left(3 + \frac{31}{6\sigma^2} + \frac{7}{6\sigma^4} - \frac{11}{6\sigma^6} + \frac{1}{2\sigma^8}\right)\right] \qquad (101)$$

The correction factor $U_2^{(c)}(\delta)/U_2^{(0)}(\delta)$ is shown in Figure 8 as a function of K_δ and $\gamma = 1.4$. In the hypersonic limit, $K_\delta = \infty$, the correction factor is approximately -0.0073, and thus the error in the first approximation is about one percent or less. As K_δ decreases, the correction becomes slightly more negative, being approximately -0.015 at $K_\delta = 1.7$. As K_δ decreases further, the correction factor increases from the minimum negative value and becomes zero at $K_\delta \simeq 1$. Further decreases in K_δ give a rapid increase in the correction factor, becoming 0.75 in the limit $K_\delta = 0$ which corresponds to linearized theory.

In the hypersonic flow range, the first approximation, obtained by neglecting $U_2^{(c)}$, is expected to be very accurate. In fact, this is true when $K_\delta > 1$. When $K_\delta < 1$, the first approximation is less accurate. Note, however, that the correct limiting results for $K_\delta = 0$, which correspond to the limiting case of linearized theory, are recovered. This is true because the perturbation U_2 itself vanishes when $\delta \rightarrow 0$ and also because the surface boundary condition $V_2(\delta) = -2V_\infty$ is enforced on the first approximation itself (which produces the first approximation for g_2). The surface boundary condition is always exactly enforced. Thus, although the linearized limit $K_\delta = 0$ is recovered, the approach to the linearized limit is in error. Because the results are correct at $K_\delta = 0$ and very nearly correct at $K_\delta = 1$, the error in the range $0 < K_\delta < 1$, while greater than for $K_\delta > 1$, is less than that indicated in Figure 8.

The above observations are born out by the results of Doty and Rasmussen (Reference 23) for hypersonic flow past a circular cone at angle of attack. Their approximate analysis was analogous to the present analysis, but the results could be compared extensively with well-known tabulated results. The agreement was very good. Thus, whereas extensive tabulated results for the

37
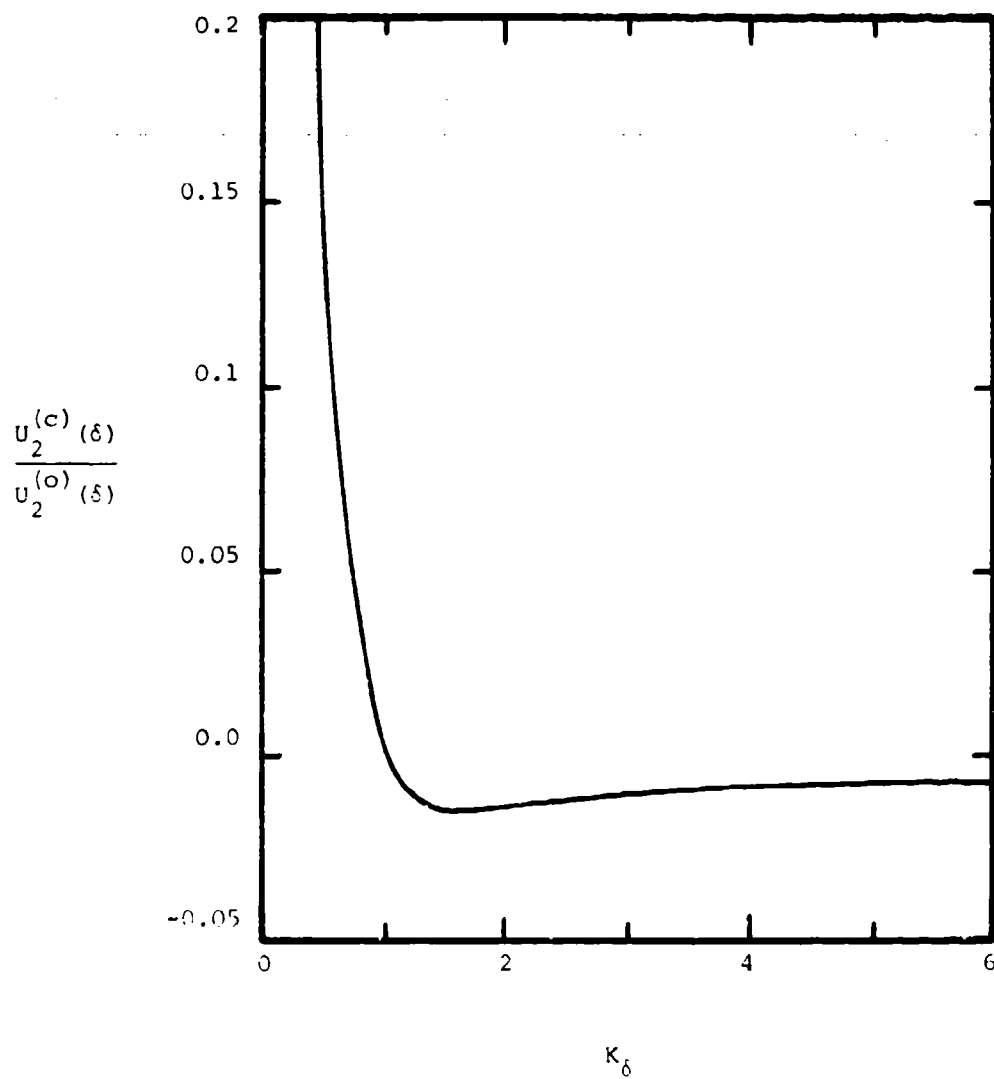
Figure 8. Correction Velocity Ratio, $\gamma = 1.4$

elliptic cone do not exist as they do for the circular cone at angle of attack, the above error analysis and the experience of Doty and Rasmussen justify confidence in the present analysis.

f.   Surface Pressure on the Elliptic Cone, Comparison with Experiment

The pressure on the surface of the cone is given by (for $\alpha = 0$)

$$p(\theta_c, \phi) = p_0(\theta_c) + \epsilon P_2(\theta_c) \cos 2\phi + 0(\epsilon_2^2) \tag{102}$$

where

$$\theta_c = \delta - \epsilon_2 \cos 2\phi + 0(\epsilon_2^2) \tag{103}$$

Transferring the expression (102) to the basic cone gives

$$p(\theta_c, \phi) = p_0(\delta) + \epsilon_2 [P_2(\delta) - (\frac{dp_0}{d\theta})_\delta] \cos 2\phi + 0(\epsilon^2) \tag{104}$$

At the cone surface, the gradient of the basic pressure, p_0, vanishes since $v_0(\delta) = 0$; that is,

$$(\frac{dp_0}{d\theta})_\delta = -\rho_0(\delta) \, v_0(\delta) \, [u_0 + \frac{dv_0}{d\theta}]_\delta = 0 \tag{105}$$

Hence

$$p(\theta_c, \phi) = p_0(\delta) + \epsilon P_2(\delta) \cos 2\phi + 0(\epsilon^2) \tag{106}$$

The pressure coefficient, C_p, is defined by

$$C_p = \frac{(p/p_\infty) - 1}{(\gamma/2) \, M_\infty^2} \tag{107}$$

Thus it can be written

$$C_p = c_{po} + \epsilon_2 c_{p2} \cos 2\phi + 0(\epsilon^2) \tag{108}$$

where

$$c_{p0} \equiv \frac{\frac{p_0(\delta)}{p_\infty} - 1}{\frac{\gamma}{2} M_\infty^2} \tag{109a}$$

$$c_{p2} \equiv \frac{2P_2(\delta)}{\gamma p_\infty M_\infty^2} \tag{109b}$$

The pressure perturbation is given by Equation (47), and since $v_0(\delta) = 0$, the result is

$$P_2(\delta) = -\rho_0(\delta)\ u_0(\delta)\ U_2(\delta) + p_0(\delta)\ F_2 \qquad (110)$$

Using the previous results for the first approximation, obtain the hypersonic similarity form

$$\frac{C_{p2}}{\delta} = \frac{2N}{K\delta^2}\ \frac{p_0(\delta)}{p_\infty}\ [\frac{g_2}{\sigma^3} - \frac{a_0^2(\beta)}{a_0^2(\delta)}\ \frac{U_2(\delta)}{V_\infty \delta}\ ] \qquad (111)$$

where

$$\frac{p_0(\delta)}{p_\infty} = 1 + \frac{\gamma}{2}\ K\delta^2\ (\frac{c_{p0}}{\delta^2}) \qquad (112)$$

and N is given by (99). From an analysis of the basic cone flow (References 21,22,23) are the expressions

$$\frac{a_0^2(\delta)}{a_0^2(\beta)} = 1 + \frac{(\gamma-1)\ \sigma^2\ [\ln \sigma^2 + \frac{1}{\sigma^2} - 1]}{(\sigma^2-1)(2\sigma^2 + \gamma + 1)} \qquad (113a)$$

$$\frac{c_{p0}}{\delta^2} = 1 + \frac{\sigma^2\ \ln \sigma^2}{\sigma^2 - 1} \qquad (113b)$$

Figure 9 shows C_{p2}/δ plotted as as function of $K\delta$ for $\gamma = 1.4$. For $K\delta = 0$, the result is $C_{p2}/\delta = -2$, in agreement with linearized theory. In the hypersonic limit, $K\delta = \infty$, C_{p2}/δ approaches the value -3.811. Thus in the hypersonic limit, the surface pressure coefficient approaches the form

$$\frac{C_p}{\delta^2} = 2.094 - 3.811\ \frac{\epsilon_2}{\delta}\ \cos 2\phi + 0(\epsilon^2) \qquad (114)$$

Surface pressures were measured on two different elliptic cone models, each at free stream Mach numbers 3.09 and 6.0, by Zakkay and Visich (Reference 26). The geometric properties of these models were as follows:
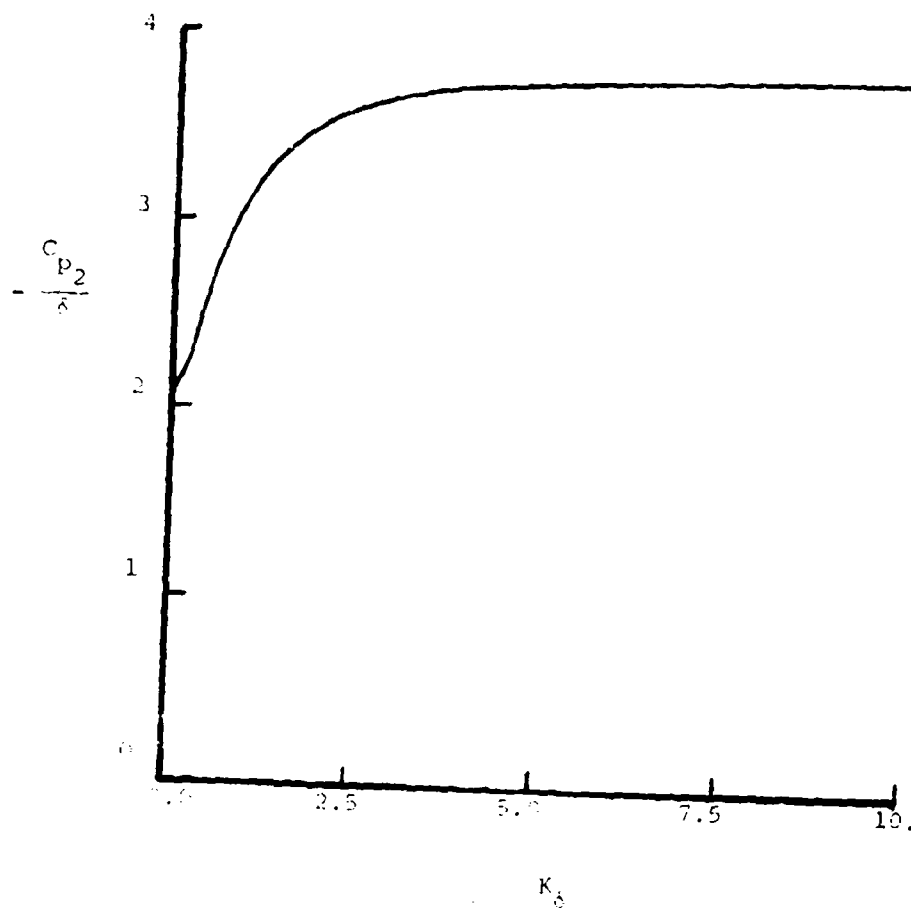
Figure 9.   Perturbation Pressure Coefficient on the Body Surface

Model I		Model II	
a	$= 0.2555$	a	$= 0.2256$
b	$= 0.3562$	b	$= 0.4034$
e	$= 0.320$	e	$= 0.523$
θ_m	$= 16.36°$	θ_m	$= 15.56°$
ε_2/δ	$= 0.155$	ε_2/δ	$= 0.266$
δ	$= 16.64° = 0.2904$ rad	δ	$= 16.28° = 0.2841$ rad

These two models have the same cross-sectional areas for the same station along the elliptic cone axis. A circular cone with the same cross-sectional area has a semivertex angle of 16.79 degrees. The experimental data are compared with the results of the present analysis and also with the analysis of Martellucci (Reference 17). Martellucci used an extension of the so-called linearized characteristics method. This method essentially uses the first-order perturbation equations utilized in the present analysis, but takes a finite number of terms in a Fourier series expansion to represent the shape of this surface. Martellucci used the first six terms. (In view of the fact that the Fourier coefficients for an ellipse decrease in magnitude like powers of the eccentricity, e, as seen in Equation (6), it would seem that a higher-order theory should be utilized to accommodate the higher-order Fourier coefficients. In this sense, the linearized-characteristics method does not seem to be entirely rational, at least for the ellipse.) The perturbation equations were integrated numerically by Martellucci, but the general results corresponding to the present analysis were not obtained.

Figure 10 shows the pressure distribution on one quadrant of model I for the elliptic cone for $M_\infty = 6.0$, which corresponds to $K_\delta = 1.747$. The present results agree very well with the data on the major and minor rays ($\phi = 90$ and 180 degrees), but give pressures that are too large in between. The overall

agreement is good considering that the perturbation theory should be strictly valid when $\varepsilon_2 \ll \delta$, and this condition is met only marginally. The results of Martellucci give slightly better agreement with the data, but probably not enough to justify the numerical computational effort.

Figure 11 shows pressure-distribution data on model II for $M_\infty = 6.0$, which corresponds to $K_\delta = 1.724$. This model is substantially more eccentric than model I, and the condition $\varepsilon_2 \ll \delta$ is certainly not satisfied. Nevertheless, fairly good agreement with the present analysis definitely represents the overall trends of the data. The results of Martellucci do not appear to give substantially better overall agreement with the data.

Figure 12 shows the pressure-distribution data on model I for the smaller Mach number, $M_\infty = 3.09$, for which $K_\delta = 0.900$. Again the present results give good agreement with the data on the semimajor ray, but the data are lower otherwise. The overall agreement does not seem to be quite as good as for the higher Mach number $M_\infty = 6.0$, which might be partially expected on the grounds that the approximate analysis is less accurate at $K_\delta = 0.900$ than for $K_\delta = 1.747$. The results of Martellucci give a little better agreement with the data between the major and minor rays.

Figure 13 shows the pressure-distribution data on model II for $M = 3.09$, for which $K_\delta = 0.888$. The agreement with the present analyses is fairly good near the major and minor rays, but poor in between. Again, for this large value of eccentricity, higher-order perturbation terms are probably required. The linearized-characteristics method used by Martellucci picks up higher-order harmonics in Fourier representation of the ellipse and thus shows somewhat better agreement with the data between the major and minor rays. In view of the large value of ε_2, however, there are probably higher-order
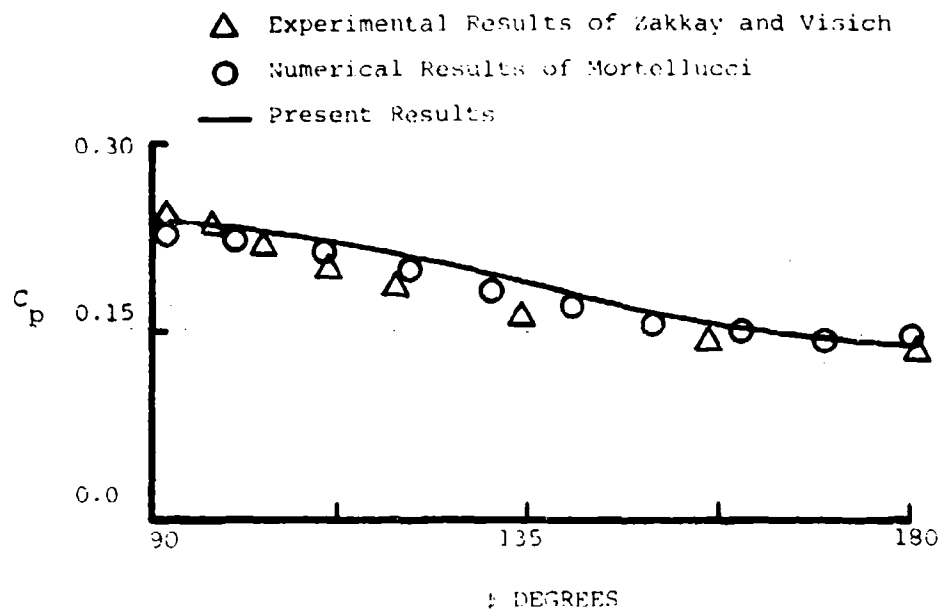
Figure 10. Pressure Coefficient on Body Surface
Model I, $M_\infty = 6$, $\gamma = 1.4$
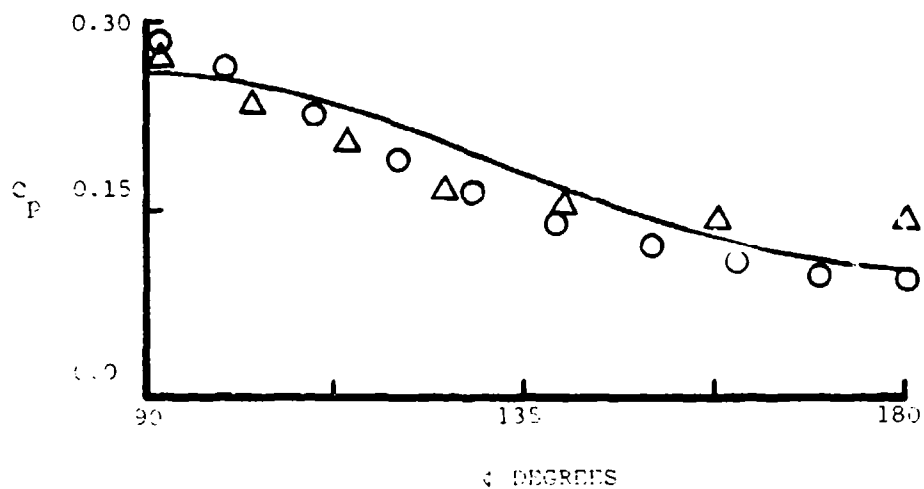
Figure 11. Pressure Coefficient on Body Surface
Model II, $M_\infty = 6$, $\gamma = 1.4$

△ Experimental Results of Bakkay and Visich

O Numerical Results of Mortellucci

— Present Results
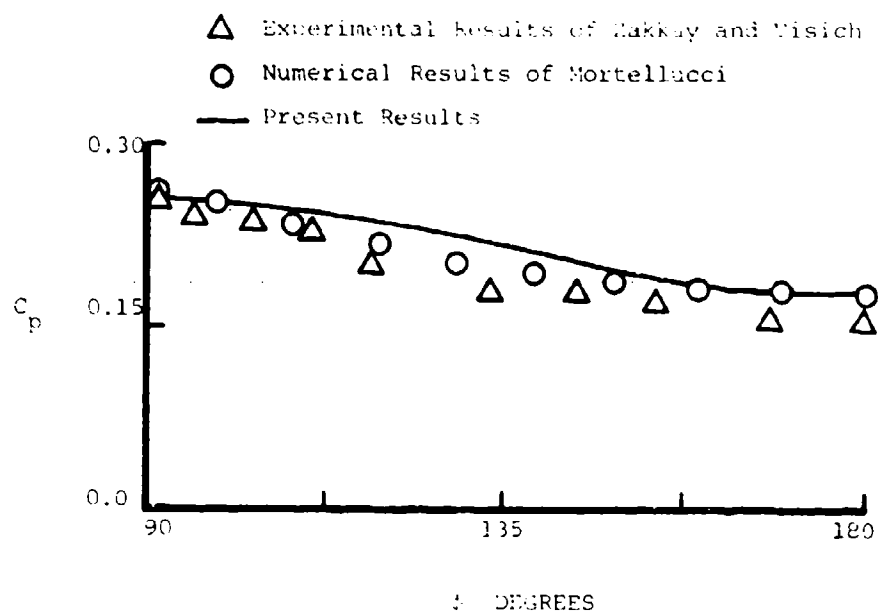
Figure 12.   Pressure Coefficient on Body Surface
Model I, M_∞ = 3.09, γ = 1.4
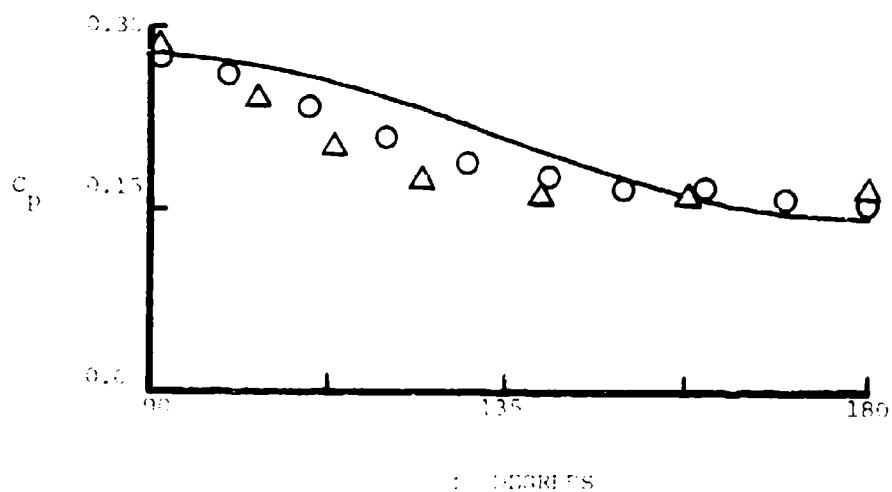
Figure 13.   Pressure Coefficient on Body Surface
Model II, M_∞ = 3.09, γ = 1.4

perturbation terms that are of the same order of magnitude as the higher-order Fourier harmonics.

The pressure force on a finite-length elliptic cone is given by

$$\vec{F} = - \iint_S p(\theta_c) \, \hat{n} \, dS \qquad (115)$$

where S is the area of the slant face, and

$$\theta_c = \delta - \varepsilon_2 \cos 2\phi + 0(\varepsilon^2) \qquad (116a)$$

$$\hat{n} = \hat{e}_\theta - \frac{2\varepsilon_2 \sin 2\phi}{\sin \delta} \hat{e}_\phi + 0(\varepsilon^2) \qquad (116b)$$

$$dS = r \sin \theta_c \, dr \, d\phi + 0(\varepsilon_2^2) \qquad (116c)$$

$$p(\theta_c) = p_0(\delta) + \varepsilon P_2(\delta) \cos 2\phi + 0(\varepsilon^2) \qquad (116d)$$

When the integration is carried out in the range $0 \leqslant \phi \leqslant 2\pi$ and $0 \leqslant z \leqslant H$, where H is the length of the cone axis, the result for the cone drag is

$$D \equiv \vec{F} \cdot \hat{e}_z = p_0(\delta)A + 0(\varepsilon_2^2) \quad , \qquad (117)$$

where

$$A = \pi H^2 \tan^2 \delta \qquad (118)$$

is the base area of the basic cone of semivertex angle δ. Thus the drag on the elliptic cone, ignoring terms of order ε_2^2, is the same as the drag on the basic cone of semivertex angle δ having the same length.

g. Elliptic Cone at Angle of Attack, Comparison with Experiment

Let the freestream wind be inclined to the axis of the elliptic cone such that the inclination angle, α, is measured in the x-z plane shown in Figure 1. Let the coordinate system remain fixed to the body so that the z-axis is the axis of the cone. The surface boundary conditions remain unchanged. The shock shape can now be represented by (Reference 22)

$$\theta_s = \beta + \alpha g_0 \cos \phi - \varepsilon_2 g_2 \cos 2\phi + 0(\alpha^2, \alpha\varepsilon_2, \varepsilon_2^2) \qquad (119)$$

where g_0 is the eccentricity factor associated with angle of attack. Assume

α and ε_2 to be small and of the same order of magnitude. Since the first-order perturbation equations and boundary conditions are linear, the angle of attack problem for the circular cone can be superposed with the elliptic-cone solution at zero angle of attack. The subsequent results for the circular-cone angle of attack problem were obtained by Doty (Reference 22) and Doty and Rasmussen (Reference 23) by an analysis very similar to the foregoing analysis for the elliptic cone. The angle-of-attack shock eccentricity factor was found to have the form

$$g_0 = \frac{3 + 2\sigma^2[3 - \dfrac{4(1+\sigma^2)}{\gamma+1}] - [\sigma(\sigma^2-1)^{1/2}]^{-1} \ln [\sigma + (\sigma^2-1)^{1/2}]}{5 - 2(1+\sigma^2)[1 + \dfrac{4\sigma^2}{\gamma+1}] - [\sigma(\sigma^2-1)^{1/2}]^{-1} \ln [\sigma + (\sigma^2-1)^{1/2}]} \tag{120}$$

where σ is given by (90) as before. This function is shown in Figure 3.

The first-order expansion for the flow variables outside the vortical layer can be written as

$$u(\theta,\phi) = u_0(\theta) + \alpha U_0(\theta) \cos \phi + \varepsilon_2 U_2(\theta) \cos 2\phi \tag{121a}$$

$$v(\theta,\phi) = v_0(\theta) + \alpha V_0(\theta) \cos \phi + \varepsilon_2 V_2(\theta) \cos 2\phi \tag{121b}$$

$$w(\theta,\phi) = \qquad \alpha W_0(\theta) \sin \phi + \varepsilon_2 W_2(\theta) \sin 2\phi \tag{121c}$$

$$\rho(\theta,\phi) = \rho_0(\theta) + \alpha R_0(\theta) \cos \phi + \varepsilon_2 R_2(\theta) \cos 2\phi \tag{121d}$$

$$p(\theta,\phi) = p_0(\theta) + \alpha P_0(\theta) \cos \phi + \varepsilon_2 P_2(\theta) \cos 2\phi \tag{121e}$$

The upper case variables with the subscript zero notation pertain to the solution for flow at angle of attack past a circular cone.

The pressure on the body surface is given by

$$p(\theta_c,\phi) = p_0(\delta) + P_0(\delta) \cos \phi + \varepsilon_2 P_2(\delta) \cos 2\phi \tag{122}$$

where

$$P_0(\delta) = -\rho_0(\delta) u_0(\delta) U_0(\delta) + \rho_0(\delta) F_0 \tag{123}$$

$$F_0 = + \gamma V_\infty^2 \delta(1 - g_0)(1 - \xi_0)^2 / a_0^2(\delta) \tag{124}$$

47

$$\frac{U_0(\delta)}{V_\infty \delta} = -2 + \frac{(1-g_0)}{\sigma^3} \left[\frac{4\sigma^5}{\gamma+1} + \sigma^3 - \frac{\sigma}{2} + 1 - \frac{\ln(\sigma + \sqrt{\sigma^2-1})}{2\sqrt{\sigma^2-1}} \right] \qquad (125)$$

which is analogous to expression (110). In terms of the pressure coefficient, is

$$C_p = c_{p0} + \alpha\, C_{p0} \cos \phi + \varepsilon_2 C_{p2} \cos 2\phi \qquad (126)$$

where

$$\frac{C_{p0}}{\delta} = \frac{2N}{K_\delta^2} \frac{p_0(\beta)}{p_\infty} \frac{p_0(\delta)}{p_0(\beta)} \left[\frac{(1-g_0)}{\sigma^3} - \frac{a_0^2(\beta)}{a_0^2(\delta)} \frac{U_0(\delta)}{V_\infty \delta} \right] \qquad (127)$$

In the calculations presented in References 22 and 23, the ratios $p_0(\delta)/p_0(\beta)$ and $a_0^2(\beta)/a_0^2(\delta)$ were set equal to unity consistent with their "constant-density" approximation.

The angle of attack perturbation pressure coefficient given by (127) is shown in Figure 14. When $K_\delta = 0$, the limiting result of linearized theory is recovered, $C_{p0}/\delta = -4$. When $K_\delta = \infty$, the limiting hypersonic value is $C_{p0}/\delta = -4.0836$. Near $K_\delta = 1$, there is a small dip in the curve. As K_δ approaches zero, there is a small overshoot in the curve which does not occur in the exact theory. Over the range of K_δ, the value of C_{p0}/δ does not differ greatly from -4. In the hypersonic limit, $K_\delta = \infty$, it is possible to write

$$\frac{C_p}{\delta^2} = 2.094 - 4.084 \left(\frac{\alpha}{\delta}\right) \cos \phi - 3.811 \left(\frac{\varepsilon_2}{\delta}\right) \cos 2\phi \qquad (128)$$

correct to first order in α and ε. Expression (128) indicates that α/δ and ε_2/δ should be sufficiently small in order for the perturbation analysis to be valid.

The present results for surface pressure at $M_\infty = 6$ and angles of attack of $\alpha = 5$ and 10 degrees are shown in Figures 15 and 16 for models I and II. The results of Martellucci are shown for comparison together with the experimental data of Zakkay and Visich for $\alpha = 10$ degrees, which is a large enough angle of attack to make for a demanding comparison. The present
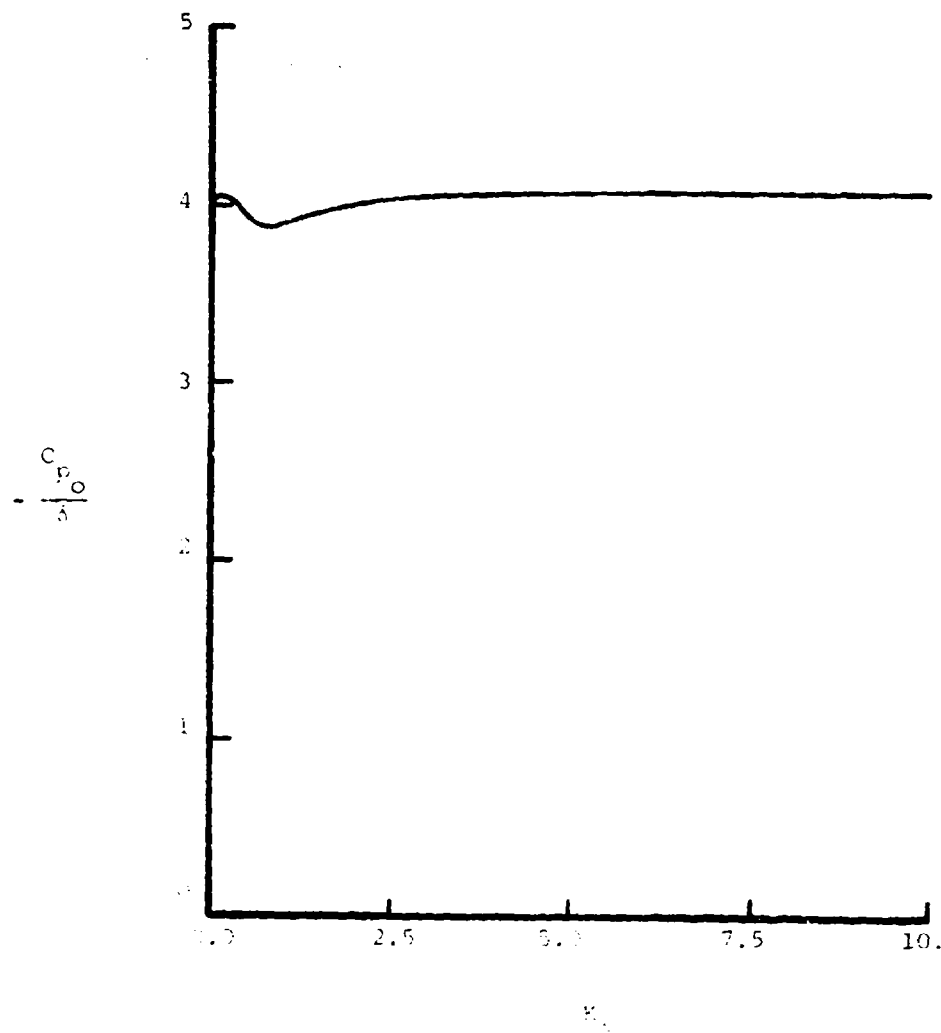
Figure 11.   Angle-of-Attack Perturbation Surface Pressure
Coefficient, $\gamma = 1.4$
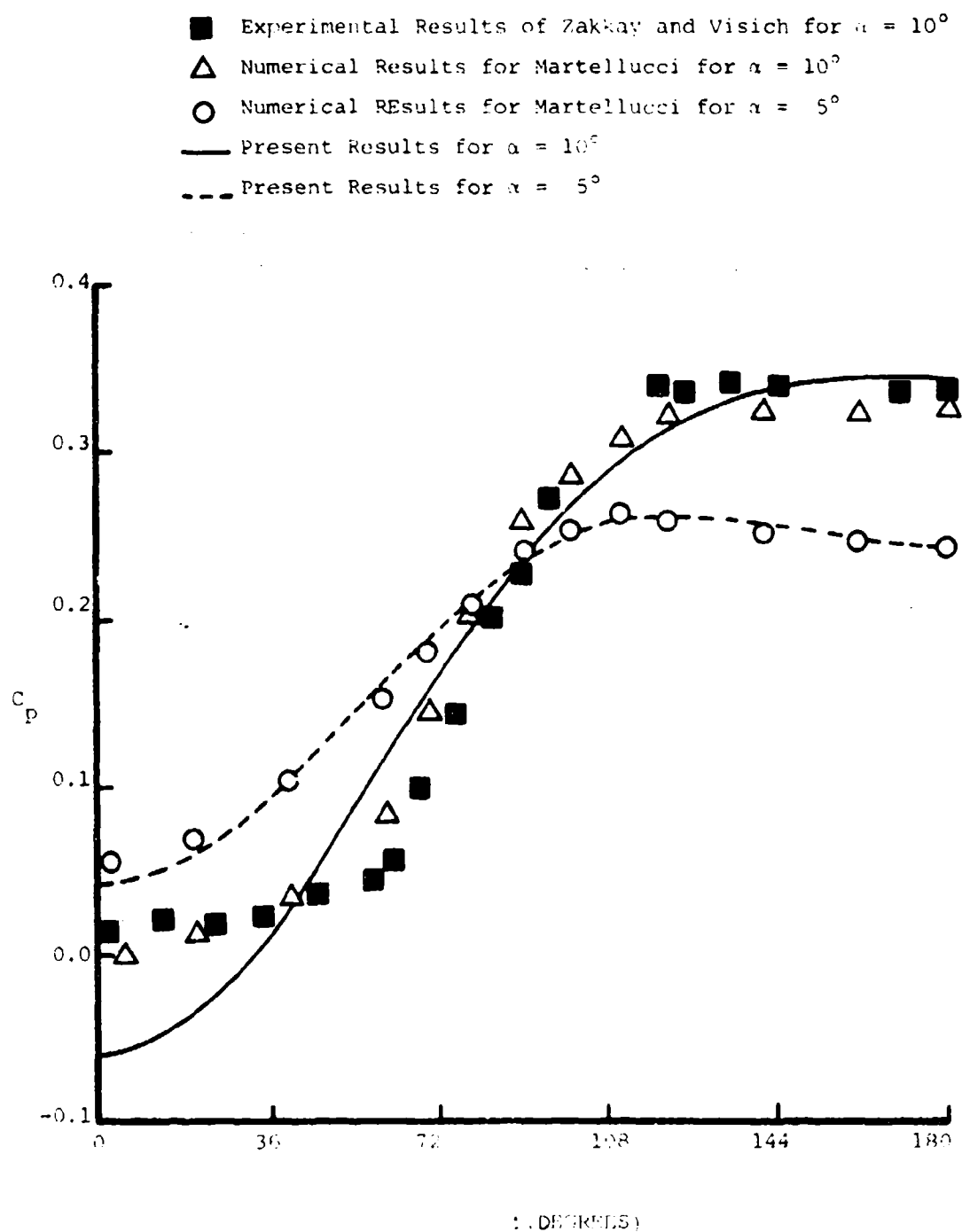
Figure 15. Comparison of Surface Pressure with Martellucci's Results, Model I, $M_\infty = 6$, $\gamma = 1.4$

50

■ Experimental Results of Zakkay and Visich for = 10°

△ Numerical Results of Martellucci for α = 10°

○ Numerical Results of Martellucci for α = 5°

—— Present Results for α = 10°

--- Present Results for α = 5°
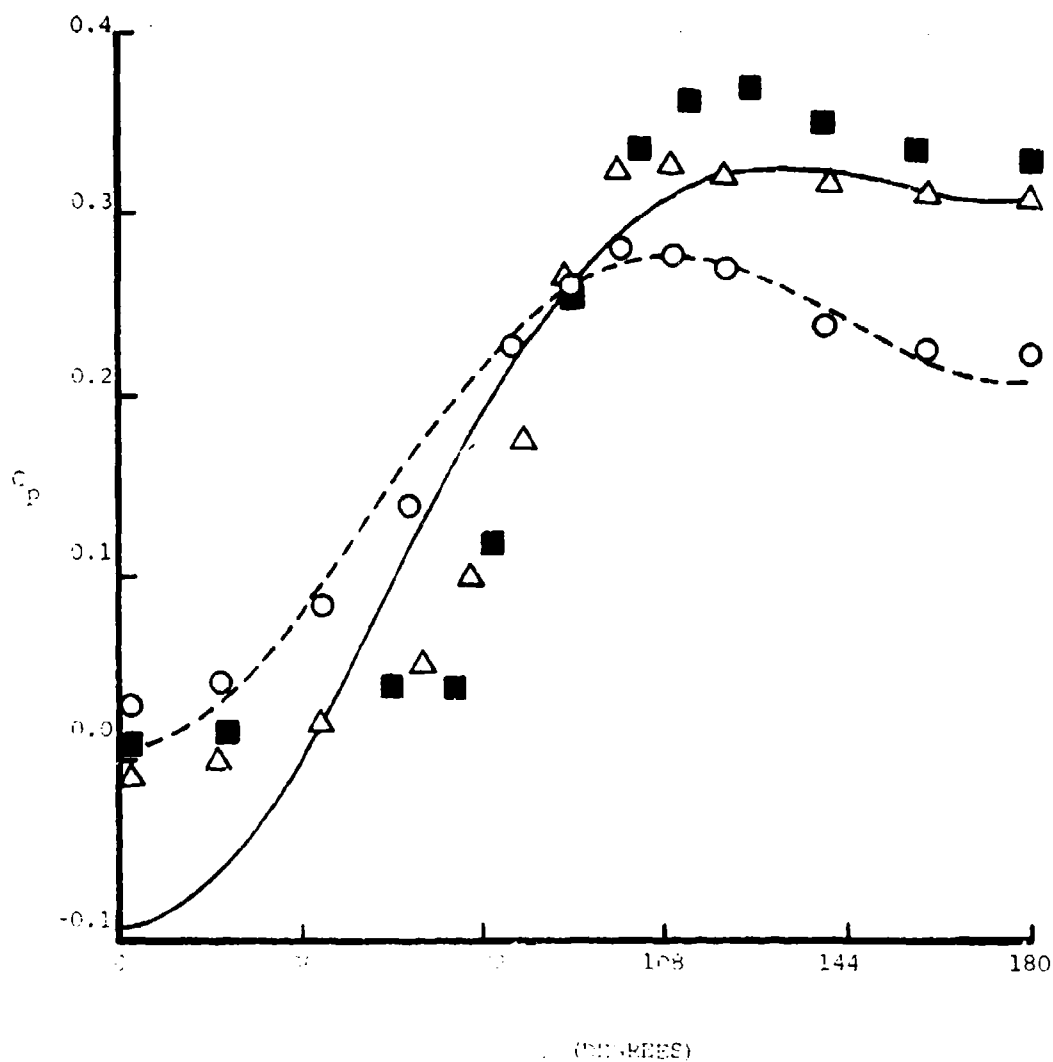
Figure 1. Comparison of Surface Pressure With Martellucci's Results, Model II, M_∞ = , = 1.

results agree well with Martellucci for both models for $\alpha = 5$ degrees, the worst agreement being on the leeward ray, $\phi = 0$ degrees. For $\alpha = 10$ degrees, the two results are in fair agreement for the small-eccentricity ellipse, model I in Figure 15, except near the leeward ray of the elliptic cone. For the large-eccentricity ellipse at $\alpha = 10$ degrees, model II in Figure 16, agreement between the two results is good only near the windward ray. For model II at $\alpha = 10$ degrees, the combined large values of $\alpha/\delta = 0.607$ and $\epsilon_2/\delta = 0.270$ render the first-order perturbation theory invalid, especially near the leeward ray where the separate perturbations are additive.

The normal-force on the cone is found to be

$$\vec{F} \cdot \hat{e}_x = C_{N\alpha} \, \alpha \, \frac{\gamma}{2} \, M_\infty^2 p_\infty A + O(\alpha^2, \epsilon_2^2, \alpha\epsilon_2) \tag{129}$$

where the force F is defined by (115), $A \equiv \pi H^2 \tan^2\delta$ is the base area of the basic cone of semivertex angle δ, and

$$C_{N\alpha} = -\frac{1}{2} \frac{C_{p0}}{\delta} \tag{130}$$

is the α-derivative of the normal-force coefficient.

The moment about the cone vertex is

$$\vec{M} = -\iint_S p(\theta_c) \, \vec{r} \times \hat{n}_c ds \tag{131}$$

Evaluation of this integral gives

$$\vec{M} = \hat{e}_y [C_{M\alpha} \, \alpha \, \frac{\gamma}{2} \, M_\infty^2 p_\infty HA] + O(\alpha^2, \epsilon_2^2, \epsilon_2\alpha) \tag{132}$$

where

$$C_{M\alpha} = \frac{2}{3} C_{N\alpha} = -\frac{1}{3} \frac{C_{p0}}{\delta} \tag{133}$$

is the α-derivative of the moment coefficient.

For completeness, the drag on the elliptic cone, (117), can be rewritten in terms of the axial-force coefficient. If the base pressure is reckoned as

p_∞ then

$$\vec{F} \cdot \hat{e}_z = C_A \frac{\gamma}{2} M_\infty^2 p_\infty A + (\alpha^2, \varepsilon_2^2, \alpha\varepsilon_2) \qquad (134)$$

where

$$C_A = c_{p0} = (\frac{c_{p0}}{\delta 2}) \delta^2 \qquad (135)$$

and c_{p0} is given by (113b).

The ratios C_{p0}/δ and c_{p0}/δ^2 depend only on K_δ and γ. They are insensitive to K_δ when K_δ is large. Thus when K_δ is large, that is, for hypersonic flow, the main effect of the cone cross-section shape is determined from δ. For slender cones (small θ_m), take from (3a) and (8a) the alternative forms

$$\delta = \sqrt{ab} \, [1 + 0(e^2)] \qquad (136)$$

$$\delta = b \sqrt{1-e} \, [1 + 0(e^2)]$$

The cross-section area of an ellipse is proportional to the product ab. Hence when the cross-section area is held fixed, the force coefficients are independent of the eccentricity e when terms of order e^2 are neglected.

On the other hand, when b is held fixed, then δ varies with the eccentricity to the first power. The normal force and moment are independent of δ when K_δ is large, but C_A decreases with increasing e when b is held fixed. Thus the lift-drag ratio increases when b is held fixed and e increases.

h. Concluding Remarks

General flowfield results for the hypersonic flow past an elliptic cone have been obtained. The results are valid for large Mach numbers and small stream deflections such that the hypersonic cimilarity parameter, $K_\delta \equiv M_\infty \delta$, is fixed in the limiting process. The results are more accurate for large K_δ ($K_\delta > 1$), but the proper linearized theory result is recovered when $K_\delta \to 0$. The

eccentricity factor, e, in the analysis must be small in the strict sense that $\varepsilon_2/\delta \ll 1$. Comparison with experimental results indicates that ε_2/δ need not be very much less than unity, but merely moderately less than unity, for acceptable engineering results. In addition, the angle of attack should be such that $\alpha/\delta \ll 1$ in the strict perturbation sense. An important feature of the analysis is that the basic circular cone angle, δ, has been well defined in terms of the geometric properties of the elliptic cone.

The methodology of this analysis can be extended to other cross-section shapes. Each term in a Fourier expansion of the cross-section shape can be handled in an analogous manner and accurate, approximate analytic results obtained. Strictly speaking, however, the cross-section shapes should deviate only slightly from a circular cone in order for the perturbation analysis to be valid. Moreover, successive Fourier coefficients should not decrease in powers of the basic expansion parameter, for then corresponding terms of higher-order perturbations become equally important.

2. ARBITRARY CROSS-SECTIONS

Here more general conical bodies are considered, whose cross-sections deviate by a small, but arbitrary, amount from a circle. The cross-section is expressed in terms of a Fourier series for the polar angle of the conical body, θ_c, as a function of the azimuthal angle ϕ,

$$\theta_c = \delta + \sum_{n=1}^{\infty} \varepsilon_n \cos(n(\phi - \phi_n)) \tag{137}$$

Here δ represents the half-angle of the basic circular cone and the ε_n are parameters that describe the deviation of the cross-sectional shape from a circle. For example, ε_2 measures the elliptical eccentricity. This perturbation scheme assumes the body deviates slightly from a circular cone at zero angle of attack and thus the ε_n are presumed to be small compared with δ.

54

The angles ϕ_n describe the relative phase of the various Fourier components.

In what follows, the governing equations and boundary conditions for these conical flows are first derived. Next using the "linearized characteristics method of Ferri et al. (Reference 13), the small disturbance equations and the simplified form of the boundary conditions are derived. A "weak polar crossflow" approximate solution to these equations is then obtained. Further results are found using the hypersonic small disturbances approximation. Comparisons of these results with experiment are then given. The stream surfaces and possible waverider geometries that derive from these stream surfaces are then discussed. The section ends with some concluding remarks.

a.   Governing Equations and Boundary Conditions

The equations expressing conservation of mass, Newton's second law, and the first law of thermodynamics (in both entropy and total enthalpy form) for an inviscid, adiabatic, steady flow are

$$\nabla \cdot (\rho \vec{V}) = 0 \tag{138}$$

$$\rho \vec{V} \cdot \nabla \vec{V} = -\nabla p \tag{139}$$

$$\vec{V} \cdot \nabla s = 0 \tag{140}$$

$$\vec{V} \cdot \nabla (h + V^2/2) = 0 \tag{141}$$

Take the state equations to be of the form

$$p = p(\rho, s) \tag{142a}$$

$$h = h(p, \rho) \tag{142b}$$

Equation (141) can be integrated to give the result that the total enthalpy $h + V^2/2$ is constant along streamlines. Since the freestream conditions are assumed to be uniform, the total enthalpy is constant everywhere. If the pressure and density are eliminated from the continuity and momentum equations, then

55

$$0 = \nabla \cdot \vec{v} - \frac{\vec{v}}{a^2} \cdot (\vec{v} \cdot \nabla v) \tag{143}$$

$$\frac{1}{\rho} \left(\frac{\partial \rho}{\partial s}\right)_p \nabla s = \frac{1}{\left(\frac{\partial h}{\partial \rho}\right)_p} \nabla \frac{(v^2)}{2} + \frac{\left(\frac{\partial h}{\partial p}\right)_\rho}{\left(\frac{\partial h}{\partial \rho}\right)_p} + \frac{1}{a^2} \vec{v} \cdot \vec{\nabla v} \tag{144}$$

It is convenient to adopt a spherical polar coordinate system (r,θ,ϕ) aligned with the basic circular cone with origin at the cone vertex (Figure 17). In this case, Equations (141), (143), and (144) become, assuming conical flow (e.g. $\partial/\partial r = 0$),

$$a^2 = \frac{\gamma-1}{2} (V_M^2 - u^2 - v^2 - w^2) \tag{145}$$

$$0 = u(2 - \frac{v^2 + w^2}{a^2}) + v \cot \theta + (1 - \frac{v^2}{a^2}) \frac{\partial v}{\partial \theta} \tag{146}$$

$$+ (1 - \frac{w^2}{a^2}) \frac{1}{\sin \theta} \frac{\partial w}{\partial \phi} - \frac{vw}{a^2} (\frac{1}{\sin \theta} \frac{\partial v}{\partial \phi} + \frac{\partial w}{\partial \theta})$$

$$0 = v \frac{\partial u}{\partial \theta} + \frac{w}{\sin \theta} \frac{\partial u}{\partial \phi} - v^2 - w^2 \tag{147}$$

$$\frac{a^2}{\gamma R} \frac{\partial s}{\partial \theta} = u \frac{\partial u}{\partial \theta} - w \frac{\partial w}{\partial \theta} + \frac{w}{\sin \theta} \frac{\partial v}{\partial \phi} + uv - w^2 \cot \theta \tag{148}$$

$$\frac{a^2}{\gamma R} \frac{\partial s}{\partial \phi} = -u \frac{\partial u}{\partial \phi} - v \frac{\partial v}{\partial \phi} + v \sin \theta \frac{\partial w}{\partial \theta} + uw \sin \theta$$

$$+ v w \cos \theta \tag{149}$$

Here V_M is the maximum attainable velocity for the given total enthalpy h_0, $V_M = \sqrt{2h_0}$, and a is the sound speed. Equations (145) through (147) also assume a perfect gas model for which Equations (142) reduce to

$$p = p_\infty (\frac{\rho}{\rho_\infty})^\gamma \exp (\frac{s-s_\infty}{c_v}) \tag{150}$$

$$h = \frac{\gamma}{\gamma-1} \frac{p}{\rho} \tag{151}$$

56
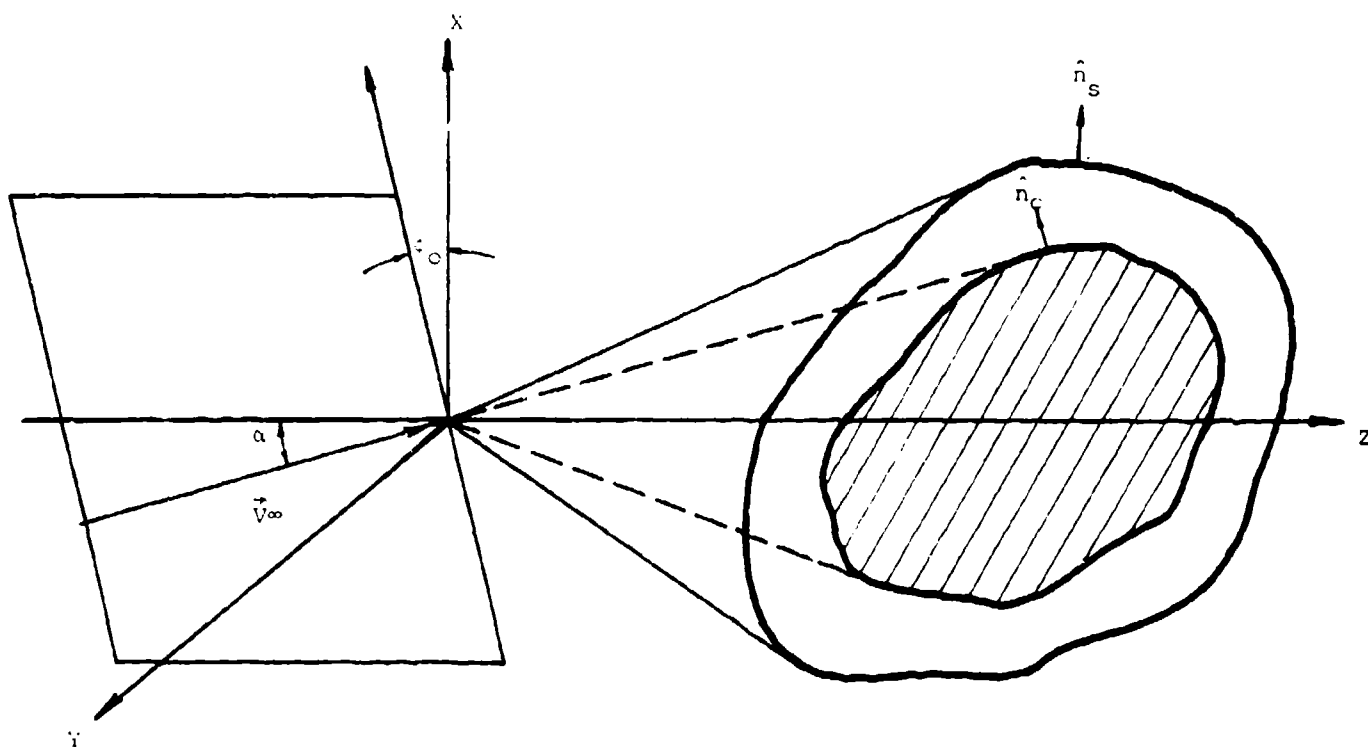
Figure 17. Geometry of Shock and Body

The boundary conditions for this problem include the shock jump relations and the condition of zero mass flux through the body -- the so-called tangency condition. The shock jump conditions can be written

$$\rho_\infty \vec{V}_\infty \cdot \hat{n}_s = \rho_s \vec{V}_s \cdot \hat{n}_s = m \tag{152}$$

$$m\vec{V}_\infty + p_\infty \hat{n}_s = m\vec{V}_s + p_s \hat{n}_s \tag{153}$$

$$m (h_\infty + V_\infty^2) = m (h_s + \frac{V_s^2}{2}) \tag{154}$$

Here the subscript s again refers to conditions just downstream of the shock wave and $\hat{n}_s$ is the unit normal to the shock (Figure 17). The freestream conditions are taken to be constant with velocity $\vec{V}_\infty$ at angle of attack α in a plane at angle ϕ_0 to the X-Z plane,

$$\vec{V}_\infty = V_\infty [\cos \alpha\ \hat{e}_z + \sin \alpha \cos \phi_0 \hat{e}_x + \sin \alpha \sin \phi_0\ \hat{e}_y] \tag{155}$$

The tangency condition on the body can be written

$$\vec{V} \cdot \hat{n}_c = 0 \qquad \text{on body} \tag{156}$$

Here $\hat{n}_c$ is the unit normal to the conical body.

The component of the freestream Mach number normal to the shock wave, $M_{\infty n}$, is given by

$$M_{\infty n} = \vec{M}_\infty \cdot \hat{n}_s \ ; \ \vec{M}_\infty = \frac{\vec{V}_\infty}{a_\infty} \tag{157}$$

For a calorically perfect gas, the shock jump conditions can be rewritten

$$\frac{\vec{V}_\infty \cdot \hat{n}_s}{\vec{V}_s \cdot \hat{n}_s} = \frac{\rho_s}{\rho_\infty} = \frac{(\gamma+1)\ M_{\infty n}^2}{(\gamma-1)\ M_{\infty n}^2 + 2} \tag{158}$$

$$\vec{V}_\infty \times \hat{n}_s = \vec{V}_s \times \hat{n}_s \tag{159}$$

$$\frac{p_s}{p_\infty} = 1 + \frac{2\gamma}{\gamma+1}\ (M_{\infty n}^2 - 1) \tag{160}$$

$$\frac{\Delta s}{c_v} = \ln \quad \frac{((2\gamma M_{\infty n}^2 - (\gamma-1))\ ((\gamma-1)M_{\infty n}^2 + 2)}{\gamma+1} \frac{}{(\gamma+1)\ M_{\infty n}^2}\Bigg)^{\gamma} \tag{161}$$

For conical flows, take the equations describing the shock wave and body as

shock wave: $\qquad\qquad \theta = \theta_s\ (\phi)$ $\hfill$ (162)

body: $\qquad\qquad\qquad \theta = \theta_c\ (\phi)$ $\hfill$ (163)

In the direct problem being considered, $\theta_c(\phi)$ is given and $\theta_s(\phi)$ is to be determined. The angles ζ and ξ are introduced so that

$$\hat{n}_s = \cos \zeta\ \hat{e}_\theta - \sin \zeta\ \hat{e}_\phi \tag{164}$$

$$\hat{n}_c = \cos \xi\ \hat{e}_\theta - \sin \xi\ \hat{e}_\phi \tag{165}$$

where

$$\tan \zeta = \frac{1}{\sin \theta_s}\ \frac{d\theta_s}{d\phi}\ ,\ \tan \xi = \frac{1}{\sin \theta_c}\ \frac{d\theta_c}{d\phi} \tag{166}$$

The expression for the normal component of the freestream Mach number can then be rewritten

$$M_{\infty n} = M_\infty\ (- \cos \alpha \sin \theta \cos \zeta \tag{167}$$
$$+ \sin \alpha \cos \theta \cos \zeta \cos (\phi - \phi_0)$$
$$+ \sin \alpha \sin \zeta \sin (\phi - \phi_0))$$

Equations (158) and (159) can be solved for the three velocity components downstream of the shock wave in the following form

$$\frac{u_s}{V_\infty} = \cos \alpha \cos \theta + \sin \alpha \sin \theta \cos (\phi - \phi_0) \tag{168}$$

$$\frac{v_s}{V_\infty} = -\cos \alpha \sin \theta + \sin \alpha \cos \theta \cos (\phi - \phi_0) \tag{169}$$
$$- \frac{2}{\gamma+1} (1 - \frac{1}{M_{\infty n}^2})\{\cos^2\zeta(-\cos \alpha \sin \theta + \sin \alpha \cos \theta \cos (\phi-\phi_0))$$
$$+ \cos \zeta \sin \zeta \sin \alpha \sin (\phi-\phi_0)\}$$

$$\frac{w_2}{V_\infty} = -\sin \alpha \sin (\phi - \phi_0) \tag{170}$$

$$+ \frac{2}{\gamma+1} (1 - \frac{1}{M_\infty n^2})[\cos \zeta \sin \zeta (-\cos \alpha \sin \theta + \sin \alpha \cos \theta \cos(\phi - \phi_0))$$

$$+ \sin^2 \zeta \sin \alpha \sin (\phi - \phi_0)]$$

Here θ is to be evaluated at $\theta_s(\phi)$. The tangency condition on the body becomes

$$0 = v_2 \cos \xi - w_2 \sin \xi \tag{171}$$

with θ evaluated at $\theta_c(\phi)$.

Equations (146) through (149) give four nonlinear partial differential equations for the four unknowns, u, v, w, and s. Equations (161) and (168) through (171) give five boundary conditions. Thus the unknown shock shape $\theta_s(\phi)$ can also be determined. Once the velocity and entropy are known, the pressure coefficient, C_p,

$$C_p = \frac{p - p_\infty}{\frac{1}{2} \rho_\infty V_\infty^2} \tag{172}$$

can be determined from

$$C_p = \frac{2}{\gamma M_\infty^2} \{(\frac{V_M^2 - v^2}{V_M^2 - V_\infty^2})^{\frac{\gamma}{\gamma-1}} \exp (- \frac{s-s_\infty}{R}) - 1\} \tag{173}$$

It is convenient to introduce the following normalized variables,

$$\vec{V}_1 = \frac{\vec{V}_1}{V_\infty} , \ \bar{p} = \frac{p}{\rho_\infty V_\infty^2} , \ \bar{s} = \frac{s - s_\infty}{c_v} , \ \bar{\rho} = \frac{\rho}{\rho_\infty} , \ \bar{a} = \frac{a}{V_\infty} \tag{174}$$

Dropping the bars for simplicity, Equations (146) through (149) can be rewritten as,

$$0 = u (2 - \frac{v^2 + w^2}{a^2}) + v \cot \theta + (1 - \frac{v^2}{a^2}) \frac{\partial v}{\partial \theta} + (1 - \frac{w^2}{a^2})$$

$$\cdot \frac{1}{\sin \theta} \frac{\partial w}{\partial \phi} - \frac{vw}{a^2} (\frac{1}{\sin \theta} \frac{\partial v}{\partial \phi} + \frac{\partial w}{\partial \theta}) \tag{175}$$

$$0 = v \frac{\partial u}{\partial \theta} + \frac{w}{\sin \theta} \frac{\partial u}{\partial \phi} - v^2 - w^2 \tag{176}$$

$$\frac{a^2}{\gamma(\gamma-1)} \frac{\partial s}{\partial \theta} = -u \frac{\partial u}{\partial \theta} - w \frac{\partial w}{\partial \theta} + \frac{w}{\sin \theta} \frac{\partial v}{\partial \phi} + uv - w^2 \cot \theta \qquad (177)$$

$$\frac{a^2}{\gamma(\gamma-1)} \frac{\partial s}{\partial \phi} = -u \frac{\partial u}{\partial \phi} - v \frac{\partial v}{\partial \phi} + v \sin \theta \frac{\partial w}{\partial \theta} + uw \sin \theta \, vw \cos \theta \qquad (178)$$

where a^2 is given by

$$a^2 = \frac{\gamma-1}{2} (V_M^2 - v^2) \quad , \quad V_M^2 = 1 + \frac{2}{(\gamma-1) M_\infty^2} \qquad (179)$$

The boundary conditions on the velocity are still given in Equations (168) through (171) with the left-hand side of Equations (169) and (170) replaced by u, v, and w, respectively. The boundary condition for the entropy s becomes

$$s = \ln \left\{ \left(\frac{2\gamma \, M_{\infty_n}^2 - (\gamma-1)}{\gamma+1}\right) \left(\frac{(\gamma-1) \, M_{\infty_n}^2 - 2}{(\gamma+1) \, M_{\infty_n}^2}\right)^\gamma \right\} \text{ at } \theta = \theta_s \qquad (180)$$

b. Linearization About Cone at Zero Angle of Attack

Assume that the flowfield is conical and deviates slightly from that for flow past a right circular cone at zero angle of attack (Figure 18). Furthermore, expand the flowfield variables in a Fourier series in the azimuthal angle ϕ,

$$u = u_0 + \alpha \, U_0(\theta) \cos(\phi-\phi_0) + \sum_{n=1}^{\infty} \epsilon_n \, U_n(\theta) \cos(n(\phi-\phi_n)) \qquad (181)$$

$$v = v_0 + \alpha \, V_0(\theta) \cos(\phi-\phi_0) + \sum_{n=1}^{\infty} \epsilon_n \, V_n(\theta) \cos(n(\phi-\phi_n)) \qquad (182)$$

$$w = \qquad \alpha \, W_0(\theta) \sin(\phi-\phi_0) + \sum_{n=1}^{\infty} \epsilon_n \, W_n(\theta) n \sin(n(\phi-\phi_n)) \qquad (183)$$

$$s = s_0 + \alpha \, S_0(\theta) \cos(\phi-\phi_0) + \sum_{n=1}^{\infty} \epsilon_n \, S_n(\theta) \cos(n(\phi-\phi_n)) \qquad (184)$$

$$\theta_s = \beta + \alpha \, g_0 \cos(\phi-\phi_0) + \sum_{n=1}^{\infty} \epsilon_n \, g_n \cos(n(\phi-\phi_n)) \qquad (185)$$

$r = r_s (\phi)$

$\theta = \delta$

$r = r_c(\phi)$
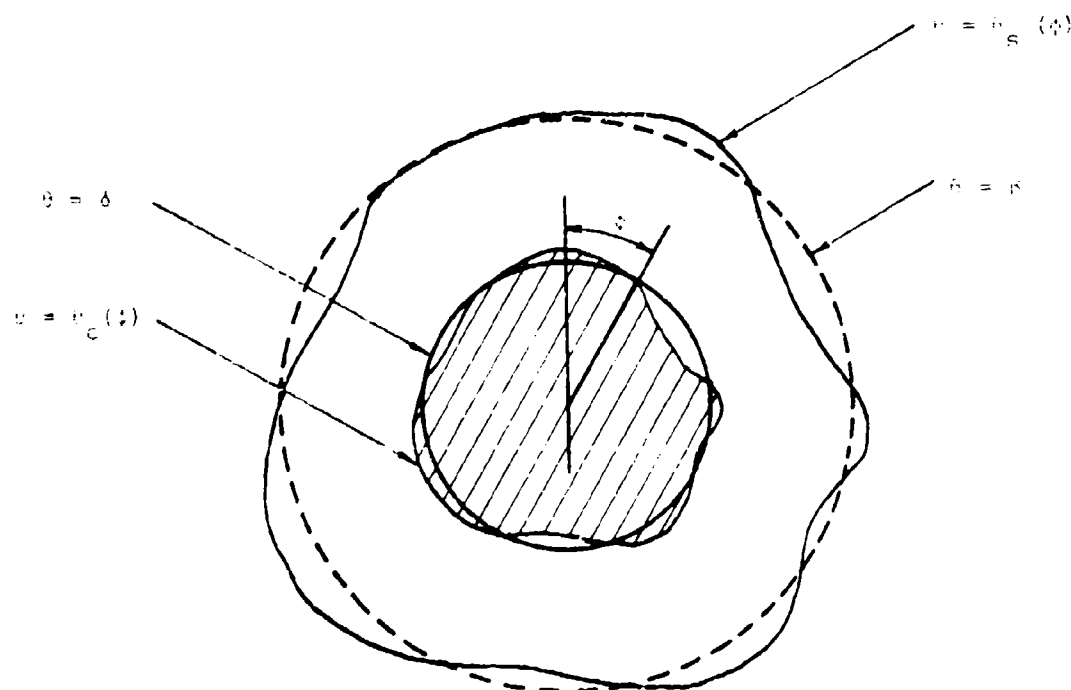
Figure 16. Schematic of Cross of Shock and Body

Lower case quantities with a subscript zero refer to the basic flow at zero angle of attack past the circular cone. The deviation from this flow due to angle of attack α and deviations of the cross-section from a circle (ε_n) are described by the U's, V's, W's, and S's which are functions of the polar angle θ and remain to be determined.

Substituting these expansions into the governing equations and boundary condition, and equating coefficients of powers of α, ε_n to zero, provides a hierarchy of problems, the first being that for flow past a right circular cone at zero angle of attack. The governing equations for that problem are

$$2 u_0 + \cot \theta \, v_0 + \frac{dv_0}{d\theta} = \frac{(v_0)^2}{a_0} \left(u_0 + \frac{dv_0}{d\theta} \right) \tag{186}$$

$$0 = v_0 \frac{du_0}{d\theta} - v_0^2 \tag{187}$$

$$\frac{a_0^2}{\gamma(\gamma-1)} \frac{ds_0}{d\theta} = - u_0 \frac{du_0}{d\theta} + u_0 v_0 \tag{188}$$

with

$$a_0^2 = \frac{-1}{2} (V_M^2 - a_0^2 - v_0^2) \tag{189}$$

The associated boundary conditions are

$$\theta = \beta: \quad u_0 = \cos \, ^\wedge \tag{190}$$

$$v_0 \qquad \frac{(V_M^2 - \cos^2 \theta)}{\sin \theta}$$

$$s_0 = \ln \left[\left(\frac{2\gamma \, M_\infty^2 \, \sin^2\theta - \gamma + 1}{\gamma + 1} \right) \left(\frac{(\gamma-1) \, M_\infty^2 \, \sin^2\theta + 2}{\gamma + 1} \right)^\gamma \right] \tag{191}$$

$$\theta = \delta: \quad v_0 = 0 \tag{192}$$

The equations for the first order (e.g. of order α, ε_n) problem are*

---

*In the case n=0 corresponding to the freestream being at angle of attack α, the form given by Equation (193) is incorrect in that the term $n^2 \, W_n \csc \theta$ does not vanish but, instead, becomes $W_n \cot \theta$.

85

$$2U_n + \cot \theta \ V_n + \frac{dV_n}{d\theta} + n^2 W_n \csc \theta \tag{193}$$

$$= (\frac{v_0}{a_0})^2 \ [U_n - 2 \ u_0 \ \frac{A_n}{a_0} + \frac{dV_n}{d\theta} - 2 \ \frac{A_n}{a_0} \ \frac{dv_0}{d\theta}$$

$$+ 2 \ V_n \ \frac{d\ln v_0}{d\theta}] + (\frac{v_0}{a_0}) \ [2 \ \frac{u_0}{a_0} \ V_n]$$

$$0 = v_0 \ \frac{dU_n}{d\theta} + V_n \ \frac{du_0}{d\theta} - 2 \ v_0 \ V_n \tag{194}$$

$$- \ \frac{a_0^2}{\gamma(\gamma-1)} \ \frac{dS_n}{d\theta} = u_0 \ (V_n - \frac{dU_n}{d\theta}) \tag{195}$$

$$- \ \frac{a_0^2}{\gamma(\gamma-2)} \ S_n = u_0 \ U_n + v_0 \ V_n + v_0 \sin \theta \ \frac{dW_n}{d\theta} \tag{196}$$

$$+ \ n \ (u_0 \sin \theta + v_0 \cos \theta)$$

$$0 = \frac{A_n}{a_0} + \frac{\gamma-1}{2} \ (\frac{u_0}{a_0} \ \frac{U_n}{a_0} + \frac{v_0}{a_0} \ \frac{V_n}{a_0}) \tag{197}$$

The associated boundary conditions are

$\theta = \beta:$ $\quad U_0 = -g_0 \ (\frac{du_0}{d\theta} + \sin \theta) + \sin \theta$

$$V_0 = -g_0 \ (\frac{dv_0}{d\theta} + v_0 \cot \theta \ \frac{2 - (\gamma-1) \ M_\infty^2 \sin^2\theta}{2 + (\gamma-1) \ M_\infty^2 \sin^2\theta})$$

$$+ \ v_0 \cot \theta \ \frac{2 - (\gamma-1) \ M_\infty^2 \sin^2\theta}{2 + (\gamma-1) \ M_\infty^2 \sin^2\theta} \tag{198}$$

$$W_0 = g_0 \ \frac{2}{\gamma+1} \ (1 - \frac{1}{M_\infty^2 \sin^2\theta}) - 1$$

$$S_0 = -g_0 \ (\frac{ds_0}{d\theta} - \frac{4\gamma(\gamma-1)(M_\infty^2 \sin^2\theta-1)^2 \cot \theta}{(2\gamma M_\infty^2 \sin^2\theta-(\gamma-1))((\gamma-1)M_\infty^2\sin^2\theta+2)}) \tag{199}$$

$$- \ \frac{4\gamma(\gamma-1)(M_\infty^2 \sin^2\theta-1)^2 \cot \theta}{(2\gamma M_\infty^2 \sin^2\theta-(\gamma-1))((\gamma-1)M_\infty^2\sin^2\theta+2)})$$

$$U_n = -g_n \ (\frac{du_0}{d\theta} + \sin \theta)$$

$$V_n = -g_n \ (\frac{dv_0}{d\theta} + v_0 \cot \theta \ \frac{2 - (\gamma-1) \ M_\infty^2 \sin^2\theta}{2 + (\gamma-1) \ M_\infty^2 \sin^2\theta} \tag{200}$$

$$W_n = g_n \frac{2}{\gamma+1} \left(1 - \frac{1}{M_\infty^2 \sin^2\theta}\right)$$

$$S_n = -q_n \left(\frac{ds_0}{d\theta} - \frac{4\gamma(\gamma-1)(M_\infty^2 \sin^2\theta-1)^2 \cot\theta}{(2\gamma M_\infty^2 \sin^2\theta-(\gamma-1))((\gamma-1) M_\infty^2 \sin^2\theta+2)}\right)$$

$$\theta = \delta: \quad V_0 = 0 \tag{201}$$

$$V_n = 2u_0 \tag{202}$$

Equations (194) and (195) can be used to show that S_n is constant and that V_n equals $dU_n/d\theta$. The result that S_n is constant is not valid on the body surface. The body surface is a streamsurface and the entropy must be constant there. The perturbation approach gives $s = s_0 + \alpha S_0 (\cos(\phi-\phi_0) + \Sigma \epsilon_n S_n \cos(n(\phi-\phi_n))$ which is not constant on the body surface. As a consequence there is a thin payer near the body surface, the so-called vortical layer, where the results of the regular perturbation scheme are not valid. Munson (Reference 27), Melnik (Reference 25), and others have studied conditions in the vortical layer and have shown that the results obtained for the pressure and azimuthal velocity by means of the regular perturbation approach are valid in the vortical layer, while the results for the radial and polar velocities and entropy are not valid there. The methods of singular perturbation theory allow correction of the inadequacies of the regular perturbation approach near the body and thereby provide a uniformly valid solution. No attempt is made here to deal with the vortical layer as it will not affect the results of interest in this report.

Equation (196) can now be rewritten

$$- \frac{a_0^2}{\gamma(\gamma-1)v_0} \epsilon_n = \frac{d}{d\theta} (U_n + W_n \sin\theta) + \frac{u_0}{v_0} (U_n + W_n \sin\theta) \tag{203}$$

which can be formally integrated to give

$$U_n + W_n \sin\theta = -\frac{S_n}{\gamma(\gamma-1)} (-v_0 \sin\theta)^{1/2} a_0^{\frac{1}{\gamma-1}} \tag{204}$$

$$\cdot \int_{\theta_{0s}}^{\theta} \frac{a_0}{v_0 \, (-v_0 \sin \theta)^{1/2}} \, d\theta^{\frac{2\gamma-3}{\gamma-1}}$$

$$= -F_n \, (\theta)$$

noting that $(U_n + W_n \sin \theta)$ vanishes at $\theta = \beta$. Eliminating V_n and W_n from Equation (193), results in*

$$\frac{d^2 U_n}{d\theta^2} + \cot \theta \, \frac{dU_n}{d\theta} + U_n \, (2-n^2 \csc^2 \theta) = n^2 F_n(\theta) \csc^2\theta \qquad (205)$$

$$+ \, 2 \, \frac{v_0}{a_0} \, \frac{u_0}{a_0} \, \frac{dU_n}{d\theta} + \left(\frac{v_0}{a_0}\right)^2 \, \left[U_n + \frac{d^2 U_n}{d\theta^2} - 2(u_0 + \frac{dv_0}{d\theta}\mu \, \frac{A_n}{a_0} + 2 \, \frac{V_n}{v_0} \, \frac{dv_0}{d\theta} \right]$$

with boundary conditions

$$\theta = \beta: \quad U_n = -g_0 \, \frac{du_0}{d\theta} + (1-g_0) \sin \theta, \quad n = 0$$

$$= -g_n \, \left(\frac{du_0}{d\theta} + \sin \theta \right) , \qquad n > 0 \qquad (206)$$

$$\frac{dU_n}{d\theta} = -g_0 \, \left(\frac{dv_0}{d\theta} + (1-g_0) \, v_0 \cot \theta \, \frac{2 - (\gamma-1) \, M_\infty^2 \sin^2\theta}{2 + (\gamma-2) \, M_\infty^2 \sin^2\theta} \right), \, n=0 \quad (207)$$

$$= -g_n \, \left(\frac{dv_0}{d\theta} + v_0 \cot \theta \, \frac{2 - (\gamma-1) \, M_\infty^2 \sin^2\theta}{2 + (\gamma-2) \, M_\infty^2 \sin^2\theta} \right), \quad n > 0$$

$$\theta = \delta: \quad \frac{dU_n}{d\theta} = 0 \quad , \quad n = 0 \qquad (208)$$

$$= 2u_0 \, , \quad n > 0$$

Once U_n is determined, W_n follows from Equation (204) and V_n follows from

$$V_n = \frac{du_n}{d\theta} \qquad (209)$$

The disturbance sound speed a_n can be evaluated from Equation (197). The constant s_n is given by Equation (198).

─────────────

*Again, on the case $n=0$, the term $n^2 \csc^2\theta \, U_n$ becomes $\csc^2\theta \, U_0$ and the term $n^2 F_n \csc^2\theta$ becomes $F_0 \csc^2\theta$.

The pressure coefficient C_p can also be expressed as a Fourier series expansion. Substituting for V and s in Equation (45), provides

$$C_p = c_{p0} + \alpha C_{p0} \cos(\phi-\phi_0) + \sum_{n=1}^{\infty} \varepsilon_n C_{pn} \cos(n(\phi-\phi_n)) \qquad (210)$$

where

$$c_{p0} = \frac{2}{\gamma M_\infty^2} \left\{ \left(\frac{V_M^2 - u_0^2 - v_0^2}{V_M^2 - 1}\right)^{\frac{\gamma}{\gamma-1}} \exp\left(\frac{-s_0}{\gamma-1}\right) - 1 \right\} \qquad (211)$$

$$C_{pn} = -\left(C_p0 + \frac{2}{\gamma M_\infty^2}\right) \left\{ \frac{s_n}{\gamma-1} + \frac{2\gamma}{\gamma-1} \frac{u_0 u_n + v_0 v_n}{V_M^2 - u_0^2 - v_0^2} \right\} \qquad (212)$$

c. Weak Polar Crossflow Approximation

An approximation introduced earlier by Rasmussen (Reference 21) that allows closed-form analytical results to be obtained is exploited here. These approximate results are surprisingly accurate over a wide range of conditions and are particularly simple to use. The approximation invoked is the "weak polar crossflow approximation" corresponding to the limit $v_0/a_0 \to 0$. The term $(v_0/a_0)^2$ varies from its maximum value at the shock to zero on the body,

$$0 < \left(\frac{v_0}{a_0}\right)^2 < \left(\frac{v_0}{a_0}\right)^2_{shock} = \frac{(\gamma-1) M_1^2 \sin^2\theta + 2}{2\gamma M_1^2 \sin^2\theta - \gamma + 1} \qquad (213)$$

For $M_\infty \sin\theta$ large, the upper bound to $(v_0/a_0)^2$ becomes $(\gamma-1)/2\gamma$ (= 1/7 if γ = 1.4). Ignoring terms of order v_0/a_0 in the governing equations reduces the equations to forms that can be solved analytically in terms of known functions.

Ignoring terms of order $(v_0/a_0)^2$ in Equation (187), the equations governing flow past a right circular cone at zero angles of attack and yaw, Equations (187) through (190), can be reduced to

$$\frac{d^2 u_0}{d\theta^2} + \cot\theta \frac{du_0}{d\theta} + 2u_0 = 0 \qquad (214)$$

$$v_0 = \frac{du_0}{d\theta} \qquad (215)$$

$$a_0^2 = \frac{\gamma-1}{2} (V_M^2 - u_0^2 - v_0^2) \tag{216}$$

$$s_0 = \ln \left\{ \left(\frac{2\gamma M_\infty^2 \sin^2\beta - \gamma+1}{(\gamma+1)} \right) \left(\frac{(\gamma-1)M_1^2 \sin^2\beta+2}{(\gamma+1)M_\infty^2 \sin^2\beta} \right)^\gamma \right\} \tag{217}$$

with boundary conditions

$$\theta = \beta: \qquad u_0 = \cos\theta \tag{218}$$

$$\frac{du_0}{d\theta} = -\frac{\gamma-1}{\gamma+1} \frac{(V_M^2 - \cos^2\theta)}{\sin\theta}$$

$$\theta = \delta: \qquad \frac{du_0}{d\theta} = 0 \tag{219}$$

Equation (214) is Legendre's equation whose solution can be written

$$u_0 = A_0 P_1(\mu) + B_0 Q_1(\mu) \tag{220}$$

($\mu = \cos\theta$). Here P_n and Q_n are the Legendre functions of the first and second kind, respectively. In particular,

$$P_1(\mu) = \mu \ , \ \ Q_1(\mu) = \frac{\mu}{2} \ln \left(\frac{1+\mu}{1-\mu} \right) - 1 \tag{221}$$

The boundary conditions, Equations (218), allow the constants A_0 and B_0 to be evaluated. The results are

$$D_0 = 1 + \left[(1-\mu^2)Q_1(\mu) \left(1 - \frac{\gamma-1}{\gamma+1} \frac{V_M^2 - \mu^2}{1-\mu^2} \right) \right]_{\mu = \mu_s} \tag{222}$$

$$E_0 = - \left[\mu(1-\mu^2) \left(1 - \frac{\gamma-1}{\gamma+1} \frac{V_M^2 - \mu^2}{1 + \mu^2} \right) \right]_{\mu = \mu_s}$$

Here $\mu_s = \cos\delta$. The cone angle δ ($= \cos^{-1} \mu_b$) follows from

$$\left(\frac{dQ_1}{d\mu} \right)_{\mu=\mu_b} = \frac{\dfrac{dQ_1}{d\mu} - \dfrac{\gamma-1}{\gamma+1} \dfrac{V_M^2-\mu^2}{1-\mu^2} Q_1}{1 - \dfrac{\gamma-1}{\gamma+1} \dfrac{V_M^2 - \mu^2}{1-\mu^2}} \bigg|_{\mu=\mu_s} \tag{223}$$

Now apply this weak crossflow approximation to the perturbation problem, Equation (205). Equation (205) contains terms on the right-hand side that are order $(u_0 v_0/a_0^2)$ and $(v_0/a_0)^2$ relative to terms on the left-hand side. The terms of order $(v_0/a_0)^2$ on the right-hand side are uniformly small compared to like terms retained on the left-hand side in this weak polar crossflow

approximation. This is not the case, however, for the term of order $(u_0 v_0/a_0^2)$. Specifically, comparison of the term $2u_0 v_0/a_0^2 \, du_0/d\theta$ on the right-hand side with the term $\cot\theta \, dU_n/d\theta$ on the left-hand side, demonstrates that their ratio varies from a maximum at the shock to zero on the body. The value of the ratio at the shock is given by

$$\left[\frac{2}{\cot\theta}\frac{(u_0)}{a_0}\frac{(v_0)}{a_0}\right]_{\theta=\theta_s} = (\gamma+1)\left[1 - \frac{(\gamma-1)}{\gamma+1}^2\left(1 + \frac{2}{(\gamma+1)M_\infty^2\sin^2\beta}\right)\right] \quad (224)$$

which is not small compared to unity. Nonetheless, the term $2(u_0 v_0/a_0^2) \, du_0/d\theta$ on the right-hand side shall be ignored for the following reasons. First, this term is relatively important only near the shock. On the body it is identically zero. Second, although the resulting governing equation is somewhat inaccurate near the shock, the solution U_n is still required to satisfy exactly the boundary conditions given by Equations (206,207). The results obtained by ignoring this term compared well with experiment and other more accurate numerical solutions.

Thus, in the weak crossflow limit, Equation (205) reduces to*

$$\frac{d^2 U_n}{d\theta^2} + \cot\theta \, \frac{dU_n}{d\theta} \, (2 - n^2\csc^2\theta) \, U_n = n^2 \csc^2\theta \, F_n(\theta) \quad (225)$$

The boundary conditions remain unchanged and are given by Equations (206,207,208). Equation (225) is formally the nonhomogeneous associated Legendre equation of order one and degree n. If it is noted that $Q_1^n(\theta)$ is a solution of the homogeneous equation**, where

$$Q_1^n = (-1)^n (1-\mu^2)^{n/2} \frac{d^n Q_1}{d\mu^n}, \quad \mu = \cos\theta \quad (226)$$

then the solution of (225) can be written as

---

*Again, when $n=0$, the term $n^2\csc^2\theta \, U_n$ becomes $\csc^2\theta \, U_0$ and the term $n^2\csc^2\theta \, F_n$ becomes $\csc^2 \, F_0$.

**The function $\sin\theta$ is also a complementary solution for the case $n = 1$.

69

$$U_n(\theta) = n^2 Q_1{}^n (\theta) \int_\theta^\beta \frac{d\theta'}{Q_1{}^n{}^2(\theta') \sin \theta'} \int_{\theta'}^\beta F_n (\theta'') \cos \theta''$$

$$\cdot Q_1{}^n (\cos \theta'') d\theta'' + A_n Q_1{}^n(\theta) \int_\theta^\beta \frac{d\theta'}{Q_1{}^n{}^2(\theta') \sin \theta'}$$

$$+ B_n Q_1{}^n (\theta) \tag{227}$$

The boundary conditions, Equations (206,207), allow the constants A_n and B_n to be evaluated as

$$A_n = [\sin \theta \frac{dQ_1}{d\theta} U_n - \sin \theta Q_1{}^n \frac{dU_n}{d\theta}]_{\theta=\beta} \tag{228}$$

$$B_n = [\frac{U_n}{Q_1{}^n}]_{\theta=\beta} \tag{229}$$

Equation (208) allows determination of the ratio g_n of the shock displacement to the body perturbation.

The integrations required to evaluate Equation (227) for $U_n(\theta)$ cannot be carried out in closed form. For this reason it is useful to consider a further approximation and to restrict attention to slender bodies. In this way, explicit results can be obtained which are quite useful.

d. Hypersonic Small Disturbance Approximation; Comparison with
Experiment

Consider now slender bodies for which, δ, $\beta \to 0$; in order to retain the essentially nonlinear character of supersonic-hypersonic flow, also require M_∞ to be large so that

$$K_\theta = M_\infty \sin \theta \tag{230}$$

is finite. The limit $\theta \to 0$, $M_\infty \to \infty$ such that $K_\theta = M_\infty \sin \theta$ is finite is the hypersonic small disturbance approximation limit.

In the hypersonic small disturbance approximation, the solution for flow past a right circular cone at zero angles of attack and yaw reduce to

Equations (76). These results allow evaluation of the function $F_n(\theta)$ that appears in Equation (204). Ignoring the variation of a_0 across the shock layer in comparison with the variation of v_0, provides

$$F_n = -\beta G \left[1 - \left(\frac{K_\theta^2 - K_b^2}{K_s^2 - K_b^2}\right)^{1/2}\right] (1-g_0) \ , \ n = 0 \tag{231}$$

$$= \beta G \left[1 - \left(\frac{K_\theta^2 - K_b^2}{K_s^2 - K_b^2}\right)^{1/2}\right] g_n \qquad , \ n > 0 \tag{232}$$

where

$$G = \frac{(K_s^2-1)^2}{K_s^2 \ (2\gamma \ K_s^2 - \gamma + 1)((\gamma-1) \ K_s^2 + 2)} \left(1 + \frac{\gamma-1}{2} \ K_b^2 \left(2 - \frac{K_b^2}{K_s^2}\right)\right) \tag{233}$$

In this hypersonic small disturbance theory limit, Equation (225) becomes*

$$\frac{d^2 U_n}{d\theta^2} + \frac{1}{\theta} \frac{dU_n}{d\theta} - \frac{n^2}{\theta^2} U_n = \frac{n^2}{\theta^2} F_n(\theta) \tag{234}$$

with boundary conditions given by Equations (206,207,208),

$$\theta = \beta : \ U_n = -g_0 \frac{\delta^2}{\theta} + \theta \quad , \quad n = 0 \tag{235}$$

$$= -g_n \frac{\delta^2}{\theta} \qquad , \quad n > 0 \tag{236}$$

$$\frac{dU_n}{d\theta} = +g_0 \left(1 + \frac{\delta^2}{\theta^2}\right) - (1 - g_0)(1 - \frac{\delta^2}{\theta^2}) \frac{2- (\gamma-1) \ K_\theta^2}{2+ (\gamma-1) \ K_\theta^2} , \ n = 0 \tag{237}$$

$$= g_n \left(1 + \frac{\delta^2}{\theta^2}\right) + g_n \left(1 - \frac{\delta^2}{\theta^2}\right) \frac{2- (\gamma-1) \ K_\theta^2}{2+ (\gamma-1) \ K_\theta^2} , \ n > 0 \tag{238}$$

$$\theta = \delta : \ \frac{dU_0}{d\theta} = 0 \tag{239}$$

$$\frac{dU_n}{d\theta} = 2 \tag{240}$$

Equation (234) has been integrated explicitly for $n = 0, 1, 2, 3, 4$. While the integrations are somewhat laborious, there is no particular impediment to consideration of larger n. The results for the first five values of n are given below.

---

*Again, when $n = 0$, the terms $n^2 U_n/\theta^2$ and $n^2 F_n/\theta^2$ become U_0/θ^2 and F_0/θ^2, respectively.

$$U_0 = -\beta G(1-g_0)\{-1 + \frac{\beta}{4\theta} + \frac{3}{4}\frac{(\theta^2-\delta^2)^{1/2}}{\beta^2-\delta^2} + \frac{2\theta^2+\delta^2}{4\theta(\beta^2-\delta^2)^{1/2}} \ln(\frac{\beta+(\beta^2-\delta^2)^{1/2}}{\theta+(\theta^2-\delta^2)^{1/2}})\}$$

$$+ A_0\theta^{-1} + B_0\theta \tag{241}$$

$$U_1 = \beta\, G_{g1}\{-1 + \frac{\beta}{4\theta} + \frac{3}{4}\frac{(\theta^2-\delta^2)^{1/2}}{\beta^2-\delta^2} + \frac{2\theta^2+\delta^2}{4\theta(\beta^2-\delta^2)^{1/2}} \ln(\frac{\beta+(\beta^2-\delta^2)^{1/2}}{\theta+(\theta^2-\delta^2)^{1/2}})\}$$

$$+ A_1\theta^{-1} + B_1\theta \tag{242}$$

$$U_2 = \beta\frac{G_{g2}}{\theta^2}\{\theta^2 - \frac{\theta^4}{2\beta^2} - \frac{\theta^4(\beta^2-\delta^2)}{2\beta^2\delta^2} + \frac{2}{5}\frac{(\theta^2-\delta^2)^{5/2}}{\delta^2(\beta^2-\delta^2)^{1/2}} + \frac{\theta^4}{2\delta^2}$$

$$- 2\frac{(3\theta^2+2\delta^2)}{15\delta^2}\frac{(\theta^2-\delta^2)^{3/2}}{(\beta^2-\delta^2)^{1/2}} - \frac{\theta^2+2\delta^2}{6}\frac{(\theta^2-\delta^2)^{1/2}}{\beta^2-\delta^2}$$

$$- \frac{\theta^4}{2\delta(\beta^2-\delta^2)^{1/2}}(\tan^{-1}\frac{(\beta^2-\delta^2)^{1/2}}{\delta^2} - \tan^{-1}\frac{(\theta^2-\delta^2)^{1/2}}{\delta^2})\}\Big|_\theta^\beta$$

$$+ A_2\theta^{-2} + B_2\theta^2 \tag{243}$$

$$U_3 = \frac{\beta\,G_{g3}}{\theta^3}\{\theta^3 - \frac{\theta^6}{2\beta\delta^2} + \frac{3\theta}{2\delta^2}\frac{(\theta^2-\delta^2)^{1/2}}{\beta^2-\delta^2}(\frac{(\theta^2-\delta^2)^2}{3} + \frac{\delta^2(\theta^2-\delta^2)}{12} - \frac{\delta^4}{8})$$

$$+ \frac{3}{16}\frac{\delta^4}{(\beta^2-\delta^2)^{1/2}} \ln(\frac{\beta+(\beta^2-\delta^2)^{1/2}}{\theta+(\theta^2-\delta^2)^{1/2}})\}\Big|_\theta^\beta$$

$$+ A_3\theta^{-3} + B_3\theta^3 \tag{244}$$

$$U_4 = \frac{\beta\,G_{g4}}{\theta^4}\{\theta^4 - \frac{4(3\theta^2+2\delta^2)}{15}\frac{(\theta^2-\delta^2)^{3/2}}{(\beta^2-\delta^2)^{1/2}} - \frac{\theta^8}{4\delta^2\beta^2}$$

$$- \frac{\theta^8}{4\delta^3(\beta^2-\delta^2)^{1/2}} \tan^{-1}\frac{(\theta^2-\delta^2)^{1/2}}{\delta^2} + \frac{2(\theta^2-\delta^2)^{3/2}}{(\beta^2-\delta^2)^{1/2}}(\frac{(\theta^2-\delta^2)^2}{7\delta^2} + \frac{2(\theta^2-\delta^2)}{5} + \frac{\delta^2}{3})$$

$$- \frac{1}{4\delta^2}\frac{(\theta^2-\delta^2)^{1/2}}{\beta^2-\delta^2}(\frac{(\theta^2-\delta^2)^3}{7} + \frac{3\delta^2(\theta^2-\delta^2)}{5} + \theta^2\delta^4))\}\Big|_\theta^\beta$$

$$+ A_4\theta^{-4} + B_4\theta^4 \tag{245}$$

The constants of integration A_n and B_n are given by

$$A_n = \frac{3}{2} \left(U_0 - \theta \frac{dU_0}{d\theta}\right)_{\theta=\beta} \quad , \quad n = 0$$

$$= \frac{\beta^n}{2} \left(U_n - \frac{\theta}{n} \frac{dU_n}{d\theta}\right)_{\theta=\beta} \quad , \quad n > 0 \qquad (246a)$$

$$B_n = \frac{1}{2\beta} \left(U_0 + \theta \frac{dU_0}{d\theta}\right)_{\theta=\beta} \quad , \quad n = 0$$

$$= \frac{\beta^{-n}}{2} \left(U_n + \frac{\theta}{n} \frac{dU_0}{d\theta}\right)_{\theta=\beta} \quad , \quad n > 0 \qquad (246b)$$

Having determined the U_n, one can then compute V_n, W_n, A_n, C_{pn}, and q_n from Equations (194), (204), (197), (212), and (240), respectively. Of particular interest is the shock--body shape relation g_n, surface pressure coefficient ($C_{pn}0$), and flow streamsurfaces. The first two quantities can be easily measured while the latter quantity is useful in developing waverider geometries.

Differentiating Equations (241)through (245) with respect to θ, results in expressions for V_0, V_1, V_2, V_3, and V_4. Evaluating these expressions at $\theta = \delta$, allows determination of the ratio of the body perturbation to the shock perturbation, g_n. The results are

$$\frac{1}{1-g_0} = 1 + G \left[- \frac{\sigma^2}{\delta} + \frac{\sigma}{\delta(\sigma^2-1)^{1/2}} \ln (\sigma + (\sigma^2-1)^{1/2})\right]$$

$$+ \frac{\sigma^2-1}{4} \frac{\sigma^4-1}{4\eta^2} \frac{2-(\gamma-1) K_s^2}{2+(\gamma-1) K_s^2} \qquad (247a)$$

$$\frac{1}{g_1} = \frac{1}{1-g_0} \qquad (247b)$$

$$\frac{1}{g_2} = G \left[- \frac{\sigma(\sigma^2+2)}{6} + \frac{\sigma}{2(\sigma^2-1)^{1/2}} \tan^{-1} ((\sigma^2-1)^{1/2})\right] \qquad (247c)$$

$$+ \frac{\sigma^4-1}{2\sigma^3} + \frac{\sigma^4+1}{4\sigma} \left(\frac{\sigma^2+1}{\sigma^2} + \frac{\sigma^2-1}{\sigma^2} \frac{2-(\gamma-1) K_s^2}{2+(\gamma-1) K_s^2}\right)$$

$$\frac{1}{g_3} = G \left[\frac{3}{4} - \frac{3}{16} \sigma^4 - \frac{9}{32} \sigma^2 - \frac{9}{32} \frac{\sigma}{(\sigma^2-1)^{1/2}} \ln(\sigma+(\sigma^2-1)^{1/2}) \right]$$

$$+ \frac{3}{4} \frac{\sigma^6-1}{\sigma^4} + \frac{\sigma^6+1}{4\sigma^2} \left(\frac{\sigma^2+1}{\sigma^2} + \frac{\sigma^2-1}{\sigma^2} \frac{2-(\gamma-1) K_s^2)}{2+(\gamma-1) K_s^2} \right) \qquad (247d)$$

$$\frac{1}{g} = G \left[\frac{1}{2\sigma} + \frac{\sigma^3}{2} - 2\sigma^5 + \frac{\sigma^7}{2} + 8(\sigma^2-1) \left(\frac{13\sigma^3}{80} - \frac{\sigma^5}{16} + \frac{23\sigma}{15} \right) \right.$$

$$+ \frac{\sigma}{2(\sigma^2-1)^{1/2}} \tan^{-1} ((\sigma^2-1)^{1/2}) \left] + \frac{\sigma^8-1}{\sigma^5} \right.$$

$$+ \frac{\sigma^8+1}{4\sigma^3} \left(\frac{\sigma^2+1}{\sigma^2} + \frac{\sigma^2-1}{\sigma^2} \frac{2-(\gamma-1) K_s^2)}{2+(\gamma-1) K_s^2} \right) \qquad (247e)$$

where σ is again the ratio of the shock angle to the cone angle for the unperturbed right circular cone, $\sigma \equiv \beta/\delta$ and is given by Equation (77) as a function of K_δ. Typical results obtained from Equations (247) are shown in Figure 19 for $\gamma = 1.4$. Note that the linearized theory result $g_n = 0$ is obtained for $K_\delta = 0$. Also as K_δ increases, the relative distortion of the shock shape decreases. Other numerical results, not shown here, show that these results are not very sensitive to changes in γ for γ in the range of 9/7 to 5/3.

Equations (216) through (212) can be used to evaluate the surface pressure coefficient. Rewriting these results in the hypersonic small disturbance theory similarity form,

$$\frac{C_p}{\delta^2} = \frac{C_{p0}}{\delta^2} + \frac{\alpha}{\delta} \frac{C_{p\alpha}}{\delta} \cos (\phi-\phi_0) + \sum_n \frac{\varepsilon_n}{\delta} \frac{C_{pn}}{\delta} \cos (n(\phi-\phi_n)) \qquad (248)$$

provides, on the surface of the body,

$$\frac{C_{p0}}{\delta^2} = 1 + \frac{(\gamma+1) K_\delta^2 + 2}{(\gamma-1) K_\delta^2 + 2} \ln \left(\frac{\gamma+1}{2} + \frac{1}{K_\delta^2} \right) \qquad (249a)$$

$$\frac{C_{pn}}{\delta} = -\gamma \left(\frac{C_{p0}}{\delta^2} + \frac{2}{\gamma K_\delta^2} \right) g_n \left\{ \frac{4(K_\beta^2-1)^2}{(2\gamma K_\beta^2-(\gamma-1))((\gamma-1)K_\beta^2+2)} \qquad (249b) \right.$$

$$+ \frac{U_n(\delta)}{\delta g_n} \frac{\gamma K_\delta^2}{1 + \frac{\gamma-1}{2} K_\delta^2(1+2\ln \sigma)} \left. \right\}$$

74

where c and the g_n are given as functions of K_δ by Equations (77) and (247), respectively. Also, for the angle of attack case (n=0), g_n in this equation becomes $-(g_0-1)$. The radial component U_n of the perturbation velocity is given on the body surface by

$$\frac{U_0(\delta)}{\delta(g_0-1)} = \sigma G \{ \sigma 1 - \frac{3}{4} (\sigma 1 - \frac{1}{(\sigma^2-1)^{1/2}} \ln (\sigma + (\sigma^2-1)^{1/2}) \}$$

$$- \frac{\sigma^2+1}{2} - \frac{(\sigma^2-1)^2}{2\sigma^2} \frac{2-(\gamma-1)K_s^2}{2+(\gamma-1)K_s^2} \qquad (250a)$$

$$\frac{U_1(\delta)}{\delta g_1} = \frac{U_0(\delta)}{\delta(g_0-1)} \qquad (250b)$$

$$\frac{U_2(\delta)}{\delta g_2} = \sigma G \{ \sigma^2-1 + \frac{(\sigma^2+1)(\sigma^2-1)^2}{2\sigma^2} - \frac{\sigma^2(\sigma^2-1)}{2} + \frac{(\sigma^2-1)^2}{10}$$

$$- \frac{(\sigma^2-1)(3\sigma^2+2)}{30} + \frac{(\sigma^2-1)}{2\sigma^2} - \frac{\sigma^2+2}{5} \qquad (250c)$$

$$+ \frac{1}{2(\sigma^2-1)^{1/2}} \tan^{-1} ((\sigma^2-1)^{1/2})$$

$$- \frac{\sigma^4+1}{2\sigma} - \frac{\sigma^4-1}{4\sigma^3} (\sigma^2 + 1 + (\sigma^2-1) \frac{2-(\gamma-1)K_s^2}{2+(\gamma-1)K_s^2} \; , \; n=2$$

$$\frac{U_3(\delta)}{\delta g_3} = \sigma G \{ \sigma^3 - 1 - \frac{\sigma^6-1}{2\sigma} + \frac{9}{2} (\sigma^2-1)(\sigma^2 - \frac{3}{4})$$

$$- \frac{3}{16} (\sigma - \frac{1}{(\sigma^2-1)^{1/2}} \ln (\sigma + (\sigma^2-1)^{1/2})$$

$$- \frac{\sigma^6+1}{2\sigma^4} - \frac{\sigma^6-1}{6\sigma^4} (\sigma^2+1+(\sigma^2-1) \frac{2-(\gamma-1) K_s^2}{2+(\gamma-1) K_s^2}) \; , \qquad (250d)$$

$$\frac{U_4(\delta)}{\delta g_4} = \sigma G \{ \quad , - \frac{4}{15} (\sigma^2-1)(3\sigma^2+2) - \frac{\sigma^8-1}{4\sigma^2} - \frac{(\sigma^2-1)^2}{4}$$

$$\frac{\sigma^2-1}{7} + \frac{3}{5}) + 2(\sigma^2-1) (\frac{(\sigma^2-1)^2}{7} + \frac{2(\sigma^2-1)}{5} + \frac{1}{3})$$

$$\frac{1}{4} (\sigma^2 - \frac{1}{(\sigma^2-1)^{1/2}} \tan^{-1} ((\sigma^2-1)^{1/2})) ; - \frac{\sigma^8+1}{2\sigma^5}$$

$$\frac{\sigma^8-1}{8\sigma^7} (\sigma^2 + 1 - (\sigma^2-1) \frac{2-(\gamma-1)K_s^2}{2+(\gamma-1)K_s^2}) \qquad (250e)$$

97
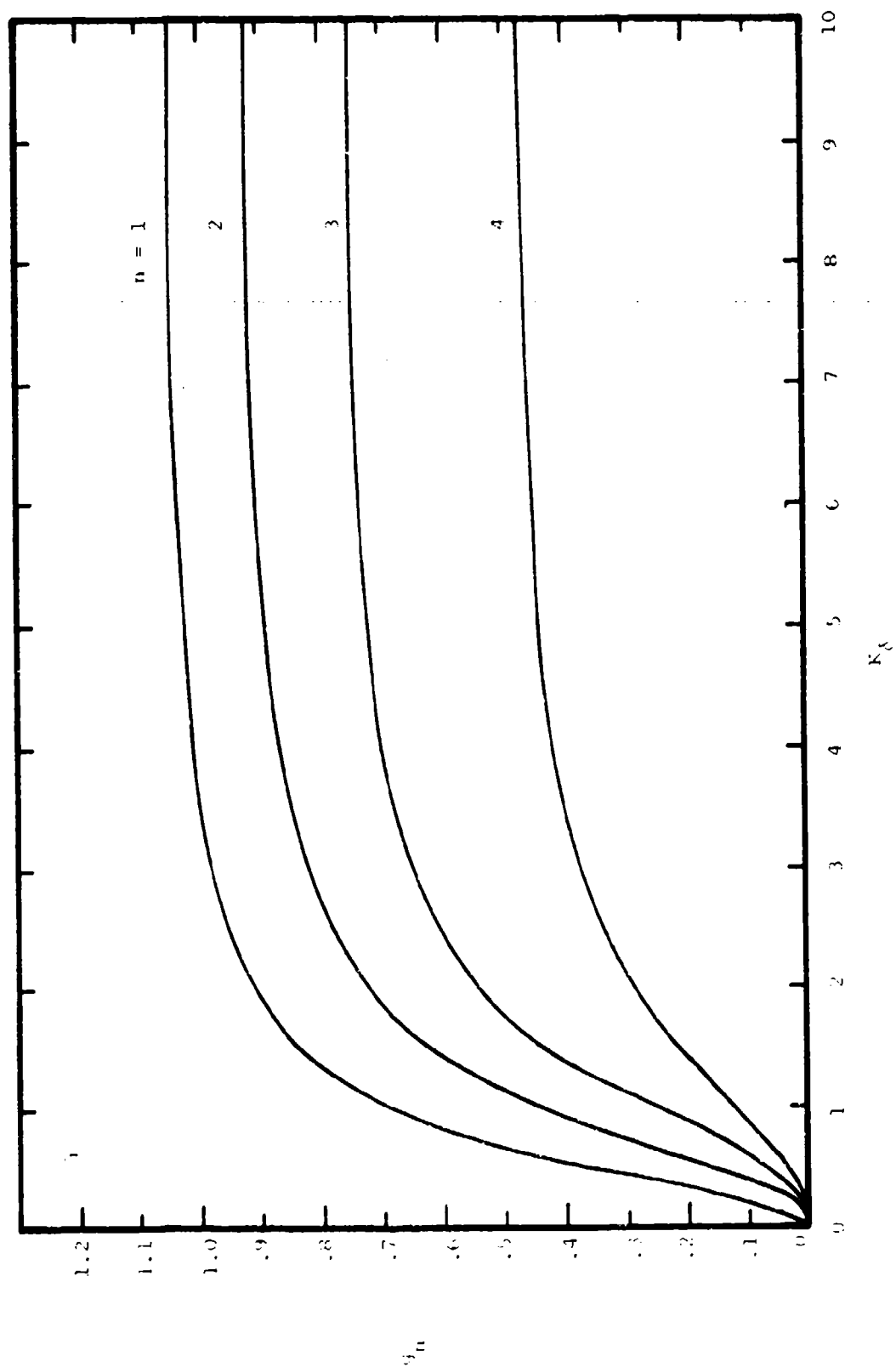
Figure 19. Relation Between Shock and Body Shapes, $\gamma = 1.4$

Typical results for the surface pressure coefficient are shown in Figure 20 for $\gamma = 1.4$. As C_{p0} is equal to the negative of C_{p1}, only the latter has been plotted. These results achieve a hypersonic limiting value as $K_\delta \to \infty$ which agrees well with other known solutions. For example, for $n = 1$, the result C_{p1}/δ takes on the value 4.046 which is to be compared with 4.088 obtained by Cheng (Reference 24) in a separate analysis. The linearized limit, $K_\delta \to 0$, of Equation (250) yields

$$\frac{C_{pn}}{\delta} \to \frac{4}{n} \quad \text{as } K_\delta \to 0 \quad , \quad n > 1 \tag{251}$$

This result agrees exactly with the linearized theory result of Mascitti (Reference 15).

Figure 21 shows a comparison of the present theory with the experimental results obtained by Chan (Reference 28) for flow past a right circular cone of half angle $\delta = 15$ degrees and freestream Mach number $M_\infty = 10.4$ and various angles of attack. Provided the angle of attack is small compared to δ, this flow corresponds to a shock wave whose shape deviates from a circle (in cross-section) by an amount proportional to $\cos \phi$. Figure 21 compares results from the present theory for the surface pressure coefficient for $n = 0$ with experimental results for $\alpha/\delta = 0$, 0.2, 0.4. The comparison is quite good, although the error does grow as α/δ increases, particularly near the symmetry lines ($\phi = 0, \pi$).

The present results for $n = 2$ are identical with those of Section II.1 and thus the comparison of the theory with experiment shall not be repeated here. While the present analysis would allow inclusion of the contribution of the $\epsilon_4 \cos(4(\phi-\phi_4))$ term to the solution, such a procedure would not be wholly systematic as it would ignore the equally important (asymptotically as $\epsilon_2 \to 0$) contribution of the second order terms proportional to ϵ_2^2. The ϵ_4 contribution does give a slight improvement in the comparison between the

77
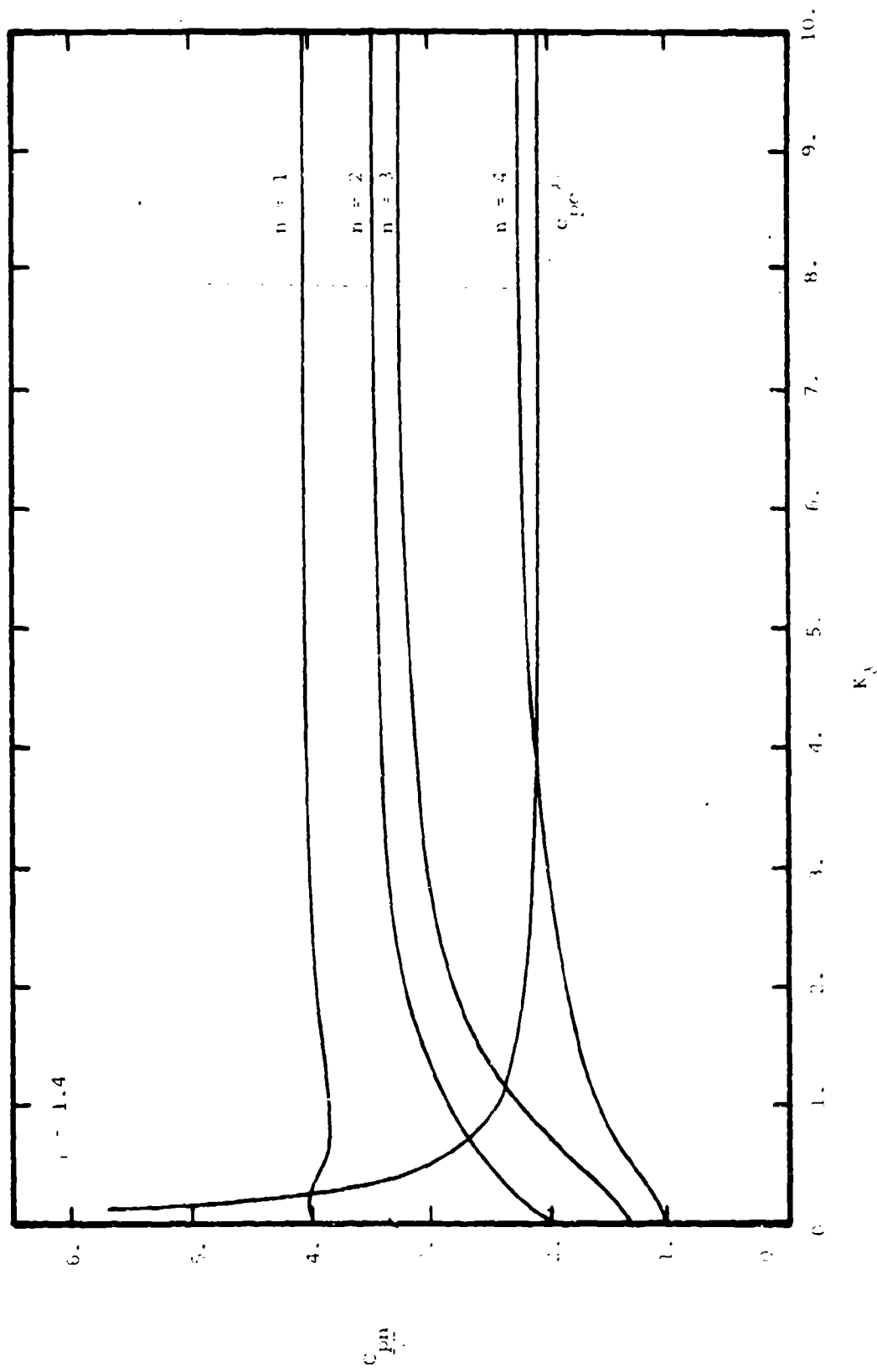
Figure 20. Surface Pressure Coefficient, $\gamma = 1.4$.
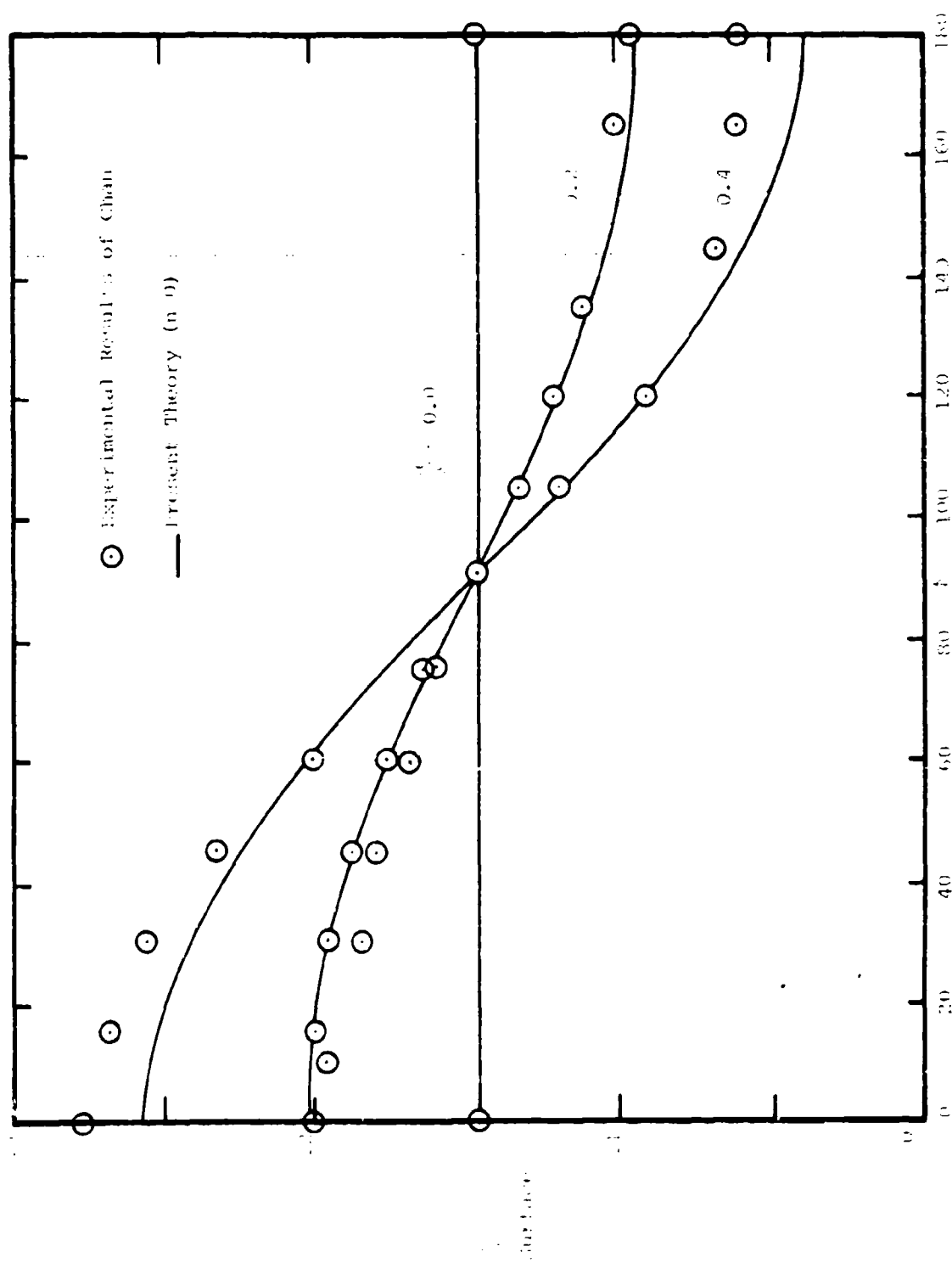
Figure 21. Circular Value of Angle of Attack (Comparison of Theory and Experiment)

experiments of Reference 26, and the theory of Section II.1. This comparison does, however, suggest that the second order terms proportional to ϵ_2^2 must be included if a useful improvement is to be obtained.

e. Streamsurfaces and Waverider Geometries

The streamsurfaces of the flowfield are surfaces composed of streamlines which, in turn, are the field lines of the velocity vector. The streamlines of a given velocity field can be determined from the solution of

$$d\vec{r} \times \vec{V} = 0 \tag{252}$$

where $\vec{r}$ is a vector giving position along the streamline. In spherical polar coordinates Equation (252) can be reduced to

$$\frac{dr}{u} = \frac{r\,d\theta}{v} = \frac{r\sin\theta\,d\phi}{w} \tag{253}$$

It is convenient in the present analysis to introduce a new polar coordinate λ, defined as

$$\lambda = \frac{\theta - \theta_c(\phi)}{\theta_s(\phi)-\theta_c(\phi)} \tag{254}$$

Then λ varies from zero on the body to unity at the shock. Now

$$d\theta = (\theta_s - \theta_c)\left[d\lambda + \left(\frac{\theta_b'}{\theta_b - \theta_s} + \lambda\,\frac{\theta_s' - \theta_b'}{\theta_s - \theta_b}\right)d\phi\right] \tag{255}$$

For geometries which deviate slightly from that of a right circular cone, $\theta_c = \delta + O(\epsilon_n)$ and $\theta_s = \beta + O(\alpha,\epsilon_n)$. In this case, Equation (255) reduces to

$$d\theta = (\beta-\delta)\,d\lambda + O(\alpha,\epsilon_n) \tag{256}$$

and Equation (253) becomes

$$\frac{dr}{u} = \frac{r(\beta-\delta)}{v}\,d\lambda = \frac{r\sin((\beta-\delta)\,\lambda)}{w}\,d\phi \tag{257}$$

with errors of order (α,ϵ_n). The velocity field is given by Equations (182 through 184)

$$u = u_0 + \alpha'J_0(\theta)\cos(\phi-\phi_0) + \sum_n \epsilon_n\,U_n(\theta)\cos(n(\phi-\phi_n))$$

30

$$v = v_0 + \alpha V_0(\theta) \cos(\phi - \phi_0) + \sum_n \varepsilon_n V_n(\theta) \cos(n(\phi - \phi_n))$$

$$w = \alpha W_0(\theta) \sin(\phi - \phi_0) + \sum_n \varepsilon_n n W_n(\theta) \sin(n(\phi - \phi_n)) \quad (258)$$

Thus, to lowest order, Equations (257) becomes

$$\frac{dr}{r} = (\beta - \delta) \frac{u_0}{v_0} d\lambda + 0 (\alpha, \varepsilon_n) \quad (259)$$

$$\frac{(\beta - \delta) \, d\lambda}{v_0 \sin((\beta - \delta) \lambda)} = \frac{d\phi}{\alpha W_0 \sin(\phi - \phi_0) + \sum_n \varepsilon_n n W_n \sin(n(\phi - \phi_n))} + O(\alpha, \varepsilon_n) \quad (260)$$

Equation (259) can be integrated to give

$$r = r_i \exp\left((\beta - \delta) \int_{\lambda_i}^{\lambda} \frac{u_0}{v_0} d\lambda\right) \quad (261)$$

where r_i and λ_i are constants of integra. and correspond to the streamline passing through the point (r_i, λ_i, ϕ_i). Inf ·tion of Equation (260) in closed form is impossible, in general. However, for geometries that can be ⁰ represented by a single Fourier component in ϕ, a rather simple result can be obtained,

$$\tan\left(\frac{n}{2}(\phi - \phi_n)\right) = \tan\left(\frac{n}{2}(\phi_i - \phi_n)\right) \exp\left[\varepsilon_n n^2 (\beta - \delta) \int_{\lambda_i}^{\lambda} \frac{W_n \, d\overline{\theta}}{v_0 \sin((\beta - \delta)\lambda)}\right] \quad (262)$$

Using the hypersonic small disturbance theory approximation, the integrals that appear in Equations (261) and (262) can be evaluated approximately. There results

$$\frac{r}{r_i} = \left(\frac{\theta_i^2 - \delta^2}{\theta^2 - \delta^2}\right)^{1/2} \quad (263)$$

$$\tan\left(\frac{n}{2}(\phi - \phi_n)\right) = \tan\left(\frac{n}{2}(\phi_i - \phi_n)\right)\left(\frac{\theta^2}{\theta_i^2} \frac{\theta_i^2 - \delta^2}{\theta^2 - \delta^2}\right)^{\frac{n^2 \varepsilon_n (F_n - u_n)_b}{2\delta^2}} \quad (264)$$

Rewritten here are the results in terms of θ rather than λ. Also, in carrying out the integration in Equation (262), $(F_n - u_n)$ has been approximated by its value on the body.

81

Typical results from Equation (264) are shown in Figures 22 through 25 for n = 1,2,3,4, respectively. These results give the projection of the streamlines on the unit sphere. These projections are referred to as the "crossflow streamlines." For a given n, the number of crossflow stagnation points is 2n. One-half of the stagnation points are of the saddle point variety while the other half are of the improper node type.

These crossflow streamline results can be used to develop a series of new waverider geometries. That is, since the streamlines of any inviscid flow can be interpreted as a solid boundary, these streamlines can be used to generate new lifting body shapes. While the generation of the new lifting body shapes will be the subject of a subsequent section, Figure 26 shows some possible results.

f. Concluding Remarks

The results obtained should be particularly useful because of their simplicity and ease of utility. The determination of the pressure acting on a body has been reduced to rather simple formulas. The dependence of the pressure force on the body shape, free-stream conditions, and ratio of specific heats is explicitly demonstrated. In addition, the associated streamsurfaces allow new classes of lifting bodies to be developed by means of the waverider notion. In this way, practical lifting geometries can be developed which avoid shape corners, wings of zero thickness, and other unrealistic features.

3. LONGITUDINAL CURVATURE

In this section is developed an approximate analytical solution that illustrates the general features of a supersonic flow past a pointed body that differs from a right circular cone as a result of small longitudinal curvature. When combined with the earlier results for the effects of angle of
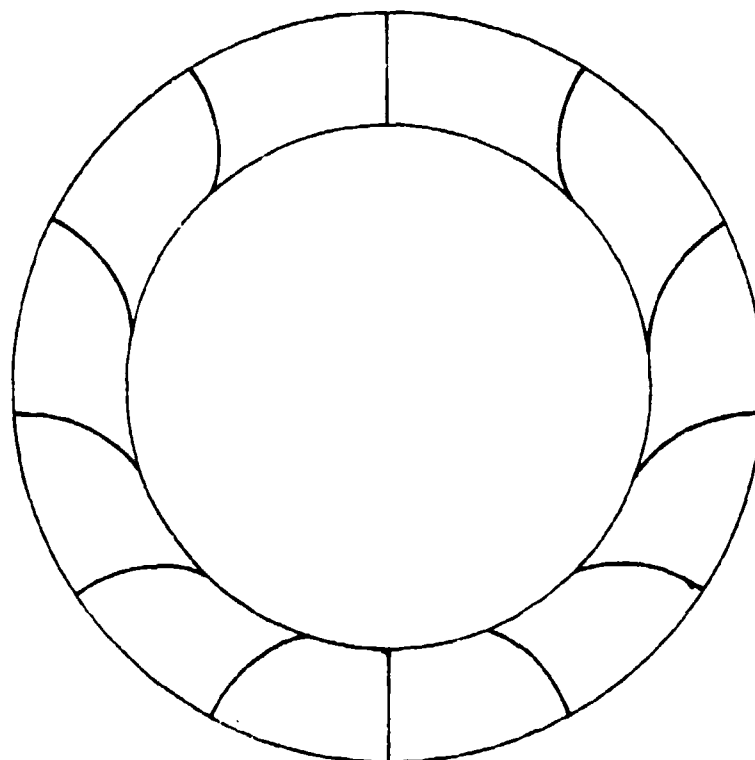
Figure. Distribution of stress

$M_\infty^2 = 1.0$

$\xi = 15°$
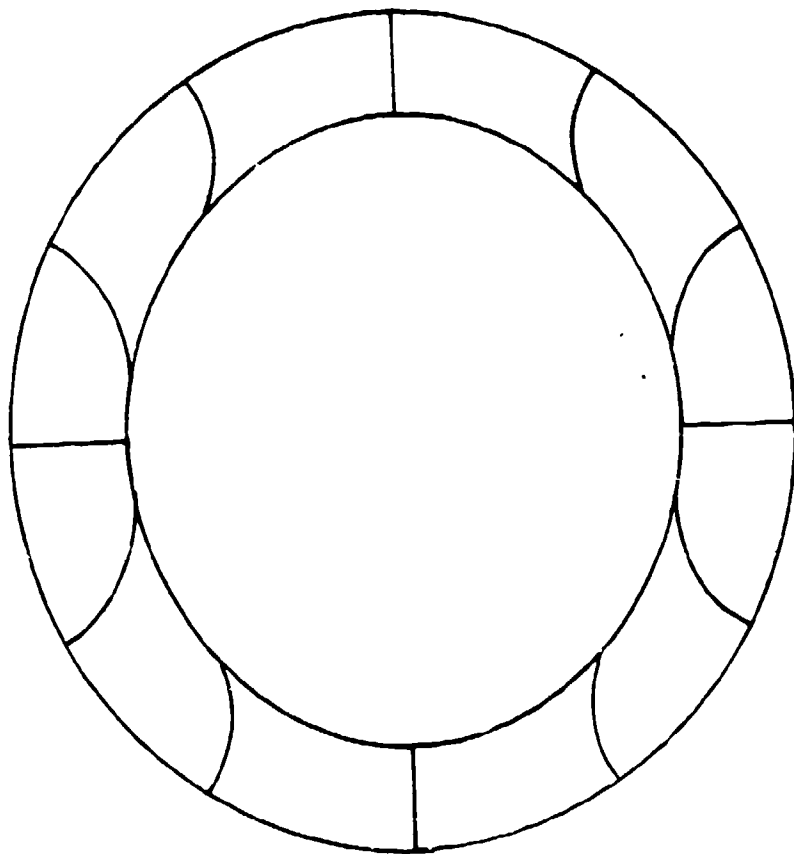
$\varphi_2 = 1.5°$

$\gamma = 1.4$

$\phi_2 = 0°$

Figure 23. Crossflow Streamlines, $\eta = \eta_0 + \eta_2 \cos(2(\phi-\phi_2))$

$$X = 1.$$

$$\omega = 15°$$

$$= 1.5$$

$$', = 1.4$$
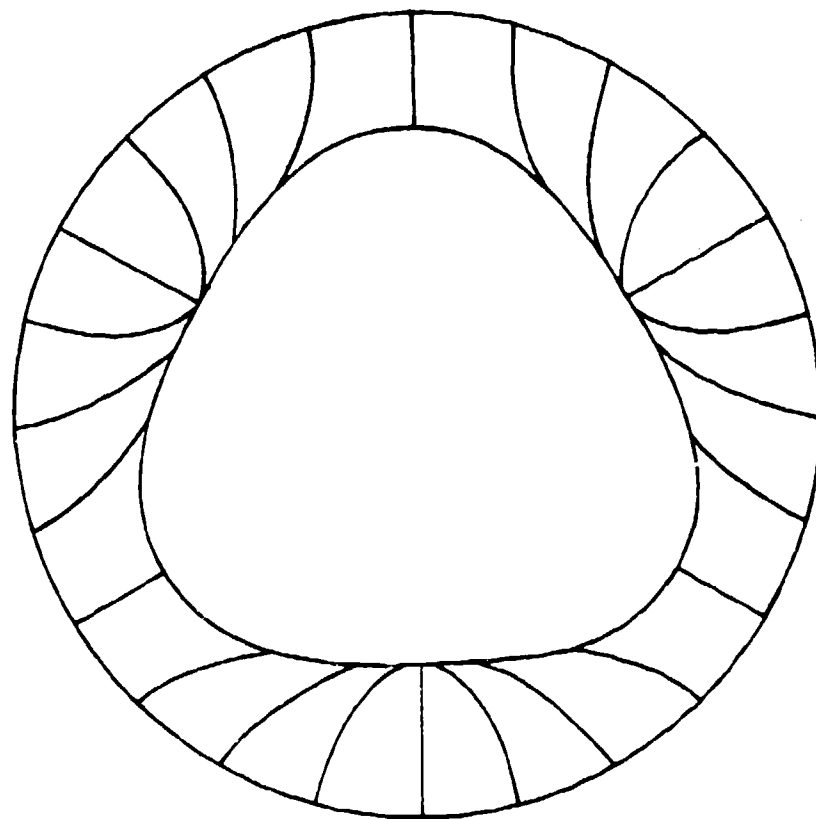
Figure 24. Crossflow Streamlines, $\cos(\zeta - \zeta_3)$
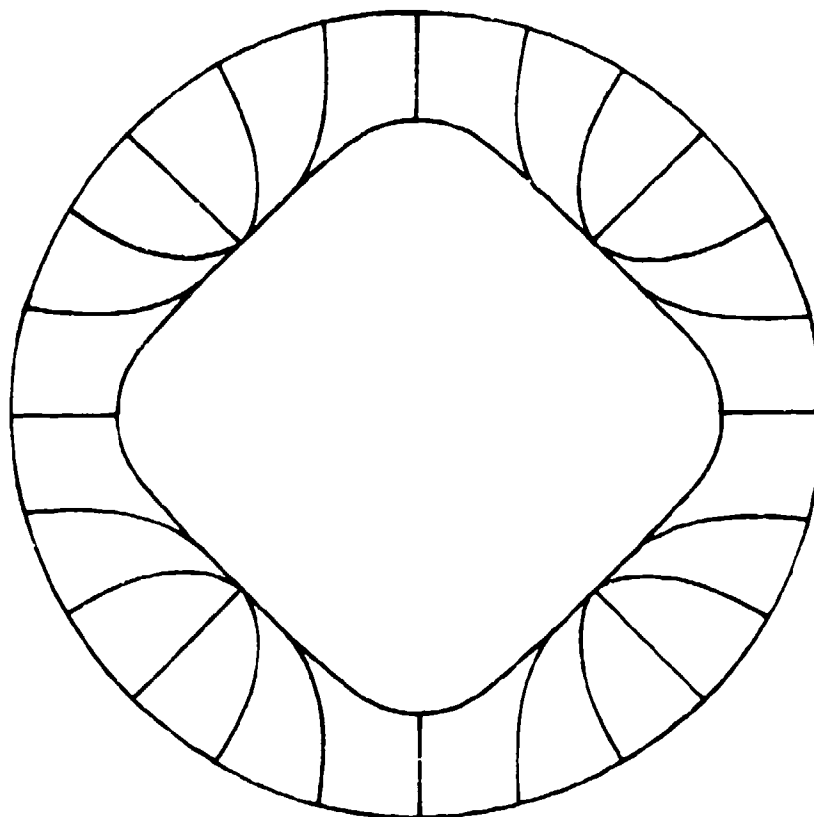
$M_\infty \delta = 1.0$

$\delta = 15°$

$\varepsilon_4 = 1.5°$

$\gamma = 1.4$

$\phi_4 = 0$

Figure 25. Crossflow Streamlines, $\omega_c = \delta + \varepsilon_4 \cos(4(\gamma - \phi_4))$

(b) $r_c = 4 + r_b \cos 2\phi$

(d) $r_c = 4 + r_b \cos 4\phi$

(a) $r_c = 4 + r_b \cos \phi$

(c) $r_c = 4 + r_b \cos 3\phi$
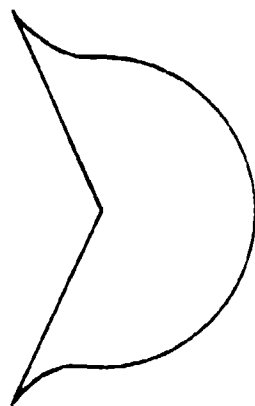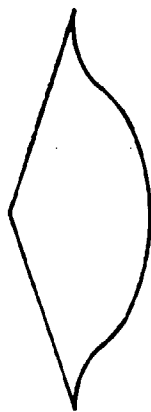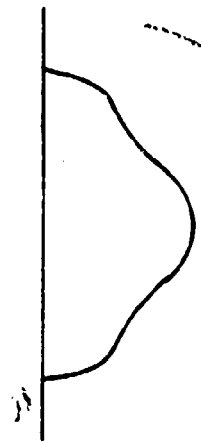
Figure 2. Waverider Geometries Derived From Flows Past Conical Bodies That Deviate Slightly From a Right Circular Cone

attack and deviations of the cross-section from a circle, these results allow the supersonic flow past rather general body shapes to be described.

Others have investigated the problem of supersonic flow past a body with longitudinal curvature. Hayes and Probstein (Reference 29) describe the well known empirical tangent cone method. The shock expansion method of Epstein (Reference 30) has also been used to analyze such flows. Van Dyke (Reference 31), using the nonlinear hypersonic small disturbance theory, has analyzed the flow past ogival-shaped bodies. However, none of these earlier approaches are completely analytical. They all require numerical integration or the use of tables. In contrast, the present work yields results which are given explicitly in closed form. As a consequence, these results are easy to use and lend themselves more readily to preliminary design applications.

a.   Governing Equations and Boundary Conditions

In spherical coordinates, as shown in Figure 27, the pointed axisymmetrical body at zero angle of attack that has slight longitudinal curvature is represented by

$$\theta_c = \delta - \epsilon f(r) \tag{265}$$

where δ is the semivertex angle of the basic right circular cone and ϵ is a small parameter. The curvature function $f(r)$ is an arbitrary function of the radial distance r and depends upon the given shape of the body. For ϵ small, the curvature is given by $\epsilon(2f' + rf'')$. The shape of the associated shock wave is represented in a similar way

$$\theta_s = \beta - \epsilon g(r) \tag{266}$$

where β is angle of the shock wave of the basic cone and $g(r)$ is a function to be determined.

Since the longitudinal curvature is proportional to the parameter ϵ, which is assumed small, the various flow field variables are expanded in
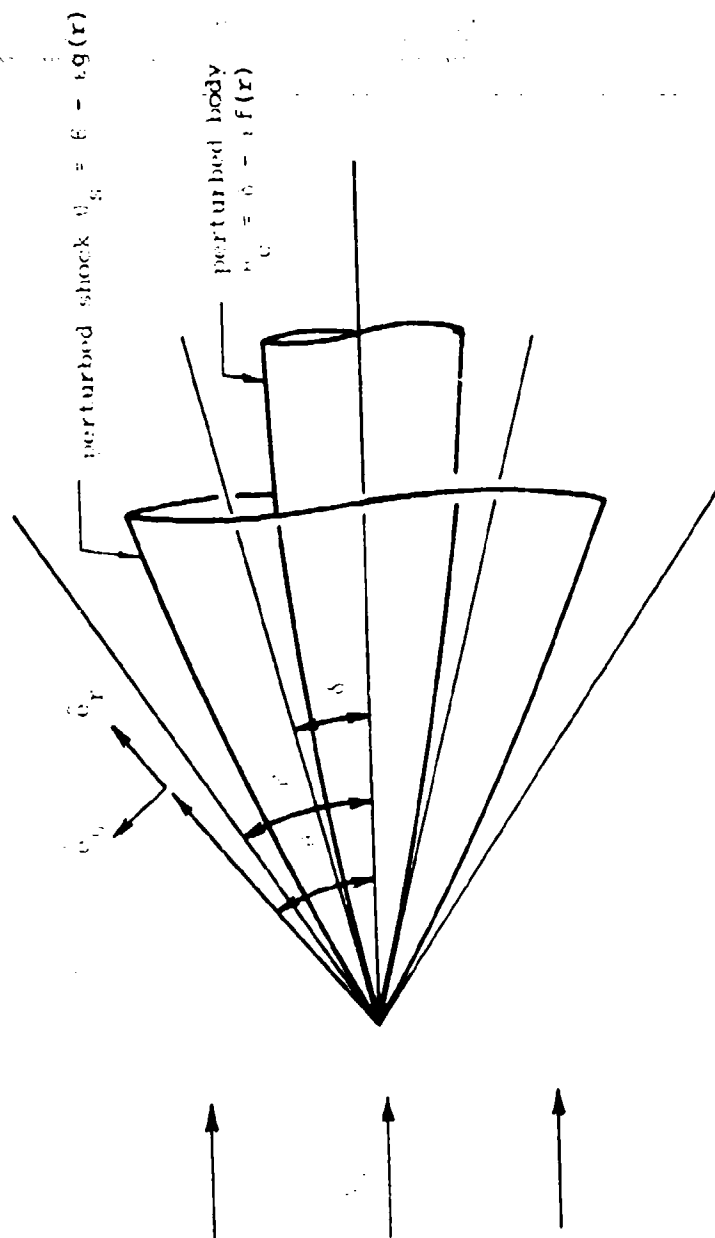
Figure 27. Geometry of Flow

powers of ϵ,

$$u(r,\theta) = u_0(\theta) + \epsilon U(r,\theta) + O(\epsilon^2)$$

$$v(r,\theta) = v_0(\theta) + \epsilon V(r,\theta) + O(\epsilon^2)$$

$$p(r,\theta) = p_0(\theta) + \epsilon P(r,\theta) + O(\epsilon^2) \tag{267}$$

$$\rho(r,\theta) = \rho_0(\theta) + \epsilon R(r,\theta) + O(\epsilon^2)$$

The variables u_0, v_0, p_0, and ρ_0 are the two components of the velocity, the pressure, and the density, respectively, of the basic right circular cone flow. They are functions of the polar angle θ only because steady, supersonic flow past a sufficiently slender right circular cone at zero angle of attack is a conical flow. The terms ϵU, ϵV, ϵP, and ϵR are the first order correction terms due to small longitudinal curvature. They depend on r and θ but are independent of the meridian angle ϕ because the perturbed flow is still axisymmetric.

The velocity, pressure, and density are governed by the equations expressing conservation of mass, Newton's second law, the first law of thermodynamics, and the various equations of state. Here, it is assumed that the flow is inviscid, adiabatic, and steady and that the gas is calorically perfect. The equations expressing conservation of mass, Newton's second law, and the first law of thermodynamics can then be written

$$\nabla \cdot (\rho \vec{V}) = 0 \tag{268}$$

$$\rho [\nabla (\frac{V^2}{2}) - \vec{V} \times (\nabla \times \vec{V})] = -\nabla p \tag{269}$$

$$\frac{V^2}{2} + \frac{\gamma}{\gamma-1} \frac{p}{\gamma} = \text{constant} \tag{270}$$

$$s = s(\rho,p) \tag{271}$$

Using these governing equations and the expansion expressions for the perturbed flow field variables, derive the equations governing the zeroth order and the first order flows for steady, homenergic flow of a perfect gas.

The expansion of the energy equation, Equation (270), by means of Equation (267) leads to

$$\frac{u_0^2 + v_0^2}{2} + \frac{\gamma}{\gamma-1} \frac{p_0}{\rho_0} = \text{constant} \qquad (272a)$$

and

$$\rho_0(\gamma-1)(u_0 U + v_0 V) + \gamma P = R a_0^2 \qquad (272b)$$

Here $a_0(\theta) = (\gamma p_0/\rho_0)^{1/2}$ is the speed of sound in the basic unperturbed flow. It is apparent that the zeroth-order equation is exactly the same as that of the unperturbed flow. The first-order equation can be interpreted as an equation giving the density perturbation in terms of pressure and velocity perturbations.

The momentum equation, Equation (269), can be expanded to give

$$\rho_0 \left[\nabla \left(\frac{\vec{v}_0 \cdot \vec{v}_0}{2} \right) - \vec{v}_0 \times \text{curl } \vec{v}_0 \right] = -\nabla p_0 \qquad (273a)$$

and

$$\rho_0 \left[\nabla(\vec{v}_0 \cdot \vec{V}) - \vec{v}_0 \times \text{curl } \vec{V} - \vec{V} \times \text{curl } \vec{v}_0 \right]$$

$$+ R \left[\nabla \left(\frac{\vec{v}_0 \cdot \vec{v}_0}{2} \right) - \vec{v}_0 \times \text{curl } \vec{v}_0 \right] = -\nabla P \qquad (273b)$$

The velocity vector $\vec{V}$ is expanded as $\vec{v}_0 + \varepsilon \vec{V}$. From the zeroth-order momentum equation, it is known that the unperturbed flow is irrotational; that is,

$$\text{curl } \vec{v}_0 = 0 .$$

The first order equation them becomes,

$$\rho_0 \left[\nabla(\vec{v}_0 \cdot \vec{V}) - \vec{v}_0 \times \text{curl } \vec{V} \right] + R \nabla \left(\frac{\vec{v}_0 \cdot \vec{v}_0}{2} \right) = -\nabla P \qquad (274)$$

Rewriting this result in spherical polar coordinates, obtains

$$\rho_0 \frac{\partial}{\partial r} (u_0 U + v_0 V) - \rho_0 v_0 \left(\frac{V}{r} + \frac{\partial V}{\partial r} - \frac{1}{r} \frac{\partial U}{\partial \theta} \right) = -\frac{\partial P}{\partial r} \qquad (275a)$$

$$\rho_0 \frac{1}{r} \frac{\partial}{\partial \theta} (u_0 U + v_0 V) + \rho_0 u_0 \left(\frac{V}{r} + \frac{\partial V}{\partial r} - \frac{1}{r} \frac{\partial U}{\partial \theta} \right) + R \frac{1}{r} \frac{d}{d\theta} \left(\frac{u_0^2 + v_0^2}{2} \right) = -\frac{1}{r} \frac{\partial P}{\partial \theta}$$

$$(275b)$$

Using the zeroth order equation, (275) can be rewritten as,

$$\rho_0 \frac{1}{r} \frac{\partial}{\partial \theta} (u_0 U + v_0 V) + \rho_0 u_0 (\frac{V}{r} + \frac{\partial V}{\partial r} - \frac{1}{r} \frac{\partial U}{\partial \theta}) - R \, a_0^2 \frac{1}{r} \frac{1}{\rho_0} \frac{d\rho_0}{d\theta} = - \frac{1}{r} \frac{\partial P}{\partial \theta} \quad (276)$$

The energy equation (272b) and the two momentum equations (275a) and (276) are three relations between the first-order perturbation variables, U, V, P, and R. Eliminating R in (276) by means of (272b) yields

$$\rho_0 \frac{1}{r} \frac{\partial}{\partial \theta} (u_0 U + v_0 V) + \rho_0 u_0 (\frac{V}{r} + \frac{\partial U}{\partial r} - \frac{1}{r} \frac{\partial U}{\partial \theta})$$

$$- \frac{1}{r} \frac{d\rho_0}{d\theta} (\gamma - 1)(u_0 U + v_0 V) - \frac{\gamma}{\rho_0} \frac{d\rho_0}{d\theta} \frac{P}{r} = - \frac{1}{r} \frac{\partial P}{\partial \theta} \quad (277)$$

Substituting for the term

$$(\frac{V}{r} + \frac{\partial V}{\partial r} - \frac{1}{r} \frac{\partial U}{\partial \theta})$$

in (277) from (275a), provides a first order partial differential equation for the quantity $L = \rho_0 u_0 U + \rho_0 v_0 V + P$,

$$u_0 \frac{\partial L}{\partial r} + \frac{v_0}{r} \frac{\partial L}{\partial \theta} + \frac{\gamma}{r} \frac{v_0^2}{a_0^2} (u_0 + \frac{dv_0}{d\theta}) L = 0 \quad (278)$$

This partial differential equation for $L(r,\theta)$ can be solved by the method of characteristics using

$$\frac{dr}{r} = \frac{d\theta}{v_0/u_0} = \frac{dL}{\gamma \frac{v_0^2}{a_0^2} (1 + u_0 \frac{dv_0}{d\theta})}$$

and appropriate boundary conditions for $L(r,\theta)$.

Here it can be seen that when $v_0^2/a_0^2 \ll 1$, $L(r,\theta)$ is constant along the streamlines of the unperturbed flow. This can be written in vector notation as

$$\vec{v}_0 \cdot \nabla L = 0 \quad \text{when } v_0^2/a_0^2 \ll 1$$

The basic right circular cone flow is conical; that is, the flowfield quantities depend only on the angle θ. As a consequence, the perturbation equations for the first-order quantities are equidimensional in r and possess

solutions that are proportional to any power of r, say r^m for any number m.
Since the perturbation equations and boundary conditions are linear, it is
possible to express the first-order quantities in the form of a series in r;

$$\epsilon U(r,\theta) = \Sigma \ \epsilon_m r^m U_m(\theta)$$

$$\epsilon V(r,\theta) = \Sigma \ \epsilon_m r^m V_m(\theta)$$

$$\epsilon P(r,\theta) = \Sigma \ \epsilon_m r^m P_m(\theta) \tag{279}$$

$$\epsilon R(r,\theta) = \Sigma \ \epsilon_m r^m R_m(\theta)$$

where here the sums are taken over all possible values of m.

The partial differential equation for $I(r,\theta)$ then becomes an ordinary
differential equation for $L_m(\theta)$.

$$\{mu_0 + \gamma \ \frac{v_0^2}{a_0^2} \ (u_0 + \frac{dv_0}{d\theta})\} \ L_m + v_0 \ \frac{dL_m}{d\theta} = 0 \tag{280}$$

where

$$L_m(\theta) = \rho_0 u_0 U_m + \rho_0 v_0 V_m + P_m \tag{281}$$

This equation can be integrated to give

$$L_m(\theta) = L_m(\beta) \ \exp \ [\int_\theta^\beta \ \frac{mu_0 + \gamma(v_0^2/a_0^2)(u_0 + v_0')}{v_0} \ d\theta] \tag{282}$$

where the constant $L_m(\beta)$ is to be obtained later from the boundary conditions.
Now that $L_m(\theta)$ is a known function, the flow variables can be expressed
in terms of $L_m(\theta)$. From Equation (281)

$$P_m = L_m - \rho_0 u_0 U_m - \rho_0 v_0 V_m \tag{283}$$

The radial momentum equation, (275a), gives

$$m\rho_0(u_0 U_m + v_0 V_m) - \rho_0 v_0 [(m+1)V_m - U_m'] = -mP_m$$

Eliminating P_m by means of (283), results in

$$V_m(\theta) = \frac{m}{m+1} \ \frac{1}{\rho_0 v_0} \ L_m + \frac{1}{m+1} \ \frac{dU_m}{d\theta} \tag{284}$$

93

Use the energy equation to determine the density function R_m,

$$R_m(\theta) = -\frac{1}{a_0^2} \left[\rho_0 u_0 U_m + \frac{\rho_0 v_0}{m+1} \frac{dU_m}{d\theta} - \left(\gamma - \frac{m}{m+1} L_m \right) \right] \tag{285}$$

Equations (283) through (285) give the pressure P_m, tangential velocity V_m, and density R_m in terms of the radial velocity U_m and the known variable L_m. To obtain U_m, use the continuity equation.

The continuity equation (268) is expanded to first order by using expressions (267) and (279) to give, in spherical coordinates,

$$2u_0 + v_0 \cot \theta + \frac{dv_0}{d\theta} + \frac{v_0}{\rho_0} \frac{d\rho_0}{d\theta} = 0 \tag{285a}$$

and

$$(m+2)(\rho_0 U_m + u_0 R_m) + (\rho_0 V_m + v_0 R_m) \cot \theta \tag{285b}$$

$$+ \frac{d}{d\theta} (\rho_0 V_m + v_0 R_m) = 0$$

Eliminating V_m and R_m by means of (284) and (285), results in a single linear, second-order ordinary differential equation for $U_m(\theta)$,

$$U_m''\left(1 - \frac{v_0^2}{a_0^2}\right)$$

$$+ U_m'\left\{ \cot \theta - \frac{v_0}{a_0} \left[\frac{v_0}{a_0} \cot \theta + (2m+3) \frac{u_0}{a_0} \right] \right.$$

$$\left. + \left(1 - \frac{v_0^2}{a_0^2}\right) \frac{d \ln \rho_0}{d\theta} + 2 \frac{v_0^2}{a_0^2} \left(\frac{d \ln a_0}{d\theta} - \frac{d \ln v_0}{d\theta} \right) \right\}$$

$$+ U_m(m+1)\left[(m+2)\left(1 - \frac{u_0^2}{a_0^2}\right) - \frac{u_0 v_0}{a_0^2} \left\{ \cot \theta + \right. \right.$$

$$\left. \frac{v_0'}{v_0} \left(1 - (2-\gamma) \frac{u_0 v_0}{a_0^2}\right) - \frac{v_0^2}{a_0^2} \left(1 - (2-\gamma) \frac{u_0^2}{a_0^2}\right) \right] \tag{286}$$

$$= \frac{(m+1)}{\rho_0 v_0} L_m \left[\frac{m}{m+1} \frac{1}{v_0} (mu_0 + v_0' - v_0 \cot \theta) \right.$$

$$+ \frac{\gamma m}{m+1} \frac{v_0(u_0 + v_0')}{a_0^2} + \frac{v_0^2}{a_0^2} \left(\gamma - \frac{m}{m+1}\right) \left\{ \frac{d \ln (v_0^2/a_0^2)}{d\theta} \right.$$

$$\left. - \cot \theta - \frac{u_0}{v_0} (m+2) + \frac{v_0'}{v_0} + \frac{mu_0}{v_0} + \frac{\gamma v_0}{a_0^2} (u_0 + v_0')\right\}]$$

where L_m is given by (282). To obtain (286), the known results of the zeroth-order equations, (272a), (273a), and (285a), are used.

Equation (286) is a linear, nonhomogeneous, second-order ordinary differential equation with variable coefficients. While numerical solutions can be readily obtained, explicit analytical solutions do not appear possible. Consequently, an approximate analytical solution is sought.

b. Weak Polar Crossflow Approximation, Hypersonic Small Disturbance

   Limit

Now adopt the weak polar crossflow approximation for slender bodies. The term $(v_0/a_0)^2$ varies from the maximum value at the shock to zero on the body. For $M_\infty \sin \beta$ large, the upper bound to (v_0^2/a_0^2) becomes $(\gamma-1)2\gamma$ ($= 1/7$ if $\gamma = 1.4$). As shall be seen, ignoring terms of order (v_0/a_0) in the governing equation for $U_m(\theta)$ reduces the equation to a form that can be solved analytically in terms of known functions. As shown in paragraph 2 for supersonic flow past a cone of small cross-sectional ellipticity, the approximate result obtained by ignoring terms of order v_0/a_0 gives a result which is accurate over the entire range of values of the hypersonic small disturbance parameter $M_\infty \delta$, especially for values of $M_\infty \delta$ greater than unity.

The speed of sound a_0 and the density ρ_0 of the basic cone flow vary smoothly and slightly across the shock layer. Hence, with little loss of accuracy, they can be replaced by $a_0(\beta)$ and $\rho_0(\beta)$. If the terms or order (v_0/a_0) and the terms proportional to $d\rho_0/d\theta$ and $da_0/d\theta$ terms in Equation (286) are ignored Equation (286) reduces to

$$U_m'' + \cot \theta \, U_m' + C_m^2 \, U_m = H_m(\theta) \tag{287}$$

95

where

$$c_m^2 = (m+1)\left[(m+2) - m\,\frac{u_0^2}{a_0^2}\right]$$

$$H_m = \frac{I_m}{\rho_0 v_0^2}\; m\left[(m+2)u_0 + 2\,\frac{dv_0}{d\theta}\right]$$

$$L_m = L_m(\beta)\,\exp\int_\theta^\beta \frac{mu_0}{v_0}\,d\theta$$

In the hypersonic small disturbance theory limit, $M_\infty \to \infty$ and $\sin\delta \to 0$ such that combination $K_\delta = K_\infty \sin\delta$ remains finite, the basic circular cone flow can be accurately approximated by Equations (76). Now assume the slender body approximation such that $\sin\theta = \theta$ and neglect second order terms in Equations (76). The zeroth-order solution then reduces to Equations (77).

In this hypersonic small disturbance limit, (287) becomes

$$\theta^2\,\frac{d^2 U_m}{d\theta^2} + \theta\,\frac{dU_m}{d\theta} + \theta^2\,c_m^2\,U_m = \theta^2\,H_m(\theta) \tag{288}$$

where

$$c_m^2 = (m+1)(m+2) - m(m+1)\,\frac{V_\infty^2}{a_0^2}$$

$$H_m(\theta) = \frac{L_m(\theta)}{\rho_0 V_\infty}\,\frac{(m^2\theta^2 - 2m\delta^2)}{(\theta^2 - \delta^2)^2}$$

$$L_m(\theta) = L_m(\beta)\left(\frac{\theta^2 - \delta^2}{\beta^2 - \delta^2}\right)^{m/2}$$

When $m = 0$, $c_m^2 = 2$ and $H_m(\theta) = 0$ then

$$\theta^2\,\frac{d^2 U_0}{d\theta^2} + \theta\,\frac{dU_0}{d\theta} + 2\theta^2\,U_0 = 0 \tag{289}$$

This is the same equation as that for supersonic conical flow past a right circular cone when the slender body assumption is made. The solution in this case is

$$v_0 = D_1 + D_2\,\ln\theta$$

For the case $m \neq 0$, the second term of c_m^2 is much greater than the first term because in the hypersonic small disturbance limit, V_∞^2/a_0^2 is large when

M_∞ is large. It is then possible to write that

$$C_m^2 \; \theta^2 = -m(m+1) \; \frac{V_\infty^2}{a_0^2} \; \theta^2 = -m(m+1) \; \frac{a_\infty^2}{a_0^2} \; K_\theta^2 \tag{290}$$

where $K_\theta^2 = M_\infty^2 \; \theta^2$. In this case, the homogeneous solution of (288) is

$$U_{m_{homo}}(\theta) = A_3 \; I_0(C_m\theta) + A_4 \; K_0(C_m\theta) \tag{291}$$

Here I_0 and K_0 are modified Bessel functions of the first and second kind of zeroth order. Using the method of variation of parameters, the nonhomogeneous solution of (288) is obtained in the form

$$U_m(\theta) = A_3 \; I_0(C_m\theta) + A_4 \; K_0(C_m\theta)$$

$$- I_0(C_m\theta) \int_\theta^\beta \theta \; K_0(C_m\theta) \; H_m(\theta) \; d\theta$$

$$+ K_0(C_m\theta) \int_\theta^\beta \theta \; I_0(C_m\theta) \; H_m(\theta) \; d\theta \tag{292}$$

The indicated integrations in this result can be carried out by using

$$L_m(\theta) = - \frac{v_0}{mu_0} \frac{dL_m(\theta)}{d\theta} \quad , \quad v_0 = \frac{du_0}{d\theta}$$

to obtain, after much algebra,

$$\int_\theta^\beta \theta \; K_0(C_m\theta)H_m(\theta)d\theta = [\; \frac{\theta^2}{\theta^2-\delta^2} \; K_0(C_m\theta)L_m(\theta)(1 - \frac{(m+1)}{(m+2)} \frac{v_0^2}{a_0^2})$$

$$+ \frac{C_m\theta}{m} \; K_1 \; (C_m\theta) \; L_m(\theta)] \Big|_\theta^\beta$$

$$\cong [\; \frac{\theta^2}{\theta^2-\delta^2} \; K_0 \; (C_m\theta)L_m(\theta) + \frac{C_m\theta}{m} \; K_1(C_m\theta)L_m(\theta)] \Big|_\theta^\beta \tag{293}$$

$$\int_\theta^\beta \theta I_0(C_m\theta) \; H_m(\theta)d\theta$$

$$= [\; \frac{\theta^2}{\theta^2-\delta^2} \; I_0(C_m\theta) \; L_m(\theta)(1 - \frac{(m+1)}{(m+2)} \frac{v_0^2}{a_0^2})$$

$$- \frac{C_m\theta}{m} \; I_1 \; (C_m\theta) \; L_m(\theta)] \Big|_\theta^\beta$$

97

$$= [\frac{\theta^2}{\theta^2-\delta^2} \, I_0(C_m\theta) \, L_m(\theta) - \frac{C_m\theta}{m} \, I_1(C_m\theta) \, L_m(\theta)]_\theta^\beta \tag{294}$$

The constants A_3, A_4 and $L_m(\beta)$ in the solution for $U_m(\theta)$ will be determined later from the associated boundary conditions. The other flowfield variables P_m, V_m, and R_m can then be obtained by using Equations (283) through (285).

c. Boundary Conditions and Flow Variables

The boundary conditions for this problem are the shock jump relations and the condition of zero mass flux through the body -- the so-called tangency condition. The shock jump conditions can be written

$$\rho_\infty \vec{V}_\infty \cdot \hat{n}_s = \rho_s \vec{V}_s \cdot \hat{n}_s = m \tag{295}$$

$$m\vec{V}_\infty \cdot \hat{n}_s + p_\infty = m\vec{V}_s \cdot \hat{n}_s \neq p_s \tag{296}$$

$$\vec{V}_\infty \times \hat{n}_s = \vec{V}_s \times \vec{n}_s \tag{297}$$

Here, again, the subscripts ∞ and s refer to conditions upstream and downstream of the shock wave and $\hat{n}_s$ is the unit normal to the shock (Figure 28). The free stream conditions are taken to be constant with

$$\vec{V}_\infty = V_\infty [\cos\theta \, \hat{e}_r - \sin\theta \, \hat{e}_\theta] \tag{298}$$

Since it is assumed that the first order quantities have the forms given by (279), the variables downstream of the shock are written as

$$\vec{V}_s = [u_0 + \Sigma \, \epsilon_m r^m \, U_m + 0(\epsilon^2)] \hat{e}_r$$

$$+ [v_0 \, \Sigma \, \epsilon_m r^m \, V_m + 0(\epsilon^2)] \hat{e}_\theta$$

$$P_s = P_0 + \Sigma \, \epsilon_m r^m \, P_m + 0(\epsilon^2) \tag{299}$$

$$\rho_s = \rho_0 + \Sigma \, \epsilon_m r^m \, R_m + 0(\epsilon^2)$$
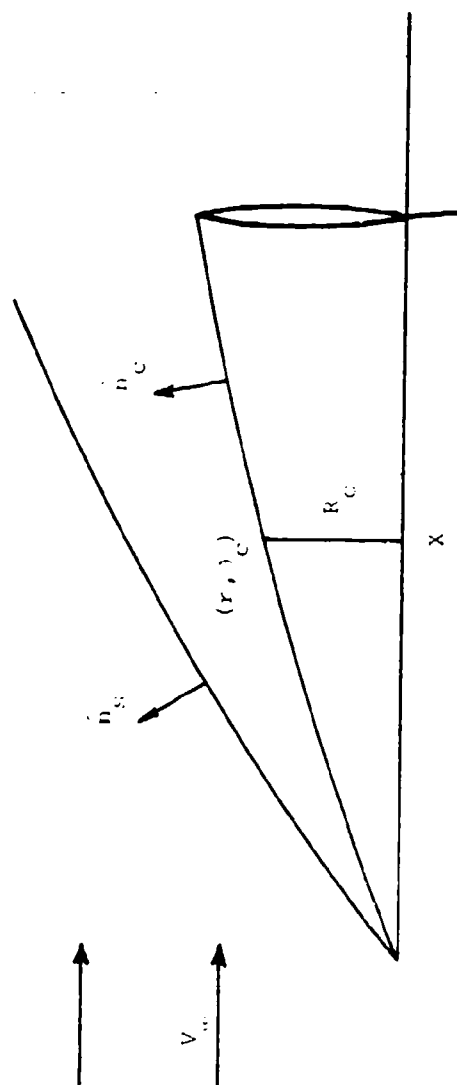
Figure 28. Shock and Body Geometry

The above representation for the perturbed flow variables suggests that the body and shock shape given in (265) and (266) should be rewritten as

$$\theta_C = \delta - \Sigma \, \epsilon_m r^m$$

$$\theta_s = \beta - \Sigma \, \epsilon_m \, G_m r^m \tag{300}$$

In cylindrical polar coordinates, the expression for the body shape is

$$R_C = z \tan \theta_b \tag{301}$$

where R_C is radius of the cross-section of the cone. Using the relation

$$r = z \sec \delta + 0(\epsilon)$$

supplies

$$\theta_b = \delta - \Sigma \, \epsilon_m (z \sec \delta)^m + 0(\epsilon^2)$$

Equation (301) can also be rewritten as

$$R_C = z \tan \delta - \Sigma \, \epsilon_m (\sec \delta)^{m+2} \, z^{m+1} + 0(\epsilon^2) \tag{302}$$

Thus, $R_C = z \tan \delta$ represents the basic circular cone and

$$\Sigma \, \epsilon_m (\sec \delta)^{m+2} \, z^{m+1} = \Sigma \, \bar{\epsilon}_m \, z^{m+1}$$

represents the perturbation terms arising from the small longitudinal curvature. The expression for the body shape, (300), can thus be re-expressed in cylindrical polar coordinates or vice versa. Also for slender bodies, the expression can be written

$$\epsilon_m = \bar{\epsilon}_m \tag{303}$$

These results will be useful later when these calculations are compared with experiment.

Using the expressions for the flow quantities upstream of the shock, (298), and downstream of the shock, (299), and the expression for shock angle, (300) with the approximation

$$\cos \left(\Sigma \, \epsilon_m r^m \, G_m \right) = 1$$

$$\sin \left(\Sigma \, \epsilon_m r^m \, G_m \right) = \Sigma \, \epsilon_m r^m \, G_m$$

It is found that (295) gives to lowest order

$$\theta = \beta: \quad \rho_0 v_0 = -\rho_\infty V_\infty \sin \beta$$

and to first order

$$\theta = \beta: \quad v_0 R_m + \rho_0 V_m = \rho_\infty V_\infty \cos \beta [(1 - \frac{\rho_0}{\rho_\infty} m+1]G_m + \frac{d}{d\theta} (\rho_0 v_0)G_m \quad (304)$$

Here, a Taylor series expansion was used to transfer the boundary conditions to the unperturbed shock location.

Again the hypersonic small disturbance approximation expressed in (77) was adopted and $\rho_0 = $ constant was assumed. In addition to (77) is the relation

$$\frac{\rho_\infty}{\rho_0(\beta)} = 1 - \frac{\delta^2}{\beta^2} \quad .$$

Then, (304) can be written in simpler form as

$$\theta = \beta: \quad v_0 R_m + \rho_0 V_m = -\rho_0 V_\infty (m+\cdots$$

Using the same procedure, the normal momentum jump condition, (296), becomes to lowest order,

$$\theta = \beta: \quad \rho_\infty V_\infty^2 \sin^2\beta + p_\infty = \rho_0 v_0^2 + p_0$$

and to first order,

$$\theta = \beta: \quad P_m + \rho_0 v_0 V_m = -\rho_0 V_\infty^2 \beta(1 - \frac{\delta^2}{\beta^2})(m+1) \frac{\delta^2}{\beta^2} G_m \quad (306)$$

The tangential velocity condition at the shock, (297), becomes to zeroth order,

$$\theta = \beta: \quad u_0 = V_\infty \cos \beta$$

and to first order

$$\theta = \beta: \quad U_m = V_\infty \beta(m+1) \frac{\delta^2}{\beta^2} G_m \quad (307)$$

The necessary boundary conditions at the shock have now been specified. For later use also note that

$$\theta = \beta: \quad L_m = \rho_0 u_0 U_m + \rho_0 v_0 V_m + P_m \quad (308)$$

$$= \rho_0 V_\infty^2 \; \beta \; \frac{\delta^4}{\beta^4} \quad (m+1) \; G_m$$

after Equations (306) and (307).

The tangency condition can be written

$$\vec{V} \cdot \hat{n}_c = 0 \quad \text{on the body} \tag{309}$$

Here $\hat{n}_c$ is the unit normal vector on the body surface, $\theta_c = \delta - \Sigma \; \epsilon_m r^m$. Using (299) and the hypersonic small disturbance limit, the tangency condition can be written as

$$V_m(\delta) = -V_\infty(m+2) \tag{310}$$

The boundary conditions needed to determine the constants D_1, D_2, D_3, D_4 and $I_m(\beta)$ of the solution for $U_m(\theta)$ are now specified. Using the two boundary conditions (307) and (310) the relation between V_m and U_m, (284), and $I_m(\beta)$, (308), the constants can be determined as

$$D_1 = \beta V_\infty \; \frac{\delta^2}{\beta^2} \; G_0 - 2\delta V_\infty \; \ell n \; \beta$$

$$D_2 = -2\delta \; V_\infty$$

$$D_3 = \frac{1}{0\beta^4\delta P} \{ K_0(C_m\delta)U_m(\beta) + (m+1)F(\delta) \; \frac{K_0(C_m\beta)}{C_m}$$

$$- (m+1)(m+2) \; V_\infty \; \frac{K_0(C_m\beta)}{C_m} \} \tag{311}$$

$$D_4 = \frac{1}{0\beta^4\delta P} \{ I_1(C_m\delta)U_m(\beta) - (m+1)F(\delta) \; \frac{I_0(C_m\beta)}{C_m}$$

$$+ (m+1)(m+2) \; V_\infty \; \frac{I_0(C_m\beta)}{C_m} \}$$

where

$$F(\theta) = \frac{\delta^4}{\beta^4} \; C_m\beta \; G_m \; V_\infty \; \{ \frac{m\beta^2}{\beta^2-\delta^2} \; 1\theta\theta\beta P + C_m\beta \; 1\theta1\beta M \}$$

and where has been introduced the notation

$$m\alpha n\beta P = I_m(C_m\alpha)K_n(C_m\beta) + K_m(C_m\alpha)I_n(C_m\beta) \tag{312}$$

$$m\alpha n\beta M = I_m(C_m\alpha)K_n(C_m\beta) - K_m(C_m\alpha)I_n(C_m\beta)$$

Thus

$$0\beta1\delta P = I_0(C_m\beta)K_1(C_m\delta) + K_0(C_m\beta)I_1(C_m\delta)$$

$$1\theta0\beta P = I_1(C_m\theta)K0(C_m\beta) + K_1(C_m\theta)I_0(C_m\beta)$$

$$1\theta1\beta M = I_1(C_m\theta)K_1(C_m\beta) - K_1(C_m\theta)I_1(C_m\beta)$$

The results for U_m then become

$$m = 0; \quad U_0(\theta) = (\beta \frac{\delta^2}{\beta^2} G_0 - 2\delta \ln \frac{\theta}{\beta}) V_\infty \tag{313a}$$

$$m \neq 0; \quad U_m(\theta) = \frac{L_m(\theta)}{\rho_0 V_\infty} + (m+1)(m+2) \frac{1}{C_m\beta} \frac{0\beta0\theta M}{0\beta1\delta P} \beta V_\infty$$

$$+ \frac{\delta^2}{\beta^2} G_m(m+1) \{\frac{0\theta1\delta P}{0\beta1\delta P} + C_m\beta \frac{\delta^2}{\beta^2} (\frac{1\beta1\delta M}{0\beta1\delta P}$$

$$+ 0\beta0\theta M - 0\theta1\beta P)\} \beta V_\infty \tag{313b}$$

When $C_m\theta \to 0$, the asymptotic expansions of the modified Bessel functions can be used; they are

$$K_0(C_m\theta) \approx -\ln \frac{C_m\theta}{2}, \quad K_1(C_m\theta) \approx \frac{1}{C_m\theta}$$

$$I_0(C_m\theta) \approx 1 \qquad , \quad I_1(C_m\theta) \approx 0$$

Then

$$1\beta1\delta M \approx 0$$

$$0\beta0\theta M \approx -\ln(\theta/\beta)$$

$$0\theta1\delta P \approx 1/C_m\delta \tag{314}$$

$$0\beta1\delta P \approx 1/C_m\delta$$

$$0\theta1\beta P \approx 1/C_m\beta$$

and the solution for $U_m(\theta)$ becomes

$$U_m(\theta) = \frac{L_m(\theta)}{\rho_0 V_\infty} - (m+1)(m+2) \ln \frac{\theta}{\beta} V_\infty\delta$$

$$+ \frac{\delta^2}{\beta^2} G_m(m+1)(1 - \frac{\delta^2}{\beta^2}) \beta V_\infty \tag{315}$$

when $C_m\theta \to 0$. It is interesting that (315) for the case $m = 0$ is identical with $U_0(\theta)$ given by (313a).

$V_m(\theta)$ can now be determined by using Equation (284). The results are

$$m = 0; \quad V_0(\theta) = -2 \, V_\infty \, \frac{\delta}{\theta} \tag{316a}$$

$$m \neq 0; \quad V_m(\theta) = \frac{\delta^2}{\beta^2} \, G_m \, V_\infty \, C_m\beta \, \{1\beta1\delta M + \frac{\delta^2}{\beta^2} \, C_m\beta \tag{316b}$$

$$(1\beta1\theta M - \frac{1\beta1\delta M}{0\beta1\delta P} \, 0\beta1\theta P)\} - (m+2)V_\infty \, \frac{0\beta1\theta P}{0\beta1\delta P}$$

When $C_m\theta \rightarrow 0$, the asymptotic forms for the modified Bessel functions give

$$1\beta1\delta M \approx 0$$

$$1\beta1\theta M \approx 0$$

$$0\beta1\theta P \approx 1/C_m\theta$$

and $V_m(\theta)$ then becomes

$$V_m(\theta) = -(m+2) \, V_\infty \, \frac{\delta}{\theta} \, , \quad C_m\theta \rightarrow 0$$

This result for $m = 0$ is identical to $V_0(\theta)$ given by (316a).

The remaining constant G_m, the ratio of the perturbations of the shock and the body angle, is calculated by using the boundary conditions, (305) and (285). The result is

$$G_m = \frac{- (1 - \beta^2 \, \frac{V_\infty^2}{a_0^2} \, D^2) \, V_{m1}}{(m+2) \, \frac{\delta^2}{\beta^2} + (m+1)\beta^2 \, \frac{V_\infty^2}{a_0^2} \, (1 - \frac{\delta^2}{\beta^2}) \, \frac{\delta^2}{\beta^2} \, (1 - \gamma \, \frac{\delta^2}{\beta^2}) + V_{m2} \, (1 - \beta^2 \, \frac{V_\infty^2}{a_0^2} \, D^2)} \tag{317a}$$

where V_{m1} and V_{m2} are defined from the boundary condition at $\theta = \beta$ as

$$V_{m1} + V_{m2}G_m = \frac{V_m(\beta)}{V_\infty}$$

and $D = (1 - \delta^2/\beta^2)$. After calculating $V_m(\beta)$ from (316), the result is

$$V_{o1} = -2 \, \frac{\delta^2}{\beta} \tag{317b}$$

$$V_{o2} = 0$$

$$V_{m1} = - \frac{(m+2) \, V_\infty}{C_m(\beta)(0\beta1\delta P)} \tag{317c}$$

$$V_{m2} = C_m \beta \frac{\delta^2}{\beta^2} \left(1 - \frac{\delta^2}{\beta^2}\right) \frac{1\beta1\delta M}{0\beta1\delta P}$$

Since $V_\infty^2 \beta^2 / a_0^2$ can be expressed in terms of γ and K_δ as

$$\frac{V_\infty^2 \beta^2}{a_0^2} = \frac{[(\gamma+1)K_\delta^2 + 2]^2}{2[(\gamma-1)K_\delta^2 + 2][\gamma K_\delta^2 + 1]}$$

It is seen that G_m is a function of β/δ, K_δ, γ and m. When m = 0, the equation for G_0 can be rewritten after some manipulation as

$$G_0 = \frac{\beta}{\delta} \left[\frac{2(\gamma + 1)K_\delta^2}{(3\gamma + 1)K_\delta^2 + 6} \right]$$

These results for G_m are plotted in Figures 29 and 30 as functions of K_δ, γ and m. G_m has the correct limiting value of linearized theory (e.g. $G_m = 0$) when $K_\delta \to 0$. Also, as $K_\delta \to \infty$, a hypersonic limiting value is achieved. In the Newtonian limit ($K_\delta \to \infty$ and $\gamma = 1$), the result is $G_m = 1$, as expected.

It is important to understand that these limits are obtained correctly in the present theory because the weak polar-cross flow approximation is applied only to the governing equation for U_m and not to the boundary conditions. The boundary conditions are satisfied exactly, within the framework of the small perturbation approximation. As a consequence, the solution achieves both the hypersonic ($K_\delta \to \infty$) and linear ($K_\delta \to 0$) limits correctly and, in general, gives a good approximation over the entire range of the similarity parameter K_δ.

A comparison is given in Figure (31) between the present result for G_1 and the initial ratio of shock to body curvature, ℓ, calculated numerically by Van Dyke (Reference 31) for an ogive body using the nonlinear hypersonic small disturbance theory. The quantity ℓ is defined such that the body and shock are given by

$$R_b = \beta(bz + \frac{1}{2} cz^2)$$

$$R_s = \beta(z + \frac{1}{2} c\ell z^2)$$

105
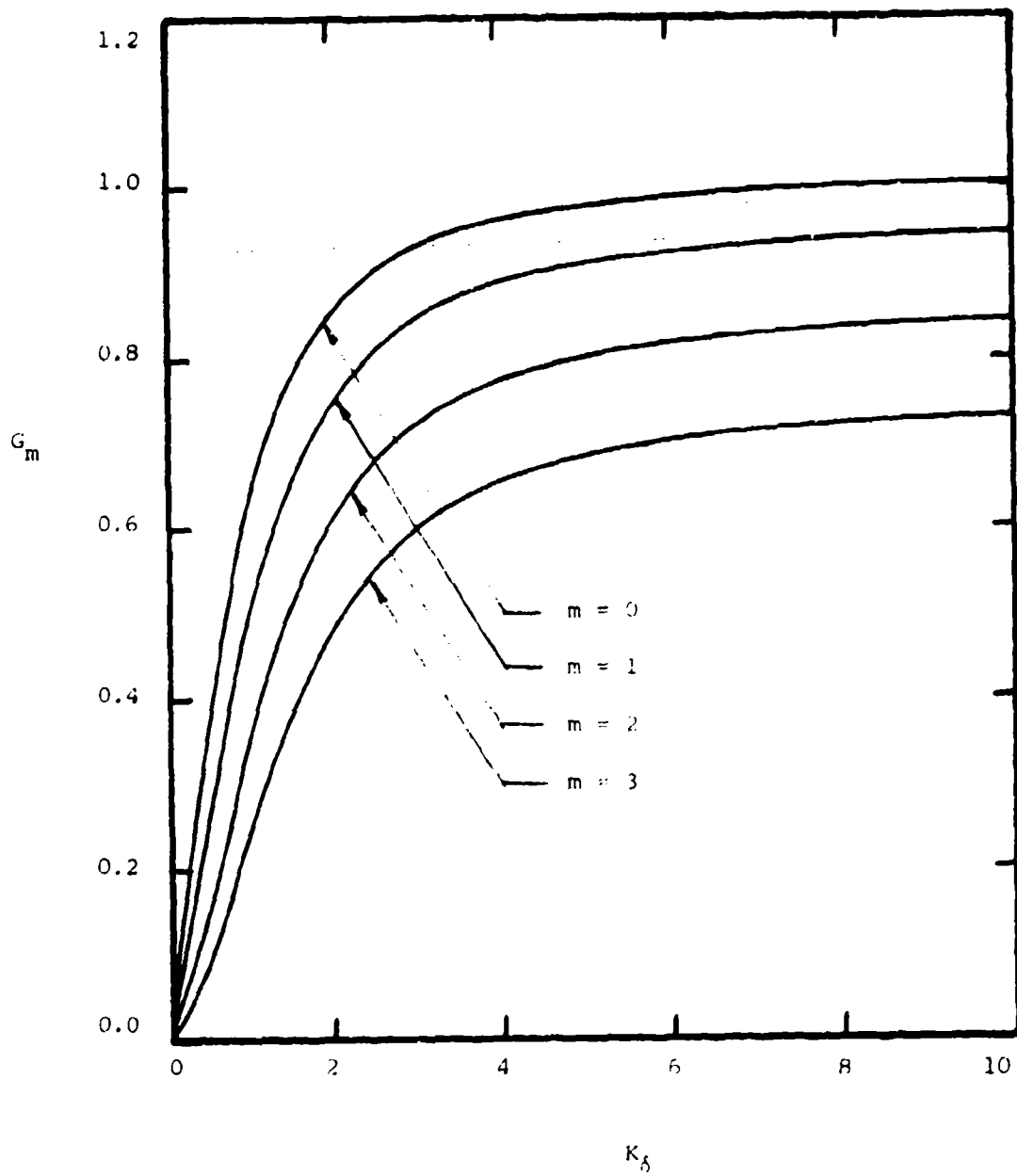
Figure 29. Ratio Between Shock and Body Perturbation, G_m, as a Function of K_δ for Various m ($\gamma = 1.4$)

Figure 30. Ratio between Shock and Body Perturbation, G_m, as a Function of K for Various m ($\gamma = 1.0$)
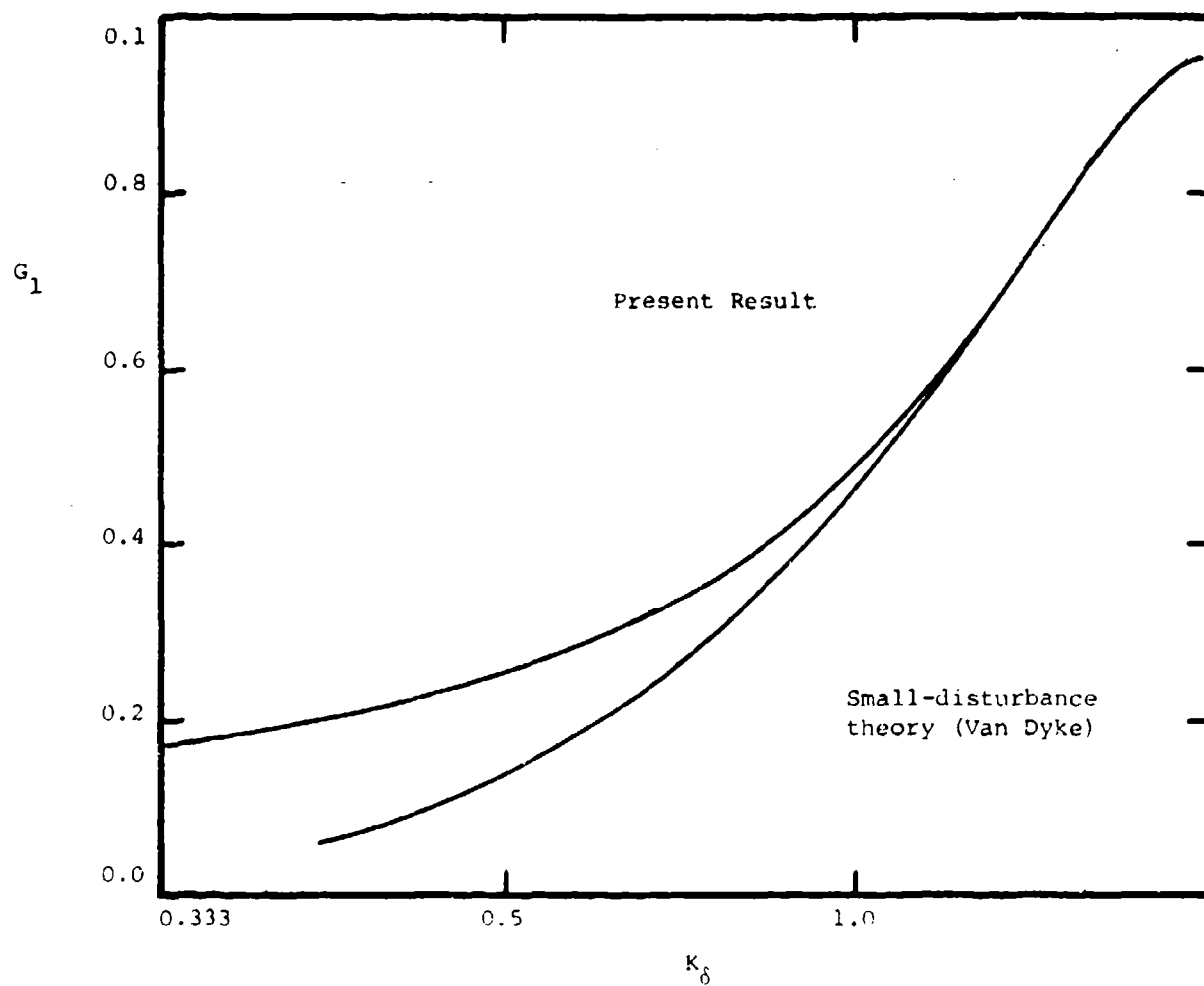
Figure 31. Comparison Between Present Result for G_1 and Numerical
Result from Hypersonic Small Disturbance Theory Due to
Van Dyke ($\gamma = 1.405$)

It can be shown that ℓ is identical to c_1 of the present theory by using (302) and (303). Figure (31) shows that the comparison between the present results and those of Van Dyke is very good, especially when K_δ is greater than unity.

The pressure and density can now be determined by using

$$P_m(\theta) = L_m(\theta) - \rho_0 V_\infty U_m(\theta) + \rho_0 V_\infty \, \theta \left(1 - \frac{\delta^2}{\theta^2}\right) V_m(\theta)$$

$$R_m(\theta) = (\gamma-1) L_m(\theta) + P_m(\theta)$$

which follow from the definition of $L_m(\theta)$ and the energy equation. $U_m(\theta)$ and $V_m(\theta)$ are given by (313) ands (316). The flow variables U_m, V_m, P_m and R_m are shown as function of $\theta' = (\theta-\delta)/(\beta-\delta)$ for various values of m and K_δ in Figure (32) through (35) for $\gamma = 1.4$.

d. Surface Perturbation Pressure Coefficient

The pressure on the surface of the cone is given by

$$p(r,\theta_b) = p_0(\theta_b) + \Sigma \, \epsilon_m r^m P_m(\theta) + O(\epsilon^2) \tag{318}$$

where

$$\theta_b = \delta - \Sigma \, \epsilon_m r^m$$

Transferring the expression (318) to the basic cone gives

$$p(r,\theta_b) = p_0(\delta) + \Sigma \, \epsilon_m r^m P_m(\delta) - \left(\frac{dp_0}{d\theta}\right)_\delta + O(\epsilon^2) \tag{319}$$

Since v_0 vanishes at the cone surface, the gradient of the zeroth-order pressure $(dp_0/d\theta)$ vanishes there also; that is,

$$\left(\frac{dp_0}{d\theta}\right)_\delta = -\rho_0(\delta)v_0(\delta)\left(u_0 + \frac{dv_0}{d\theta}\right)_\delta = 0 \tag{320}$$

Hence

$$p(r,\theta_b) = p_0(\delta) + \Sigma \, \epsilon_m r^m P_m(\delta) + O(\epsilon^2) \tag{321}$$

The pressure coefficient C_p is defined by

$$C_p = \frac{\dfrac{p}{p_\infty} - 1}{\dfrac{\gamma}{2} M_\infty^2}$$

109
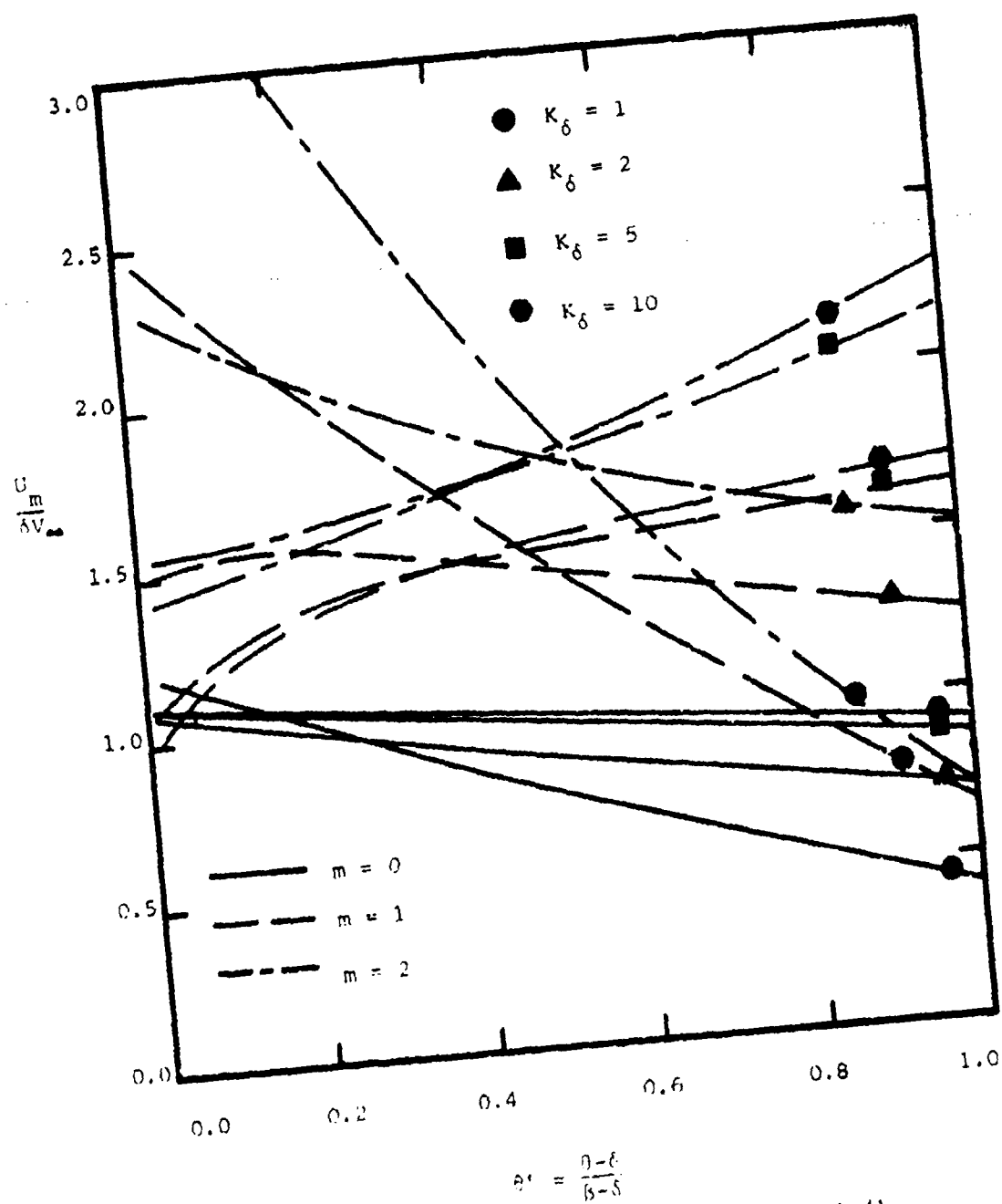
Figure 32. Radial Velocity Function, U_m ($\gamma = 1.4$)

The plot legend shows:
- $K_\delta = 1$
- $K_\delta = 2$
- $K_\delta = 5$
- $K_\delta = 10$

- $m = 0$
- $m = 1$
- $m = 2$

Vertical axis: $\dfrac{U_m}{\delta V_\infty}$

Horizontal axis: $\theta' = \dfrac{\theta - \delta}{\beta - \delta}$

113
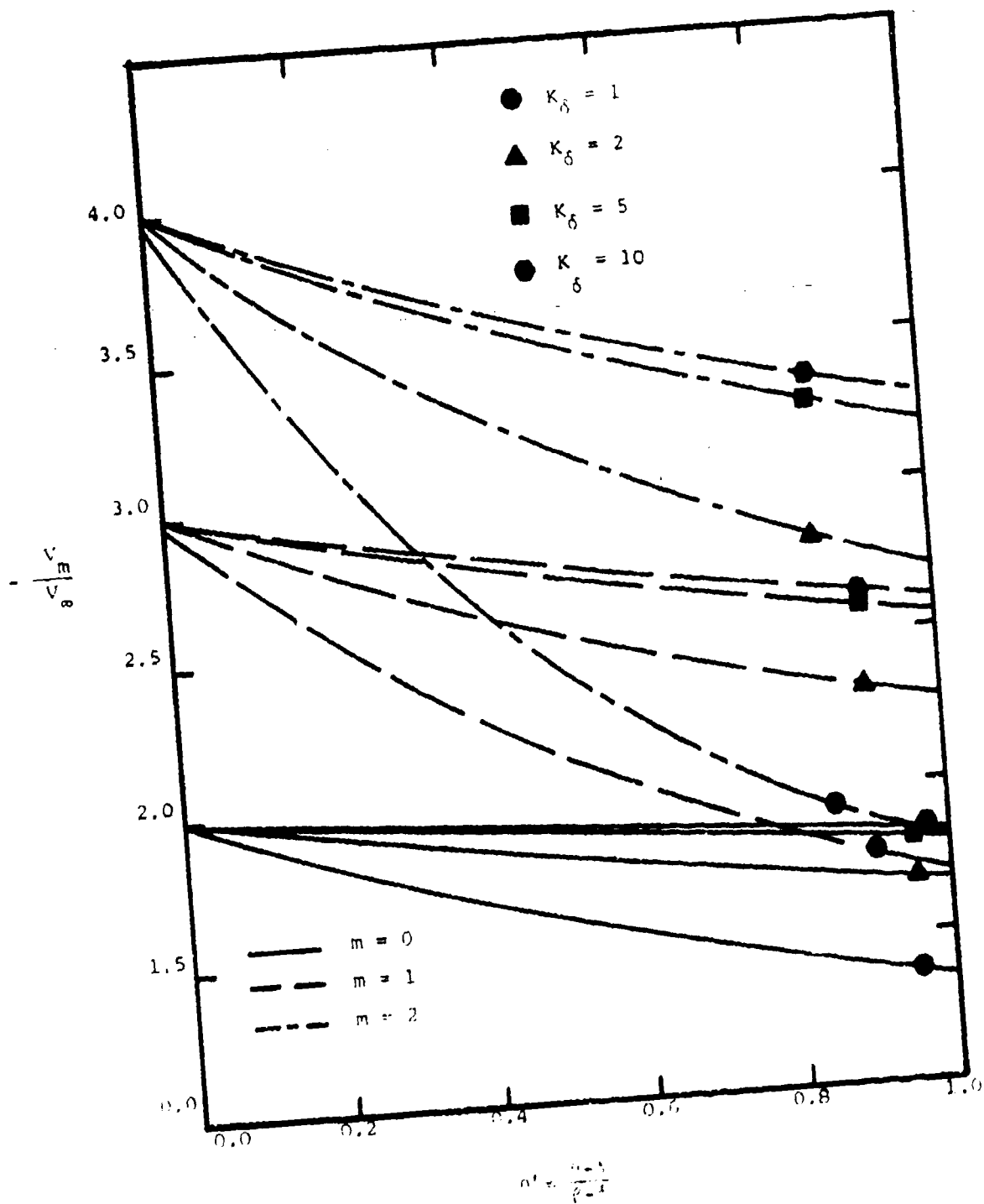
Figure 33.   Polar Velocity Function, V_m ($\gamma = 1.4$)

$$\frac{2P_m}{P_\infty V_\infty \delta}$$

Legend:
- ● $K_\delta = 1$
- ▲ $K_\delta = 2$
- ■ $K_\delta = 5$
- ⬡ $K_\delta = 10$
- —— $m = 0$
- — — $m = 1$
- -- -- $m = 2$

$$\theta' = \frac{\theta - \delta}{\kappa - \delta}$$
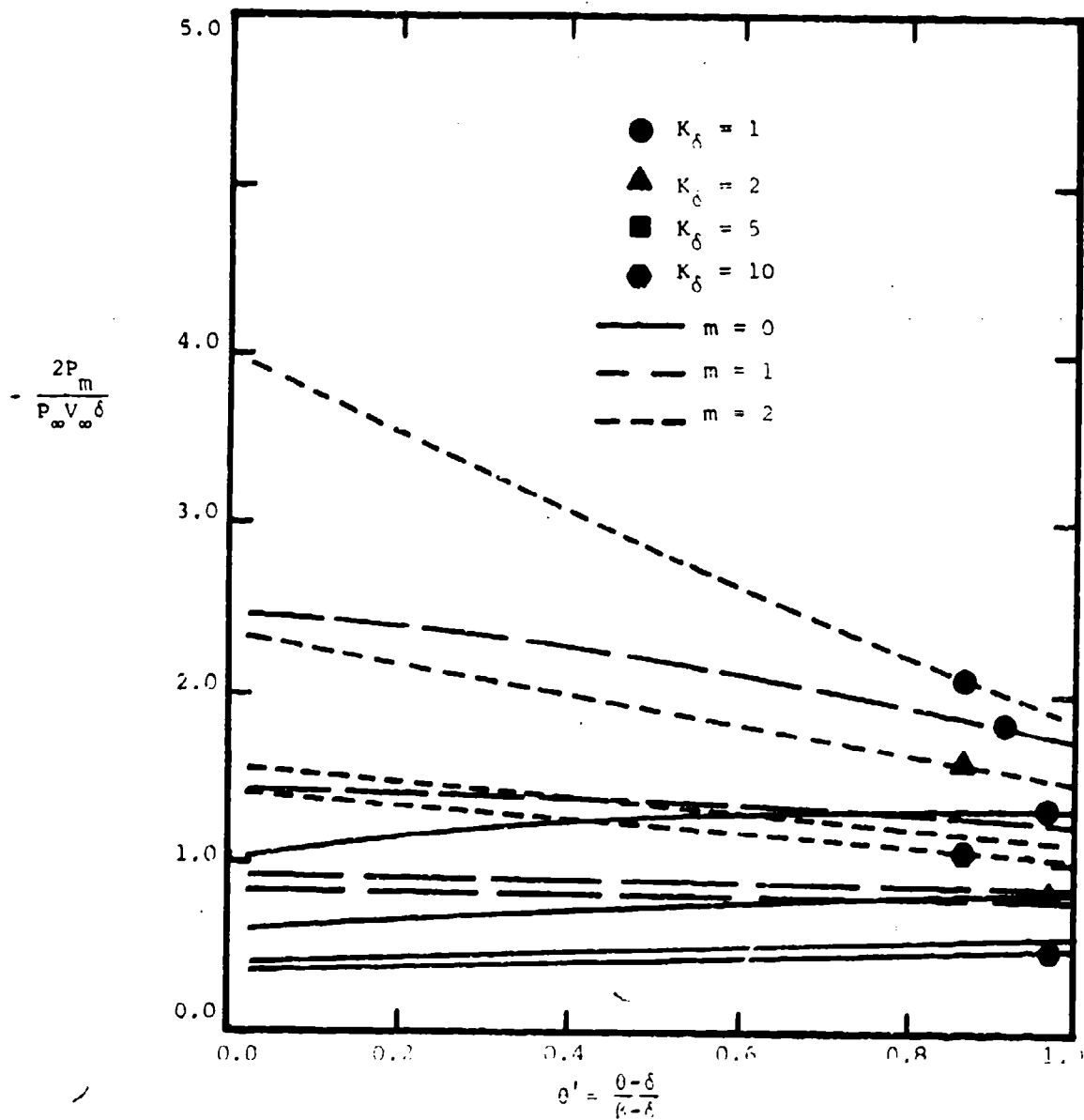
Figure 34. Pressure Function, P_m ($\gamma = 1.4$)
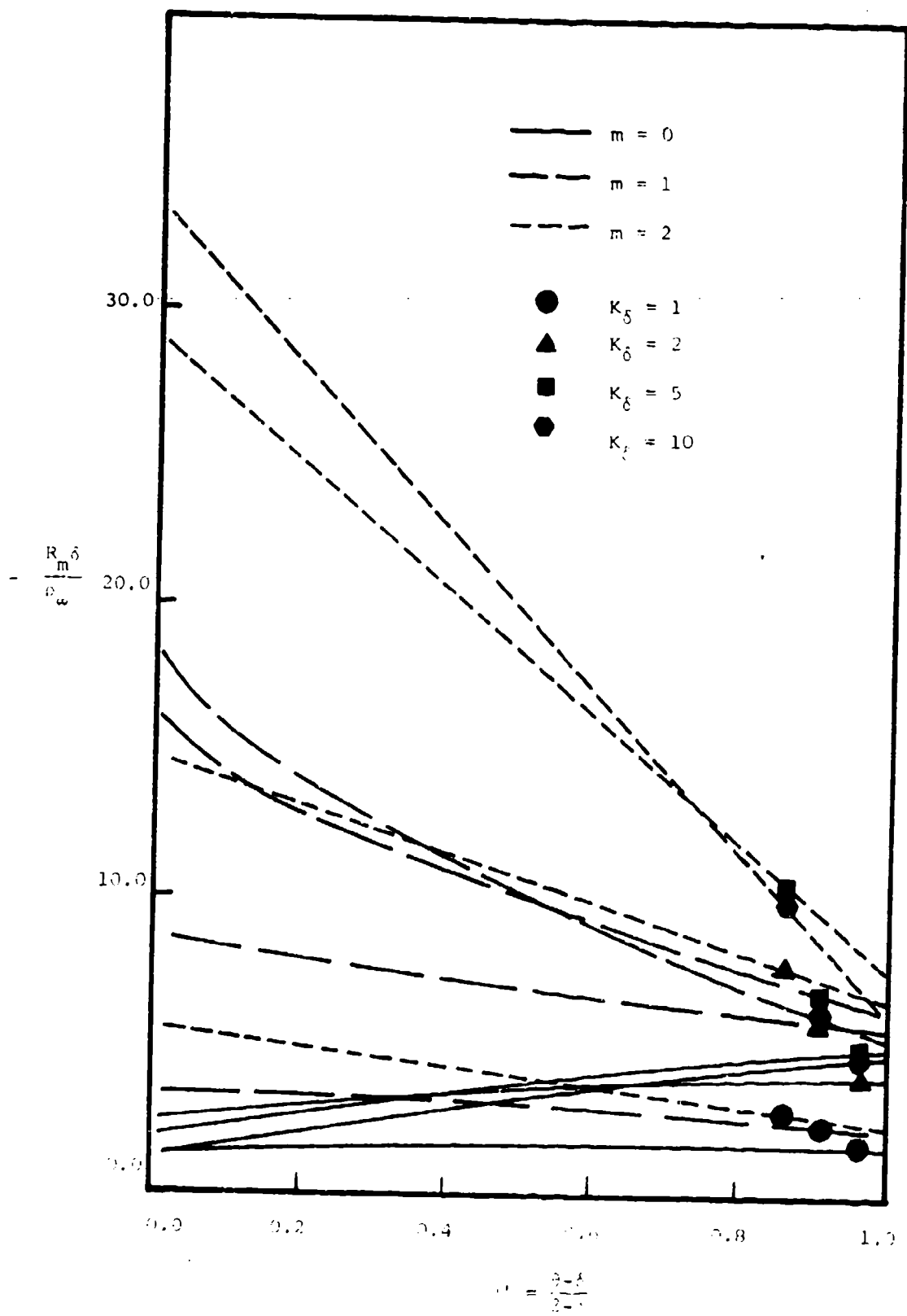
Figure 35. Density function, R_m ($\gamma = 1.4$)

115

Thus the surface pressure coefficient, C_{pc}, can be written as

$$C_{pc} = c_{p0}(\delta) + \Sigma \; \varepsilon_m r_m \; C_{pm}(\delta) + 0(\varepsilon^2) \tag{322}$$

where

$$C_{p0}(\delta) = (\underline{p_0(\delta)} - 1)/(\underline{\gamma} \; M_\infty^2)$$
$$\phantom{C_{p0}(\delta) = } p_\infty \qquad 2$$

$$C_{pm}(\delta) = P_m(\delta)/\underline{\gamma} \; M_\infty^2$$
$$\phantom{C_{pm}(\delta) = P_m(\delta)/} 2$$

$$= -\rho_0 V_\infty U_m(\delta)/(\underline{\gamma} \; M_\infty^2)$$
$$ 2$$

The velocity perturbation $U_m(\delta)$ can be calculated from (313), and $p_0(\delta)$ is known from the unperturbed flow results. Using the relation

$$M_\infty^2 = \underline{V_\infty^2} = V_\infty^2 \rho_\infty / \gamma p_\infty$$
$$ a_\infty^2$$

the expression for the perturbation pressure coefficient C_{pm} as can be written as

$$m = 0; \quad C_{pm} = [\underline{4 \; \ell n(\delta/\beta)} - 2 \; \underline{\delta} \; G_0]\delta$$
$$\phantom{m = 0; \quad C_{pm} = [} (1 - \underline{\xi^2}) \qquad \beta$$
$$\phantom{m = 0; \quad C_{pm} = [4 \; \ell n(\delta/\beta)} \beta^2$$

$$m \neq 0; \quad C_{pm} = - \; \underline{2\delta} \quad [(m+1)(m+2) \; \underline{1} \; \underline{0\beta0\delta M}$$
$$\phantom{m \neq 0; \quad C_{pm} = - } (1 - \underline{\delta^2}) \qquad\qquad C_m\delta \; 0\beta1\delta P$$
$$\phantom{m \neq 0; \quad C_{pm} = - 2\delta} \beta^2$$

$$+ \; \underline{\delta} \; G_m(m+1) \; \{\underline{0\delta1\delta P} + C_m\beta \; \underline{\delta^2} \; (1\beta1\delta M \; 0\beta0\delta M - 0\delta1\beta P)\}]$$
$$ \beta \qquad\qquad 0\beta1\delta P \qquad\quad \beta^2 \; 0\beta1\delta P$$

These results can be shown to agree exactly with linearized theory in the limit $K_\delta \to 0$ and with the modified Newtonian theory (e.g. Newtonian plus Bussmann correction) in the double limit $K_\delta \to \infty$, $\gamma \to 1$. Figure 36 shows a comparison of the results of the present theory with those of other methods for the initial pressure gradient on the ogive body represented by

$$R_c = R_0'z + \underline{1} \; R_0'' \; z^2 + \underline{1} \; R_0''' \; z^3 + \ldots$$
$$ 2 \qquad\qquad 6$$

The value of $-C_{p1}/2\delta$, which gives the initial pressure gradient at the tip of the ogive, is plotted versus to K for $\gamma = 1.405$. The present results agree

114
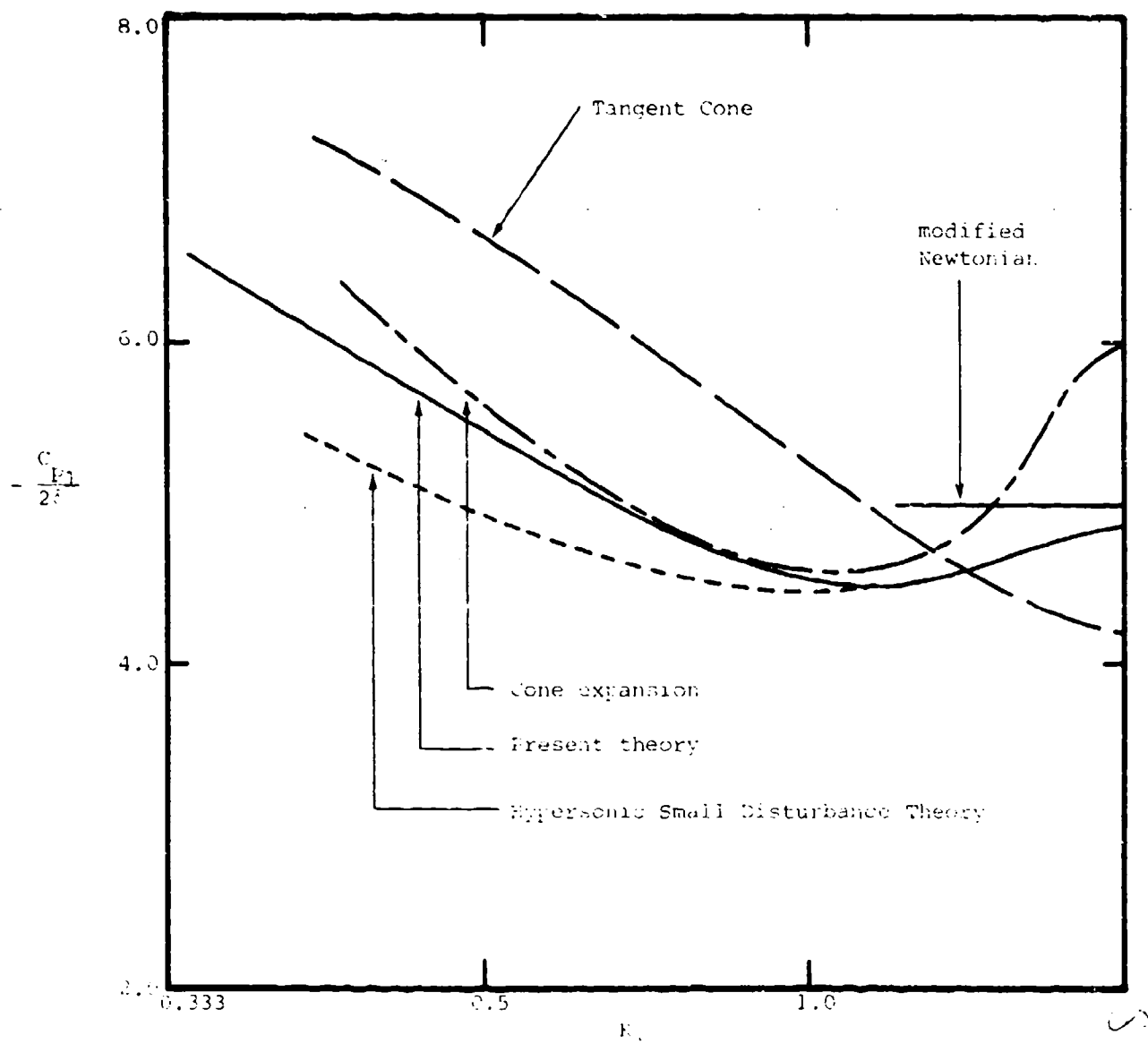
Figure 36.   Initial Pressure Gradient on Ogive Body (γ = 1.405)

well with the numerical calculation of Van Dyke (Reference 31) based on the nonlinear hypersonic small disturbance theory when $K_\delta > 1$. Also, the results in Figure 37 show that the present theory goes to the limit of modified Newtonian theory when $K_\delta \rightarrow \infty$ and $\gamma \rightarrow 1$.

Figure 38 shows a comparison of the surface pressure coefficient calculated by means of the present theory with experimental data (Reference 32) for an ogival shape given by

$$\frac{dR}{dx} = \delta(1-z)$$

This expression can be used along with (302) to obtain

$$\theta_c = \delta(1 - \frac{r}{2})$$

Figure 38 shows that the present theory works well provided the correction (here $\delta r/2$) is small compared to basic cone angle (here δ); that is, if $r/2 \ll 1$. The results show that this condition is satisfied if $r < 0.2$.

An improved comparison of theory and experiment can be obtained using an empirical "secant cone" method. This result is obtained by taking the perturbation solution

$$c_{pc} = \delta^2 c_{p0}(K_\delta, \gamma) + \delta \frac{r}{2} c_{p1}(K_\delta, \gamma)$$

and replacing δ with the local secant angle given by,

$$\bar{\theta} = \delta(1 - \frac{r}{2})$$

at every station x along the axis of the ogive.

The comparison between theory and experiment is shown in Figure 39 and is now remarkably good. The well known tangent-cone result is also included in Figure 39 for comparison. In the empirical tangent cone method, the pressure coefficient is assumed to be given by

116
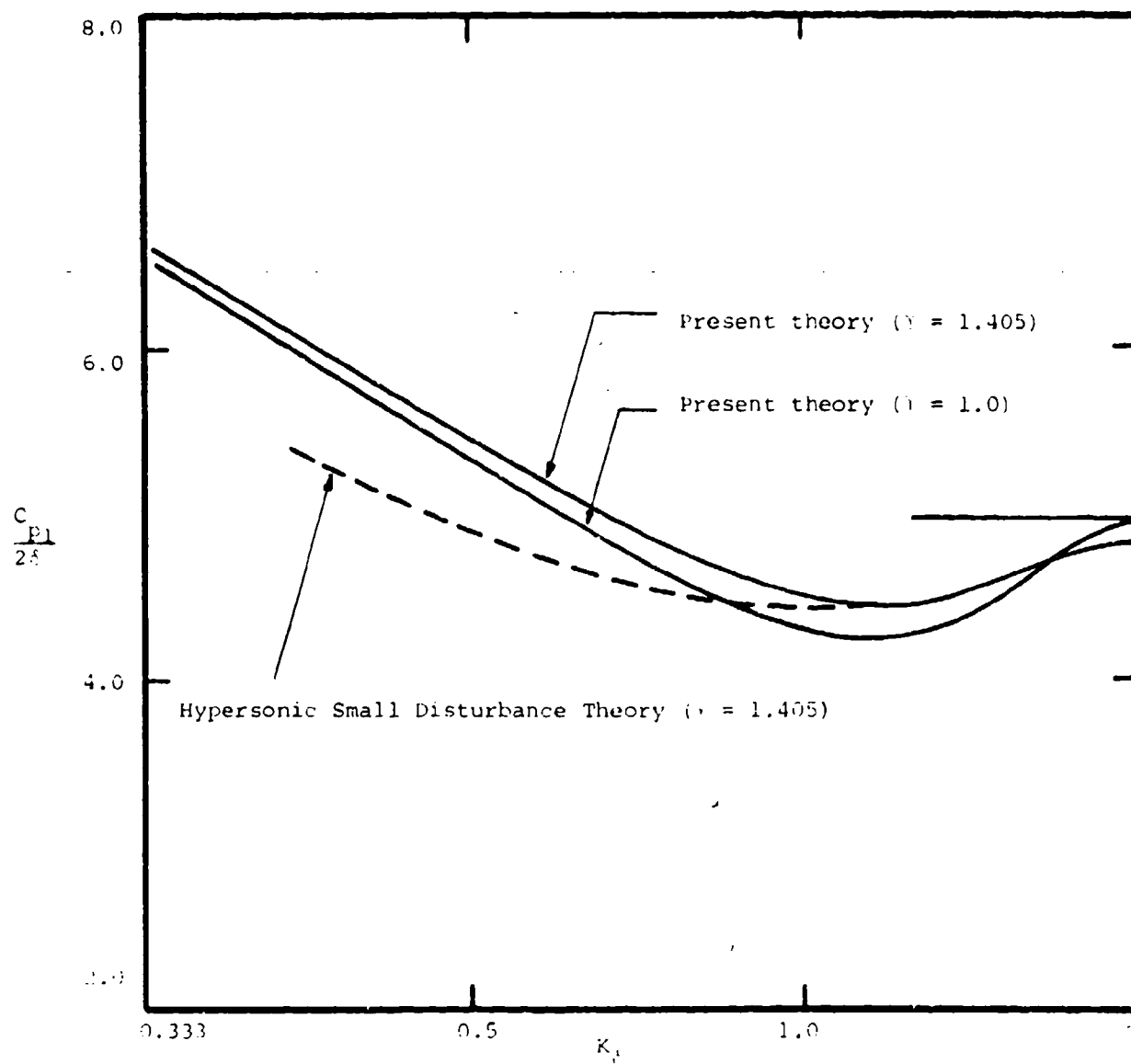
Figure 3?. Initial Pressure Gradient on Ogive Body (= 1.0,) = 1.405)
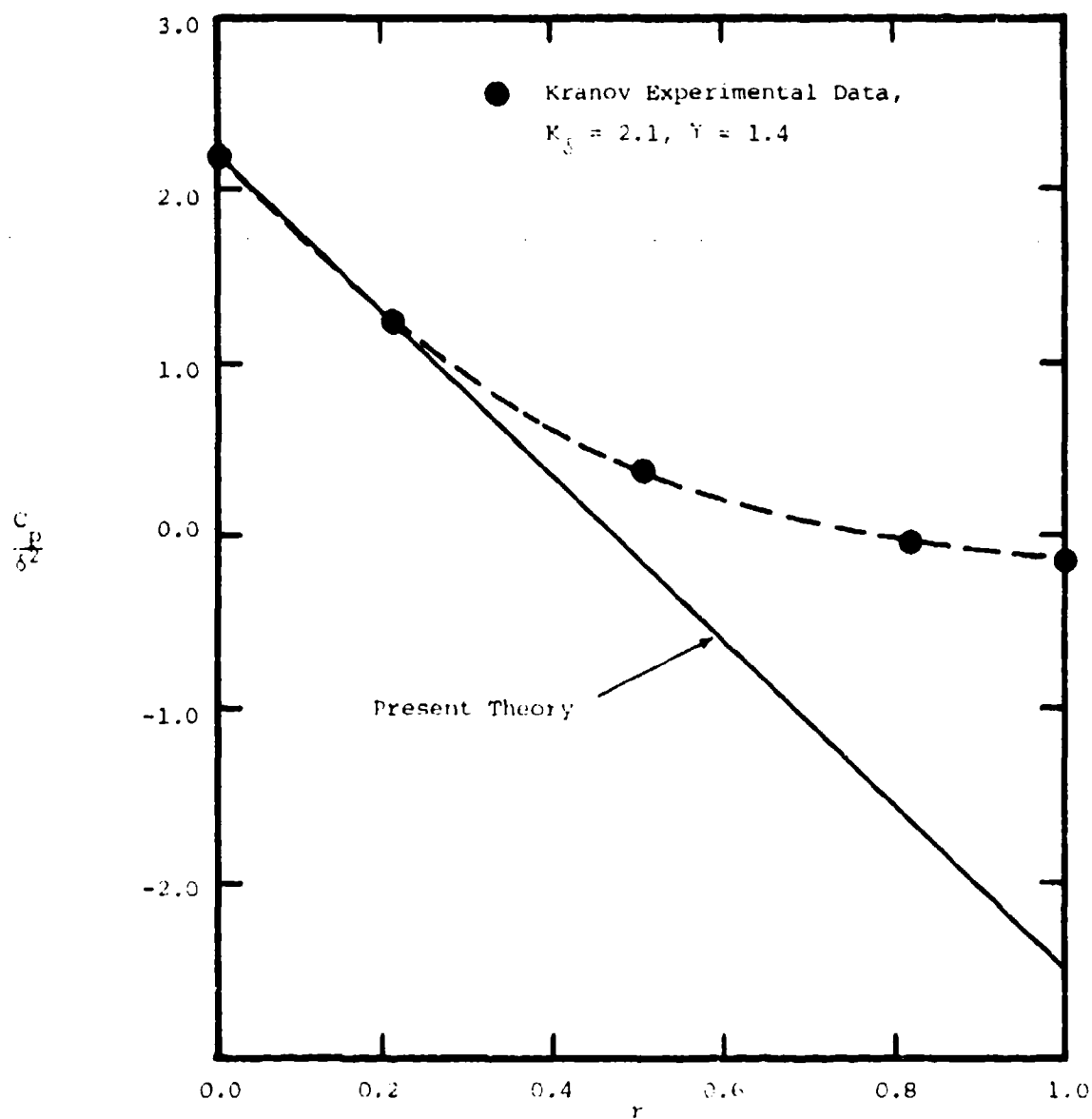
Figure 38. Surface Pressure Coefficient on the Ogive $P_c = \delta(1 - r/2)$
Comparison of Theory and Experiment.
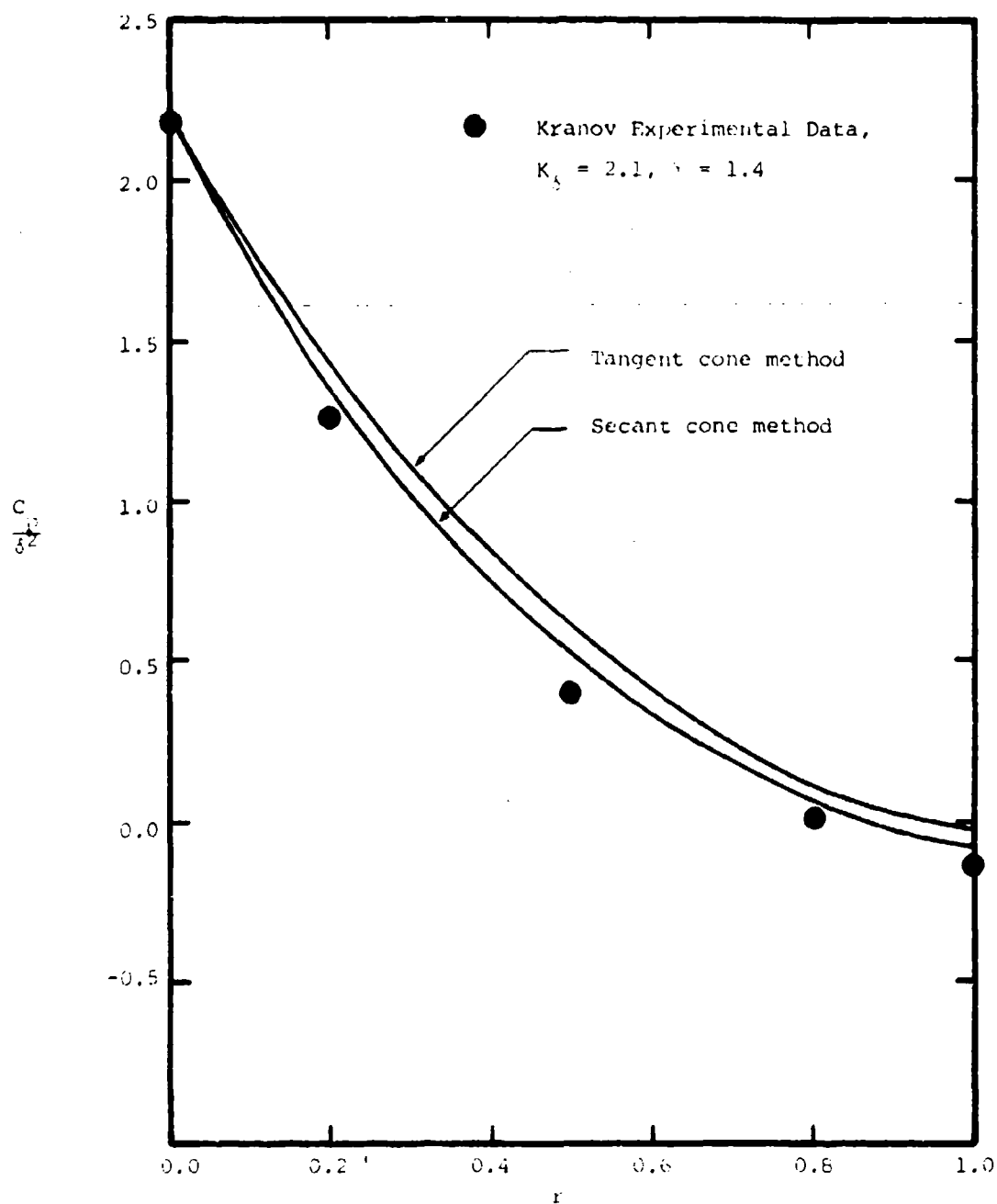
Figure 39.   Surface Pressure Coefficient on the Ogive $r_c = A(1-r^2)$
Comparison of the Secant Cone Method and Experiment

$$c_{pc} = \theta^2 \, c_{p0}(K_\theta, \gamma)$$

where the local inclination θ is given by

$$\theta \approx \delta(1-r)$$

While the comparison between theory and experiment is better than that for the regular perturbation scheme, it is not as good as that for the secant cone method.

e. Concluding Remarks

Approximate flowfield results for the supersonic flow past an axisymmetric body which has slightly longitudinal curvature have been obtained explicitly in closed form. The results appear to be accurate when the perturbation of the body angle is less than ten percent of the body angle of the basic right circular cone. The range of accuracy for the pressure coefficient can be enlarged by using the empirical secant cone method. The present results are useful over the entire range of K_δ from the linearized theory limit ($K_\delta \to 0$) to the hypersonic limit ($K_\delta \to \infty$). The results are especially accurate for $K_\delta > 1$. Further comparisons of the results of the present theory with experimental data would be desirable as the basis for more carefully delineating the accuracy of the present calculations.

4. UNSTEADY MOTIONS

In the design and analysis of missiles and aircraft undergoing dynamical motions in supersonic and hypersonic flight, the time-varying behavior of the flowfield, shock-wave shape, and forces and moments are of paramount interest. The methods for dealing with these factors on an approximate and relatively simple, but accurate, basis, however, seem to be in a primitive state. It is safe to say 'hat approximate methods of analysis for unsteady supersonic flows are now   ir as broad or as useful as the myriad of

12)

analytical methods available for related steady flows. The general usage of digital computers has obviated this need somewhat, but the insight and practical utility of approximate analytical results are still needed.

For hypersonic flow the simplest method for calculating the forces and moments on a body is that of Newtonian theory. Stability derivatives for combinations of cones, cone frustums, and hemispheres are given by Fisher (Reference 33). Newtonian theory, however, is valid strictly when streamline curvature is negligible and in the double limit $M_\infty \to \infty$ and $\gamma \to 1$. Because of these shortcomings, various modifications, such as that of Ericsson (Reference 34), have been devised. Such methods, by their nature, are subject to significant error, as pointed out by Mahoud and Hui (Reference 35). Other methods have also been devised, such as those of Khalid and East (References 36,37) which make use of shock-expansion concepts to generate closed-form formulas for stability derivatives for certain missile shapes. These results, however, are not valid in the limit $M_\infty \to \infty$. The aforementioned methods calculate results for body forces and moments and are not useful for predicting flowfields and shock shapes. They are used because they are simple and because there is a lack of anything better that does not involve lengthy computer calculations. Thus there appears to be a need for rational approximate analyses, even for simple shapes, that consider the entire flowfield in addition to the forces and moments.

Unsteady supersonic two-dimensional flows appear to be more amenable to analysis than flows past axisymmetric bodies. For oscillating wedges and airfoils, the works of McIntosh (Reference 38), Barron (Reference 39), Barron and Mandl (Reference 40), and Fleeter and Riffel (Reference 41), as well as others, are noteworthy. On the other hand, the analogous unsteady-flow problem for oscillating cones seems to be much more difficult. The use of

121

potential theory by Tobak and Wehrend (Reference 42) and such methods as piston theory by Zartarian, Hsu, and Ashlev (Reference 43) have not led to accurate results when the Mach number is high enough that nonlinear effects are important, which is generally the case. As mentioned previously, the shock-expansion results of Khalid and Fas (Reference 37) for dynamic stability derivatives of sharp cones are invalid when $M_\infty \to \infty$. Likewise, pure numerical methods, such as the method of characteristics by Kawamura and Tsien (Reference 44) are cumbersome and are not useful for parametric studies.

Another method of attack for the problem of an oscillating cone has been by means of perturbation of the steady axisymmetric flow past a circular cone. By such means Brong (Reference 45,46) and Hsu (Reference 47) dealt with the full perturbation problem, and McIntosh (Reference 48) utilized the methods of hypersonic small-disturbance theory. Although these methods lead to sets of ordinary differential equations to solve, their solutions were obtained by numerical methods on digital computers. As a result, a good deal of useful information was obtained, and yet the cohesiveness and utility of analytic representations were still missing. In part, Orlik-Ruckemann (Reference 49) overcame some of these deficiencies by devising empirical formulas to represent the results of McIntosh. The results were then more readily applicable to other problems, such as in the analysis by Orlik-Ruckemann (Reference 50) of an oscillating cone in viscous hypersonic flow.

The motivation for the present work is to obtain approximate analytic results, on some sort of rational basis, that describe the shock shape, flowfield structure, and forces and moments on a harmonically pitching and plunging cone. Such results are thus more useful for various purposes, such as parametric studies and possibly also for investigations of unsteady motions

of other bodies, for instance cone-derived waveriders (Reference 51). It has
been found that steady flows past conical bodies generated by perturbation of
the basic axisymmetric flow past a circular cone can be handled accurately by
approximate analytic methods when the basic cone flow is described by the
approximate formulas of Rasmussen (Reference 21). In this way accurate
approximate analytic results were obtained for steady flows past inclined
cones (Reference 23), elliptic cones (Reference 52), and arbitrary cones
(Reference 53). In this study, it is planned to apply this method of analysis
to obtain approximate analytic results for the harmonically pitching and
plunging cone.

a. Coordinate Systems

To describe the unsteady motion of a body, two coordinate systems, a
body-fixed coordinate system (x,y,z) and an inertial coordinate system (X,Y,Z)
are utilized. The unsteady motion is regarded as a small perturbation about a
basic steady motion in which the body (a circular cone) is aligned with a
uniform free stream flowing past it. The basic freestream velocity V_∞ is
aligned with the Z axis of the inertial coordinate system, that is,

$$\vec{V}_\infty = V_\infty \hat{e}_Z .$$

In the steady, basic, unperturbed motion, the body-fixed coordinate system is
coincident with the inertial coordinate system. Now the body is allowed to
undergo a small unsteady motion such that the unsteady disturbances in the
flow produced by this motion are regarded as small. The unsteady motion of
the body is comprised of two parts: a rotational motion about a point z_0 on
the z axis of the body in the X-Z plane of the inertial system, represented by
the angle $\psi(t)$ which is regarded as small, and a rectilinear motion of the
body-fixed point z_0 in the X direction of X-Z inertial plane, represented by
the displacement

$$\vec{h} = h(t)\hat{e}_X$$

which is also regarded as appropriately small. The configuration of the body and the coordinate systems are shown in Figure 40. Spherical coordinates are shown in Figure 41. The rotational motion is referred to as a pitching motion and the rectilinear motion is referred to as a plunging motion. The motions are indicated in Figures 42 and 43.

The angle $\psi(t)$ is the angle measured from the inertial Z-axis to the body-fixed z axis. The angular velocity vector for the rotational rate is thus

$$\vec{\omega} = -\dot{\psi}(t)\ \hat{e}_Y\ ,\tag{325}$$

and the angular velocity about the inertial Y-axis is

$$q = \dot{\psi}(t)\ .$$

The relative wind seen by an observer fixed at z_0 on the body is

$$\vec{V}_r = V_\infty\hat{e}_Z - \dot{h}(t)\ \hat{e}_X.\tag{326}$$

Thus the angle of attack measured from the relative wind to the body z axis is

$$\alpha(t) = \psi(t) - \frac{\dot{h}(t)}{V_\infty}\ ,\tag{327}$$

where $\dot{h}/V_\infty$ is assumed small. It thus follows that

$$\frac{\ddot{h}}{V_\infty} = \dot{\psi}(t) - \dot{\alpha}(t)\ ,$$

$$= -(q + \dot{\alpha})\ .\tag{328}$$

The relation between the position vector r measured from the origin of the inertial system to a field point and the position vector r_h measured from the origin of the body-fixed system to the same field point is

$$\vec{r} = z_0\ \hat{e}_Z + h\ \hat{e}_X = z_0\ \hat{e}_Z + \vec{r}_h\ .\tag{329}$$

124

$$\gamma = \tan^{-1}\left(\frac{\dot{h}}{V_\infty}\right) \simeq \frac{\dot{h}}{V_\infty}$$
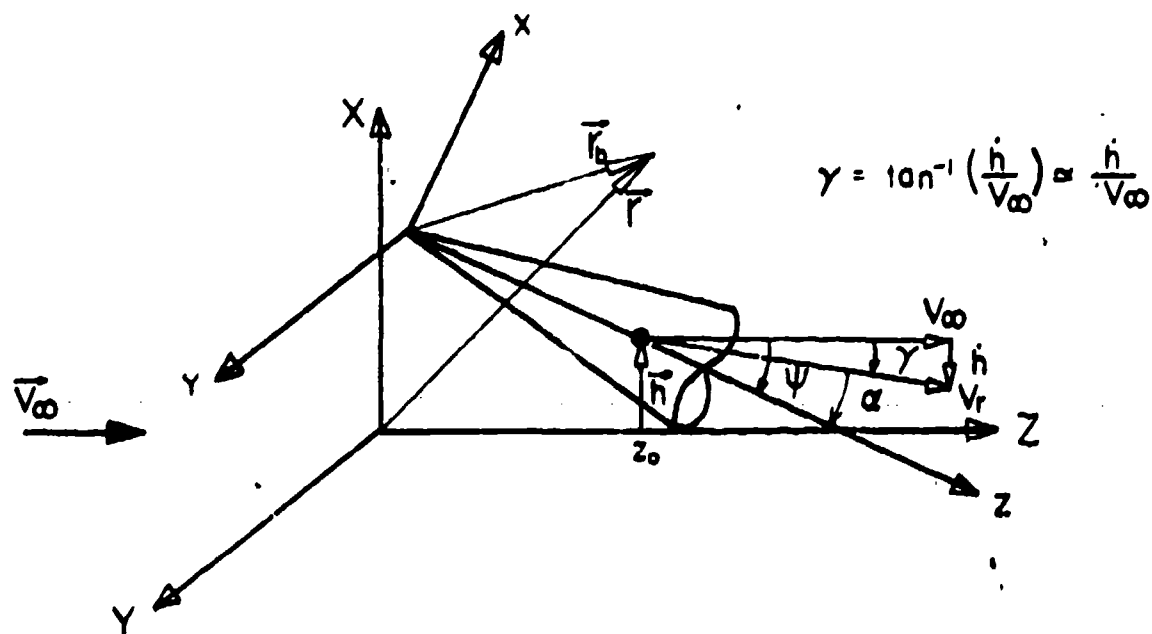
Figure 40. Geometrical Configuration and Coordinate Systems
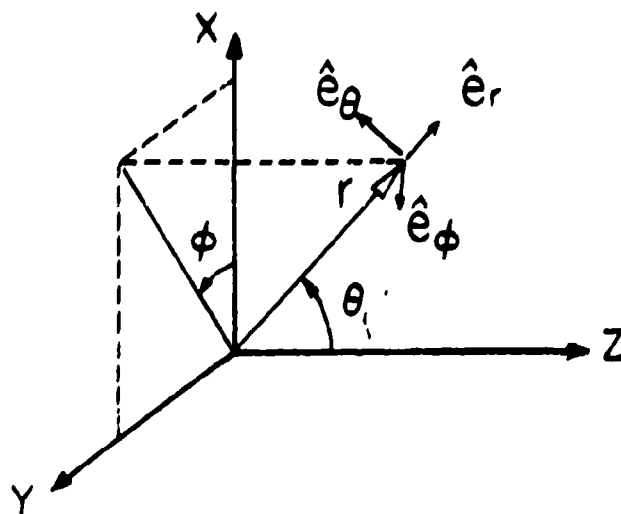
Figure 41. Spherical Coordinates
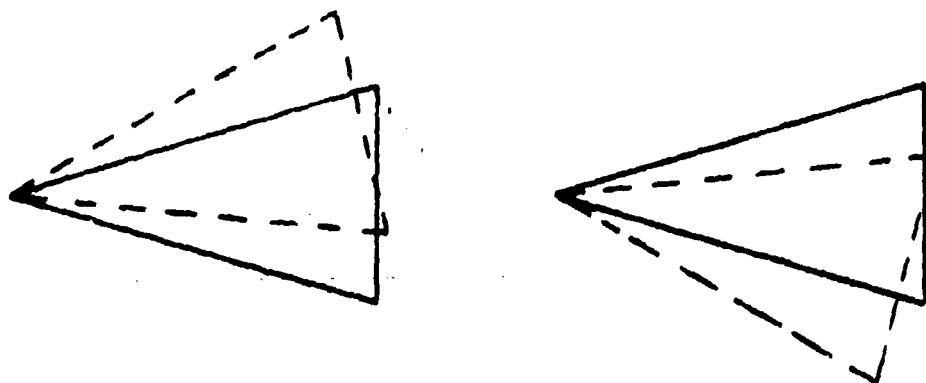
Figure 42.   Oscillation of a Cone about its Vertex
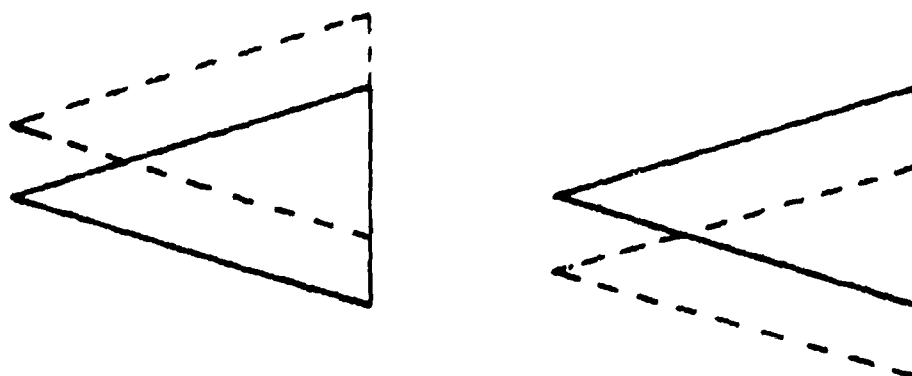
Figure 43.   Pure Oscillatory Plunging Motion of a Cone

From geometrical considerations, it is easily seen that the orthonormal Cartesian basis vectors in the body-fixed system are related to their counterparts in the inertial coordinate system by

$$\hat{e}_x = \cos\psi\,\hat{e}_X + \sin\psi\,\hat{e}_Z \quad ,$$

$$\hat{e}_y = \hat{e}_Y \quad , \qquad\qquad (330)$$

$$\hat{e}_z = -\sin\psi\,\hat{e}_X + \cos\psi\,\hat{e}_Z \quad .$$

Equations (330) together with Equation (329) are enough to establish relations between the pairs of Cartesian coordinates (x,y,z) and (X,Y,Z). It is more useful, however, to develop relations between spherical coordinates in the two systems. Towards this end, therefore, write

$$X = r\sin\theta\cos\phi \quad , \qquad x = r_b\sin\theta_b\cos\phi_b \quad ,$$

$$Y = r\sin\theta\sin\phi \quad , \qquad y = r_b\sin\theta_b\sin\phi_b \quad , \qquad (331)$$

$$Z = r\cos\theta \qquad\qquad , \qquad z = r_b\cos\theta_b \qquad .$$

The spherical coordinates (r,θ,ϕ) thus describe a field point in the inertial coordinate system, and the spherical coordinates (r_b,θ_b,ϕ_b) describe the same field point as reckoned in the body-fixed system. The geometrical description of the spherical coordinates is shown in Figure 41. When θ, ψ, and h are all regarded as small, the following relations can be obtained between the two systems of coordinates to lowest order:

$$r_b = r[1 - \frac{\psi z_0 + h}{r}\,\theta\cos\phi] \quad , \qquad (332a)$$

$$\theta_b = \theta + [\psi - \frac{\psi z_0 + h}{r}]\cos\phi \quad , \qquad (332b)$$

$$\phi_b = \phi - [\psi - \frac{\psi z_0 + h}{r}]\,\frac{\sin\phi}{\theta} \quad . \qquad (332c)$$

The perturbation terms in Equation (332a) for r_b are actually negligible since they involve products of ψ, h, and θ. When z_0 and h are nonzero, these

relations are singular at the origins $r = 0$ and $r_b = 0$.

It is also useful to have relations for the velocity components between the two coordinate systems. Let (u,v,w) denote the spherical velocity components in the inertial (r,θ,ϕ) directions, and let (u_b,v_b,w_b) denote the body-fixed components in the (r_b,θ_b,ϕ_b) directions. Then for small θ, ψ, and h, it can be established that, to lowest order,

$$u_b = u - \frac{\psi z_0 + h}{r}\, (v \cos\phi - w \sin\phi) \quad , \tag{333a}$$

$$v_b = v + \frac{\psi z_0 + h}{r}\, v \cos\phi - \left(\psi - \frac{\psi z_0 + h}{r}\right) \frac{w}{\theta} \sin\phi \quad , \tag{333b}$$

$$w_b = w - \frac{\psi z_0 + h}{r}\, u \sin\phi + \left(\psi - \frac{\psi z_0 + h}{r}\right) \frac{v}{\theta} \sin\phi \quad . \tag{333c}$$

Thus when the velocity components are known in the inertial system, they can be obtained immediately in the body-fixed system.

The problem as it has thus been formulated corresponds to the motion observed in a wind tunnel of a model immersed in a uniform stream undergoing combined pitching and plunging motions in a plane.

b.   Surface Boundary Conditions

A conical body is described in the body-fixed coordinates by an equation of the form

$$\theta_b = \theta_c(\phi) \quad . \tag{334}$$

Equation (332b) can be used to describe the same body in the inertial coordinate system:

$$\theta = \theta_c(\phi) - \left[\psi(t) - \frac{\psi(t)z_0 + h(t)}{r}\right] \cos\phi$$

or

$$F(r,\theta,\phi,t) \equiv \theta - \theta_c(\phi) + \left[\psi(t) - \frac{\psi(t)z_0 + h(t)}{r}\right] \cos\phi = 0 \quad . \tag{335}$$

For this problem, the body is simply a right circular cone of semivertex angle

129

δ. Thus $\theta_c = \delta$, and the surface function F is

$$F(r,\theta,\phi,t) \equiv \theta - \delta + \left[\psi(t) - \frac{\psi(t)z_0 + h(t)}{r}\right] \cos \phi = 0 . \tag{336}$$

The surface tangency condition for unsteady inviscid flow is

$$\frac{\partial F}{\partial t} + \vec{V} \cdot \nabla F = 0 \quad \text{on } F = 0 . \tag{337}$$

For the spherical velocity components (u,v,w), this surface boundary condition becomes

$$\left[\dot{\psi} - \frac{\dot{\psi}z_0 + \dot{h}}{r}\right] \cos \phi + u \frac{\psi z_0 + h}{r^2} \cos \phi + \frac{v}{r}$$

$$-w\left[\psi - \frac{\psi z_0 + h}{r}\right] \frac{\sin \phi}{r\theta} = 0 \quad \text{on } F = 0 . \tag{338}$$

When the small parameters ψ and h are set equal to zero, the basic flow is recovered, which is steady axisymmetric flow past the cone of semivertex angle δ. The basic axisymmetric flow is denoted by $u_0 = u_0(\theta)$, $v = v_0(\theta)$, and $w = w_0(\theta) = 0$. The perturbed velocity components are denoted by $u'(r,\theta,\phi,t)$, $v'(r,\theta,\phi,t)$, and $w'(r,\theta,\phi,t)$, which are of the order of smallness of ψ and h, that is,

$$u = u_0(\theta) + u'(r,\theta,\phi,t) ,$$

$$v = v_0(\theta) + v'(r,\theta,\phi,t) , \tag{339}$$

$$w = 0 + w'(r,\theta,\phi,t) .$$

It is further necessary in the perturbation process to transfer the boundary condition to the basic-cone surface by means of a Taylor series expansion:

$$v_0(\theta) = v_0(\delta) - \left(\frac{dv_0}{d\theta}\right)_\delta \left[\psi - \frac{\psi z_0 + h}{r}\right] \cos \phi$$

$$+ \text{higher-order terms, on } F = 0. \tag{340}$$

The surface boundary conditions for the basic cone and the first-order perturbation then become

$$v_0(\delta) = 0 \quad , \qquad \qquad (341a)$$

$$v'(r,\delta,\phi,t) = [-r\dot{\psi} + \psi(\frac{dv_0}{d\theta})_\delta] \cos\phi$$

$$+ [\dot{\psi}z_0 + \dot{h} - \frac{\psi z_0 + h}{r} \{u_0(\delta) + (\frac{dv_0}{d\theta})_\delta\}] \cos\phi \qquad (341b)$$

$$+ \text{higher-order terms.}$$

The surface boundary condition (341b) for the first-order θ-velocity

perturbation suggests the functional form for the dependency on r, θ, ϕ, and

t. It also suggests that the problem can be decomposed into two parts. The

terms in the first set of brackets on the right side of Equation (341b)

describe pure pitching motion about the vertex of the cone, that is, the

motion for $z_0 \equiv 0$ and $h \equiv 0$. The terms in the second set of brackets on the

right side of that equation occur in the combination of $\psi z_0 + h$. If ψ were

zero, this would describe pure plunging motion. When $z_0 \neq 0$, pitching about a

point along the z-axis thus leads to an additional pitching contribution that

has the same form as a pure plunging motion. There are thus two basic

problems to be solved: (1) a pure pitching motion about the vertex, and (2) a

pure plunging motion. If $\psi(t)$ has the same form as $h(t)$, then the pitching

contribution for $z_0 \neq 0$ can be obtained from the pure plunging motion.

c. Decomposition of the Problem

The boundary condition, Equation (341b), suggests not only that small

contributions of pitching and plunging can be separated, but also that the

independent variables can be partially separated. Assume that the pitching

occurs at a frequency ω and the plunging occurs at a frequency ω_1 such that

$$\psi(t) = \psi_0 e^{i\omega t} \quad ,$$

$$h(t) = h_0 e^{i\omega_1 t + i\Omega} \quad , \qquad (342)$$

where ψ_0 and h_0 are constants, the small perturbations of pitching and

plunging, and Ω is some constant phase angle. The complex notation in Equations (342) indicates that either the real or imaginary part is to be taken in obtaining the final results.

It is now enlightening to write the boundary condition in nondimensional form by introducing three nondimensional small parameters:

$$\epsilon_0 \equiv \psi_0 \quad ,$$

$$\epsilon_z \equiv \frac{i\omega\psi_0 z_0}{V_\infty} \quad , \tag{343}$$

$$\epsilon_p \equiv \frac{i\omega_1 h_0 e^{i\Omega}}{V_\infty} \quad .$$

The boundary condition (341b) can now be expressed in nondimensional form as

$$\frac{v'(r,\delta,\phi,t)}{V_\infty} = \epsilon_0 [-(\frac{i\omega r}{V_\infty}) + \frac{1}{V_\infty} (\frac{dv_0}{d\theta})_\delta] e^{i\omega t} \cos\phi$$

$$+ \epsilon_z [1 - (\frac{i\omega r}{V_\infty})^{-1} C] e^{i\omega t} \cos\phi$$

$$+ \epsilon_p [1 - (\frac{i\omega_1 r}{V_\infty})^{-1} C] e^{i\omega_1 t} \cos\phi \quad , \tag{344}$$

where

$$C \equiv \frac{1}{V_\infty} [u_0(\delta) + (\frac{dv_0}{d\theta})_\delta] \quad .$$

The three small parameters ϵ_0, ϵ_z, and ϵ_p are linearly independent with regard to ψ_0, z_0, and h_0. Thus any one of these contributions could be represented separately by the form

$$v'(r,\delta,\phi,t) = \epsilon f(r) e^{i\omega t} \cos\phi \quad , \tag{345}$$

where ϵ represents any one of ϵ_0, ϵ_z, or ϵ_p and $f(r)$ is the corresponding coefficient that depends on r only. Likewise the frequency, ω or ω_1, separates out along with the dependency on t and ϕ. It can also be pointed out that the plunging motion could be represented in a different plane from the pitching motion by replacing $\cos\phi$ by $\cos(\phi - \phi_0)$ in the coefficient of ϵ_p, where $\phi = \phi_0$ represents the plane of plunging motion.

As can be seen from Equation (344) the function $f(r)$ is the same for both ε_z and ε_p, that is, for the contribution of pitching about $z_0 \neq 0$ and for plunging. Thus there are only two independent problems to be solved: one for pure pitching about the vertex, $\varepsilon = \varepsilon_0$, and the other for pure plunging, $\varepsilon = \varepsilon_p$. When the pure plunging problem is solved, the pitching contribution about $z_0 \neq 0$, that is, for $\varepsilon = \varepsilon_z$, can then be obtained by a suitable change in notation. The general solution is a linear combination of the three solutions for the three reduced problems.

d. Shock Conditions

It is assumed that a shock wave is attached to the vertex of the oscillating cone. The shape of the cone surface, given by Equations (335) or (336), and the surface boundary condition (345) suggest that the shock-wave surface should have the form

$$\theta \equiv \theta_s = \beta - \varepsilon q(r) e^{i\omega t} \cos \phi \quad , \tag{346a}$$

or

$$G(r, \theta, \phi, t) \equiv \theta - \beta + \varepsilon q(r) e^{i\omega t} \cos \phi \equiv 0 \quad , \tag{346b}$$

for the first-order perturbation problem. Here β is the semivertex angle of the basic axisymmetric conical shock, and $\varepsilon \equiv \varepsilon_0$, ε_z, or ε_p for any of the reduced motions corresponding to the reduced boundary condition (345). The function $g(r)$ is to be determined as part of the analysis.

The unsteady shock jump conditions for mass, normal momentum, tangential momentum, and energy can be written in terms of the shock-shape function $G = 0$ as

$$\rho_\infty \left(\frac{DG}{Dt} \right)_\infty = \rho_s \left(\frac{DG}{Dt} \right)_s \quad , \tag{347a}$$

$$p_\infty (\nabla G)^2 + \rho_\infty \left(\frac{DG}{Dt} \right)_\infty^2 = p_s (\nabla G)^2 + \rho_s \left(\frac{DG}{Dt} \right)_s^2 \quad , \tag{347b}$$

$$\vec{V}_\infty \times \nabla G = \vec{V}_s \times \nabla G \quad , \tag{347c}$$

132

$$h_\infty(\nabla G)^2 + \frac{1}{2}\left(\frac{DG}{Dt}\right)^2_\infty = h_s(\nabla G)^2 + \frac{1}{2}\left(\frac{DG}{Dt}\right)^2_s \quad , \tag{347d}$$

where ρ, p, h, and $\vec{V}$ denote the density, pressure, specific enthalpy, and
velocity. The subscripts ∞ and s again denote the values on the two _ides of
the shock discontinuity surface. The material derivative is defined as $D/Dt \equiv$
$\partial/\partial t + v\cdot\nabla$. In addition it is assumed that the gas is thermally and
calorically perfect such that

$$\frac{p_s}{p_\infty} = \frac{\rho_s h_s}{\rho_\infty h_\infty} \tag{347e}$$

In spherical components the freestream velocity is given by

$$\vec{V}_\infty = V_\infty[\cos\theta\ \hat{e}_r - \sin\theta\ \hat{e}_\theta]. \tag{348}$$

Assume that downstream of the shock the spherical velocity components,
density, pressure, and specific enthalpy, have the following first-order
forms:

$$u(r,\theta,\phi,t) = u_0(\theta) + \varepsilon u_1(r,\theta)e^{i\omega t}\cos\phi \quad ,$$

$$v(r,\theta,\phi,t) = v_0(\theta) + \varepsilon v_1(r,\theta)e^{i\omega t}\cos\phi \quad ,$$

$$w(r,\theta,\phi,t) = \qquad \varepsilon w_1(r,\theta)e^{i\omega t}\sin\phi \quad ,$$

$$\rho(r,\theta,\phi,t) = \rho_0(\theta)[1 + \varepsilon\rho_1(r,\theta)e^{i\omega t}\cos\phi],$$

$$p(r,\theta,\phi,t) = p_0(\theta)[1 + \varepsilon p_1(r,\theta)e^{i\omega t}\cos\phi],$$

$$h(r,\theta,\phi,t) = h_0(\theta)[1 + \varepsilon h_1(r,\theta)e^{i\omega t}\cos\phi]. \tag{349}$$

Further, it is part of the perturbation process to transfer the shock
conditions to the basic conical shock. Thus for any variable $Q(\theta)$

$$Q(\theta) = Q(\beta) - \varepsilon\left(\frac{dQ}{d\theta}\right)_\beta g(r)e^{i\omega t}\cos\phi, \text{ on } G = 0. \tag{350}$$

Substitution of Equations (348), (349), and (350) into the shock
conditions (347) and sorting out the zeroth and first-order problems lead,

133

after a lengthy analysis, to the following results

Basic Conical Shock

$$-\rho_\infty V_\infty \sin\beta = \rho_0(\beta)v_0(\beta) \qquad ,$$

$$p_\infty + \rho_\infty V_\infty^2 \sin^2\beta = p_0(\beta) + \rho_0(\beta)v_0^2(\beta) \qquad ,$$

$$h_\infty + \frac{1}{2}V_\infty^2\sin^2\beta = h_0(\beta) + \frac{1}{2}v_0^2(\beta) \qquad ,$$

$$\frac{p_0(\beta)}{p_\infty} = \frac{\rho_0(\beta)}{\rho_\infty}\frac{h_0(\beta)}{h_\infty} \qquad , \qquad (351)$$

First-Order Perturbation

$$u_1(r,\beta) = [V_\infty \sin\beta + v_0(\beta)](q + rq'),$$

$$v_1(r,\beta) = [V_\infty \cos\beta(q + rq') + i\omega rg]\left[\frac{2(\gamma-1)}{\gamma+1} - \zeta_0\right]$$

$$-i\omega rg - u_0(\beta)rq' + \left(\frac{dv_0}{d\theta}\right)_\beta g \qquad ,$$

$$w_1(r,\beta) = -\left[V_\infty + \frac{v_0(\beta)}{\sin\beta}\right]g \qquad ,$$

$$p_1(r,\beta) = \frac{4\gamma}{\gamma+1}\frac{v_0(\beta)}{a_0^2(\beta)}[V_\infty \cos\beta(g + rq') + i\omega rg]$$

$$+ \left(\frac{dp_0}{d\theta}\right)_\beta \frac{q}{p_0(\beta)} \qquad ,$$

$$\rho_1(r,\beta) = \frac{2}{v_0(\beta)}[V_\infty \cos\beta(g + rq') + i\omega rg]\left[\zeta_0 - \frac{\gamma-1}{\gamma+1}\right]$$

$$+ \left(\frac{d\rho_0}{d\theta}\right)_\beta \frac{q}{\rho_0(\beta)} \qquad ,$$

$$h_1(r,\beta) = p_1(r,\beta) - \rho_1(r,\beta) \qquad . \qquad (352)$$

These definitions have been used

$$\xi_0 \equiv \rho_\infty/\rho_0(\beta) \qquad ,$$

$$a_0^2(\beta) \equiv \gamma\, p_0(\beta)/\rho_0(\beta) \qquad ,$$

$$\gamma \equiv c_p/c_v \qquad . \qquad (353)$$

The basic conical shock conditions (351) are the usual shock jump conditions across an oblique shock. The first-order perturbation relations (352) are the boundary conditions the first-order perturbation variables must satisfy at $\theta = \beta$.

e. Perturbation Equations

The governing equations for inviscid, nonconducting, unsteady flow are

mass:

$$\frac{\partial \rho}{\partial t} + \vec{V} \cdot \nabla \rho + \rho \ \text{div} \ \vec{V} = 0 \quad , \tag{354a}$$

momentum:

$$\rho [\frac{\partial \vec{V}}{\partial t} + \nabla (\frac{V^2}{2}) - \vec{V} \times \text{curl} \ \vec{V}] = -\nabla p \quad , \tag{354b}$$

energy:

$$(\frac{\partial}{\partial t} + \vec{V} \cdot \nabla)(\frac{p}{\rho^{\gamma}}) = 0 \quad . \tag{354c}$$

In writing the energy equation (354c) a thermally and calorically perfect gas has been assumed. Although Equations (354) form a closed set, it is useful in the ensuing analysis to replace one of them by the equation for total enthalpy:

$$\rho (\frac{\partial}{\partial t} + \vec{V} \cdot \nabla)(h + \frac{V^2}{2}) = \frac{\partial p}{\partial t} \quad . \tag{355}$$

Now assume for the basic flow and the perturbation variables the forms given by Equations (349). After these expressions are substituted into the governing equations, the basic-flow problem and the perturbation problem can be sorted out. The governing equations for the basic flow are

$$v_0 \frac{d\rho_0}{d\theta} + \rho_0 [2u_0 + \frac{dv_0}{d\theta} + \cot \theta \ v_0] = 0 \quad , \tag{356a}$$

$$\rho_0 [u_0 \frac{du_0}{d\theta} + v_0 \frac{dv_0}{d\theta}] = - \frac{d\rho_0}{d\theta} \quad , \tag{356b}$$

$$v_0 = \frac{du_0}{d\theta} \quad , \tag{356c}$$

135

$$\frac{p_0}{\rho_0{}^\gamma} = \text{constant (homentropic)} \quad . \quad (356d)$$

In addition, Equation (355) yields for the basic flow

$$h_0 + \frac{u_0{}^2 + v_0{}^2}{2} = h_\infty + \frac{V_\infty{}^2}{2} = \text{constant} . \quad (357)$$

To express the equations for the first-order perturbation variables, it is useful to utilize the operator

$$D \equiv i\omega r + u_0 r \frac{\partial}{\partial r} + v_0 \frac{\partial}{\partial \theta} \quad , \quad (358)$$

which represents r times the lowest-order material derivative to produce mass:

$$D\rho_1 + 2u_1 + r \frac{\partial u_1}{\partial r} + [\frac{d \ln \rho_0}{d\theta} + \cot \theta]v_1 + \frac{\partial v_1}{\partial \theta} + w_1 \csc \theta = 0 \quad , \quad (359a)$$

r-mom:

$$Du_1 - v_0 v_1 = -\frac{a_0{}^2}{\gamma} r \frac{\partial p_1}{\partial r} \quad , \quad (359b)$$

ϕ-mom:

$$\sin \theta \, Dw_1 + (u_0 \sin \theta + v_0 \cos \theta)w_1 = \frac{a_0{}^2}{\gamma} p_1 , \quad (359c)$$

total-enthalpy:

$$D[\frac{a_0{}^2}{\gamma-1} (p_1-\rho_1) + u_0 u_1 + v_0 v_1] = \frac{a_0{}^2}{\gamma} i\omega r \, p_1 \quad , \quad (359d)$$

energy:

$$D(p_1-\gamma\rho_1) = 0 \quad , \quad (359e)$$

where use has been made of the results

$$h_1 = p_1 - \rho_1 \quad , \quad (360a)$$

$$a_0{}^2 = \gamma p_0/\rho_0 \quad , \quad (360b)$$

$$h_0 = a_0{}^2/(\gamma-1). \quad (360c)$$

Equation (360a) follows from the thermal equation of state

$$\frac{p}{p_0} = \frac{\rho h}{\rho_0 h_0} \quad . \quad (361)$$

The solution for the basic axisymmetric flow past a cone will be considered as known since a very accurate approximate solution for slender

136

cones is available. Now direct attention to the solution of the first-order perturbation equations (359) by means of series expansions.

f.   Solution by Series Expansion

The appearance of the radial coordinate r and its derivative in the equidimensional combination $r(\partial/\partial r)$ suggests that any one of the perturbation functions $\rho_1(r,\theta)$, $p_1(r,\theta)$, $u_1(r,\theta)$, $v_1(r,\theta)$, $w_1(r,\theta)$, for instance $Q(r,\theta)$, can be expanded in the form

$$Q(r,\theta) \equiv \sum_{n=-1}^{\infty} \left(\frac{i\omega r}{V_\infty}\right)^n Q_n(\theta), \qquad (362)$$

where the functions $Q_n(\theta)$ depend only on θ. Here it has been anticipated that the first term in the series may start with $n = -1$ since the boundary condition (344) includes a term proportional to r^{-1}. Further, since the angular frequence ω appears in the combination $i\omega r$ in the perturbation equations, it is useful to use the combination $i\omega r/V_\infty$ as a nondimensional representation of r. It can now be seen that

$$r \frac{\partial Q}{\partial r} \equiv \sum_{n=-1}^{\infty} n\left(\frac{i\omega r}{V_\infty}\right)^n Q_n(\theta) \quad , \qquad (363a)$$

$$\frac{\partial Q}{\partial \theta} \equiv \sum_{n=-1}^{\infty} \left(\frac{i\omega r}{V_\infty}\right)^n Q_n{}'(\theta) \quad , \qquad (363b)$$

$$DQ \equiv \left(\frac{i\omega r}{V_\infty}\right)^{-1} [-u_0 Q_{-1} + v_0 Q'_{-1}] + V_\infty Q_{-1} + v_0 Q_0{}'$$

$$+ \sum_{n=1}^{\infty} \left(\frac{i\omega r}{V_\infty}\right)^n [V_\infty Q_{n-1} + n u_0 Q_n + v_0 Q_n{}'] \quad . \qquad (363c)$$

With these results in mind, assume the following expansions:

$$\frac{u_1(r,\theta)}{V_\infty} = \sum_{n=-1}^{\infty} \left(\frac{i\omega r}{V_\infty}\right)^n U_n(\theta),$$

$$\frac{v_1(r,\theta)}{V_\infty} = \sum_{n=-1}^{\infty} \left(\frac{i\omega r}{V_\infty}\right)^n V_n(\theta),$$

$$\frac{w_1(r,\theta)}{V_\infty} = \sum_{n=-1}^{\infty} \left(\frac{i\omega r}{V_\infty}\right)^n W_n(\theta),$$

$$p_1(r,\theta) = \sum_{n=-1}^{\infty} \left(\frac{i\omega r}{V_\infty}\right)^n P_n(\theta),$$

$$\rho_1(r,\theta) = \sum_{n=-1}^{\infty} \left(\frac{i\omega r}{V_\infty}\right)^n R_n(\theta). \tag{364}$$

The functions U_n, V_n, W_n, P_n, and R_n are all dimensionless. Better approximations for the sum of the series can be anticipated as the value of the dimensionless combination, $\omega r/V_\infty$, becomes smaller.

Expansions (364) can be substituted into the perturbation equations (359), and the coefficients of like powers of $(i\omega r/V_\infty)$ can then be collected and collectively set to zero for each power. These can be expressed as a set of equations for $n = -1$, $n = 0$, and $n \geq 1$. For $n = -1$:

$$-\frac{u_0}{V_\infty} R_{-1} + \frac{v_0}{V_\infty} R_{-1}' + U_{-1} + \left[\frac{d\ln\rho_0}{d\theta} + \cot\theta\right]V_{-1} + V_{-1}' + W_{-1} \csc\theta = 0, \tag{365a}$$

$$-u_0 U_{-1} + v_0 U_{-1}' - v_0 V_{-1} - \frac{a_0^2}{\gamma V_\infty} P_{-1} = 0, \tag{365b}$$

$$v_0 [\sin\theta\, W_{-1}]' - \frac{a_0^2}{\gamma V_\infty} P_{-1} = 0, \tag{365c}$$

$$-u_0 J_{-1} + v_0 J'_{-1} = 0, \tag{365d}$$

$$-u_0(P_{-1} - \gamma R_{-1}) + v_0(P_{-1}' - \gamma R_{-1}') = 0, \tag{365e}$$

where

$$J_{-1} \equiv \frac{a_0^2}{(\gamma-1)V_\infty^2} (P_{-1} - R_{-1}) + \frac{u_0}{V_\infty} U_{-1} + \frac{v_0}{V_\infty} V_{-1}. \tag{365f}$$

The defined function J_{-1} represents a perturbation of the total enthalpy. The governing equations (365) are homogeneous.

For $n = 0$,

$$\frac{v_0}{V_\infty} R_0' + 2U_0 + \left[\frac{d\ln\rho_0}{d\theta} + \cot\theta\right]V_0 + V_0' + W_0 \csc\theta = -R_{-1}, \tag{366a}$$

$$v_0[U_0' - V_0] = -V_\infty U_{-1}, \tag{366b}$$

$$\sin \theta \; v_0 W_0' + (u_0 \sin \theta + v_0 \cos \theta)W_0 - \frac{a_0^2}{\gamma V_\infty}P_0 = -V_\infty \sin \theta \; W_{-1} \quad , \qquad (366c)$$

$$v_0 J_0' = \frac{a_0^2}{\gamma V_\infty}P_{-1} - V_\infty J_{-1} \quad , \qquad (366d)$$

$$v_0(P_0' - \gamma R_0') = -V_\infty(P_{-1} - \gamma R_{-1}) \quad , \qquad (366e)$$

where

$$J_0 \equiv \frac{a_0^2}{(\gamma-1)V_\infty^2}(P_0 - R_0) + \frac{u_0}{V_\infty}U_0 + \frac{v_0}{V_\infty}V_0 \quad . \qquad (366f)$$

The terms on the right side of these equations depend on the leading functions in the series expansions, U_{-1}, V_{-1}, W_{-1}, P_{-1}, and R_{-1}, which are to be determined from the homogeneous equations (365).

Correspondingly, the set of equations for $n \geq 1$ is given by

$n \geq 1$:

$$\frac{n u_0}{V_\infty}R_n + \frac{v_0}{V_\infty}R_n' + (2+n)U_n + [\frac{d \ell n \rho_0}{d\theta} + \cot \theta]V_n + V_n' + W_n \csc \theta = -R_{n-1}, \quad (367a)$$

$$n \; u_0 U_n + v_0 U_n' - v_0 V_n + \frac{a_0^2}{\gamma V_\infty}n \; P_n = -V_\infty U_{n-1} \quad , \qquad (367b)$$

$$v_0 (\sin \theta \; W_n)' + (n+1) \; u_0 \sin \theta \; W_n$$
$$- \frac{a_0^2}{\gamma V_\infty} P_n = -V_\infty \sin \theta \; W_{n-1} \quad , \qquad (367c)$$

$$n \; u_0 \; J_n + v_0 \; J_n' = \frac{a_0^2}{\gamma V_\infty}P_{n-1} - V_\infty J_{n-1} \quad , \qquad (367d)$$

$$n \; u_0(P_n - \gamma R_n) + v_0(P_n' - \gamma R_n') = -V_\infty(P_{n-1} - \gamma R_{n-1}) \quad , \qquad (367e)$$

where

$$J_n \equiv \frac{a_0^2}{(\gamma-1)V_\infty^2} (P_n - R_n) + \frac{u_0}{V_\infty} U_n + \frac{v_0}{V_\infty} V_n \quad . \qquad (367f)$$

Again, these equations are inhomogeneous, and the right sides of the equations for the Ω_n variables depend on the Ω_{n-1} variables.

For the case of pure pitching motion about the vertex, the perturbation parameter is $\varepsilon \equiv \psi_0$, and Equation (343) becomes

$$\frac{v_1(r,\delta)}{V_\infty} = \frac{1}{V_\infty} \left(\frac{dv_0}{d\theta}\right)_\delta - \left(\frac{i\omega r}{V_\infty}\right) . \tag{368}$$

In terms of the series variables, thus are obtained

$$V_{-1}(\delta) = 0 \qquad , \tag{369a}$$

$$V_0(\delta) = \frac{1}{V_\infty} \left(\frac{dv_0}{d\theta}\right)_\delta \qquad , \tag{369b}$$

$$V_1(\delta) = -1 \qquad , \tag{369c}$$

$$V_n(\delta) = 0 \quad , \quad n \geq 2 . \tag{369d}$$

Since the set of Equations (365) that governs the Q_{-1} variables is homogeneous, the boundary condition (369a) leads to the conclusion that all the Q_{-1} variables are zero for the reduced problem of pure pitching about the vertex. Hence $U_{-1} = V_{-1} = W_{-1} = P_{-1} = R_{-1} = 0$ for this reduced problem. As shall be seen, the shock condition is thus satisfied correspondingly by $q_{-1} = 0$.

The lowest-order problem is thus the set of equations (366), which now becomes homogeneous, with the boundary condition (369b).

For pure plunging motion it is convenient to choose the perturbation parameter ε as the nondimensional form $\varepsilon \equiv i\omega h_0 e^{i\Omega}/V_\infty$. The surface boundary condition (344) now becomes

$$\frac{v_1(r,\delta)}{V_\infty} = -\left(\frac{i\omega r}{V_\infty}\right)^{-1} \left[\frac{u_0(\delta)}{V_\infty} + \frac{1}{V_\infty} \left(\frac{dv_0}{d\theta}\right)_\delta \right] + 1 . \tag{370}$$

In terms of the series variables,

$$V_{-1} = -\frac{1}{V_\infty} \left[u_0(\delta) + \left(\frac{dv_0}{d\theta}\right)_\delta \right] , \tag{371a}$$

$$V_0(\delta) = 1 \qquad , \tag{371b}$$

$$V_n(\delta) = 0 \quad , \quad n \geq 1 \qquad . \tag{371c}$$

The contribution for pitching motion about the point $z_0 \neq 0$ is obtained by choosing the perturbation parameter as $\varepsilon \equiv i\omega\psi_0 z_0/V_\infty$. The surface boundary conditions are thus the same as Equations (333) and (334), and the results of the pure plunging problem can be utilized directly. The results for the total

pitching and plunging problem will thus be a linear combination of the three reduced problems.

The series expansions (364) suggest that the function $g(r)$ in the shock-shape equation (346a) can be expanded in the form

$$g(r) = \sum_{n=-1}^{\infty} \left(\frac{i\omega r}{V_\infty}\right)^n g_n \ , \tag{372}$$

where the parameters g_n are constants to be determined.

For the case of pure pitching about the vertex, $\varepsilon = \psi_0$ and all the Q_{-1} variables are zero. It follows that $g_{-1} = 0$. From Equations (352) are obtained for $n = 0$:

$$U_0(\beta) = g_0 \left[\sin \beta + \frac{v_0(\beta)}{V_\infty} \right] \ , \tag{373a}$$

$$V_0(\beta) = g_0 \left[\left\{ \frac{2(\gamma-1)}{\gamma+1} - \xi_0 \right\} \cos \beta + \frac{1}{V_\infty} \left(\frac{dv_0}{d\theta}\right)_\beta \right] \ , \tag{373b}$$

$$W_0(\beta) = -g_0 \left[1 + \frac{v_0(\beta)}{V_\infty \sin \beta} \right] \ , \tag{373c}$$

$$P_0(\beta) = g_0 \left[\frac{4\gamma}{\gamma+1} \frac{V_\infty\, v_0(\beta)}{a_0{}^2(\beta)} \cos \beta + \frac{1}{p_0(\beta)} \left(\frac{dp_0}{d\theta}\right)_\beta \right] \ , \tag{373d}$$

$$R_0(\beta) = g_0 \left[\frac{2V_\infty \cos \beta}{v_0(\beta)} \left\{ \xi_0 - \frac{\gamma-1}{\gamma+1} \right\} + \frac{1}{\rho_0(\beta)} \left(\frac{d\rho_0}{d\theta}\right)_\beta \right] \ . \tag{373e}$$

For $n \geqslant 1$, are obtained

$$U_n(\beta) = \left[\sin \beta + \frac{v_0(\beta)}{V_\infty} \right] (1+n) g_n \ , \tag{374a}$$

$$V_n(\beta) = \left[\cos \beta (1+n) g_n + g_{n-1} \right] \frac{[2(\gamma-1) - \xi_0]}{\gamma+1}$$

$$- g_{n-1} + \left[-n \cos \beta + \frac{1}{V_\infty} \left(\frac{dv_0}{d\theta}\right)_\beta \right] g_n \ , \tag{374b}$$

$$W_n(\beta) = -g_n \left[1 + \frac{v_0(\beta)}{V_\infty \sin \beta} \right] \ , \tag{374c}$$

$$P_n(\beta) = \frac{4\gamma}{\gamma+1} \frac{V_\infty v_0(\beta)}{a_0{}^2(\beta)} \left[\cos \beta (1+n) g_n + g_{n-1} \right] + \left(\frac{dp_0}{d\theta}\right)_\beta \frac{g_n}{p_0(\beta)} \ , \tag{374d}$$

141

$$R_n(\beta) = \frac{2V_\infty}{v_0(\beta)} \left[\cos \beta (1+n) q_n + q_{n-1} \right] \left(\xi_0 - \frac{\gamma-1}{\gamma+1} \right) + \left(\frac{d\rho_0}{d\theta} \right)_\beta \frac{q_n}{\rho_0(\beta)} \ . \tag{374e}$$

Note for all cases that

$$\sin \beta \ W_n(\beta) + \frac{U_n(\beta)}{n+1} = 0 \ , \quad n > 0 \ . \tag{375}$$

For pure plunging motion, the perturbation parameter is given by $\epsilon \equiv i\omega h_0 e^{i\Omega}/V_\infty$. From Equations (352) and (372) there exists for $n = -1$:

$$U_{-1}(\beta) = 0 \qquad , \tag{376a}$$

$$V_{-1}(\beta) = \left[\cos \beta + \frac{1}{V_\infty} \left(\frac{dv_0}{d\theta} \right)_\beta \right] q_{-1} \quad , \tag{376b}$$

$$W_{-1}(\beta) = -\left(1 + \frac{v_0(\beta)}{V_\infty \sin \beta} \right) q_{-1} \quad , \tag{376c}$$

$$P_{-1}(\beta) = \left(\frac{dp_0}{d\theta} \right)_\beta \frac{q_{-1}}{\rho_0(\beta)} \qquad , \tag{376d}$$

$$R_{-1}(\beta) = \left(\frac{d\rho_0}{d\theta} \right)_\beta \frac{q_{-1}}{\rho_0(\beta)} \qquad . \tag{376e}$$

The results for $n > 0$ are the same as given by Equations (374).

Some integrations of Equations (367) for $n > 0$ can be accomplished when the basic-flow velocities $u_0(\theta)$ and $v_0(\theta)$ are regarded as known. Now is introduced the factor

$$I(\theta) \equiv \exp \left\{ \int_\beta^\theta \frac{u_0(\theta)}{v_0(\theta)} d\theta \right\} \ , \tag{377}$$

where it is noted that $I(\beta) = 1$. The energy equation (367e) can now be integrated by means of an integrating factor, and gives

$$P_n - \gamma R_n = \frac{S_n(\beta)}{I^n} - \frac{V_\infty}{I^n} \int_\beta^\theta \frac{I^n}{v_0} (P_{n-1} - \gamma R_{n-1}) d\theta \ , \tag{378}$$

where $S_n(\beta) \equiv P_n(\beta) - \gamma R_n(\beta)$.

The function $S_n(\beta)$ is the nth-order entropy function evaluated at the basic shock. To see this, note for a thermally and calorically perfect

gas that

$$\frac{s-s_0}{c_v} = \ln\left[\frac{p}{p_0}\left(\frac{\rho}{\rho_0}\right)^{-\gamma}\right] \quad . \tag{379}$$

Now if the notation is written

$$\frac{s-s_0}{c_v} = \epsilon\left[\sum_{n=-1}^{\infty} \left(\frac{i\omega r}{V_\infty}\right)^n S_n(\theta)\right]e^{i\omega t}\cos\phi \quad , \tag{380}$$

then with the use of Equations (349) and (364) it is found that

$$S_n(\theta) \equiv P_n(\theta) - \gamma R_n(\theta) \quad . \tag{381}$$

With the aid of the shock conditions (374d,e)

$$S_n(\beta) = \frac{2\gamma V_\infty v_0(\beta)}{a_0^2(\beta)}\left\{\frac{2}{\gamma+1} + \frac{a_0^2(\beta)}{v_0^2(\beta)}\frac{(\gamma-1}{\gamma+1} - \zeta_0)\right\}[(1+n)g_n\cos\beta + g_{n-1}] \quad . \tag{382a}$$

By means of the basic-flow shock relations (251), this can be simplified to the form

$$S_n(\beta) = -\frac{V_\infty^2\gamma(\gamma-1)(1-\zeta_0)^2\sin\beta}{a_0^2(\beta)}[(1+n)g_n\cos\beta + g_{n-1}] \quad . \tag{382b}$$

The total-enthalpy equation (367d) can be integrated similarly and gives

$$J_n(\theta) = \frac{J_n(\beta)}{I^n} + \frac{V_\infty}{I^n}\int_\beta^\theta \frac{I^n}{v_0}\left\{\frac{a_0^2}{\gamma V^2_\infty}P_{n-1} - J_{n-1}\right\}d\theta \quad , \tag{383}$$

where $J_n(\theta)$ is defined by (367f). From the shock conditions (374) and (351) it can be established that

$$J_n(\beta) = -(1-\zeta_0)\sin\beta\, g_{n-1} \quad ,$$

$$= -U_{n-1}(\beta)/n \qquad , \; n \neq 0 \quad . \tag{384}$$

Equations (378) and (383) can be regarded as two equations for P_n and R_n. Elimination of R_n between these two equations yields

$$\frac{a_0^2(\theta)P_n(\theta)}{\gamma V_\infty^2} = -\left\{\frac{u_0}{V_\infty}U_n + \frac{v_0}{V_\infty}V_n\right\} + \frac{1}{I^n}\left[J_n(\beta) - \frac{S_n(\beta)a_0^2(\theta)}{\gamma(\gamma-1)V_\infty^2}\right]$$

$$- \frac{1}{I^n}\int_\beta^\theta \frac{I^n}{v_0}(u_0 U_{n-1} + v_0 V_{n-1})d\theta \quad . \tag{385}$$

When the identity

143

$$\frac{u_0}{v_0} I^n U_{n-1} \equiv \frac{1}{n} \frac{d}{d\theta} (I^n U_{n-1}) - \frac{I^n}{n} U'_{n-1} \qquad (386)$$

is substituted into the integral in Equation (385), one integration can be performed, and the equation can be rewritten with the use of (384) to read

$$\frac{a_0^2(\theta) P_n(\theta)}{\gamma V_\infty^2} = -\left[\frac{u_0}{V_\infty} U_n + \frac{v_0}{V_\infty} V_n + \frac{U_{n-1}}{n}\right] - \frac{S_n(\beta) a_0^2(\theta)}{\gamma(\gamma-1) V_\infty^2 I^n}$$

$$+ \frac{1}{I^n} \int_\beta^\theta I^n \left[\frac{U'_{n-1}}{n} - V_{n-1}\right] d\theta \quad . \qquad (387)$$

This equation gives the pressure perturbation P_n as a function of the velocity perturbations U_n and V_n. Thus when the velocity is known the pressure can be determined.

The density function is found to be

$$\frac{a_0^2(\theta) R_n(\theta)}{V_\infty^2} = -\left[\frac{u_0}{V_\infty} U_n + \frac{v_0}{V_\infty} V_n + \frac{U_{n-1}}{n}\right] - \frac{S_n(\beta) a_0^2(\theta)}{(\gamma-1) V_\infty^2 I^n}$$

$$+ 1 \int_\beta^\theta I^n \left[\frac{U'_{n-1}}{n} - V_{n-1} + \frac{a_0^2}{\gamma V_\infty v_0} (P_{n-1} - \gamma R_{n-1})\right] d\theta \quad . \qquad (388)$$

When the pressure equation (387) is substituted into the r-momentum equation (367b), the result is

$$v_0 [U_n' - (1+n) V_n] = \frac{n S_n(\beta) a_0^2(\theta)}{\gamma(\gamma-1) V_\infty I^n} - \frac{n V_\infty}{I^n} \int_\beta^\theta I^n \left[\frac{U'_{n-1}}{n} - V_{n-1}\right] d\theta \quad . \qquad (389)$$

This equation gives a relation between the velocity components U_n and V_n. At the cone surface $\theta = \delta$, the velocity $V_n(\delta)$ is prescribed and $v_0(\delta) = 0$. Thus when $n > 1$, U_n' at the cone surface is not analytic. This feature must be accounted for properly in the analysis, especially in any numerical computation.

When V_n is solved for from Equation (389) and substituted into Equation (387) for the pressure, the computation results in

$$\frac{a_0^2(\theta) P_n(\theta)}{\gamma V_\infty^2} = -\left[\frac{u_0}{V_\infty} U_n + \frac{v_0}{V_\infty} \frac{U_n'}{1+n} + \frac{U_{n-1}}{n}\right] - \frac{S_n(\beta) a_0^2(\theta)}{(1+n)\gamma(\gamma-1) V_\infty^2 I^n}$$

$$+ \frac{1}{(1+n)I^n} \int_\beta^\theta I^n \left[\frac{U'_{n-1}}{n} - V_{n-1} \right] d\theta \quad . \tag{390}$$

This expression gives the pressure in terms of the velocity component U_n only.

After the pressure equation (390) is substituted into the ϕ-momentum equation (367c), the outcome is

$$v_0 \left[\sin\theta\, W_n + \frac{U_n}{1+n} \right]' + (1+n)u_0 \left[\sin\theta\, W_n + \frac{U_n}{1+n} \right] =$$

$$- V_\infty \left[W_{n-1} \sin\theta + \frac{U_{n-1}}{n} \right] - \frac{S_n(\beta)a_0^2(\theta)}{(1+n)\gamma(\gamma-1)V_\infty I^n}$$

$$+ \frac{V_\infty}{(1+n)I^n} \int_\beta^\theta I^n \left[\frac{U'_{n-1}}{n} - V_{n-1} \right] d\theta \quad . \tag{391}$$

An integrating factor for this equation is I^{1+n}/v_0, and a straightforward integration thus gives

$$\sin\theta\, W_n + \frac{U_n}{1+n} = - \frac{V_\infty}{I^{1+n}} \int_\beta^\theta \frac{I^{1+n}}{v_0} \left[\sin\theta\, W_{n-1} + \frac{U_{n-1}}{n} \right] d\theta$$

$$- \frac{S_n(\beta)}{(1+n)\gamma(\gamma-1)V_\infty I^{n+1}} \int_\beta^\theta \frac{I\, a_0^2(\theta)}{v_0} d\theta$$

$$+ \frac{V_\infty}{(1+n)I^{1+n}} \int_\beta^\theta \frac{I}{v_0} \left[\int_\beta^\theta I^n \left(\frac{U'_{n-1}}{n} - V_{n-1} \right) d\theta \right] d\theta \quad . \tag{392}$$

The shock condition (375) was taken into account. This equation gives the azimuthal velocity W_n as a function of the radial velocity U_n.

When the function U_n is known, all of the other functions can be determined in terms of it. It thus remains to establish the governing equation for U_n. By means of Equation (367e), first eliminate the density in favor of the pressure in the continuity equation (367a):

$$n \frac{u_0}{V_\infty} \frac{P_n}{\gamma} + \frac{v_0}{V_\infty} \frac{P_n'}{\gamma} + (2+n)U_n + \left[\frac{d\,\ell n\, \rho_0}{d\theta} + \cot\theta \right] V_n$$

$$+ V_n' + W_n \csc\theta = -P_{n-1}/\gamma \quad . \tag{393}$$

Now note the identity

$$n u_0 P_n + v_0 P_n' \equiv [n \frac{u_0}{a_0^2} - \frac{v_0}{a_0^2} (\ln a_0^2)'](a_0^2 P_n) + \frac{v_0}{a_0^2} (a_0^2 P_n)' .$$

$$(394)$$

The combination $a_0^2 P_n$ is given in terms of U_n by Equation (390), and V_n and W_n are given in terms of U_n by Equations (389) and (392). When the necessary operations are performed and substituted into Equation (373), a single differential equation for U_n results. To simplify the form of this equation, note the following results obtained from the homentropic basic flow:

$$(\ln a_0^2)' = (\gamma-1)(\ln \rho_0)' = \frac{\gamma-1}{\gamma} (\ln p_0)' = -(\gamma-1) \frac{v_0}{a_0^2} (u_0 + v_0') . \quad (395)$$

Using these results, it is now possible to obtain

$$(1 - \frac{v_0^2}{a_0^2})U_n'' + [\cot \theta - \frac{v_0}{a_0^2} \{2nu_0 + (u_0 + v_0')(2 + (\gamma-1) \frac{v_0^2}{a_0^2}\}]U_n' +$$

$$(1+n)[2 + n(1 - \frac{u_0^2}{a_0^2}) - \frac{\csc^2\theta}{1+n} - \frac{v_0^2}{a_0^2} \{1 + (\gamma-1) \frac{u_0}{a_0^2} (u_0+v_0')\}]U_n = T_n . \quad (396)$$

The inhomogeneous term, T_n, for the right-hand side is given by

$$T_n \equiv - \frac{1+n}{\gamma} P_{n-1} + \frac{1+n}{n} [\frac{nu_0}{a_0^2} + \frac{v_0^2}{a_0^4} (\gamma-1)(u_0 + v_0')]V_\infty U_{n-1}$$

$$+ \frac{1+n}{n} \frac{V_\infty v_0}{a_0^2} U'_{n-1} - \frac{V_\infty}{v_0} (U'_{n-1} - V_{n-1})(n + \frac{v_0^2}{a_0^2})$$

$$+ \frac{nS_n(\beta)}{\gamma(\gamma-1)V_\infty} \frac{a_0^2}{v_0^2 I^n} [v_0 \cot \theta - \gamma \frac{v_0^2}{a_0^2} (u_0 + v_0') - nu_0 - v_0']$$

$$+ [nv_0 \cot \theta - \frac{v_0^2}{a_0^2} (u_0 + v_0)\{n - (\gamma-1) \frac{v_0^2}{a_0^2}\} - n^2 u_0] \frac{V_\infty}{v_0^2 I^n} \int_\beta^\theta I^n(\frac{U'_{n-1}}{n}$$

$$- V_{n-1})d\theta + \csc^2\theta [\frac{S_n(\beta)}{\gamma(\gamma-1)V_\infty I^{n+1}} \int_\beta^\theta \frac{I a_0^2}{v_0} d\theta$$

$$+ \frac{(1+n)V_\infty}{I^{1+n}} \int_\beta^\theta \frac{I^{1+n}}{v_0} (\sin \theta W_{n-1} + \frac{U_{n-1}}{n})d\theta$$

$$- \frac{V_\infty}{I^{1+n}} \int_\beta^\theta \frac{I}{v_0} \int_\beta^\theta I^n(\frac{U'_{n-1}}{n} - V_{n-1})d\theta]d\theta] . \quad (397)$$

The inhomogeneous term, T_n, depends on the previously obtained functions Q_{n-1} and the entropy function at the shock $S_n(\beta)$. Equation (395) is a linear

146

differential equation with variable coefficients. Now these equations are to be solved by approximate methods.

g. Approximate Solution for the Basic Flow

For the basic axisymmetric flow past a slender cone, the approximate solution developed in Reference 21, which has proven successful in the analysis of steady-flow problems (Reference 22,52,53) similar in nature to the present unsteady-flow problem, shall be utilized. It shall be assumed that the cone is slender such that $\sin \theta \simeq \theta$. In addition it shall be assumed that the freestream Mach number M_∞ is large such that when $M_\infty \to \infty$ and $\theta \to 0$, the combination $M_\infty \theta$ remains finite. The pertinent parameter in this hypersonic small-disturbance limit is the similarity parameter $K_\delta \equiv M_\infty \delta$. Thus the basic-flow velocity components are approximated by

$$u_0(\theta) \simeq V_\infty [1 - \frac{\delta^2}{2} \{\frac{\theta^2}{\delta^2} + \ln(\frac{\beta^2}{\theta^2})\}] \quad , \tag{398a}$$

$$v_0(\theta) \simeq -V_\infty \theta \ (1 - \frac{\delta^2}{\theta^2}) \quad . \tag{398b}$$

The basic-flow shock angle is determined by

$$\sigma \equiv \frac{\beta}{\delta} \cong [\frac{\gamma+1}{2} + \frac{1}{K_\delta^2}]^{1/2} \quad . \tag{399}$$

The temperature and pressure in the shock layer increase only a small amount from the shock to the cone surface. Hence it is possible to establish the following formulas:

$$\frac{T_0(\theta)}{T_\infty} = \frac{a^2_0(\theta)}{a_\infty^2} \equiv 1 + \frac{\gamma-1}{2} K_\delta^2 \ [2 + \ln(\frac{\beta}{\theta})^2 - (\frac{\delta}{\theta})^2] \quad , \tag{400a}$$

$$\frac{p_0(\theta)}{p_\infty} \equiv 1 + \frac{\gamma}{2} K_\delta^2 \ [1 + \frac{\sigma^2}{\sigma^2-1} \{1 + \ln(\frac{\beta}{\theta})^2 - (\frac{\delta}{\theta})^2\}] \quad . \tag{400b}$$

Also availble are the formulas

$$v_0' \equiv -V_\infty(1 + \frac{\delta^2}{\theta^2}) \quad , \tag{401a}$$

$$(\ln p_0)' = \gamma(\ln \rho_0)' \equiv - \frac{\gamma v_0}{a_0^2}(u_0 + v_0') \quad ,$$

147

$$\equiv - \frac{\gamma V_\infty^2}{a_0^2(\theta)} \frac{\delta^2}{\theta} \left(1 - \frac{\delta^2}{\theta^2}\right), \tag{401b}$$

$$\zeta_0 \equiv \frac{\rho_\infty}{\rho_0(\beta)} \equiv \frac{\sigma^2-1}{\sigma^2} \quad . \tag{401c}$$

h. Approximate Solution for the Plunging Cone (n=-1)

The approximate solution to Equations (365) for n = -1 can now be obtained when the basic-flow solution is known. The n = -1 order of perturbation amounts to a shift in the origin of coordinates along the inertial X axis. With this taken into account, the velocity perturbations can be obtained from Equations (333) when the transformation (332b) is taken into account (with $\psi = 0$). This produces

$$U_{-1}(\theta) = 0 \quad ,$$

$$V_{-1}(\theta) = \frac{\delta^2}{\theta^2} \quad ,$$

$$W_{-1}(\theta) = \frac{\delta^2}{\theta^2} \quad , \tag{402}$$

The scalar perturbation variables can also be determined by the translation of the origin, and gives

$$P_{-1}(\theta) = \frac{\gamma V_\infty^2}{a_0^2} \frac{\delta^2}{\theta}\left(1 - \frac{\delta^2}{\theta^2}\right) \quad ,$$

$$R_{-1}(\theta) = \frac{V_\infty^2}{a_0^2} \frac{\delta^2}{\theta}\left(1 - \frac{\delta^2}{\theta^2}\right) \quad ,$$

$$J_{-1}(\theta) = 0 \quad . \tag{403}$$

These results satisfy Equations (365b,c,d,e) exactly. Equation (365a) is also satisfied approximately to within the accuracy of the basic-flow approximation. The surface boundary condition (371a), $V_{-1}(\delta) = 1$, is satisfied, and the shock-boundary conditions (375) are satisfied when

$$g_{-1} = -1 \quad ,$$

which provides the perturbed shock shape.

i. Approximate Solution for the Pure Pitching Problem for n = 0

For the pure pitching problem the $n = -1$ variables are all zero, and the inhomogeneous terms in Equations (366) for $n = 0$ vanish. The surface boundary condition is Equation (369b), which becomes

$$v_0(\delta) = -2 \quad . \tag{405}$$

The shock boundary conditions, at $\theta = \beta$, are given by Equations (375).

The pressure and density functions are given by the appropriate forms of Equations (387) and (388):

$$P_0(\theta) = - \frac{\gamma V_\infty}{a_0^2}[u_0 U_0 + v_0 v_0] - \frac{S_0(\beta)}{(\gamma-1)} \quad , \tag{406a}$$

$$R_0(\theta) = - \frac{V_\infty}{a_0^2}[u_0 U_0 + v_0 v_0] - \frac{S_0(\beta)}{\gamma-1} \quad , \tag{406b}$$

where

$$S_0(\beta) = -V_\infty^2 \, \gamma(\gamma-1)(1-\xi_0)^2 \beta g_0/a_0^2(\beta) \tag{407}$$

is determined from Equation (382b). The velocity components V_0 and W_0 are determined from Equations (389), or (366b) and (392):

$$V_0(\theta) = U_0{}'(\theta) \quad , \tag{408}$$

$$\theta W_0(\theta) = -U_0 - \frac{S_0(\beta)}{\gamma(\gamma-1)V_\infty} \frac{1}{I} \int_\beta^\theta \frac{I a_0^2}{v_0} d\theta \quad . \tag{409}$$

The governing equation for U_0 is given by (396), which for small angles is given by

$$\left(1 - \frac{v_0^2}{a_0^2}\right)U_0{}'' + \left[\frac{1}{\theta} - \frac{v_0(u_0 + v_0{}')}{a_0^2}\{2 + (\gamma-1)\frac{v_0^2}{a_0^2}\}\right]U_0{}'$$

$$+ \left[2 - \frac{1}{\theta^2} - \frac{v_0^2}{a_0^2}\{1 + (\gamma-1)\frac{u_0(u_0 + v_0{}')}{a_0^2}\}\right] U_0 = T_0 \quad , \tag{410a}$$

where

$$T_0 \equiv \frac{1}{\theta^2} \frac{S_0(\beta)}{\gamma(\gamma-1)V_\infty I} \int_\beta^\theta \frac{I a_0^2}{v_0} d\theta \quad . \tag{410b}$$

Now the variable coefficients of U_0, $U_0{}'$, and $U_0{}''$ are considered. The combination v_0/a_0 vanishes at the body and, for large values of K_δ, is small at the shock. It is thus reasonable to neglect v_0/a_0 compared to unity where it appears on the left side of Equation (410). This is tantamount to a

149

constant-density approximation, and it has been found to yield excellent results for all values of κ_δ (References 23, 52, 53). Consistent with this approximation is the assumption that $1/\theta$ is large compared to unity. Finally, since $a_0^2(\theta)$ varies very slowly across the shock layer, it is replaced by its value at the shock. Thus the problem (410) is approximated by

$$U_0'' + \frac{1}{\theta}U_0' - \frac{1}{\theta^2}U_0 = T_0 \quad , \tag{411a}$$

where

$$T_0 \cong \frac{1}{\theta^2} \frac{S_0(\beta)a_0^2(\beta)}{\gamma(\gamma-1)V_\infty I} \int_{\beta v_0}^{\theta} \frac{I}{v_0} \, d\theta \quad .$$

The complementary solutions to Equation (411a) are θ and θ^{-1}, and thus it is easy to establish, since $V_0 = U_0'$, that the general solution that satisfies the shock conditions for U_0 and V_0 is

$$U_0(\theta) = U_0(\beta) \frac{\theta}{\beta} + \frac{1}{2} [\beta V_0(\beta) - U_0(\beta)] [\frac{\theta}{\beta} - \frac{\beta}{\theta}]$$

$$+ \frac{\theta}{2} \int_\beta^\theta T_0 d\theta - \frac{1}{2\theta} \int_\beta^\theta \theta^2 T_0 \, d\theta \quad . \tag{412}$$

The solution can be completed by the evaluation of I (Equation (377)) and the quadratures of T_0. By means of $u_0 = V_\infty$ and $v_0 \cong -\theta V_\infty(1-\frac{\delta^2}{\theta^2})$, are obtained

$$I(\theta) = [\frac{\beta^2-\delta^2}{\theta^2-\delta^2}]^{1/2} \quad , \tag{413}$$

and

$$T_0(\theta) = \frac{S_0(\beta)a_0^2(\beta)}{\gamma(\gamma-1)V_\infty^2} \frac{1}{\theta^2} [1 - \sqrt{\frac{\theta^2-\delta^2}{\beta^2-\delta^2}}] \quad . \tag{414}$$

When the quadratures on T_0 are evaluated and the shock conditions (373a,b), (407b), and (401c) utilized, the velocity U_0 can be written in terms of $z \equiv \theta/\delta$ and $\sigma \equiv \beta/\delta$ as

$$U_0(\theta) = g_0 \delta \{\frac{z}{\sigma^2} - \frac{1}{2} (\frac{4}{\gamma+1} + \frac{1}{\sigma^2})(z - \frac{\sigma^2}{z})$$

$$- \frac{1}{\sigma^3} \{-1 + \frac{\sigma}{4z} + \frac{3}{4} \sqrt{\frac{z^2-1}{\sigma^2-1}} + \frac{2z^2+1}{4z\sqrt{\sigma^2-1}} \ln'\frac{\sigma+\sqrt{\sigma^2-1}}{z+\sqrt{z^2-1}} \}\} . \tag{415}$$

The velocity V_0 is determined by $V_0 = U_0'$:

$$V_0(\theta) = g_0 [\frac{1}{\sigma^2} - \frac{1}{2} (\frac{4}{\gamma+1} + \frac{1}{\sigma^2})(1 + \frac{\sigma^2}{z^2})$$

$$- \frac{1}{4\sigma^3} \{- \frac{\sigma}{z^2} + \frac{1}{z} \sqrt{\frac{z^2-1}{\sigma^2-1}} + \frac{2z^2-1}{z^2\sqrt{\sigma^2-1}} \ln[\frac{\sigma+\sqrt{\sigma^2-1}}{z+\sqrt{z^2-1}}]\}] . \tag{416}$$

The shock-shape factor g_0 is determined by imposing the surface boundary condition $V_0(\delta) = -2$. Solving for g_0 then gives

$$\frac{1}{g_0} = - \frac{3}{8\sigma^2} + \frac{\sigma^2+1}{\gamma+1} + \frac{1}{4} + \frac{\ln[\sigma + \sqrt{\sigma^2-1}]}{8\sigma^3\sqrt{\sigma^2-1}} . \tag{417}$$

The shock-shape factor g_0 is thus given as a function of σ and γ, or, alternatively, as a function of K_δ and γ by means of (399). The factor g_0 is shown in Figure 44, which will be discussed later.

The pressure can be obtained from Equation (406a) and is

$$\frac{a_0^2(\theta)P_0(\theta)}{\gamma V_\infty^2 \delta} = g_0 [- \frac{1}{\sigma^2 z} + \frac{1}{2z} (\frac{4}{\gamma+1} + \frac{1}{\sigma^2})(1 - 2\sigma^2 + \frac{\sigma^2}{z^2})$$

$$+ \frac{1}{4\sigma^3} \{2\sigma - \frac{\sigma}{z} - \frac{\sigma}{z^3} + \sqrt{\frac{z^2-1}{\sigma^2-1}} (2 + \frac{1}{z^2})$$

$$+ (\frac{4}{z} - \frac{1}{z^3}) \frac{\ln[\sigma + \sqrt{\sigma^2-1}]}{\frac{z + \sqrt{z^2-1}}{\sqrt{\sigma^2-1}}} \} + \frac{1}{\sigma^3} \{\frac{a_0^2(\theta)}{a_0^2(\beta)} - 1\}] . \tag{418}$$

The results for $n = 0$ correspond to the results of steady flow at an angle of attack ψ. Thus, these results are equivalent to the results of Doty and Rasmussen (Reference 23).

151
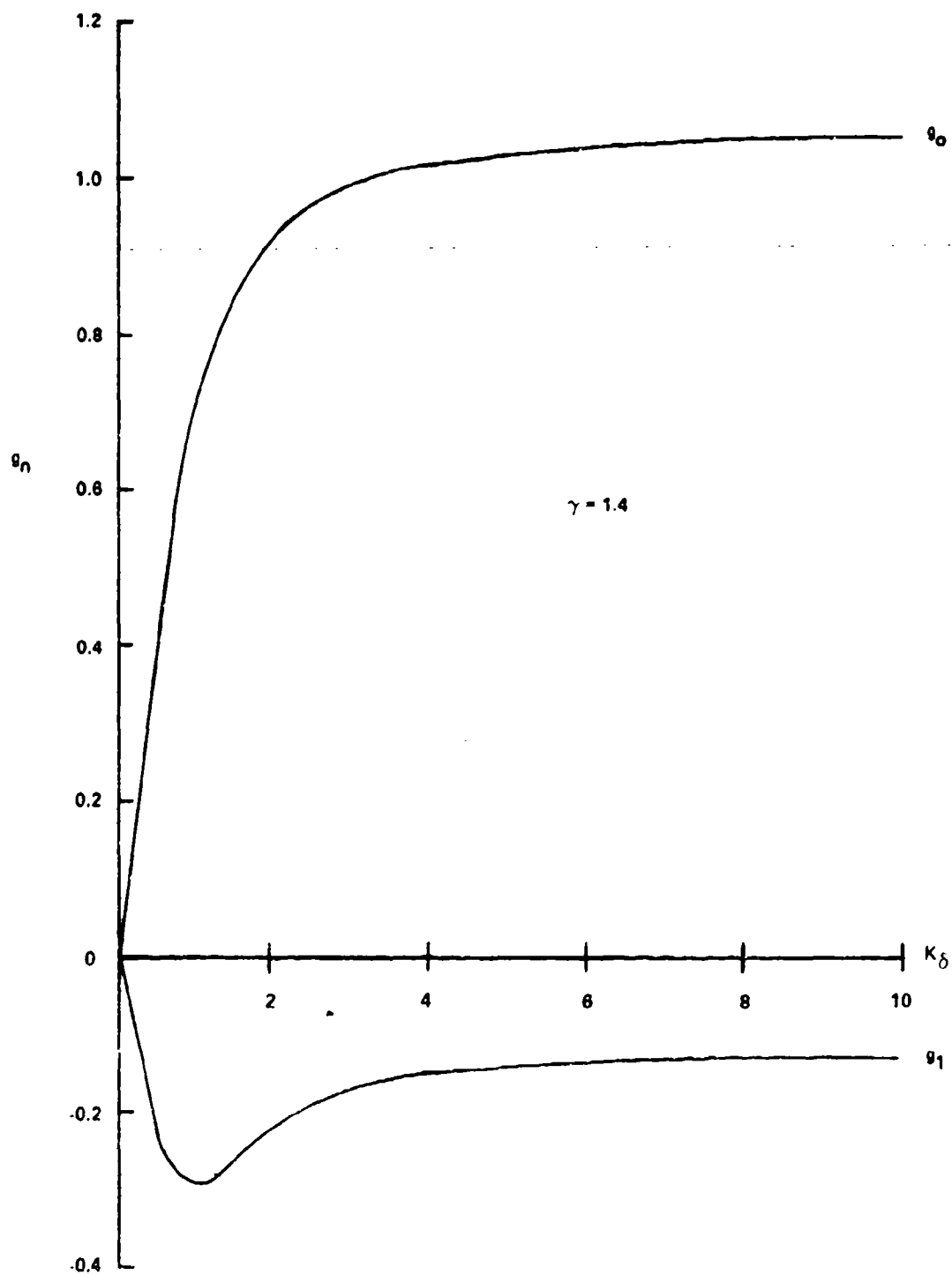
Figure 44.   Shock-Shape Parameters g_0 and g_1 for Pure Pitching About
the Vertex ($\gamma = 1.4$)

j. Approximate Solution for the Pure Pitching Problem for n = 1.

For n = 1, the problem is governed by the inhomogeneous equations, Equation (367). The surface boundary condition is $V_1(\delta) = -1$, as given by Equation (369c), and the shock boundary conditions are given by Equations (374). The pressure and density integrals are given in terms of the velocity by Equations (387) and (388):

$$\frac{a_0^2(\theta)P_1(\theta)}{\gamma V_\infty^2} = -\left[\frac{u_0}{V_\infty}U_1 + \frac{v_0}{V_\infty}V_1 + U_0\right] - \frac{S_1(\beta)a_0^2(\theta)}{\gamma(\gamma-1)V_\infty^2 I} \quad , \tag{419}$$

$$\frac{a_0^2(\theta)R_1(\theta)}{V_\infty^2} = -\left[\frac{u_0}{V_\infty}U_1 + \frac{v_0}{V_\infty}V_1 + U_0\right] - \frac{S_1(\beta)a_0^2(\theta)}{(\gamma-1)V_\infty^2 I}$$

$$+ \frac{1}{\gamma V_\infty I}\int_\beta^\theta \frac{Ia_0^2}{v_0}(P_0 - \gamma R_0)d\theta \quad . \tag{420}$$

The velocity components V_1 and U_1 are related by Equation (389):

$$v_0[U_1' - 2V_1] = \frac{S_1(\beta)a_0^2(\theta)}{\gamma(\gamma-1)V_\infty I} \quad . \tag{421}$$

The azimuthal velocity component is determined by

$$2\theta W_1 + U_1 = -\frac{2V_\infty}{I^2}\int_\beta^\theta \frac{I^2}{v_0}[\theta W_0 + U_0]d\theta$$

$$- \frac{S_1(\beta)}{\gamma(\gamma-1)V_\infty I^2}\int_\beta^\theta \frac{Ia_0^2}{v_0}d\theta \quad . \tag{422}$$

Finally, the velocity function U_1 is governed by Equation (396):

$$\left(1 - \frac{v_0^2}{a_0^2}\right)U_1'' + \left[\frac{1}{\theta} - \frac{v_0}{a_0^2}\left\{2u_0 + (u_0 + v_0')(2 + (\gamma-1)\frac{v_0^2}{a_0^2})\right\}\right]U_1' +$$

$$2\left[3 - \frac{u_0^2}{a_0^2} - \frac{1}{2\theta^2} - \frac{v_0^2}{a_0^2}\left\{1 + (\gamma-1)\frac{u_0}{a_0^2}(u_0+v_0')\right\}\right]U_1 = T_1, \tag{423a}$$

where

153

$$T_1 \equiv - \frac{2}{\gamma} P_0 + 2V_\infty [\frac{u_0}{a_0^2} + \frac{v_0^2}{a_0^4} (\gamma-1)(u_0 + v_0')]U_0$$

$$+ \frac{2V_\infty v_0}{a_0^2} V_0 + \frac{S_1(\beta)}{\gamma(\gamma-1)V_\infty} \frac{a_0^2}{v_0^2 I} [\frac{v_0}{\theta} - (1 + \frac{\gamma v_0^2}{a_0^2})(u_0 + v_0')]$$

$$+ \frac{1}{\theta^2} [\frac{S_1(\beta)}{\gamma(\gamma-1)V_\infty I^2} \int_\beta^\theta \frac{I a_0^2}{v_0} d\theta$$

$$+ \frac{2V_\infty}{I^2} \int_\beta^\theta \frac{I^2}{v_0} (\theta W_0 + U_0) d\theta] \quad . \tag{423b}$$

Equation (421) shows that U' is singular at $\theta = \delta$ since $v_0(\delta) = 0$. It is useful to introduce a new variable $U_1^*(\theta)$, which is not singular, to replace $U_1(\theta)$. As suggested by Equation (421), write

$$U_1(\theta) = 2U_1^*(\theta) + \frac{S_1(\beta)}{\gamma(\gamma-1)V_\infty} \int_\beta^\theta \frac{a_0^2(\theta)}{v_0 I} d\theta \tag{424a}$$

such that

$$V_1(\theta) = U_1^{*'}(\theta) \quad , \tag{424b}$$

in agreement with Equation (421). Substitution of Equation (424a) into Equation (423a) gives

$$(1 - \frac{v_0^2}{a_0^2})U_1^{*''} + [\frac{1}{\theta} - \frac{v_0}{a_0^2} \{2u_0 + (u_0 + v_0')(2 + (\gamma-1) \frac{v_0^2}{a_0^2})\}]U_1^{*'} +$$

$$2[3 - \frac{u_0^2}{a_0^2} - \frac{1}{2\theta^2} - \frac{v_0^2}{a_0^2} \{1 + (\gamma-1) \frac{u_0}{a_0^2} (u_0 + v_0')\}] U_1^* = T_1^* , \tag{425a}$$

where

$$T_1^* = - \frac{P_0}{\gamma} + \frac{V_\infty}{a_0^2} [u_0 + \frac{v_0^2}{a_0^2} (\gamma-1)(u_0 + v_0')]U_0 + \frac{V_\infty v_0}{a_0^2} V_0$$

$$+ \frac{S_1(\beta)}{\gamma(\gamma-1)V_\infty} \frac{u_0}{I} [u_0 - \{3 - \frac{u_0^2}{a_0^2} - \frac{1}{2\theta^2} - \frac{v_0^2}{a_0^2} (1 + \frac{\gamma-1}{a_0^2} u_0(u_0 + v_0'))\} \int_\beta^\theta \frac{a_0^2}{v_0 I} d\theta]$$

$$+ \frac{1}{2\theta^2} [\frac{S_1(\beta)}{\gamma(\gamma-1)V_\infty} \frac{1}{I^2} \int_\beta^\theta \frac{I a_0^2}{v_0} d\theta + \frac{2V_\infty}{I^2} \int_\beta^\theta \frac{I^2}{v_0} (\theta W_0 + U_0) d\theta] \quad . \tag{425b}$$

154

The singular behavior has been removed from the inhomogeneous term.

An approximate solution to Equation (425a) is obtained by a process analogous to the previous analysis for U_0. To begin, the ratio v_0/a_0 on the left side of Equation (423a) is ignored since it vanishes at the body and is small at the shock at least for large K_δ. In the coefficient of U_1^*, however, the ratio u_0^2/a_0^2 is not small for large M_∞. Since $u_0 \simeq V_\infty$ and $a_0 \simeq a_0(\beta)$, the result is

$$\frac{u_0^2(\theta)}{a_0^2(\theta)} \simeq \frac{V_\infty^2}{a_0^2(\beta)} = \frac{\kappa^2}{2\delta^2} \quad , \tag{426a}$$

where

$$\kappa^2 \equiv \frac{2K_\delta^2(1 + \frac{\gamma+1}{2} K_\delta^2)}{(1 + \gamma K_\delta^2)(1 + \frac{\gamma-1}{2} K_\delta^2)} \quad . \tag{426b}$$

Use was made of expression (400a). Consistent with the hypersonic small-disturbance approximations, it can be seen that the factor u_0^2/a_0^2 should be retained since it is of order $1/\delta^2$ when K_δ is held fixed. Thus Equation (425a) is approximated by the equation

$$U_1^{*\prime\prime} + \frac{1}{\theta} U_1^{*\prime} - (\frac{\kappa^2}{\delta^2} + \frac{1}{\theta^2})U_1^* = T_1^* \quad . \tag{427}$$

Before dealing with this equation, an alternative form for the inhomogeneous term T_1^* is obtained

When $a_0^2(\theta) \simeq a_0^2(\beta)$ is treated as a constant in the integrals in Equation (425b) for T_1^*, and Equation (409) is used to evaluate the integral with $\theta W_0 + U_0$, the results are

$$T_1^* = - \frac{P_0}{\gamma} + \frac{V_\infty}{a_0^2} (u_0 U_0 + v_0 V_0) + \frac{V_\infty v_0^2}{a_0^4} (\gamma-1)(u_0 + v_0')U_0$$

$$+ \frac{S_1(\beta)}{\gamma(\gamma-1)} [1 + \frac{a_0^2}{V_\infty^2} \{-3 + \frac{v_0^2}{a_0^2} (1 + \frac{(\gamma-1)}{a_0^2} u_0(u_0 + v_0'))\}(1 - \frac{1}{I})]$$

$$+ \frac{1}{2\theta^2} \frac{a_0^2(\beta)}{\gamma(\gamma-1)V_\infty^2} [S_1(\beta) \frac{I^2-1}{I^2} - S_0(\beta) \frac{(I-1)^2}{I^2}] \quad . \tag{428}$$

The term $a_0{}^2/V_\infty{}^2$ is of order δ^2 when $K\delta$ is fixed and can be neglected in the coefficient of $S_1(\beta)$. Further, the second term on the right side of Equation (428) can be replaced by means of (406a), and $T_1{}^*$ can be approximated by the hypersonic-similarity form

$$T_1{}^* \equiv - \frac{2P_0}{\gamma} + \frac{V_\infty v_0{}^2}{a_0{}^4} (\gamma-1)(u_0 + v_0{}')U_0$$

$$+ \frac{S_1(\beta) - S_0(\beta)}{\gamma(\gamma-1)}$$

$$+ \frac{1}{2\theta^2} \frac{a_0{}^2(\beta)}{\gamma(\gamma-1)V_\infty{}^2} [S_1(\beta) \frac{I^2-1}{I^2} - S_0(\beta) \frac{(I-1)^2}{I^2}] . \tag{429}$$

It can be established that $T_1{}^*$ is of order $1/\delta$.

Now return to Equation (427) which, by defining the new variable

$$\phi \equiv \kappa \frac{\theta}{\delta} = \kappa z , \tag{430}$$

can be rewritten in the form

$$\frac{d^2}{d\phi^2} U_1{}^* + \frac{1}{\phi} \frac{dU_1{}^*}{d\phi} - (1 + \frac{1}{\phi^2})U_1{}^* = \frac{\delta^2}{\kappa^2} T_1{}^* . \tag{431}$$

This is the inhomogeneous form of the equation for the modified Bessel functions of the first and second kinds, $I_1(\phi)$ and $K_1(\phi)$. The solution that satisfies the initial shock conditions $U_1{}^*(\theta = \beta) = \frac{1}{2} U_1(\beta)$ and $U_1{}^{*'}(\theta = \beta) = V_1(\beta)$ is

$$U_1{}^*(\theta) = A I_1(\phi) + B K_1(\phi)$$

$$+ \frac{\delta^2}{\kappa^2} [I_1(\phi) \int_{\kappa\sigma}^{\phi} \phi K_1(\phi)T_1{}^* d\phi - K_1(\phi) \int_{\kappa\sigma}^{\phi} \phi I_1(\phi)T_1{}^* d\phi] , \tag{432}$$

$$U_1{}^{*'}(\theta) \equiv V_1(\theta) = \frac{\kappa}{\delta} [A I_1{}'(\phi) + B K_1{}'(\phi)]$$

$$+ \frac{\delta}{\kappa} [I_1{}'(\phi) \int_{\kappa\sigma}^{\phi} \phi K_1(\phi)T_1{}^* d\phi - K_1{}'(\phi) \int_{\kappa\sigma}^{\phi} \phi I_1(\phi)T_1{}^* d\phi] , \tag{433}$$

where

$$A \equiv \beta V_1(\beta) K_1(\kappa\sigma) - \kappa\sigma U_1{}^*(\beta)K_1{}'(\kappa\sigma) , \tag{434a}$$

$$B \equiv \kappa\sigma U_1{}^*(\beta)I_1{}'(\kappa\sigma) - \beta V_1(\beta) I_1(\kappa\sigma) , \tag{434b}$$

156

and the Wronskian is

$$K_1(\phi)\, I_1'(\phi) - I_1(\phi)\, K_1'(\phi) \equiv 1/\phi \quad . \tag{435}$$

The shock boundary conditions, from Equations (374a,b), are

$$U_1{}^*(\beta) = \frac{1}{2}\, U_1(\beta) = \frac{\delta g_1}{\sigma} \quad , \tag{436a}$$

$$V_1(\beta) = g_1\left[-\frac{8}{\gamma+1} + \frac{1}{\sigma^2}\right] + g_0\left[-\frac{4}{\gamma+1} + \frac{1}{\sigma^2}\right] \quad . \tag{436b}$$

Further, the entropy functions are, from Equation (382b),

$$\frac{S_0(\beta)}{\gamma(\gamma-1)} = -\frac{\kappa^2}{2\delta\sigma^3}\, g_0 \quad , \tag{437a}$$

$$\frac{S1(\beta)}{\gamma(\gamma-1)} = -\frac{\kappa^2}{2\delta\sigma^3}(2g_1 + g_0) \quad . \tag{437b}$$

The shock-shape parameter g_1 is determined by imposing the surface boundary condition $V_1(\delta) = -1$. Equation (433) then gives

$$-1 = \frac{\kappa}{\delta}[A I_1'(\kappa) + B K_1{}^1(\kappa)]$$

$$+ \frac{\delta}{\kappa}[I_1'(\kappa) \int_{\kappa\sigma}^{\kappa} \phi K_1(\phi) T_1{}^* d\phi - K_1'(\kappa) \int_{\kappa\sigma}^{\kappa} \phi I_1(\phi) T_1{}^* d\phi] \quad . \tag{438}$$

The factor $g_1 = g_1(K_\delta, \gamma)$ can be factored out and solved for explicitly in terms of quadratures, but the quadratures must be evaluated numerically. Figure 44 shows g_1 as a function of K_δ, which will be discussed later. With g_1 determined, the flow variables describing the shock-layer structure can then be obtained in terms of quadratures which must be evaluated numerically. These results will also be discussed later.

k. Approximate Solution for the Pure Plunging Problem for $n = 0$.

For the pure plunging problem, the $n = -1$ variables given by Equations (402) and (403) constitute the inhomogeneous terms in Equations (366) for the $n = 0$ variables. Equation (366e) yields the integral

$$P_0 - \gamma R_0 = S_0{}^P(\beta) \equiv p_0(\beta) - \gamma R_0(\beta) \quad ,$$

$$= -\frac{\kappa^2\gamma(\gamma-1)}{2\delta\sigma^3}(g_0 + g_{-1}) \tag{439}$$

Here recall that $q_{-1} = -1$. The total enthalpy equation (366d) becomes

$$J_0' = \frac{-\delta^2}{\theta^2} \quad , \tag{440}$$

which has the integral

$$J_0(\theta) = J_0^P(\beta) + \delta^2\left(\frac{1}{\theta} - \frac{1}{\beta}\right) \quad , \tag{441}$$

$$= \frac{\delta^2}{\theta}$$

Here it was determined that $J_0^P(\beta)$ has t'$\quad$value as prescribed by Equation (384):

$$J_0^P(\beta) = -\frac{\delta}{\sigma} q_{-1} = \frac{\delta}{\sigma} \quad . \tag{442}$$

Equations (439) and (441) allow the pressure and density functions to be determined in terms of the velocities. Thus are obtained

$$P_0(\theta) = -\frac{\gamma V_\infty^2}{a_0^2(\theta)}\left[\frac{u_0}{V_\infty} u_0 + \frac{v_0}{V_\infty} V_0 - \frac{\delta^2}{\theta}\right] - \frac{S_0^P(\beta)}{\gamma-1} \quad , \tag{443}$$

$$R_0(\theta) = -\frac{V_\infty^2}{a_0^2(\theta)}\left[\frac{u_0}{V_\infty} U_0 + \frac{v_0}{V_\infty} V_0 - \frac{\delta^2}{\theta}\right] - \frac{S_0^P(\beta)}{\gamma-1} \quad . \tag{444}$$

Since $U_{-1} = 0$, Equation (366a) yields the same result as for the pure pitching problem:

$$V_0 = U_0' \quad . \tag{445}$$

With this result, Equation (366c) can be dealt with analogously to the pure pitching problem, and thus is obtained

$$\theta W_0 + U_0 = -\frac{S_0^P(\beta)}{\gamma(\gamma-1)V_\infty I} \int_\beta^\theta \frac{I a_0^2}{v_0} d\theta \quad . \tag{446}$$

The previous results can now be substituted into the continuity equation (366a) to obtain a single equation for U_0:

$$\left(1 - \frac{v_0^2}{a_0^2}\right)U_0'' + \frac{1}{\theta}\left[1 - \frac{v_0(u_0 + v_0')}{a_0^2}\left(2 + (\gamma-1)\frac{v_0^2}{a_0^2}\right)\right] U_0'$$

$$+ \left[2 - \frac{1}{\theta^2} - \frac{v_0^2}{a_0^2}\left(1 + (\gamma-1)\frac{u_0(u_0 + v_0')}{a_0^2}\right)\right]U_0 = T_0^P \quad , \tag{447}$$

158

where

$$T_0{}^P = - \frac{P_{-1}}{\gamma} - \delta^2 V_\infty v_0 \left(\frac{1}{\theta a_0{}^2}\right)' + \frac{1}{\theta^2} \frac{S_0{}^P(\beta)}{\gamma(\gamma-1)V_\infty I} \int_\beta^\theta \frac{I a_0{}^2}{v_0} d\theta \quad,$$

$$= - \frac{2V_\infty{}^2}{a_0{}^2} \frac{\delta^2}{\theta} (1 - \frac{\delta^2}{\theta})[1 - \frac{\gamma-1}{2} \frac{v_0}{a_0{}^2} (u_0 + v_0')] + \frac{1}{\theta^2} \frac{S_0{}^P(\beta)}{\gamma(\gamma-1)V_\infty I} \int_\beta^\theta \frac{I a_0 a_0{}^2}{v_0} d\theta \quad,$$

$$= - \frac{2V_\infty{}^2}{a_0{}^2} \frac{\delta^2}{\theta} (1 - \frac{\delta^2}{\theta^2})[1 - \frac{\gamma-1}{2} \frac{V_\infty{}^2 \delta^2}{a_0{}^2} (1 - \frac{\delta^2}{\theta^2})] + \frac{1}{\theta^2} \frac{S_0{}^P(\beta)}{\gamma(\gamma-1)V_\infty I} \int_\beta^\theta \frac{I a_0 a_0{}^2}{v_0} d\theta \quad.$$

$$(448)$$

This equation has the same form as the pure pitching case, but the inhomogeneous function $T_0{}^P$ is different.

The same approximations for the left side of Equation (447) can be made as for the pure pitching problem, and the approximating equation is thus

$$U_0'' + \frac{1}{\theta} U_0' - \frac{1}{\theta^2} U_0 = T_0{}^P \quad. \tag{449}$$

The solution to this equation that satisfies the shock conditions for U_0 and V_0 has the same form as Equation (412):

$$U_0(\theta) = U_0(\beta) \frac{\theta}{\beta} + \frac{1}{2} [\beta V_0(\beta) - U_0(\beta)][\frac{\theta}{\beta} - \frac{\beta}{\theta}]$$

$$+ \frac{\theta}{2} \int_\beta^\theta T_0{}^P d\theta - \frac{1}{2\theta} \int_\beta^\theta \theta^2 T_0{}^P d\theta \quad. \tag{450}$$

The shock bo. .ary conditions from Equations (374a,b) are

$$U_0(\beta) = \delta q_0/\sigma \quad, \tag{451}$$

$$V_0(\beta) = -(q_0 + q_{-1})(\frac{4}{\gamma+1}) + \frac{1}{\sigma^2} q_{-1} \quad. \tag{452}$$

Recalling that $q_{-1} = -1$, evaluate the integrals in Equation (450) and obtain (with $z = \theta/\delta$)

$$U_0(\theta) = \delta(q_0-1)[\frac{z}{\sigma^2} - \frac{1}{2} (\frac{4}{\gamma+1} + \frac{1}{\sigma^2})(z - \frac{\sigma^2}{z})$$

$$- \frac{1}{\sigma^3} \left\{ -1 + \frac{\sigma}{4z} + \frac{3}{4} \sqrt{\frac{z^2-1}{\sigma^2-1}} + \frac{2z^2 + 1}{4z\sqrt{\sigma^2-1}} \ln \left[\frac{\sigma + \sqrt{\sigma^2-1}}{z + \sqrt{z^2-1}} \right] \right\}$$

$$+ \frac{\delta}{z} + \frac{\kappa^2\delta}{2} \left[\left\{ \frac{(z^2+1)}{z} \ln \frac{\sigma}{z} + \frac{1+\sigma^2}{2\sigma^2} \frac{(z^2-\sigma^2)}{z} \right\} \right.$$

$$- \frac{\gamma-1}{4} \kappa^2 \left\{ \frac{(z^2+2)}{z} \ln \frac{\sigma}{z} + \frac{z}{4\sigma^4} (2\sigma^4 + 4\sigma^2 - 1) \right.$$

$$\left. \left. + \frac{1}{2\sigma^2z} (1 - 2\sigma^2 - \sigma^4) - \frac{1}{4z^3} \right\} \right] \quad . \tag{453}$$

The polar velocity is given by

$$V_0(\theta) = U_0'(\theta) = (g_0-1) \left[\frac{1}{\sigma^2} - \frac{1}{2} \left(\frac{4}{\gamma+1} + \frac{1}{\sigma^2} \right)(1 + \frac{\sigma^2}{z^2}) \right.$$

$$- \frac{1}{4\sigma^3} \left\{ - \frac{\sigma}{z^2} + \frac{1}{z} \sqrt{\frac{z^2-1}{\sigma^2-1}} + \frac{2z^2-1}{z^2\sqrt{\sigma^2-1}} \ln \left[\frac{\sigma + \sqrt{\sigma^2-1}}{z + \sqrt{z^2-1}} \right] \right\}$$

$$- \frac{1}{z^2} + \frac{\kappa^2}{2} \left[\left\{ \frac{z^2-1}{z^2} \ln \frac{\sigma}{z} + \frac{(\sigma^2-1)(\sigma^2-z^2)}{2\sigma^2z^2} \right. \right.$$

$$- \frac{\gamma-1}{4} \kappa^2 \left\{ \frac{z^2-2}{z^2} \ln \frac{\sigma}{z} - \frac{z^2+2}{z^2} + \frac{1}{4\sigma^4} (2\sigma^4 + 4\sigma^2 - 1) \right.$$

$$\left. \left. - \frac{1}{2\sigma^2z^2} (1 - 2\sigma^2 - \sigma^4) + \frac{3}{4z^4} \right\} \right] \quad . \tag{454}$$

The shock-shape factor is determined by imposition of the surface boundary condition $V_0(\delta) = 1$. Solving for g_0 gives

$$\frac{1}{1-g_0} = \frac{- \frac{3}{8\sigma^2} + \frac{\sigma^2+1}{\gamma+1} + \frac{1}{4} + \frac{\ln[\sigma + a\sqrt{\sigma^2-1}]}{8\sigma^3 \sqrt{\sigma^2-1}}}{1 - \frac{\kappa^2}{4} \left[\frac{(\sigma^2-1)^2}{2\sigma^2} - \frac{\gamma-1}{4} \kappa^2 \left(-\ln \sigma + \frac{(\sigma^2-1)(2\sigma^4-\sigma^2+1)}{4\sigma^4} \right) \right]} \tag{455}$$

which is written in a form analogous to formula (417) for the pure pitching problem. The factor g_0 for the pure plunging problem is shown in Figure 45, and it will be discussed later.
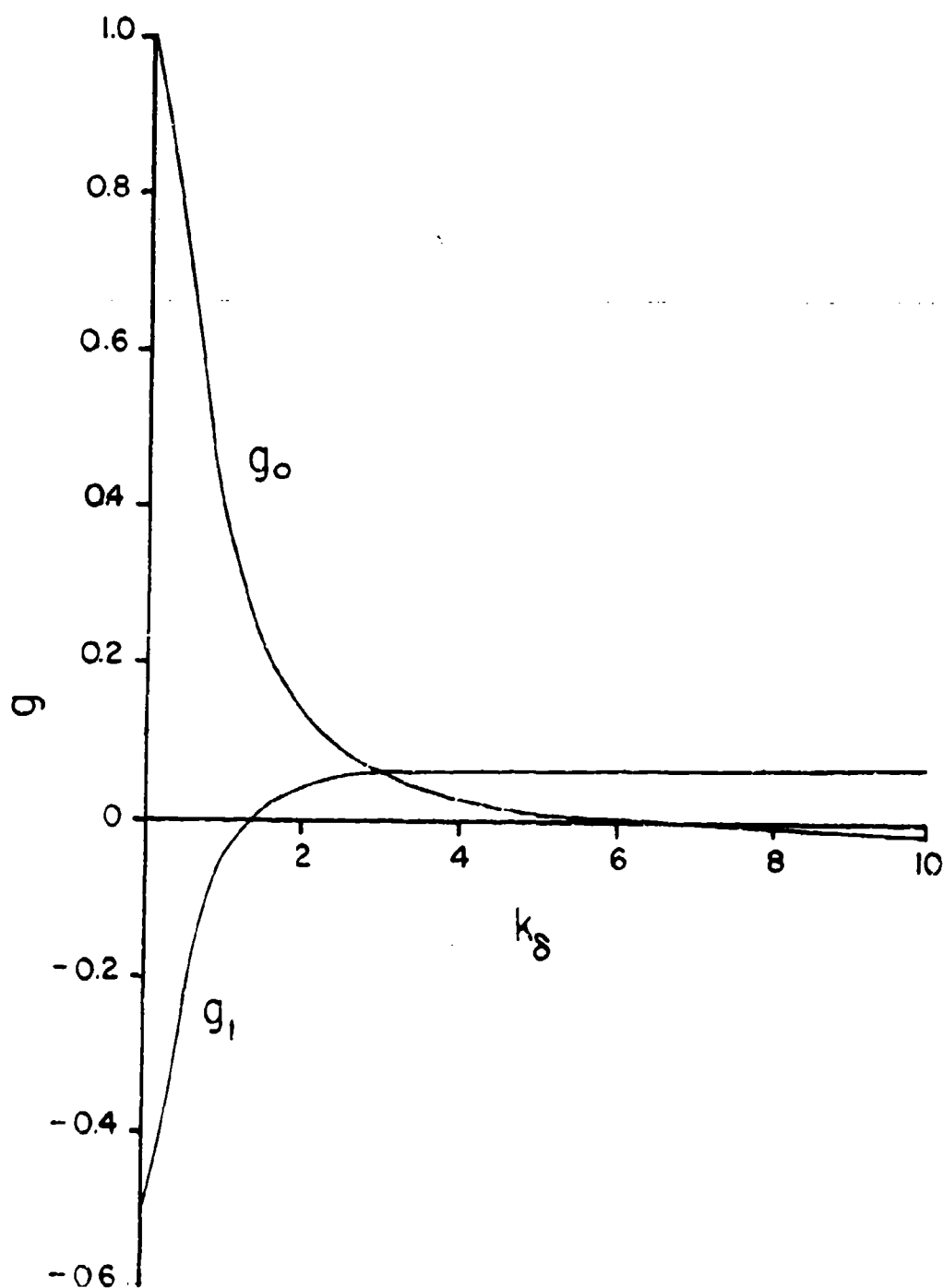
Figure 45. Shock-Shape Parameters g_0 and g_1 for Pure Plunging ($\gamma = 1.4$)

With U_0 and V_0 known, the pressure can be obtained from Equation (443). The solution is

$$\frac{a_0^2(\theta)}{\gamma V_\infty^2} \frac{P_0(\theta)}{\delta} = (g_0-1)\Big[-\frac{1}{\sigma^2 z} + \frac{1}{2z}\Big(\frac{4}{\gamma+1} + \frac{1}{\sigma^2}\Big)(1 - 2\sigma^2 + \frac{\sigma^2}{z^2})$$

$$+ \frac{1}{4\sigma^3}\Big\{\frac{2\sigma}{z} - \frac{\sigma}{z^3} + \sqrt{\frac{z^2-1}{\sigma^2-1}}\ (2 + \frac{1}{z^2})$$

$$\frac{\ln(\sigma + \sqrt{\sigma^2-1}}{}$$

$$+ \Big(\frac{4}{z} - \frac{1}{z^3}\Big) \frac{z + \sqrt{z^2-1})}{\sqrt{\sigma^2-1}}\Big\} + \frac{1-z^2}{z^3} + \frac{\kappa^2}{2}\Big[\frac{1-3z^2}{z^3}\ \ln\frac{\sigma}{z}$$

$$+ \frac{(\sigma^2-z^2)(2\sigma^2 z^2-\sigma^2+1)}{2\sigma^2 z^3} - \frac{\gamma-1}{4}\ \kappa^2\Big\{\frac{2-5z^2}{z^3}\ \ln\frac{\sigma}{z}$$

$$+ \frac{(\sigma^2-z^2)[2\sigma^4 z^2(2z^2-1) - z^2 + \sigma^2(8z^2-3)]}{4\sigma^4 z^5}\Big\}\Big]$$

$$+ \frac{(g_0-1)}{\sigma^3}\ \Big[\frac{a_0^2(\theta)}{a_0^2(\beta)} - 1\Big]\ . \tag{456}$$

Numerical results for these functions will be discussed later.

1. Approximate Solution for the Pure Plunging Problem for $n = 1$.

The equations for $n = 1$ for pure plunging take the same form as the equations in Section II-4i for pure pitching about the vertex, only with $S_0(\beta)$ replaced by $S_0^P(\beta)$ and the inhomogeneous $n = 0$ terms evaluated by the appropriate plunging functions. The appropriate equation for $U_1^*(\theta)$, defined by Equation (424a), is Equation (431), which is rewritten here:

$$\frac{d^2 U_1^*}{d\phi^2} + \frac{1}{\phi}\ \frac{dU_1^*}{d\phi} - (1 + \frac{1}{\phi^2})U_1^* = \frac{\delta^2 T_1^* P}{\kappa^2}\ , \tag{457}$$

where

$$T_1^* P \equiv -\frac{2P_0}{\gamma} + \frac{V_\infty v_0^2}{a_0^4}(\gamma-1)(u_0 + v_0')U_0 + \frac{V_\infty^2}{a_0^2}\ \frac{\delta^2}{\theta}$$

$$+ \frac{S_1(\beta) - S_0^P(\beta)}{\gamma(\gamma-1)}$$

162

$$+ \frac{1}{2\theta^2} \frac{a_0^2(\beta)}{\gamma(\gamma-1)V_\infty^2} \left[S_1(\beta) \frac{I^2-1}{I^2} - S_0 P(\beta) \frac{(I-1)^2}{I^2} \right] . \quad (458)$$

The solution to this problem that satisfies the shock conditions, which a e the same as Equations (436a,b), is given in terms of the modified Bessel functions by Equations (432) and (433), with T_1^* replaced by $T_1^* P$.

The surface boundary condition for the $n = 1$ pure plunging problem is given by Equation (371c): $V_1(\delta) = 0$. This condition is different from the corresponding pure pitching case. Thus the condition that determines the shock shape parameter g_1 should be written

$$0 = \frac{\kappa}{\delta} [AI_1'(\kappa) + BK_1'(\kappa)]$$

$$+ \frac{\delta}{\kappa} [I_1'(\kappa) \int_{\kappa\sigma}^{\kappa} \phi K_1(\phi) T_1^* P \, d\phi - K_1'(\kappa) \int_{\kappa\sigma}^{\kappa} \phi I_1(\phi) T_1^* P \, d\phi] . \quad (459)$$

This equation is analogous to Equation (438) with the left side replaced by zero. The factor $g_1(K_\delta, \gamma)$ is shown in Figure 45. All the other variables can now be computed.

m. Results for the Shock Layer

Figure 44 shows g_0 and g_1 as functions of K_δ for $\gamma = 1.4$ for pure pitching about the vertex. The function g_0 is computed from Equation (417) and g_1 from Equation (438). The function g_0 is equivalent to that obtained for the steady-flow inclined cone by Doty and Rasmussen (Reference 23). As K_δ goes to infinity, g_0 tends asymptotically to $g_0 = 1.057$. The function g_1 is negative and has a minimum near $K_\delta = 1$.

For pure plunging motion, the shock parameter g_{-1} has the value $g_{-1} = -1$. Figure 45 shows g_0 and g_1 for pure plunging as functions of K_δ for $\gamma = 1.4$. The functions g_0 and g_1 are computed by means of Equations (455) and (459). For pure plunging the factor g_0 is positive for small K_δ and tends to $g_0 = -0.016$ as K_δ tends to infinity. The function g_1 is negative for small values

163

of K_δ, being $g_1 = 0.5$ at $K_\delta = 0$, becomes zero at $K_\delta = 1.27$, and tends to a positive asymptote $g_1 = 0.075$ as K_δ goes to infinity.

The shock shape in the inertial coordinate system is given by Equation (346a), which is written here as

$$\theta_s = \beta - [\psi_0 \sum_{n=0}^{\infty} \left(\frac{i\omega r}{V_\infty}\right)^n g_n + \epsilon_z \sum_{n=-1}^{\infty} \left(\frac{i\omega r}{V_\infty}\right)^n g_n{}^p$$

$$+ \epsilon_p \sum_{n=-1}^{\infty} \left(\frac{i\omega r}{V_\infty}\right)^n g_n{}^p] e^{i\omega t} \cos \phi \quad , \tag{460}$$

where

$$\epsilon_z \equiv \frac{i\omega\psi_0 z_0}{V_\infty} , \tag{461a}$$

$$\epsilon_p \equiv \frac{i\omega h_0}{V_\infty} e^{i\Omega} , \tag{461b}$$

and $g_n{}^p$ represents g_n for the pure plunging problem. Note that $\epsilon = \psi_0$ denotes the contribution from pure pitching about the vertex ($z_0 = 0$), ϵ_z denotes the contribution from pitching about $z_0 \neq 0$, and ϵ_p denotes the contribution from pure plunging. This representation is singular at $r = 0$ owing to the terms $n = -1$ arising from pitching about $z_0 \neq 0$ and plunging.

The transformation to the body-fixed system is done by means of Equation (332b):

$$\theta_b = \theta + [\psi_0 - (\epsilon_z + \epsilon_p)\left(\frac{i\omega r}{V_\infty}\right)^{-1}]e^{i\omega t} \cos \phi . \tag{462}$$

Substituting Equation (460) into Equation (462) evaluated at the shock, the result is that the r^{-1} terms cancel out since $g_{-1} = -1$, leaving

$$\theta_{bs} = \beta - [\psi_0\{(g_0-1) + \left(\frac{i\omega r}{V_\infty}\right)g_1 + \ldots\}$$

$$+ \epsilon_z \{g_0{}^p + \left(\frac{i\omega r}{V_\infty}\right) g_1{}^p + \ldots\}$$

$$+ \epsilon_p \{g_0{}^p + \left(\frac{i\omega r}{V_\infty}\right) g_1{}^p + \ldots\}]e^{i\omega t} \cos \phi . \tag{463}$$

Thus the shock shape represented in the body-fixed system is not singular at r = 0. Since ε_z and ε_p are proportional to $i \equiv e^{i\pi/2}$, it can be seen that there is a 90 degree time phase shift associated with pitching about $z_0 \neq 0$ and with plunging, relative to pure pitching about the vertex. When $\omega r/V_\infty$ is sufficiently small, it can be expected that the higher-order terms in the series expansions will be negligible.

The flow variables $Q_n(\theta)$ have been computed in an inertial coordinate system. The series representation in this system is singular as $r \to 0$ owing to the terms for n = -1. It is thus useful to describe the flow in the body-fixed system which is not singular as $r \to 0$ for pitching about $z_0 \neq 0$ and plunging.

Denote variables described in a body-fixed system with a subscript b. Then for any scalar variable write

$$Q_b(\theta_b) = Q(\theta)$$

$$= Q(\theta_b + (\theta - \theta_b)) \ . \tag{464}$$

Since $(\theta - \theta_b)$ is small according to Equation (462), it is possible to use the first term of a Taylor-series expansion and obtain

$$Q_b(\theta_b) = Q(\theta_b) - \left(\frac{\partial Q}{\partial \theta}\right)_{\theta_b} [\psi_0 - (\varepsilon_z + \varepsilon_p)(\frac{i\omega r}{V_\infty})^{-1}]e^{i\omega t} \cos \phi \ . \tag{465}$$

This transformation, when applied to both the scalar and vector variables, is tantamount to removing the n = -1 terms from the series description in the body-fixed coordinates. In addition, however, the n = 0 term for pure pitching about the vertex is affected, as Equation (465) shows. This can also be seen in the expression (464) for the shock shape. Thus for the pressure for pure pitching about the vertex, write

$$P_{b0}(\theta_b) = P_0(\theta_b) - \left(\frac{d \ln p_0}{d\theta}\right)_{\theta_b} \ ,$$

$$= P_0(\theta_b) + [\frac{\gamma v_0}{a_0^2} (u_0 + v_0')]_{\theta_b} \ ,$$

$$= P_0(\theta_b) + \frac{\gamma V_\infty}{a_0{}^2(\theta_b)} \frac{\delta^2}{\theta_b} (1 - \frac{\delta^2}{\theta_b{}^2}) \ . \tag{466}$$

For the velocity components, first use Equations (333) before applying the transformation (465). For the radial velocity, then, the result for the case of pure pitching about the vertex is

$$U_{b0} = U_0(\theta_b) - \frac{v_0(\theta_b)}{V_\infty} \qquad ,$$

$$= U_0(\theta_b) + \theta_b (1 - \frac{\delta^2}{\theta_b{}^2}) \ , \tag{467a}$$

$$V_{b0}(\theta_b) = V_0(\theta_b) - \frac{v_0{}'(\theta_b)}{V_\infty} \qquad ,$$

$$= V_0(\theta_b) + (1 + \frac{\delta^2}{\theta_b{}^2}) \ , \tag{467b}$$

$$W_{b0}(\theta_b) = W_0(\theta_b) - \frac{v_0(\theta_b)}{V_\infty \theta_b} \qquad ,$$

$$= W_0(\theta_b) - (1 - \frac{\delta^2}{\theta_b{}^2}) \ . \tag{467c}$$

For $n > 1$, the first order perturbation problem is $Q_{bn}(\theta_b) = Q_n(\theta)$. Thus in the body-fixed coordinates the functions for $n = -1$ are not present, and only the $n = 0$ functions for pure pitching about the vertex are altered, as shown above.

To illustrate the variation of the velocity and pressure functions between the shock and the body is introduced the normalized angle variable

$$\theta' \equiv \frac{\theta - \delta}{\beta - \delta} \ , \tag{468a}$$

such that $\theta' = 0$ at the body and $\theta' = 1$ at the shock. Equation (468a) represents the inertial coordinate system. For body-fixed coordinates, the corresponding variable is

$$\theta_b{}' \equiv \frac{\theta_b - \delta}{\beta - \delta} \ . \tag{468b}$$

The two variables differ by the order of ε.

Figures 46, 47, and 48 show the variation of U_0/δ, V_0, and W_0, for pure pitching about $z_0 = 0$, across the shock layer with different values of K_δ taken as a parameter and for $\gamma = 1.4$. These representations are for inertial coordinates. The function U_0/δ is positive and decreases from the body to the shock. The function V_0 is negative and increases from the body to the shock. The azimuthal velocity W_0, however, is negative and increases from the body to the shock for small values of K_δ but decreases from the body to the shock for larger values of K_δ. For K_δ of about 2, W_0 is nearly uniform.

Figures 49a, b, and c show the corresponding variations of U_{b0}/δ, V_{b0}, and W_{b0} for pure pitching about $z_0 = 0$ in body-fixed coordinates. These are essentially the same as could be calculated from Doty and Rasmussen (Reference 23). For U_{0b}/δ and W_{b0}, the values at the body, $\theta_b' = 0$, are the same as for these corresponding variables evaluated at the body in the inertial coordinate systems. Comparison of the results in the two different coordinate systems shows the different appearance the functions take in the different representations.

Figure 50 shows the pressure function $a_0^2(\theta)P_0(\theta)/\gamma V_\infty^2 \delta$ for pure plunging about the vertex as it varies across the shock layer, with K_δ as a parameter and $\gamma = 1.4$. The pressure perturbation P_0 is negative and decreases a small amount from the body to the shock for large values of K_δ. For small values of K_δ, P_0 decreases, reaches a minimum, and then increases. Figure 51 shows the corresponding pressure function for body-fixed coordinates, P_{0b}. The pressure P_{0b} shows the same trends as P_0, but the values increase from the body to the shock monotonically.

The reason the two pressure perturbation functions in the two coordinate systems are not the same is associated with the transferral of the actual shock and body locations to the location of the basic shock and basic cone.
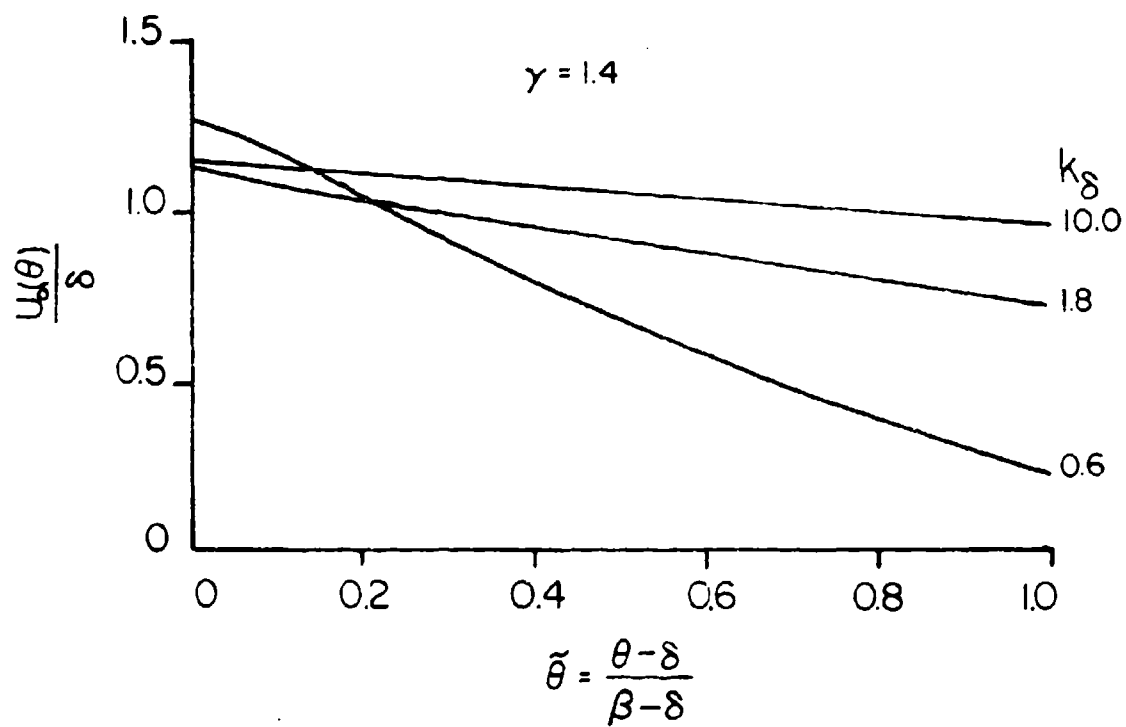
Figure 46   Variation of U_0 Across the Shock Layer in Inertial Coordinates
($\gamma = 1.4$): Pure Pitching About $z_0 = 0$

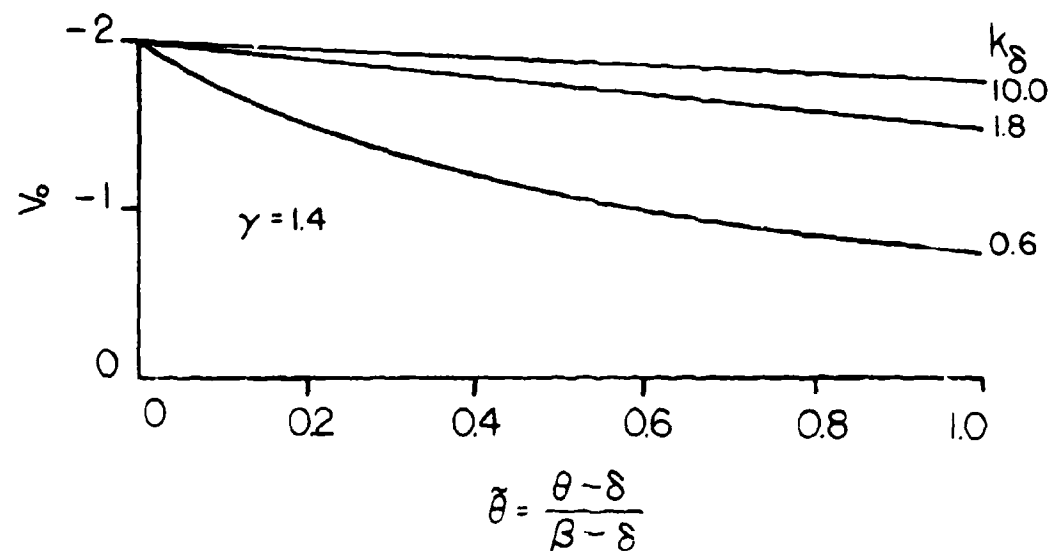Figure 47   Variation of V_θ across the Shock Layer in Inertial Coordinates ($\gamma = 1.4$): Pure Pitching About $z_0 = 0$

Figure 48. Variation of W_0 Across the Shock Layer in Inertial Coordinates ($\gamma = 1.4$); Pure Pitching About $z_0 = 0$

Figure 49.   ...ion of U_{b_0}, V_{b_0}, and W_{b_0} Across the Shock Layer in
                 Fixed Coordinates ($\gamma = 1.4$): Pure Pitching About $z_0 = 0$.
                 U_{b_0}/δ, (b) V_{b_0}, (c) W_0
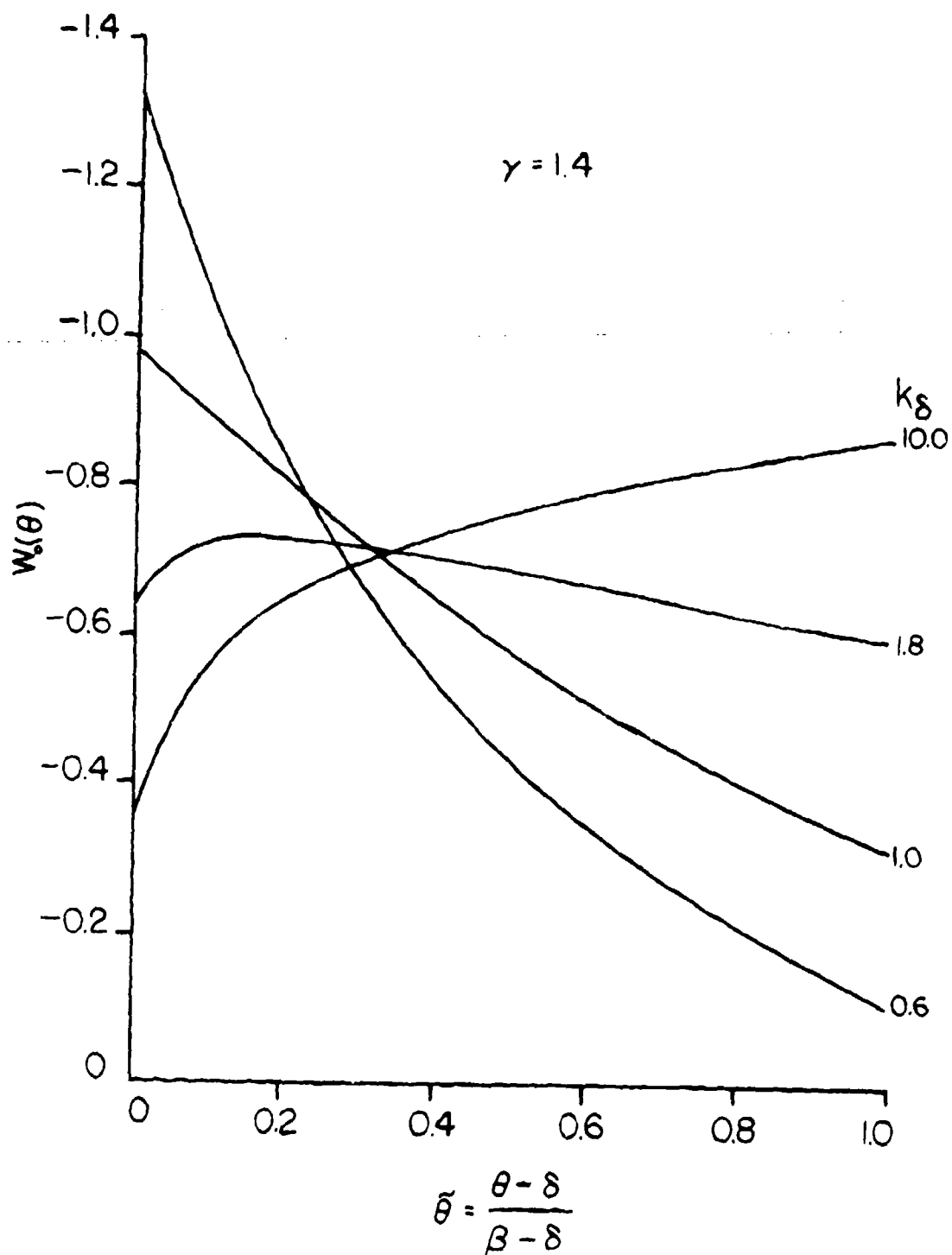
171

Figure 50. Variation of P_0 Across the Shock Layer in Inertial Coordinates ($\gamma = 1.4$): Pure Pitching About $z_0 = 0$

194

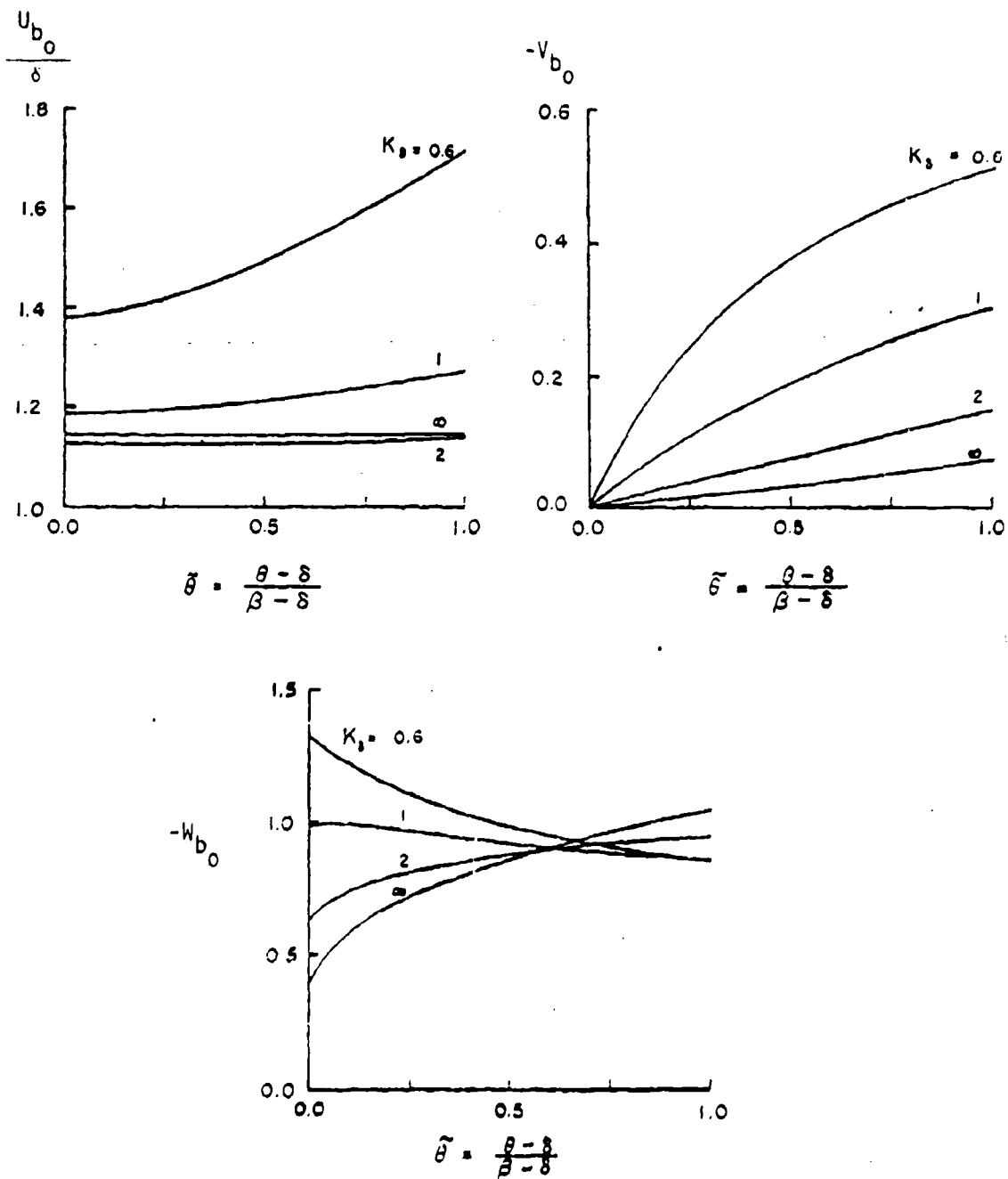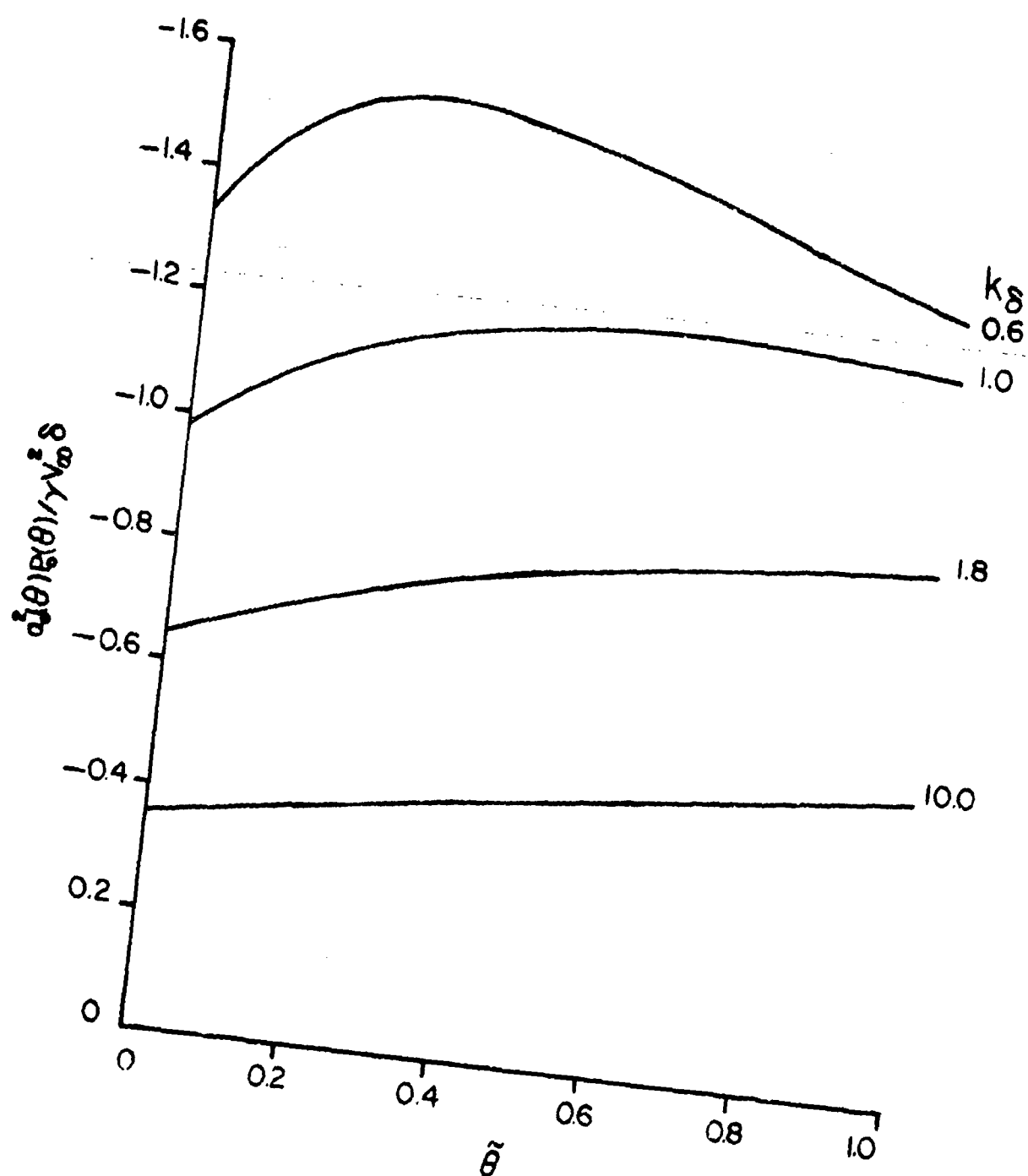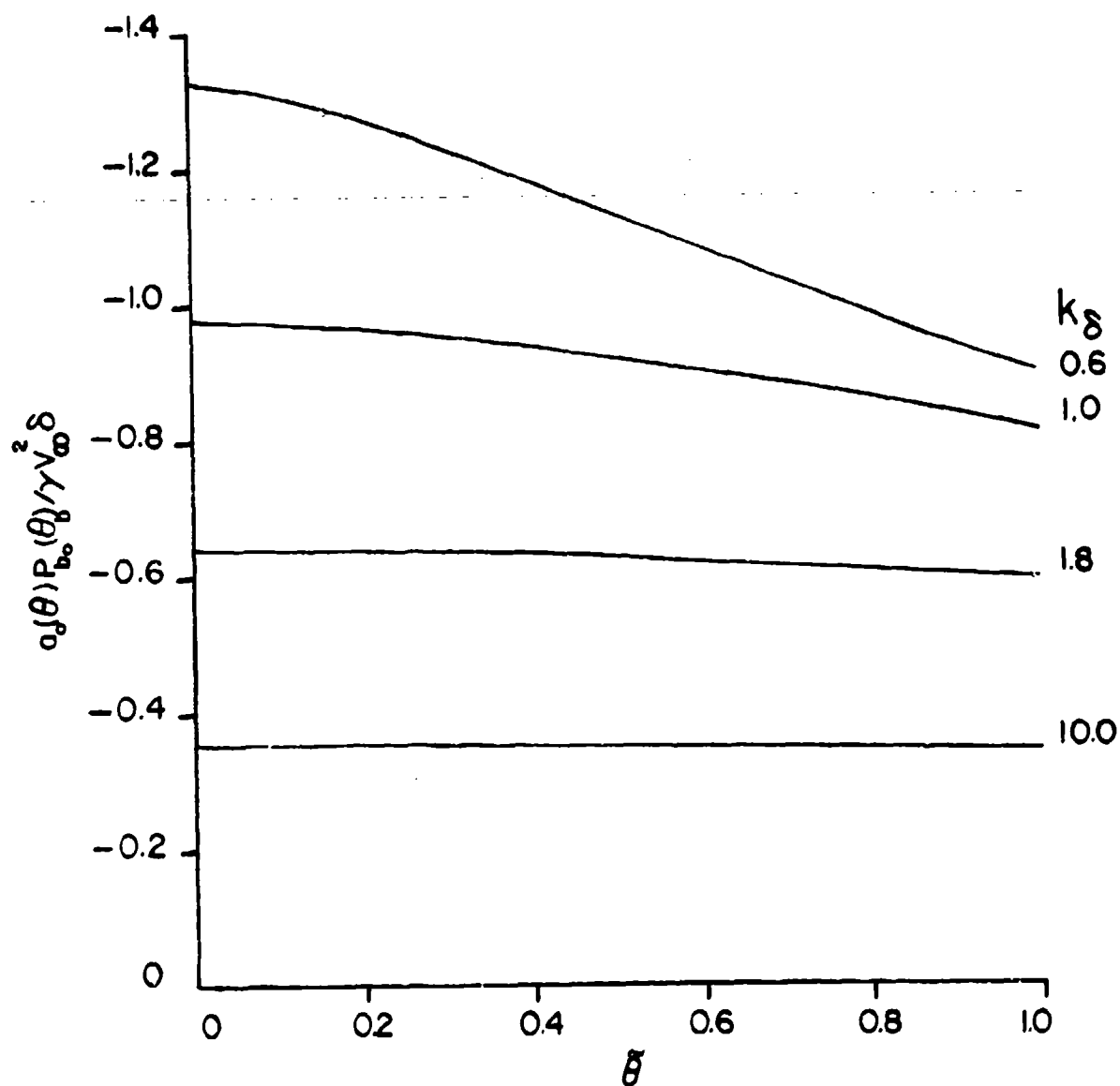Figure 51. Variation of P_b Across the Shock Layer in Body-Fixed Coordinates ($\gamma = 1.4$): Pure Pitching About $z_o = 0$

173

For instance, the pressure at the shock in the two systems can be written to the first order of perturbation as

$$p(\theta_s) = p_0(\beta) + \left(\frac{dp_0}{d\theta}\right)_\beta (\theta_s - \beta) + \epsilon p_0 P_0(\beta) e^{i\omega t} \cos \phi \ , \qquad (469a)$$

$$p(\theta_{bs}) = p_0(\beta) + \left(\frac{dp_0}{d\theta}\right)_\beta (\theta_{bs} - \beta) + \epsilon p_0 P_{b0}(\beta) e^{i\omega t} \cos \phi \ . \qquad (469b)$$

The actual pressure perturbations are given by the second two terms on the right. These two terms must be taken in combination, in either coordinate system, to determine the correct total perturbation.

The variations of U_0/δ, V_0, and W_0 across the shock layer for pure plunging are shown in Figures 52, 53, and 54. These functions are the same for both the inertial and body-fixed coordinate system representations. In these computations the terms arising from the variation of a_0^2 across the shock layer, proportional to $(\gamma-1)$ in Equations (448), (453), (454), (455), and (456), were neglected. The velocity U_0 is negative at the body and increases toward the shock. For large values of K_δ, U_0 is negative at the shock also, but it is positive for smaller values of K_δ. The velocity function V_1 is positive and decreases from the body to the shock. The azimuthal velocity W_0 increases from the body to the shock when K_δ is large, but decreases from the body to the shock when K_δ is small.

The pressure function $a_0^2(\theta)P_0(\theta)/\gamma V_\infty^2 \delta$ for pure plunging is shown as it varies across the shock layer in Figure 55 for $\gamma = 1.4$ and various values of K_δ. The perturbation P_0 is positive and decreases from the body to the shock.

For pure pitching about the vertex, the velocity functions U_1/δ, V_1, and W_1 are shown in Figures 56, 57, and 58 as functions of θ'. Again various values of K_δ are shown and $\gamma = 1.4$. In these computations the second term in Equation (429) for T_1^*, proportional to $(\gamma-1)$, is negligile since it arises out of variations of a_0^2 and is small. For large values of K_δ, U_1 is negative

174
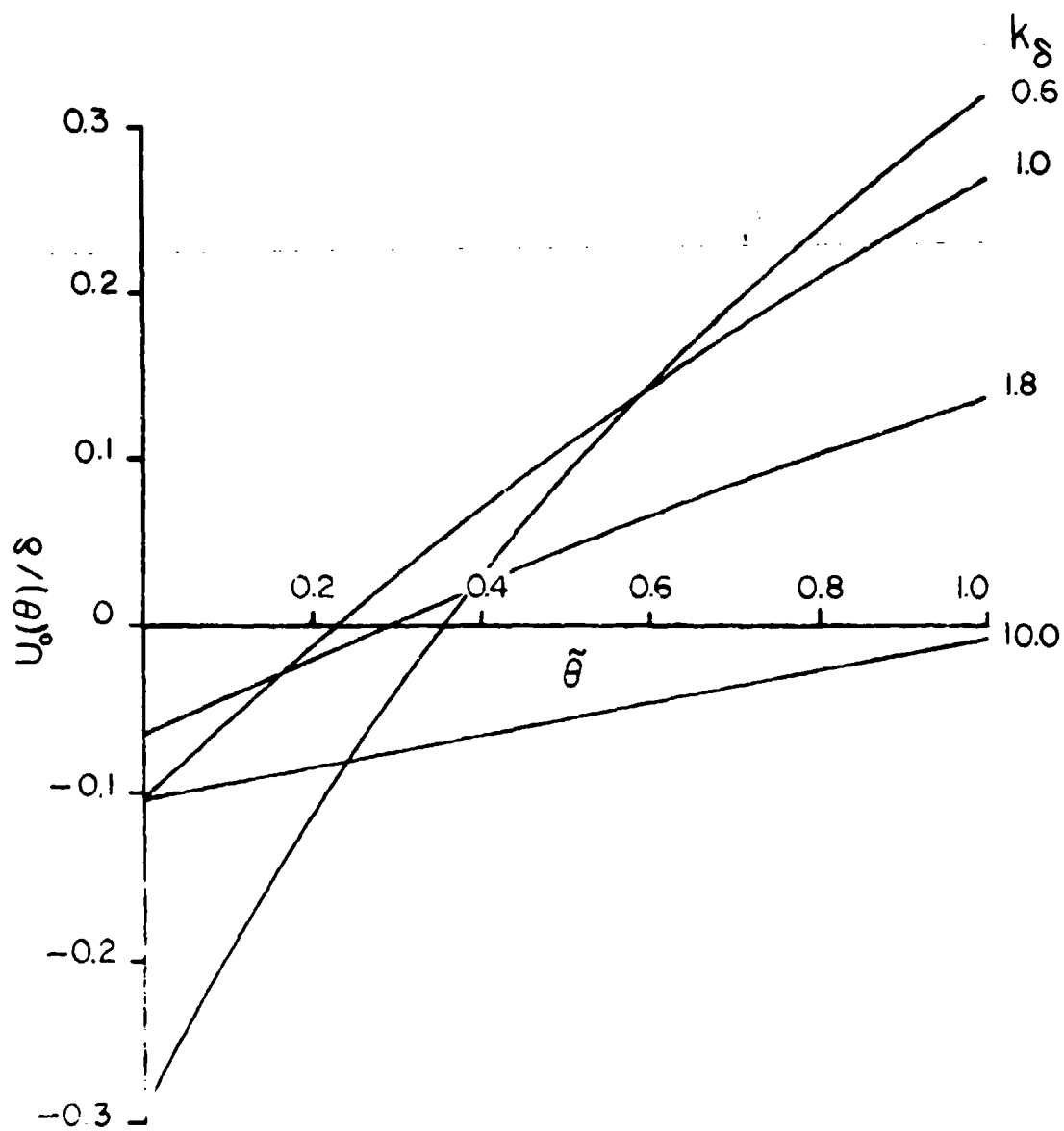
Variation of U_0 Across the Shock Layer ($\gamma = 1.4$): Pure Plunging

Figure 52.   Variation of V_0 Across the Shock Layer ($\gamma = 1.4$): Pure Plunging

Figure   . Variation of W_0 Across the Shock Layer ($\gamma = 1.4$): Pure Plunging

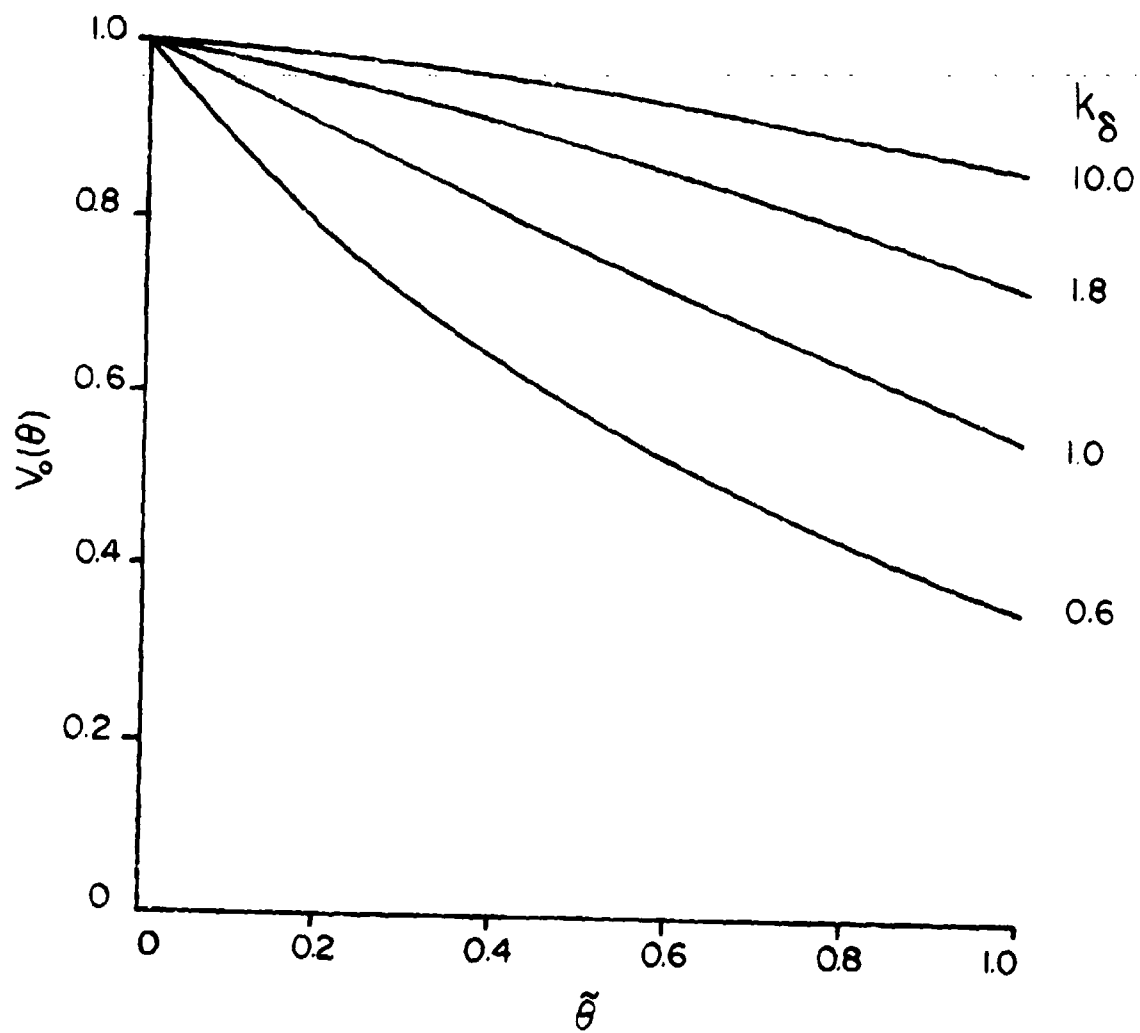Figure 55.   Variation of P_0 Across the Shock Layer (γ = 1.4): Pure Plunging

Figure 56.   Variation of U_1 Across the Shock Layer ($\gamma = 1.4$): Pure Pitching About $z_0 = 0$
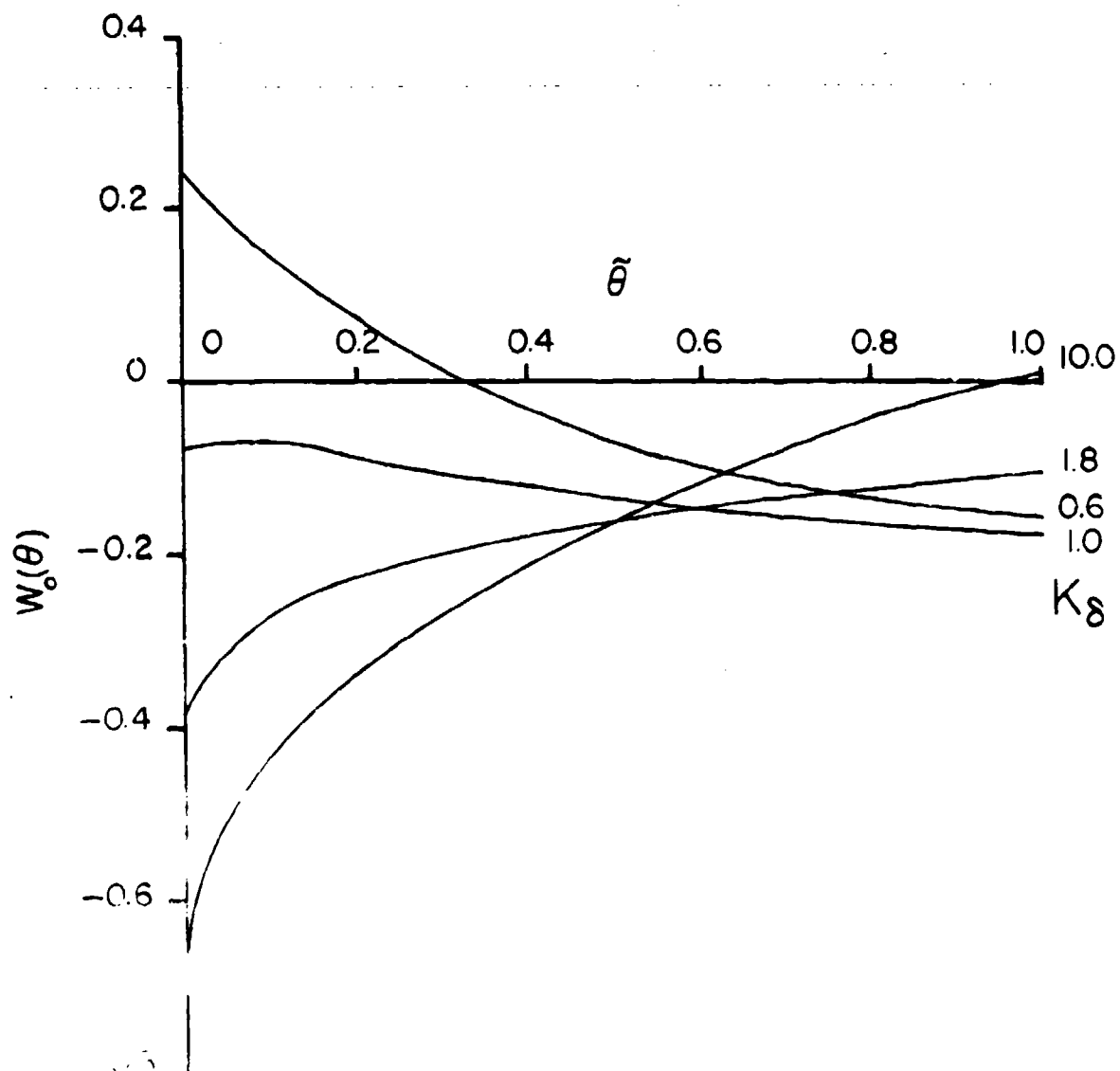
Figure 57.   Variation of V_1 Across the Shock Layer ($\gamma = 1.4$): Pure Pitching
About $z_0 = 0$

202

Figure 58. Variation of W_1 Across the Shock Layer ($\gamma = 1.4$): Pure Pitching About $z_0 = 0$

at the body and increases to positive values at the shock. For K_δ about 2, U_1 varies only slightly across the shock layer. The polar velocity perturbation V_1 decreases from the body to the shock. For small values of K_δ, V_1 is negative at the shock, being positive otherwise. For large values of K_δ, the azimuthal velocity perturbation W_1 is negative and increases from the body to the shock. For small values of K_δ, W_1 decreases from a positive value at the body to a negative value at the shock. The functions are the same in both inertial and body-fixed coordinate descriptions.

For pure pitching about the vertex, the variation of $a_0^2(\theta)P_1(\theta)/\gamma V_\infty^2\delta$ across the shock layer is shown in Figure 59. The pressure perturbation P_1 is positive on the body surface and decreases toward the shock, becoming negative for small values of K_δ.

For pure plunging motions, the velocity perturbations U_1/δ, V_1, and W_1 are shown in Figures 60, 61, and 62 as functions of θ. In these computations the second term in Equation (458) for T_1^*P, proportional to $(\gamma-1)$, is negligible since it arises from the small variation of a_0^2 across shock layer. The velocity perturbation U_1 is positive at the body and increases toward the shock for large values of K_δ. For small values of K_δ, it is positive at the body and decreases to negative values at the shock. The polar velocity perturbation V_1 decreases from zero at the body to negative values at the shock. The azimuthal velocity W_1 increases from negative values at the body, becoming positive at the shock for small K_δ.

For pure plunging, the variation of $a_0^2(\theta)P_1(\theta)/\gamma V_\infty^2\delta$ across the shock layer is shown in Figure 63. The pressure perturbation P_1 is positive at the body and decreases to negative values at the shock for all K_δ.

n. Forces

For inviscid flow, the forces on a body arise from the pressures exerted

182

Figure 59.   Variation of P_1 Across the Shock Layer ($\gamma = 1.4$): Pure Pitching
About $z_0 = 0$

Figure 60.   Variation of U_1 Across the Shock Layer ($\gamma = 1.4$): Pure Plunging

Figure 61.   Variation of V_1 Across the Shock Layer ($\gamma = 1.4$): Pure Plunging

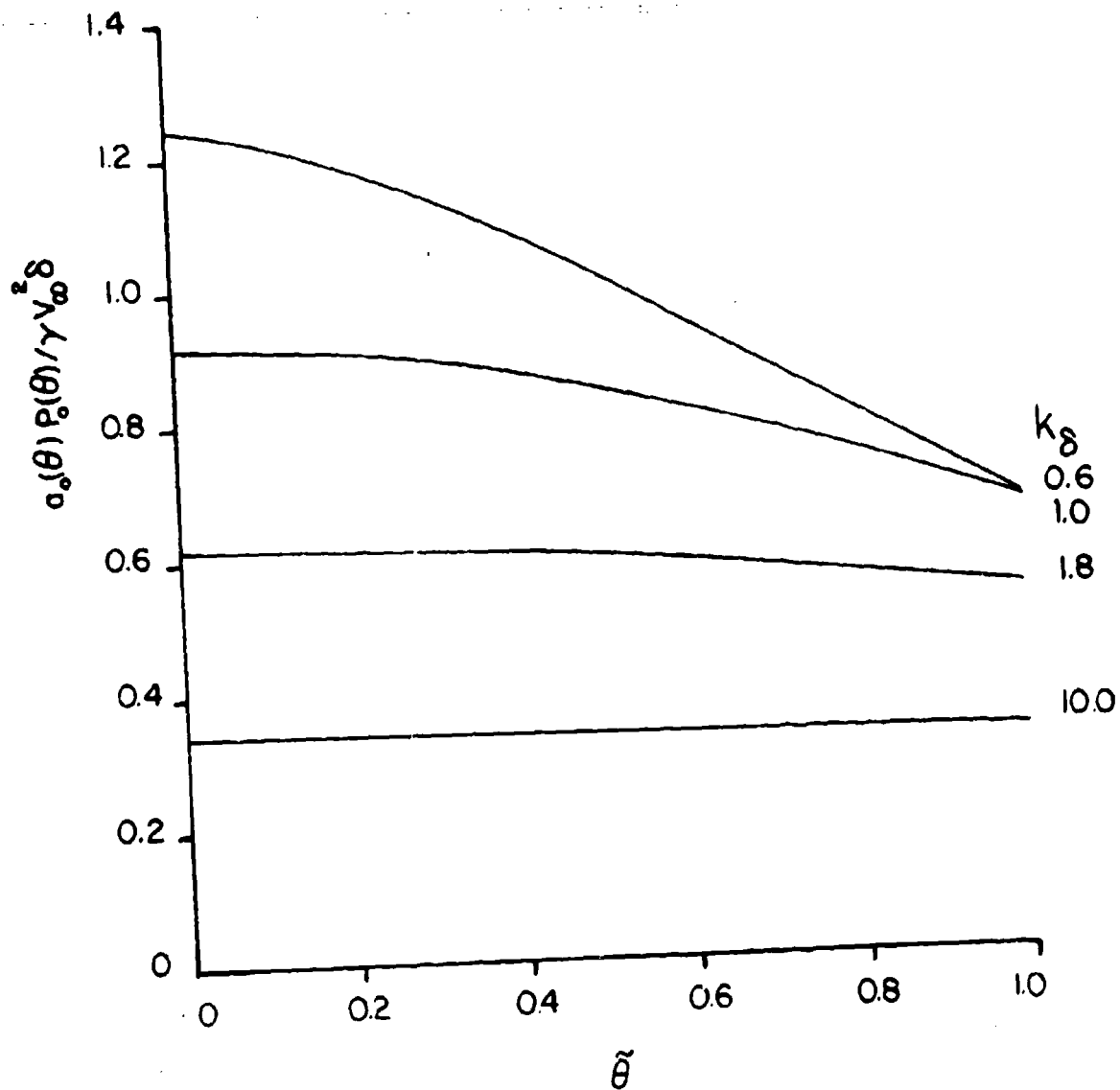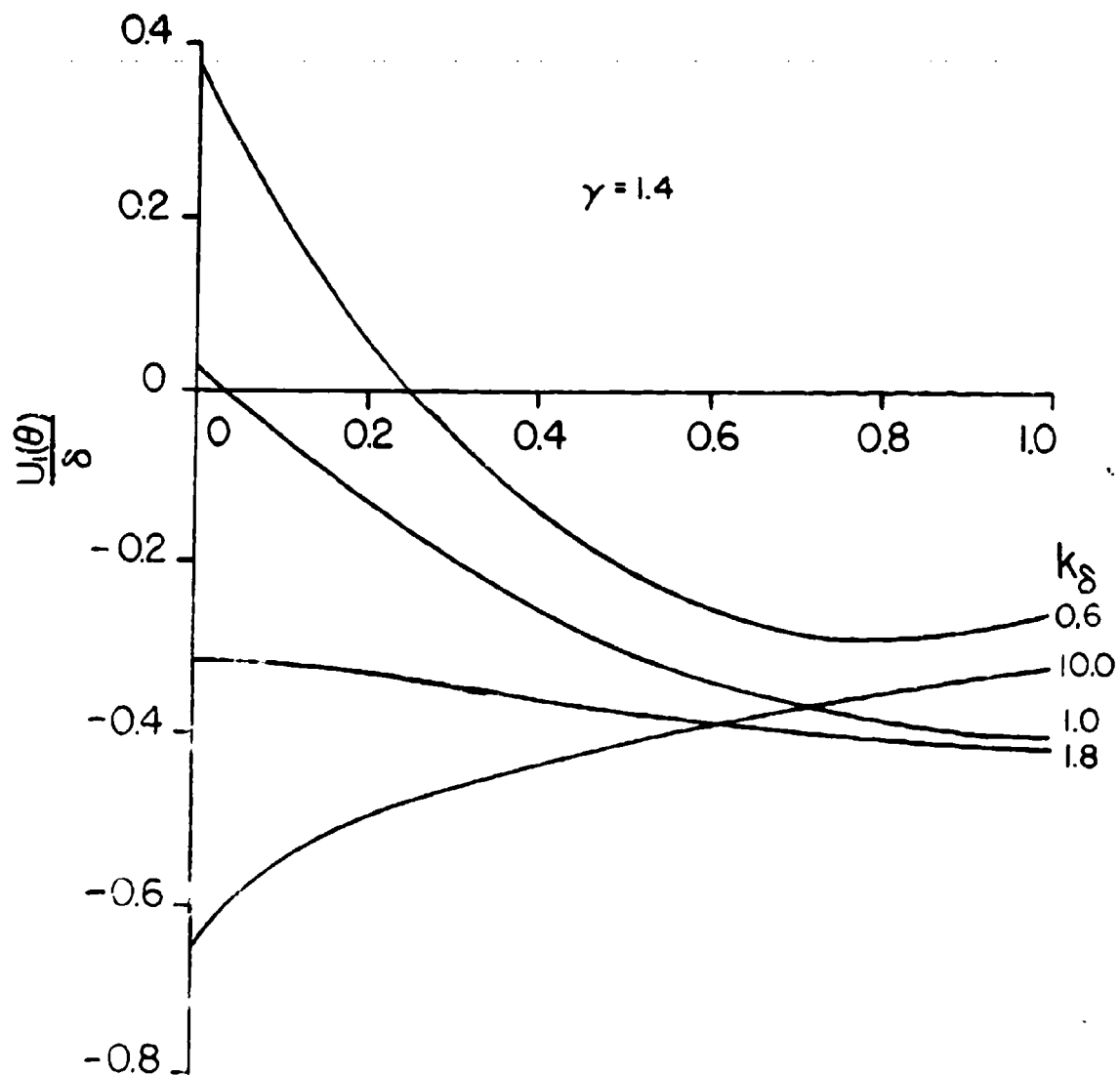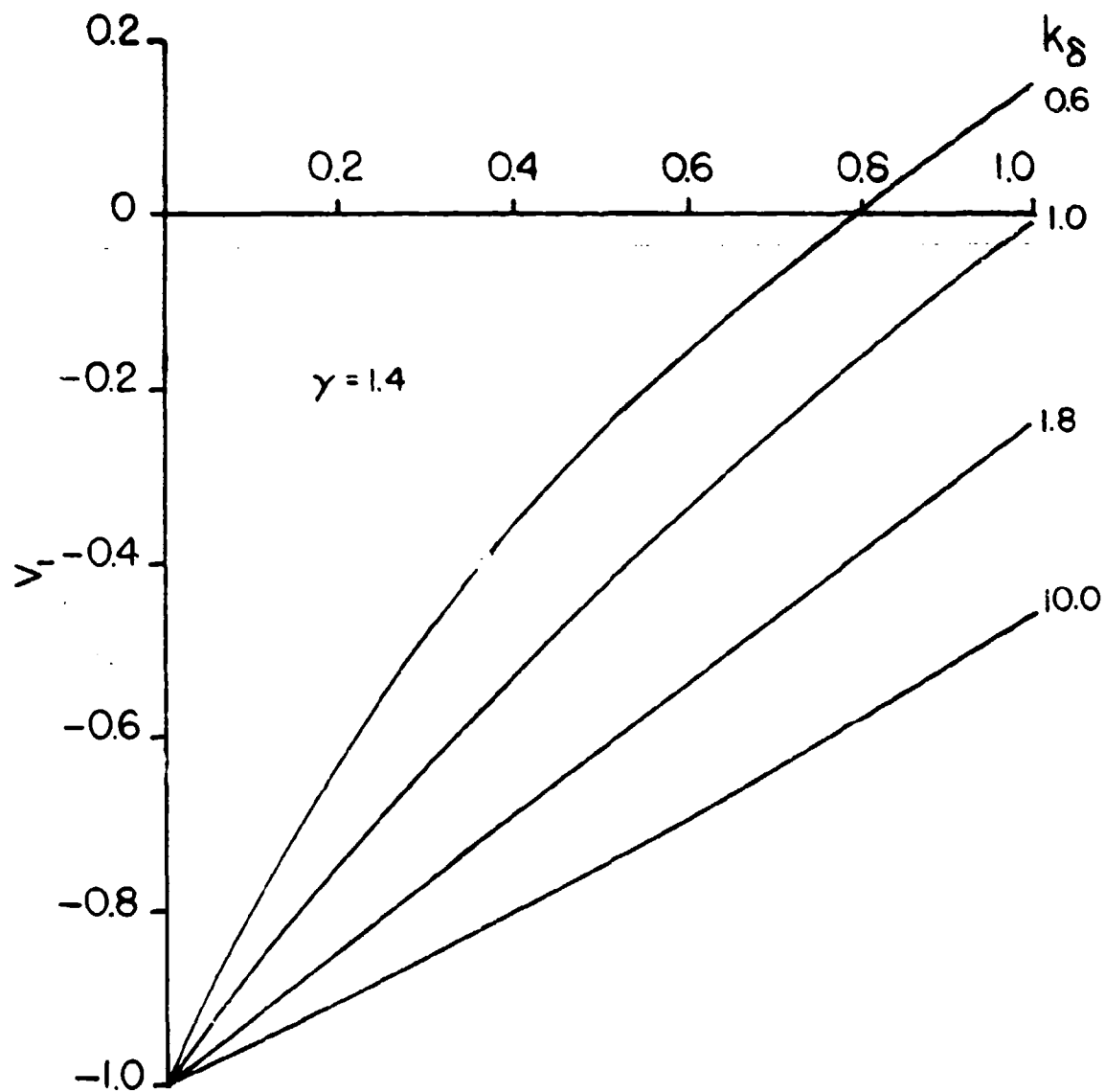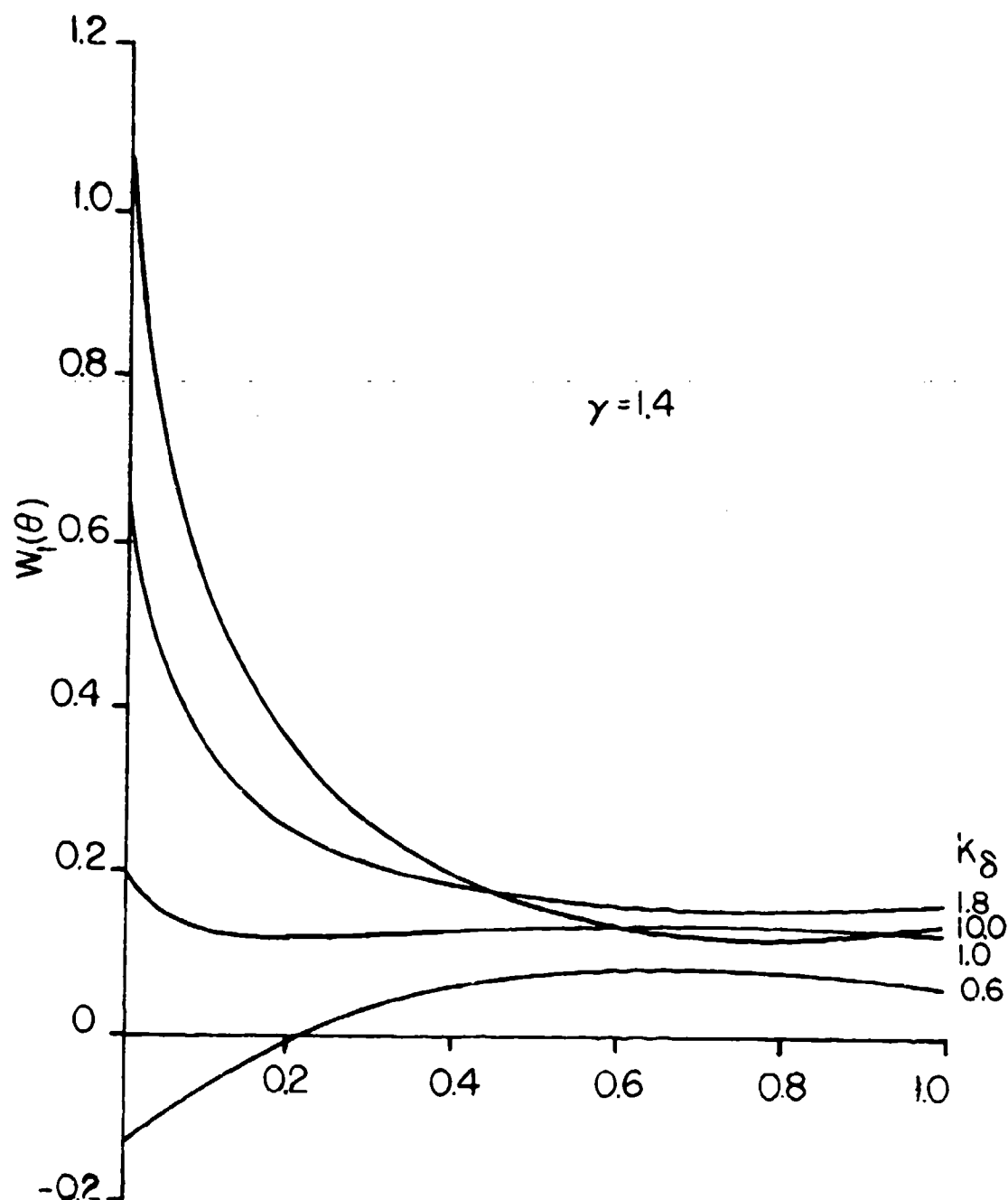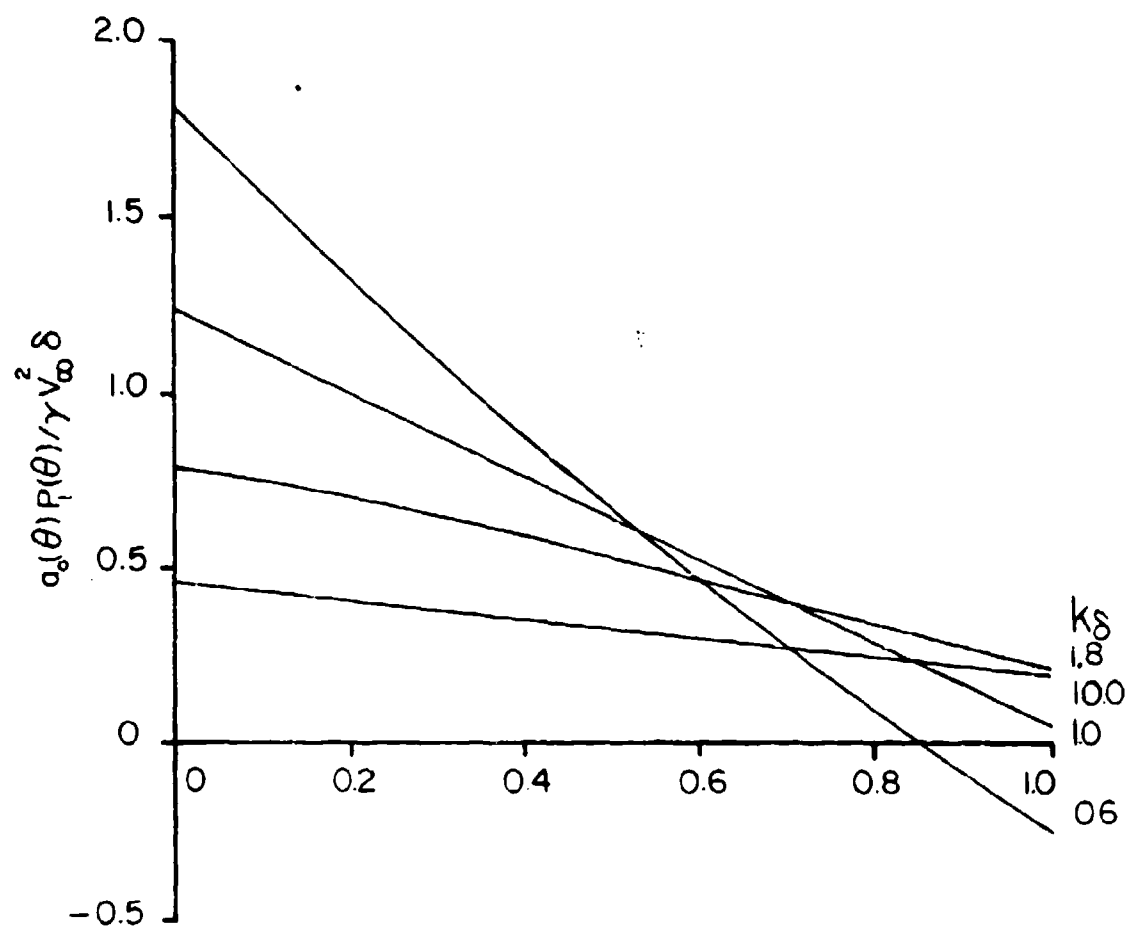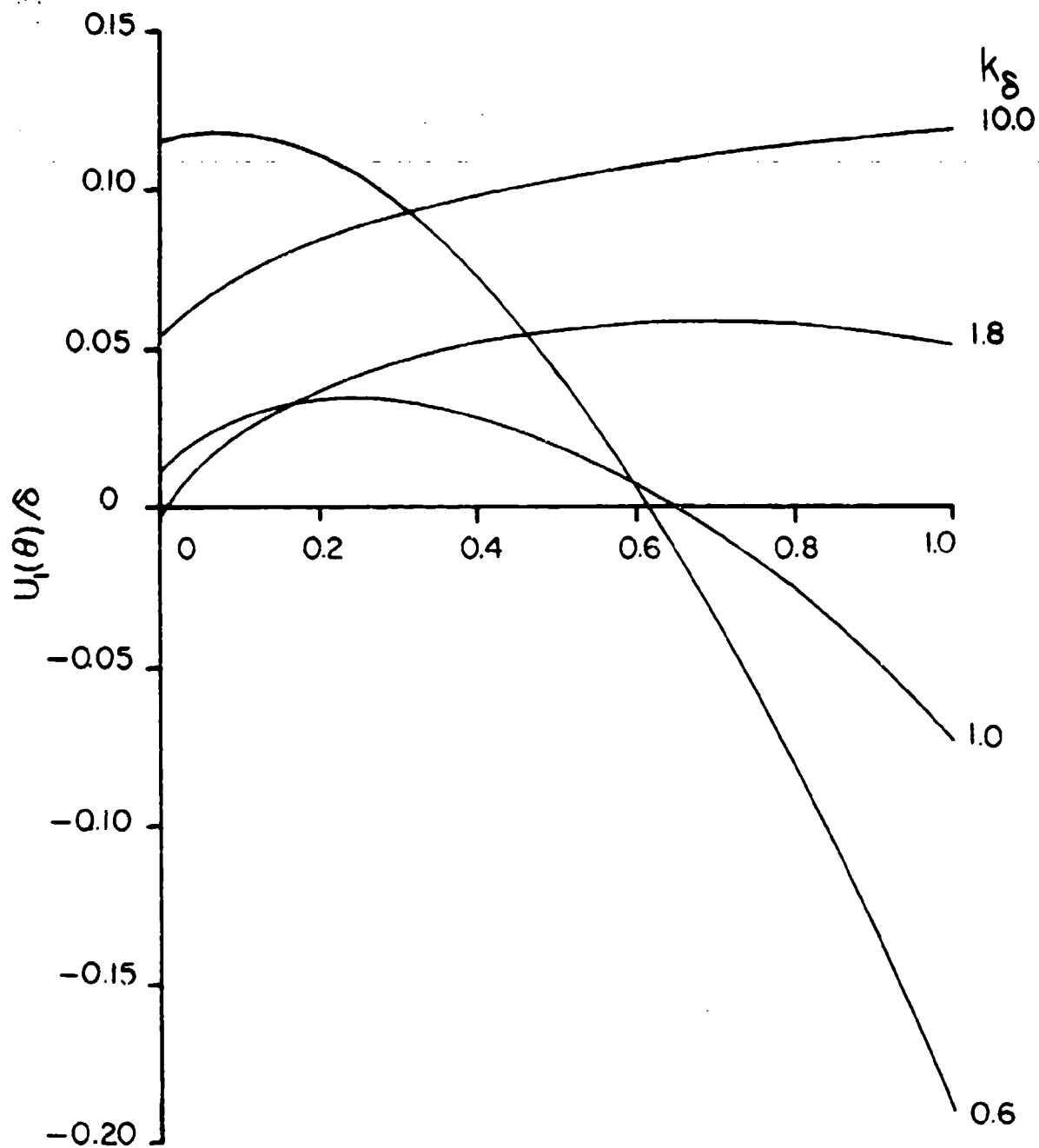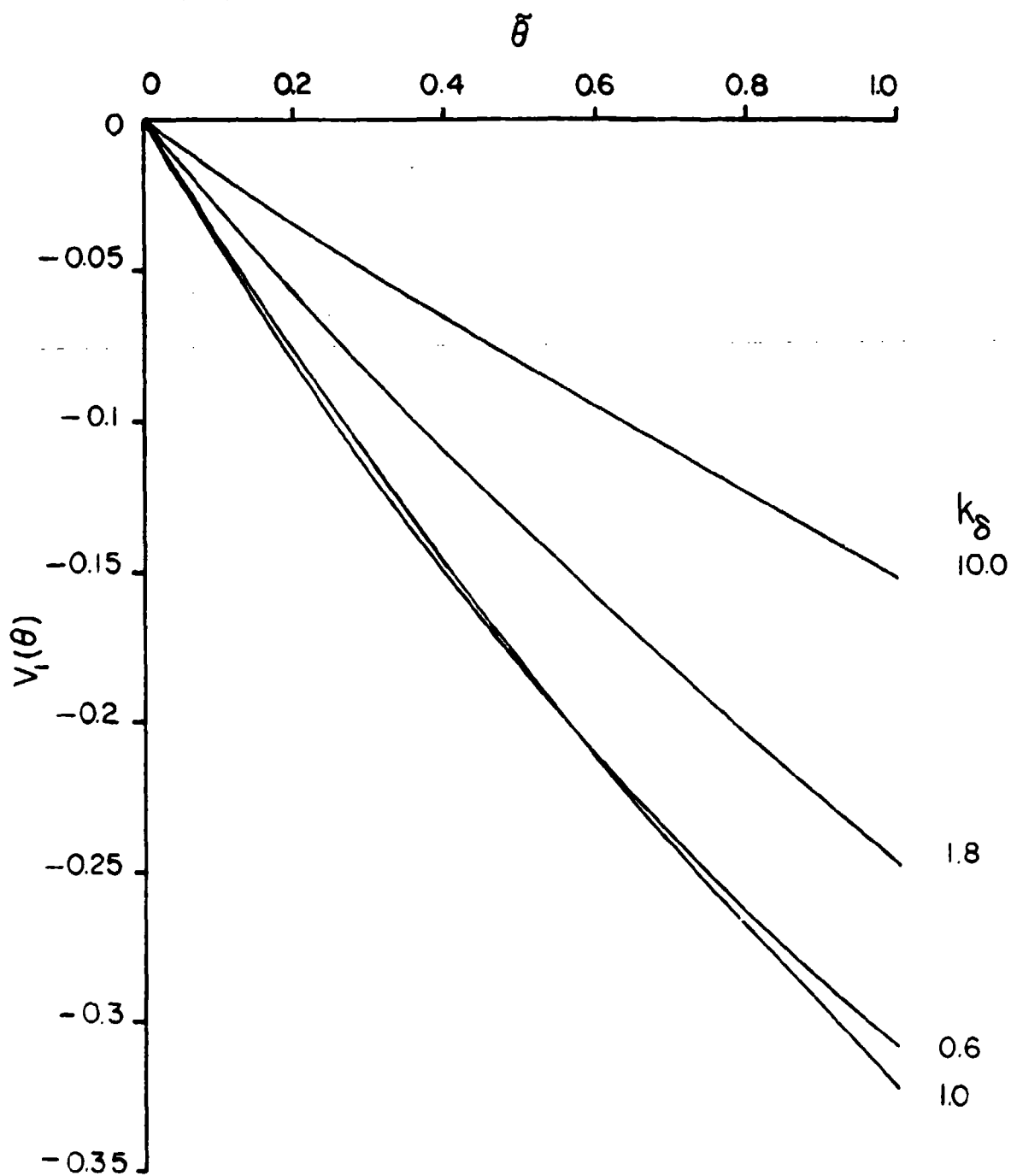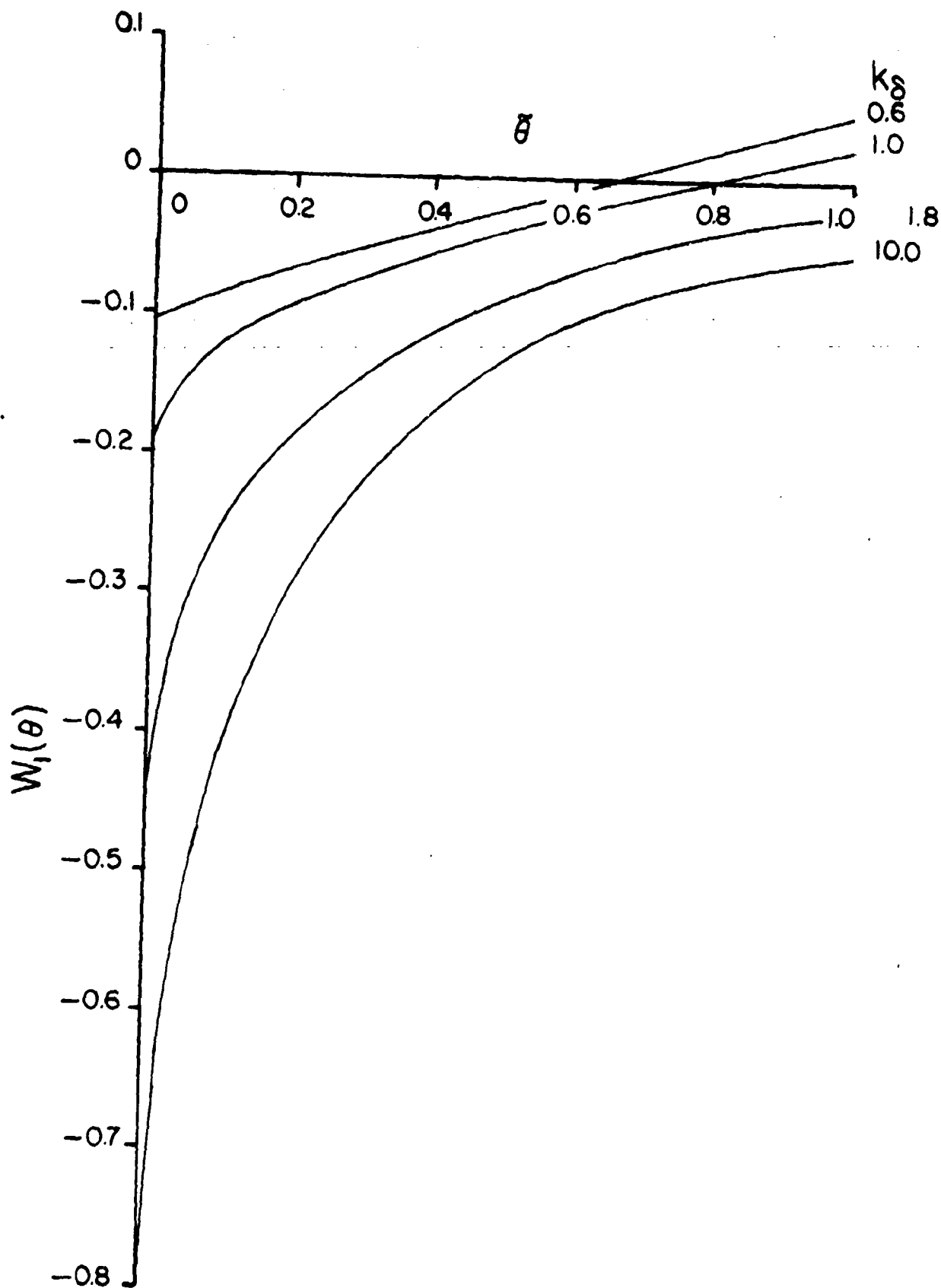Figure 62. Variation of W_1 Across the Shock Layer ($\gamma = 1.4$): Pure Plunging

136
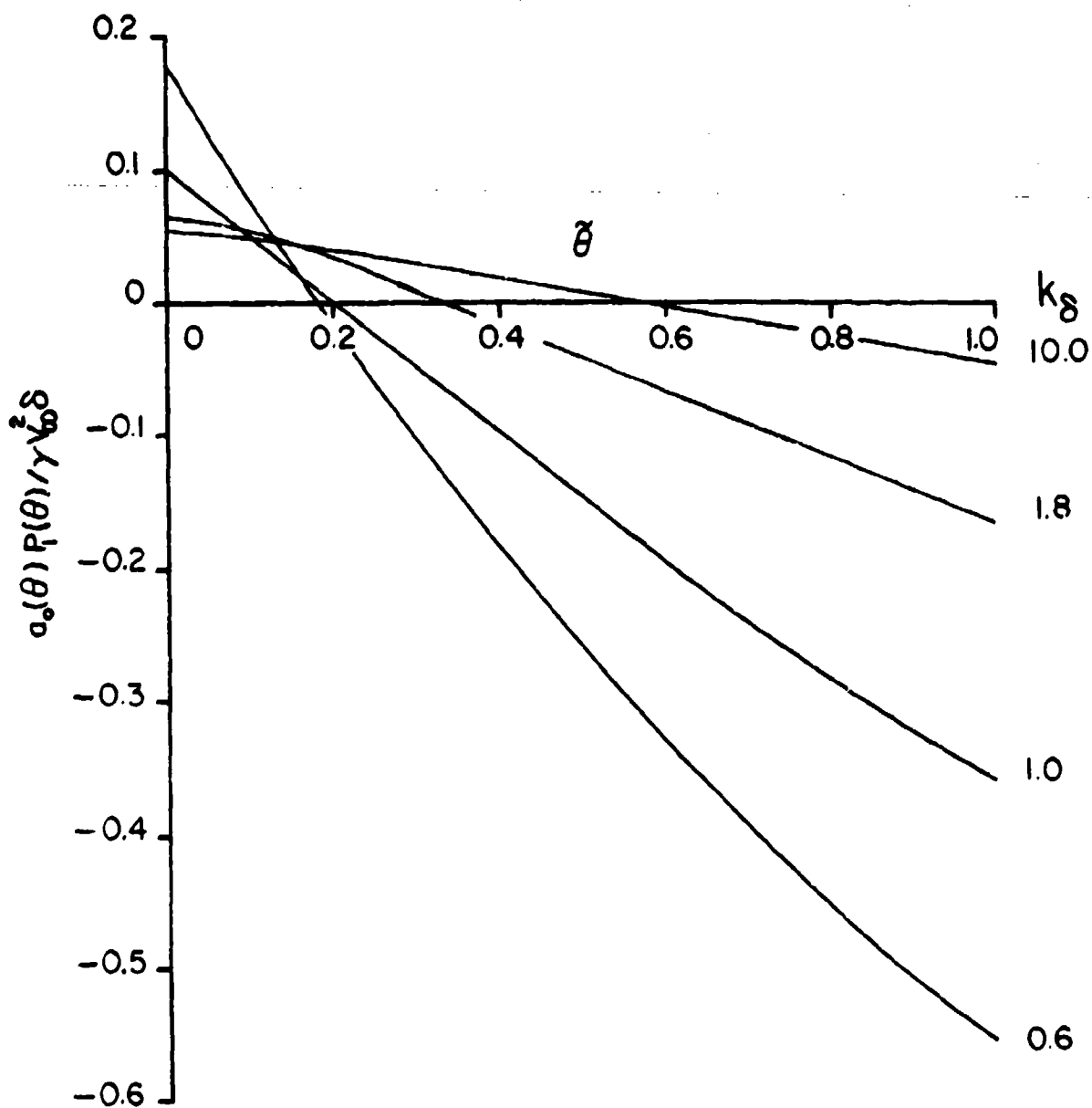
Figure 63. Variation of P_1 Across the Shock Layer ($\gamma = 1.4$): Pure Plunging

on the body surface by the flow. Omitting the force contribution from the base pressure, the force is given by

$$\vec{F} = -\iint_S p\,\hat{n}\,dS ,\qquad (470)$$

where S is the slant surface of the cone and $\hat{n}$ is the outward unit normal on the surface. The force is easy to reckon in body-fixed coordinates. In this case

$$\hat{n}\,dS = \hat{e}_{\theta b}(\theta = \delta)\sin\delta\; r\,dr\,d\phi$$

$$= (\cos\delta\cos\phi\,\hat{e}_x + \cos\delta\sin\phi\,\hat{e}_y - \sin\delta\,\hat{e}_z)\sin\delta\; r\,dr\,d\phi .\qquad (471)$$

Owing to symmetry, there will be no side forces in the y direction, and thus for a cone of axial length L,

$$\vec{F} = [-\cos\delta\sin\delta\int_0^{2\pi}\int_0^{L\sec\delta} p\cos\phi\; r\,dr\,d\phi]\,\hat{e}_x$$

$$+ [\sin^2\delta\int_0^{2\pi}\int_0^{L\sec\delta} p\; r\,dr\,d\phi]\,\hat{e}_z \qquad (472)$$

To first order in ϵ, the axial force in the z direction will arise only from the basic cone pressure p_0. The main concern is now with the component of force in the x-direction, which is called the normal force:

$$F_x \equiv -\cos\delta\sin\delta\int_0^{2\pi}\int_0^{L\sec\delta} p(\delta)\cos\phi\; r\,dr\,d\phi .\qquad (473)$$

In body-fixed coordinates, the surface pressure can be written

$$p(\delta) = p_0(\delta)[1 + \psi_0\{P_{b0}(\delta) + \frac{(i\omega r)}{V_\infty} P_{b1}(\delta) + \ldots\}$$

$$+ (\epsilon_z + \epsilon_p)\{P_{b0}{}^P(\delta) + \frac{(i\omega r)}{V_\infty} P_{b1}{}^P(\delta) + \ldots\}]e^{i\omega t}\cos\phi ,\qquad (474)$$

where $P_{b0}{}^P$ and $P_{b1}{}^P$ represent P_{b0} and P_{b1} calculated for the pure plunging problem. The normal force can now be written

$$F_x = -\frac{\pi}{2} (L \tan \delta)^2 \cot \delta \; p_0(\delta) \{ \psi_0 P_{b0}(\delta) + (\epsilon_z + \epsilon_p) P_{b0}{}^P(\delta)$$

$$+ \frac{2}{3} \sec \delta \; (\frac{i\omega L}{V_\infty}) \{ \psi_0 P_{b1}(\delta) + (\epsilon_z + \epsilon_p) P_{b1}{}^P(\delta) \}$$

$$+ O((\frac{\omega L}{V_\infty})^2)] e^{i\omega t} \quad . \tag{475}$$

Now $S_b \equiv \pi(L \tan \delta)^2$ can be recognized as the base area of the cone and the normal force coefficient can be defined as

$$C_N \equiv \frac{F_x}{\frac{1}{2}\rho_\infty V_\infty{}^2 S_b} \quad . \tag{476}$$

The result is then

$$C_N = -\cot \delta \; \frac{p_0(\delta)}{\rho_\infty} \; \frac{a_0{}^2(\delta)}{\gamma V_\infty{}^2} \{ \psi_0 \; P_{b0}(\delta) + (\epsilon_z + \epsilon_p) \; P_{b0}{}^P(\delta)$$

$$+ \frac{2}{3} \sec \delta \; (\frac{i\omega L}{V_\infty}) \{ \psi_0 \; P_{b1}(\delta) + (\epsilon_z + \epsilon_p) \; P_{b1}{}^P(\delta) \}$$

$$+ O((\frac{\omega L}{V_\infty})^2))] \; e^{i\omega t} \quad . \tag{477}$$

This expression is exact and becomes approximate to the extent that the functions P_{b0}, $P_{p0}{}^b$, P_{b1}, and $P_{b1}{}^P$ are approximate.

Now recall that

$$\psi = \psi_0 \; e^{i\omega t} \quad ,$$

$$h = h_0 \; e^{i\omega t} + i\Omega \quad ,$$

then Equation (477) can also be written as

$$C_N = -\cot \delta \; \frac{p_0(\delta)}{\rho_\infty} \; \frac{a_0{}^2(\delta)}{\gamma V_\infty{}^2} \{ \psi \; P_{b0}(\delta) + (\frac{\dot{\psi} z_0}{V_\infty} + \frac{\dot{h}}{V_\infty}) \; P_{b0}{}^P(\delta)$$

$$+ \frac{2}{3} \sec \delta \; \{ \frac{\dot{\psi} L}{V_\infty} P_{b1}(\delta) + (\frac{\ddot{\psi} z_0 L}{V_\infty{}^2} + \frac{\ddot{h} L}{V_\infty{}^2}) P_{b1}{}^P(\delta) \}$$

$$+ \frac{1}{2} \sec^2 \delta \; \{ \frac{\ddot{\psi} L^2}{V_\infty{}^2} P_{b2}(\delta) + (\frac{\ddot{\psi} z_0 L^2}{V_\infty{}^3} + \frac{\ddot{h} L^2}{V_\infty{}^3}) P_{b2}{}^P(\delta) \} + . .] \quad . \tag{478}$$

The last terms involving $P_{b2}(\delta)$ and $P_{b2}P(\delta)$ illustrate the nature of the next terms in the series that have not been evaluated.

When the higher-order terms proportional to $P_{b2}(\delta)$ and $P_{b2}P(\delta)$ are ignored in Equation (478), the normal-force coefficient depends on four independent terms. These terms are proportional to the pressure perturbations $P_{b0}(\delta)$, $P_{b0}P(\delta)$, $P_{b1}(\delta)$, and $P_{b1}P(\delta)$. It is useful to delineate these effects by expressing the normal-force coefficient as a linear combination of the effects due to ψ, $\dot{\psi}$, $\dot{h}$, and $\ddot{h}$. Thus write C_N as

$$C_N = C_{N\psi}\psi + C_{N\dot{h}} \left(\frac{\dot{\psi}z_0}{V_\infty} + \frac{\dot{h}}{V_\infty} \right)$$

$$+ C_{N\dot{\psi}}\ddot{\psi} + C_{N\ddot{h}} \left(\frac{\ddot{\psi}z_0 L}{V_\infty^2} + \frac{\ddot{h}L}{V_\infty^2} \right) \quad , \qquad (479)$$

where the higher-order terms in the series have been ignored and where

$$C_{N\psi} \equiv -\cot\delta \; \frac{\rho_0(\delta)}{\rho_\infty} \; \frac{a_0^2(\delta)}{\gamma V_\infty^2} \; P_{b0}(\delta) \quad , \qquad (480a)$$

$$C_{N\dot{h}} \equiv -\cot\delta \; \frac{\rho_0(\delta)}{\rho_\infty} \; \frac{a_0^2(\delta)}{\gamma V_\infty^2} \; P_{b0}P(\delta) \quad , \qquad (480b)$$

$$C_{N\dot{\psi}} \equiv -\frac{2}{3} \cot\delta \; \sec\delta \; \frac{\rho_0(\delta)}{\rho_\infty} \; \frac{a_0^2(\delta)}{\gamma V_\infty^2} \; P_{b1}(\delta) \quad , \qquad (480c)$$

$$C_{N\ddot{h}} \equiv -\frac{2}{3} \cot\delta \; \sec\delta \; \frac{\rho_0(\delta)}{\rho_\infty} \; \frac{a_0^2(\delta)}{\gamma V_\infty^2} \; P_{b1}P(\delta) \quad . \qquad (480d)$$

The coefficients defined by Equations (480) are called stability derivatives. The stability derivatives $C_{N\psi}$ and $C_{N\dot{\psi}}$ arise from pure pitching about the vertex, and the stability derivatives $C_{N\dot{h}}$ and $C_{N\ddot{h}}$ arise from pure plunging. The coefficient $C_{N\psi}$ is a static derivative since it depends upon the instantaneous inclination of the cone and not upon its time rate of change. The other stability derivatives, $C_{N\dot{\psi}}$, $C_{N\dot{h}}$, and $C_{N\ddot{h}}$ are dynamic stability derivatives since they depend upon the time rates of change of ψ and h.

Although the form of Equation (479) follows directly from the analysis, it is not in the form more appropriate for describing the dynamical motion of a missile. The reason is that the analysis was performed in an inertial coordinate system and Equation (479) follows directly from that analysis. The forces acting on a missile undergoing a general dynamical motion are more appropriately perceived from an observer in a body-fixed coordinate system. The forces acting on a missile are more appropriately described in terms of the orientation of the wind relative to the body; thus the angle of attack, α, is more appropriate than the rotation angle ψ, which is essentially an Euler angle. Thus the primary variables $(\psi, \dot{\psi}, \dot{h}, \ddot{h})$ are changed to a new set of primary variables $(\alpha, \dot{\alpha}, q, \dot{h})$ by means of the transformations (325), (327), and (328):

$$\dot{\psi}(t) \equiv -q(t) \quad ,$$

$$\psi(t) = \alpha(t) + \dot{h}(t)/V_\infty \quad ,$$

$$\ddot{h}(t) = -[q(t) + \dot{\alpha}(t)] \quad . \tag{481}$$

Equation (479) can thus be written

$$C_N = C_{N\alpha}\, \alpha - C_{Nh} \left(\frac{qz_0}{V_\infty}\right) + (C_{N\alpha} + C_{Nh})\left(\frac{\dot{h}}{V_\infty}\right)$$

$$- C_{Nq} \left(\frac{qL}{V_\infty}\right) + C_{N\alpha}\left[\left(\frac{\dot{\alpha}L}{V_\infty}\right) + \frac{qz_0 L}{V_\infty^2}\right] \quad , \tag{482}$$

where definitions have been made

$$C_{N\alpha} \equiv C_{N\psi} \quad , \tag{483a}$$

$$C_{N\alpha} \equiv -C_{Nh} \tag{483b}$$

$$C_{N\alpha} \equiv C_{N\psi} + C_{Nh} \tag{483c}$$

or

$$C_{N\psi} \equiv C_{Nq} + C_{N\alpha}$$

These definitions may differ with those of other authors. Since there seems

to be no definite uniformity, care should be taken when comparing the present results with others.

The static normal-force coefficient $C_{N\alpha} = C_{N\psi}$ is shown in Figures 64, 65, and 66 and compared with other results. The static coefficient $C_{N\alpha}$ is the same coefficient that is obtained for steady flow past an inclined cone. If the density ratio $\rho(\delta)/\rho(\beta)$ were set equal to unity, the present result would be the same as that obtained by Doty and Rasmussen (Reference 23). The Newtonian result (Reference 33), valid strictly for $K_\delta \to \infty$ and $\gamma \to 1$, is $C_{N\alpha}/\cos^2\delta = 2$. Figure 64 shows a comparison with the exact numerical results of Sims (Reference 54) and the empirical curve of Orlik-Ruckeman (Reference 49). The present result shows a characteristic dip in the curve nea For $K_\delta > 1$, the agreement with Sims is very good, becoming better as u accordance with the underlying requirements of hypersonic small-disturbance theory. As $K_\delta \to 0$, the present result overshoots the correct linearized value $C_{N\alpha} = 2$ by a small amount before it actually obtains the correct result at $K_\delta = 0$. The empirical values of Orlik-Ruckemann are slightly too large for large K_δ and do not tend to the correct behavior ɜ $K_\delta \to 0$. Figure 65 shows a comparison of the present results with McIntosh (Reference 48) and again with Orlik-Ruckemann. The hypersonic small-disturbance results of McIntosh, which are numerical and limited to the range $K_\delta < 4$ are very accurate and agree well with the present results when $K_\delta > 1$; the disagreement when $K_\delta < 1$ is less than 5 percent. Figure 66 shows a comparison of the present results with the numerical results of Brong (References 45, 46). Agreement is good for large K_δ, and the deviation from the results of small-disturbance theory owing to finite cone angles is illustrated.

The dynamic stability derivative C_{Nh}, which arises from plunging, is shown in Figure 67 as a function of K_δ. It has nearly the same shape as $C_{N\alpha}$,
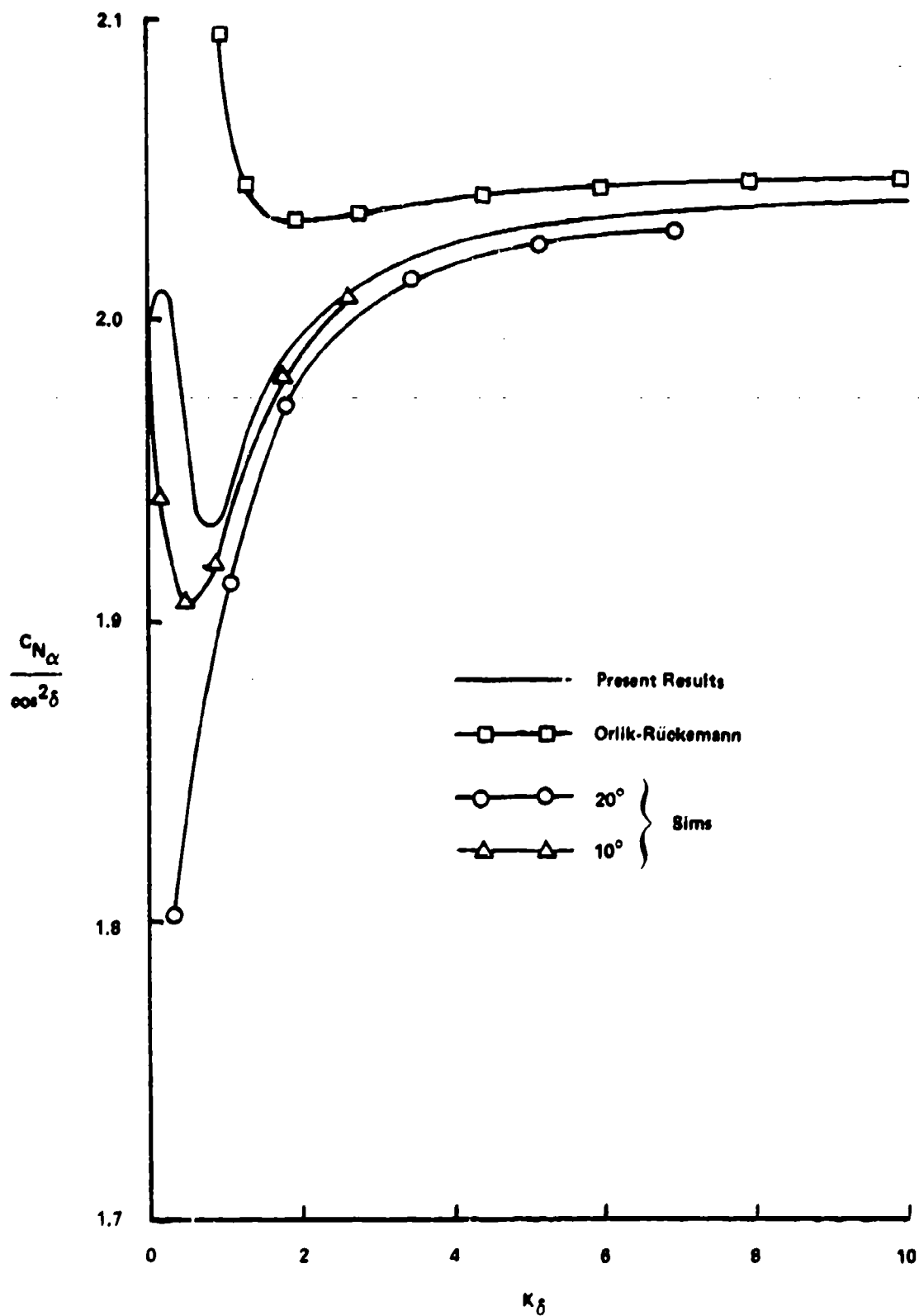
Figure 64. C_{N_α} Versus K_δ for $\gamma = 1.4$: Comparison With Sims and Orlik-Ruckemann

193

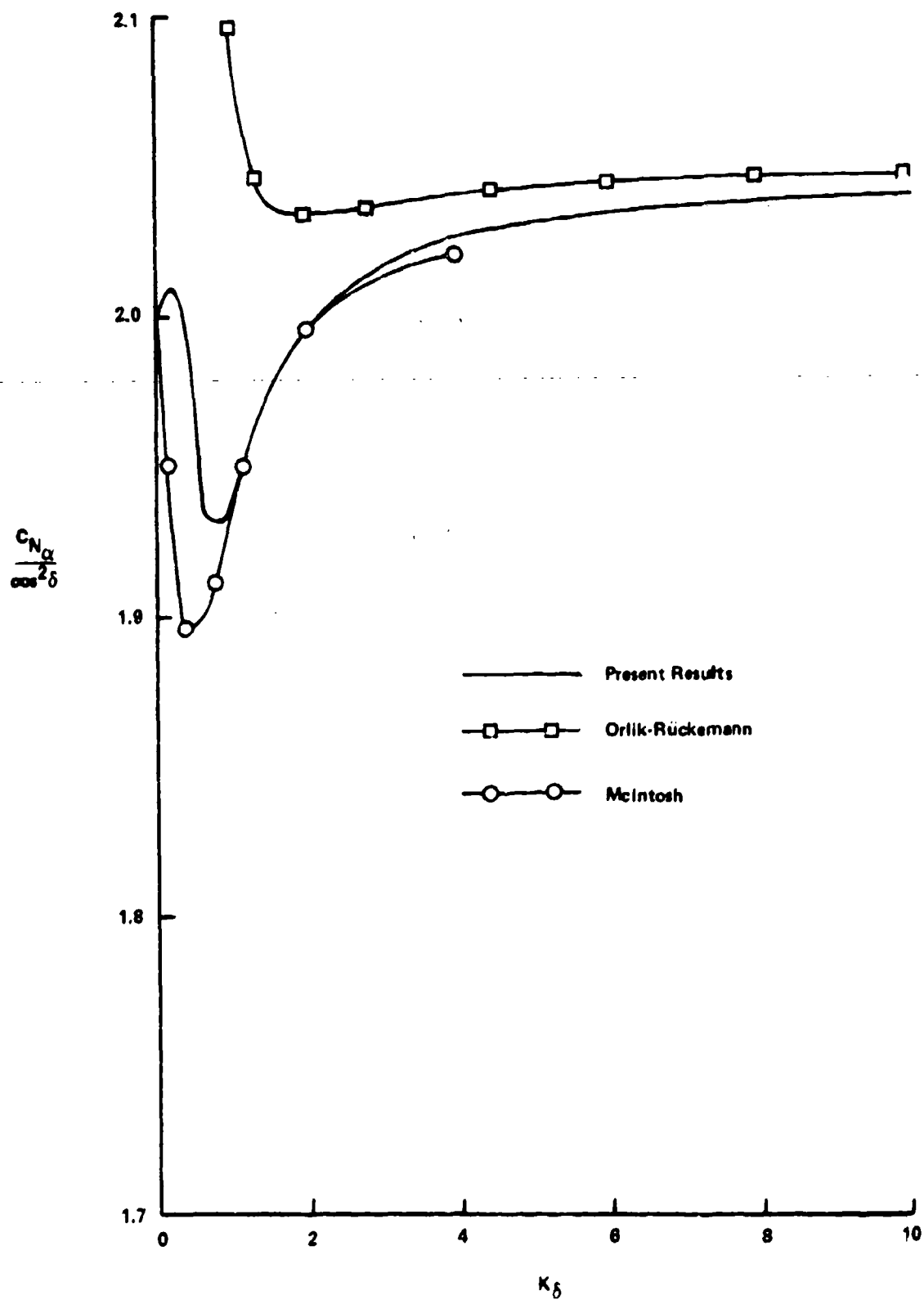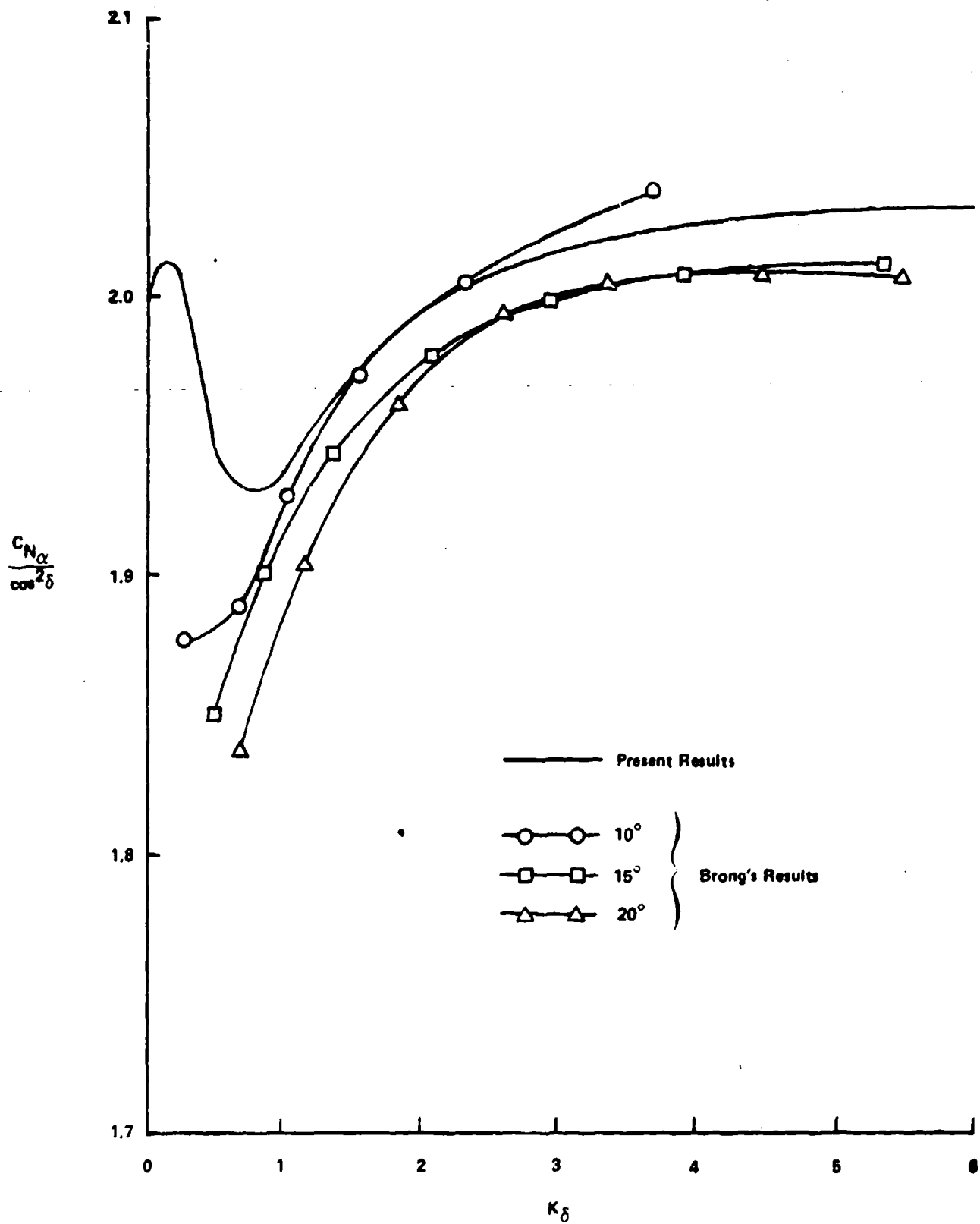Figure 65. C_{N_α} Versus K_δ for $\gamma = 1.4$: Comparison With McIntosh and Orlik-Ruckemann

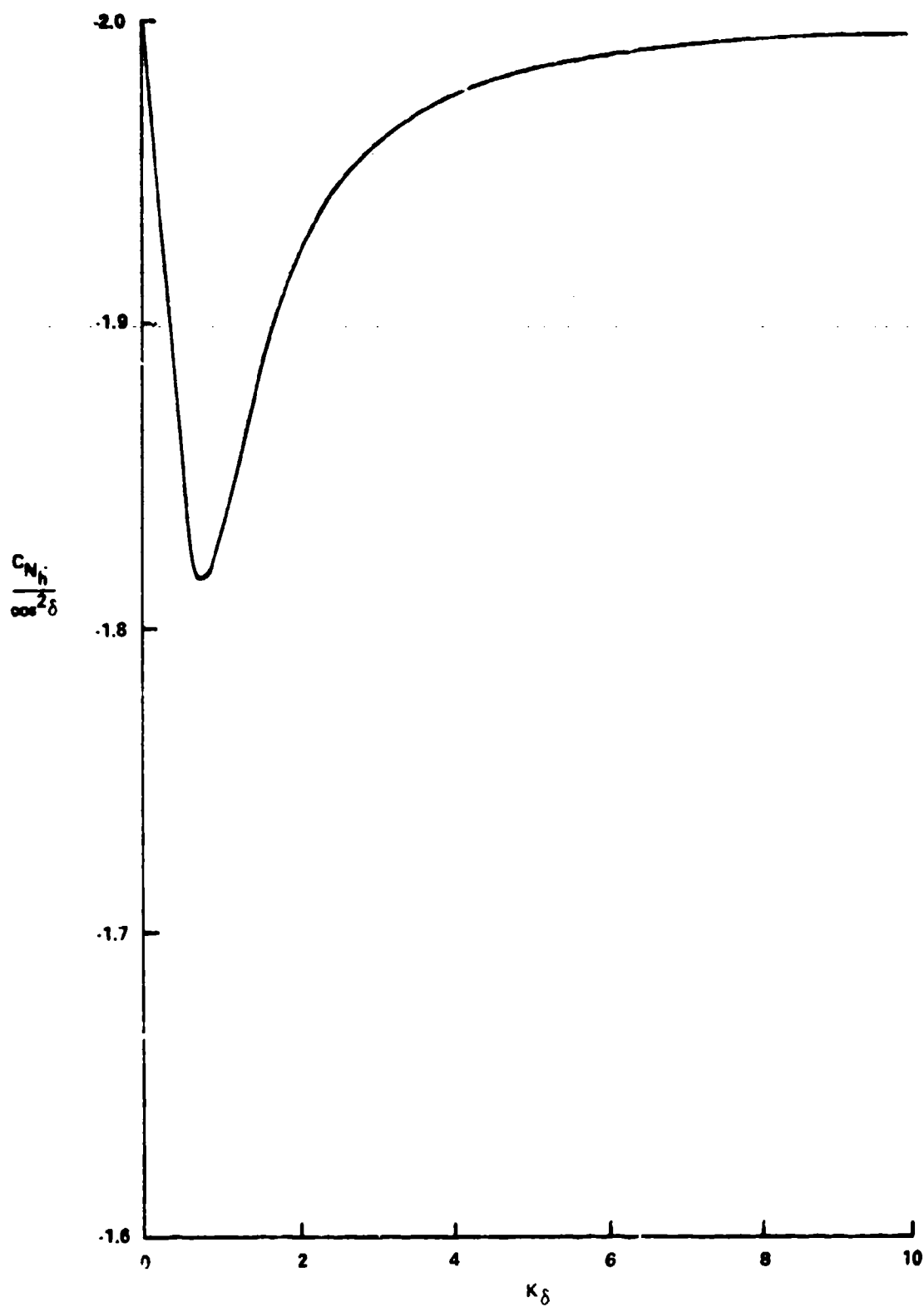Figure 66. C_{N_α} Versus K_δ for $\gamma = 1.4$: Comparison With Brong

195

Figure 67. C_{N_h} Versus K_δ for   = 1.4

although of opposite sign, but does not tend to quite as large a value as K_δ $\rightarrow \infty$. Again there is a characteristic dip in the curve near $K_\delta = 1$.

Figure 68 shows the dynamic stability derivative $C_{N\alpha} \equiv -C_{Nh}$, which arises from plunging, as a function of K_δ. A comparison with the results of McIntosh (Reference 48) and Orlik-Ruckemann (Reference 49) are also shown. The Newtonian result (Reference 33) is $C_{N\alpha} = 0$. The present results agree well with the hypersonic small-disturbance results of McIntosh, which were limited to the range $K_\delta < 2$. The correct limit of linearized theory, $CN_\alpha = 2/3$, is obtained when $K_\delta \rightarrow 0$, and the present results are only slightly smaller than those of McIntosh when $1 < K_\delta < 2$. The empirical curve of Orlik-Ruckemann produces values that are slightly larger than the other two results, and it does not behave quite correctly as $K_\delta \rightarrow 0$. A characteristic dip near $K_\delta = 1$ is shown in all three results. Figure 69 compares the results of Brong (References 45, 46) with the present results, as well as those of McIntosh. The results of Brong show the same trends as the present results, but are somewhat larger.

Figure 70 shows the dynamic derivative $C_{N\psi} \equiv C_{N\alpha} + C_{N\dot{\alpha}}$ as a function of K_δ when compared with the results of McIntosh and Orlik-Ruckemann. The Newtonian result (Reference 33) is $CN_{\dot{\psi}} = 4/3$, and the linearized-theory result, valid for $K_\delta \rightarrow 0$, is $CN_{\dot{\psi}} = 8/3$. The present results show the same trend as the numerical small-distrubance results of McIntosh, agreeing with the correct linearized-theory result at $K_\delta = 0$ and being slightly larger than McIntosh for $0.8 < K_\delta < 2$. The empirical results of Orlik-Ruckemann are too large for small K_δ and slightly smaller than the present results for large K_δ. Figure 71 shows a comparison with McIntosh and with Tobak and Wehrend (Reference 42) on a different scale for   The present results agree will with the potential-theory results of Tobak and Wehrend when $K_\delta\delta \rightarrow 0$. Figure

197
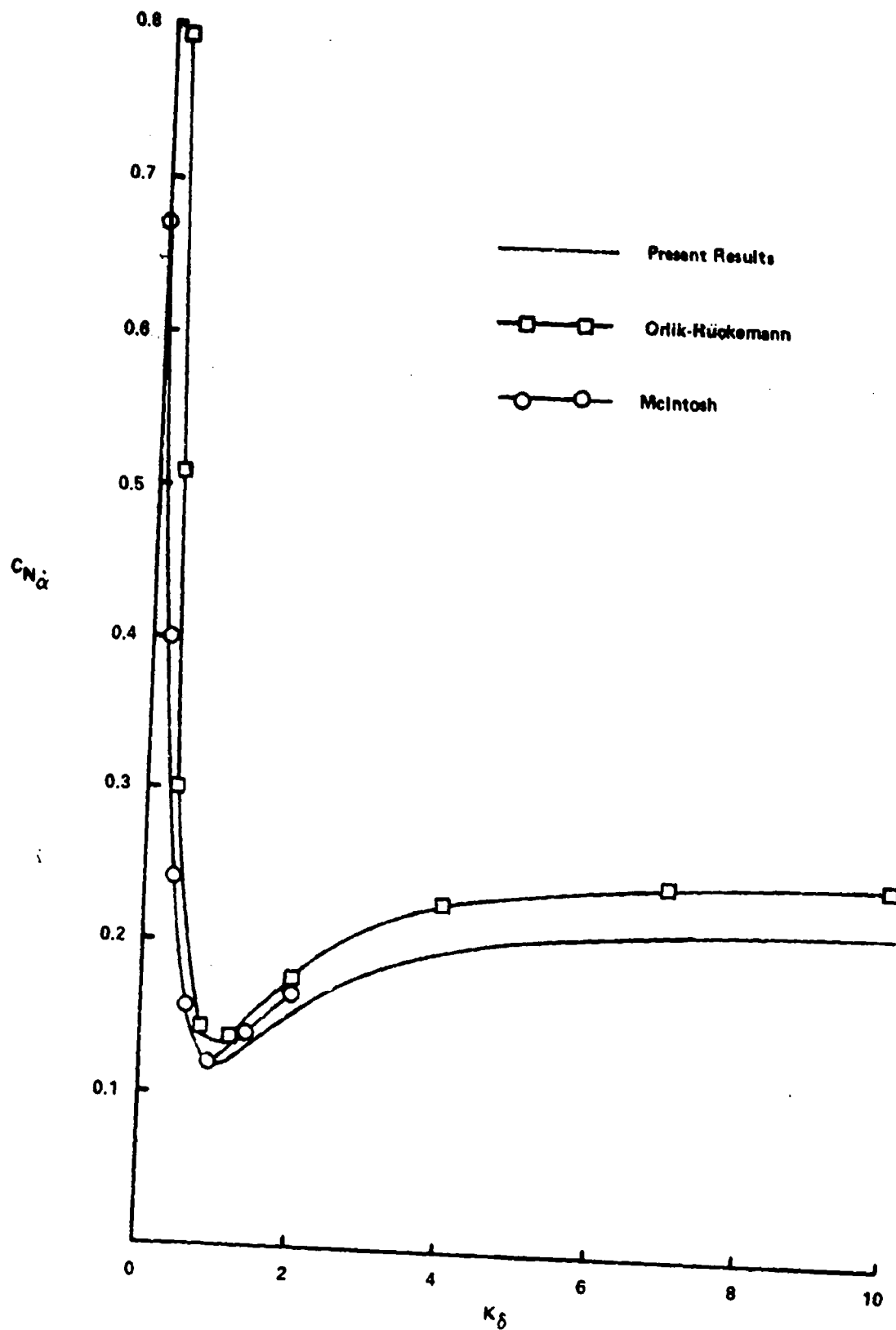
Figure 68. $C_{N_{\dot{\alpha}}}$ Versus K_δ for $\gamma = 1.4$: Comparison With McIntosh and Orlik-Ruckemann
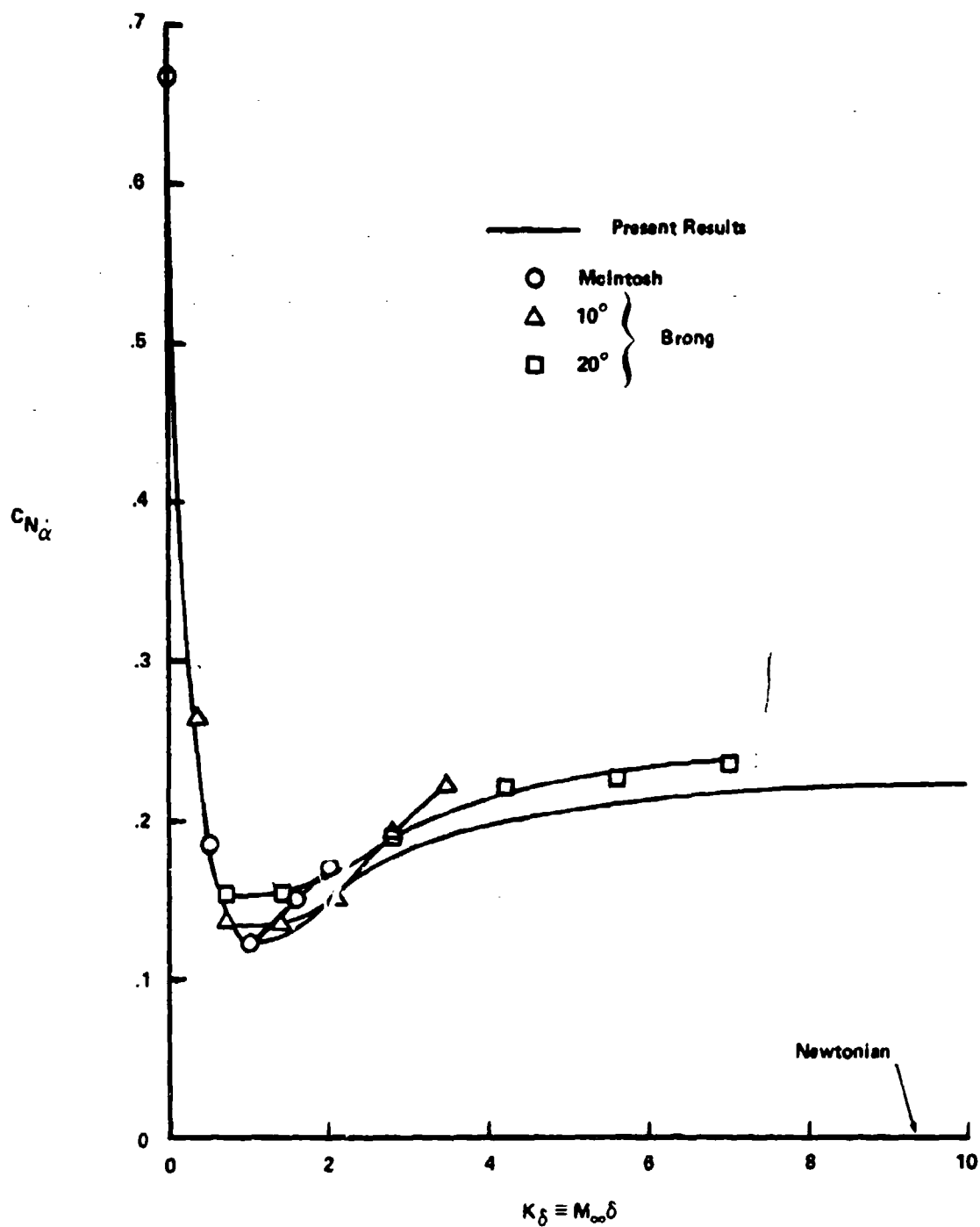
Figure 69. $C_{N_{\dot{\alpha}}}$ Versus K_{δ} for $\gamma = 1.4$: Comparison With McIntosh and Brong
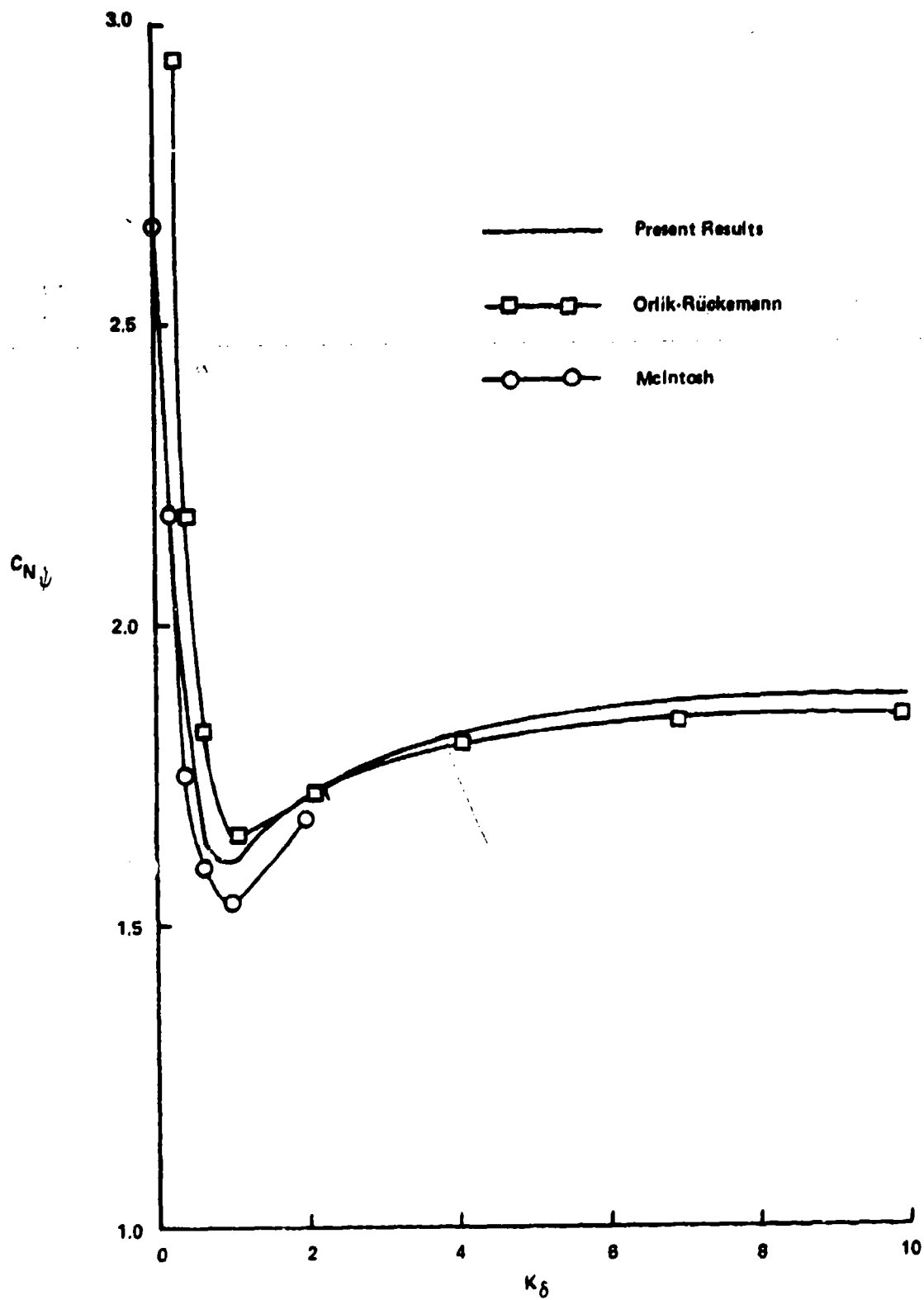
Figure 70. $C_{N_{\dot{\psi}}}$ Versus K_{δ} for $= 1.4$: Comparison With McIntosh and Orlik-Ruckemann

200
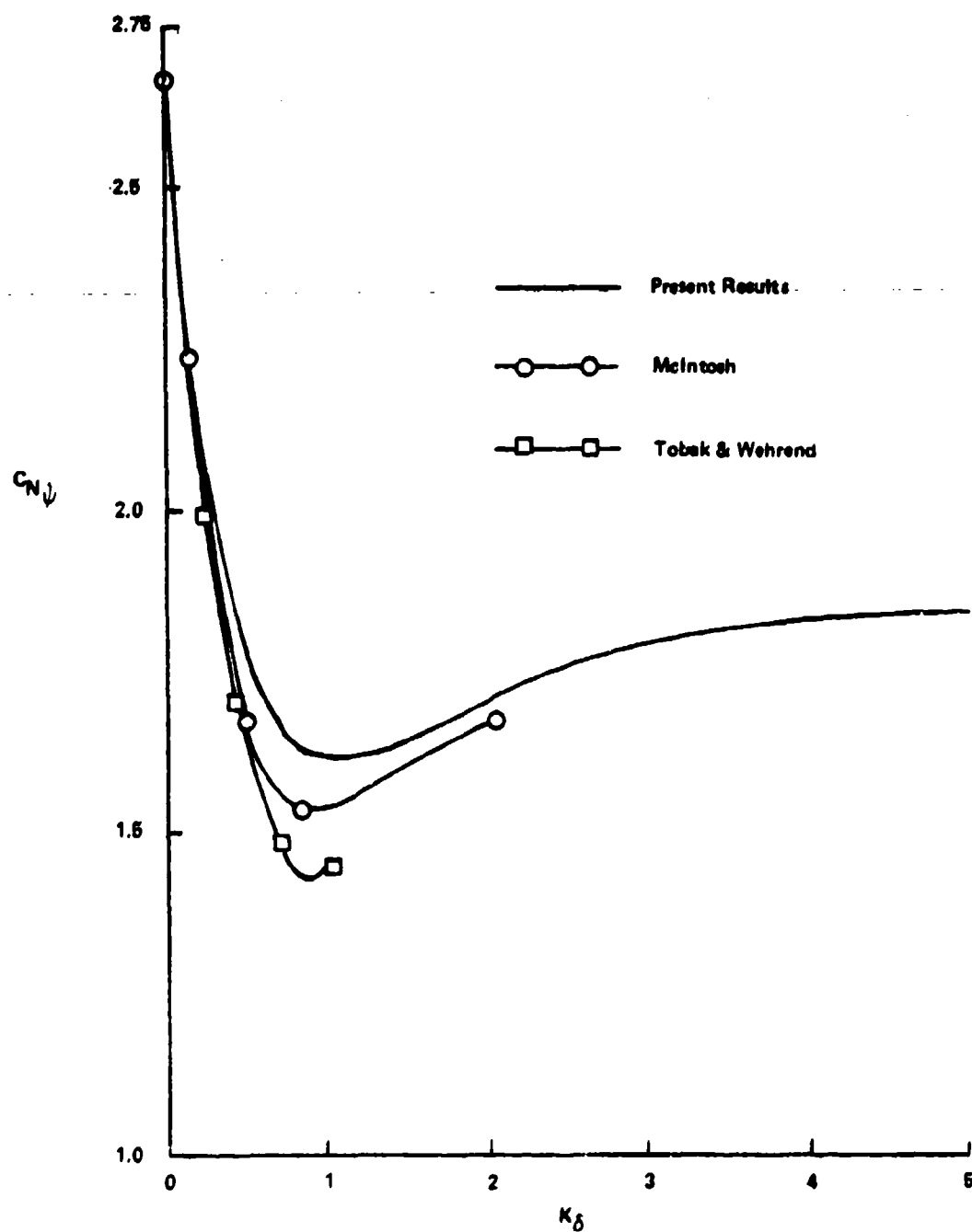
Figure 71. C_N Versus K_δ for $\gamma = 1.4$: Comparison With McIntosh and Tobak and Wehrend

72 shows further comparison of the present results with Brong (References 45, 46) as well as with McIntosh (Reference 49) again. The results of Brong show good overall agreement with the present results, especially for large K_δ.

Figure 73 shows a comparison of the dynamic stability derivative $C_{Nq} \equiv (C_{N\psi} - C_{N\alpha})$, reckoned about the vertex, with the results of McIntosh and Brong. The present results tend to the correct limit of linearized theory, $C_{Nq} = 2$, as $K_\delta \to 0$, but otherwise they are larger than both the results of McIntosh and Brong. The differences between the present results are not great. A characteristic dip at $K_\delta \simeq 1$ is shown in all three results:

o. Moment About the Vertex

The moment about any point z_1 on the cone axis is given by

$$\vec{M}_1 = -\iint_S (\vec{r} - z_1\hat{e}_z) \times p\,\hat{n}\,dS \quad ,$$

$$= \vec{M}_0 - z_1\hat{e}_z \times \vec{F} \quad ,$$

$$= \vec{M}_0 - \frac{1}{2} \rho_\infty V_\infty^2 \, S_b \, z_1 \, C_N \, \hat{e}_v \quad , \tag{484}$$

where

$$\vec{M}_0 = -\iint_S (\vec{r} \times p\hat{n})\,dS \tag{485}$$

is the moment about the vertex of the cone. When $\vec{M}_0$ is expanded out, the result is

$$\vec{M}_0 = -\iint_S p\,\hat{e}_\phi \, r\,dS \quad ,$$

$$= -\sin\delta \int_0^{2\pi} \int_0^{L\,\sec\delta} p[\cos\phi\,\hat{e}_y + \sin\phi\,\hat{e}_x]r^2\,dr\,d\phi \quad ,$$

$$= [-\sin\delta \int_0^{2\pi} \int_0^{L\,\sec\delta} p\,\cos\phi\,r^2\,dr\,d\phi]\,\hat{e}_v \quad . \tag{486}$$
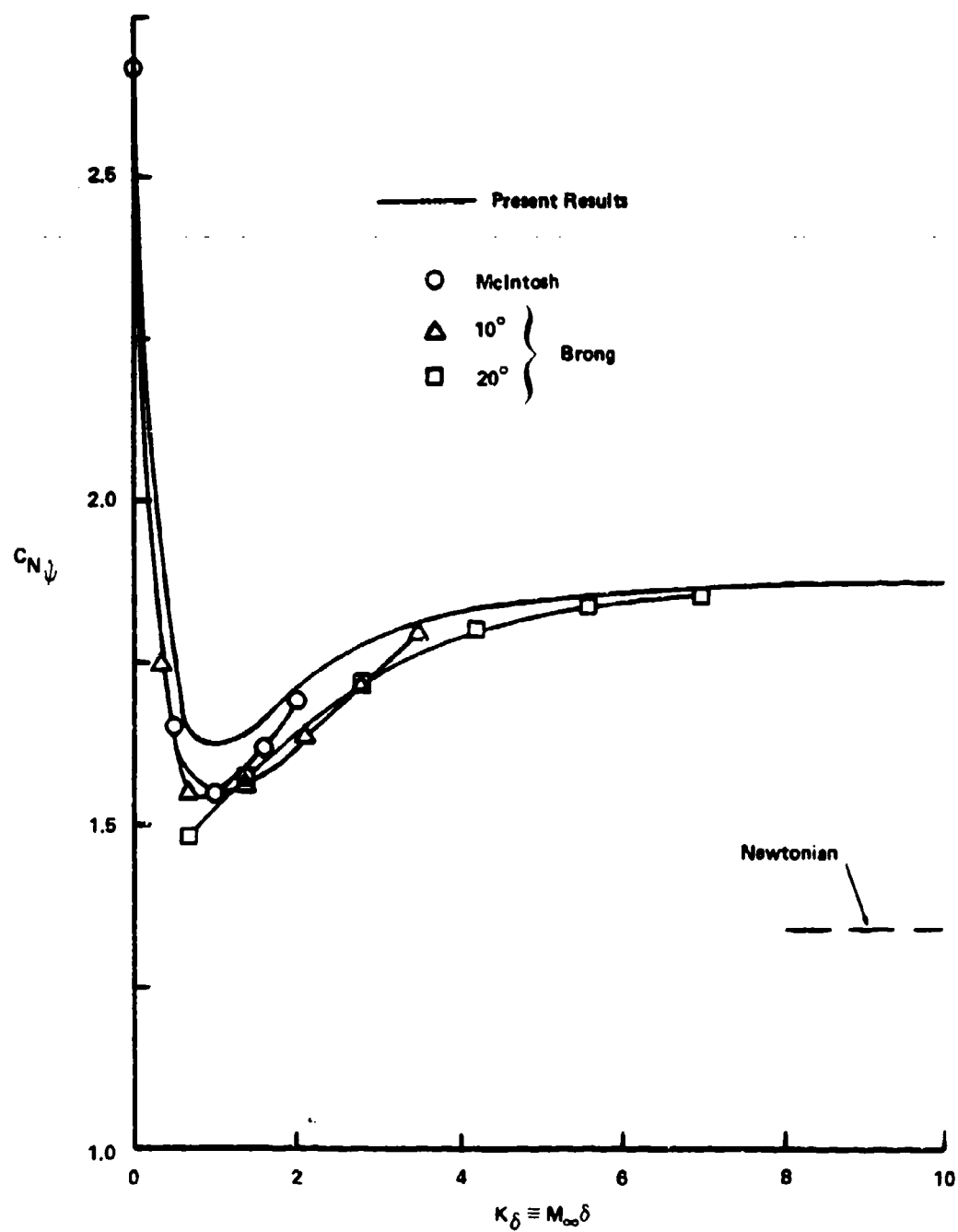
Figure 72. C_{N_ψ} Versus K_δ for $\gamma = 1.4$: Comparison With Brong and McIntosh

203
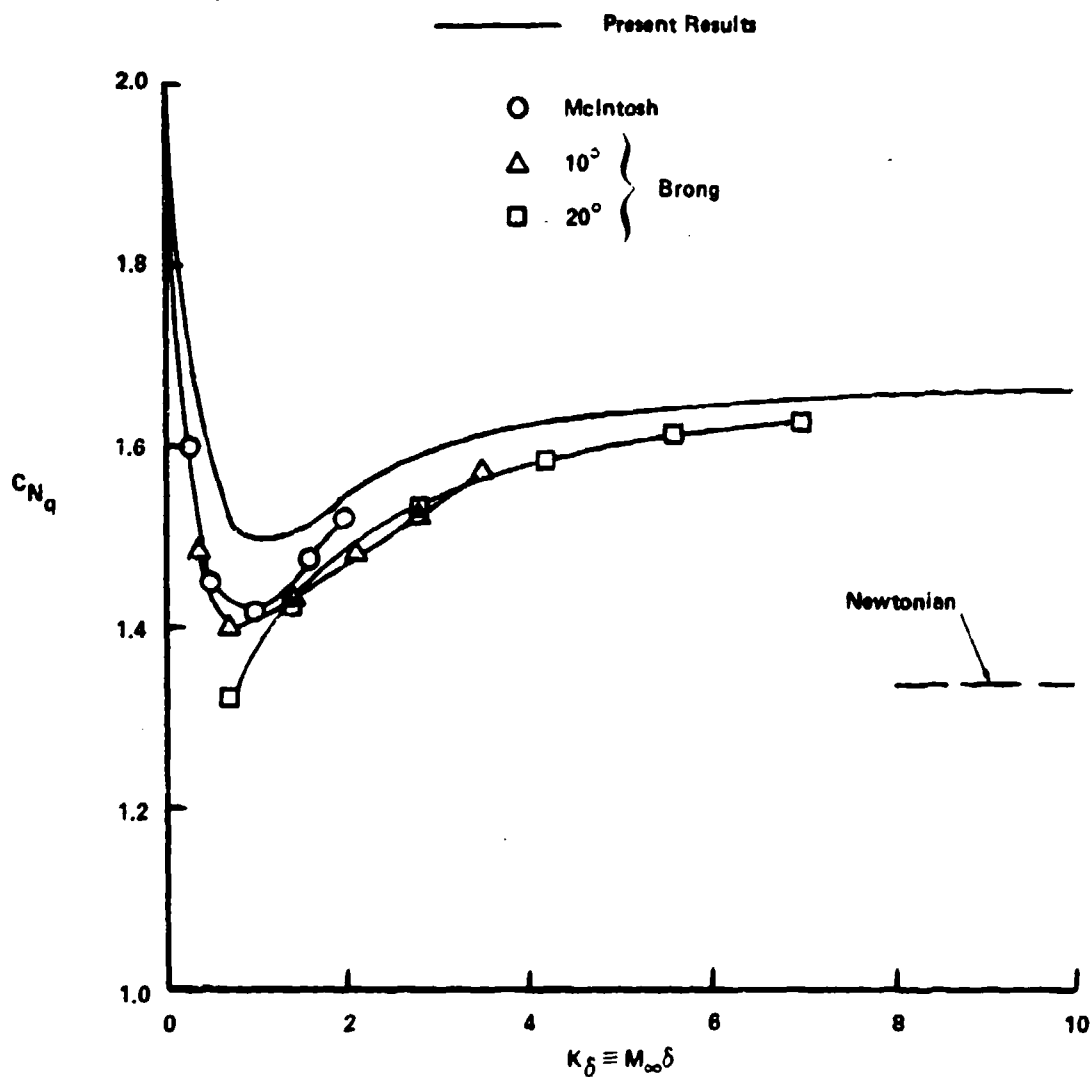
Figure 73. $C_{N_{qo}}$ Versus K_δ for $\gamma = 1.4$: Comparison With McIntosh and Brong

Thus by symmetry there is only a moment about the y axis.

A moment coefficient is defined by

$$C_{M0} \equiv \frac{(M_0)_y}{\frac{1}{2}\rho_\infty V_\infty^2 S_b L} \quad . \tag{487}$$

An analogous means to obtaining the normal-force coefficient provides

$$C_{M0} = C_{M\psi}\,\psi + C_{M\dot{h}}\left(\frac{\dot{\psi}z_0}{V_\infty} + \frac{\dot{h}}{V_\infty}\right)$$

$$+ C_{M\ddot{\psi}}\,\dot{\psi} + C_{N\dot{h}}\left(\frac{\ddot{\psi}z_0 L}{V_\infty^2} + \frac{\ddot{h}L}{V_\infty^2}\right) \quad , \tag{488}$$

where the higher-order ter   n the series have been neglected, and where

$$C_{M\psi} \equiv \frac{2}{3}\sec^2\delta\;C_{N\psi} \quad , \tag{489a}$$

$$C_{Mh} \equiv \frac{2}{3}\sec^2\delta\;C_{Nh} \quad , \tag{489b}$$

$$C_{M\psi} \equiv \frac{3}{4}\sec^2\delta\;C_{N\psi} \quad , \tag{489c}$$

$$C_{Mh} \equiv \frac{3}{4}\sec^2\delta\;C_{Nh} \quad . \tag{489d}$$

In terms of the variables α, $\dot{\alpha}$, q, and $\dot{h}$, the results are

$$C_{M0} = C_{M\alpha}\,\alpha - C_{Mh}\left(\frac{qz_0}{V_\infty}\right) + (C_{M\alpha} + C_{Mh})\left(\frac{\dot{h}}{V_\infty}\right)$$

$$- C_{Mq}\left(\frac{qL}{V_\infty}\right) + C_{M\dot{\alpha}}\left[\frac{\dot{\alpha}L}{V_\infty} + \frac{qz_0 L}{V_\infty^2}\right] \quad , \tag{490}$$

where

$$C_{M\alpha} \equiv C_{M\psi} \quad , \tag{491a}$$

$$C_{M\dot{\alpha}} \equiv -C_{Mh} \quad , \tag{491b}$$

$$C_{Mq} \equiv C_{M\psi} + C_{Mh}$$

or

$$C_{M\psi} \equiv C_{Mq} + C_{M\dot{\alpha}} \tag{491c}$$

The moment coefficients are proportional to the normal-force coefficients, as can be seen from Equations (489).

Unsteady supersonic flow past a circular cone undergoing harmonic pitching and plunging motions in a plane has been analyzed. The goal was to obtain approximate analytic results that are accurate and useful in a wide range of practical and theoretical applications. The results were cast in the similarity form of hypersonic small-disturbance theory. Whereas the first terms in the perturbations series (U_0, V_0, W_0, P_0) were obtained in relatively simple analytic form, the second terms (U_1, V_1, W_1, P_1) involved quadratures of Bessel functions which, while being in analytic form, required numerical evaluation of the quadratures. From comparisons with other related works involving numerical integrations of the governing differential equations, the present results showed all the proper trends when $K_\delta \equiv M_\infty \delta$ was varied. For the static and dynamic stability derivatives, the correct linearized-theory results were recovered when $K_\delta \to 0$, and a characteristic dip in the curves was shown near $K_\delta = 1$. While being more accurate for large K_δ, a good approximation is given over the whole range of K_δ. This is in accordance with results obtained previously for steady flows by means of the same methodology.

5. EFFECTS OF BLUNTNESS

The desire for increased maneuverability in the high supersonic, low hypersonic Mach number regime has led to a renewed interest in the aerodynamics of nonsymmetric lifting bodies (References 55, 56). For example, lift-to-drag ratios near unity can be achieved with slender bodies possessing elliptical cross-sections whose major-to-minor axis ratio is of the order of two or more. Circular cross-sections, in contrast, achieve maximum lift-to-drag ratios well below unity. Significantly higher lift-to-drag

ratios can be achieved at hypersonic conditions with so-called waverider configurations (References 57, 58). Recent work has shown that rather attractive waverider vehicles can be developed from the conical flow solutions for supersonic flow past cones whose cross-section deviates slightly from a circle (see Figure 74). These vehicles efficiently integrate volumetric storage and lifting requirements, can achieve lift-to-drag ratios of three or more at Mach numbers ranging from three to five, and behave surprisingly well at off-design conditions.

Because these new waverider configurations are derived from conical flow solutions, they all have sharply pointed noses. These pointed noses invite serious heating problems at higher Mach numbers. One approach to alleviating these heat transfer problems is to slightly blunt the nose of the vehicle.

The effects of nose bluntness on supersonic and hypersonic flow past axisymmetric vehicles was studied extensively in the 1960's. Numerical work by Sychev (Reference 59) and Guiraud (Reference 60) as well as analytical work by Yakura, Fiorino, and Schneider (References 61,62, and 63, respectively) using both direct and inverse methods showed that slight blunting of the nose of a slender vehicle in a hypersonic flow can significantly change the forces on the vehicle. In particular, the fluid wetting the body passes through the normal portion of the bow shock wave at the nose of the vehicle and, as a consequence, will have a higher entropy and lower density than the fluid which passes through the more oblique portions of the shock wave. The use of the hypersonic small disturbance equations to calculate the flow past a slender body overestimates the entropy near the body and thus overestimates the surface pressure. Yakura (Reference 61), using the method of matched asymptotic expansions, and Fiorino (Reference 62), using an inverse method, have shown how to eliminate this error that results from using the small
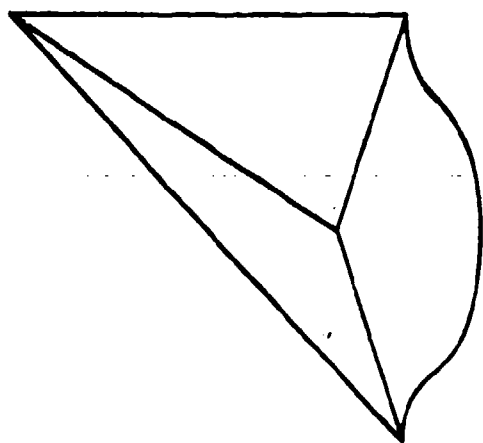
(b) Elliptical-cone Body
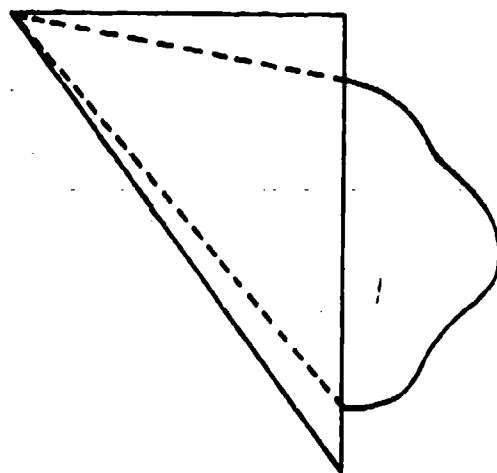
(d) "cos 4θ" Body
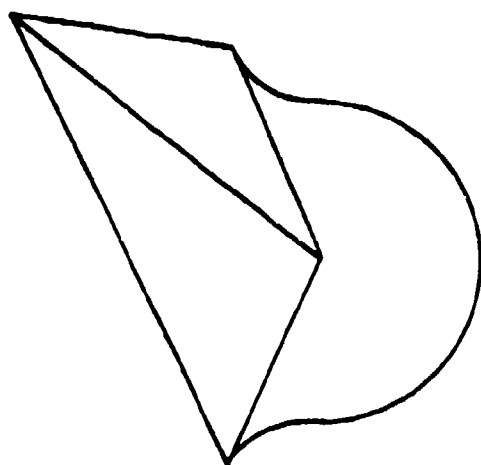
(a) Cone-at-angle-of-attack Body

(c) "cos 3θ" Body
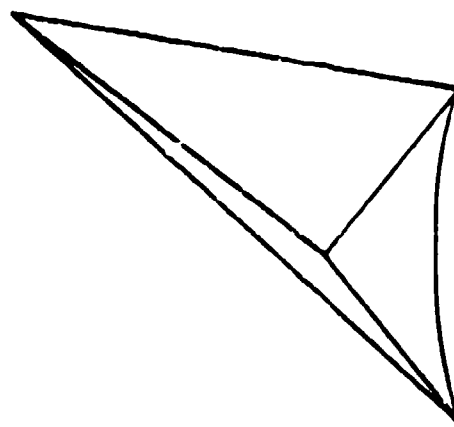
Figure 74. Waveriders Derived From Conical Flow Solutions

disturbance equations for the case of axisymmetric flows.

This section deals with the effects of nose bluntness on hypersonic flow past nonsymmetric vehicles such as might arise for flow past a slender body at angle of attack or a body with an elliptical cross-section. To allow analytical progress, this work is restricted to slender bodies whose cross-section deviates slightly from that of a circle and employs a regular perturbation technique. By adopting an inverse approach in which the shock wave is specified and the associated body is determined, analytical results are obtained that are easily interpreted. The approach is a generalization of that of Fiorino and Rasmussen (Reference 64) for axisymmetric shapes.

The governing equations and boundary conditions for inviscid, hypersonic flow past a slender body, using the equivalence principle of Hayes (Reference 65) are developed in the following paragraphs. Using a regular perturbation scheme, equations are derived to describe the effects of small nonsymmetries. These equations are solved and explicit results are obtained for infinite Mach numbers and power law shock shapes. The section ends with a discussion of the results and suggestions for future work.

a. Formulation of the Governing Equations

Consider the steady, hypersonic flow of an otherwise uniform stream past a slender, nonsymmetric body with a blunted nose such as that shown in Figure 75a. Later, the assumption shall be that the asymmetric cross-section deviates slightly from a circle. The z-axis of the rectangular coordinate system in Figure 75a is aligned with the freestream velocity vector. The cross-flow plane is then defined by a constant value of z. Hayes (Reference 65) has shown that the steady, three-dimensional, hypersonic flow past a slender body is equivalent* to an unsteady, two-dimensional flow in the cross-flow plane

―――――――――――
*to within an error of the order of the square of the slenderness ratio.
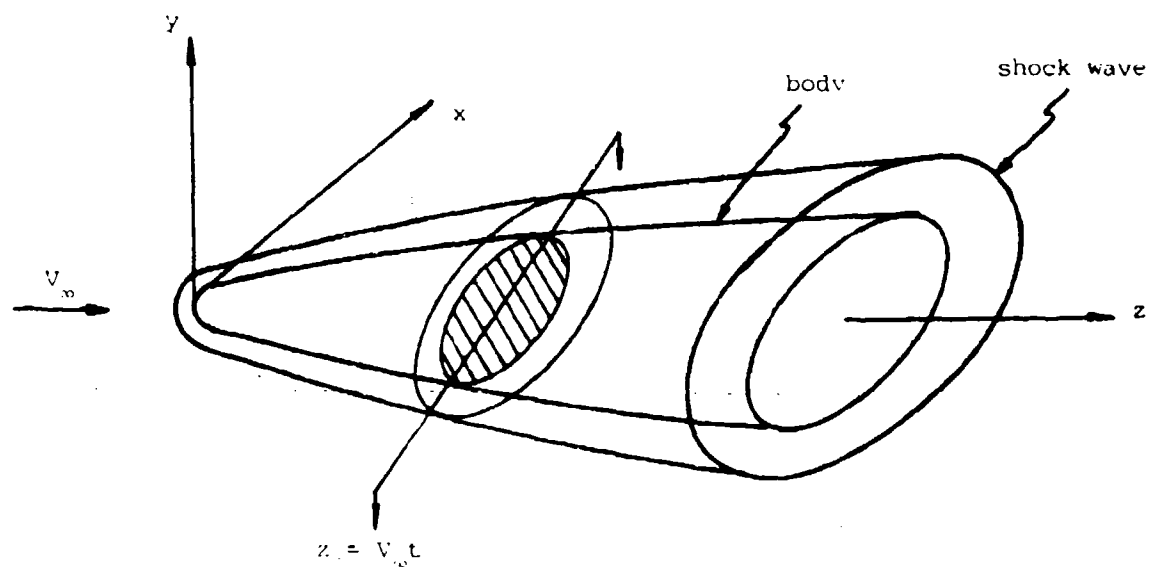
(a)   Three-Dimensional Steady Flow
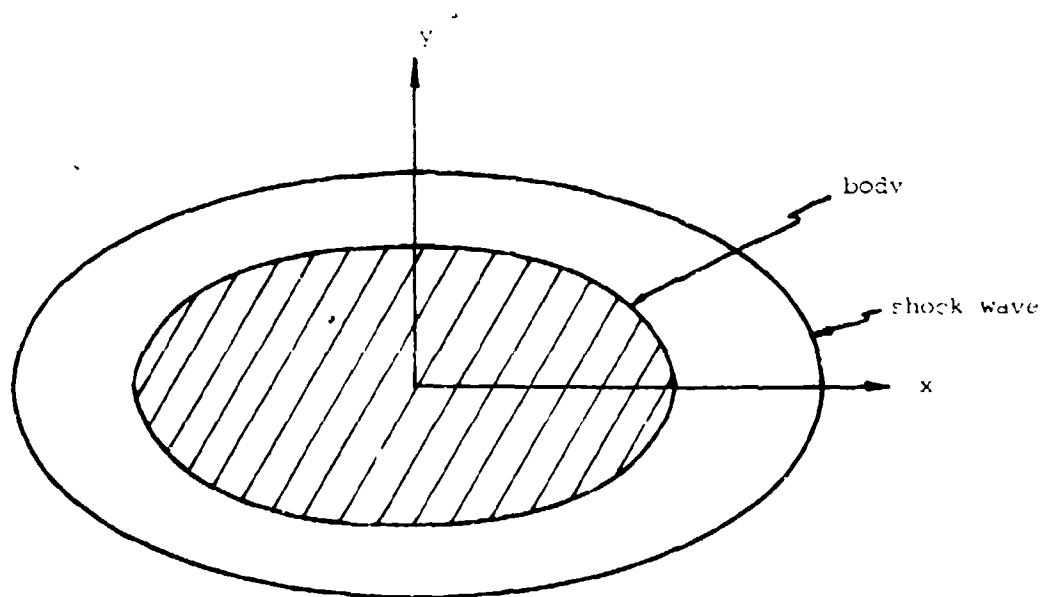
(b)   Equivalent Two-Dimensional Flow

Figure 75.   Equivalence Principle for Hypersonic Flow
Past Slender Bodies

normal to the freestream velocity vector as shown in Figure 75b. The equivalent two-dimensional, unsteady flow is thus in the x-y plane and can be viewed as being due to a two-dimensional piston, whose shape at any time t is that of the original slender body at the axial position $z = V_\infty t$, propagating into an atmosphere at rest.

Now derive the integral form of the conservation equations for an arbitrary sector of the cross-flow plane defined by the angle ϕ_0 as shown in Figure 76. Assume that the body and the resulting flowfield are symmetric with respect to the y-axis. The volume V, shown in Figure 76, is defined as being of unit depth in the z-direction and bounded by the body, a cylindrical surface Σ lying outside the shock wave and on which the velocity vanishes, and the sector of extent ϕ_0.

When applied to the volume V, the equations expressing conservation of mass, Newton's second law, and the first law of thermodynamics become

$$\frac{d}{dt} \iiint_V \rho \, dV + \iint_{S_0} \rho \vec{V} \cdot \hat{n} \, dS = 0 \tag{492}$$

$$\frac{d}{dt} \iiint_V \rho \vec{V} \, dV + \iint_{S_0} \rho \vec{V}\vec{V} \cdot \hat{n} \, dS = - \iint_S p \hat{n} \, dS \tag{493}$$

$$\frac{d}{dt} \iiint_V \rho (e + \frac{V^2}{2}) dV + \iint_{S_0} \rho (e + \frac{V^2}{2}) \vec{V} \cdot \hat{n} \, dS = - \iint_S p\vec{V} \cdot \hat{n} \, dS \tag{494}$$

Here the assumption is an inviscid, adiabatic flow without body forces. The closed surface S bounds the Volume V and has an outward unit normal n. The open surface S_0 is a plane of unit depth at angle ϕ_0 and extends from the body $(r = r_b(\phi,t))$ to the shock wave $(r = r_s(\phi,t))$.

Before proceeding further with the development of these equations, it is useful to discuss the basic structure of the flowfield. In this way, the various approximations that will be made subsequently can be motivated.
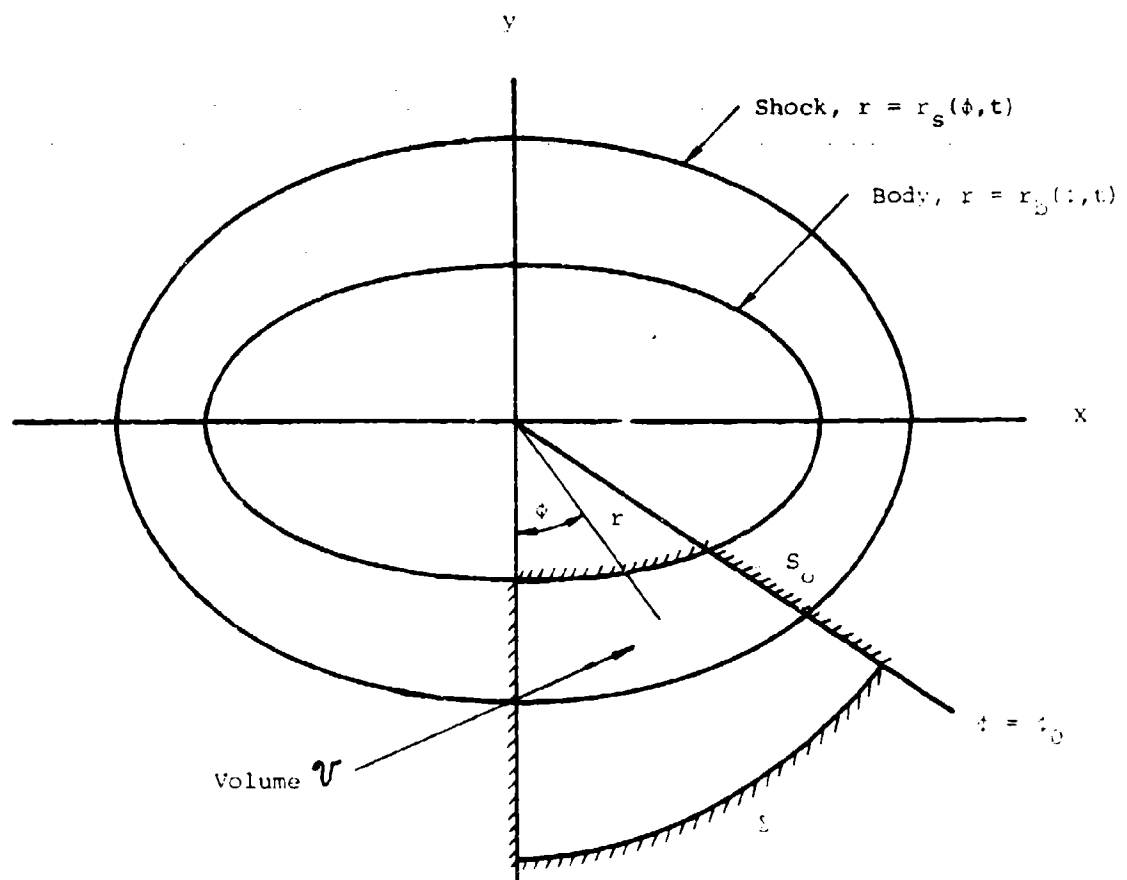
211

Figure 76. Geometry of the Cross-Flow Plane

While the hypersonic flow past blunt-nosed lifting bodies will eventually be considered, it is instructive to first consider the axisymmetric case.

If, except for the region near the nose, the body is slender and the free-stream Mach number is sufficiently large that $M_\infty r_b'$ is of order unity or larger, the shock layer between the body and bow shock wave is thin and consists of a region of high density near the shock wave in which most of the shock layer mass is concentrated and a low density, high entropy region adjacent to the body. This high entropy layer near the body arises from the nose bluntness since the streamlines wetting the surface must pass through the normal or nearly normal portions of the bow shock wave near the nose. Because the pressure does not vary significantly outside the high density region near the bow shock wave, the high entrophy near the body implies a relatively low density there. The pressure variation across the shock layer occurs primarily in the high density region near the shock wave. The pressure at the edge of the high density region is approximately equal to the value given by the shock jump relations plus a centripetal correction, first described by Busemann (Reference 66). The radial velocity varies smoothly and weakly from the given value at the body to that just downstream of the bow shock wave. Figure 77 shows, qualitatively, the variations of the density ρ, the pressure p, and the radial velocity u across the shock layer for this axisymmetric case. Fiorino (Reference 62) has obtained useful analytical results for this problem with an inverse approach by assuming the density is negligibly small outside the high density layer near the shock. With this approximation, the pressure is constant outside the high density region. The results obtained are quite like the results of modified Newtonian theory except that the effects of nose bluntness are retained.

The chock layer structure for a slightly nonsymmetric body is expected to
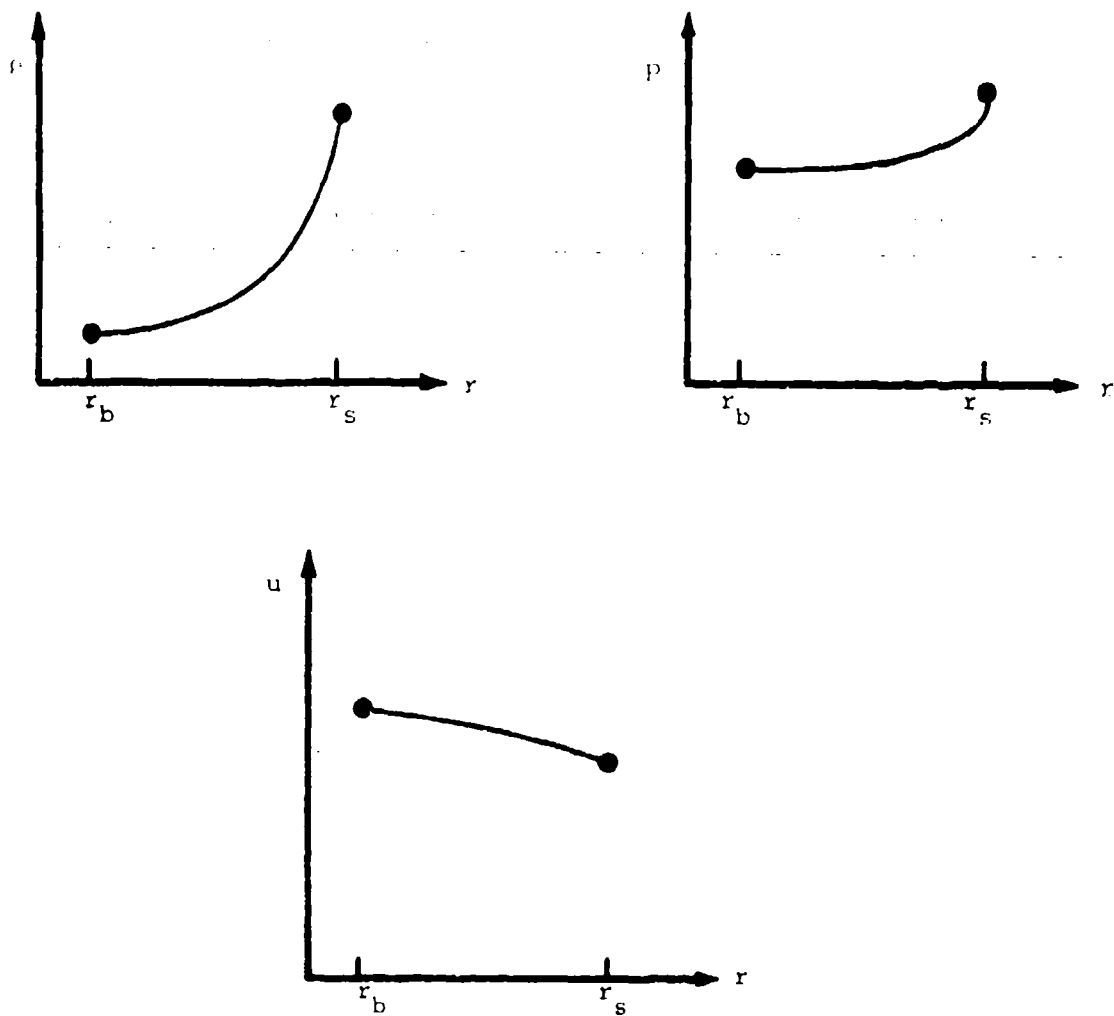
Figure 77. Qualitative Shock Layer Profiles
(Axisymmetric Case)

be quite similar except for the nonzero crossflow velocity v in the ϕ-direction. Of course, for a symmetric body, v is identically zero. The shock wave associated with a nonsymmetric body will also be nonsymmetric although the degree of nonsymmetry is typically different from that of the body. Consequently, the crossflow velocity is expected to vary across the shock layer. Figure 78 illustrates the qualitative behavior of the radial shock layer profiles for the nonsymmetric case.

Approximate forms of the integral conservation equations for the case of a nonsymmetric body are developed in the following paragraphs. For this case, assume that the shock layer is divided into a high density zone of thickness η near the shock wave and a relatively low density region in the remaining part of the shock layer between the high density zone and the body. Assume also that the pressure does not vary radially outside the high density zone and ignore any radial variations of the radial velocity u. Finally, use a linear variation across the shock layer for the azimuthal velocity v. These assumed profiles are shown in Figure 79.

To proceed, first integrate the mass conservation equation, Equation (492), with respect to time to obtain

$$
\iiint_{V_s} \rho \, dV = - \int_0^t dt \iint_{S_0} \rho \vec{V} \cdot \hat{n} \, dS + \rho_\infty \, V_\infty \tag{495}
$$

Here ρ_∞ is the freestream density and V_∞ is the volume of unit depth bounded by the shock wave and the sector of extent ϕ_0,

$$
V_\infty = \int_0^{\phi_0} \frac{r_s^2}{2} \, d\phi \tag{496}
$$

Also, V_s is the volume of unit depth bounded by the shock wave, the body, and the sector of extent ϕ_0. The volume V_s is bounded by the surface S_s. Making use of the assumed radial variation of the velocity v and density ρ, it is possible to rewrite the mass conservation equation as
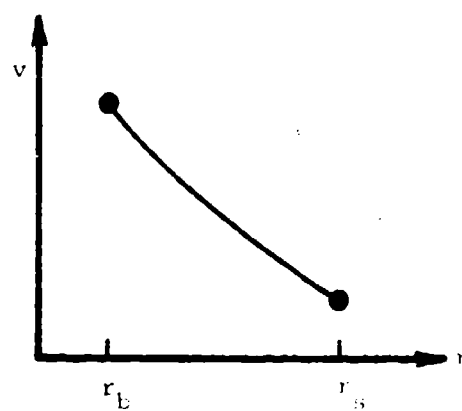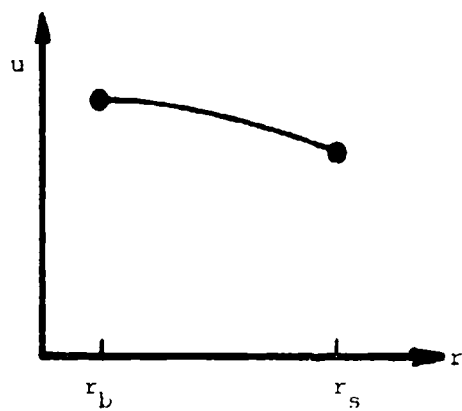
215
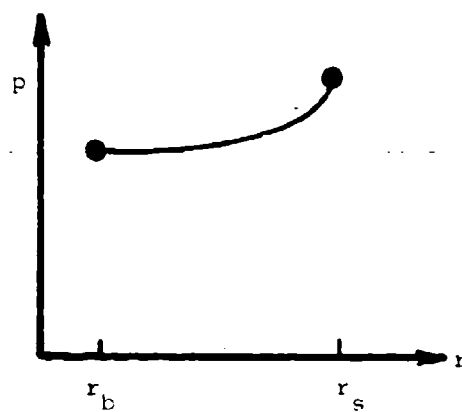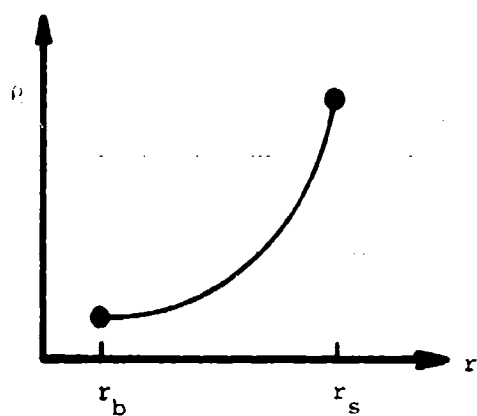
Figure 78. Qualitative Shock Layer Profiles
(Nonsymmetric Case)
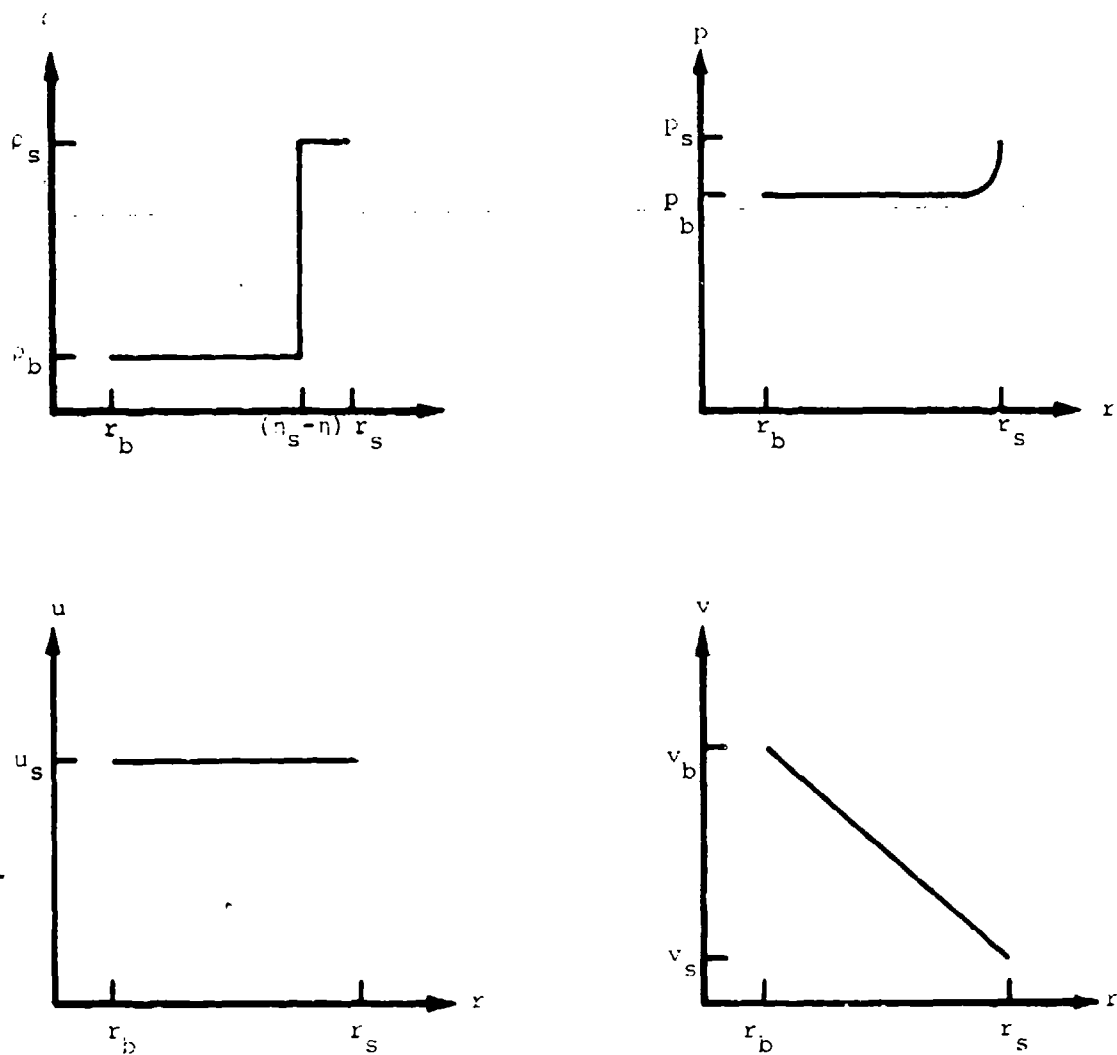
Figure 79. Assumed Shock Layer Profiles

$$\int_0^{\phi_0} \{(\rho_s-\rho_b)\eta\, r_s + \rho_b \frac{(r_s^2-r_b^2)}{2} - (\rho_s-\rho_b)\frac{\eta^2}{2} - \rho_\infty \frac{r_s^2}{2}\}\, d\phi \quad (497)$$

$$= -\int_0^t \{(\rho_s-\rho_b)v_s\eta + \rho_b(r_s-r_b)\frac{(v_s+v_b)}{2} + (\rho_s-\rho_b)\frac{(v_s-v_2)\eta^2}{2(r_s-r_b)}\}\, dt \Big|_{\phi=\phi_0}$$

The subscript s refers to conditions just downstream of the shock, b refers to conditions on the body, and ∞ refers to the freestream conditions. If the bow shock wave is assumed to be sufficiently strong that ρ_s/ρ_∞ is large and η is small compared to (r_s-r_b), it is possible to ignore terms of order η^2 and to obtain

$$\int_0^{\phi_0} \{(\rho_s-\rho_b)\eta\, r_s + \rho_b \frac{(r_s^2-r_b^2)}{2} - \rho_\infty \frac{r_s^2}{2}\}\, d\phi \quad (498)$$

$$= -\int_0^t \{(\rho_s-\rho_b)\, v_s\, \eta + \rho_b\, (r_s-r_b)\frac{(v_s+v_b)}{2}\}\, dt \Big|_{\phi=\phi_0}$$

An even simpler result is obtained if ρ_b compared to ρ_s is ignored , where the two are directly compared,

$$\int_0^{\phi_0} \{\rho_2\, \eta\, r_s - \rho_\infty \frac{r_s^2}{2}\}\, d\phi = -\int_0^t \{\rho_2\, v_s\, \eta + \rho_b(r_s-r_b)\frac{(v_s+v_b)}{2}\}\, dt \Big|_{\phi=\phi_0} \quad (499)$$

Newton's second law, Equation (493), contains an integral giving the net pressure force acting on the surface S. This expression for the net pressure force can be rewritten as

$$-\iint_S p\hat{n}\, dS = -p_\infty \int_0^{\phi_0} r_s\, \hat{n}_s\, d\phi - \int_{r_b}^{r_s} p\hat{n}\, dr\Big|_{\phi=0} \quad (500)$$

$$- \int_{r_b}^{r_s} p\hat{n}\, dr\Big|_{\phi=\phi_0} + \int_0^{\phi_0} p_b\, \hat{n}_b\, r_b\, d\phi$$

where here n_b is the outward unit normal to the body. Also, use has been made of the fact that the pressure p is equal to the constant freestream value p_∞ ahead of the shock wave. Using Green's theorem in the plane, Equation (500)

can be rewritten as

$$- \iint_S p \, \hat{n} \, dS = \int_0^{\phi_0} (p_{b0} - p_\infty) \hat{n}_b \, r_b \, d\phi + \int_0^{\phi_0} (p_b - p_{b0}) \hat{n}_b \, r_b \, d\phi$$

$$- \int_{r_b}^{r_s} (p - p_b) \hat{n} \, dr \bigg|_{\phi=0} - \int_{r_b}^{r_s} (p - p_b) \hat{n} \, dr \bigg|_{\phi=\phi_0} \qquad (501)$$

$$- \int_{r_b}^{r_s} (p_b - p_\infty) \hat{n} \, dr \bigg|_{\phi=0} - \int_{r_b}^{r_s} (p_b - p_\infty) \hat{n} \, dr \bigg|_{\phi=\phi_0}$$

where p_{b0} is a reference value of the surface pressure that will be specified more precisely later. Since $(p_{b0} - p_\infty)$ is a constant, Green's theorem can be used to obtain

$$\int_0^{\phi_0} (p_{b0} - p_\infty) \hat{n}_b \, r_b \, d\phi = - \int_0^{r_b} (p_{b0} - p_\infty) \hat{n} \, dr \bigg|_{\phi=0} - \int_0^{r_b} (p_{b0} - p_\infty) \hat{n} \, dr \bigg|_{\phi=\phi_0} \qquad (502)$$

Thus, the expression for the net pressure force becomes

$$- \iint_S p\hat{n} \, dS = \int_0^{\phi_0} (p_b - p_{b0}) \, \hat{n}_b \, r_b \, d\phi \qquad (503)$$

$$- (p_{b0} - p_\infty) \hat{n} \, r_s \big|_{\phi=0} - (p_{b0} - p_\infty) \, \hat{n} \, r_s \big|_{\phi=\phi_0}$$

$$- \int_{r_b}^{r_s} (p - p_{b0}) \hat{n} \, dr \bigg|_{\phi=0} - \int_{r_b}^{r_s} (p - p_{b0}) \hat{n} \, dr \bigg|_{\phi=\phi_0}$$

Using the profiles shown in Figure 79, the integrals on the left-hand side of Equation (493) can be evaluated and thus produce the following form of Newton's second law,

$$\frac{d}{dt} \int_0^{\phi_0} \{\vec{v}_2 [\rho_b \frac{r_s^2 - r_b^2}{2} + (\rho_s - \rho_b) r_s \, \eta] + \hat{e}_\phi (v_b - v_s) \rho_b \frac{(r_s + 2r_b)}{6} (r_s - r_b)\} \, d\phi$$

$$+ \{\rho_b (r_s - r_b) [\hat{e}_r \, u_s \, \frac{v_s + v_b}{2} + \hat{e}_\phi \, \frac{v_s^2 + v_s v_b + v_b^2}{3}]$$

$$+ (\rho_s - \rho_b)[\vec{v}_s \ (v_s n + \frac{v_b - v_s}{r_s - r_b} \frac{n^2}{2}) + \hat{e}_\phi \ \frac{v_b - v_s}{r_s - r_b} n)(v_s n + (v_b - v_s n^2))]\}_{\phi = \phi_0}$$

$$= \int_0^{\phi_0} (p_b - p_{b0}) \hat{n}_b r_b \ d\phi \tag{504}$$

$$- \{(p_{b0} - p_\infty) r_s \hat{n} + (\bar{p} - p_{b0})(r_s - r_b) \hat{n}\}_{\phi = \phi_0}$$

$$- \{(p_{b0} - p_\infty) r_s \hat{n} + (\bar{p} - p_{b0})(r_s - r_b) \hat{n}\}_{\phi = 0}$$

Here the terms of order n^2 have been ignored when they are directly compared with terms of order n. Also, $\bar{p}$ represents the radially averaged value of the pressure in the shock layer.

In order to eliminate the internal energy e as a variable, the following discussion is restricted to calorically perfect gases for which

$$\rho e = \frac{p}{\gamma - 1} \tag{505}$$

In this case, the energy equation , Equation (494), can be rewritten

$$\frac{d}{dt} \iiint_V (\frac{p}{\gamma - 1} + \frac{1}{2} \rho v^2) \ dV \ + \iint_{S_0} (\frac{p}{\gamma - 1} + \frac{1}{2} \rho v^2) \vec{v} \cdot \hat{n} \ dS$$

$$= - \iint_S p\vec{v} \cdot \hat{n} \ dS \tag{506}$$

Since $\vec{v} \cdot \hat{n}$ vanishes on $\phi = 0$, because of symmetry there, as well as on Σ because $\vec{v}$ vanishes on Σ, Equation (506) can be rewritten as

$$\frac{d}{dt} \iiint_V (\frac{p}{\gamma - 1} + \frac{1}{2} \rho v^2) dV \ + \iint_{S_0} \frac{1}{2} \rho v^2 \ \vec{v} \cdot \hat{n} \ dS$$

$$= \int_0^{\phi_0} p_b \ \vec{v}_b \cdot \hat{n}_b \ d\phi - \int_{r_b}^{r_s} \frac{\gamma}{\gamma - 1} pv \ dr|_{\phi = \phi_0} \tag{507}$$

Since the pressure p equals p_∞ on Σ, then

$$\iiint_V \frac{p}{\gamma - 1} \ dV \ = \frac{p_\infty}{\gamma - 1} \iiint_{V - V_s} dV + \iiint_{V_s} \frac{p}{\gamma - 1} \ dV \tag{508}$$

or

220

$$\iiint_V \frac{p}{\gamma-1}\, dV = \frac{p_\infty}{\gamma-1}\left[V - \int_0^{\phi_0} \frac{1}{2}\, r_s^2\, d\phi\right] \tag{509}$$

$$+ \int_0^{\phi_0} \frac{p_b}{\gamma-1}\, \frac{r_s^2-r_b^2}{2}\, d\phi + \iiint_{V_s} \frac{p-p_b}{\gamma-1}\, dV$$

Making use of the profiles shown in Figure 79, evaluate the integrals
on the left-hand side of Equation (507) and thus obtain the following form of
the energy equation,

$$\frac{d}{dt} \int_0^{\phi_0} \left\{ \frac{p_b}{\gamma-1}\, \frac{r_s^2-r_b^2}{2} + (\rho_2-\rho_b)\left[\frac{v_s^2}{2}\, r_s\, \eta - \frac{v_s(v_b-v_s)}{2(r_s-r_b)}\, r_s\, \eta^2 + \frac{(v_b-v_s)^2}{6(r_s-r_b)^2}\, r_s\, \eta^3\right] \right.$$

$$+ \rho_b\left[\frac{v_s^2}{2}\, \frac{r_s^2-r_b^2}{2} + \frac{v_s(v_b-v_s)}{6}\, (2r_b+r_s)(r_s-r_b) + \frac{(v_b-v_s)^2}{24}\, (r_s+3r_b)(r_s-r_b)\right]\right\}d\phi$$

$$+ \left\{\frac{1}{2}\, \rho_b\left[u_s^2\, \frac{v_s+v_b}{2} + \frac{v_s^3+v_b v_s^2+v_b^2 v_s+v_b^3}{4}\right](r_s-r_b)\right.$$

$$+ \frac{1}{2}\, (\rho_2-\rho_b)\left[v_s^2 v_s \eta + \frac{(v_b-v_s)}{r_s-r_b}\, \eta\right)\, \frac{\eta}{2}\, (u_s^2+3v_s^2) + \left(\frac{v_b-v_s}{r_s-r_b}\, \eta\right)^2 v_s \eta$$

$$\left.\left. + \left(\frac{v_b-v_s}{r_s-r_b}\, \eta\right)^3\, \frac{\eta}{4}\right]\right\}_{\phi=\phi_0}$$

$$= \int_0^{\phi_0} p_b\, \vec{v}_b\cdot\hat{n}_b\, r_b\, d\phi + \frac{p_\infty}{\gamma-1}\, \frac{d}{dt} \int_0^{\phi_0} \frac{1}{2}\, r_s^2\, d\phi \tag{510}$$

$$- \frac{\gamma}{\gamma-1}\left(p_b\, \frac{v_s+v_b}{2}\, (r_s-r_b) + (\bar{p}-p_b)v_s \eta\right)_{\phi=\phi_0}$$

$$- \frac{d}{dt} \iiint_{V_s} \frac{p-p_b}{\gamma-1}\, dV$$

In addition to satisfying the conservation equations, the flow quantities
must also satisfy the shock jump relations. For a three-dimensional steady
flow, these jump relations are

$$\rho_\infty\, \vec{V}_\infty\cdot\hat{n}_s = \rho_s\, \vec{V}_s\cdot\hat{n}_s = m \tag{511}$$

$$m\, \vec{V}_\infty + p_\infty\, \hat{n}_s = m\, \vec{V}_s + p_s\, \hat{n}_s \tag{512}$$

$$m\, (h_\infty + \frac{V_\infty^2}{2}) = m(h_s + \frac{V_s^2}{2}) \tag{513}$$

221

Here h is the enthalpy per unit mass and n_s is a unit vector normal to the shock wave. For a calorically perfect gas,

$$h = \frac{1}{\gamma - 1} \frac{p}{\rho} \tag{514}$$

In this case, the shock jump relations can be manipulated to yield

$$\frac{\rho_s}{\rho_\infty} = \frac{(\gamma + 1) M_n^2}{(\gamma - 1) M_n^2 + 2} \tag{515}$$

where M_n is the normal component of the freestream Mach number,

$$M_n = \frac{\vec{V}_\infty \cdot \hat{n}_s}{a_\infty} \tag{516}$$

$$= M_\infty \hat{e}_z \cdot \hat{n}_s$$

The sound speed a is related to the pressure and density by

$$a^2 = \frac{\gamma p}{\rho} \tag{517}$$

Using Equation (515), it is possible to solve for the normal component of the velocity downstream of the shock wave as

$$\frac{\vec{V}_s \cdot \hat{n}_s}{\vec{V}_\infty \cdot \hat{n}_s} = \frac{\gamma - 1}{\gamma + 1} + \frac{2}{(\gamma + 1) M_\infty^2 (\hat{n}_s \cdot \hat{e}_z)^2}. \tag{518}$$

while Equation (512) can be used to show that the tangential component of velocity is conserved across the shock wave,

$$\vec{V}_s \times \hat{n}_s = \vec{V}_\infty \times \hat{n}_s \tag{519}$$

In the steady, three-dimensional flow, the shock wave is represented by $r = r_s(\phi, z)$. Here (r, ϕ, z) are orthogonal cylindrical polar coordinates. The velocity just downstream of the shock, $\vec{V}_s$, is then expressed in these cylindrical polar coordinates as

$$\vec{V}_s = u_s \hat{e}_r + v_s \hat{e}_\phi + w_s \hat{e}_z \tag{520}$$

and the outward unit normal to the shock wave is given by

$$\hat{n}_s = \frac{\hat{e}_r - \frac{\partial \ln r_s}{\partial \phi} \hat{e}_\phi - \frac{\partial r_s}{\partial z} \hat{e}_z}{[1 + (\frac{\partial \ln r_s}{\partial \phi})^2 + (\frac{\partial r_s}{\partial z})^2]^{1/2}} \tag{521}$$

222

Equations (518) and (519) can then be used to determine the jump relations

for the three components of the velocity; the results are

$$\frac{u_s}{V_\infty} = \frac{2}{\gamma+1} \frac{\partial r_s}{\partial z} [1 - \frac{1 + (\frac{\partial \ln r_s}{\partial \phi})^2 (\frac{\partial r_s}{\partial z})^2}{M_\infty^2 (\frac{\partial r_s}{\partial z})^2}] / [1 + (\frac{\partial \ln r_s}{\partial \phi})^2 + (\frac{\partial r_s}{\partial z})^2] \quad (522)$$

$$\frac{v_s}{V_\infty} = -\frac{2}{\gamma+1} \frac{\partial r_s}{\partial z} \frac{\partial \ln r_s}{\partial \phi} [1 - \frac{1 + (\frac{\partial \ln r_s}{\partial \phi})^2 (\frac{\partial r_s}{\partial z})^2}{M_\infty^2 (\frac{\partial r_s}{\partial z})^2}] / [1 + (\frac{\partial \ln r_s}{\partial \phi})^2 + (\frac{\partial r_s}{\partial z})^2]$$

$$(523)$$

$$\frac{w_s}{V_\infty} = [1 + (\frac{\partial \ln r_s}{\partial \phi})^2 + (\frac{\partial r_s}{\partial z})^2 \{\frac{\gamma-1}{\gamma+1} + \frac{2}{\gamma+1} \frac{1 + (\frac{\partial \ln r_s}{\partial \phi})^2 (\frac{\partial r_s}{\partial z})^2}{M_\infty^2 (\frac{\partial r_s}{\partial z})^2}\}]$$

$$+ [1 + (\frac{\partial \ln r_s}{\partial \phi})^2 + (\frac{\partial r_s}{\partial z})^2] \quad (524)$$

Also, the density ratio can be expressed as

$$\frac{\rho_s}{\rho_\infty} = [\frac{(\gamma+1) M_\infty^2 (\partial r_s/\partial z)^2}{1 + (\frac{\partial \ln r_s}{\partial \phi})^2 + (\frac{\partial r_s}{\partial z})^2}] / [\frac{(\gamma-1) M_\infty^2 (\partial r_s/\partial z)^2}{1 + (\frac{\partial \ln r_s}{\partial \phi})^2 + (\frac{\partial r_s}{\partial z})^2} + 2] \quad (525)$$

In the hypersonic small disturbance theory limit, corresponding to $M_\infty \to \infty$ and

$\partial r_s/\partial z \to 0$ such that the product $M_\infty \partial r_s/\partial z$ is finite, exists

$$\frac{u_s}{V_\infty} = \frac{2}{\gamma+1} \frac{\partial r_s}{\partial z} [1 - \frac{1}{(M_\infty \frac{\partial r_s}{\partial z})^2}] \quad (526)$$

$$\frac{v_s}{V_\infty} = -\frac{2}{\gamma+1} \frac{\partial r_s}{\partial z} \frac{\partial \ln r_s}{\partial \phi} [1 - \frac{1}{(M_\infty \frac{\partial r_s}{\partial z})^2}] \quad (527)$$

$$\frac{w_s}{V_\infty} = 1 \quad (528)$$

$$\frac{\rho_s}{\rho_\infty} = \frac{(\gamma+1)(M_\infty \partial r_s/\partial z)^2}{(\gamma-1)(M_\infty \partial r_s/\partial z)^2 + 2} \quad (529)$$

neglecting terms of order $(\partial r_s/\partial z)^2$. Because flows past bodies which are only slightly nonsymmetric are considered later, terms of order $(\partial \ln r_s/\partial \phi)^2$ have also been neglected. In the Hayes equivalence principle, one replaces z everywhere it appears in these shock relations with $V_\infty t$.

b. The Axisymmetric Problem

It is instructive to see how the developed equations reduce to the axisymmetric case considered earlier by Fiorino (Reference 62). In this case, all scalar physical quantities are independent of ϕ and v vanishes identically. Equations (491), (504), and (510) then reduce to

$$(\rho_s-\rho_b)\eta\, r_s + \rho_b \frac{r_s^2-r_b^2}{2} = \rho_\infty \frac{r_s^2}{2} \tag{530}$$

$$\frac{d}{dt}\,[\rho_\infty\, u_s\, \frac{r_s^2}{2}] \int_0^{\phi_0} \hat{e}_r\cdot\hat{e}\; d\phi] = -(p_b-p_\infty)r_s[(\hat{e}_\phi\cdot\hat{e})_{\phi=\phi_0} - (\hat{e}_\phi\cdot\hat{e})_{\phi=0}] \tag{531}$$

$$\frac{d}{dt}\,[\frac{p_b}{\gamma-1} \frac{r_s^2-r_b^2}{2} + \rho_\infty \frac{u_s^2}{2} \frac{r_s^2}{2}] = \frac{p_\infty}{\gamma-1} \frac{d}{dt} (\frac{r_s^2}{2}) + p_b\, u_b\, r_b \tag{532}$$

where terms of relative order η have been ignored as unimportant. Also, the e-component of the momentum equation has been taken, where e is any constant unit vector. Since

$$\int_0^{\phi_0} \hat{e}_r\cdot\hat{e}\; d\phi = \hat{e}_\phi\cdot\hat{e})_{\phi=0} - \hat{e}_\phi\cdot\hat{e})_{\phi=\phi_0}$$

Equation (531) can be rewritten

$$\frac{d}{dt} (\rho_\infty\, u_s\, \frac{r_s^2}{2}) = (p_b-p_\infty)\, r_s \tag{533}$$

Provided the shock trajectory $r_s(t)$ is known, the body trajectory $r_b(t)$ and pressure $p_b(t)$ can be calculated exactly and explicitly from these equations. Fiorino (Reference 62) was the first to solve this inverse problem. The resulting solution is

$$p_b = p_\infty + \frac{1}{r_s} \frac{d}{dt} (\rho_\infty\, u_s\, \frac{r_s^2}{2}) \tag{534}$$

$$r_b{}^2 = p_b{}^{-1/\gamma} \{I_0 + \int_0^t p_b{}^{\frac{1-\gamma}{\gamma}} [\frac{\gamma-1}{2\gamma} \frac{d}{dt} (\rho_\infty u_s{}^2 r_s{}^2) + \frac{d}{dt} (\frac{r_s}{2\gamma} \frac{d}{dt} (\rho_\infty u_g r_s{}^2))] dt\}$$

<div align="right">(535)</div>

where

$$u_g = \frac{2}{\gamma+1} \frac{dr_s}{dt} [1 - (a_\infty / \frac{dr_s}{dt})^2] \qquad (536)$$

The constant of integration I_0 is determined by the initial conditions at $t=0$ and can be viewed as being due to the effects of nose bluntness. That is, examination of Equation (535) for the case of a power law shock (e.g. $r_s \sim z^m$) shows that the integral term gives a result that is identical to that obtained assuming a self-similar solution (e.g., $r_b \sim z^m$). The first term in Equation (535) gives a contribution for power law shocks that grows like $z^{1/2\gamma}$, the same result obtained by Yakura (Reference 6l) and Sychev (Reference 59) in their studies of the effects of nose bluntness. This bluntness term can be interpreted as giving the difference between the actual body shape and the body shape given by the self-similar solution, for a given shock shape. Because the small-disturbance equations overestimate the surface entropy and thus underestimate the surface density, the actual body radius is greater than that given by the self-similar solution alone. In this sense, the bluntness term is determined as giving a negative entropy displacement effect. Because of the use of the slender body approximation and the equivalence principle, these results are not strictly valid in the nose region where dr_s/dt is of the order of V_∞ or larger. As a consequence, the constant of integration I_0, which determines the relative contribution of nose bluntness, must be specified or determined from considerations that lie outside the present theory. Fiorino (Reference 62) obtained results that compared well with other calculations by determining I_0 from the condition that the shock radius r_s and body radius r_b are equal (to within the accuracy of the theory) when the shock

dr_s/dt equals V_∞. This is equivalent to a "patching" procedure (not a "matching" condition in the sense of the theory of matched asymptotic expansions) in which the small disturbance solution valid downstream of the nose region is patched to a rather crude nose region solution at a point that corresponds roughly to the boundary to the two regions.

Note that Equations (534) and (535) do not contain ρ_b. Thus, these results are valid for nonzero ρ_b, although terms of relative order η have been neglected. The density on the body, ρ_b, for a blunt-nosed body can be estimated from the normal shock relations and the state equation. The entropy on the body streamline follows from the normal shock relations,

$$\frac{s_b - s_\infty}{c_p} = \frac{1}{\gamma} \ell n \frac{p_{sn}}{p_\infty} - \ell n \frac{\rho_{sn}}{\rho_\infty}$$

$$= \frac{1}{\gamma} \ell n \left[\frac{2\gamma M_\infty^2 - \gamma + 1}{\gamma + 1} \right] - \ell n \left[\frac{(\gamma+1) M_\infty^2}{(\gamma-1)M_\infty^2 + 2} \right]$$

The density on the body follows from the state equation as

$$\frac{\rho_b}{\rho_\infty} = \left(\frac{p_b}{p_\infty} \right)^{1/\gamma} \exp \left(- \frac{s_b - s_\infty}{c_p} \right)$$

Substituting for the body pressure and entropy, gives

$$\frac{\rho_b}{\rho_\infty} = \left(1 + \frac{\gamma}{r_s} \frac{d}{dt} \frac{(u_s r_s^2)}{z \, a_\infty^2} \right)^{1/\gamma} \left(\frac{(\gamma+1)M_\infty^2}{(\gamma-1)M_\infty^2 + 2} \right) \left(\frac{2\gamma M_\infty^2 - \gamma + 1}{\gamma + 1} \right)^{-1/\gamma}$$

Hence it can be seen that, in the hypersonic small disturbance theory limit, ρ_b is quite small for blunt-nosed bodies (viz. $\rho_b/\rho_\infty \sim M_\infty^{-2/\gamma}$).

c. Perturbation Expansion

To study the effects of slight asymmetries in the body shape, expand the various flow quantities in Fourier cosine series (the sine terms are absent because of the presumed symmetry about $\phi = 0$),

$$r_b(\phi,t) = r_{b0}(t) + \sum_{n=1} \varepsilon_n r_{bn}(t) \cos n\phi \qquad (537a)$$

$$r_s(\phi,t) = r_{s0}(t) + \sum_{n=1} \epsilon_n r_{sn}(t) \cos n\phi \tag{537b}$$

$$p(\phi,t) = p_0(t) + \sum_{n=1} \epsilon_n p_n(t) \cos n\phi \tag{537c}$$

$$\rho(\phi,t) = \rho_0(t) + \sum_{n=1} \epsilon_n \rho_n(t) \cos n\phi \tag{537d}$$

$$\eta(\phi,t) = \eta_0(t) + \sum_{n=1} \epsilon_n \eta_n(t) \cos n\phi \tag{537e}$$

$$u(\phi,t) = u_0(t) + \sum_{n=1} \epsilon_n u_n(t) \cos n\phi \tag{537f}$$

$$v(\phi,t) = \sum_{n=1} \epsilon_n v_n(t) \frac{\sin n\phi}{n} \tag{537g}$$

Here the subscript zero refers to the axisymmetric solution. The ϵ_n are small parameters that characterize the contributions of the various Fourier components. Provided the ϵ_n are small, n=1 gives the effects of angle of attack while n=2 corresponds to a slightly elliptical cross-section.

Before proceeding to the derivation of the equations governing these perturbation quantities, it is useful to rewrite the momentum equation, Equation (504), in the following form

$$\int_0^{\phi_0} (e_r \hat{A} + e_\phi \hat{B}) d\phi + (e_r \hat{C} + e_\phi \hat{D})\bigg|_{\phi=0}^{\phi=\phi_0} = 0 \tag{538}$$

where

$$\hat{A} = \frac{\partial}{\partial t} [u_s(\rho_b \frac{r_s^2 - r_b^2}{2} + (\rho_s - \rho_b)r_s\eta)] - (p_b - p_{b0})r_b \tag{539a}$$

$$\hat{B} = \frac{d}{dt} [v_s(\rho_b \frac{r_s^2 - r_b^2}{2} + (\rho_s - \rho_b)r_s\eta) + \rho_b(v_b - v_s) \frac{r_s + 2r_b}{6}(r_s - r_b)] \tag{539b}$$

$$\hat{C} = \rho_b(r_s - r_b) u_s \frac{(v_s + v_b)}{2} + (\rho_s - \rho_b)\eta u_s(v_s + \frac{v_b - v_s}{r_s - r_b} \frac{\eta}{2}) \tag{539c}$$

$$\hat{D} = \rho_b(r_s - r_b) \frac{v_s^2 + v_s v_b + v_b^2}{3} + (\rho_s - \rho_b)\eta v_s (v_s + \frac{v_b - v_s}{r_s - r_b} \frac{\eta}{2})$$

$$+ (\rho_s - \rho_b) \frac{v_b - v_s}{r_s - r_b} \eta^2 (v_s + \frac{v_b - v_s}{r_s - r_b} \frac{\eta}{3}) \tag{539d}$$

$$+ (p_{b0} - p_\infty)r_s + (\bar{p} - p_{b0})(r_s - r_b)$$

Here use has been made of the fact that $n_b = e_r$ to within an error of order ε_n. Since

$$\frac{d\hat{e}_\phi}{d\phi} = -\hat{e}_r \quad , \quad \frac{d\hat{e}_r}{d\phi} = \hat{e}_\phi$$

Equation (538) can be rewritten as

$$\int_0^{\phi_0} \{\hat{e}_r [A + \frac{dC}{d\phi} - D] + \hat{e}_\phi [B + \frac{dD}{d\phi} + C]\}d\phi = 0 \tag{540}$$

The assumed Fourier expansions given by Equations (537) imply the following forms for the expansions of A, B, C, and D,

$$A = A_0 + \sum_n \varepsilon_n A_n \cos n\phi \tag{541a}$$

$$B = \sum_n \varepsilon_n B_n \frac{\sin n\phi}{n} \tag{541b}$$

$$C = \sum_n \varepsilon_n C_n \frac{\sin n\phi}{n} \tag{541c}$$

$$D = D_0 + \sum_n \varepsilon_n D_n \cos n\phi \tag{541d}$$

where

$$A_0 = \frac{d}{dt} [u_{s0}(\rho_{b0} \frac{r_{s0}^2 - r_{b0}^2}{2} + (\rho_{s0} - \rho_{b0})r_{s0} \eta_0)] \tag{542a}$$

$$D_0 = (p_{b0} - p_\infty)r_{s0} + (\bar{p}_0 - p_{b0})(r_{s0} - r_{b0}) \tag{542b}$$

$$A_n = \frac{d}{dt} [u_{sn}(\rho_{b0} \frac{r_{s0}^2 - r_{b0}^2}{2} + (\rho_{s0} - \rho_{b0})r_{s0} \eta_0)$$

$$+ u_{s0}(\rho_{bn} \frac{r_{s0}^2 - r_{b0}^2}{2} + \rho_{b0}(r_{s0}r_{sn} - r_{b0}r_{bn}) \tag{542c}$$

$$+ (\rho_{sn} - \rho_{bn})r_{s0} \eta_0 + (\rho_{s0} - \rho_{b0})(r_{sn}\eta_0 + r_{s0}\eta_n))] - p_{bn}r_{b0}$$

$$B_n = \frac{d}{dt} [v_{sn}(\rho_{b0} \frac{r_{s0}^2 - r_{b0}^2}{2} + (\rho_{b0} - \rho_{b0})r_{s0}\eta_0)] + \rho_{b0}(v_{bn} - v_{sn})\frac{(r_{s0} + 2r_{b0})}{6}(r_{s0} - r_{b0}) \tag{542d}$$

$$C_n = \rho_{b0}(r_{s0} - r_{b0}) u_{s0} \frac{v_{sn} + v_{bn}}{2} + (\rho_{s0} - \rho_{b0})\eta_0 u_{s0}(v_{sn} + \frac{v_{bn} - v_{sn}}{r_{s0} - r_{b0}} \frac{\eta_0}{2}) \tag{542e}$$

$$D_n = (p_{b0} - p_\infty) r_{sn} + \bar{p}_n (r_{s0} - r_{b0}) + (\bar{p}_0 - p_{b0})(r_{sn} - r_{bn}) \tag{542f}$$

250

ignoring all terms of order ε_n^2.

To proceed, substitute these Fourier expansions into the governing equations and collect the coefficients of the various ε_n. In this way, a sequence of equations is obtained, the lowest order of which govern the axisymmetric problem and are identical to the axisymmetric case considered earlier provided $(\bar{p}_0-p_{b0})(r_{s0}-r_{b0})$ compared to $(p_{b0}-p_\infty)r_{s0}$ is ignored.

From Equation (508), the first-order mass conservation equation is written as

$$(\rho_{sn}-\rho_{bn})\eta_0 \, r_{s0} + (\rho_{s0}-\rho_{b0})(\eta_n \, r_{s0} + \eta_0 \, r_{sn})$$

$$+ \rho_{bn} \frac{r_{s0}^2 - r_{b0}^2}{2} + \rho_{b0}(r_{s0}r_{sn} - r_{b0}r_{bn}) - \rho_\infty \, r_{s0} \, r_{sn} \qquad (543)$$

$$= -\int_0^t [(\rho_{s0}-\rho_\infty)\eta_0 \, v_{sn} + \rho_{b0}(r_{s0}-r_{b0}) \frac{v_{sn}+v_{bn}}{2}]dt$$

Substituting Equations (541) into Equation (540), gives

$$(A_0-D_0) \int_0^{\phi_0} \hat{e}_r \, d\phi + \sum_n \varepsilon_n(A_n + C_n - D_n) \int_0^{\phi_0} \hat{e}_r \cos n\phi \, d\phi \qquad (544)$$

$$+ \sum_n \frac{\varepsilon_n}{n} (B_n - n^2D_n + C_n) \int_0^{\phi_0} \hat{e}_\phi \sin d\phi \, d\phi = 0$$

To lowest order, $A_0 = D_0$, which is identical to the axisymmetric momentum equation, Equation (533) is used. Since ϕ_0 is arbitrary, the first-order momentum equations are obtained as

$$A_n + C_n - D_n = 0 \qquad (545a)$$

and

$$B_n - n^2D_n + C_n = 0 \qquad (545b)$$

or

$$\frac{d}{dt} \, [u_{sn}(\rho_{b0} \frac{r_{s0}^2-r_{b0}^2}{2} + (\rho_{s0}-\rho_{b0})r_{s0}\eta_0)$$

$$+ u_{s0}(\rho_{bn} \frac{r_{s0}^2 - r_{b0}^2}{2} + \rho_{b0}(r_{s0}r_{sn} - r_{b0}r_{bn}) + (\rho_{sn} - \rho_{bn})r_{s0}\eta_0 +$$

$$(\rho_{s0} - \rho_{b0})(r_{sn}\eta + r_{s0}\eta_n))]$$

$$+ \rho_{b0}(r_{s0} - r_{b0})u_{s0} \frac{v_{sn} + v_{bn}}{2} + (\rho_{s0} - \rho_{b0})\eta_0 u_{s0}(v_{sn} + \frac{v_{bn} - v_{sn}}{r_{s0} - r_{b0}} \frac{\eta_0}{2})$$

$$- p_{bn} r_{b0} - (p_{b0} - p_\infty)r_{sn} = 0 \tag{546}$$

and

$$\frac{d}{dt} [v_{sn}(\rho_{b0} \frac{r_{s0}^2 - r_{b0}^2}{2} + (\rho_{s0} - \rho_{b0})r_{s0}\eta_0)] + \rho_{b0}(v_{bn} - v_{sn}) \frac{(r_{s0} + 2r_{b0})}{6} (r_{s0} - r_{b0}) -$$

$$- n^2(p_{b0} - p_\infty)r_{sn}$$

$$+ \rho_{b0}(r_{s0} - r_{b0})u_{s0} \frac{v_{sn} + v_{bn}}{2} + (\rho_{s0} - \rho_{b0})\eta_0 u_{s0}(v_{sn} + \frac{v_{bn} - v_{sn}}{r_{s0} - r_{b0}} \frac{\eta_0}{2}) = 0$$

$$\tag{547}$$

The first-order energy equation can be obtained from Equation (510) as

$$\frac{d}{dt} [\frac{p_{bn}}{\gamma - 1} \frac{r_{s0}^2 - r_{b0}^2}{2} + \frac{p_{b0}}{\gamma - 1} (r_{sn}r_{s0} - r_{bn}r_{b0}) + (\rho_{sn} - \rho_{bn}) \frac{u_{s0}^2}{2} r_{s0}\eta_0$$

$$+ (\rho_{s0} - \rho_{b0})(u_{s0}u_{sn} r_{s0}\eta_0 + \frac{u_{s0}^2}{2} r_{sn}\eta_0 + \frac{u_{s0}^2}{2} r_{s0}\eta_n)$$

$$+ \rho_{bn} \frac{u_{s0}^2}{2} (\frac{r_{s0}^2 - r_{b0}^2}{2}) + \rho_{b0}(u_{s0}u_{sn} \frac{r_{s0}^2 - r_{b0}^2}{2} + \frac{u_{s0}^2}{2} (r_{s0}r_{sn} - r_{b0}r_{bn}))]$$

$$+ \frac{1}{2} \rho_{b0}u_{s0}^2 \frac{v_{sn} + v_{bn}}{2} (r_{s0} - r_{b0}) + \frac{1}{2}(\rho_{s0} - \rho_{b0})(u_{s0}^2 v_{sn}\eta_0 + \frac{v_{bn} - v_{sn}}{r_{s0} - r_{b0}} \frac{\eta_0^2}{2} u_{s0}^2)$$

$$= p_{bn} r_{b0} \frac{dr_{b0}}{dt} + p_{b0} \frac{d}{dt} (r_{b0} - r_{bn}) \tag{548}$$

$$+ \frac{p_\infty}{\gamma - 1} \frac{d}{dt} (r_{s0}r_{sn}) - \frac{\gamma}{\gamma - 1} p_{b0} \frac{v_{sn} + v_{bn}}{2} (r_{s0} - r_{b0})$$

ignoring terms of order $\bar{p}_n(r_{s0} - r_{b0})$ compared to $(p_{b0} - p_\infty)r_{sn}$.

Equations (543), (546) and (547) are valid for either pointed or blunt-nosed bodies. As interest in this work is with the effects of bluntness in hypersonic flow, this discussion is restricted to this case and consideration of the limit $\rho_b \to 0$. Taking ρ_b to zero, produces a simplified form of the first-order equations,

$$\frac{d}{dt} (\rho_{sn}\eta_0 r_{s0} + \rho_{s0}\eta_n r_{s0} + \rho_{s0}\eta_0 r_{sn} - \rho_\infty r_{s0} r_{sn}) + \rho_{s0}\eta_0 v_{sn} = 0 \tag{549}$$

$$\frac{d}{dt} (\rho_{s0} r_{s0}\eta_0 u_{sn} + \rho_{sn} r_{s0} u_{s0} + \rho_{s0} r_{s0}\eta_n u_{s0} + \rho_{s0} r_{sn}\eta_0 u_{s0}) \tag{550}$$

$$+ \rho_{s0}\eta_0 u_{s0} (v_{sn} + \frac{v_{bn}-v_{sn}}{r_{s0}-r_{b0}} \frac{\eta_0}{2}) - p_{bn} r_{b0} - (p_{b0}-p_\infty) r_{sn} = 0$$

$$\frac{d}{dt} (\rho_{s0} r_{s0}\eta_0 u_{sn}) - n^2 (p_{b0}-p_\infty) r_{sn} + \rho_{s0}\eta_0 u_{s0}(v_{sn} + \frac{v_{bn}-u_{sn}}{r_{s0}-r_{b0}} \frac{\eta_0}{2}) = 0 \tag{551}$$

$$\frac{d}{dt} [\frac{p_{bn}}{\gamma-1} \frac{r_{s0}^2-r_{b0}^2}{2} + \frac{p_{b0}}{\gamma-1} (r_{sn}r_{s0}-r_{bn}r_{b0}) + \rho_{sn} \frac{u_{s0}^2}{2} r_{s0}\eta_0$$

$$+ \rho_{s0} (u_{s0}u_{sn}r_{s0}\eta_0 + \frac{u_{s0}^2}{2} r_{sn}\eta_0 + \frac{u_{s0}^2}{2} r_{s0}\eta_n)]$$

$$+ \frac{1}{2} \rho_{s0} u_{s0}^2 \eta_0 (v_{sn} + \frac{v_{bn}-v_{sn}}{r_{s0}-r_{b0}} \frac{\eta_0}{2}) - p_{bn} r_{b0} \frac{dr_{b0}}{dt} \tag{552}$$

$$- p_{b0} \frac{d}{dt} (r_{b0}r_{bn}) - \frac{p_\infty}{\gamma-1} \frac{d}{dt} (r_{s0}r_{sn}) + \frac{\gamma}{\gamma-1} p_{b0}(r_{s0}-r_{b0}) \frac{v_{sn}+v_{bn}}{2} = 0$$

d. Solution to the Inverse Problem

Equations (549) through (552) can be solved exactly and explicitly if the shock trajectory $r_{sn}(t)$ is known. In this inverse approach in which the shock trajectory is given and the body trajectory $r_{bn}(t)$ is calculated, all shock quantities are known in terms of r_{sn},

$$u_{sn} = \frac{2}{\gamma+1} (1 + a_\infty^2/\dot{r}_{s0}^2) \frac{dr_{sn}}{dt} \tag{553}$$

$$v_{sn} = \frac{2}{\gamma+1} n^2 \frac{\dot{r}_{s0}}{r_{s0}} (1 - a_\infty^2/\dot{r}_{s0}^2) r_{sn} \tag{554}$$

$$\rho_{sn} = \rho_\infty \frac{2(\gamma+1)\dot{r}_{s0}}{(\gamma-1)\dot{r}_{s0}^2 + 2a_\infty^2} (1 - \frac{(\gamma-1)\dot{r}_{s0}^2}{(\gamma-1)\dot{r}_{s0}^2 + 2a_\infty^2}) \frac{dr_{sn}}{dt} \tag{555}$$

Here the dot over r_{s0} is a short-hand notation for dr_{s0}/dt. Thus, integrating the mass conservation equation, Equation (549), gives

231

$$\rho_{s0} r_{s0} \eta_n = \rho_\infty r_{s0} r_{sn} - \rho_{s0} \eta_0 r_{sn} - \rho_{sn} \eta_0 r_{s0}$$

$$- \int_0^t \rho_{s0} \eta_0 v_{sn} dt + J_n \tag{556}$$

where J_n is a constant of integration. Specification of the shock trajectory r_{sn} and knowledge of the zeroth-order, axisymmetric solution allows explicit evaluation of the right-hand side of Equation (556), once the initial value of η_n is known. Subtracting Equation (551) from Equation (550) eliminates v_{bn} and allows determination of the pressure on the body, p_{bn}. The result is

$$p_{bn} = (n^2 - 1) \frac{r_{sn}}{r_{b0}} (p_{b0} - p_\infty) \tag{557}$$

$$+ \frac{1}{r_{b0}} \frac{d}{dt} \left(\rho_{s0} r_{s0} \eta_0 (u_{sn} - v_{sn}) + \rho_{s0} u_{s0} (r_{sn} \eta_0 + r_{s0} \eta_n) + \rho_{sn} r_{s0} \eta_0 u_{s0} \right)$$

Either of the momentum equations can then be solved for the azimuthal velocity in the body, v_{bn}. The result is

$$v_{bn} = v_{sn} - \frac{2(r_{s0} - r_{b0})}{\eta_0} \left\{ v_{sn} + \frac{1}{\rho_{s0} u_{s0} \eta_0} \left(\frac{d}{dt} (\rho_{s0} r_{s0} \eta_0 v_{sn}) - n^2 (p_{b0} - p_\infty) r_{sn} \right) \right\}$$

$$\tag{558}$$

Having determined η_n, p_{bn}, and v_{bn}, the energy equation can now be used to evaluate the body shape r_{bn}. To this end, it is convenient to rewrite Equation (552) as

$$\gamma p_{b0} \frac{d}{dt} (r_{b0} r_{bn}) + r_{b0} r_{bn} \frac{dp_{b0}}{dt}$$

$$= \frac{d}{dt} \left[p_{bn} \left(\frac{r_{s0}^2 - r_{b0}^2}{2} \right) + p_{b0} r_{sn} r_{s0} + \frac{(\gamma - 1)}{2} \rho_{sn} u_{s0}^2 r_{s0} \eta_0 \right.$$

$$+ (\gamma - 1) \rho_{s0} \left(u_{s0} u_{sn} r_{s0} \eta_0 + \frac{u_{s0}^2}{2} r_{sn} \eta_0 + \frac{u_{s0}^2}{2} r_{s0} \eta_n \right) \right] \tag{559}$$

$$+ \frac{(\gamma - 1)}{2} \rho_{s0} u_{s0}^2 \eta_0 \left(v_{sn} + \frac{v_{bn} - v_{sn}}{r_{s0} - r_{b0}} \frac{\eta_0}{2} \right) + (\gamma - 1) p_{bn} r_{b0} \frac{dr_{b0}}{dt}$$

$$- p_\infty \frac{d}{dt} (r_{s0} r_{sn}) + \gamma p_{b0} (r_{s0} - r_{b0}) \frac{v_{sn} + v_{bn}}{2}$$

$$= G_n(t)$$

232

where $G_n(t)$ is known from the given shock trajectory $r_{sn}(t)$ and the solutions for η_n, p_{bn}, and v_{bn}. Solving Equation (559) for r_{bn}, furnishes

$$r_{bn} = \frac{1}{r_{b0}p_{b0}^{1/\gamma}} \left\{ I_n + \int_0^t p_{b0}^{\frac{1-\gamma}{\gamma}} G_n(t')dt' \right\} \tag{560}$$

where I_n is the constant of integration. As with the zeroth-order, axisymmetric solution, the constant I_n is identified with the effects of bluntness. With reference to the equivalent three-dimensional (steady) flow, the slender body formulation becomes invalid for a blunt body near $z = 0$ where the local shock and body inclinations are not small. The effects of this localized bluntness manifest themselves in the constant I_n which gives the value of r_{bn} near $z = 0$, e.g., near the blunt nose. To complete the solution, this constant of integration must be specified because its determination depends upon the details of conditions near the nose region where the small disturbance approximation is not valid. This question shall be answered later when power law shock trajectories are considered.

e. Lift and Drag Forces, Pitching Moment

Results for the pressure and body trajectory allow estimation of the forces and moments acting on a vehicle. General expressions for the force $\vec{F}$ and moment $\vec{M}$ can be written as

$$\vec{F} = - \iint_{S_b} p_b \, \hat{n}_b \, dS \tag{561}$$

$$\vec{M} = - \iint_{S_b} p_b \, \vec{r}_b \times \hat{n}_b \, dS \tag{562}$$

Recall, the three-dimensional body is given by $r = r_b(\phi, z)$. Thus the outward unit normal to the body, $\hat{n}_b$, is given by

$$\hat{n}_b = \frac{\hat{e}_r - \left(\frac{\partial \ln r_b}{\partial \phi}\right) \hat{e}_\phi - \left(\frac{\partial r_b}{\partial z}\right) \hat{e}_z}{\left\{1 + \left(\frac{\partial \ln r_b}{\partial \phi}\right)^2 + \left(\frac{\partial r_b}{\partial z}\right)^2\right\}^{1/2}} \tag{563}$$

233

Also, if the pitching moment about the nose is computed,

$$\vec{r_b} = r \; \hat{e_r} + z \; \hat{e_z} \; .$$

Because of symmetry with respect to the y-axis (Figure 75), the force has only drag and lift components while the only nonzero component of the moment is the pitching moment.

$$\vec{F} = D \; \hat{e_x} + L \; \hat{e_y} \tag{564}$$

$$\vec{M} = M \; \hat{e_x} \tag{565}$$

Substituting the expressions for the body shape r_b and body pressure p_b given by Equations (537a) and (537c) into Equations (561) and (562), provides, after some manipulation in which terms of order ϵ_n^2 are ignored,

$$D = 2\pi \int_0^\ell p_{b0} \; r_{b0} \; \frac{dr_{b0}}{dz} \; dz \tag{566}$$

$$L = \pi \; \epsilon_1 \int_0^\ell p_{b1} \; r_{b0} \; dz \tag{567}$$

$$M = -\pi \; \epsilon_1 \int_0^\ell \{ p_{b0} r_{b0} (r_{b0} \frac{dr_{b1}}{dz} + 2r_{b1} \frac{dr_{b0}}{dz})$$
$$+ p_{b1} (z \; r_{b0} + r_{b0}^2 \frac{dr_{b0}}{dz}) \} dz \tag{568}$$

Here ℓ is the length of the body. Equations (566, 567, 568) give the forces and moments due to the pressure acting on the forebody; base pressure effects are ignored. The expressions for the drag given by Equation (566) can be rewritten by making use of the lowest-order energy equation, Equation (532). There results

$$D = \frac{\pi}{\gamma-1} (r_{s0}^2 - r_{b0}^2)(p_\infty + \frac{V_\infty}{r_{s0}} \frac{d}{dz} (\rho_\infty u_{s0} \frac{r_{s0}^2}{2})) + \frac{\pi}{2} r_{s0}^2 \rho_\infty u_{s0}^2 - \frac{\pi}{\gamma-1} r_{b0}^2 p_\infty \tag{569}$$

Similarly, making use of the solution for the pressure perturbation given in

Equation (557), the expression for the lift, L, can be rewritten as

$$L = \pi V_\infty \epsilon_1 \{ \rho_{s0} r_{s0} \eta_0 (u_{s1} - v_{s1}) + \rho_{s1} u_{s0} r_{s0} \eta_0 + \rho_{s0} u_{s0} r_{s0} \eta_1 + \rho_{s0} u_{s0} \eta_0 r_{s1} \}$$

(570)

f. Power Law Shock Waves

Power law shock waves are rather attractive to study in that the resulting formulas are easy to obtain and interpret. In the absence of nose bluntness effects, hypersonic small disturbance theory can be used to show that axisymmetric power law shocks give rise to similar power law bodies. Thus, the effects of nose bluntness are rather easy to identify in this case. In addition, the results of other authors are available for comparison in the case of power law shocks. Thus, assume

$$r_{s0} = A_0 \, t^m$$

(571a)

$$r_{sn} = A_n \, t^{m'}$$

(571b)

In the equivalent three-dimensional steady flow, write

$$r_{s0} = a_0 \, z^m$$

(572a)

$$r_{sn} = a_n \, z^{m'}$$

(572b)

where, because of the equivalence principle, $a_0 = A_0 V_\infty^{-m}$ and $a_n = A_n V_\infty^{-m'}$.

Equations (534), (535) and (536) and the shock jump relations then allow the zeroth-order, axisymmetric solution to be determined in the hypersonic limit $(M_\infty \to \infty)$ as

$$p_{b0} = \rho_\infty V_\infty^2 \, \frac{m(3m-1)}{\gamma+1} \, (a_0 z^{m-1})^2$$

(573a)

$$r_{b0}^2 = I_0 \, z^{2(1-m)/\gamma} + \frac{(2m-1)(5\gamma+1)m-\gamma-1)}{(\gamma+1)(3m-1)((\gamma+1)m-1)} \, (a_0 z^m)^2$$

(573b)

$$u_{s0} = \frac{2}{\gamma+1} \, V_\infty a_0 m z^{m-1}$$

(573c)

$$\rho_{s0} = \frac{\gamma+1}{\gamma-1} \, \rho_\infty$$

(573d)

$$\eta_0 = \frac{1}{2} \frac{\gamma-1}{\gamma+1} \, a_0 \, z^m$$

(573e)

235

where $\bar{I}_0$ is a constant proportional to I_0 and which gives the effects of nose bluntness. If Fiorino (Reference 62) is followed and $r_{b0} = rs_0$ at $z = z_0$ (where $dr_{s0}/dt = V_\infty$) is assumed, the result is

$$r_{b0}^2 = a_0^2 z^{2m} \{ (1-\zeta)(\frac{z}{z_0})^{\frac{2(1-m)}{\gamma}} + \zeta(\frac{z}{z_0})^{2m} \}$$ (573f)

where

$$\zeta = \frac{(2m-1)((5\gamma+1)m-\gamma-1)}{(\gamma+1)(3m-1)((\gamma+1)m-1)}$$ (573g)

$$z_0 = (a_0 m)^{1/(1-m)}$$ (573h)

In the equivalent two-dimensional unsteady flow, $z = V_\infty t$. Sychev (Reference 59) and others have shown that the bluntness term makes a significant contribution to the body shape if m is in the range

$$\frac{1}{2} < m < \frac{\gamma+1}{2\gamma+1}$$ (574)

For m less than 1/2, the self-similar term becomes negative and the basic axisymmetric solution is physically unrealistic. For m greater than $(\gamma+1)/(2\gamma+1)$, but less than unity, the displacement effect of the entropy layer is of smaller order than the errors introduced by the small disturbance equations.

In the hypersonic limit ($M_\infty \to \infty$), this power law shock assumption reduces the inverse solution to the perturbation problem to

$$u_{sn} = \frac{2V_\infty}{\gamma+1} a_n \, m' z^{m'-1}$$ (575a)

$$v_{sn} = \frac{2V_\infty}{\gamma+1} a_n n^2 \, m \, z^{m'-1}$$ (575b)

$$\rho_{sn} = 0$$ (575c)

$$\eta_n = \frac{\gamma-1}{\gamma+1} \{ \frac{a_n z^{m'}}{2} (1 - \frac{2n^2}{\gamma+1} \frac{m}{m'+m}) + \frac{J_n}{\rho_\infty a_0} z^{-m} \}$$ (575d)

236

$$p_{bn} = \frac{\rho_\infty V_\infty^2}{\gamma+1} a_0 a_n z^{m'+m-2} m\{(n^2-1)(3m-1) + \frac{r_{s0}}{r_{b0}}(2m+m'-1)(2-n^2+\frac{m'}{m} - \frac{2n^2}{\gamma+1}\frac{m}{m+m'}))\}$$

$$+ \rho_\infty V_\infty^2 \frac{r_{s0}}{r_{b0}}(m-1)\frac{J_n}{\rho_\infty} z^{-2} \qquad (575e)$$

$$v_{bn} = V_\infty n^2 a_n z^{m'-1}\{\frac{2m}{\gamma+1} - 4(\frac{\gamma+1}{\gamma-1})(1 - \frac{r_{b0}}{rs0})(\frac{2m}{\gamma+1}+m'-m)\} \qquad (575f)$$

$$r_{bn} = r_{bn}(z_0)\frac{r_{b0}(z_0)}{r_{b0}}\frac{p_{b0}(z_0)}{p_{b0}}^{1/\gamma} + \frac{1}{r_{b0}p_{b0}^{1/\gamma}}\int_{z_0}^{z} p_{b0}^{\frac{1-\gamma}{\gamma}} G_n\, dz \qquad (575g)$$

where

$$G_n = \frac{d}{dz}[\frac{p_{bn}}{2}(r_{s0}^2-r_{bn}^2) + (p_{b0}-p_\infty)r_{s0}r_{sn} + \rho_\infty(\gamma+1)(u_{s0}r_{s0}\eta_0 u_{sn}$$

$$+ \frac{u_{s0}^2}{2}r_{s0}\eta_n + \frac{u_{s0}^2}{2}r_{sn}\eta_0)]$$

$$+ \frac{\gamma-1}{4}\rho_\infty u_{s0}^2 r_{s0}(\frac{v_{sn}}{V_\infty} + \frac{1}{2}\frac{\eta_0}{r_{s0}-r_{b0}}\frac{v_{bn}-v_{sn}}{V_\infty}) + (\gamma-1)p_{bn}r_{b0}\frac{dr_{b0}}{dz}$$

$$+ \gamma p_{bn}\frac{r_{s0}-r_{b0}}{V_\infty}\frac{v_{sn}+v_{bn}}{2} \qquad (575g)$$

and r_{b0}/r_{s0} is given by Equation (573f) as a function of z. The quadrature that appears in the expression for r_{bn} apparently cannot be evaluated analytically in closed form and thus must be computed numerically.

Typical flowfield results for power law shocks are shown in Figures 80 through 85 where the flowfield solutions are sketched for various m and m' with γ equal to 1.4 and M_∞ equal to ∞. Figures 80, 81, and 82 give results r n = 1 corresponding to an axisymmetric body at small angle of attack. Figures 83, 84, and 85 give results for n = 2, corresponding to a body with a slightly elliptical cross-section. The range of values of m and m' in Figures 80 through 85 corresponds to the limits given by Equation (574), for γ = 1.4. Also, in all cases $a_n = 1$ has been taken. Because of the linearity of the perturbation problem, the results for other values of a_n follow directly by multiplying the results in Figures 80 through 85 by a_n.
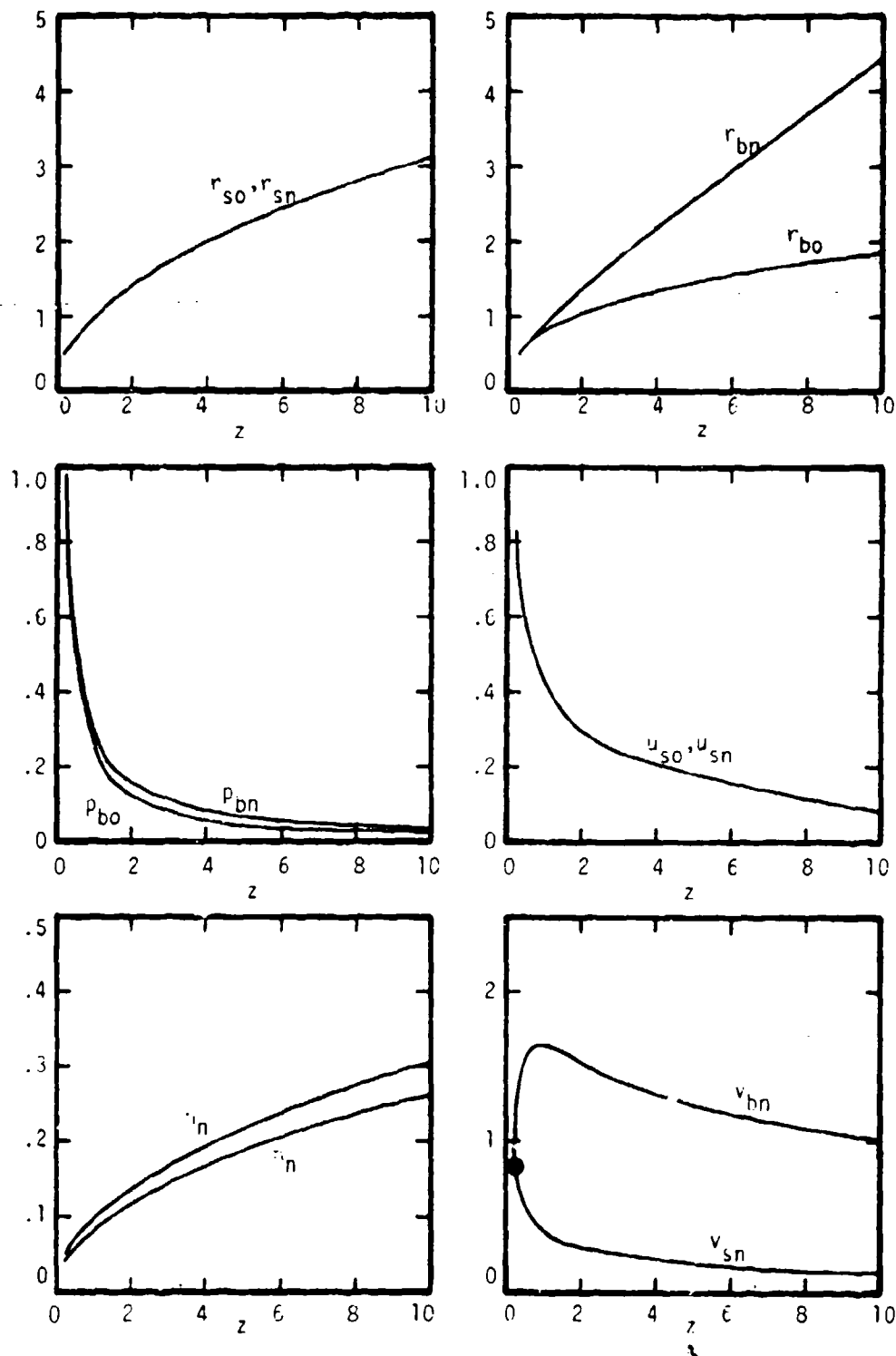
Figure 80. Flow field Solution for Power Law-Shock (Π = , n=1, m=n'= 0.5 $a_0=a_1=1$, =1.4, J_n= 0.0)

238

Figure ... The variation in ... for a low-law shock ... r_{so}, r_{sn}, r_{bo}, r_{bn} ...
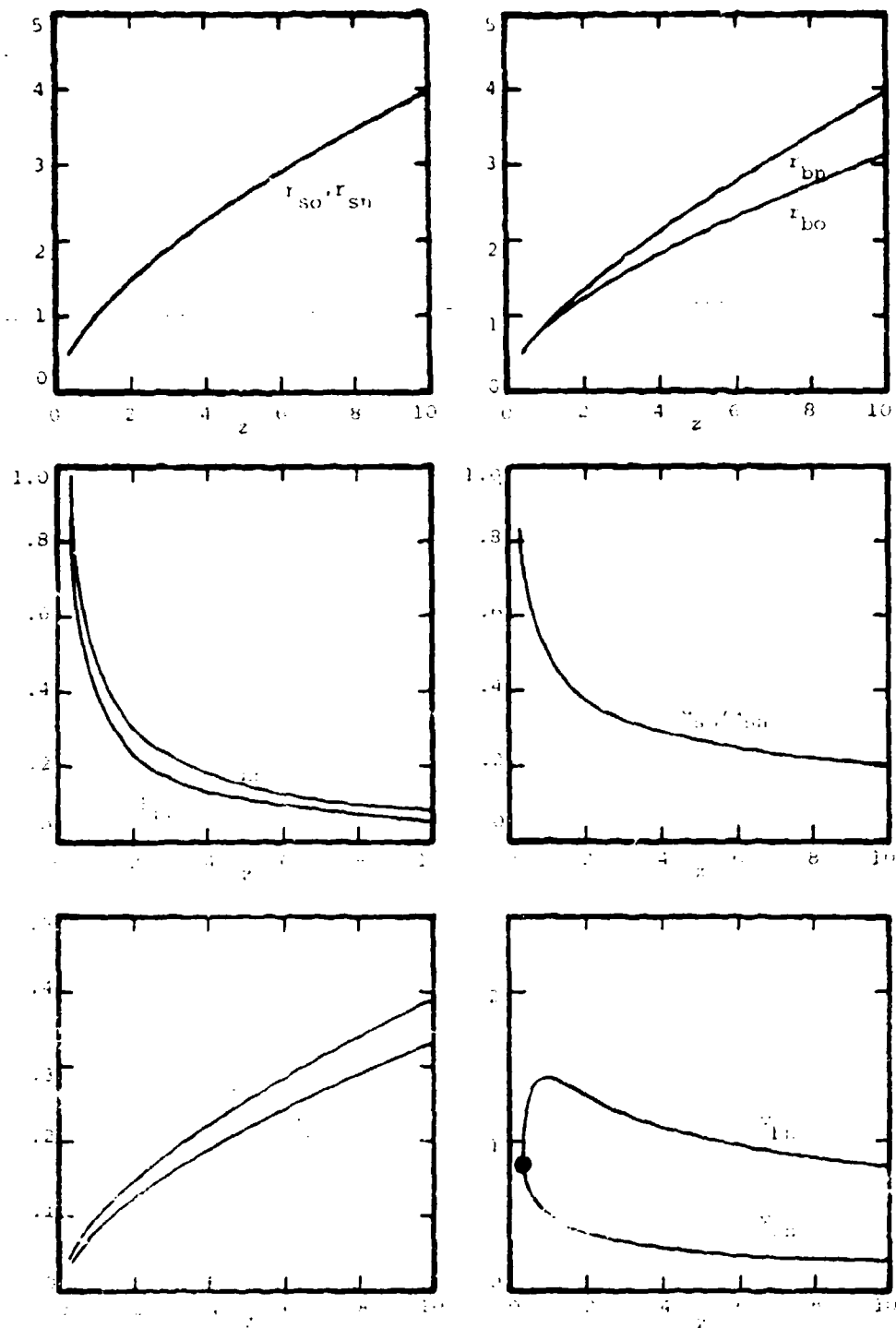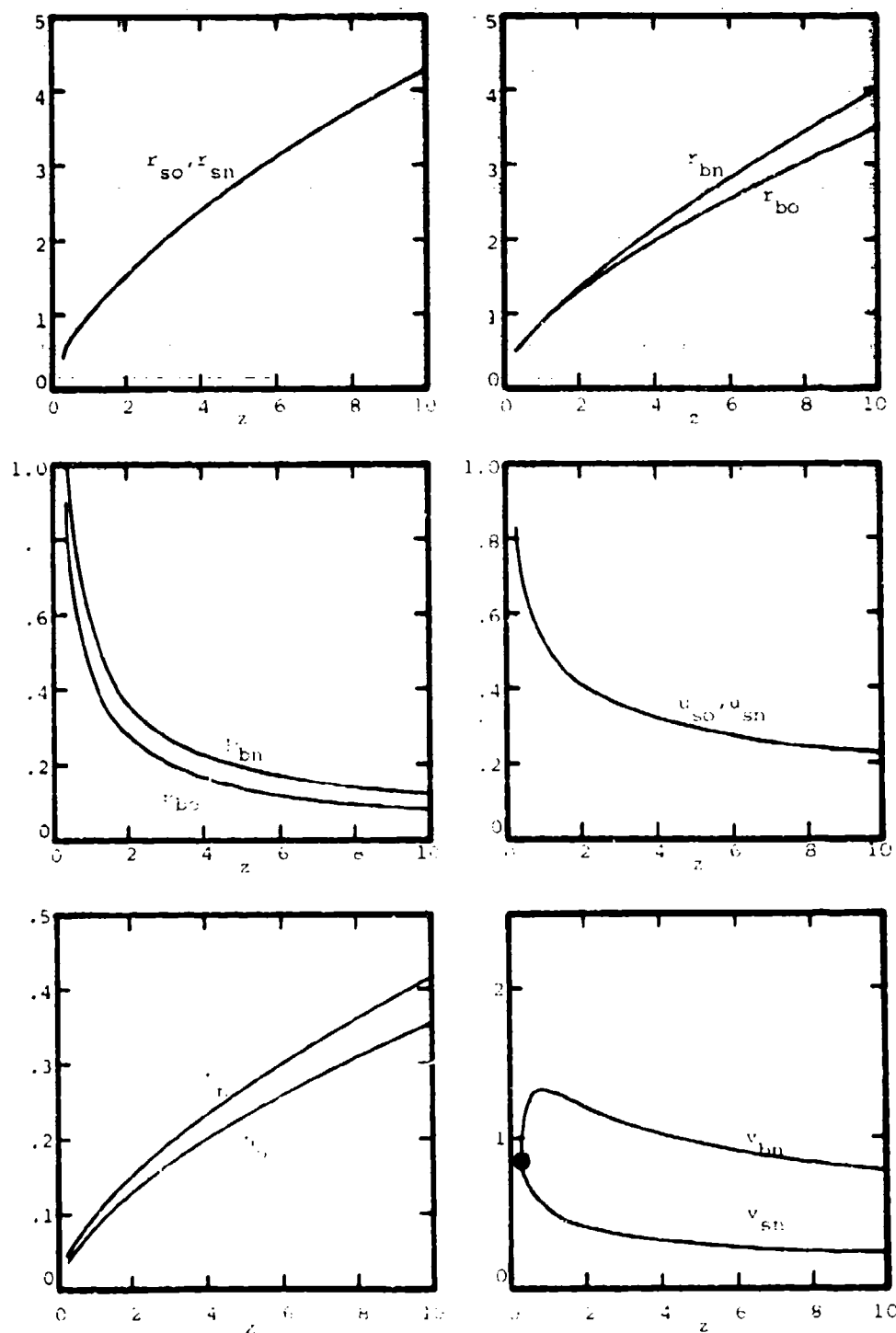
Figure 82. Flow field solution for [...] Shock (M[...], n=1, m=m'= 0.63158, [...] 1.0, [...], [...])

24
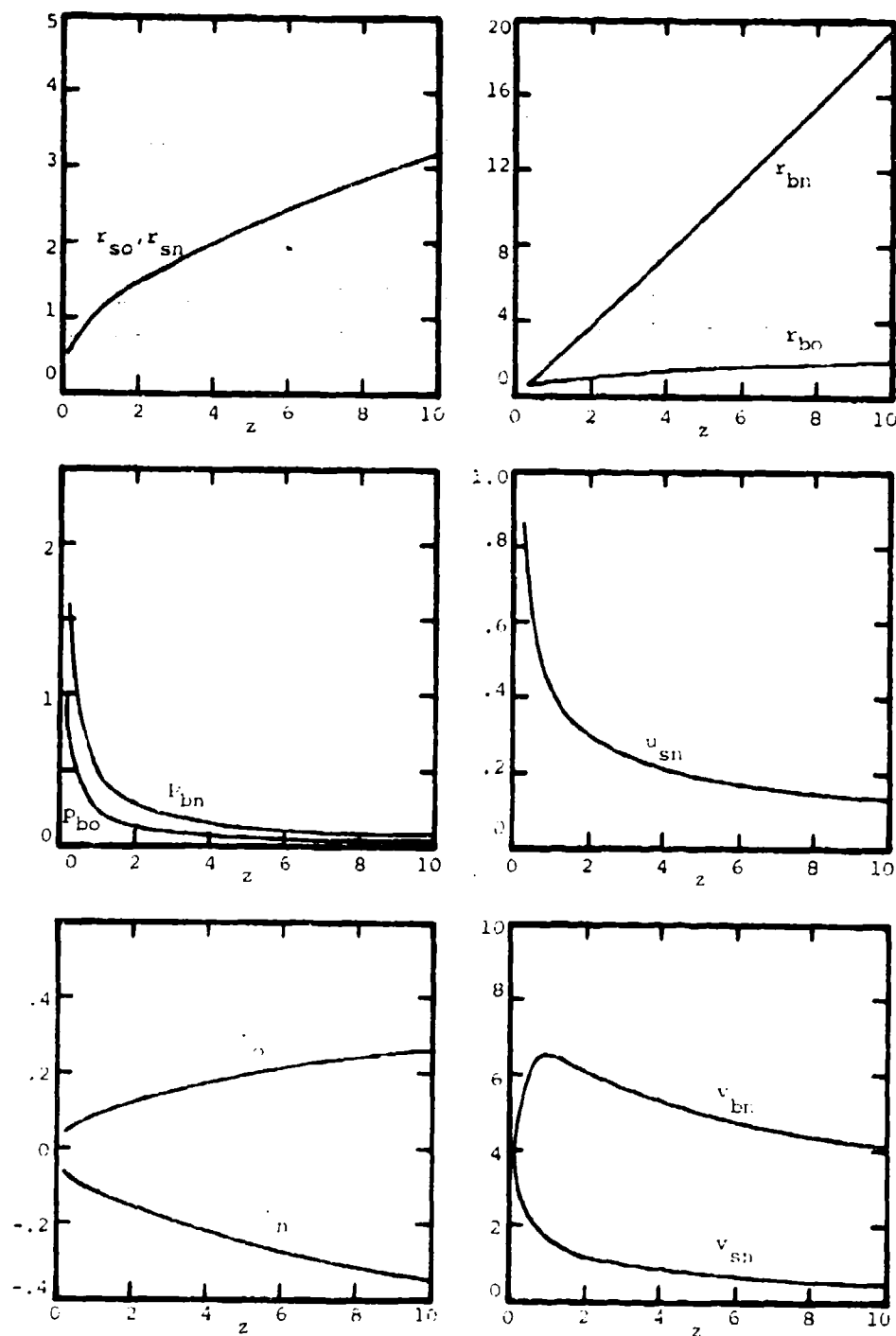
Fig. 2.83.   Flowfield Solution for Power-Law Shock ($\eta_c = 0$, n=2, m=m'= 0.5, $q_m = q_g = 1.0$, $\gamma = 1.4$, $c_n = 0.5$)

241

Figure 84. Flowfield Solution for Power-Law Shock ($M_\infty = \infty$, $n = 2$, $m=m'= 0.6$
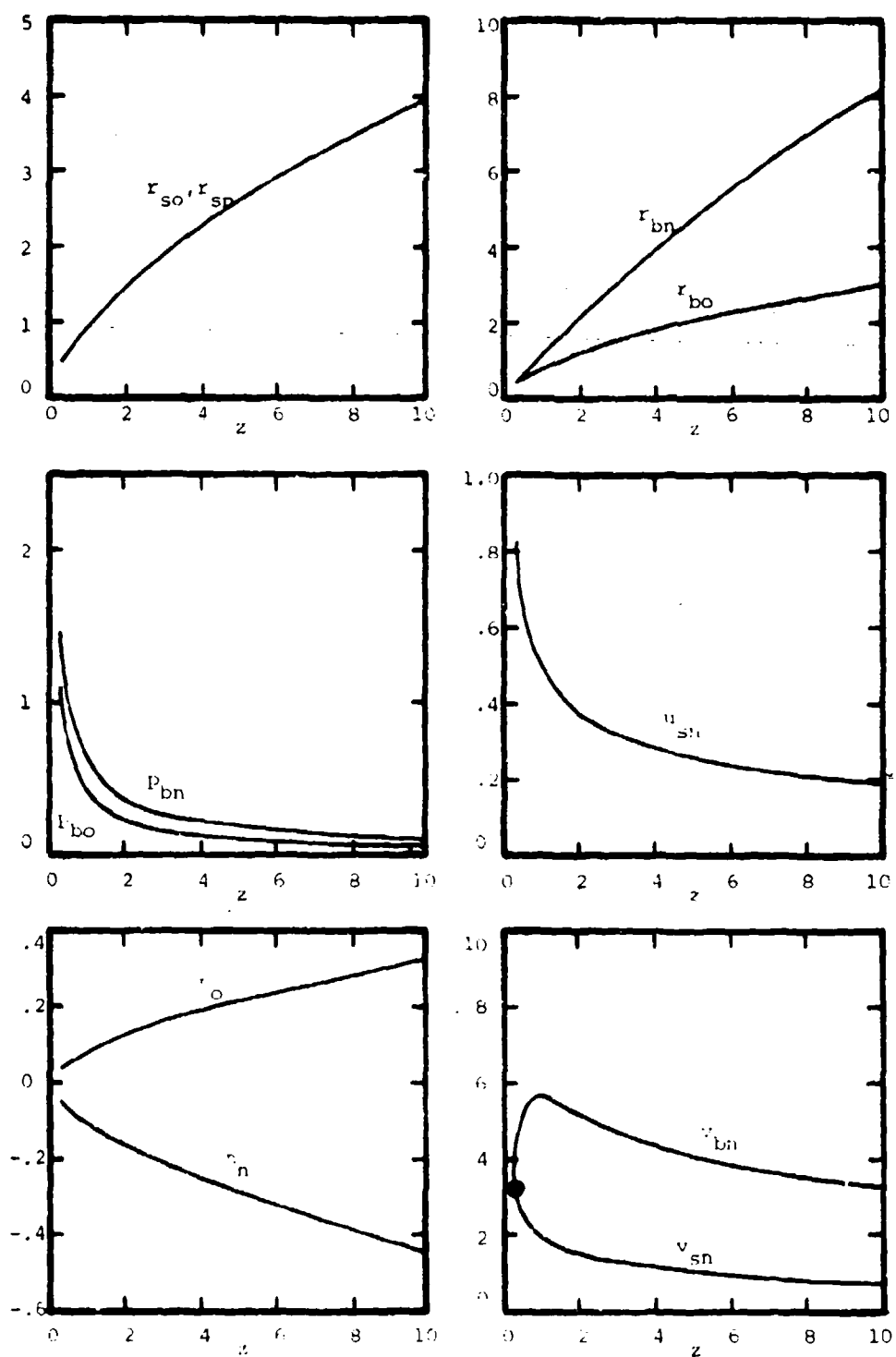$a_0=a_2=1.6$, $\gamma = 1.4$, $\theta_n = 0.0$)

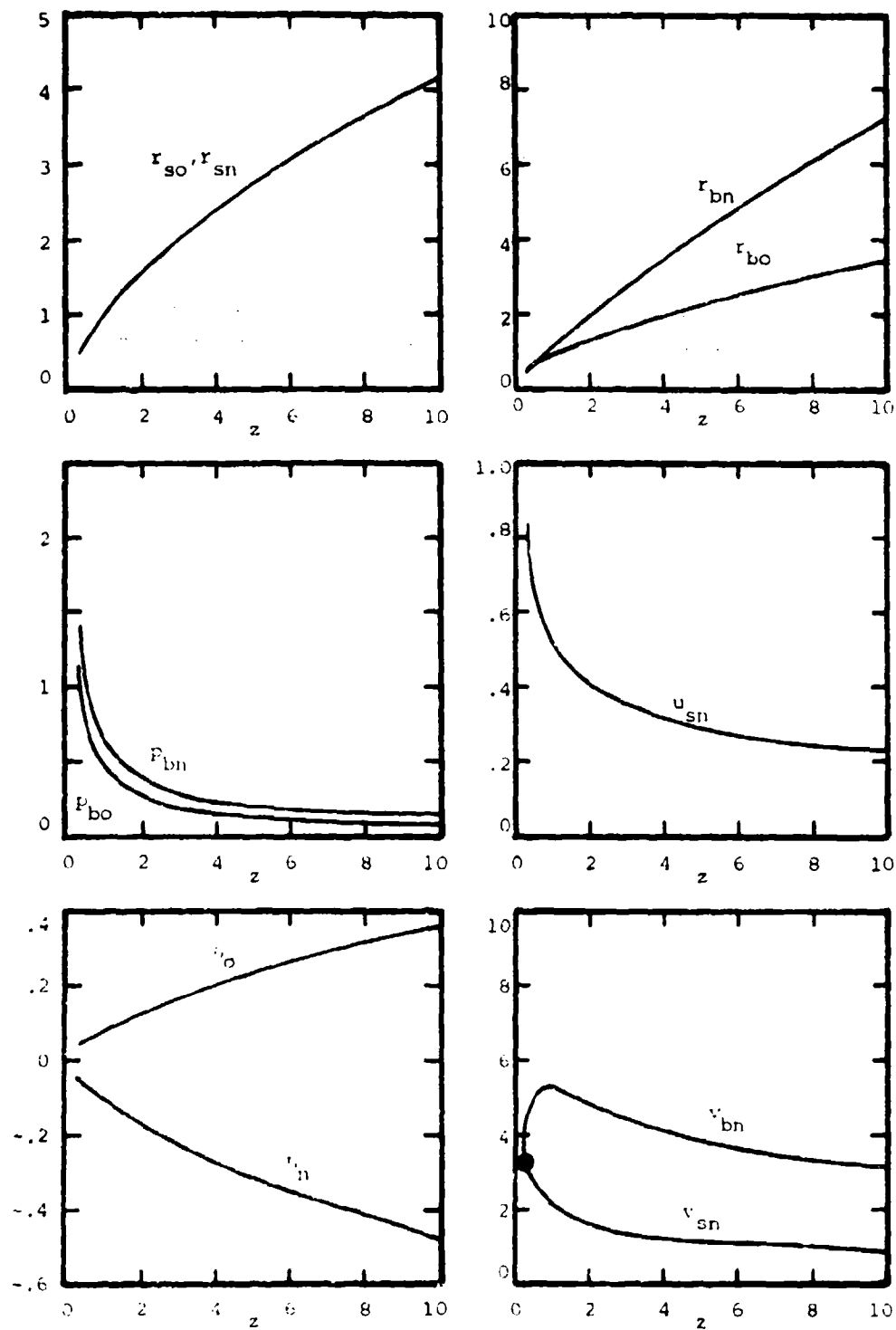Figure 95. Flowfield solution for power-law shock ($M_∞$ = 9, n = 2, m=m'= 0.63158, c_0=c_2=1.0, γ = 1.4, θ_n = 0.0)

Some general observations can be made from these results. First, r_{bn} always is greater than r_{b0}, even though r_{s0} and r_{sn} are equal. That is, the relative body shape perturbation (e.g., r_{bn}/r_{sn}) is greater than the basic axisymmetric result (e.g., r_{b0}/r_{s0}). Because the basic axisymmetric flowfield has a very low density near the body, a relatively large perturbation in the body shape is required to achieve a given shock shape perturbation.

Second, in spite of some small numerical differences, the axisymmetric and perturbation body pressures -- p_{b0} and p_{bn}, respectively -- have very similar distributions along the body. A rather rapid expansion takes place just downstream of the nose and the surface pressure decreases rapidly.

Third, the crossflow induced by the nonsymmetric cross-section can be rather strong compared to the radial velocity perturbation, especially near the body. That is, v_{bn} is typically several times u_{sn}.

Figures 86, 87, and 88 give results for the drag coefficient, the lift coefficient, and moment coefficient, respectively, as functions of the body length ℓ. In all cases, $M_\infty = \infty$, $\gamma = 1.4$, $a_0 = a_1 = 1$, and $J_n = 0$.

The drag coefficient is unaffected by perturbations of the sort considered here and thus depends only on the basic axisymmetric solution. The results presented in Figure 86 are identical to those obtained earlier by Fiorino; they show that the decreasing pressure downstream of the nose contributes less and less to the drag as the body length is increased and the base area increases.

The lift force L is proportional to ε_1, the angle of attack. Figure 87 shows that the coefficient of proportionality depends weakly on m. As with the drag coefficient, the lift coefficient decreases with increasing body length because the base area used in the definition of the lift coefficient increases and the pressure decreases.
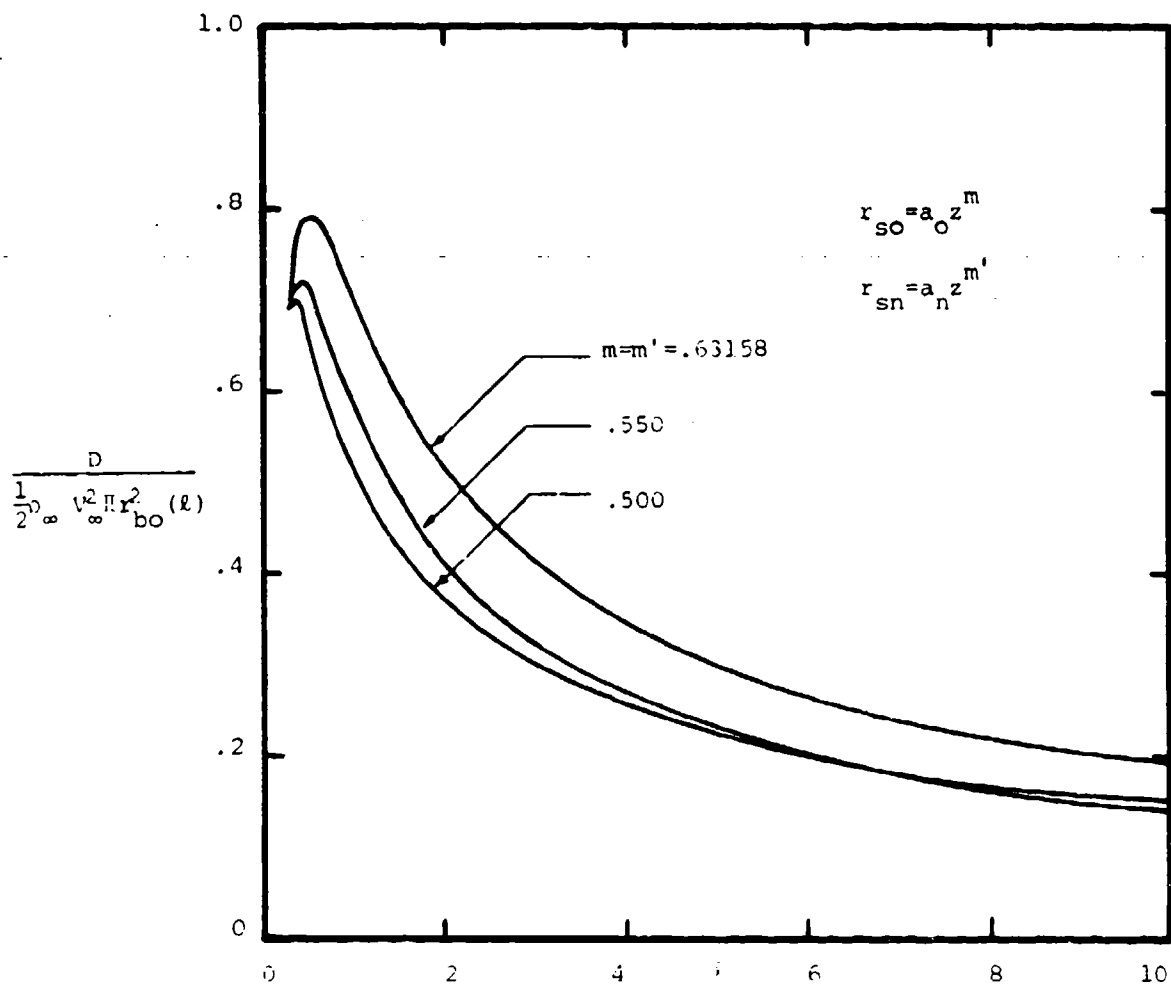
244

Figure 86. Drag Coefficient Versus Body Length for
Various Power-Law Shocks ($M_\infty = \infty$, $\gamma = 1.4$,
$J_n = 0.0$, $a_0 = 1.0$, m=m')

$$r_{so} = a_o z^m$$

$$r_{sn} = a_n z^{m'}$$

$$\frac{L}{\frac{1}{2}\rho_\infty u_\infty^2 \pi r_{bo}^2(\ell)\, \epsilon_1}$$
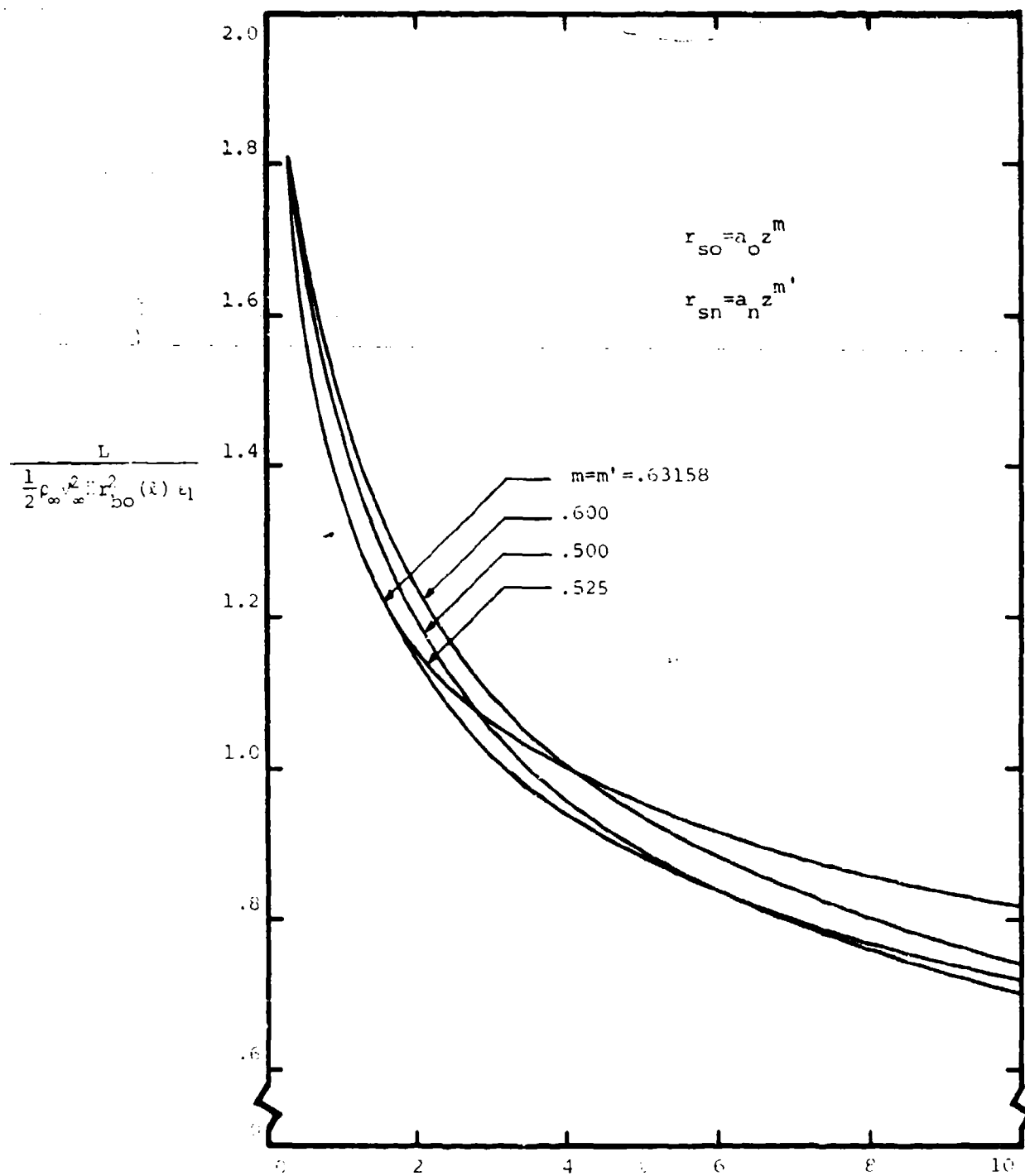
m=m' = .63158

.600

.500

.525

Figure 87. Lift Coefficient Versus Body Length for Various
Power-Law Shocks $M_\infty = \infty$, $\gamma = 1.4$, $J_n = 0.6$, $a_o = a_1 = 1.0$,
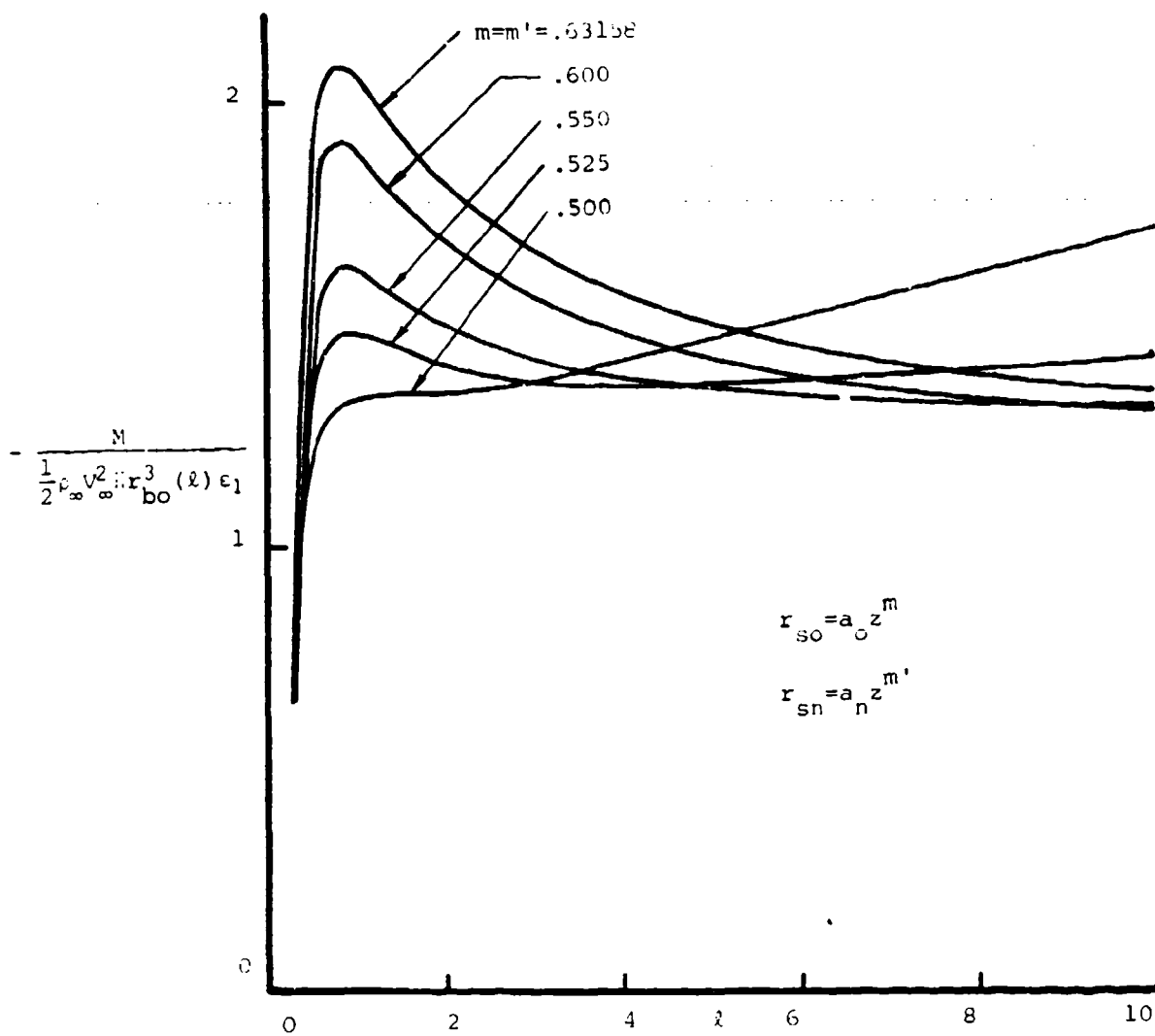m=m')

Figure 88. Moment Coefficient Versus Body Length for Various Power-Law Shocks ($M_\infty = \infty$, $\gamma = 1.4$, $J_n = 0.0$, $a_o = a_i = 1.0$, m=m')

Finally, Figure 88 gives results for the pitching moment coefficient. These numerical results show that a relative maximum is achieved near ℓ equal to unity. The pitching moment coefficient then decreases and at some value of ℓ begins to increase again. The value of ℓ at which the relative minimum is achieved depends upon n, the power law exponent.

g. Concluding Remarks

The effect of nose bluntness on hypersonic flow past slightly nonsymmetric bodies has been studied by means of a perturbation approximation within the framework of an integral method. These results, which are a generalization of the axisymmetric results obtained by Fiorino and Rasmussen (Reference 64), have been applied in an inverse approach to the study of power law shock waves. Results have been obtained for the flowfield variables and the force and moment coefficients.

Further work remains to be done on this problem. First, the results obtained herein should be compared with other calculations and/or experiment. Second, results should be obtained for hyperbolic shock shapes. Analyses by Yakura and Fiorino (References 61 and 62) for axisymmetric bodies show that such shocks are associated with blunted cones, a shape of practical interest. Third, it would be of interest to more carefully and rigorously match the asymptotic solutions obtained herein with solutions valid in the nose region. The methods of matched asymptotic expansions offer a useful methodology with which to carry out such a calculation.

SECTION III

LIFTING BODIES DERIVED FROM

SUPERSONIC FLOWS PAST INCLINED CIRCULAR

AND ELLIPTIC CONES

1. INTRODUCTION

The design of an aircraft for high supersonic flight that achieves desirable aerodynamic behavior and still accomodates such demands as propulsion, structures, materials, and operations is a very challenging task. A discussion of the requirements of hypersonic aircraft is given in References 2 and 3. When the Mach numbers are sufficiently high that the flow disturbances are intrinsically nonlinear, a treatment of the problem by means of linearized theory is not appropriate. A generalized study of the problem by means of numerical solutions of the nonlinear governing equations of fluid mechanics is very formidable indeed. For this reason the few known exact solutions for flows past elementary geometries are extremely important. These basic exact solutions provide insight and a knowledge of fundamental physical features associated with high-speed flow. In addition, they can also be used as building blocks for flows past more complex geometries.

A basic scheme for deriving exact solutions for three-dimensional lifting bodies by means of simple two-dimensional wedge flows was set forth in Reference 1. These results were elaborated upon by Venn and Flower (Reference 67), Nardo (Reference 68), and others. The simplest configurations thus derived are called caret wings, or caret waveriders, because of their caret shape. Because these aerodynamic shapes are derived from basic two-dimensional flows, they generally involve flat surfaces and concomitant sharp corners where these surfaces intersect. These sharp corners may be undesirable when factors such as viscous and heating effects are taken into account.

Corresponding to the flat surfaces generated by the basic wedge-shock flow, curved surfaces can be generated by utilization of the stream surfaces associated with the axisymmetric supersonic flow past a circular cone. Such surfaces were devised by Jones and Woods (References 5 and 69). These constructions generate curved surfaces and curved shocks that are attached to sharp leading edges. The flows for both the cone-generated surfaces and the wedge-generated surfaces can be classified as conical flows.

Besides the axisymmetrical conical flows, there are also conical flows associated with inclined circular cones and with non-circular cones. These flows generate stream surfaces that could be attractive for construction of lifting bodies with curved surfaces. The analytical description of these flows, as contrasted with a numerical description, generally involves a perturbation analysis, which is not uniformly valid in all the variables but fails in a vortical layer adjacent to the body surface. The pressure and azimuthal velocity, however, are uniformly valid across the vortical layer (References 24, 25, 28). This is very important because the azimuthal perturbation velocity is pertinent in determining the flow stream surfaces and the pressure is important in determining the relevant forces on the surfaces. Thus the first-order straight forward perturbation expansion, while being suspect at first glance, is thus pertinent in determining the stream surfaces and related forces on waverider configurations generated by the perturbation results. The object of this investigation is to generate various waverider configurations by means of angle-of-attack and cross-section eccentricity perturbations of the basic axisymmetric cone flow.

The present study rests heavily on the fact that approximate analytical expressions are available for the perturbed flows past circular (Reference 22,

23) and elliptical (Reference 52) cones at small angles of attack. These results allow for an analytical, as opposed to a numerical, investigation to be performed that leads to results that are simple and easily understood. The effects of free-stream Mach number, pertinent cone angle, angle of attack, cross-section eccentricity, and ratio of specific heats on the shock shape, shock-layer structure, stream-surface shape, and surface conditions can be readily established. Although the results are approximate, they are accurate enough for the parametric and design considerations that are of primary concern here. When the trends and concepts have become clear, more precise and elaborate schemes of analysis can be undertaken for numerical accuracy.

The main concern of this section is the generation of stream surfaces that can be used as solid surfaces in lifting-body waverider configurations. How the pressure distributions can be obtained is outlined, but no actual lift, drag, or moment results are presented here. Such results, and other results of interest such as reported by Squire (Reference 70), will be the subject of further research.

2. FUNDAMENTAL WEDGE-DERIVED WAVERIDER

The fundamental wedge-derived waverider, sometimes called the caret waverider, is derived from the basic exact flowfield produced by supersonic flow through a plane oblique shock wave, as shown in Figures 89 and 90. The f` is deflected by the angle Δ when passing through the shock. The plane shock wave is inclined at angle β with the freestream flow. Let the line formed by the common intersection of the planes parallel and perpendicular to the freestream flow with the plane of the shock denote the leading edge of a solid wedge. The upper surface of the wedge is parallel to the freestream flow; and the lower surface of the wedge, inclined downward at an angle Δ with the upper surface, is the stream surface of the flow that has passed through
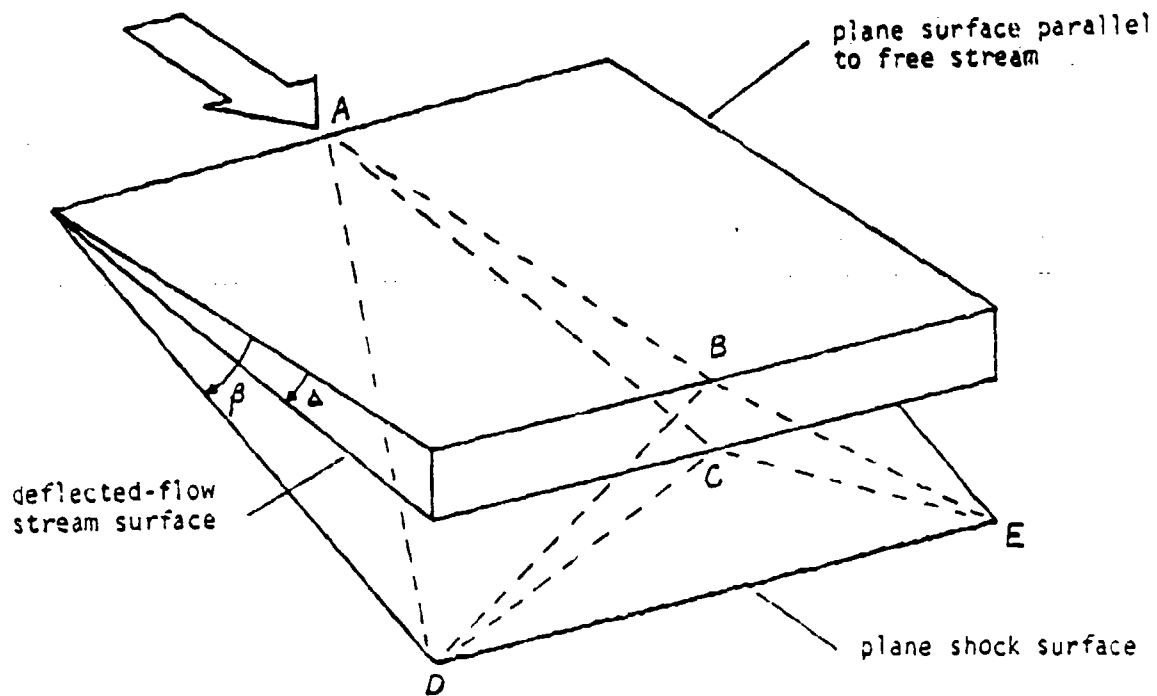
251

plane surface parallel
to free stream

A

B

deflected-flow
stream surface

C

E

plane shock surface

D

Fig. 90. Wedge Shock Configuration

β
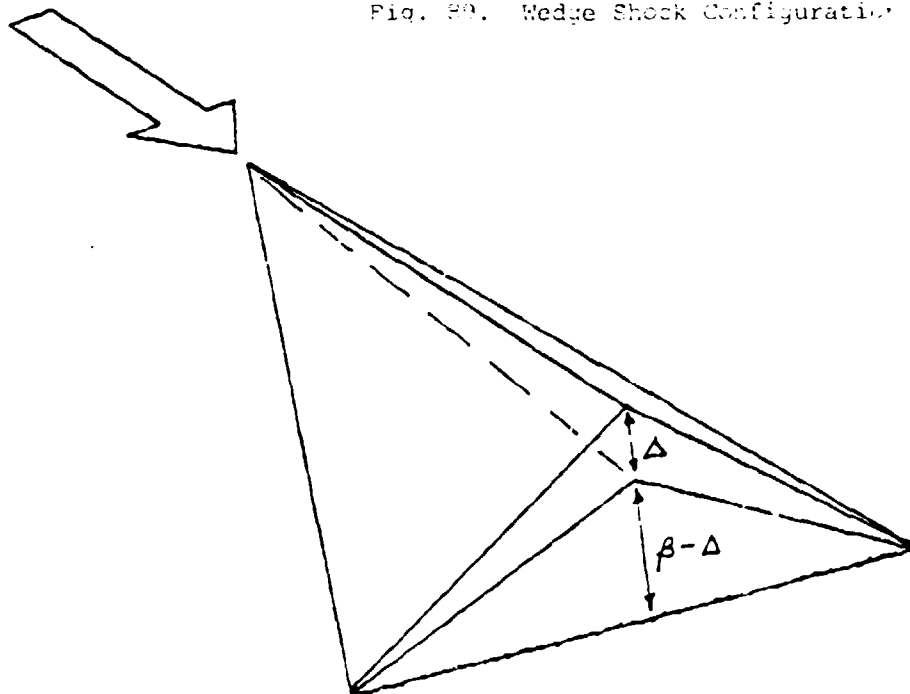
Δ

Δ

$\beta - \Delta$

Figure 90. Wedge-Derived Waverider

the shock at the common-line intersection denoting the leading edge of the wedge. The flowfield between the lower surface of the wedge and the shock wave is parallel and uniform and has properties obtainable from the oblique-shock relations.

The oblique-shock relations are well known and can be expressed in analytical form exactly for a thermally and calorically perfect gas. Owing to the intrinsic interaction of the variables, however, the shock angle, β, cannot be obtained explicitily as a function of the deflection angle, Δ. It is thus useful to utilize the approximate results of hypersonic small disturbance theory, valid for large freestream Mach numbers, M_∞, and small deflection and shock angles. This shock-angle relation originally obtained by Linnell (Reference 71) is

$$\frac{\sin \beta}{\sin \Delta} = \frac{\gamma+1}{4} + \sqrt{\frac{(\gamma+1)^2}{4} + \frac{1}{(M_\infty \sin \Delta)^2}} \quad , \qquad (576)$$

The corresponding relation for the pressure coefficient is

$$C_p \equiv \frac{p-p_\infty}{\frac{1}{2} \rho_\infty V_\infty^2} \quad ,$$

$$\frac{C_p}{(\sin \Delta)^2} = \frac{\gamma+1}{2} = \sqrt{\frac{(\gamma+1)^2}{2} + \frac{4}{(M_\infty \sin \Delta)^2}} \quad . \qquad (577)$$

In inviscid steady flow, any stream surface can be utilized as a solid surface since no flow crosses a stream surface. To visualize further stream surfaces in Figure 89 and utilize them as solid surfaces in a new configuration, mark out the axis AB aligned with the freestream flow and lying in the top surface of the wedge. The normal projection of the axis AB onto the lower surface of the wedge is denoted by AC. Any plane passing through the axis AB is aligned with the freestream flow, and any plane passing through the axis AC is aligned with the shock deflected flow. Now select the points D and E on the shock surface, positioned symm... ically (but not necessarily) on

253

either side of the axes AB and AC. The two plane surfaces passing through the pair of three points ACD and ACE are stream surfaces in the shock deflected flow. The two plane surfaces passing through the pairs of three points ABD and ABE are stream surfaces in the freestream flow. If these four new stream surfaces are chosen as the relevant solid surfaces of an aerodynamic body, then the new configuration appears as shown in Figure 90. This aerodynamic configuration is called a caret waverider since it appears to ride on the plane shock wave attached to its under surface. The upper surface is parallel to the freestream and hence at freestream conditions. The under surface of the caret shape is at a uniform pressure given by formula (577), and the shock stand-off angle is given by formula (576). For given caret waverider configuration, the shock wave will be attached as shown in Figure 90 only for the particular Mach number determined from Equation(576) with β and Δ given. The caret waverider is a lifting aerodynamic shape since the pressure is higher on the under surface.

3. GENERAL CONSIDERATIONS FOR CONICAL FLOWS

To determine the stream surfaces of conical flows past slender elliptic cones at small angles of attack, use spherical coordinates in a body-fixed system as shown in Figure 91. Let $a \equiv \tan \theta_a$ and $b \equiv \tan \theta_b$ be the semivertex angles of the semiminor and simimajor axes of the elliptic cone. Then the elliptic cone is described by

$$\tan \theta_c = \frac{\tan \theta_m}{\sqrt{1+e \cos 2\phi}} \qquad (578)$$

where

$$\tan \theta_m = \frac{\sqrt{2} \ ab}{\sqrt{a^2+b^2}} = b \sqrt{1-e} = a \sqrt{1+e} ,$$
$$\sqrt{a^2+b^2} = \sqrt{ab} \ (1-e^2)^{1/4} , \qquad (579a)$$
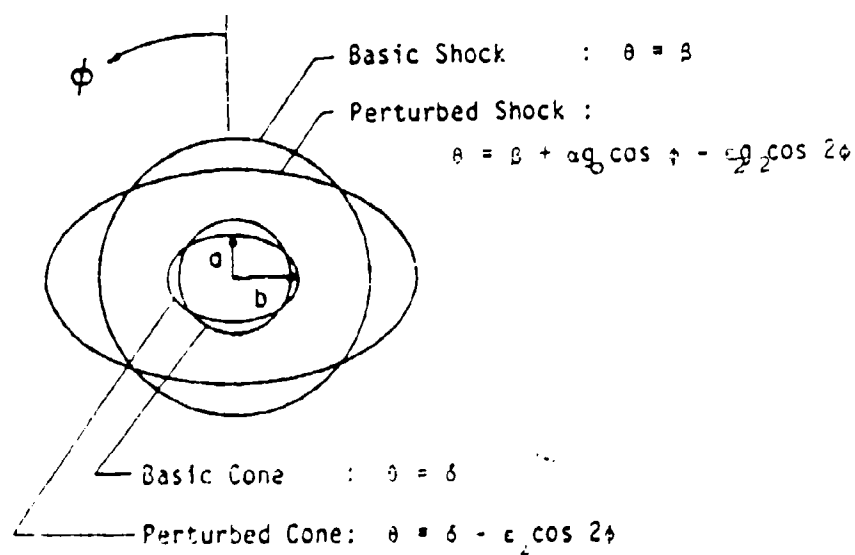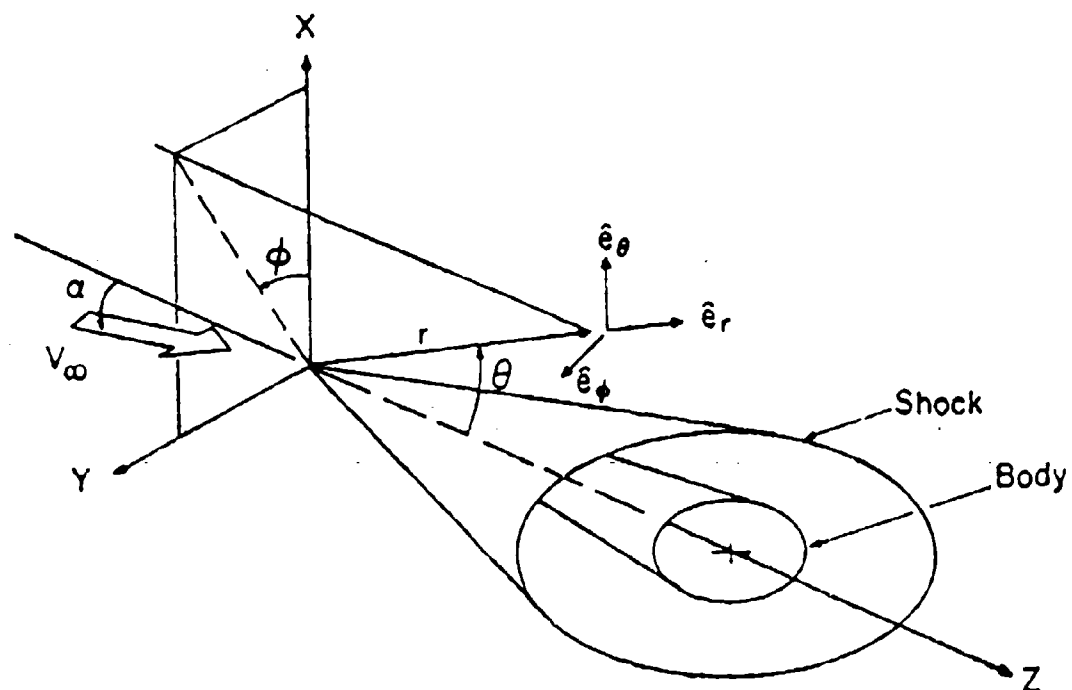
Figure 41. Cone Coordinates and Geometry

$$-e \equiv \frac{b^2 - a^2}{b^2 + a^2} \qquad . \tag{579b}$$

The paramet e is a measure of the eccentricity of the elliptic cone. For small eccentricities, expand Equation (578) in a Fourier series, the first two terms of which are

$$\theta_c = \delta - \varepsilon_2 \cos 2\phi + O(\varepsilon^2) \qquad , \tag{580}$$

where

$$\delta \equiv \theta_m + \frac{e^2}{32} [3 - 2 \sin^2\theta_m] \sin 2\theta_m + O(e^4) \quad , \tag{581a}$$

$$\varepsilon_2 \equiv \frac{e}{4} \{1 + \frac{e^2}{32} \{15 - 20 \sin^2\theta_m + 8 \sin^4\theta_m\} + O(e^4)\} \sin 2\theta_m. \tag{581b}$$

The parameter ε_2 is a new measure of the eccentricity and is the appropriate small parameter in a perturbation procedure. The parameter δ specifies the simivertex angle of the basic circular cone about which the perturbation expansion is performed.

The conical shock wave attached to the elliptic cone has the form (Reference 52) small α and ε_2,

$$\theta_s = \beta + \alpha g_0 \cos \phi - \varepsilon_2 g_2 \cos 2\phi \quad , \tag{582}$$

where

$$\beta/\delta = \{\frac{\gamma+1}{2} + \frac{1}{K_\delta^2}\}^{1/2} \quad , \tag{583}$$

and $K_\delta \equiv M_\infty \delta$ is the hypersonic similarity parameter. The parameters g_0 and g_2 are the shock eccentricity factors associated with angle of attack and elliptic cone eccentricity. They are functions of K_δ and are shown in Figure 92.

Let u, v, and w denote the r, θ, and ϕ spherical components of velocity, and let p denote the pressure. Outside the surface vortical layer and the viscous boundary layer, the variables have the following expansions for small α and ε_2:

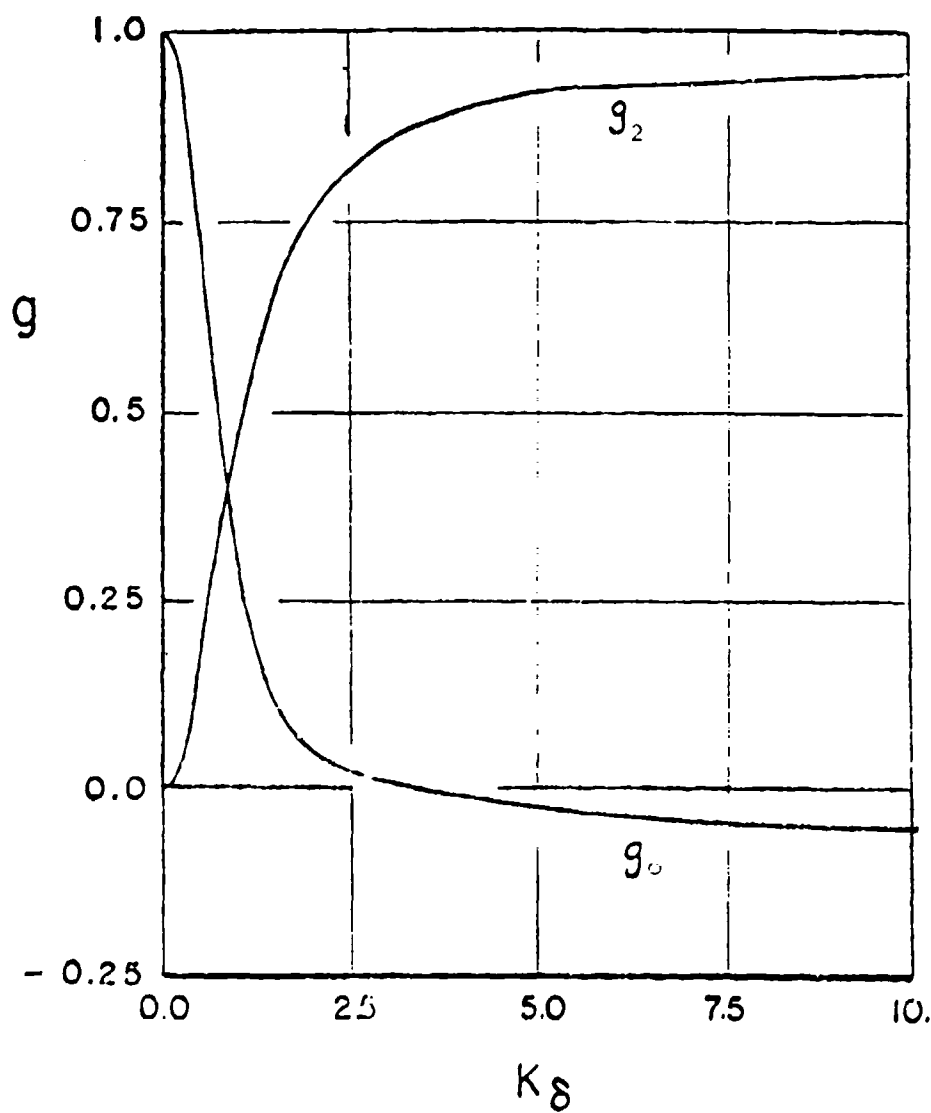$$\Theta_s = \beta + \alpha g_0 \cos \phi - \epsilon g_2 \cos 2\phi$$

Figure ... Shock Eccentricity Factors, $\gamma = 1.4$

$$u(\theta,\phi) = u_0(\theta) + \alpha U_0(\theta) \cos \phi + \varepsilon_2 U_2(\theta) \cos 2\phi$$

$$v(\theta,\phi) = v_0(\theta) + \alpha V_0(\theta) \cos \phi + \varepsilon_2 V_2(\theta) \cos 2\phi$$

$$w(\theta,\phi) = \alpha w_0(\theta) \sin \phi + \varepsilon_2 w_2(\theta) \sin 2\phi \qquad (584)$$

The lower case terms in the expansions, with the subscript zero, pertain to the basic-cone solution. The first-order, capitalized terms with the subscript zero notation pertain to the angle-of-attack perturbation, and the capitalized terms with the subscripts pertain to the elliptic-cone eccentricity perturbation. The pressure and the azimuthal velocity components, $W_0(\theta)$ and $W_2(\theta)$, are uniformly valid across the vortical layer.

As calculated by Doty and Rasmussen (Reference 23), the angle-of-attack velocity perturbations $U_0/(V_\infty \delta)$, V_0/V_∞, and W_0/V_∞ are functions of θ and K_δ within the fabrication of hypersonic small-disturbance theory. Correct to the first order expansion of interest, the shock-layer structure can be normalized by the variable

$$\theta' \equiv \frac{\theta - \delta}{\beta - \delta} \qquad (585)$$

At the cone surface, $\theta' = 0$, and at the shock, $\theta' = 1$. The angle-of-attack velocity components are shown in Figure 93 as a function of θ' and various values of K_δ. The corresponding elliptic eccentricity velocity components (Section II.1) are shown in Figure 94. The body-surface values of the azimuthal velocity components, $W_0(\theta_c)$ and $W_2(\theta_c)$, are shown in Figure 95 as a function of K_δ. The body surface perturbation pressure coefficients, C_{p0} and C_{p2}, are shown in Figure 96 as a function of K_δ.
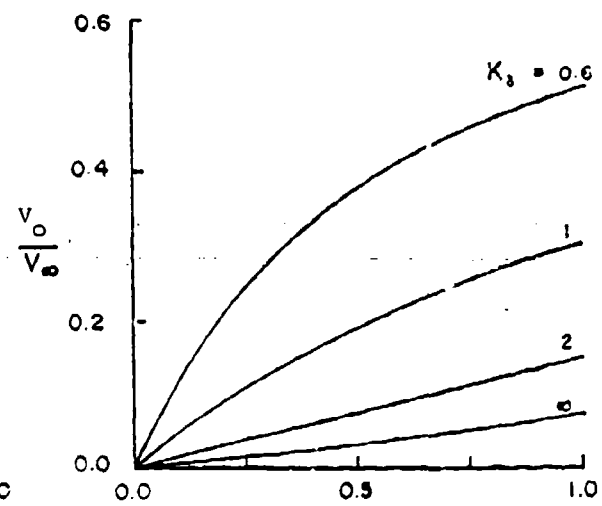
4. CONICAL STREAM SURFACES

The vector equation for a streamline, $\vec{V} \times d\vec{s} = 0$, can be written in spherical coordinates as

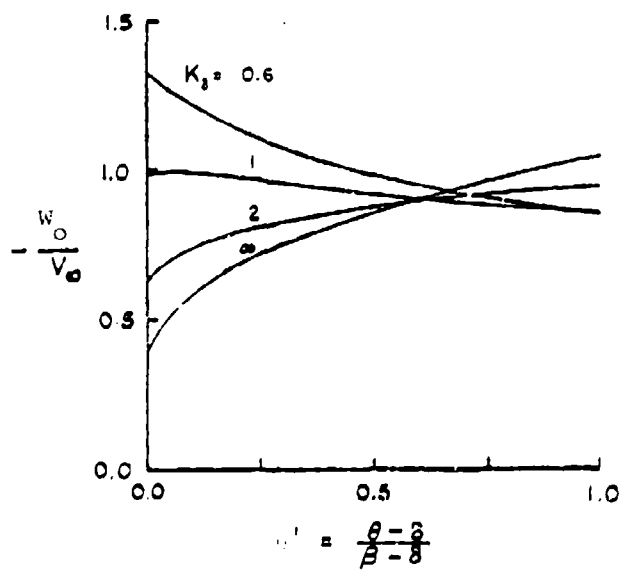$$\frac{dr}{u(\theta,\phi)} = \frac{r d\theta}{v(\theta,\phi)} = \frac{r \sin \theta d\phi}{w(\theta,\phi)} \qquad . \qquad (586)$$
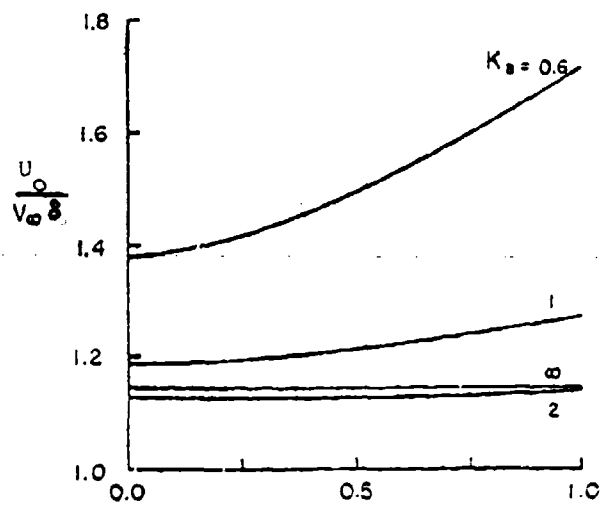
(a) Radial

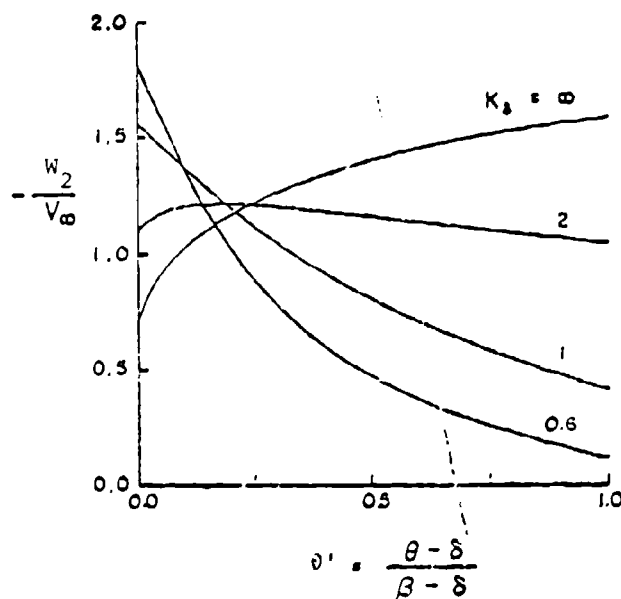(b) Polar

(c) Azimuthal

Figure 9?. Inclined-Cone Velocity Perturbations
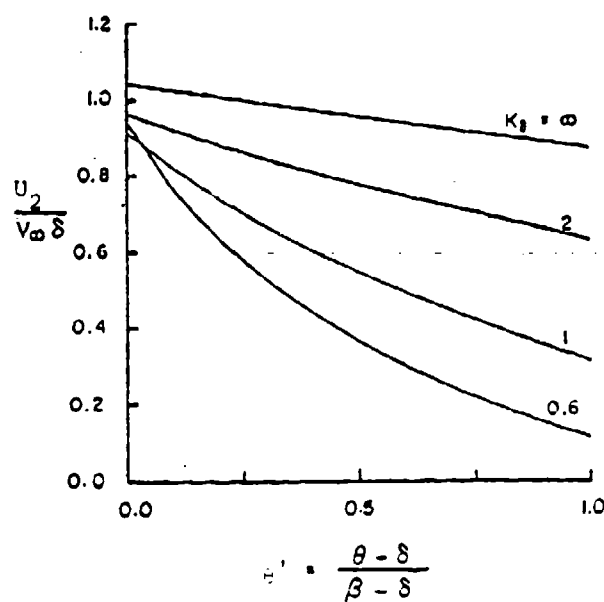
(a) Radial
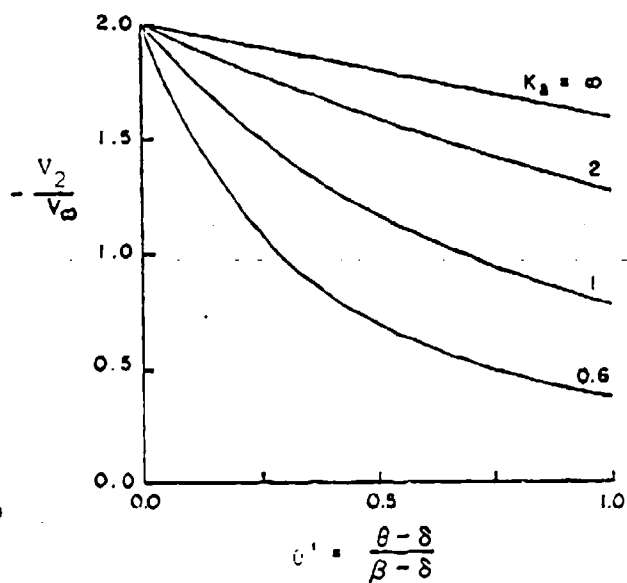
(b) Polar

(c) Azimuthal
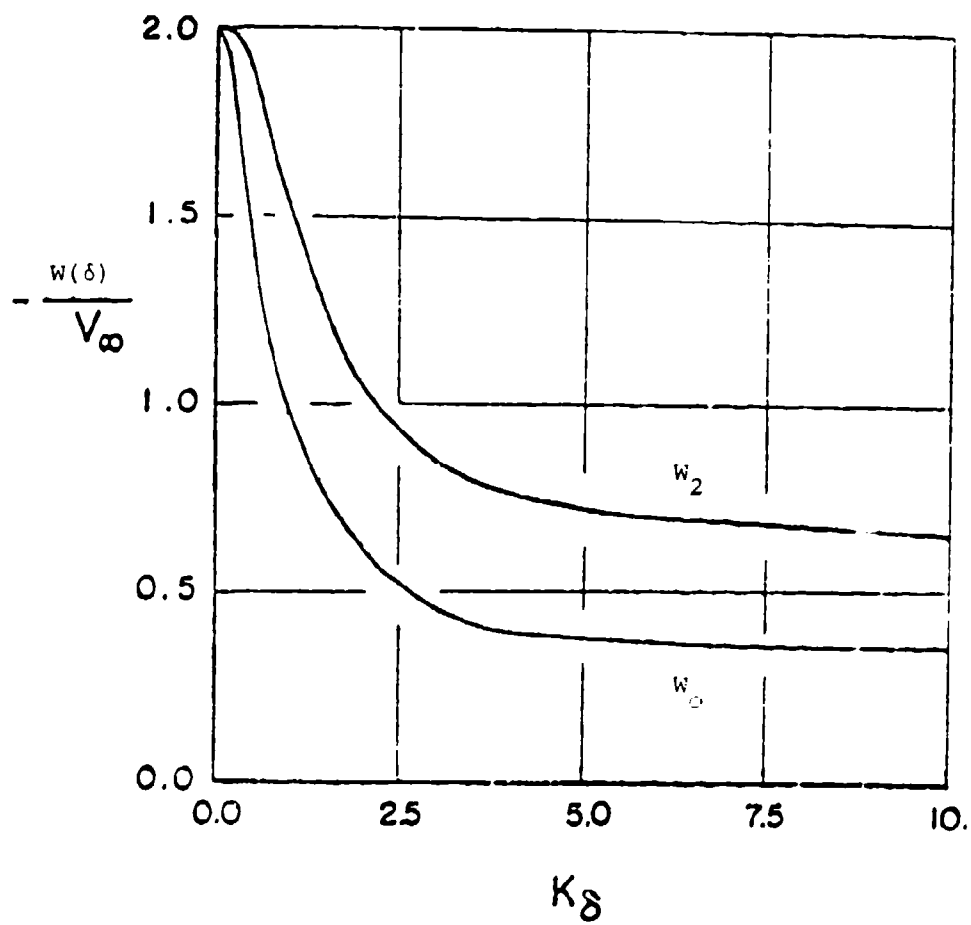
Figure ? Elliptic-Cone Velocity Perturbations

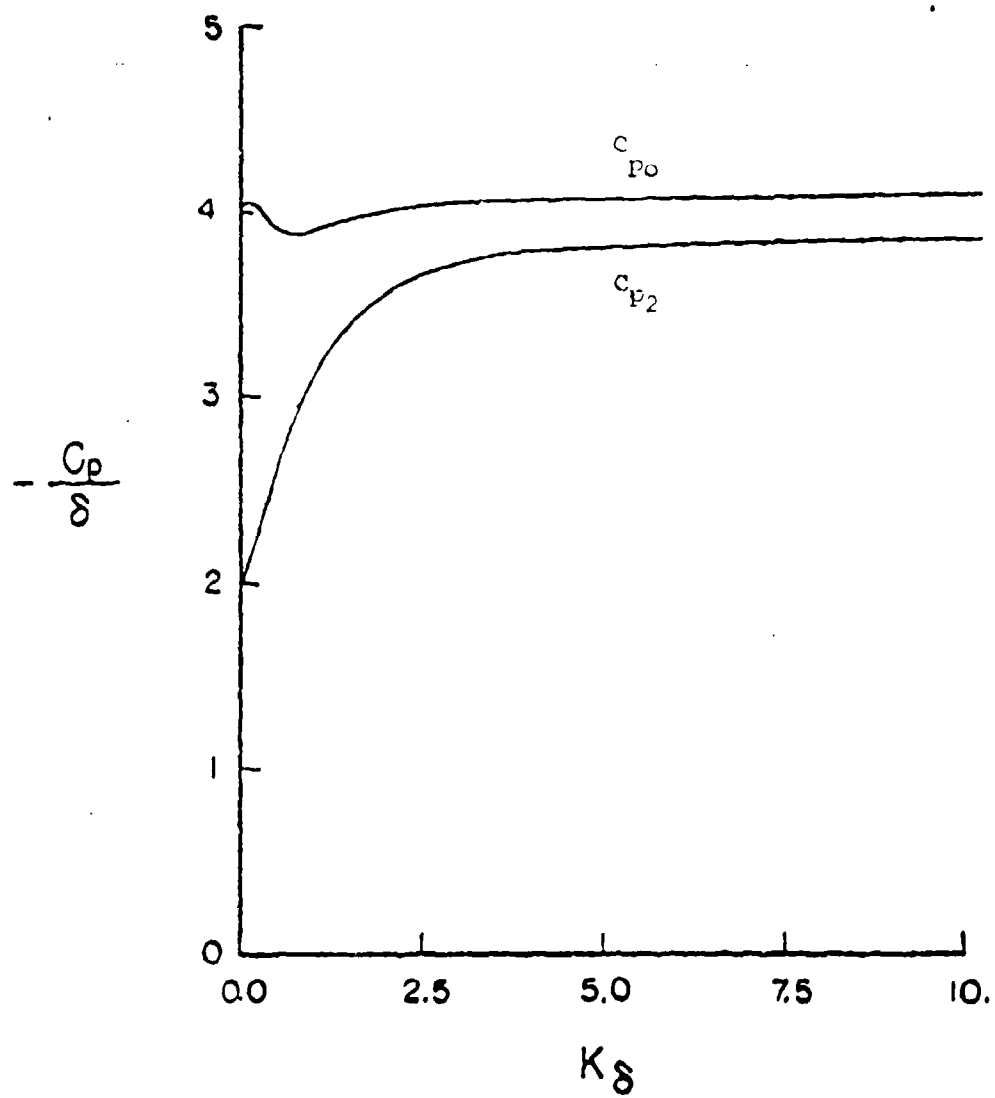Figure 45. Azimuthal Velocity at the Body Surface, $\gamma = 1.4$

Figure 6.. Surface Pressure Perturbations

The conical stream surfaces are determined by the last two terms of Equation (586). For small angles and to lowest order,

$$\frac{d\theta}{\theta v_0(\theta)} = \frac{d\phi}{\alpha w_0(\theta) \sin \phi + \epsilon_2 w_2(\theta) \sin 2\phi} \qquad (587)$$

To lowest order, only the zeroth-order polar velocity, $v_0(\theta)$, for the basic cone and the uniformly valid azimuthal perturbaton velocities, $W_0(\theta)$ and $W_2(\theta)$, enter the analysis. Even though these velocity functions are known, it does not appear possible to obtain an integral of Equation (587) analytically. In the cases when α or ϵ_2 vanish separately, the variables in Equation (587) can be separated, and integration can then be obtained at least by quadratures. Formulas for the basic-cone flow and the perturbed flow are given in Section II.1.

5.   WAVERIDERS DERIVED FROM INCLINED CIRCULAR CONES

a.   Stream Surfaces

First consider the case when $\epsilon_2 = 0$, that is, a circular cone at angle of attack. When $\epsilon_2 = 0$, the variables in Equation (587) can be separated and the integration on θ can be performed. The following results can be obtained

$$- \frac{\alpha}{V_\infty} \int_{\theta_s^*}^{\theta} \frac{w_0(\theta) d\theta}{\theta^2 - \delta^2} = \ln \left[\frac{\tan \phi/2}{\tan \phi_s/2} \right] , \qquad (588)$$

where

$$\theta_s^* \equiv \beta + \alpha g_0 \cos \phi_s , \qquad (589)$$

and ϕ_s is the azimuthal angle where the stream surface intersects the shock. The function $W_0(\theta)$ is known (Reference 52) and shown in Figure 93, and thus the quadrature in expression (588) can be evaluated numerically. When θ proceeds to the cone surface, $\theta \to \delta$, the quadrature on the left side of (588) diverges, and the left side of (588) tends to zero. Thus all the stream surfaces become tangent to the body surface at $\phi=0$, the leeward ray on the cone.

263

b.   Approximate Integration

Inspection of the function $W_0(\theta)$ in Figure 93 suggests that W_0 can be approximated by the relation

$$W_0(\theta) = A + \frac{\delta B}{\theta} \qquad , \qquad (590a)$$

where

$$A \equiv \frac{\sigma W_0(\beta) - W_0(\delta)}{\sigma - 1} \qquad , \qquad (590b)$$

$$B \equiv \frac{\sigma[W_0(\delta) - W_0(\beta)]}{\sigma - 1} \quad , \qquad (590c)$$

and $\sigma \equiv \beta/\delta$. When this approximation is substituted into the integral in Equation (588) and the integral evaluated, the result is

$$k_1 \ln \left[\frac{\theta-\delta}{\theta_s{}^*-\delta}\right] + k_2 \ln \left[\frac{\theta+\delta}{\theta_s{}^*+\delta}\right] - (k_1 + k_2) \ln \left[\frac{\theta}{\theta_s{}^*}\right] = \ln \left[\frac{\tan \phi/2}{\tan \phi_s/2}\right] \; , \quad (591)$$

where

$$k_1 \equiv -\frac{1}{2}\frac{\alpha}{\delta}\frac{W_0(\delta)}{V_\infty} \qquad , \qquad (592a)$$

$$k_2 \equiv -\frac{\alpha}{\delta}\frac{(\sigma+1)W_0(\delta) - 2\sigma W_0(\beta)}{2(\sigma-1)V_\infty} \quad . \qquad (592b)$$

Equation (591) can also be written as

$$\left[\frac{\theta - \delta}{\theta_s{}^*-\delta} \cdot \frac{\theta_s{}^*}{\theta}\right]^{k_1} \left[\frac{\theta + \delta}{\theta_s{}^*+\delta} \cdot \frac{\theta_s{}^*}{\theta}\right]^{k_2} = \frac{\tan \phi/2}{\tan \phi_s/2} \qquad (593)$$

Expression (593) gives a relation between θ/δ and ϕ, with ϕ_s, α/δ, and K_δ as parameters. (Recall that $\sigma \equiv \beta/\delta$ is given by Equation (583).) The parameter k_1 is always positive since $W_0(\delta)$ is negative when α is positive, and vice versa. The dependency of k_1 on K_δ can be determined with the aid of Figure 94. The parameter k_2 changes sign as K_δ varies, as might be anticipated from Figure 93. It can be shown that (References 22,23)

$$\frac{W_0(\beta)}{V_\infty} = -(\sigma^2 - g_0)/\sigma^2 \; . \qquad (594)$$

Thus k_2 can be written as

$$k_2 = -\frac{\alpha}{\delta} \frac{\sigma^2(\sigma+1)\{W_0(\delta)/V_\infty\} + 2\sigma(\sigma^2-g_0)}{2\sigma^2(\sigma-1)} \; . \tag{595a}$$

The dependency of k_2 on K_δ is shown in Figure 97. At $K_\delta = 0$ and $K_\delta = 0.9$, the parameter k_2 is zero. It is positive when $0<K<0.9$ and negative when $K_\delta>0.9$. Several typical stream surfaces (plotted as $Z \tan \theta$ versus ϕ, with $Z = $ constant and $\tan \theta \approx \theta$; that is, projections on a plane perpendicular to the cone axis) are shown in Figure 98 for $K_\delta = 1.3$, $\alpha/\delta = 0.2$, and $\gamma = 1.4$.

c. Lip Angle

The portion of a stream surface adjacent to the shock is referred to as the lip of t'~ stream surface. The acute angle between the lip of a stream surface a' ~he plane surface passing through the lip and the axis of the body cone is referred to as the lip angle, denoted by λ_0. If $\phi = \phi(\theta)$ denotes the functional form for a stream surface, then the unit normal vector to a stream surface is given by

$$n = \frac{e_\phi - \sin \theta \, d\phi/d\theta \; e_\theta}{[1 + \sin^2\theta(d\phi/d\theta)^2]^{1/2}} \; , \tag{596}$$

where e_ϕ and e_θ are the azimuthal and polar spherical unit basis vectors. The lip angle is determined by $\cos \lambda_0 = e_\phi \cdot n$, and, for small angles θ,

$$\tan \lambda_0 = \theta_s \cdot (d\phi/d\theta)_s \; . \tag{597}$$

From Equation (593) it is determined that

$$\theta_s \cdot (d\phi/d\theta)_s = \frac{W_0(\beta) \sin \phi_s}{v_0(\beta)} = -\frac{\alpha}{\delta} \frac{W_0(\beta)}{V_\infty} \frac{\sigma \sin \phi_s}{\sigma^2-1} \; . \tag{598}$$

Utilizing Equation (594) the lip angle is determined to be

$$\tan \lambda_0 = \frac{\alpha}{\delta} \frac{\sigma^2 - g_0}{\sigma(\sigma^2-1)} \sin \phi_s \; . \tag{599}$$

The dependency of λ_0 on K_δ is shown in Figure 99. The ratio $(\tan \lambda_0)\csc^2 \phi_s/(\alpha/\delta)$ increases from zero to the asymptotic value 5.5 as K_δ increases from zero to infinity. The lip angle thus becomes thicker as α/δ and K_δ increase separately, and it is a maximum when $\phi_s = 90$ degrees.
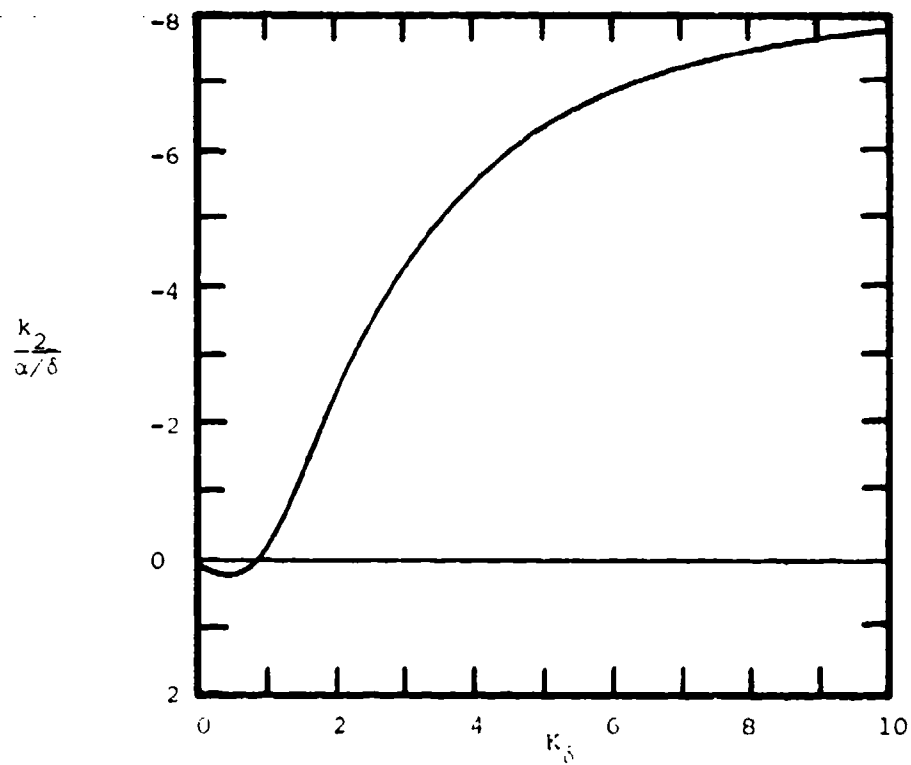
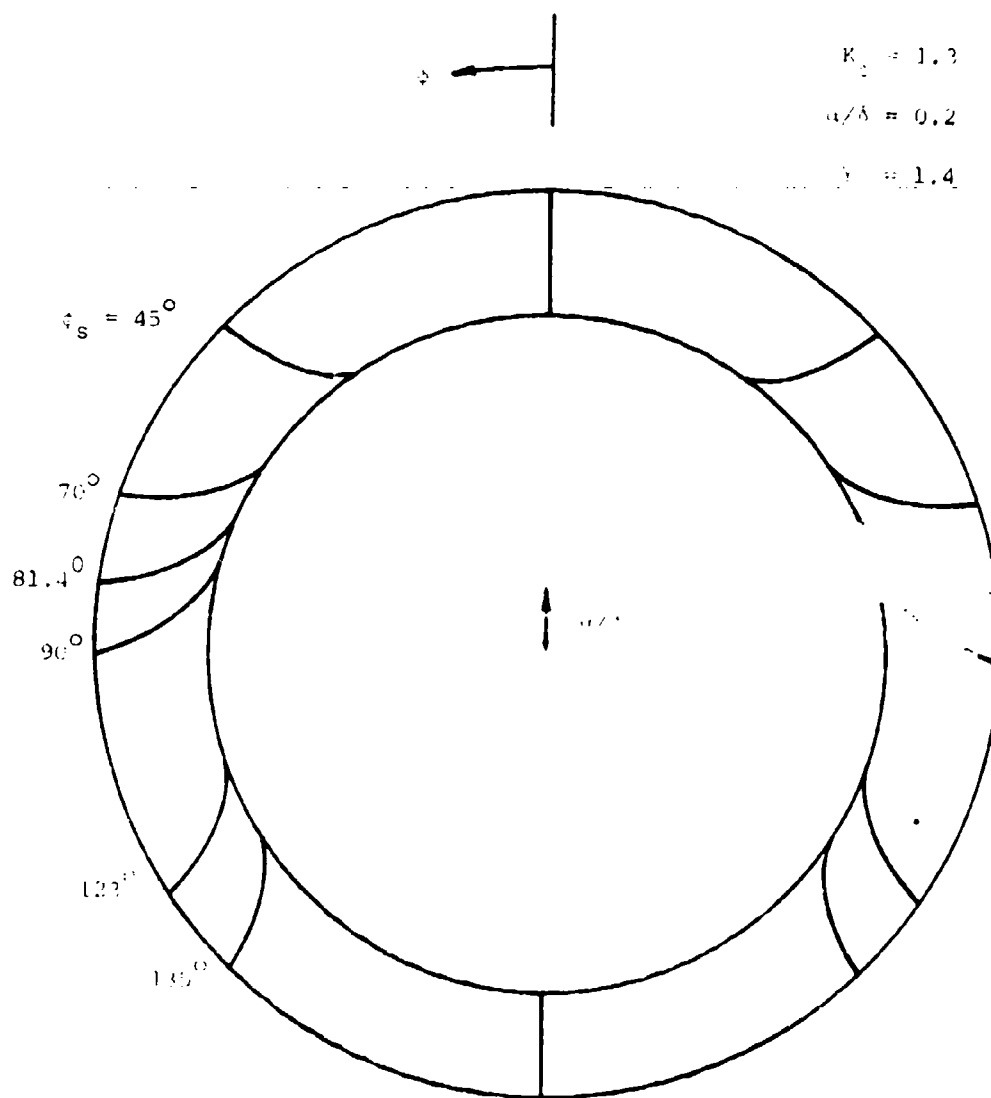Figure 97. Circular-Cone Stream-Surface Function

$K_s = 1.3$

$a/\delta = 0.2$

$\gamma = 1.4$

$\phi_s = 45°$

$70°$

$81.4°$

$90°$

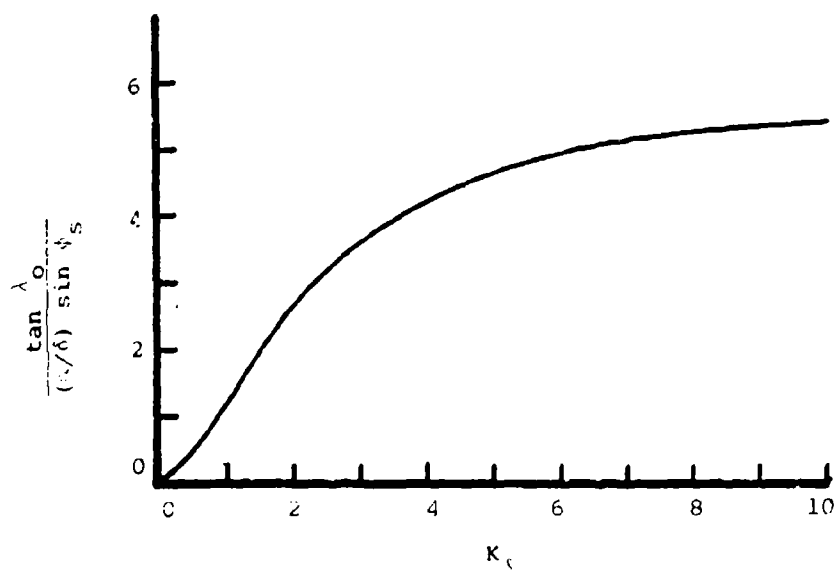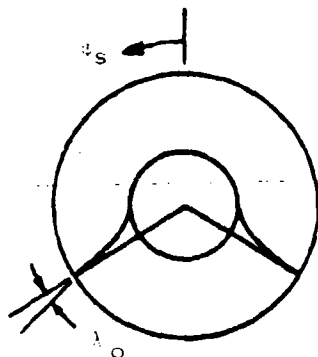$120°$

$135°$

Figure ... Stream Surface for Inclined Cone

Figure 99. Circular-Cone Lip Angle

d. Spacing of the Stream Surfaces

In Equations (588) or (593), the value of ϕ_S designates a particular stream surface, and a stream surface can be represented functionally by $\phi_S = \phi_S(\theta,\phi) = $ constant. How closely the stream surfaces are spaced as θ is varied outward from the cone surface, for a fixed azimuthal angle ϕ, can be evaluated by the derivative $(\partial\phi_S/\partial\theta)$ with ϕ held constant. From Equation (588) is obtained

$$\left(\frac{\partial\phi_S}{\partial\theta}\right)_\phi = - \frac{W_0(\theta)\,\sin\phi}{\theta v_0(\theta)},$$

$$= \frac{\alpha}{\delta}\,\frac{W_0(\theta)}{V_\infty}\,\frac{\sin\phi}{\theta^2-\delta^2}. \tag{600}$$

In terms of the normalized shock-layer variable θ' defined by expression (585),

$$\left(\frac{\partial\phi_S}{\partial\theta}\right)_\phi \frac{\alpha}{\delta}\,\frac{W_0(\theta',K_\delta)}{V_\infty}\,\frac{\sin\phi}{\theta'[2+(\sigma-1)\theta']}. \tag{601}$$

This derivative   creases when α increases and goes to infinity when θ' goes to zero ($\theta \to \delta$), and the stream surfaces become more closely spaced correspondingly. As seen from Figure 93, the derivative is insensitive to variation; in K_δ when θ' is about 0.7. When θ' is less than 0.7, the derivative decreases as K_δ increases, and vice versa when θ' is greater than 0.7, but to a lesser degree.

e. Waveriders with a Freestream Upper Surface

Any stream surface just described can be utilized as a solid surface, but a complementary surface remains to be described in order to fashion a closed aerodynamic body. Here such surfaces are chosen to be parallel to the freestream. First demarcate the axis passing through the vertex that is aligned with the freestream. This axis is inclined by an angle α with the cone axis. Any plane passing through this freestream axis is parallel to the freestream. Select pairs of these freestream planes that pass through the

lip-shock intersection of the conical stream surfaces, and a closed
aerodynamic body is thus formed. The upper surfaces are pairs of freestream
planes passing through the freestream vertex axis, and the lower surface is a
stream surface of the inclined circular-cone flowfield. These surfaces join
together at the lip-shock intersection. An example is shown in Figure 100 for
which the lip-shock intersection occurs at $\phi_s = 90$ degrees.

There are an infinite number of such aerodynamic waveriders, depending on
how the freestream planes are selected. As a step towards distinguishing
between the different configurations, determine the lip angle, λ_{0w}, between
the freestream planes and the conical stream surfaces. The normal unit vector
to a freestream plane intersecting the shock at ϕ_s is, for small angles

$$\hat{n}_\infty = \frac{[\sigma - (\alpha/\delta)(1-g_0) \cos \phi_s] \hat{e}_\phi - (\alpha/\delta) \sin \phi_s \hat{e}_\beta}{\sqrt{[\sigma - (\alpha/\delta)(1-g_0) \cos \phi_s]^2 + (\alpha/\delta)^2 \sin^2\phi_s}} \quad . \tag{602}$$

The lip angle, λ_{0w}, is determined by the condition

$$\cos \lambda_{0w} = \hat{n}_\infty \cdot \hat{n} , \tag{603}$$

where $\hat{n}$ is the unit normal vector of the conical stream surface evaluated at
the shock, given by Equation (596). For small ratios $\alpha/\delta \ll 1$,

$$\tan \lambda_{0w} \approx \frac{\alpha}{\delta} \left[\frac{\sigma^2-g_0}{\sigma(\sigma^2-1)} - \frac{1}{\sigma - \alpha/\delta (1-g_0) \cos \phi_s} \right] \sin \phi_s \quad . \tag{604}$$

If the waverider lip angle is ever to be a cusp, then $\lambda_{0w}=0$ is necessary.
The right side of Equation (604) can vanish only when $\sin \phi_s = 0$ or when

$$\frac{\alpha}{\delta} \cos \phi_s = \frac{\sigma}{\sigma^2-g_0} \quad . \tag{605}$$

The right-hand side of Equation (605) vanishes when $K_\delta \to 0$ and increases to
0.87 when $K_\delta \to \infty$. When $K_\delta = 0.5$ and $\alpha/\delta = 0.5$, then Equation (605) yields ϕ_s
= 0, and a cusp can occur only at $\phi_s = 0$. When K_δ is larger than 0.5 and α/δ
is less than 0.5 a cusp cannot occur except at $\phi_s = 0$ or 180 degrees. These
are generally conditions of interest and, as such, the possibility of a cusp
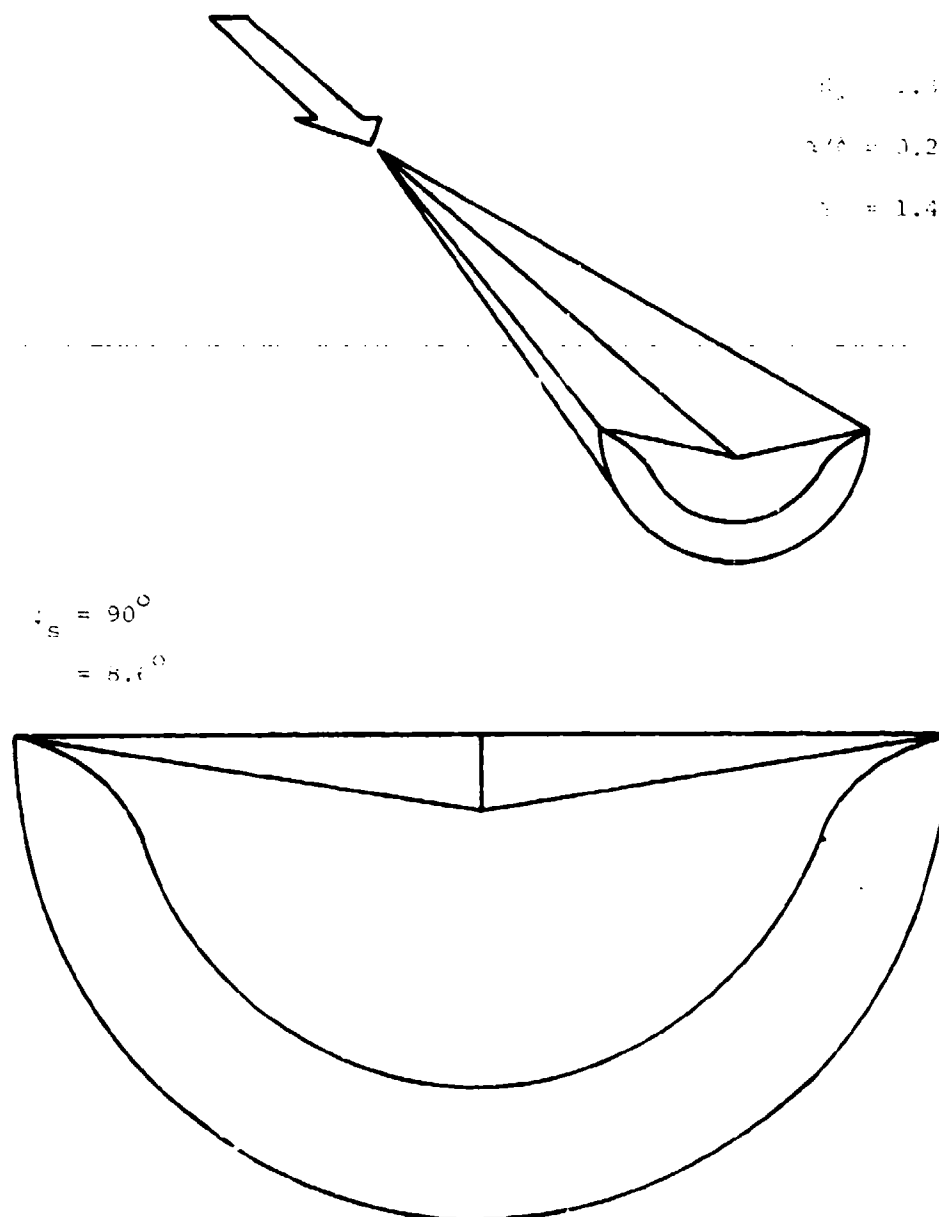
$M^2 = 0.2$

$\gamma = 1.4$

$\theta_s = 90°$

$= 5.6°$

Figure ... Circular-Arc Waverider with Freestream Upper Surface: Positive Dihedral

is of no concern.

From structural or heating considerations, the condition where the lip angle λ_{0w} is a maximum is of interest. Setting the derivative of λ_{0w} with respect to ϕ_s equal to zero yields, for small α/δ,

$$\cos \phi_s = - \frac{\sigma^2-1}{\sigma} \frac{\alpha}{\delta} \quad . \qquad (606)$$

When the right-hand side is less than minus unity, no relative maximum occurs. When the right-hand side is small, the result is

$$\phi_s = \frac{\pi}{2} + \frac{\sigma^2-1}{\sigma} \frac{\alpha}{\delta} \quad , \qquad (607)$$

which illustrates that the maximum value of λ_{0w} occurs when $\phi_s > \pi/2$. When $K_\delta = 1.3$, $\gamma = 1.4$, and $\alpha/\delta = 0.2$, $\lambda_{0w} = 8.6$ degrees is a maximum when $\phi_s = 96.8$ degrees. This particular waverider is similar in shape to that shown in Figure 100, for which $\phi_s = 90$ degrees and $\lambda_{0w} = 8.57$ degrees. The upper surfaces in these cases appear to have positive dihedral angle.

Another waverider can be formed in which the two upper freestream planes are parallel, that is, the upper surface is flat. An example is shown in Figure 101. From geometrical considerations, this situation occurs when, for small α/δ,

$$\cos \phi_s = \frac{(\alpha/\delta)}{\sigma} \quad . \qquad (608)$$

$K_\delta = 1.3$, $\gamma = 1.4$, and $\alpha/\delta = 0.2$ results in $\phi_s = 81.4$ degrees and $\lambda_{0w} = 8.2$ degrees. This waverider is akin to the waverider formed from a half cone at zero angle of attack with a symmetry plane through the cone axis identified as a flat, zero-thickness delta wing. The waverider shown in Figure 101, however, while having a flat upper surface, has a faired under surface with a "wing" of finite thickness. This waverider can be said to have zero dihedral angle.

Other waveriders in this family can be formed that have negative dihedral
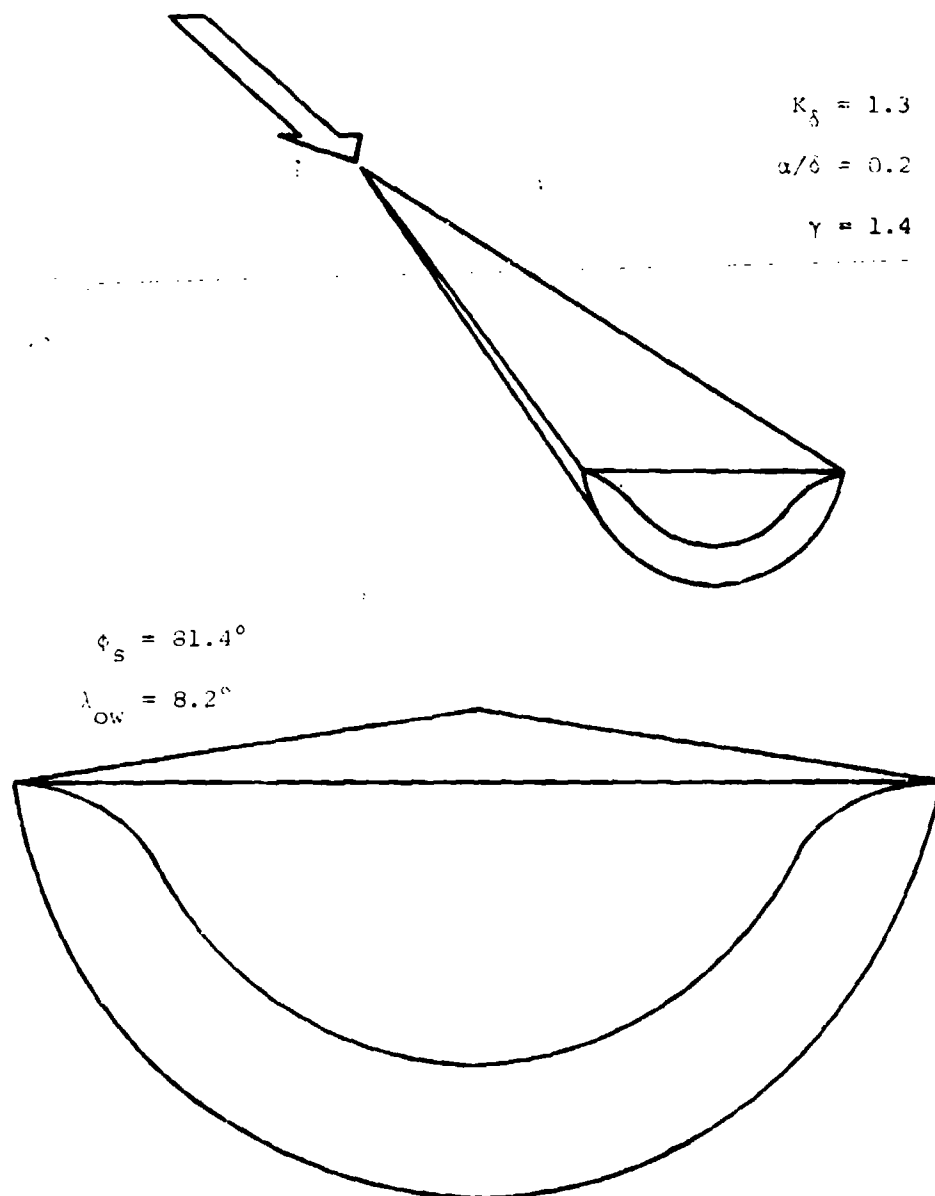
272

$$K_\delta = 1.3$$
$$\alpha/\delta = 0.2$$
$$\gamma = 1.4$$

$$\phi_s = 81.4°$$
$$\lambda_{ow} = 8.2°$$

Figure 101. Circular-Cone Waverider With Freestream Upper
Surface: Zero Dihedral

angles. These exist when ϕ_s is less than the value given by Equation (608).
An example is shown in Figure 102 for $\phi_s = 70$ degrees and $\lambda_{0w} = 7.6$ degrees.
All of the waveriders in this section are lifting bodies since the lower
conical surface is at a higher pressure than the upper freestream surfaces.

f. Waveriders with a Complementary Wedge Surface

Another means of deriving a closed aerodynamic shape in conjunction with
a conical stream surface is to use plane surfaces passing through the cone
axis. In these cases the freestream flow must be deflected by the angle α.
Thus the formulas for the fundamental wedge-derived waverider obtained in
Section III.2 can be used, setting $\Delta = \alpha$. Let the angle between the two
cone-axis plane surfaces be denoted by 2ψ, where ψ is the dihedral angle, as
shown in Figure 103. The plane (or wedge) shock wave across the top of the
waverider is oriented at an angle β_w with the freestream, and it is related
to the cone shock by the relation

$$\beta_w - \alpha = \theta_s{}^* \cos \psi$$
$$= (\beta + \alpha\, g_0 \cos \phi_s) \cos \psi \,. \tag{609}$$

Note that now $\phi_s = \pi - \psi$ and that β_w is given by Equation (576), with $\sin \beta \to \beta_w$
and $\sin \Delta \to \alpha$. Equation (609) is rewritten as

$$\frac{\alpha}{\delta} \left[\frac{\gamma+1}{4} + \sqrt{\frac{(\gamma+1)^2}{4} + \frac{1}{K_\delta^2} \frac{(\delta)^2}{\alpha}} \right] = \left[\frac{\beta}{\delta} - \frac{\alpha}{\delta}\, g_0 \cos \psi \right] \cos \psi \,. \tag{610}$$

Recalling that $\sigma \equiv \beta/\delta$ is given by Equation (583), note that Equation (610)
provides a relation between σ/δ, K_δ, and ψ. Solving for α/δ, obtains

$$\frac{\alpha}{\delta} = \frac{B\sigma \cos \psi \pm \sqrt{\frac{(\gamma+1)}{4}\sigma \cos \psi)^2 - \frac{1}{K_\delta^2}\left(\frac{(\gamma+1)^2}{4} - B^2\right)}}{\frac{(\gamma+1)^2}{4} - B^2} \tag{611}$$

where

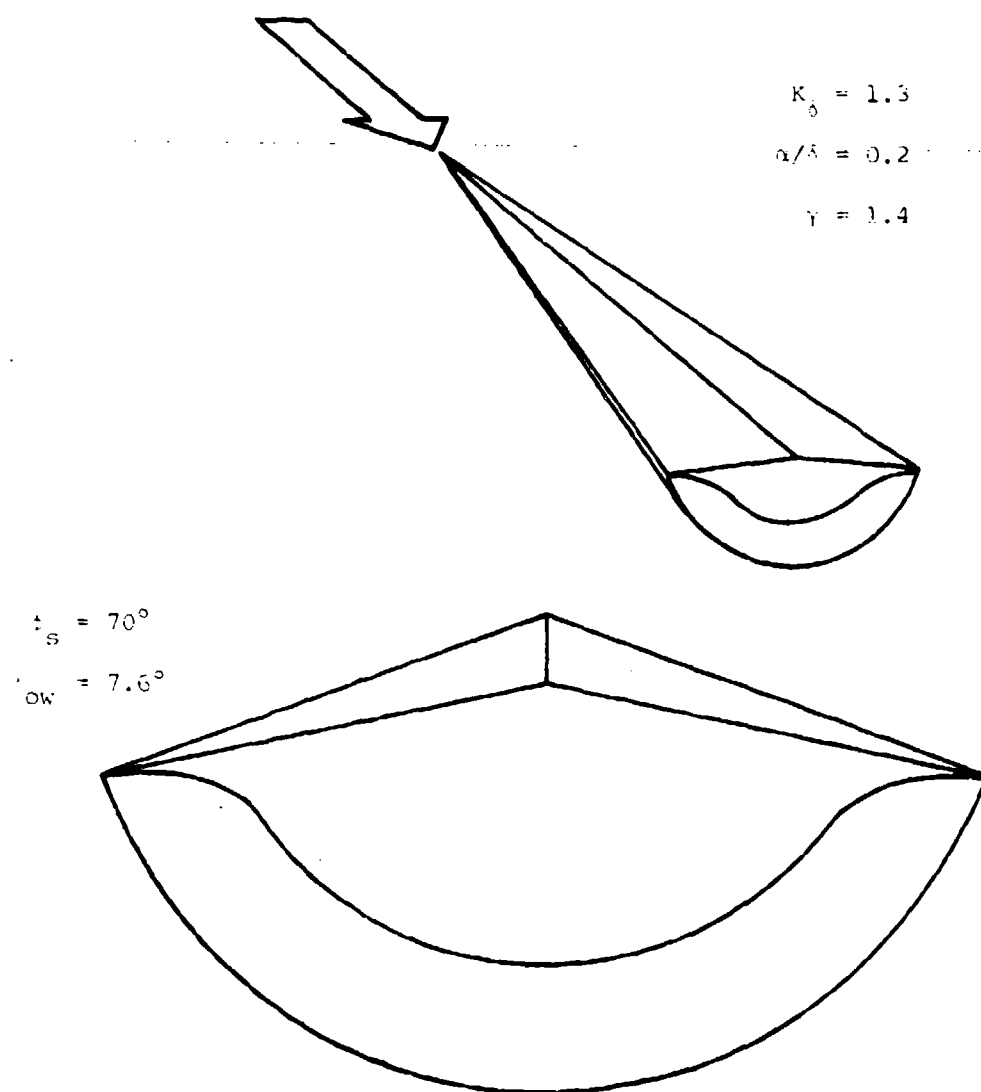$$B \equiv \frac{3-\gamma}{4} - g_0 \cos \psi \,. \tag{612}$$

274

$K_\delta = 1.3$

$\sigma/\lambda = 0.2$

$\gamma = 1.4$

$\xi_s = 70°$

$\delta_w = 7.6°$

Figure 132. Circular-Cone Waverider With Freestream Upper Surface: Negative Dihedral

275

$K_A = 1.3$

$\alpha/\delta = 0.2$

$\gamma = 1.4$

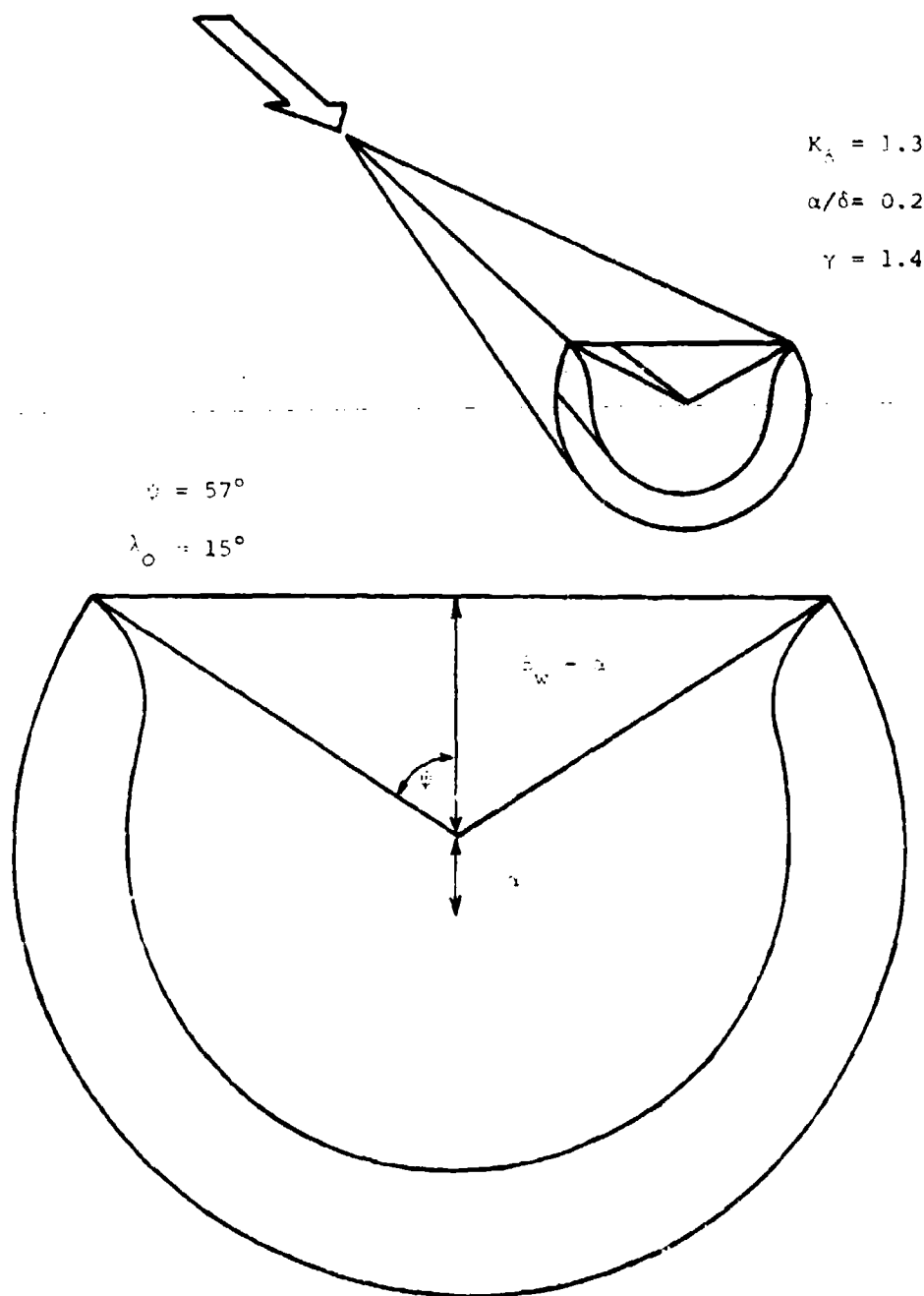$\psi = 57°$

$\lambda_o = 15°$

Figure 133. Circular-Cone Waverider With Wedge-Shock Upper Surface

Figure 104 shows α/δ plotted as a function of K_δ for various values of the dihedral angle ψ and for $\gamma = 1.4$. Observe that α/δ is double valued for fixed values of K_δ and ψ, but this is only apparent for $\psi > 75$ degrees since the curves are plotted for only the realistic values of $\alpha/\delta < 1$. The condition $\alpha/\delta = 0$ corresponds to zero flow deflection over the upper surface; the dihedral angle ψ is such that a plane Mach surface sits on the lip of the waverider, and the lips extend to the cone surface as a pair of infinitesimally thin delta wings.

The lift on the waveriders in this section may be positive or negative depending on the value of α/δ. The pressure in the conical flow field is given by

$$\frac{C_{pc}(\theta,\phi)}{\delta^2} = \frac{c_{p0}(\theta)}{\delta^2} + \frac{\alpha}{\delta} \frac{C_{p0}(\theta)}{\delta} \cos\phi + 0(\alpha^2) \quad , \tag{613}$$

and the pressure in the wedge flowfield is given by (from Equation (577))

$$\frac{C_{pw}}{\delta^2} = \frac{\gamma+1}{2}\left(\frac{\alpha}{\delta}\right)^2 + \sqrt{\frac{(\gamma+1)^2}{2}\left(\frac{\alpha}{\delta}\right)^4 + \frac{4}{K_\delta^2}\left(\frac{\alpha}{\delta}\right)^2} \quad . \tag{614}$$

The minimum pressure on the conical stream surface occurs at the symmetry plane, $\theta = \delta$ and $\phi = 0$. The minimum lifting pressure differential is thus given by

$$\frac{\Delta C_{pm}}{\delta^2} \equiv \frac{C_{pc}(\delta,0)}{\delta^2} - \frac{C_{pw}}{\delta^2} \tag{615}$$

Also note (References 20,21,and 22) that

$$\frac{C_{p0}(\delta)}{\delta^2} = 1 + \frac{\sigma^2 \ln \sigma^2}{\sigma^2 - 1} \tag{616}$$

Further, from Figure 96, note that $C_{p0}(\delta)/\delta = -4$. A lower bound for the value of α/δ corresponding to zero lift can now be found by setting $\Delta C_{pm} = 0$:

$$1 + \frac{\sigma^2 \ln \sigma^2}{\sigma^2-1} - 4\left(\frac{\alpha}{\delta}\right) - \frac{\gamma+1}{2}\left(\frac{\alpha}{\delta}\right)^2 - \sqrt{\frac{(\gamma+1)^2}{2}\left(\frac{\alpha}{\delta}\right)^4 + \frac{4}{K_\delta^2}\left(\frac{\alpha}{\delta}\right)^2} = 0 \quad . \tag{617}$$

This relation provides α/δ for zero lift as a function of K_δ and is shown in Figure 103. The waveriders described by conditions below this line are lifting
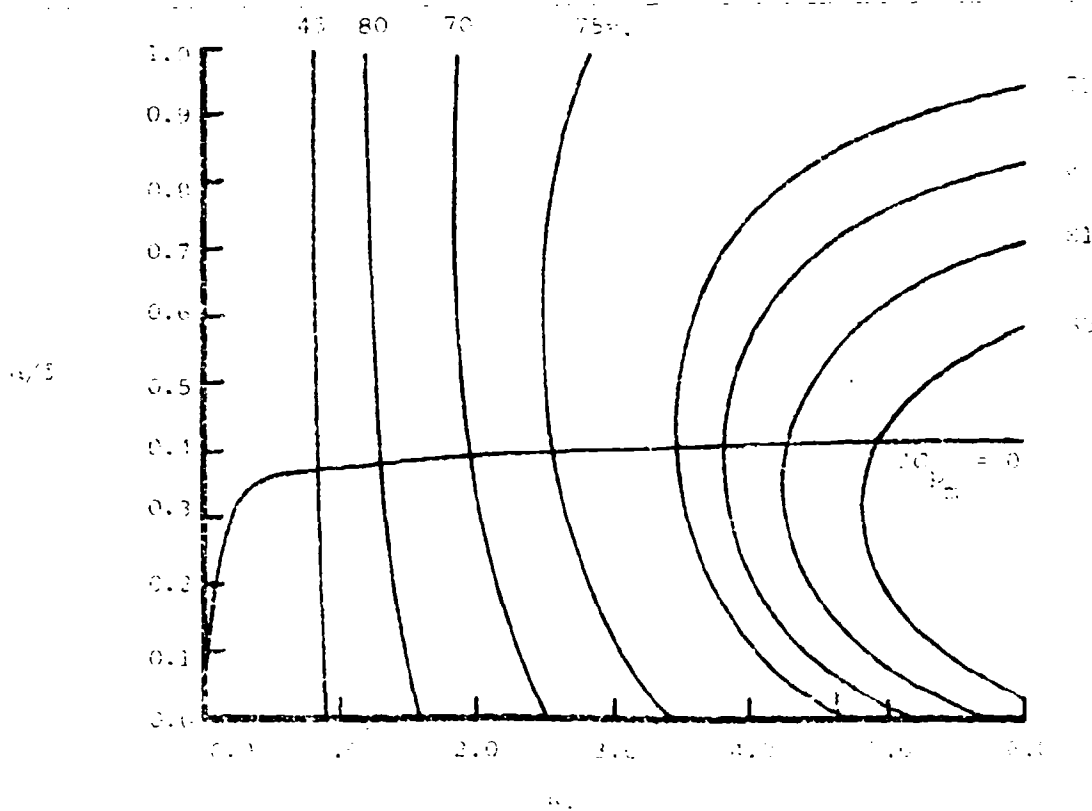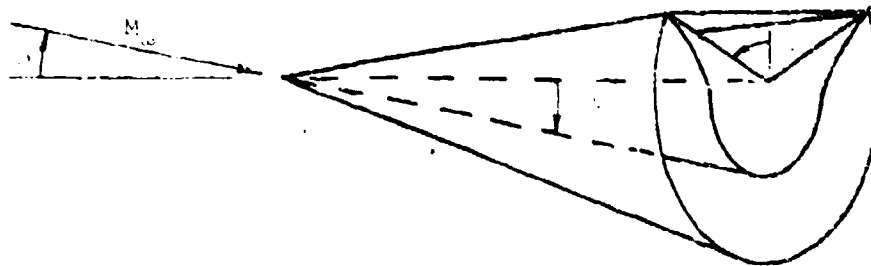
277

Figure 104. a/r Versus K For Various Internal Angles

when the conical surface is underneath, and the waveriders described by conditions above the line are lifting when the wedge surface is underneath. Approximately, the zero lift conditions occur when $\alpha/\delta = 0.4$ for $K\delta > 1$.

A systematic variation of the cone-wedge waverider cross section geometries is shown in Figures 105 through 110 for $\alpha/\delta = 0.1, 0.2, 0.3, 0.4,$ 0.5, 0.6. For each value of α/δ, dihedral angles of $\psi = 45, 60, 70, 75,$ 80 degrees are shown along with their corresponding values of $K\delta$ as determined from Equations (612) or (613). For $\alpha/\delta = 0.1, 0.2, 0.3$, the bodies are lifting when the conical surface is underneath. At α/δ 0.4, the body is nearly at zero lift. For $\alpha/\delta = 0.5$ and 0.6, the bodies are lifting when the wedge surface is underneath. The shock lies closer to the body when $K\delta$ is larger, and hence when ψ is larger. The standard conditions $K\delta = 1.3$, $\gamma = 1.4$, and $\alpha/\delta = 0.2$ are represented in Figure 103, in which case $\psi = 57$ degrees and $\lambda_{0w} = 15$ degrees.

6. WAVERIDERS DERIVED FROM ELLIPTIC CONES

   a. Stream Surfaces

The case when $\alpha = 0$, that is, an elliptic cone at zero angle of attack is considered. When $\alpha = 0$, separate the variables in Equation (587), perform the integration on θ, and obtain

$$-\frac{2\varepsilon_2}{V_\alpha} \int_{\theta_s}^{\theta} * \frac{w_1(\theta) \, d\theta}{\theta^2 - \theta_c^2} = \ln \left[\frac{\tan \phi}{\tan \phi_s} \right] \quad , \tag{618}$$

where

$$\theta_s^* \equiv \beta - \varepsilon_2 a_2 \cos 2\phi_s \quad , \tag{619}$$

and where δ that appears in Equation (586) has been replaced by θ_c, the elliptic cone angle,

$$\theta_c \equiv \delta - \varepsilon_2 \cos 2\phi \quad . \tag{620}$$

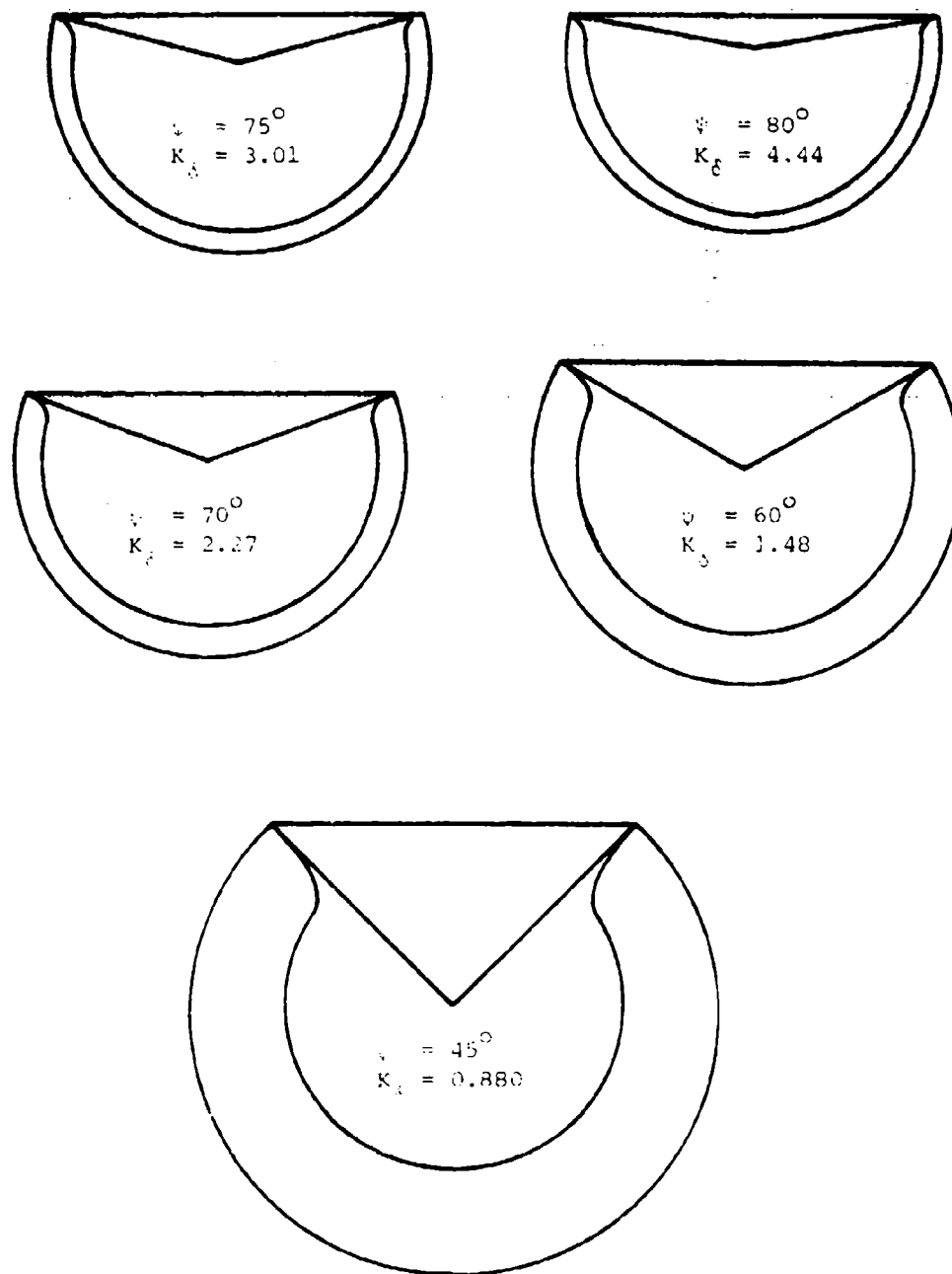The variation of ϕ that occurs in θ_c is to be ignored in the integration.

$\psi = 75^{\circ}$
$K_{\delta} = 3.01$

$\psi = 80^{\circ}$
$K_{\delta} = 4.44$

$\psi = 70^{\circ}$
$K_{\delta} = 2.27$

$\psi = 60^{\circ}$
$K_{\delta} = 1.48$

$\psi = 45^{\circ}$
$K_{\delta} = 0.880$
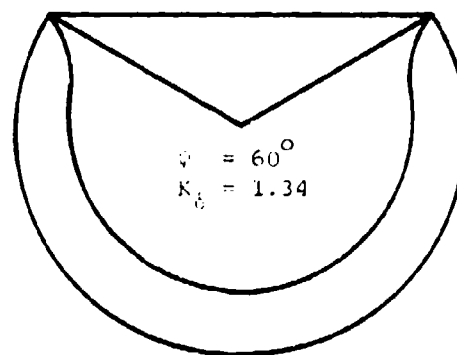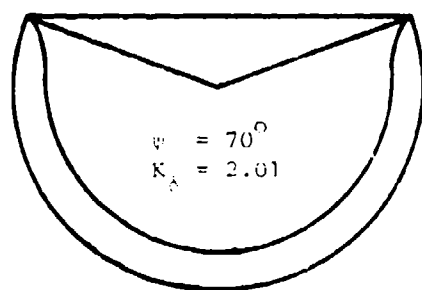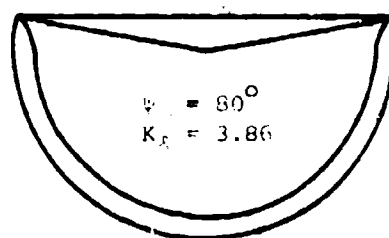
Figure 165.   Wedge Shock-Circular Cone Waveriders,
$\eta = 0.1$

$\alpha = 75^\circ$
$K_A = 2.79$

$\alpha = 80^\circ$
$K_A = 4.05$

$\alpha = 70^\circ$
$K_A = 2.12$

$\alpha = 60^\circ$
$K_A = 1.40$

$\alpha = 45^\circ$
$K_A = 0.96$
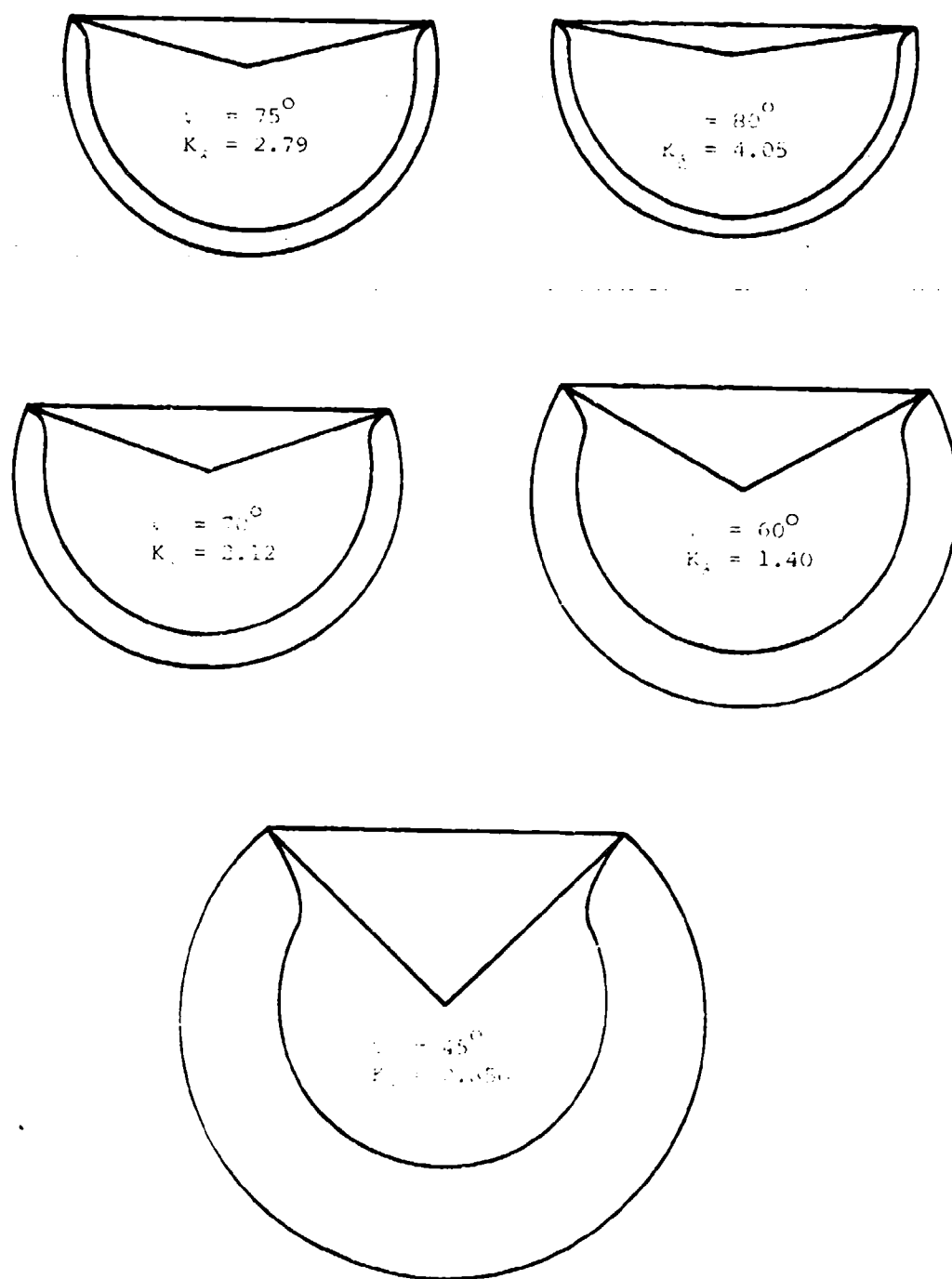
Figure 84. Active Stress-Strain Line Eccentricity, $x/L = 0.2$
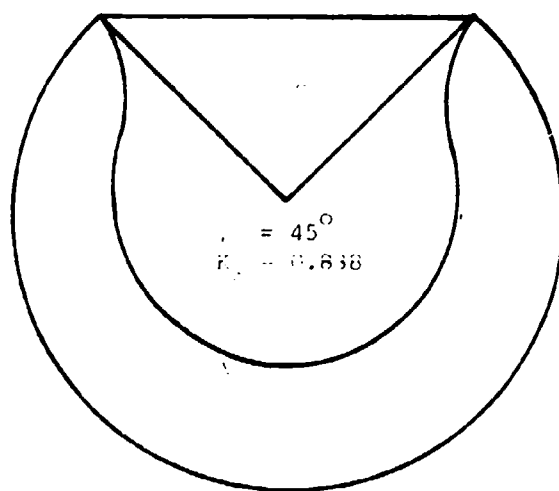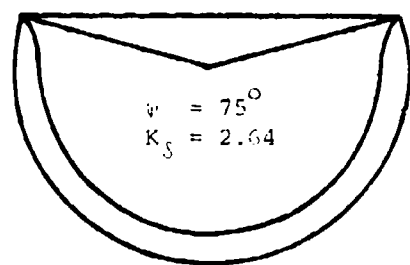
Figure 107. Wedge Shock-Circular Cone Waveriders, x/s = 0.3

282

$\psi = 75^{o}$
$K_{\delta} = 2.55$

$\psi = 80^{o}$
$K_{\delta} = 3.81$

$\psi = 70^{o}$
$K_{\delta} = 1.93$

$\psi = 60^{o}$
$K_{\delta} = 1.29$

$\psi = 45^{o}$
$K_{\delta} = 0.825$
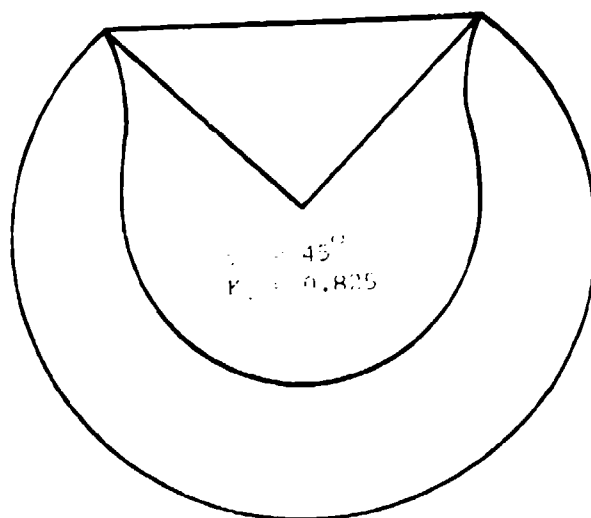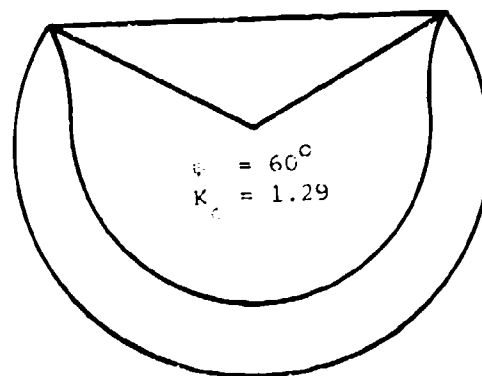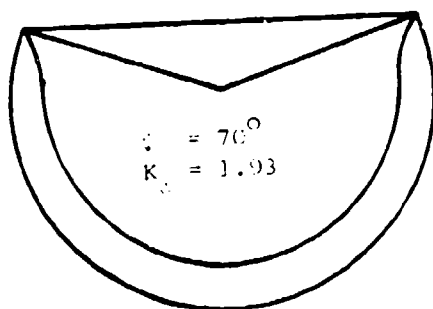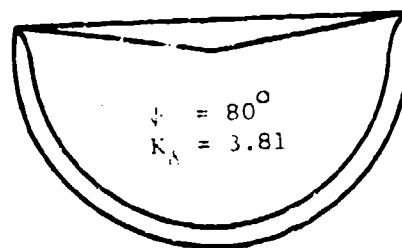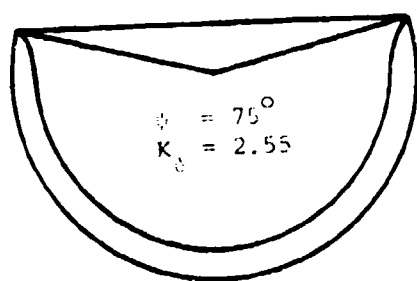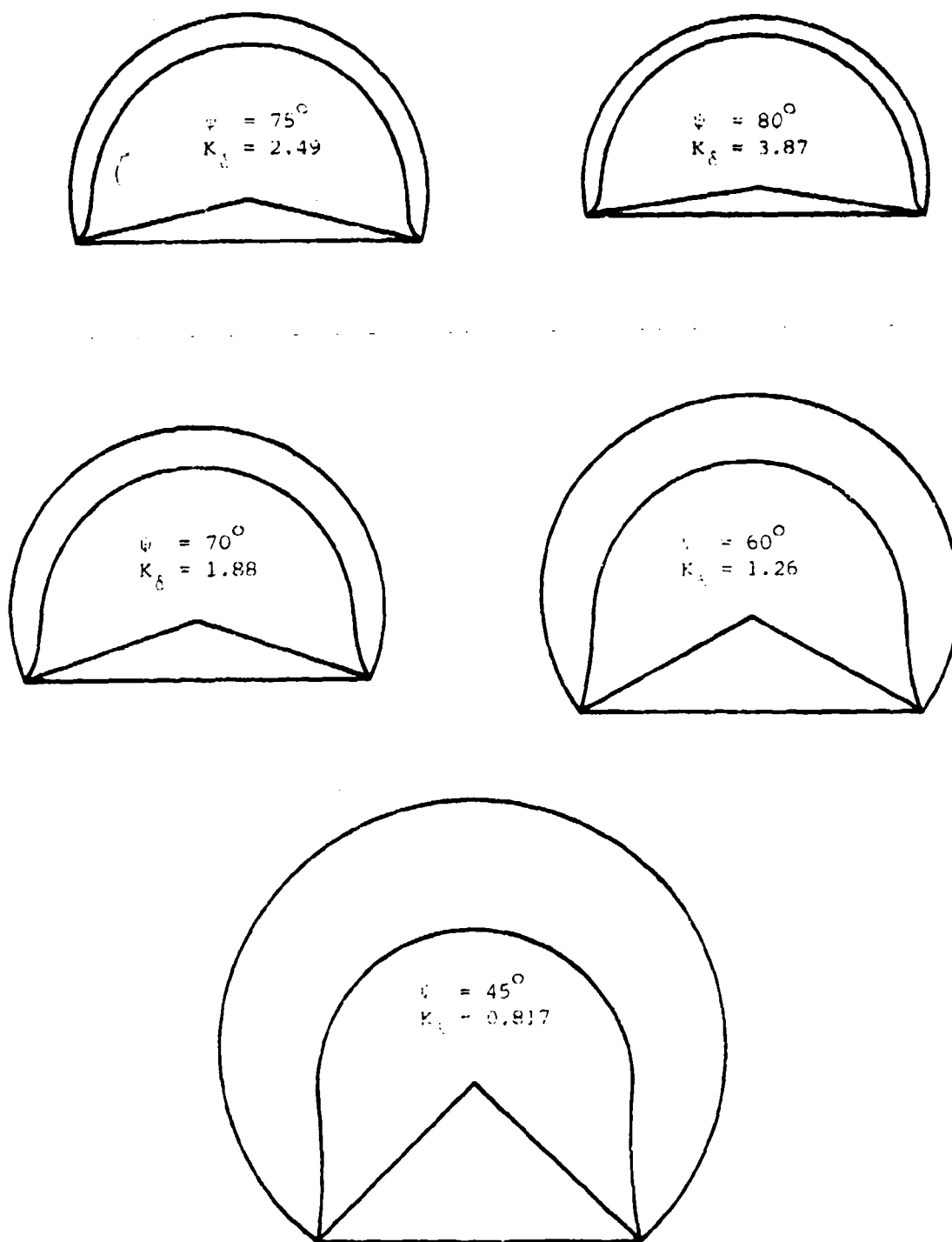
Figure 109. Wedge shock-Circular cone Waveriders, ψ = 0.5

$\psi = 75^{\circ}$
$K_\delta = 2.48$

$= 80^{\circ}$
$K_\delta = 4.08$

$= 75^{\circ}$
$K_\delta = 1.64$

$= 60^{\circ}$
$K_\delta = 1.23$

$= 45^{\circ}$
$K_\delta = 0.818$
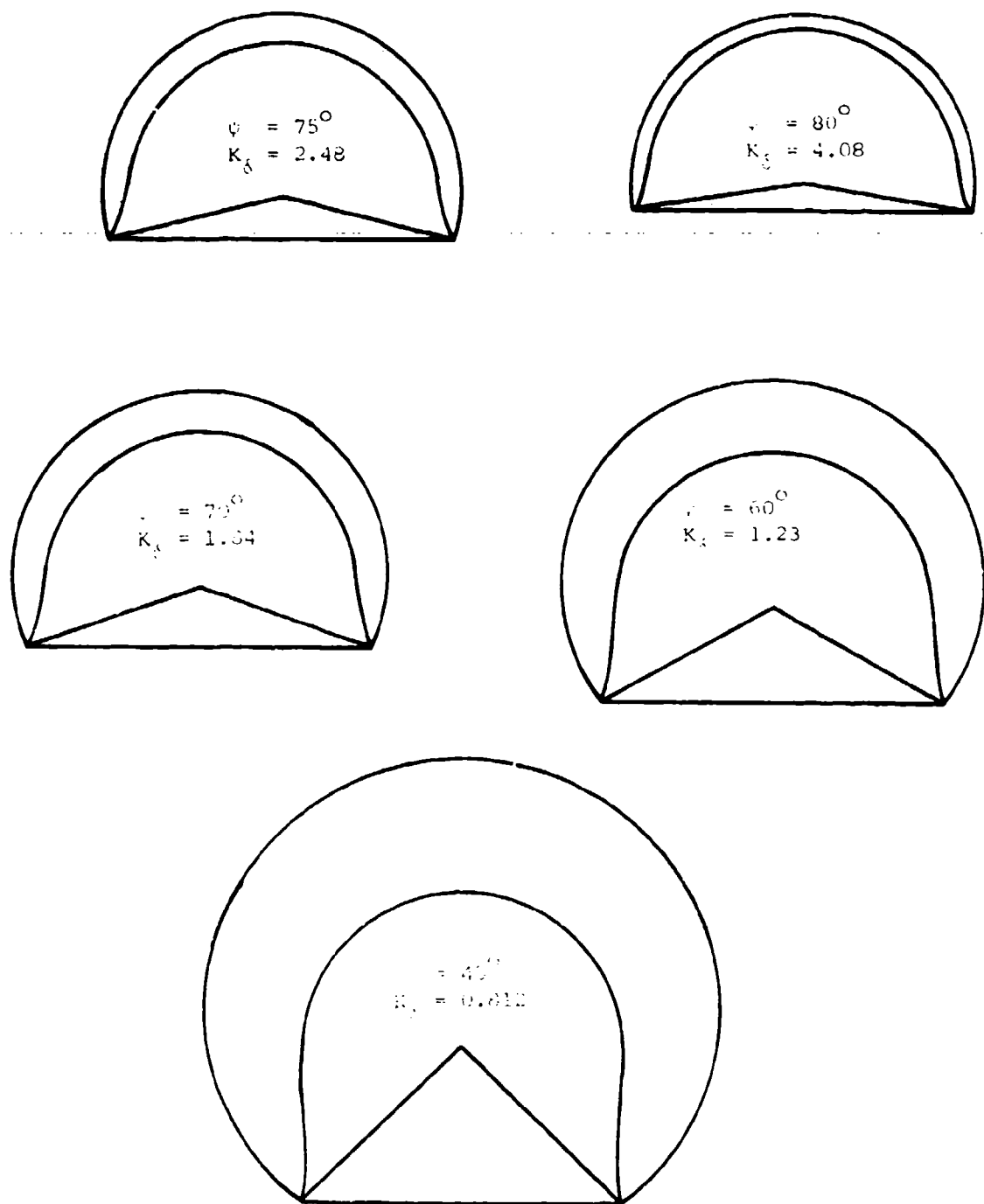
Figure 11.6. Radial semi-circular lane barricade, $= 0.6$

These operations are consistent in present first-order accuracy. The azimuthal velocity $W_2(\theta)$ is known [Equation (84)] and is illustrated in Figure 94. The quadrature thus can be evaluated numerically. When θ proceeds to the cone surface, $\theta \to \theta_c$, the quadrature on the left side of Equation (618) diverges, and the right side tends to minus infinity. Correspondingly, when the shock location of the stream surface, ϕ_s, is less than 90 degree, the angle ϕ tends to zero. When ϕ_s is greater than 90 degree, the angle tends to 180 degrees. Thus the stream surfaces that begin at the shock for $\phi_s < 90$ degrees become tangent to the cone surface at $\phi = 0$, and the stream surfaces that begin at the shock for $\phi_s > 90$ degrees become tangent to the cone at $\phi = 180$ degrees. The stream surface $\phi_s = 90$ degree is a symmetry plane that is perpendicular to the body at $\phi = 90$ degree. Examples of stream srufaces are shown in Figure 111.

b. Approximate Integration

Figure 94 suggests that $W_2(\theta)$ can be approximated by the relation

$$W_2(\theta) = A + \frac{\theta_c B}{\theta} , \qquad (621a)$$

where

$$A \equiv \frac{\sigma' W_2(\theta_s) - W_2(\theta_c)}{\sigma' - 1} , \qquad (621b)$$

$$B \equiv \frac{[W_2(\theta_c) - W_2(\theta_s)]}{\sigma' - 1} , \qquad (621c)$$

where $\sigma' \equiv \theta_s/\theta_c = \sigma + 0(\varepsilon)$, $\theta_s = \beta + 0(\varepsilon)$, and $\theta_c = \delta + 0(\varepsilon)$. The errors of order ε in Equations (621) will subsequently be neglected. When this approximation is used to evaluate the integral in Equation (618), the result is

$$k_3 \ln \left[\frac{\theta - \theta_c}{\theta_s - \theta_c}\right] + k_4 \ln \left[\frac{\theta + \theta_c}{\theta_s + \theta_c}\right] - (k_3 + k_4) \ln \left[\frac{\theta}{\theta_s}\right] = \ln \left[\frac{\tan \phi}{\tan \phi_s}\right] , \quad (622)$$
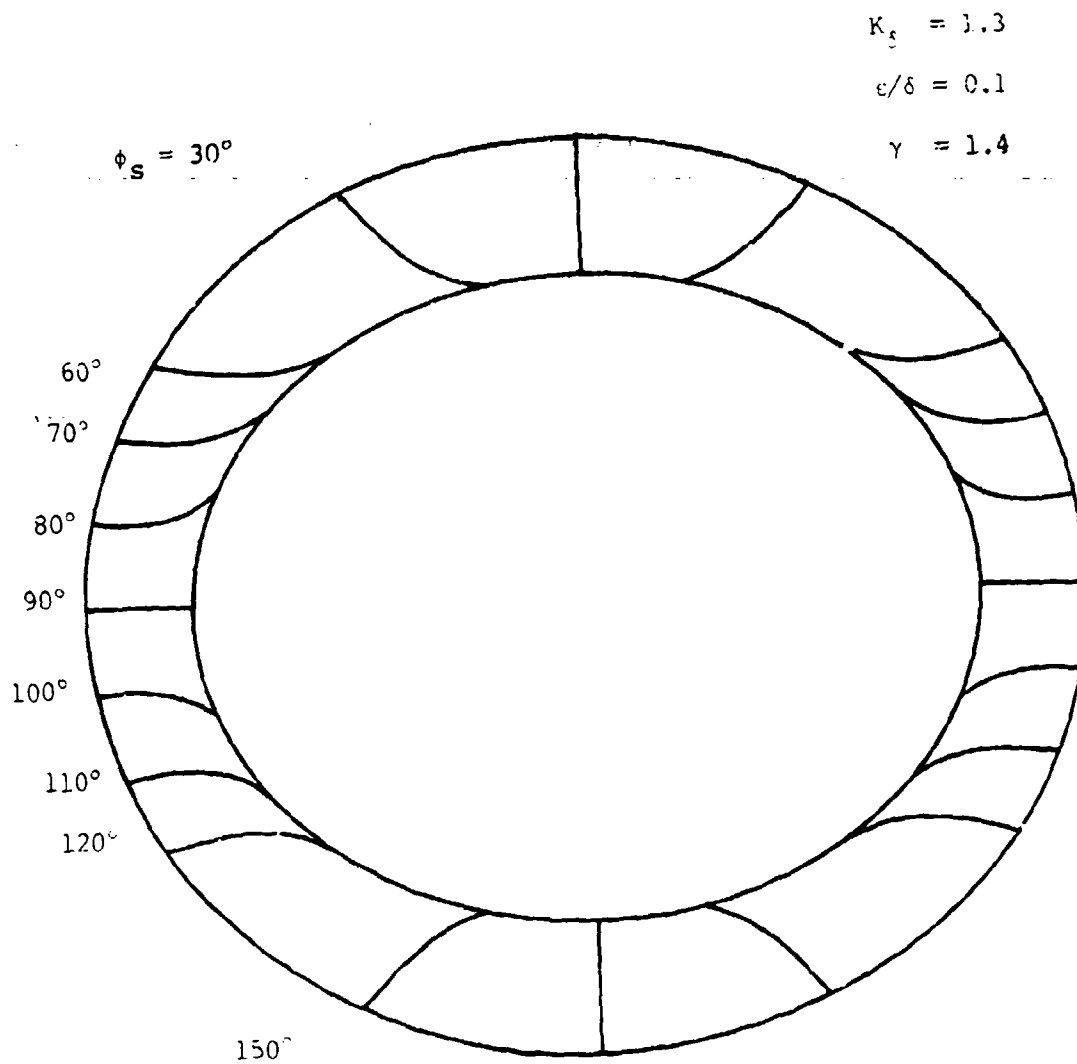
where

Figure 111. Stream Surfaces for Elliptic Cone

287

$$k_3 \equiv - \frac{\varepsilon_2}{\delta} \frac{W_2(\delta)}{V_\infty} \quad , \tag{623a}$$

$$k_4 \equiv - \frac{\varepsilon_2}{\delta} \frac{(\sigma+1)W_2(\delta) - 2\sigma W_2(\beta)}{(\sigma-1) V_\infty} \quad . \tag{623b}$$

Equation (622) can also be written as

$$\left[\frac{\theta - \theta_c}{\theta_s^* - \theta_c} \cdot \frac{\theta_s^*}{\theta} \right]^{k_3} \left[\frac{\theta + \theta_c}{\theta^*_s + \theta_c} \cdot \frac{\theta_s^*}{\theta} \right]^{k_4} = \frac{\tan \phi}{\tan \phi_s} \tag{624}$$

Expression (624) is a relation between θ/δ and ϕ_s, with ϕ_s, ε/δ, and K_δ as parameters. The parameter k_3 is always positive since $W_2(\delta)$ is negative when ε is positive, and vice versa. Figure 95 illustrates the dependency of k_3 on K_δ. The parameter k_4 changes sign as K_δ varies, which is suggested by the behavior of $W_2(\theta)$ shown in Figure 94. It can be shown that [Equation (84)]

$$\frac{W_2(\beta)}{V_\infty} = - 2g/\sigma^2 \quad . \tag{625}$$

Now k_4 can be written as

$$k_4 = - \frac{\varepsilon_2}{\delta} \frac{4g + \sigma(\sigma+1) \{w_1(\delta)/V_\infty\}}{\sigma(\sigma-1)} \tag{626}$$

Figure 112 shows how k_4 depends on K_δ. The parameter k_4 vanishes at $K_\delta \approx 1.9$. In the range $0 < K_\delta < 1.9$, k_2 is positive, and it is negative when $K_\delta > 1.9$.

c. Lip Angle

The lip angle is defined by $\cos \lambda_2 = e\hat{\phi} \cdot \hat{n}$, and for the elliptic conical surfaces is determined by

$$\tan \lambda_2 = - \frac{\varepsilon_2}{\delta} \frac{W_2(\beta)}{V_\infty} \frac{\sigma \sin 2\phi_s}{\sigma^2 - 1}$$

$$= \frac{\varepsilon_2}{\delta} \frac{2g_2 \sin 2\phi_s}{\sigma(\sigma^2-1)} \quad . \tag{627}$$

Figure 113 shows the dependency of λ_2 on K_δ. The ratio $(\tan \lambda_2)(\csc 2\phi_s)/(\varepsilon_2/\delta)$ increases from zero to the asymptotic value 8.7 as K_δ increases from zero to infinity. The lip angle becomes thicker as K_δ and ε/δ increase
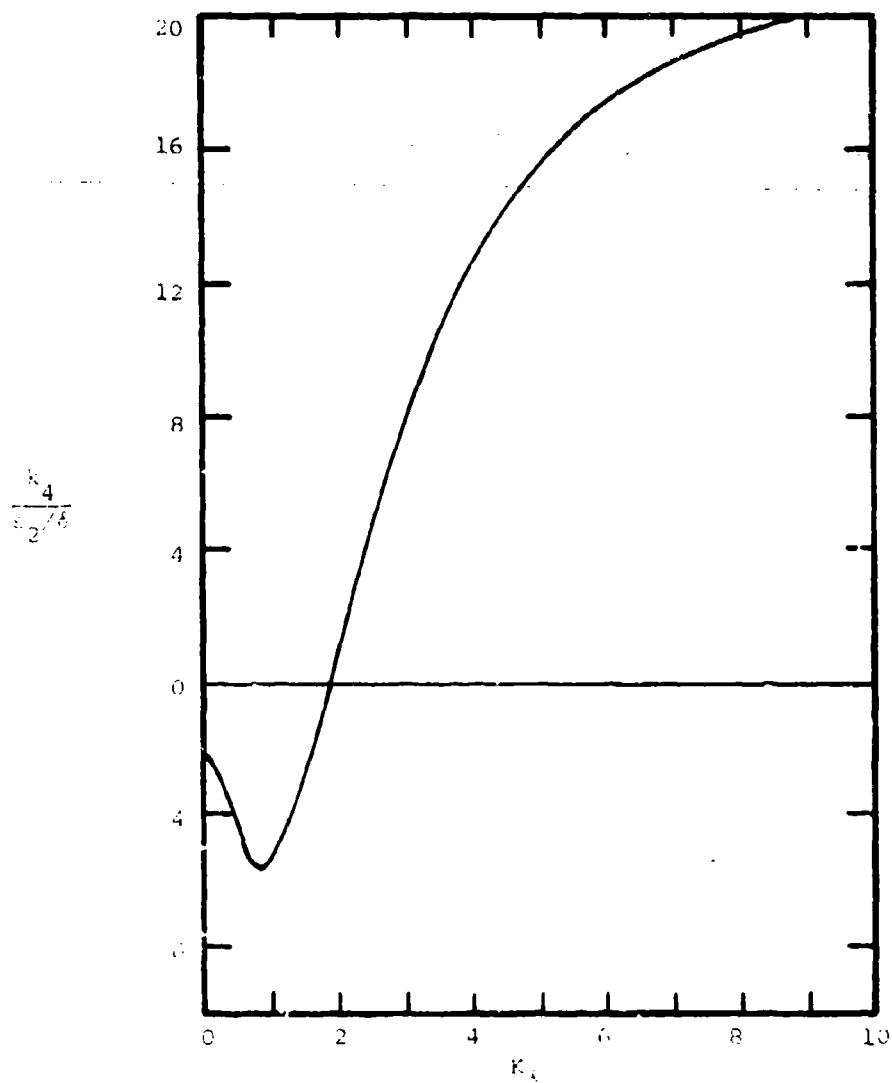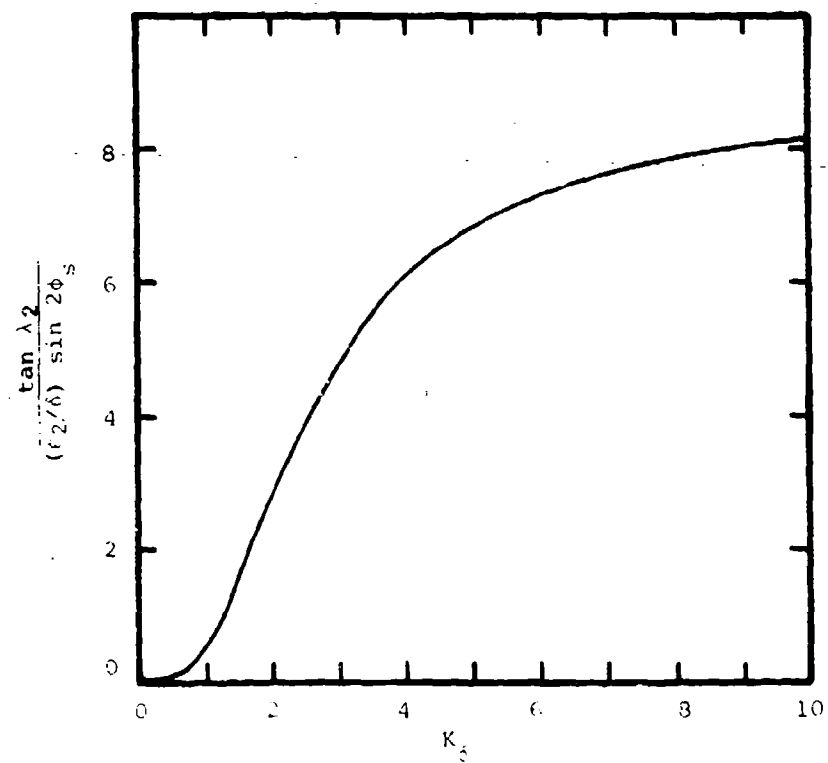
288

Figure 112. Elliptic-Cone Stream-Surface Function

Figure 113. Elliptic-Cone Lip Angle

separately. The lip angle is a maximum when $\phi_s = 45$ and 135 degrees, and it is zero at the symmetry planes $\phi_s = 0$ and 90 degrees.

d. Waveriders with a Freestream Upper Surface

The axis of the elliptic cone at zero angle of attack is parallel to the freestream, and any plane that passes through the cone axis is parallel to the freestream. Pairs of plane surfaces that pass through the cone axis and intersect the shock at the lips of a conical stream surface were chosen. When the plane surfaces are the upper surfaces and the conical surface is the lower surface, a lifting aerodynamic waverider is formed. Two examples are shown in Figure 114 for $K_\delta = 1.3$, $\epsilon/\delta = 0.1$, and $\lambda = 1.4$. These configurations correspond to lip positions of $\phi_s = 100$ and 110 degrees. The respective lip angles are found to be $|\lambda_2| = 2.2$ and 4.0 degrees. These elliptic-cone shapes are similar in form to the circular cone shape shown in Figure 102. The elliptic cone shapes are flatter on the bottom and have thinner lip angles.

The pressure coefficient on the undersurface is given by

$$\frac{C_p(\theta,\phi)}{\delta^2} = \frac{c_{p0}(\theta)}{\delta^2} + \left(\frac{\epsilon_2}{\delta}\right) \frac{C_{p2}(\theta)}{\delta} \cos 2\phi \qquad (628)$$

When Equation (624) is used to determine θ as a function of ϕ, the surface pressure as a function of ϕ can be determined.

7. WAVERIDERS DERIVED FROM INCLINED ELLIPTIC CONES

a. Stream Surfaces

The general stream-surface structure for flow past an inclined elliptic cone can be studied by rewriting Equation (587) in the form

$$\frac{(\alpha W_0 + 2\epsilon_2 W_2)}{V_\infty(\theta^2 - \theta_c^2)} \, d\theta = \frac{d\mu}{(1-\mu^2)(k_5+k_6\mu)} \qquad , \qquad (629)$$

where

$$\mu \equiv \cos \phi \qquad , \qquad (630a)$$

$$k_5 \equiv \frac{\alpha W_0(\theta)}{\alpha W_0(\theta)+2\epsilon_2 W_2(\theta)} \qquad , \qquad (630b)$$

$K_c = 1.3$

$\varepsilon_3/\delta = 0.1$

$\gamma = 1.4$

$\phi_s = 100^o$
$\lambda_2 = 2.2^o$

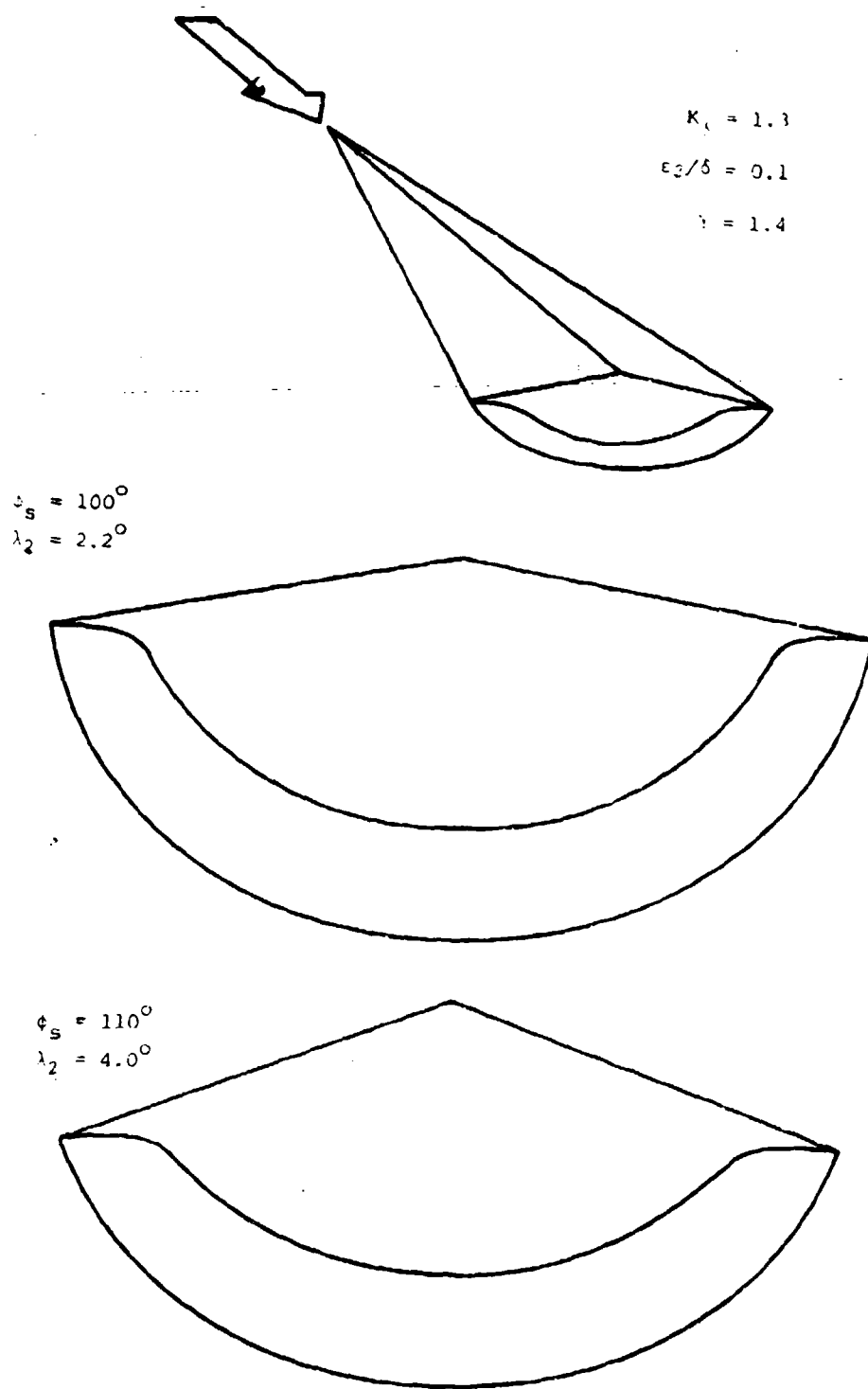$\phi_s = 110^o$
$\lambda_2 = 4.0^o$

Figure 114. Elliptic Cone Waveriders with Freestream Upper Surface.

$$k_6 \equiv \frac{2\epsilon_2 W_2(\theta)}{\alpha W_0(\theta)+2\epsilon_2 W_2(\theta)} \qquad . \qquad (630c)$$

The difficulty with the integration of Equation (629) comes from the combination

$$w^*(\theta,\mu) \equiv k_5 + k_6\mu \qquad (631)$$

which may vanish in the shock layer. The azimuthal velocity vanishes between the shock and the body when $w^* = 0$. The azimuthal location ϕ_0 where w^* vanishes is determined by

$$\cos \phi_0 = - \frac{\alpha}{2\epsilon_2} \frac{W_0(\theta)}{W_2(\theta)} \qquad (632)$$

The surface for $w^* = 0$ (dashed curve) is shown in Figure 115 for $K_\delta = 1.3$, $\gamma = 1.4$, $\alpha/\delta = 0.2$, and $\epsilon_2/\delta = 0.1$. The position where this surface intersects the body surface is denoted by $\phi_0 = \phi_{0c}$ and is determined by

$$\cos \phi_{0c} = - \frac{\alpha}{2\epsilon_2} \frac{W_0(\theta_c)}{W_2(\theta_c)}$$

$$= - \frac{\alpha}{2\epsilon_2} \frac{W_0(\delta)}{W_2(\delta)} \qquad . \qquad (633)$$

For the conditions in Figure 115 there is $\phi_{0c} = 127°$. The surface for $w^* = 0$ lies on the windward side of the body. Between the body and the surface $w^* = 0$ the azimuthal velocity is positive, and it is negative between the $w^* = 0$ surface and the shock. For other conditions, $\cos \phi_{0c}$ can be calculated with the use of Figure 116 which shows the ratio $W_2(\delta)/W_0(\delta)$ as a function of K_δ for $\gamma = 1.4$. Also shown is the ratio at the shock, $W_2(\beta)/W_0(\beta)$. For a given value of K_δ, the ratio $W_2(\theta)/W_0(\theta)$ increases from the shock value to the surface value.

A straightforward approximate integration of Equation (629) is obtained by treating k_5 and k_6 as constants. Experience shows that the best values to use for these constants are the values at the body. For this choice, the body surface conditions are correctly given , which is especially important for
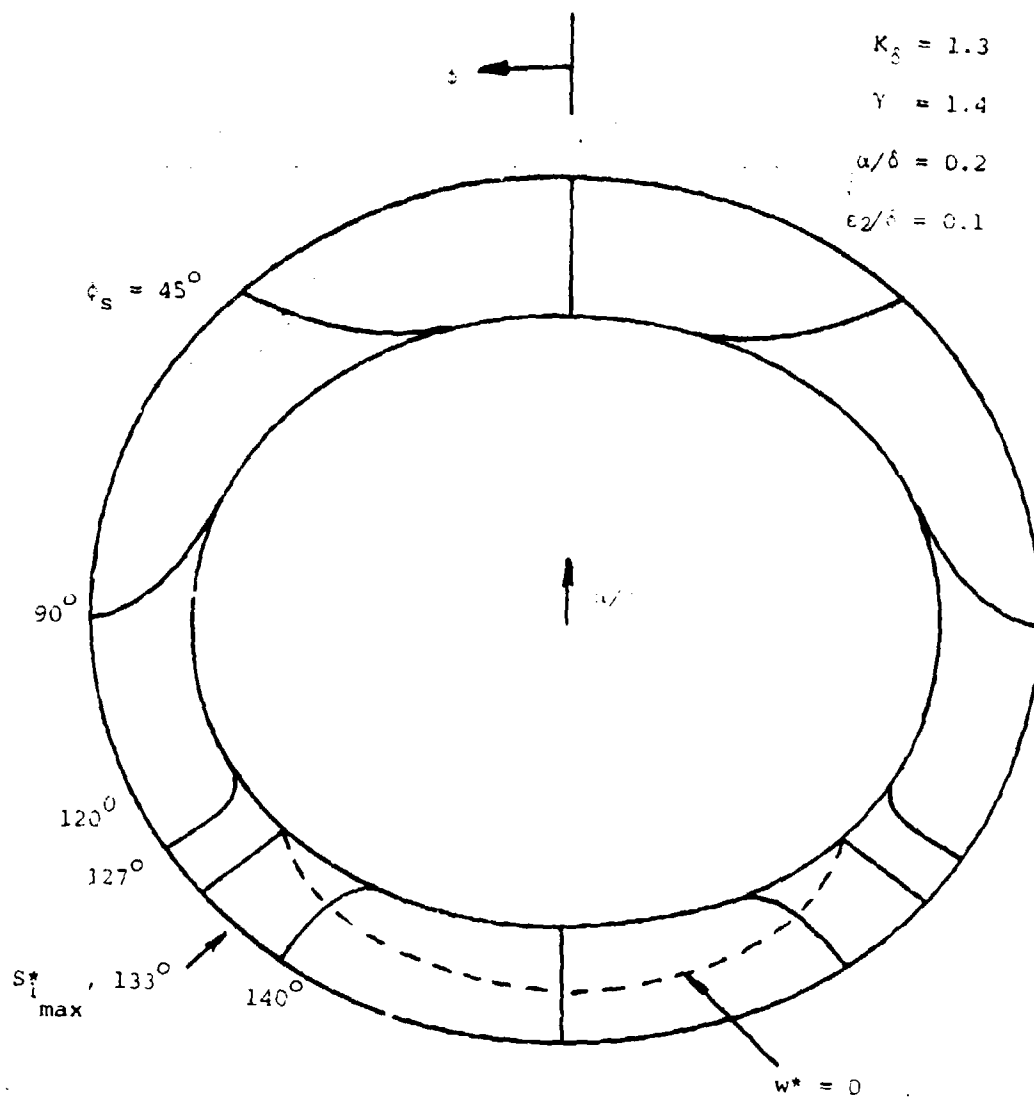
293

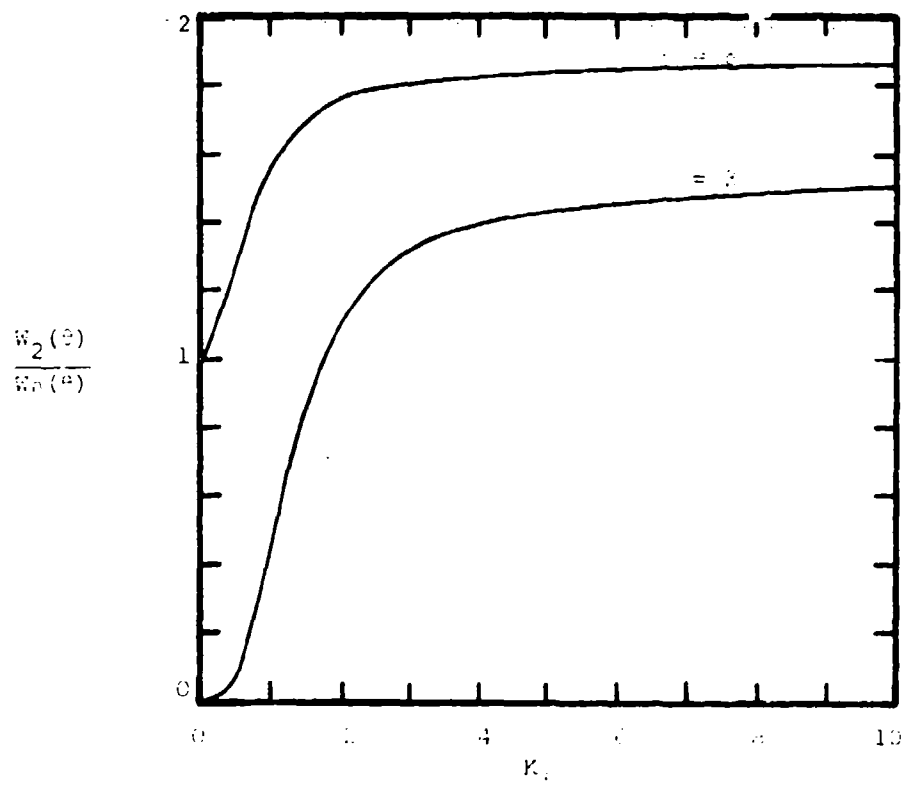Figure 115. Stream Surfaces for Inclined Elliptic Cone

Figure 116. Azimuthal Velocity Ratios at Shock and Body

the position of the intersection of the windward-leeward dividing stream surface with the body, denoted by ϕ_{0c}.

With the left side of Equation (629) evaluated as for the previous cases, the approximate integral of Equation (629) is determined to be

$$\left|\frac{\theta - \theta_c}{\theta_s^* - \theta_c} \cdot \frac{\theta_s^*}{\theta}\right|^{k_1+k_3} \left|\frac{\theta + \theta_c}{\theta_s^* + \theta_c} \cdot \frac{\theta_s^*}{\theta}\right|^{k_2+k_4} =$$

$$\frac{\left|\tan\frac{\phi}{2}\right|^{k_7}}{\left|\tan\frac{\phi_s}{2}\right|} \left|\frac{k_1 \csc\phi + k_3 \cot\phi}{k_1 \csc\phi_s + k_3 \cot\phi_s}\right| \qquad , \qquad (634)$$

where

$$k_7 \equiv k_1/(k_1-k_3) \qquad , \qquad (635a)$$

$$k_8 \equiv k_1/(k_1-k_3) \qquad , \qquad (635b)$$

$$\theta_c \equiv \delta - \varepsilon_2 \cos 2\phi \qquad , \qquad (635c)$$

$$\theta_s^* \equiv \beta + \alpha g_0 \cos\phi_s - \varepsilon_2 g_2 \cos 2\phi_s \qquad . \qquad (635d)$$

Equation (634) reduces to Equation (593) or (594) in the separate limits $\varepsilon_2 \rightarrow$ 0 and $\alpha \rightarrow 0$. If the conditions are such that $k_1 = k_3$, then the appropriate limit must be taken on the right-hand side of Equation (634), which corresponds to setting $k_5 = k_6$ in the original differential equation, Equation (629).

Figure 115 shows stream surfaces generated by Equation (634) for the conditions $K_\delta = 1.3$, $\gamma = 1.4$, $\alpha/\delta = 0.2$, and $\varepsilon_2/\delta = 0.1$. The dividing stream surface which separates the flow that proceeds toward the leeward ray from the flow that proceeds toward the windward ray occurs at $\phi_s = 127$ degrees . This dividing surface is a plane surface in this approximation. The actual stream surfaces should appear slightly different near the dividing stream surface and toward the windward ray. In this region the actual stream surfaces have a negative value of azimuthal velocity at the shock and hence should slope towards the leeward direction before curving into the radial direction at the

surface $w^* = 0$ and then curving further towards the windward ray as shown. The slope $(\partial\phi/\partial\theta)_{\phi_s}$ should actually be positive in the windward region whereas the approximation (634) yields a slightly negative slope. Because the details of the azimuthal velocity field have not been taken into account, the dividing stream surface and its intersection with the body surface are not precisely described by the plane surface shown, even though the location of the body intersection is correct. Both the actual slopes and the approximation slopes at the shock are small in the windward region, and hence the description shown in Figure 115 is qualitatively valid except for the aforementioned discrepancies.

b. Maximum-Entropy Surface

Outside the vortical and viscous boundary layers, the entropy has the expansion

$$s(\theta,\phi) = s_0(\theta) + \alpha S_0 \cos\phi + \varepsilon_2 S_2 \cos 2\phi \quad , \qquad (636)$$

where S_0 and S_2 are constants associated with the angle-of-attack and eccentricity perturbations. Let

$$s_1^* = \alpha s/S_0 \cos\phi_s + \varepsilon_2 S_2 \cos 2\phi_s \qquad (637)$$

denote the entropy perturbation at the shock. It can be shown (References 22 and 52) that

$$\frac{s_1^*}{c_v} = -\gamma(\gamma-1)\beta(1-\varepsilon_0)^2 \frac{V_\infty^2}{a_0^2(\beta)} [\alpha(1-g_0)\cos\phi_s + \varepsilon_2 g_2 \cos 2\phi_s] \quad , \qquad (638)$$

where $\xi_0 = \rho_\infty/\rho_0(\beta)$ and $a_0^2(\beta) = \gamma p_0(\beta)/\rho_0(\beta)$. The maximum entropy perturbation at the shock occurs where the derivative with respect to ϕ_s of Equation (638) vanishes. This occurs where

$$\cos\phi_{gm} = \frac{-\alpha(1-g_0)}{4\varepsilon_2 g_2} \cdot \qquad (639)$$

If the value of the right side is less than or equal to minus unity, the maximum occurs at the windward ray, $\phi_s = 180$ degrees. For the conditions of

297

Figure 115 ($K_\delta = 1.3$, $\gamma = 1.4$, $\alpha/\delta = 0.2$, $\epsilon_2/\delta = 0.1$), the maximum-entropy stream surface originates at the shock at $\phi_s = 133$ degrees. This is on the windward side of the dividing stream surface which is located in Figure 115 at $\phi_s = 127$ degrees. Thus the maximum-entropy stream surface does not wet the body surface but lies in the windward part of the shock layer. That the body surface and maximum-entropy surface are not necessarily identical is also true for hypersonic blunt-body flows (see Hayes and Probstein Reference 29, page 399). Melnik (Reference 25) on the other hand, in his analysis of conical flows assumed that the body was a maximum entropy surface. The conical results holds for all values of K_δ. The ratio of $\cos \phi_{sm}$ and $\cos \phi_{0c}$, given by Equation (633) is

$$\frac{\cos \phi_{sm}}{\cos \phi_{0c}} = \frac{1-g_0}{2g_2} \frac{w_1(\delta)}{w_1'(\delta)} \quad . \tag{640}$$

For $\gamma = 1.4$ this ratio is greater than unity for $K_\delta > 0$, and hence the conclusion is that $\phi_{sm} > \phi_{0c}$ for $K_\delta > 0$.

c. Lip Angle

Corresponding to Equations (599) and (627), the lip angle, λ^*, for the shock-stream surface intersection for an inclined elliptic cone is determined to be given by

$$\tan \lambda^* = \tan \lambda_0 + \tan \lambda_2$$
$$= \frac{\alpha}{\delta} \frac{\sigma^2 - g_0}{\sigma(\sigma^2-1)} \sin \phi_s + \frac{\epsilon_2}{\delta} \frac{2q}{\sigma(\sigma^2-1)} \sin 2\phi_s \quad . \tag{641}$$

When the angles are small, the lip angle for an inclined elliptic-cone stream surface is equal to the sum of the lip angles for the corresponding inclined circular-cone stream surface and the aligned elliptic-cone stream surface.

d. Waveriders with Freestream Upper Surfaces

As before, waverider configurations can be formed by utilizing freestream plane surfaces that pass through the vertex along an axis inclined at an angle

α with the cone axis, and intersect the shock at the lips of an underneath conical stream surface. The conditions shown in Figure 115 with the lip located $\phi_s = 90$ degrees were chosen as an example. The waverider formed is shown in Figure 117. The freestream surface intersecting the shock at ϕ_s has a unit normal vector given by

$$\hat{n}_\infty = \frac{[\sigma - (\frac{\alpha}{\delta})(1-g_0)\cos\phi_s - (\frac{\varepsilon}{\delta})g_2\cos 2\phi_s]\,\hat{e}_\phi - \frac{\alpha}{\delta}\sin\phi_s\,\hat{e}_\theta}{\sqrt{[\sigma - (\frac{\alpha}{\delta})(1-g_0)\cos\phi_s - (\frac{\varepsilon_2}{\delta})g_2\cos 2\phi_s]^2 + (\frac{\alpha}{\delta})^2\sin^2\phi_s}} \qquad (642)$$

The waverider lip angle, λ_w, is determined by the condition $\cos\lambda_w = \hat{n}_\infty \cdot \hat{n}$, where $\hat{n}$ is given by Equation (596). For small α/δ, the result is

$$\tan\lambda_w \approx \tan\lambda^* - \frac{\frac{\alpha}{\delta}\sin\phi_s}{\sigma - (\frac{\alpha}{\delta})(1-g_0)\cos\phi_s - (\frac{\varepsilon}{\delta})g\cos 2\phi_s} \qquad . \qquad (643)$$

The waverider lip angle in Figure 117 is found to be $\lambda_w = 8.9$ degrees. This waverider has a positive dihedral and is analogous to the circular cone waverider shown in Figure 100. The elliptic-cone waverider in Figure 117 is shallower and flatter on the bottom than its circular-cone counterpart in Figure 100. It also has a slightly greater span since the attached shock is broader for the ellipse. The pressure on the windward ray of the elliptic-cone waverider is less than that of its circular-cone counterpart, but the pressure at the lips is greater owing to the greater inclination of the shock. There are also elliptic cone waveriders with zero and negative dehidral, corresponding to the circular-cone waveriders shown in Figures 101 and 102, but these will not be discussed here.

e. Further Remarks

Elliptic waveriders with wedge-shock upper surfaces can also be constructed, such as was done for the circular cone configuration shown in Figure 103. Because there is an additional parameter, ε_2/δ, involved in

$K_s = 1.3$

$\epsilon/\delta = 0.2$

$\epsilon_2/\delta = 0.1$

$\gamma = 1.4$

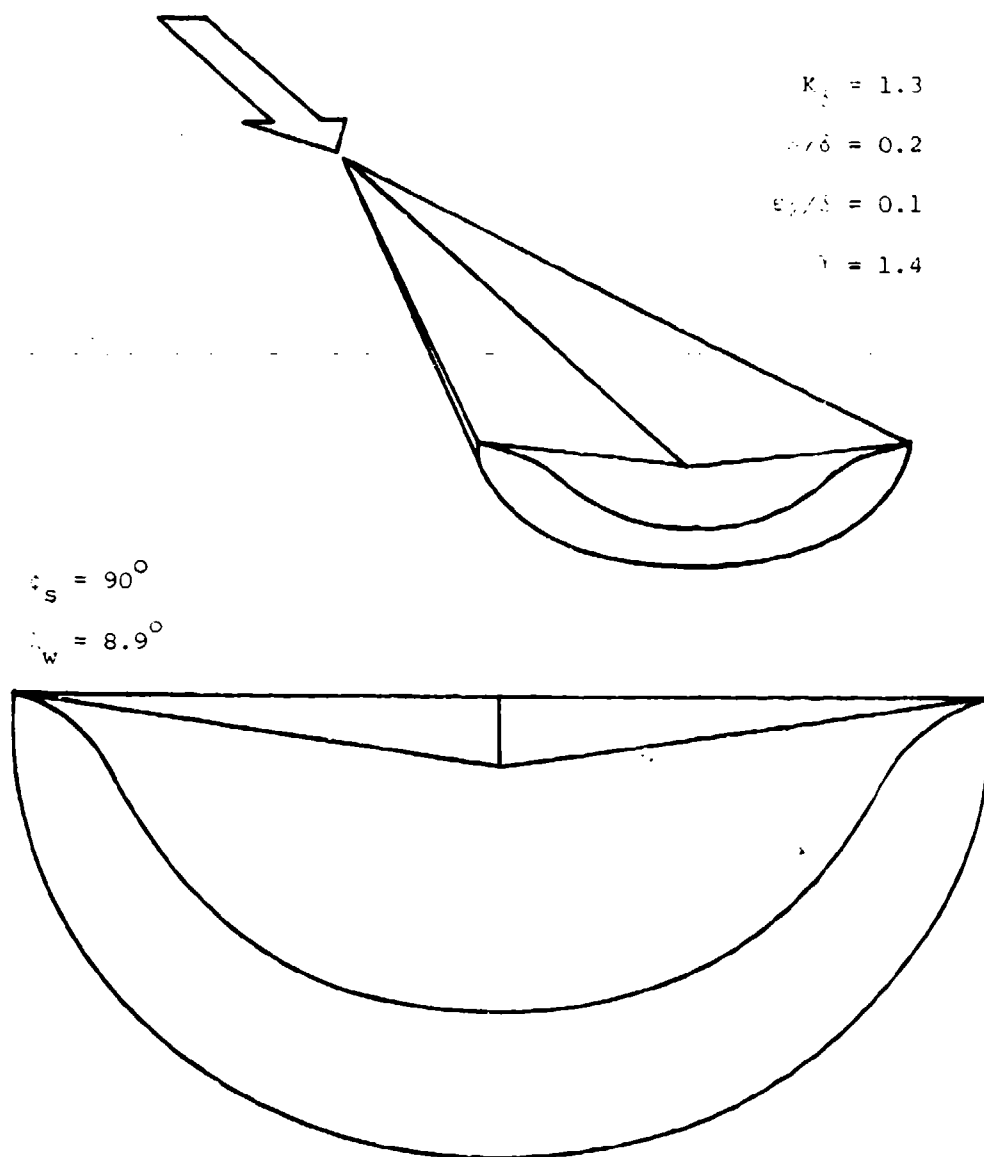$\theta_s = 90^\circ$

$\theta_w = 8.9^\circ$

Figure 117. Inclined Elliptic-Cone Waverider With Freestream
Upper Surface: Positive Dihedral

fitting the wedge-shock to the waverider, the analysis is very involved and will not be considered here.

Other characteristics of interest for the families of waveriders presented here are lift, drag, and stability. The pressure coefficient on the conical stream surface can be obtained from the equation

$$\frac{c_p}{\delta^2}(\theta,\delta) = \frac{c_{p0}(\theta)}{\delta} \cos \phi + \frac{\varepsilon_2}{\delta} \frac{c_{p2}(\theta)}{\delta} \cos 2\phi \ , \quad (644)$$

which is in hypersonic similarity form and can be regarded as known (Reference 52). The lift and drag characteristics can thus be determined without great difficulty. The pitching moment can also be determined, but general stability characteristics require a knowledge of off-design flow conditions. These considerations are fruitful subjects for further research.

8. SOME CONSIDERATIONS REGARDING CONTROL SURFACES

a. Control Flaps

For controlled flight, control surfaces are necessary for changing and maintaining pitching, yawing, and rolling motions as well as for aerodynamic trim. The waverider configurations that have been derived so far generally have horizontal or nearly horizontal surfaces where flaps can be placed to produce nearly vertical forces by their deflections. If enough dihedral is present, it may be possible that the flaps could produce the behavior of a vee tail and thus obviate the need of a vertical fin. In general, however, the design of controlled flight necessitates the consideration of vertical control surfaces. In this section is formulated the analysis of vertical fins that are themselves waverider configurations.

b. Vertical-Fin Control Surfaces

Consider a wedge-shock caret waverider, such as shown in Figures 89 and 90, but that is nonsymmetric, that is, the polar angles describing the freestream surfaces are unequal. A typical configuration that shall be

utilized as a vertical fin is shown in Figure 118. Let one freestream surface be denoted by $\tan \theta_{s\infty} = \theta_{s\infty}$ (for small angles) to represent the angle between a freestream cone axis and the corresponding cone shock. The other freestream surface which shall represent the left half of a vertical fin is denoted by the conical angle θ_f. The flow deflection angle is denoted by Δ and the shock angle is denoted by β_w. All these polar angles are regarded as small and are shown as projections on a fixed Z plane. The dihedral angle between the two freestream surfaces is denoted by ψ_∞.

From geometrical considerations, the law of cosines yields

$$\theta_{s\infty}^2 - 2\theta_{s\infty}\theta_f \cos \psi_\infty + \theta_f^2 = [(\theta s_\infty^2 - \beta_w^2)^{1/2} + (\theta_f^2 - \beta_w^2)^{1/2}]^2. \tag{645}$$

Expanding this equation and solving for θ_f yields

$$\frac{\theta_{s\infty}}{\theta_f} = \cos \psi_\infty \pm \sin \psi_\infty \left[\left(\frac{\theta_{s\infty}}{\beta_w}\right)^2 - 1\right]^{1/2} . \tag{646}$$

Since $\theta_{s\infty}/\theta_f$ is always positive the plus sign must be chosen when $\psi_\infty > 90$ degrees since $\cos \psi_\infty$ is then negative. For a continuous variation, a change in sign occurs when the radical vanishes. This does not occur since $\theta_{s\infty}/\beta_w > 1$. Hence the plus sign is to be selected in Equation (646).

Equation (646) follows from the geometry of the configuration. The shock conditions of gas dynamics, however, require that β_w be determined by the flow deflection Δ and the freestream Mach number as given by Equation (576). Thus Equation (646) can be rewritten as

$$\frac{\theta_{s\infty}}{\theta_f} = \cos \psi_\infty + \sin \psi_\infty \left[\left(\frac{\theta_{s\infty}}{\delta}\right)^2 \left(\frac{\delta}{\beta_w}\right)^2 - 1\right]^{1/2} , \tag{647}$$

and δ/β_w can be determined from

$$\frac{\delta}{\beta_w} = \kappa_\delta \left[- \frac{\gamma+1}{4} \kappa_\delta \left(\frac{\Delta}{\delta}\right) + \sqrt{\frac{(\gamma+1)^2 \kappa_\delta^2 (\frac{\Delta}{\delta})^2 + 1}{4}} \right] . \tag{648}$$

Thus (θ_f/δ) is a function of $\theta_{s\infty}/\delta$, κ_δ, γ, $\cos \psi$, and Δ/δ, where δ is taken as the characteristic angle of the cone flow. When $\Delta = 0$, β_w takes the Mach angle as its minimum value, and θ_f takes a minimum value given by

302

Figure 112. Geometry for the Vertical Fin

$$\frac{\theta_{g\infty}}{\theta_{fmin}} = \cos\psi_\infty + \sin\psi_\infty \left[\left(\frac{\theta_{g\infty}}{\delta}\right)^2 \kappa_\delta^2 - 1\right]^{1/2} \qquad . \qquad (649)$$

c. Vertical Fin for the Elliptic-Cone Waverider

The elliptic-cone waveriders considered are those shown in Figure 114 with the conditions $\kappa_\delta = 1.3$, $\gamma = 1.4$, and $\varepsilon_2/\delta = 0.1$. In this case the freestream upper surfaces of the cone waverider are matched with the freestream surface of the half-fin analyzed in Section 7b. Thus $\psi_\infty = \phi_s$ is set and

$$\theta_{g\infty} = \theta_s^* \equiv \beta - \varepsilon_2 q_2 \cos 2\phi_s \qquad . \qquad (650)$$

For the lip at $\phi_s = 100$ degrees, the outcomes for various values of Δ/δ are

Δ/δ	θ_f/δ
0	1.06
0.1	1.21
0.2	1.40

Since the freestream surfaces are matched, the vertical fin can start at the cone vertex, or at some other position. The configuration for which the fin starts at the vertex is shown in Figure 119 for $\Delta/\delta = 0.2$. In this case the fin shock is attached to the conical lip. The case where the fin begins half-way back on the elliptic-cone undersurface is shown in Figure 120 for $\Delta/\delta = 0.2$. In a real flow, owing to viscous boundary-layer shock interaction, the flow would not be as well behaved as illustrated here.

d. Vertical Fin for the Inclined-Cone Waveriders

When the basic conical waverider surfaces are derived from cones at angle-of-attack, the freestream surfaces are inclined at an angle α with the geometric cone axis. The formulas in paragraph 7b must be adapted to these situations by the appropriate evaluation of ψ_∞ and $\theta_{g\infty}$. The unit normal vector to the freestream surface passing through lip shock and the freestream cone axis is given by $\hat{n}_\infty$, defined by Equation (642). If $\hat{e}_y$ denotes the unit
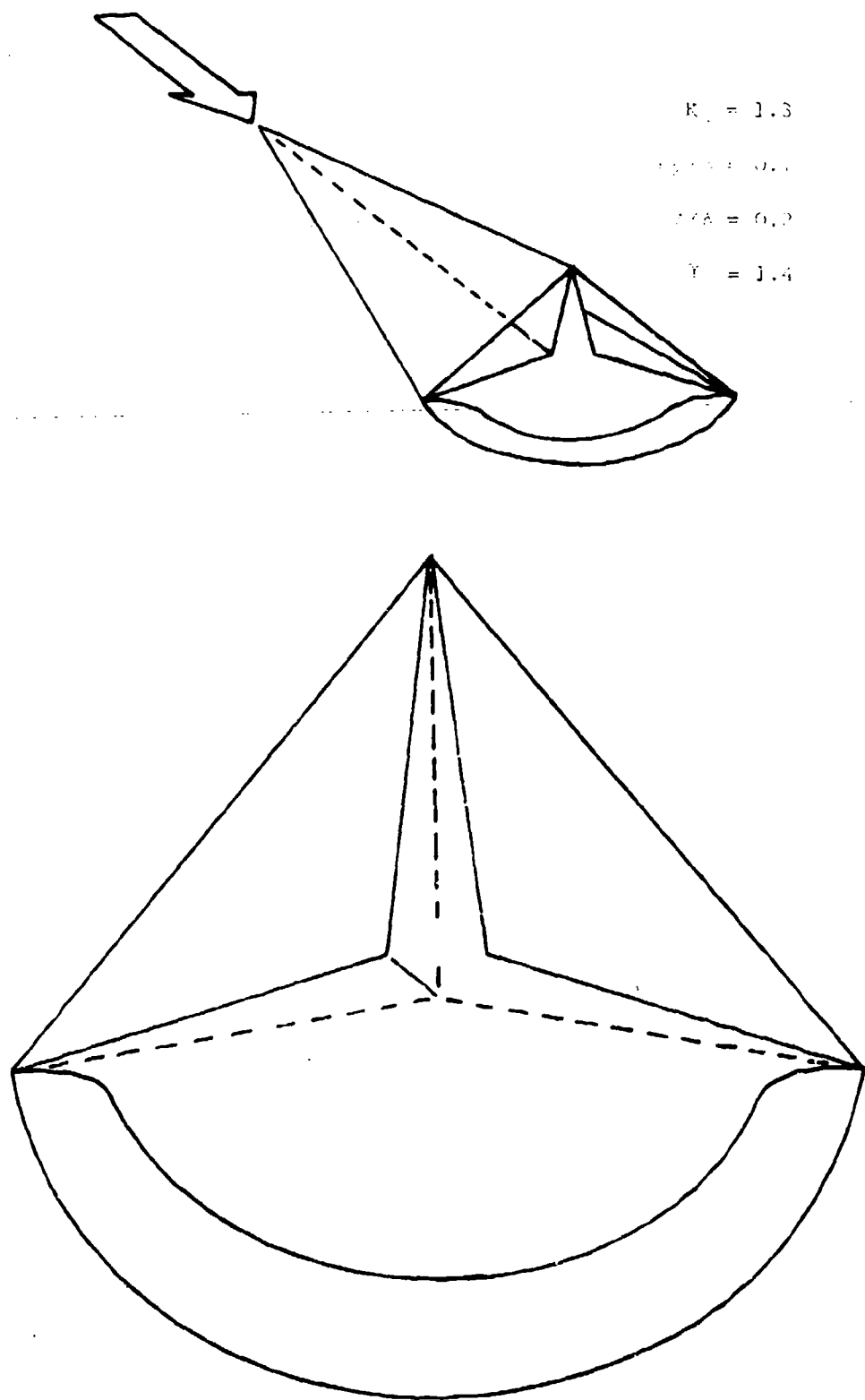
304

$R_1 = 1.3$

$\cdots = 0.5$

$2/A = 0.9$

$Y = 1.4$

Figure 129. Elliptic-Cone Waverider with Fin Starting at Vertex

$$K_1 = 1.3$$

$$c2/c = 0.1$$
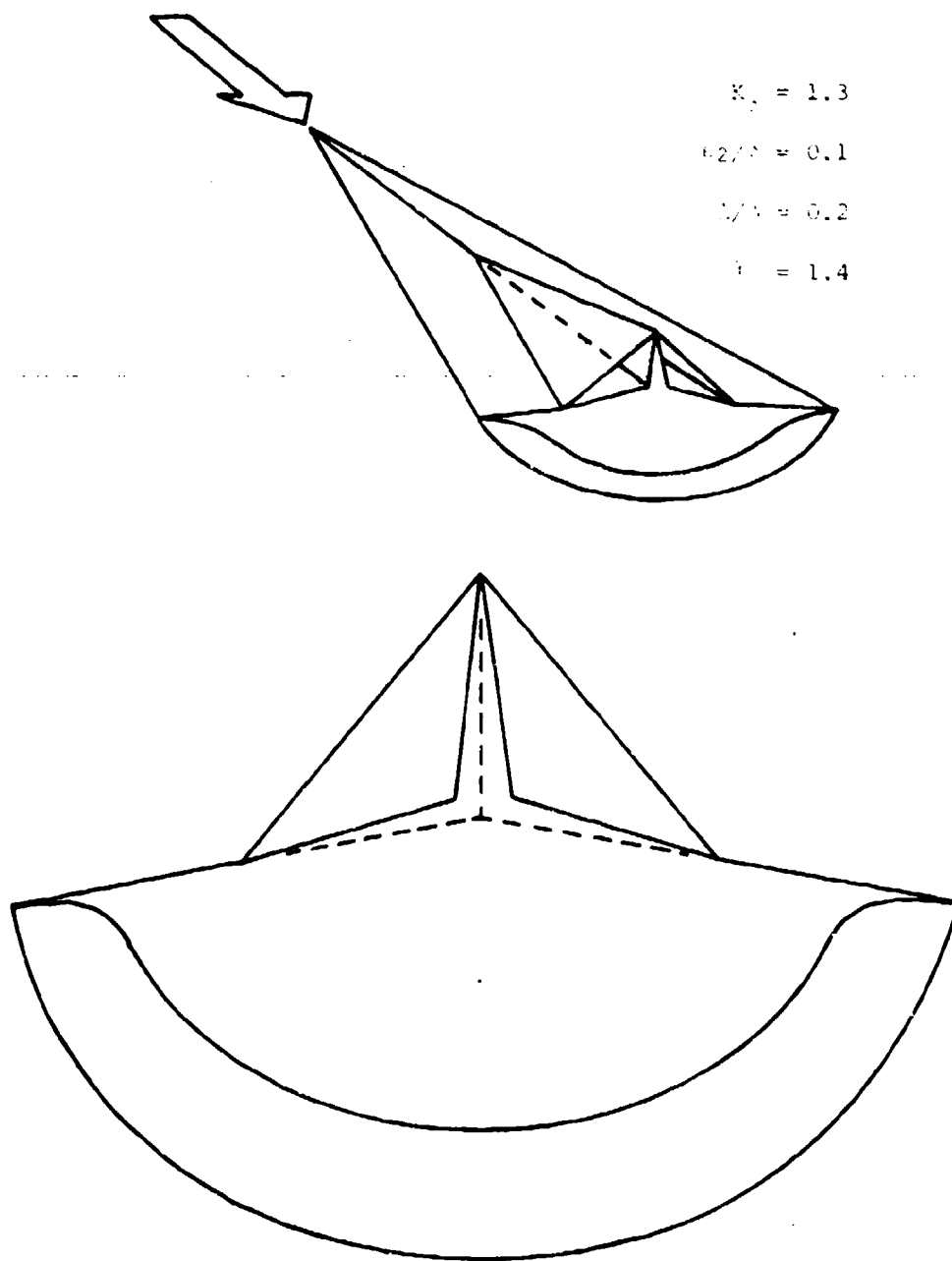
$$b/c = 0.2$$

$$\lambda = 1.4$$

Figure 120. Elliptic-cone bareorder with fin station at half length.

normal vector to the vertical plane, then ψ_∞ from the condition $\cos \hat\psi_\infty = -\hat{n}_\infty$.
$\hat{e}_y$ is obtained

$$\cos \psi_\infty = \frac{[\sigma - (\frac{\alpha}{\delta})(1-g_0) \cos \phi_s - (\frac{\varepsilon_2}{\delta}) g_2 \cos 2\phi_s] \cos \phi_s + \frac{\alpha}{\delta} \sin^2 \phi_s}{\sqrt{[\sigma - (\frac{\alpha}{\delta})(1-g_0) \cos \phi_s - (\frac{\varepsilon_2}{\delta}) g_2 \cos 2\phi_s]^2 + (\frac{\alpha}{\delta})^2 \sin^2 \phi_s}}$$

(651)

When $\alpha = 0$, this reduces to the result $\psi_\infty = \pi - \phi_s$. There is no discrepancy
in this result compared to Section III if it is realized that the windward ray
was taken as $\phi = 0$ for the inclined-cone waveriders, whereas the noninclined
elliptic-cone waverider utilized $\phi_s > \pi/2$ for the conical surface.

From geometrical considerations also comes

$$\theta_{s\infty} = [\theta_s^{*2} + \alpha^2 - 2\theta_s^* \alpha \cos \phi_s]^{1/2} \quad , \tag{652}$$

where

$$\theta_s^* = \beta + \alpha g \cos \phi_s - 2\varepsilon q \cos 2\phi_s \quad . \tag{653}$$

No further calculations are considered here.

9. CONCLUDING REMARKS

By means of stream surfaces obtained from angle-of-attack and
cross-section eccentricity perturbations of the basic supersonic axisymmetric
flow past a circular cone, aerodynamic lifting-body configurations have been
derived. The emphasis has been on a systematic parametric study of the
various configurations that can be obtained. The configurations have attached
shocks on sharp leading edges and thus can be described as conical waveriders.
Utilization of wedge-shock caret-waverider results leads to a combination of
configurations and to vertical-fin control surfaces. Generalization of the
perturbed flow past a circular cone to allow for generalized noncircular cross
sections (Reference 58) can lead to further aerodynamic combinations.

The analysis has proceeded within the framework of hypersonic small-disturbance theory, and approximate analytic formulas have been derived that apply over a wide range of conditions. Although pressure distributions have not been calculated, the pertinent formulas have been presented. Further calculations by interested investigators can be performed readily.

The lifting-body configurations that have been presented appear attractive in terms of high lift-drag ratio requirements. Further work is required to account for other aerodynamic factors. Some of these are

 (1) lift, drag, and moment characteristics,

 (2) boundary-layer growth and related viscous effects,

 (3) off-design effects,

 (4) details of flaps and other control surfaces.

SECTION IV

EXPERIMENTAL STUDIES

1. INTRODUCTION

In this section extensive experimental results are presented for the forces, moments, and surface pressure distributions on two fundamental cone-derived waveriders. These two waverider configurations were selected from examples illustrated and discussed in Section III. To provide a basis for comparison, experiments were also conducted on two other basic configurations: an elliptic cone with a major-minor axis ratio of 1.87, and this same elliptic cone with thin delta winglets attached on the major-axis plane. Six component force and moment data and surface pressure data were obtained for a variation of ± 20 degrees in angle of attack and sideslip over a Mach number range of 3 to 5. Schlieren and surface oil-flow visual data were also obtained.

2. DESCRIPTION OF MODELS

Figure 121 illustrates the model configurations that were tested. All the models were constructed of stainless steel and had the same length, $L = 60$ cm $\simeq 23.62$ inches, measured along the basic cone-axis from which they were derived. The other dimensions are indicated in Figure 121 and given in inches in Table 1, along with the base area, A_b, in square inches.

TABLE 1. MODEL DIMENSIONS (INCHES)

	L	W	T	R	A_b in.^{2}
Circular Cone Waverider	23.62	21.98	7.96	4.46	103.60
Elliptic Cone Waverider	23.62	21.50	7.11	4.62	75.83
Elliptic Cone	23.62	22.68	12.16	6.08	216.60
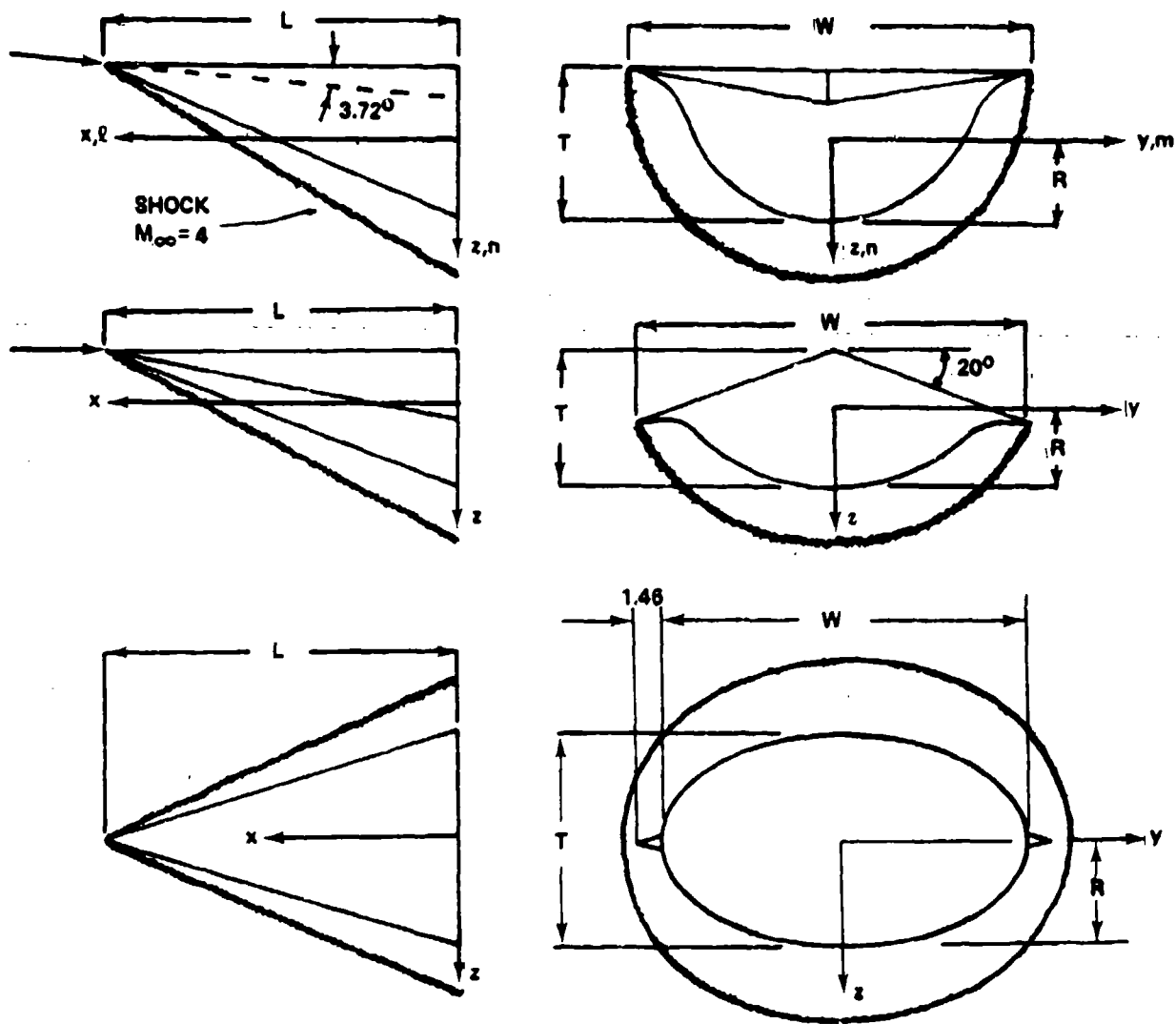
Figure 121. Model Configurations (a) Circular-cone Waverider (b) Elliptic-cone Waverider (c) Elliptic cone with wiglets

The position of the body-fixed (or string) coordinate system, to which the six force and moment components are referred, is also shown (note that this coordinate system differs from that used in the previous analysis; here the freestream direction is given by the x-axis). The jagged curves in Figure 121 indicate the theoretical position of the shock wave at the design condition, $M_\infty = 4$.

The model shown in Figure 121a was derived from the flow past a circular cone at angle of attack, as explained in Section III. It is referred to as the circular-cone waverider. The flow in the shock layer is the same as the flow on the leeward side of an inclined circular cone. The shape of the curved surface, which is a stream surface in the inclined-cone flow, has been approximated by the method of analysis in Section III and is given in spherical coordinates by

$$\frac{\theta}{\delta} = 1 + 0.34 \left[\tan\left(\frac{\pi}{2} - \frac{\phi}{2}\right)\right]12.5 \qquad , \tag{654}$$

where θ is the polar angle measured from the basic-cone axis (parallel to the x axis but passing through the vertex), and ϕ is the azimuthal angle measured around the basic-cone axis such that $\phi = \pi$ in the z direction. The semi-vertex angle for the basic cone is denoted by δ, which for this model is $\delta = 19.62$ degrees. The angle of attack defining this waverider configuration was selected as $\alpha/\delta = 0.2$, or $\alpha = 3.72$ degrees, which determined the angle between the basic-cone axis and the symmetry ray of the upper surface.

The model shown in Figure 121b was derived from the flow past an elliptic cone at zero angle of attack and is referred to as the elliptic-cone waverider. The shape of the curved surface, which is a stream surface for the elliptic-cone flow, is given approximately by

$$\frac{\theta}{\delta} = 1 - 0.1 \cos 2\phi + (0.39 + 0.1 \cos 2\phi) \frac{\left[\tan(\pi-\phi)\right]7.69}{2.75} \qquad . \tag{655}$$

311

The basic-cone angle for this model was also selected as $\delta = 18.62$ degrees. The eccentricity as defined by the Fourier series representation of Section II was selected such that $\epsilon_2/\delta = 0.1$.

The design Mach number for these waverider models is $M_\infty = 4$. Thus the pertinent hypersonic similarity parameter is $K_\delta = M_\infty \delta = 1.3$. According to Section III the circular-cone waverider, model a, is said to have a positive dihedral, and the elliptic-cone waverider, model b, is said to have a negative dihedral. A photograph of the underside of the elliptic-cone waverider is shown in Figure 122.

For the design condition, the theoretical shock shape for model a is

$$\frac{\theta_a}{\delta} = 1.34 - 0.04 \cos \phi \qquad , \tag{656}$$

and for model b the shock shape is

$$\frac{\theta_s}{\delta} = 1.34 - 0.06 \cos 2\phi \qquad . \tag{657}$$

These shocks are attached to the waverider lips at $\phi = 90$ degrees for model a and at $\phi = 110$ degrees for model b.

Figure 121c shows the elliptic cone model with winglets attached on the plane of the major axis. The equation for the elliptic cone in spherical coordinates is

$$\tan \theta = \frac{\tan \theta_m}{\sqrt{1 + e \cos 2\phi}} \tag{658}$$

with $\theta_m = 17.79$ degrees and $e = 0.5534$. These values correspond to a major-minor axis ratio of 1.97. According to the perturbation analysis of Section II the corresponding basic-cone angle is 18.63 degrees , which is nearly the same as for the two waverider models. The pertinent hypersonic similarity parameter is thus also about $K_\delta = 1.3$ for $M_\infty = 4$. The perturbation analysis of Section II yields eccentricity factor of $\epsilon_2/\delta = 0.478$. This elliptic cone is thus much more eccentric than the elliptic cone from which

312

(a) sideview

(b) bottom view

Figure 1.7. Elliptic-cone Waverider

313

waverider b was derived. The delta winglets that could be attached on the major-axis plane were wedge-shaped with a five degree included angle at the sharp leading edge, and they were 1.46 inches wide at the base. The winglets were designed to extend out to the shock position that would exist at $M_\infty = 4$ without the winglets. Tests were run with and without winglets attached.

3. EXPERIMENTAL CONDITIONS

The tests were run in wind tunnel A of the von Karman Facility at the USAF Arnold Engineering Development Center. Tunnel A is a continuous, closed-circuit, variable-density wind tunnel with an automatically driven flexible-plate-type nozzle and a 40-inch by 40-inch test section. The tunnel is equipped with a model injection system which allows removal of the model from the test section while the tunnel remains in operation. A complete description of the tunnel and airflow calibration information may be found in Reference 72.

The experiments were conducted at Mach numbers 3.0, 3.5, 4.0, 4.5, and 5.0. On-design conditions for the waveriders were at $M_\infty = 4.0$ and $\alpha = -3.72$ degrees for the circular-cone waverider and $\alpha = 0$ for the elliptic-cone waverider, both with zero sideslip. All other conditions were off-design conditions. Six components of force and moment data were recorded for angles of attack and sideslip in the range of ±20 degrees. Visual Schlieren data were recorded during these tests from which shock-wave positions could be measured and flow patterns observed. Oil-flow tests were conducted separately.

The nominal unit Reynolds number for the tests was 2 million per foot. Tests were also conducted at a unit Reynolds number of 1 million per foot on the circular cone waverider Mach numbers of 3.0, 3.5, 4.0, and 4.5. Because there was no noticeable effect of unit Reynolds number in this range, all the

314

remaining tests were conducted at the nominal unit Reynolds number of 2 million per foot. A complete summary of the test conditions is given in Reference 73.

4. FORCES AND MOMENTS

The data for the forces and moments are presented in three comparative groups. First, the six components of force and moment coefficients are presented in body-fixed coordinates for $M_\infty = 4$, comparing the four aerodynamic configurations. The second group compares the corresponding lift and drag coefficients of the four configurations at $M_\infty = 4$. The third group is concerned with the effects of variation in freestream Mach number. The forces and moment are all for the forebody contribution only.

The discussion of these results is facilitated by the use of simple approximate formulas for the normal force and axial force coefficients of the cone-derived waveriders at the design conditions, referred to the axis of the basic cone. These formulas, which are derived in Appendix A, are

$$C_N \simeq \left(\frac{C_p}{\delta^2}\right) \frac{2\delta}{\pi} \frac{\sigma \cos \Lambda}{1 + \frac{2\Lambda}{\pi}} \quad , \tag{659}$$

$$C_A \simeq \left(\frac{C_p}{\delta^2}\right) \delta^2 \quad . \tag{660}$$

These coefficients are normalized with the base area of the waveriders and were obtained under the assumption of small deviations from an axisymmetric basic-cone flow, consistent with the analysis of Section III. The semivertex angle of the basic cone is δ, and C_p is an average pressure coefficient which can be taken as the pressure coefficient on the basic cone, $C_p \simeq c_{p0}$. According to hypersonic small disturbance theory, the ratio C_p/δ^2 is a function of the similarity parameter K_δ. The ratio of the basic shock angle to the basic-cone angle, $\sigma \equiv \beta/\delta$, is also a function of K_δ as given in

Appendix A. The angle Λ is a basic dihedral angle, the angle measured from the horizontal plane through the basic-cone axis to the plane passing through the basic-cone axis and the waverider lip intersection with the shock. For the present circular-cone waverider, $\Lambda = 0$, whereas for the elliptic-cone waverider, $\Lambda = -20$ degrees. For the present on-design conditions, $K_\delta = 1.3$, $\sigma = 1.34$, $c_{p0}/\delta^2 = 2.32$, and $\delta = 18.6$ degrees. The approximate formulas (659) and (660) suggest how the present results can be extended to other conditions and configurations.

Figures 123 and 124 show the normal-force and axial-force coefficients for the different models at $M_\infty = 4$ as a function of angle of attack and at unit Reynolds number of 2 million per foot and zero sideslip angle. The on-design conditions for the circular-cone waverider is $\alpha = -3.72$ degrees, and for the elliptic-cone waverider the on-design condition is $\alpha = 0$. At these conditions the shocks are attached as indicated in Figure 121a and b. Increasing the angle of attack amounts to a positive rotation of the bodies about the y axes. The force and moment coefficients were normalized with the individual base areas of the models, and this should be kept in mind when comparing the actual forces on the models. The elliptic-cone waverider produces the largest normal-force coefficient at $\alpha = 20$ degrees and also the largest negative value at $\alpha = -20$ degrees. The C_N versus α curve is nearly linear over this angle of attack range and also has the largest slope, $C_{N\alpha}$. The normal-force coefficient for the circular-cone waverider is nearly bilinear, that is, the slope $C_{N\alpha}$ has one value for positive α and another value for negative α. Even when the larger reference base area of the circular-cone waverider is taken into account, the elliptic-cone waverider produces a larger normal force than the circular-cone waverider for on-design

316
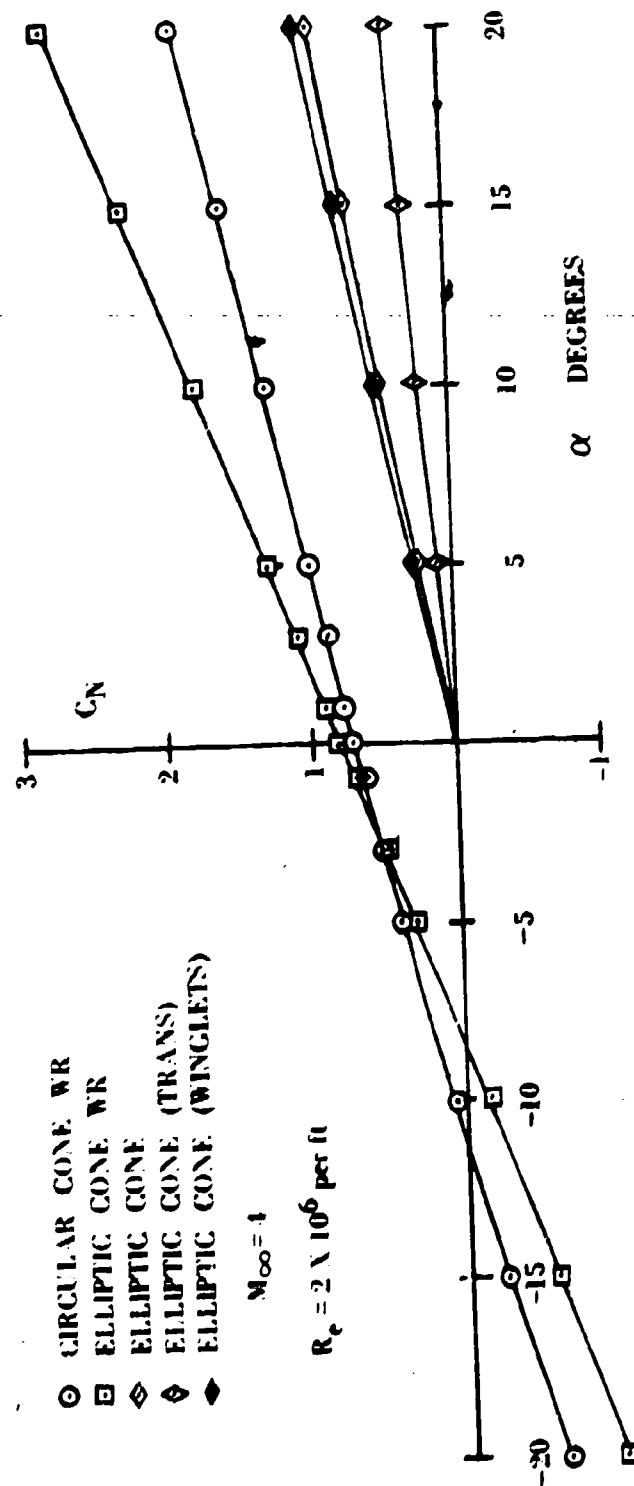
Figure 123. Normal-force Coefficient Versus Angle of Attack at $M_\infty = 4$

CIRCULAR CONE WR
ELLIPTIC CONE WR
ELLIPTIC CONE
ELLIPTIC CONE (TRANS)
ELLIPTIC CONE (WINGLETS)

$M_\infty = 4$

$R_e = 2 \times 10^6$ per ft
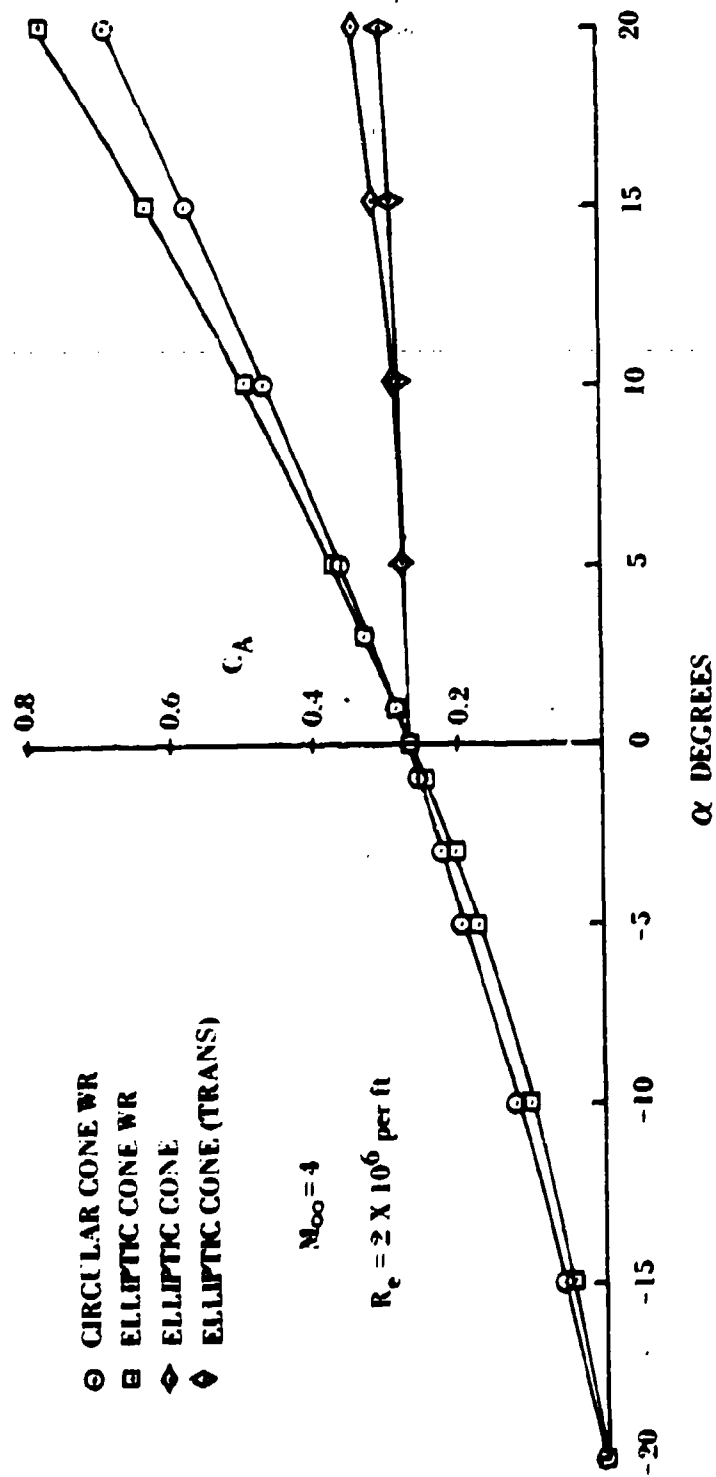
Figure 34. Axial-Force Coefficient Versus Angle of Attack at $M_\infty = 4$

conditions and positive angles of attack. Equation (659) gives a slightly low value for C_N for the on-design elliptic-cone waverider ($\alpha = 0$) and a slightly high value for the on-design circular-cone waverider (= -3.72 degrees).

As a basis for comparison, Figure 123 also shows the normal-force coefficients for the elliptic cone. When the cross flow is perpendicular to the minor axis of the elliptic cone, the orientation is referred to as the transverse condition (trans). Without this restriction the cross flow is understood to be perpendicular to the major axis. The slope of the normal-force curve for non-transverse condition is approximately 2.25 times greater than the transverse condition. The winglets attached to the elliptic cone produce about a 14 percent increase in the slope of the normal-force curve over the elliptic cone without winglets. The effects of the winglets are found to be small compared to the differences between the other configurations.

At $\alpha = 20$ degrees the value of C_N for the elliptic cone is only 10 percent larger than for the on-design ($\alpha = 0$) condition for the elliptic-cone waverider. The actual normal force for the elliptic cone, however, is significantly larger since its base area is 2.86 times greater than that of the elliptic cone waverider. At $\alpha = 20$ degrees the C_N for the elliptic-cone waverider is 3.15 times greater than for the elliptic cone, and 1.49 times greater than for the circular-cone waverider. The elliptic-cone waverider produces the largest actual normal force. The angle of zero normal force occurs at $\alpha = -8.4$ degrees for the elliptic-cone waverider and at $\alpha = -11.2$ degrees for the circular-cone waverider.

The axial-force coefficients are shown in Figure 124. The base drag has been subtracted from the force contribution on the models. The elliptic-cone waverider has the largest values of C_A for positive angles of attack. At $\alpha =$

0, all the configurations have about the same value of $C_A = 0.266$, which is consistent with Equation (660) since K_δ and δ are nearly the same for all. The theoretical value of C_A from Equation (660) is 8 percent lower than the experimental value. The axial force on the waveriders vanishes when $\alpha = -20$ degrees. The effect of the winglets on C_A for the elliptic cone is very small and thus is not shown.

Figure 125 shows the side-force coefficients for $M_\infty = 4$ as a function of side-slip angle, β, for $\alpha = 0$. (A negative side-slip angle corresponds to a positive rotation about the z-axis.) Because the models are all symmetric about the x-z plane, only values for negative β are shown. The data for the circular-cone waverider illustrate the negligible change when unit Reynolds number is varied between 1 and 2 million per foot. The side-force coefficients are nearly linear with β. The side-force coefficients for the circular-cone waverider are the largest, and the smallest for the elliptic-cone waverider, with transverse flow past the elliptic cone in between. The actual side force for the transverse elliptic cone is really the largest of the three shown since it has a reference base area 2.09 times greater than that of the circular-cone waverider.

Figures 126, 127, and 128 show the moment coefficients C_ℓ, C_m, and C_n for the moments about the x, y, and z axes for $M_\infty = 4$. Figure 126 shows the rolling moment coefficient C_ℓ as a function of side-slip angle (with $\alpha = 0$). The circular-cone waverider illustrates negligible change with unit Reynolds numbers in the range 1 to 2 million per foot. The rolling moments are nearly linear with β, with C_ℓ for the circular-cone waverider being about 3.1 times greater than that for the elliptic-cone waverider. The rolling moments for cross flows perpendicular to the major or minor axes of the elliptic cone are zero owing to symmetry.
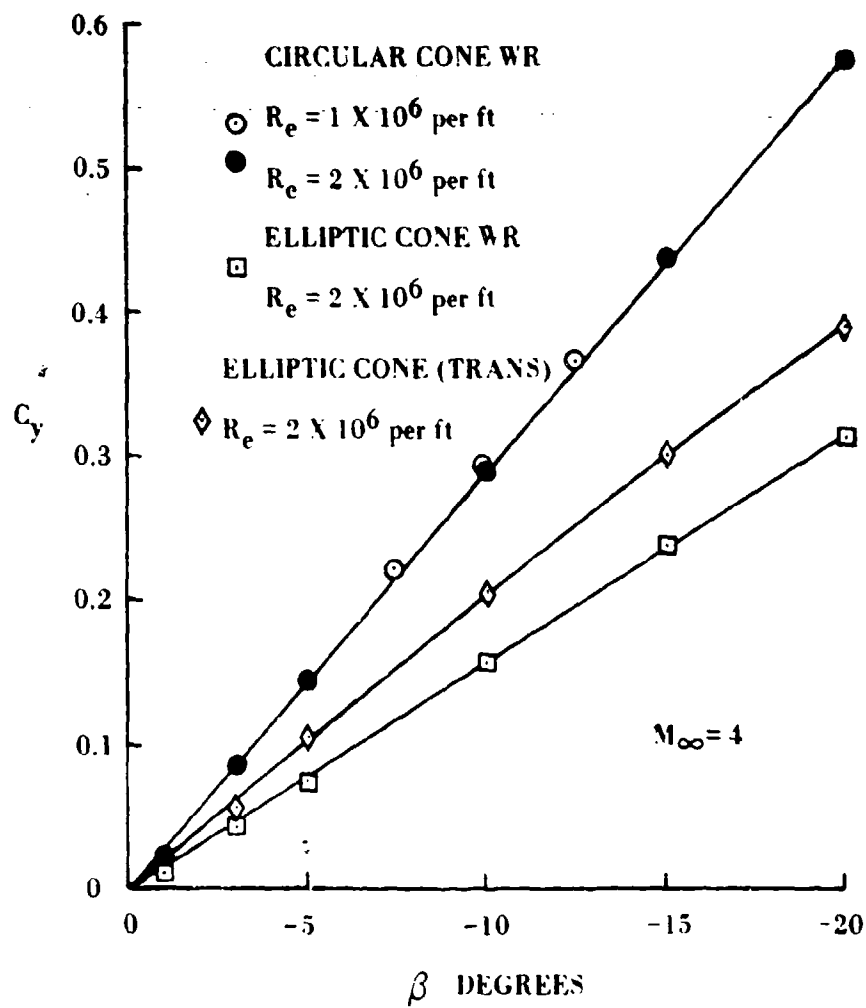
Figure 125. Side-Force Coefficient Versus Sideslip Angle at $M_\infty = 4$
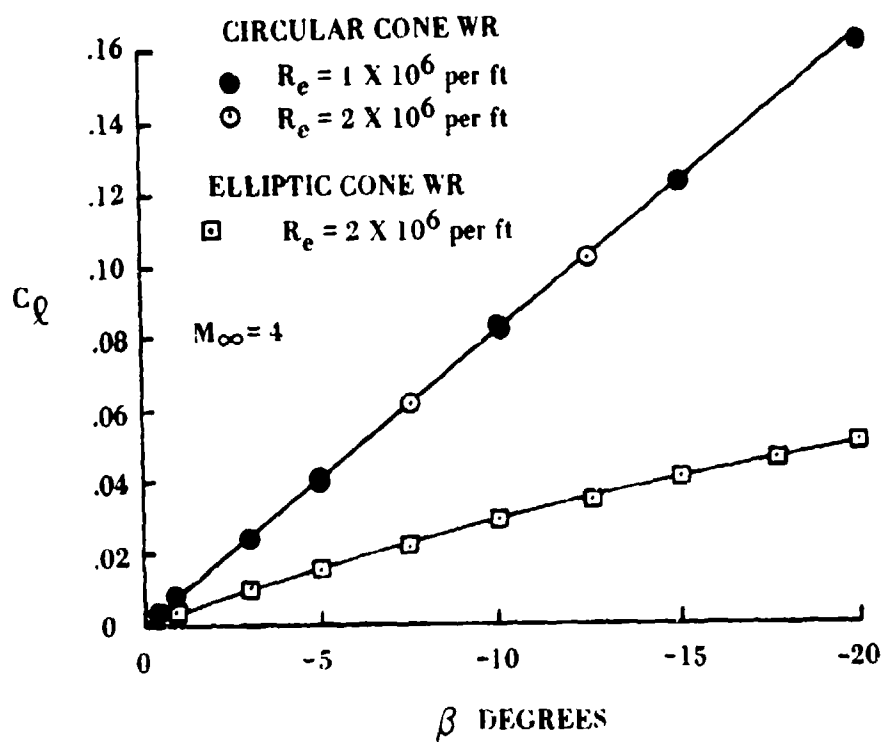
Figure 126. Rolling-Moment Coefficient Versus Sideslip Angle at $M_\infty = 4$
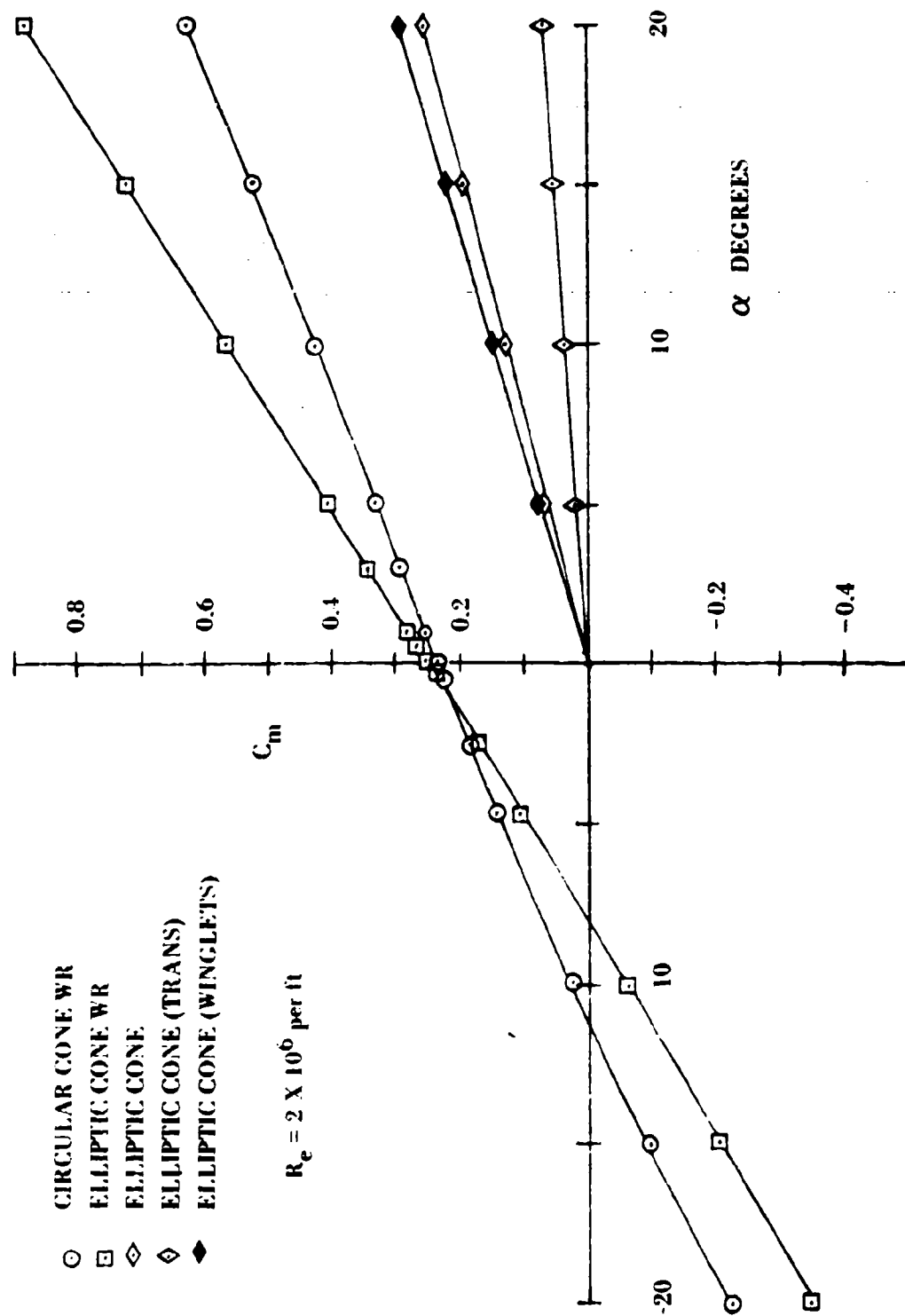
Figure 127. Pitching-Moment Coefficient Versus Angle of Attack at $M_\alpha = 4$

323
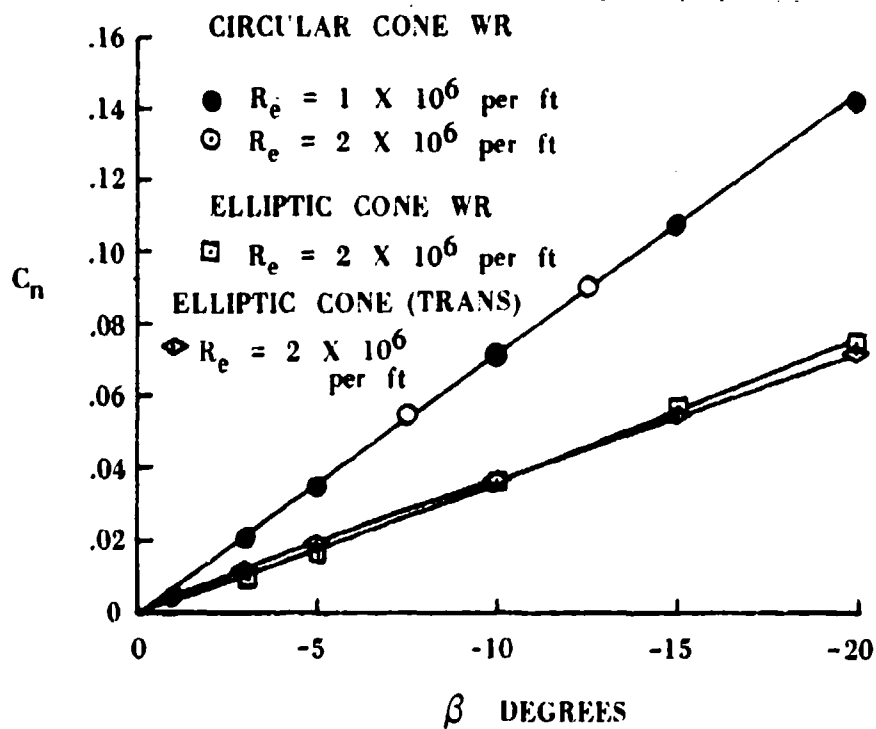
Figure 128. Yawing-Moment Coefficient Versus Sideslip Angle at $M_\infty = 4$

Figure 127 shows the pitching-moment coefficients as a function of angle of attack (with $\beta = 0$), reckoned about the y axes located on the bases of the models. The pitching-moment curves are similar in appearance to the normal-force curves in Figure 123. The ratios C_m/C_N yield the center of pressure for pitching rotations, measured in percent of L from the base. Since the curves are nearly linear, the elliptic-cone waverider has an average center-of-pressure over the range $\alpha = \pm 20$ degrees of about $C_m/C_N = 0.32$, and the circular-cone waverider has an average value of $C_m/C_N = 0.33$ for the elliptic cone, the corresponding values are $C_m/C_N = 0.29$ and $C_m/C_N = 0.18$ for the transverse orientation. The center-of-pressure for pitching is thus more towards the vertex for the waveriders than for the elliptic cones. The center-of-pressure for the basic cone is $C_m/C_N = 1 - (2/3) \sec^2\delta = 0.26$.

The yawing-moment coefficients, corresponding to moments about the z axis, are shown in Figure 128 as a function of side-slip angle (with $\alpha = 0$). The curves for the waveriders are nearly linear. The center-of-pressure position for yawing motion is given by the ratio C_n/C_y, measured in percent of L from the base. For the elliptic-cone waverider, the center-of-pressure is $C_n/C_y = 0.24$, and for the circular-cone waverider the value is $C_n/C_y = 0.25$. The curve for the transverse elliptic-cone is not so linear as for the elliptic-cone waverider, starting off above the elliptic-cone waverider for · nall β and ending slightly below it for large β; the average value of C_n/C_y is about 0.18.

Figures 129, 130, and 131 show the lift coefficients, the drag coefficients, and the L/D ratios as functions of angle of attack. The curves for C_L in Figure 129 are similar to the corresponding curves for C_N, but are noticeably nonlinear as should be expected from the geometrically related definitions. The elliptic-cone waverider shows the greatest lifting ability
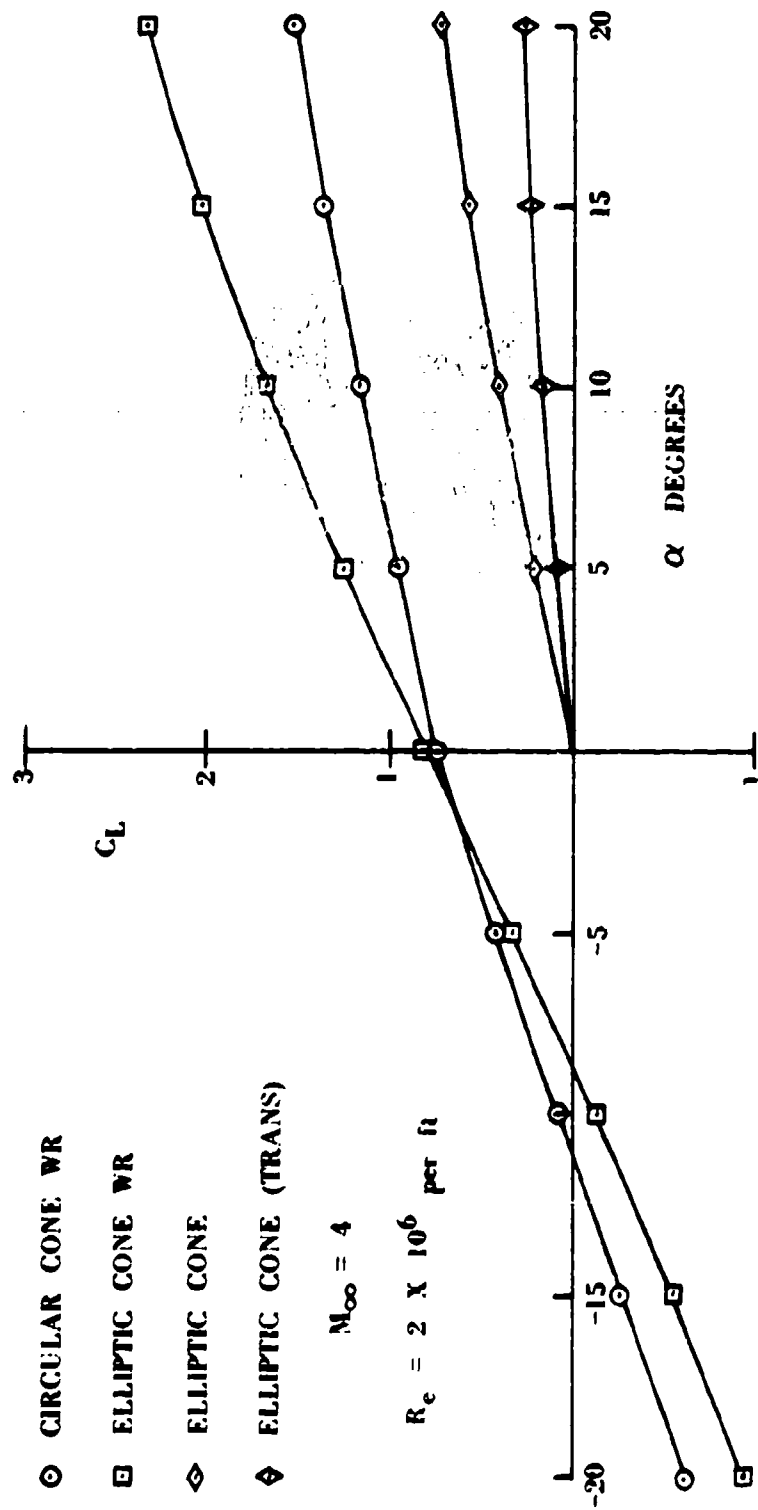
Figure 129. Lift Coefficient Versus Angle of Attack at $M_\infty = 4$
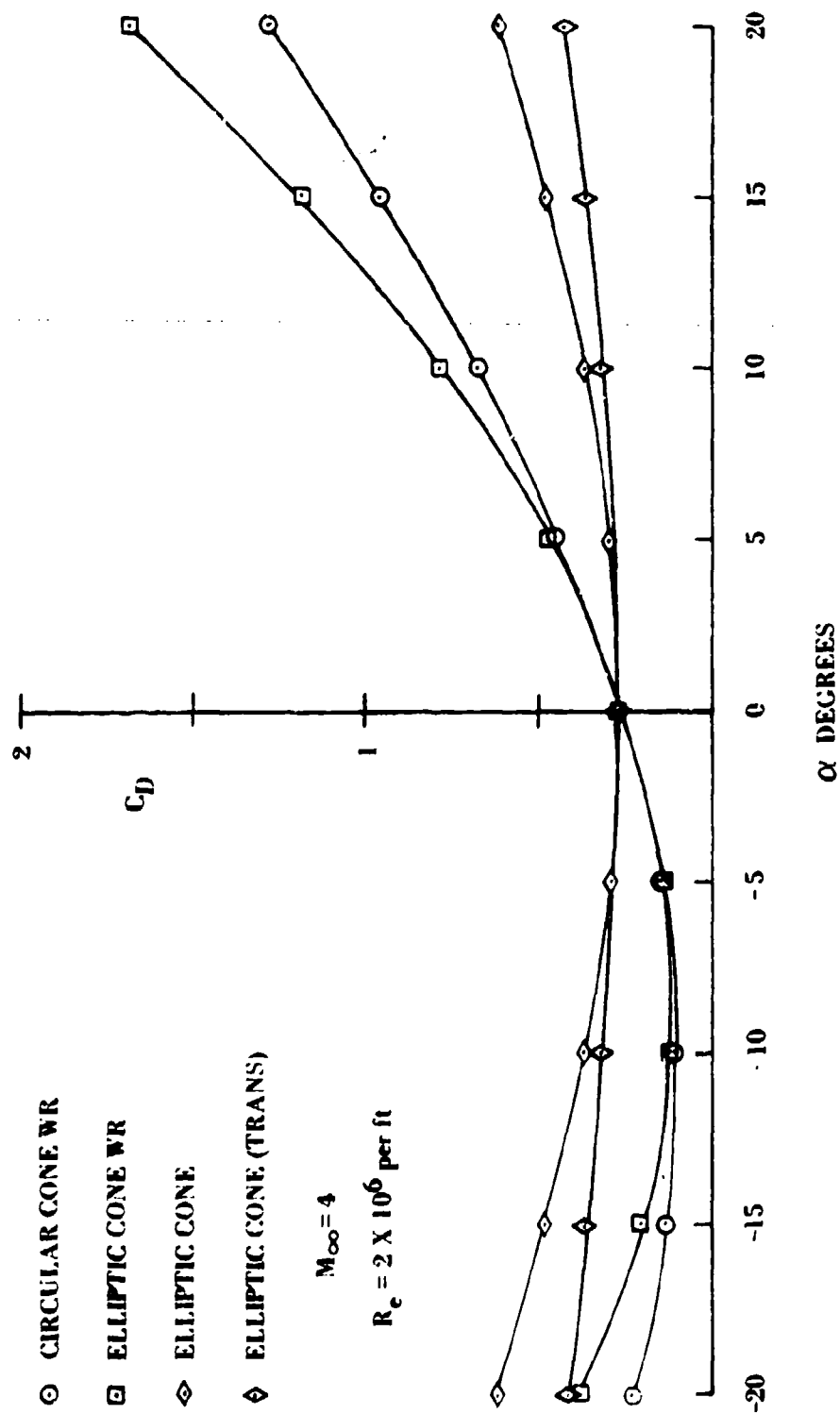
Figure 130. Drag Coefficient Versus Angle of Attack at $M_\infty = 4$

The plot shows C_D versus α DEGREES with the following legend:

⊙ CIRCULAR CONE WR
⊡ ELLIPTIC CONE WR
◇ ELLIPTIC CONE
◈ ELLIPTIC CONE (TRANS)

$M_\infty = 4$

$R_e = 2 \times 10^6$ per ft
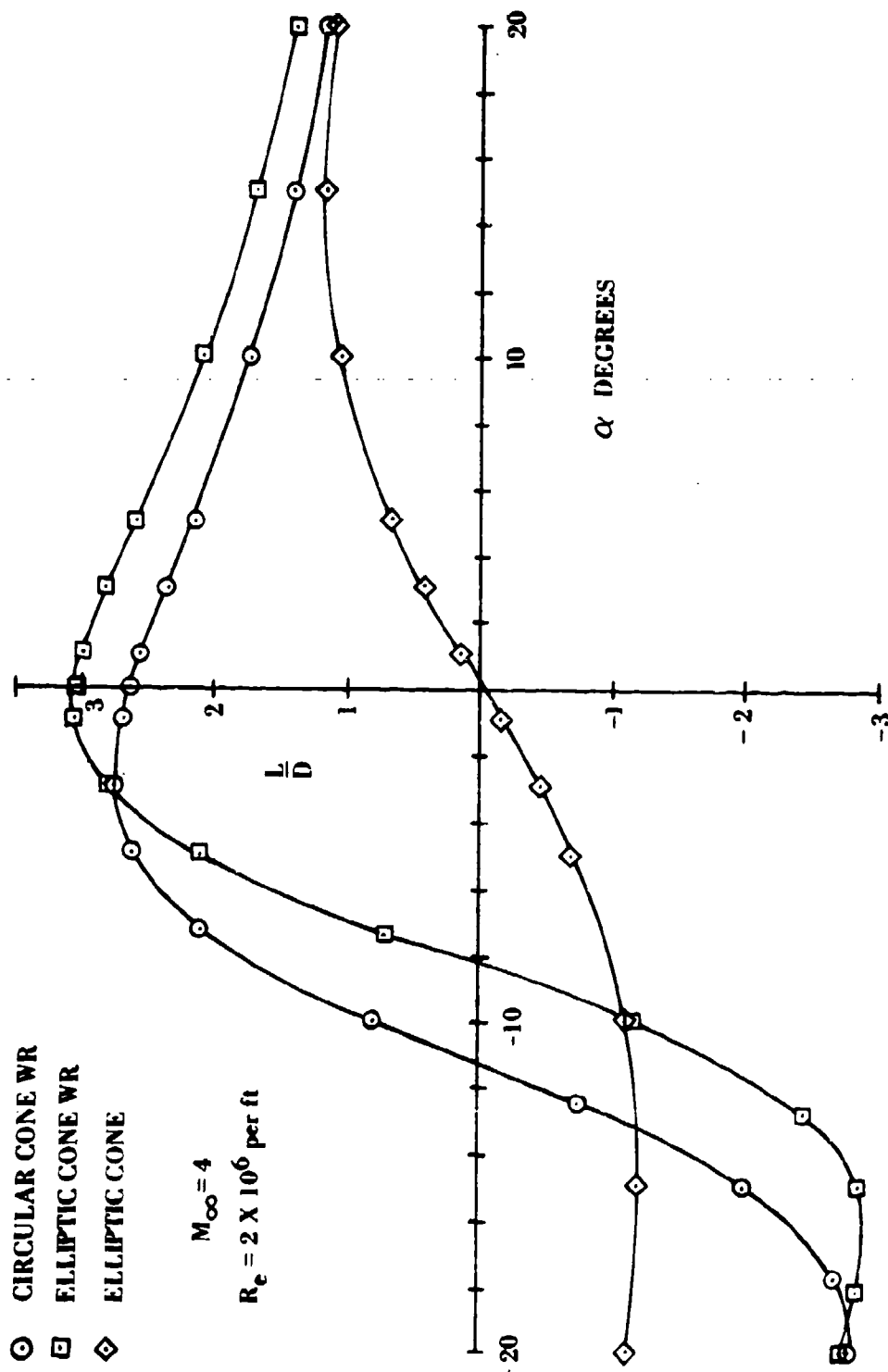
Figure 131.   Lift-to-Drag Ratio Versus Angle of Attack at $M_\infty = 4$

328

of the four models. The values of $C_L = C_N$ at on-design conditions are approximated by Equation (659) for the waveriders. The drag coefficients shown in Figure 130 are decidedly nonlinear, varying approximately as α squared about the angle of zero lift, which is -8.5 degrees for the elliptic-cone waverider and -11.2 degrees for the circular-cone waverider. The drag coefficients are approximately the same for all the models at $\alpha = 0$, in accordance with Equation (660). At design conditions, the circular-cone waverider drag coefficient is less than the elliptic-cone waverider drag coefficient, but the actual drags are nearly the same when the differences in base areas are taken into account. The drags for the on-design waveriders are much less than those for the elliptic cone generating the same lift.

Figure 131 shows the L/D ratios, which are an important measure of aerodynamic efficiency, especially with regard to range. The L/D ratios are independent of the base areas of reference for the different models. The waverider models achieve their maximum value of L/D at their design orientations, with the elliptic-cone waverider having the largest value. The maximum value of L/D for the elliptic-cone waverider (at $\alpha = 0$) is 2.5 times greater than the maximum value of L/D for the elliptic cone (at $\alpha = 15$ degrees). The waverider models also have negative values of L/D which occur at negative angles of attack, the minimum L/D values have nearly the same absolute values as the on-design conditions. The ratio of Equations (659) and (660) gives a good approximation for the maximum L/D for the waveriders:

$$\left(\frac{C_L}{C_D}\right)_{max} \approx \frac{2}{\pi\delta} \frac{\sigma \cos \Lambda}{1 + \frac{2\Lambda}{\pi}} \quad . \tag{661}$$

Equation (661) shows simply how δ, σ, and Λ affect the maximum L/D ratios for the waveriders on-design. Smaller values of δ, that is, more slender bodies, increase the value of L/D, and negative dihedral tends also to increase L/D.

Figures 132, 133, and 134 illustrate the effects of Mach number changes from 3 to 5 for the waveriders. The Mach number effects for the elliptic cones were much smaller, and thus only their results for $M_\infty = 4$ are shown for comparison purposes. For example, for the elliptic cone at $\alpha = 20$ degrees, C_N decreased from 0.90 to 0.85 as M_∞ increased from 3 to 5, but the maximum value of L/D did not vary significantly from 1.2. The largest effects of changes of Mach number for the waverider configurations were on the normal-force coefficients and the rolling-moment coefficients. The variation of C_N with Mach number is shown in Figure 132 for the circular-cone waverider and in Figure 133 for the elliptic-cone waverider. As M_∞ increases from 3 to 5, the absolute value of C_N decreases. The waveriders have a higher C_N for Mach numbers smaller than the design value. The axial-force coefficients (not shown) show much smaller variations with Mach number. For the elliptic-cone waverider at $\alpha = 0$, L/D decreased from 3.2 to 2.90 as M_∞ increased from 3 to 5. Figure 134 shows the effect of Mach number changes on the rolling moment coefficients C_ℓ for the waveriders. Increasing the Mach number causes the rolling moment to decrease.

5. SHOCK-WAVE CONFIGURATIONS

Some of the features of the flowfield and shock-wave configurations were determined from Schlieren photography. Schlieren photographs were taken at selected angles of attack and sideslip angles during the force and moment measurements. In addition, photographs were taken at 10 degrees in roll about the x axis. Examples of these Schlieren data are shown in Figure 135 for the elliptic-cone waverider at $\alpha = 0$, for roll angles of 0 and 90 degrees and for Mach numbers of 3, 3.5, 4, 4.5, and 5. The first column of these photographs shows the side view of the waverider (zero roll). The lower part of the shock wave can be seen and measured. For the upper part of the flow, no shock

330
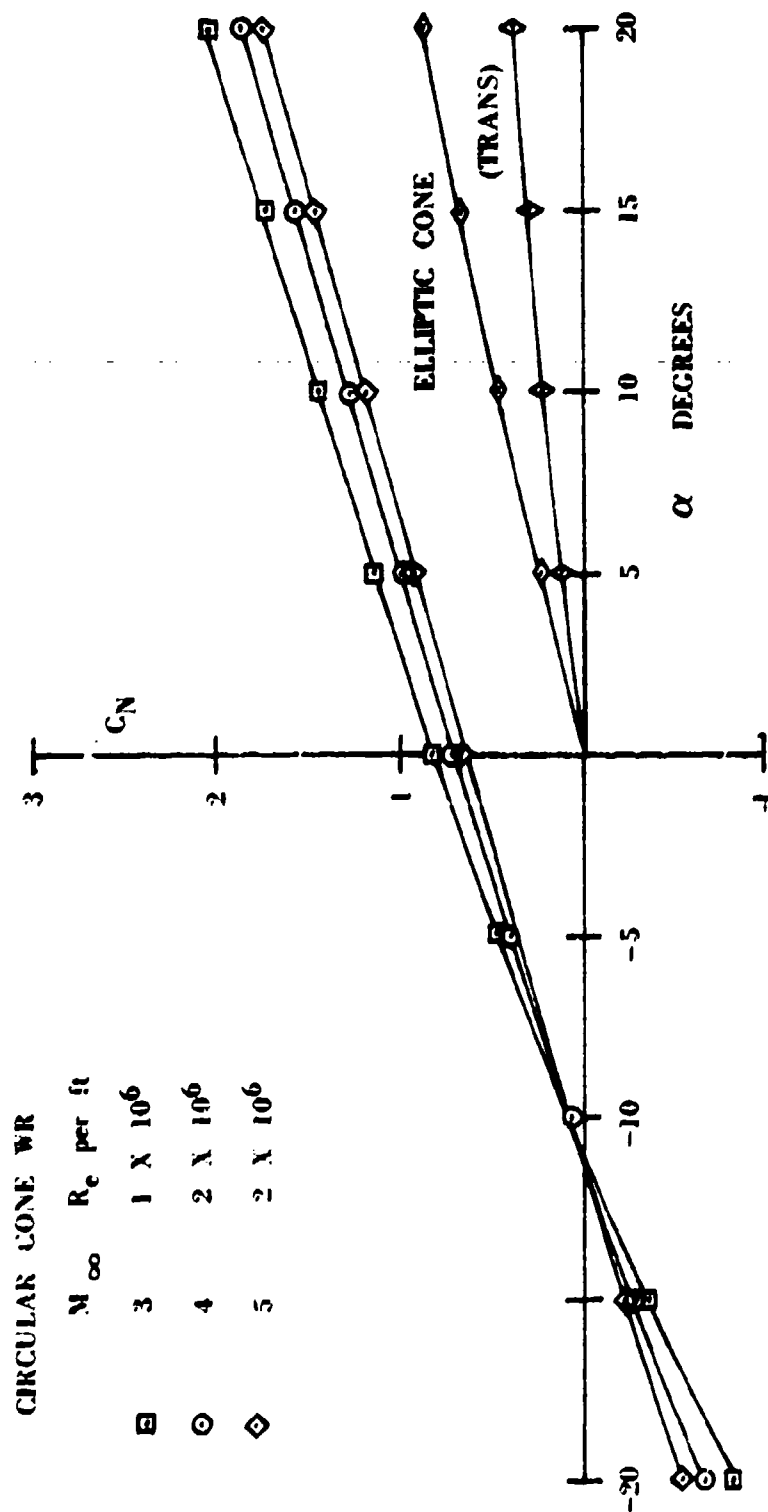
Figure 132. Mach Number Variation of C_N versus Angle of Attack for Circular-Cone Waverider
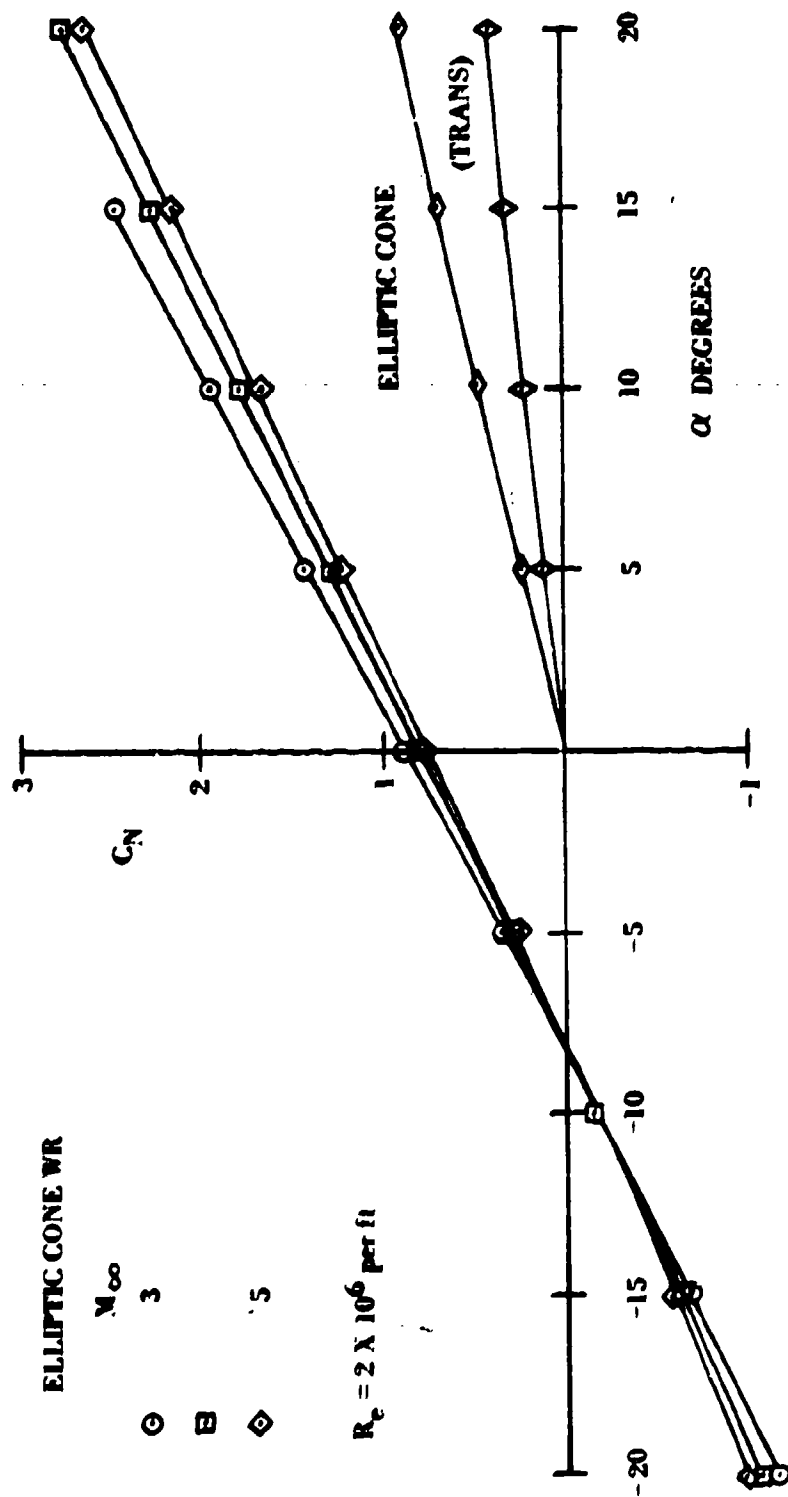
Figure 133.   M Number Variation of C_N versus Angle of Attack for Elliptic-Cone Waverider
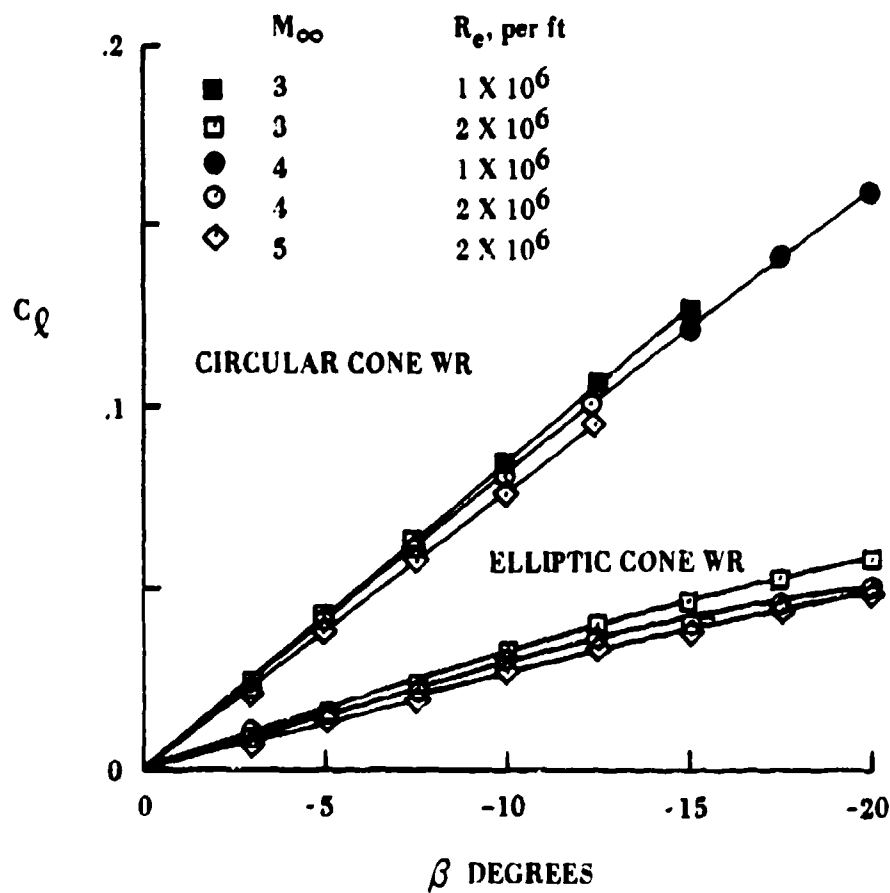
Figure 134. Mach Number Variation of C_{ℓ} Versus Sideslip Angle for Waveriders
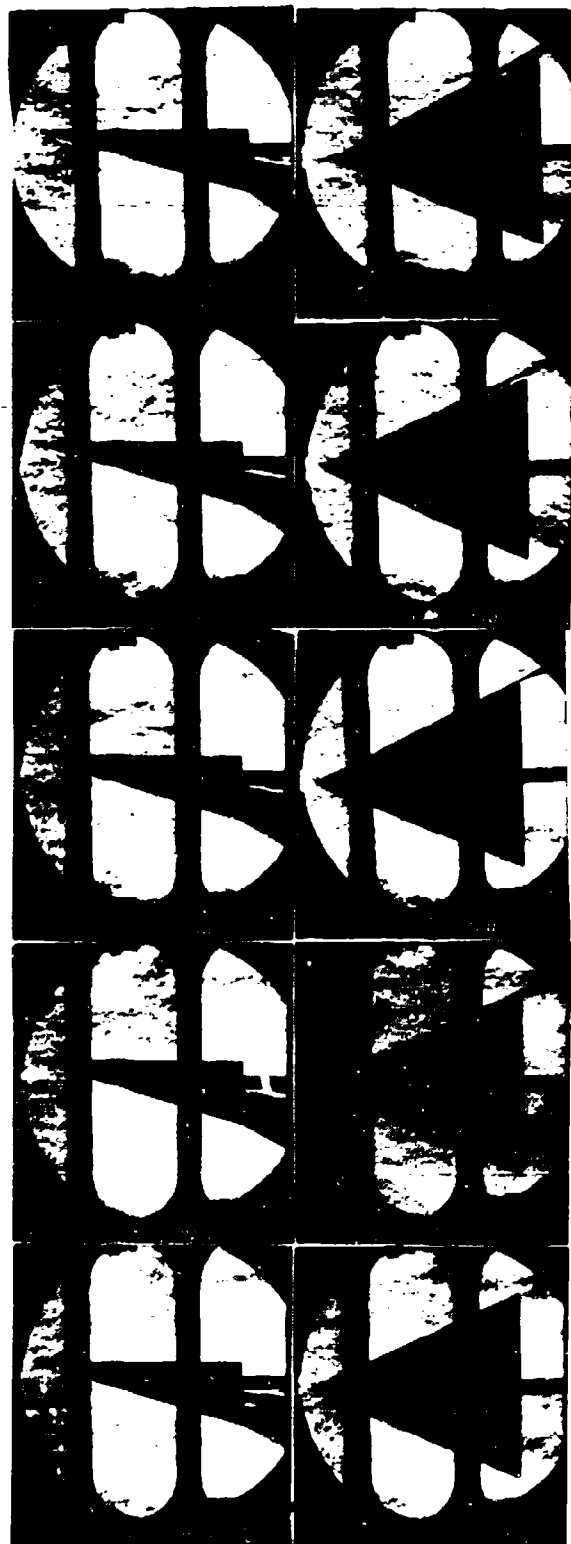
Figure 135.   Schlieren Photographs of Side Views and
Plan Views of Elliptic-Cont Waverider

disturbance can be seen. This is in accordance with the on-design condition of the waverider at $M_\infty = 4$ since the flow is aligned with the upper surface, and the entire flow disturbance is meant to be contained in the attached shock layer beneath the waverider. For the off-design conditions $M_\infty = 3$ and 3.5; in the first two photographs of the second column showing the planform configuration at 90 degrees roll, the shock wave is seen to be detached from the lip. Since there is no upper shock wave seen in the corresponding side views, the detached conical shock degenerates to a Mach wave at the upper ray in the symmetry plane. At the upper off-design conditions $M_\infty = 4.5$ and 5, the lower planform views in the second column show the shock-wave to be attached to the waverider.

The data from the Schlieren photographs in Figure 135 can be used to infer the shock shapes in the y-z plane as shown in Figure 136. The attached shock underneath the waverider is the theoretical on-design shock shape for $M_\infty = 4$ computed from Equation (657). The actual shock angle at the lower ray for $M_\infty = 4$ measured from the photograph is slightly greater than the theoretical result; in fact, the actual shock at $M_\infty = 4$ appears very slightly detached from the body. For the higher Mach numbers 4.5 and 5, the shock waves are attached underneath the body, and the lower ray comes closer to the body as M_∞ increases. For the lower Mach numbers 3 and 3.5 the conical shock wave is de .ched, (except at the vertex) and the faired shock-curves through the data points in Figure 136 are inferred. The data points for the top ray ($\phi = 0$) are the theoretical Mach angles extending from the vertex since no disturbance was observed from the Schlieren photographs. The dashed curve above the waverider is the theoretical Mach surface for the on-design condition $M_\infty = 4$. Similar Mach surfaces also exist for $M_\infty = 4.5$ and 5, but they are not shown. The shock waves above the waverider approach the Mach surface as M_∞ approaches 4 from below.

INFERRED SHOCK

$M_\infty = 3$

$M_\infty = 3.5$

THEORETICAL
MACH SURFACE

$M_\infty = 4$

ϕ

SCHLIEREN DATA

$M_\infty = 3$ ○

$M_\infty = 3.5$ ◗

$M_\infty = 4$ ◇

$M_\infty = 4.5$ △

$M_\infty = 5$ ◺

THEORY $M_\infty = 4$
EQ. (4)

Figure 176. Symmetrisation Shock Shapes of Elliptic-Cone Waverider
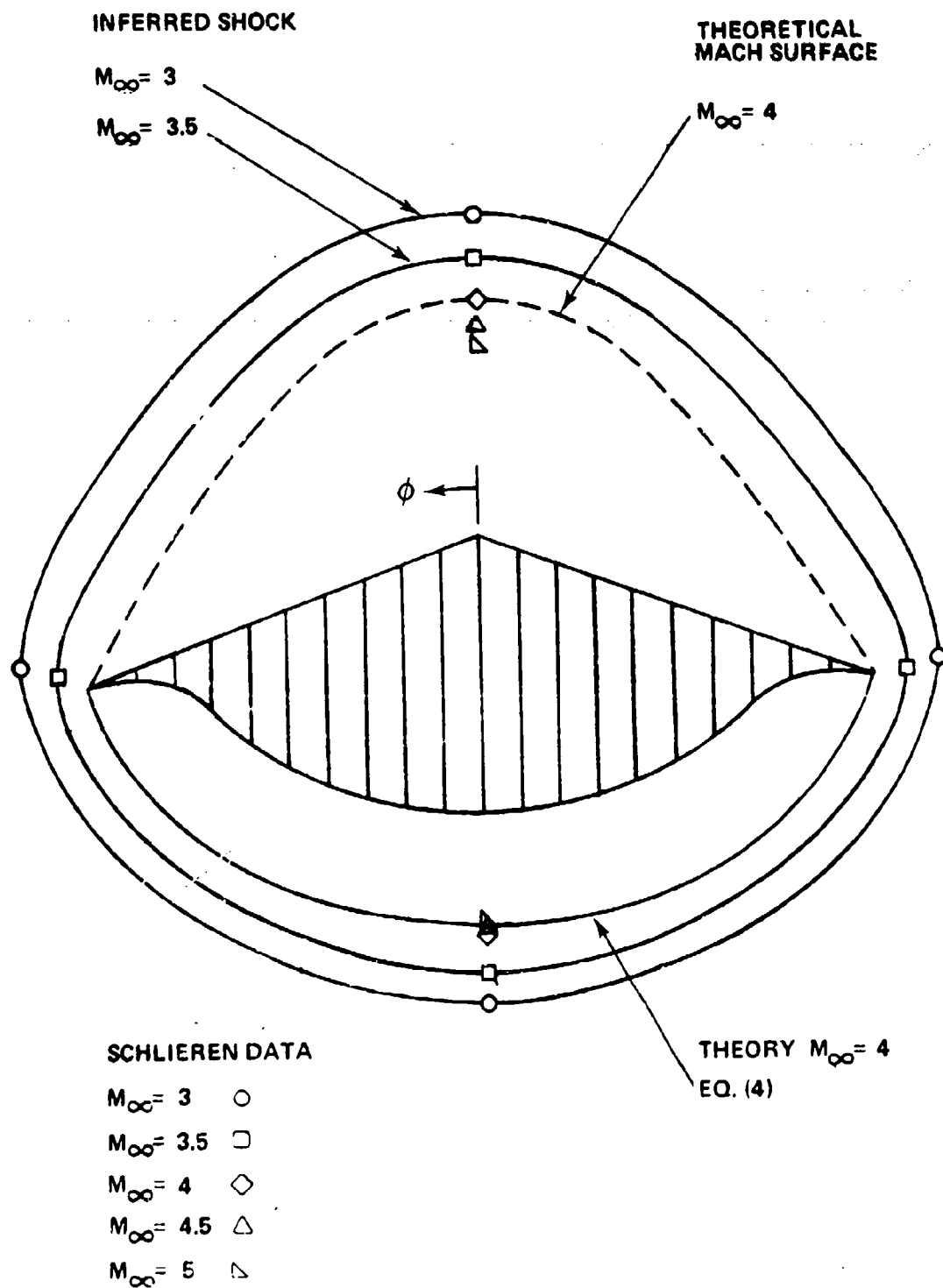
Similar results were found for the circular-cone waverider. The shock was found to be very slightly detached from the lip at $M_\infty = 4$, and attached as for the elliptic cone waverider for the higher Mach numbers.

From the Schlieren photographs it was determined for the elliptic cone at $M_\infty = 4$ that the shock stood off from the base at the body 2.27 inches from the major axis and 4.40 inches from the minor axis. The original intention in the design of the winglets was for them to extend out to the shock at $M_\infty = 4$. The base dimension of the 1.96 inches for the winglet was determined on the basis of a numerical calculation which now seems to have been in error since the actual standoff distance of 2.27 inches is somewhat larger. The shock position shown in Figure 121c thus reflects the anticipated shock position and not the actual one determined from the Schlieren photographs.

6. OIL FLOW RESULTS

Oil-flow visualization data were obtained on each model configuration at $M_\infty = 3.5$, 4, and 4.5 and at a unit Reynolds number of 2 million per foot. The top and bottom surfaces of the models were photographed simultaneously at angles of attack of -10, -3.7, 10, and 11.5 degrees with zero sideslip and at a sideslip angle of -10 degrees for zero angle of attack. From these photographs the boundary layer always appeared to be a laminar flow, and no transition to turbulence was observed. No separation of the boundary layer was observed on the waverider models. A kind of cleaning of the oil from the surface near sharp corners occurred, and distinctive patterns of oil flow occurred on the curved surfaces near the nose, apparently owing to viscous shear effects. The flow overall appeared very clean and did not deviate from what was expected from a purely conical inviscid flow outside the boundary layer. Representative oil-flow photographs for the circular cone waverider at $M_\infty = 4$, $\alpha = 10$ degrees, and $R_e = 2$ million per foot are shown in Figure 137.
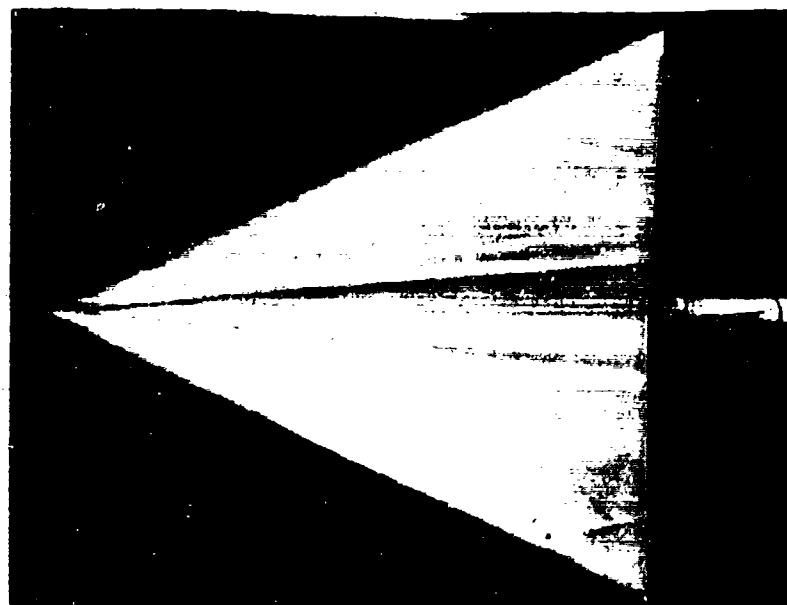
a. Top view   M=4   a = 10° $R_e = 2 \times 10^6$/ft
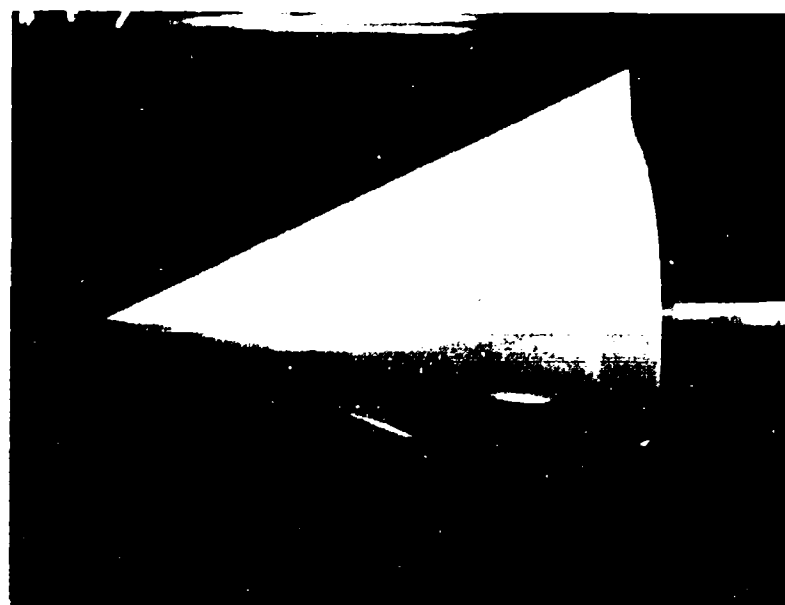
b. Bottom view   M=4 $\alpha = 10°$

Figure 137. Oil-Flow Pattern on Circular-Cone Waverider at $M_\infty = 4$
$\iota = 10°$, and $R_e = 2$ million per foot

338

7. SURFACE PRESSURE DISTRIBUTIONS

After the force and moment tests, Schlieren photography, and oil flow studies were completed, two waveriders and the elliptic cone models were tapped and instrumented with 43 to 48 flush-mounted pressure tubes. The location and designation of each surface pressure and base pressure orifice for each model tested are shown in Figures 138 through 141. For these pressure tests, the elliptical cone with winglets was not tested as it was impossible to place pressure ports in the winglets because of the thinness of the winglet. Prior to the pressure tests, several orifices at the most forward model station of the two waverider locations were found to be leaking. These orifices could not be reached for repair because of the manner in which they had been fabricated due to the restricted space available internally at this model station.

All of the pressure tests were conducted at a fixed Reynolds number of 2 x 10^6 per foot. The experiments were conducted at Mach numbers of 3.0, 3.5, 4.0, 4.5, and 5.0. Model orientations were varied from +20 to -20 degrees sideslip angle at zero angle of attack. A complete description of the tunnel and airflow calibration information is given in Reference 73.

Figures 142, 143, and 144 show results for the surface pressure coefficient at a freestream Mach number of 4.0 or at various angles of attack from -20 to +20 degrees at zero sideslip angle. These pressure coefficient data are plotted along rays through the vertex of the model. For example, ports 2, 6, 11, 21, 30, and 35 all lie along a ray at ϕ = 225 degrees through the vertex of the circular-cone waverider.

Presenting the measurements in this manner provides a useful check of the basic conical flow assumption that is part of the theory used to derive these waverider shapes. If the flow is in fact conical, there should be no

339

Figure 138. Pressure orifice location and Designation, Elliptic Cone

34

TOP VIEW

BOTTOM VIEW

MS 0.0   MS 3.940 MS 7.874 MS 11.811 MS15.748 MS19685 MS23.247
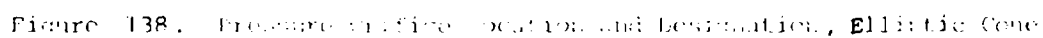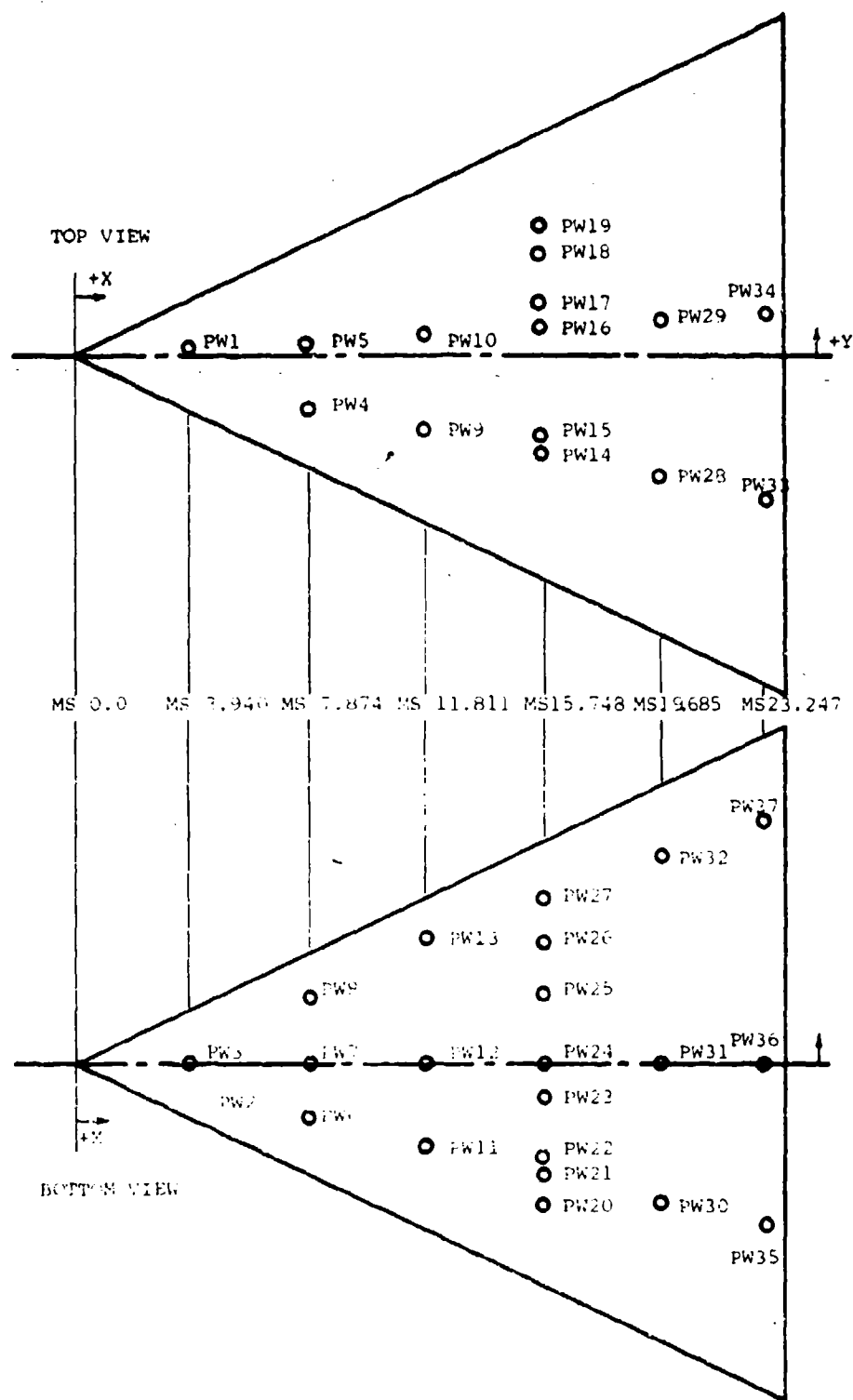
Figure 139. Transducer Orifice Location and Designation, Circular Cone Waverider

TOP VIEW

PW42
PW37
PW25
PW12
PW24
PW7
PW23
PW2
PW22
PW21
PW20
PW1
PW6
PW19
PW11
PW18
PW17
PW36
PW41
PW16

+X
+Y

MS 0.0 MS 4.750 MS 7.874 MS 11.811 MS 15.748 MS 19.685 MS 23.247

PW35
PW34
PW33
PW40
PW45
PW32
PW15
PW5
PW10
PW31
PW4
PW9
PW14
PW30
PW39 PW44
PW3
PW29
PW8
PW28
PW13
PW27
PW26
PW38
PW43

+X

BOTTOM VIEW
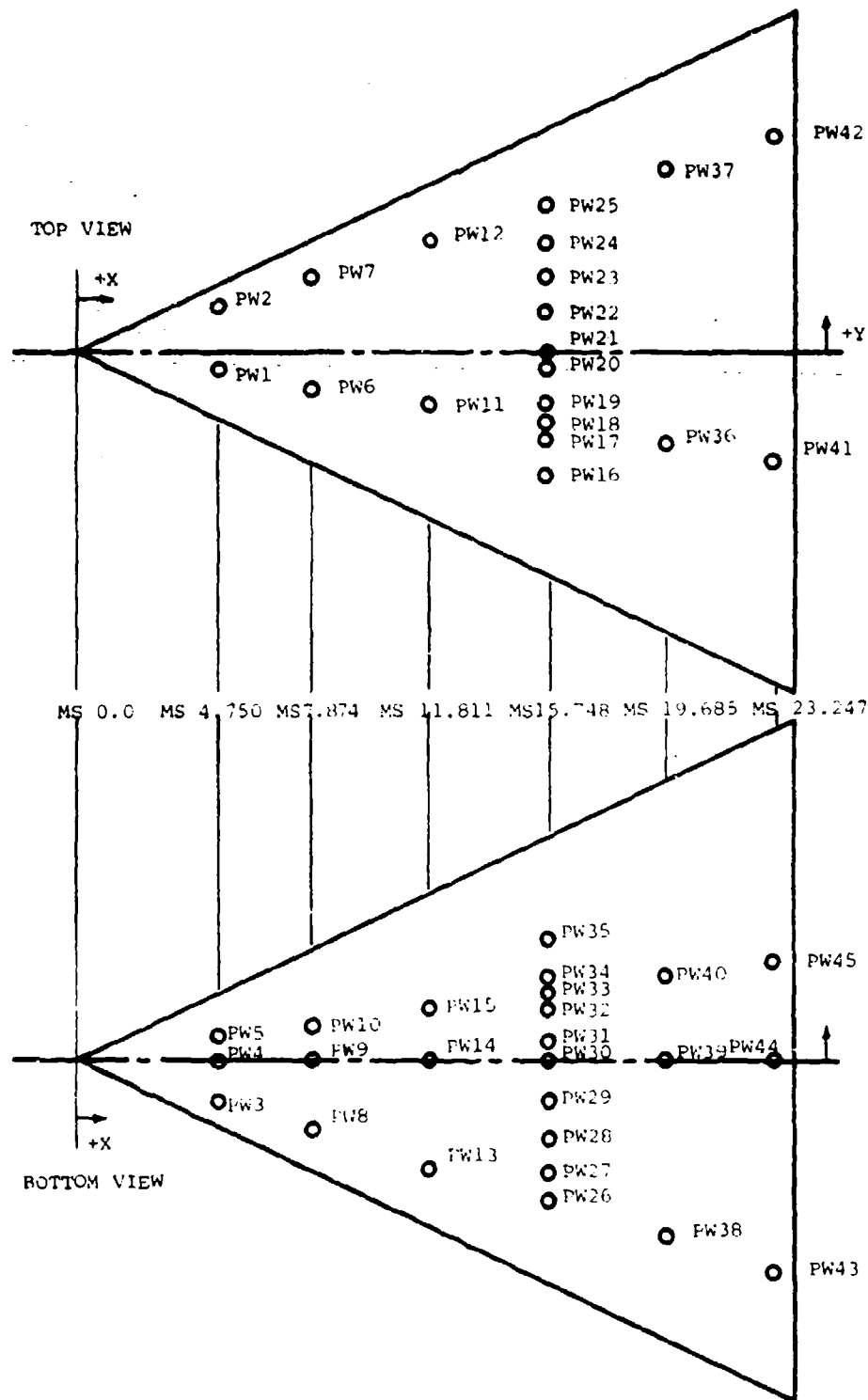
Figure 140 . Pressure orifice location and designation Elliptic Cone Waverider Model
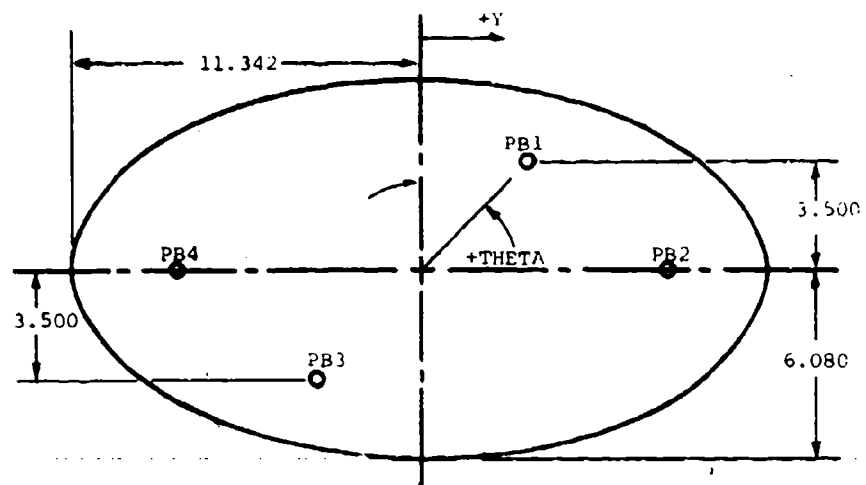
Elliptic Cone
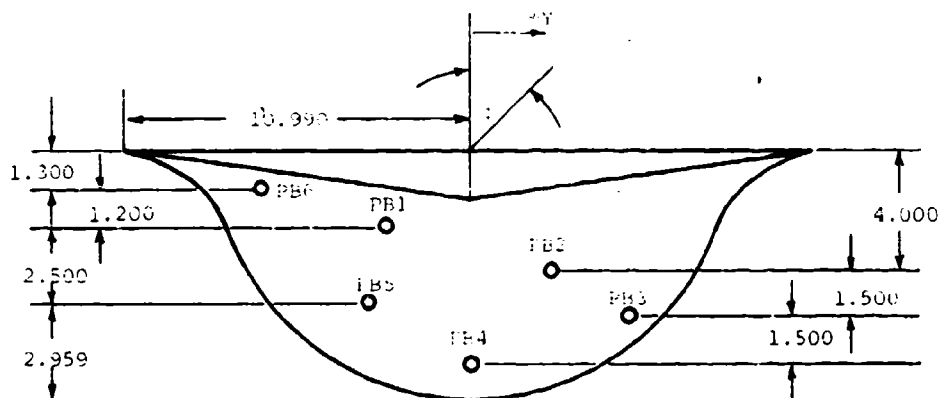
Circular Cone Waverider
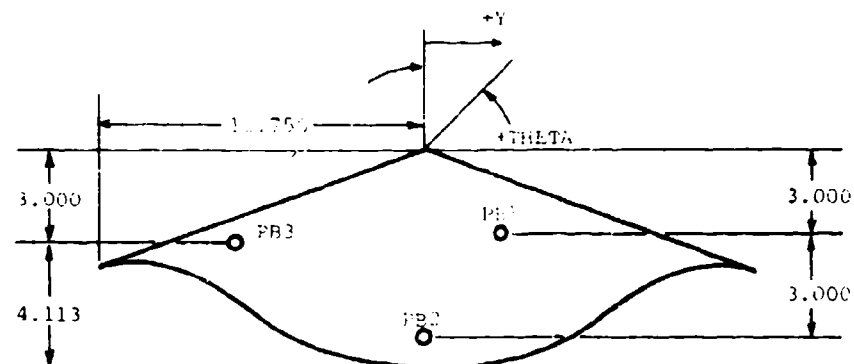
Elliptic Cone Waverider

Figure 141. Pressure Orifice Location and Designation; Base Pressure Orifices

343
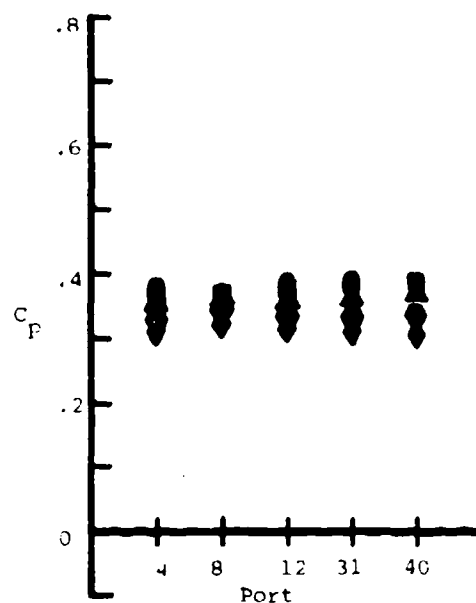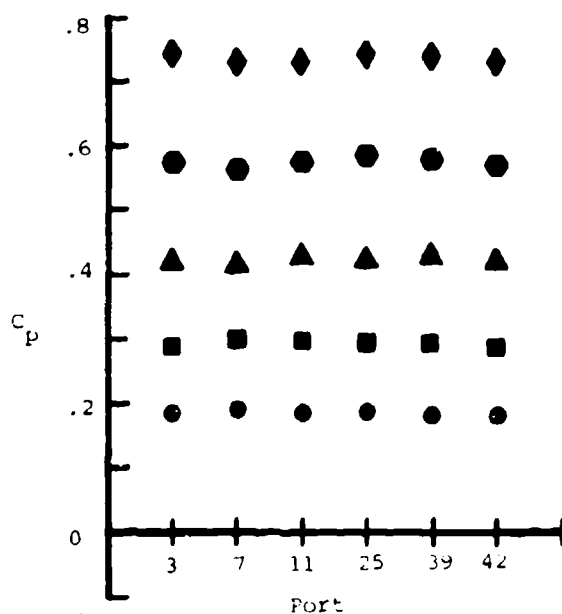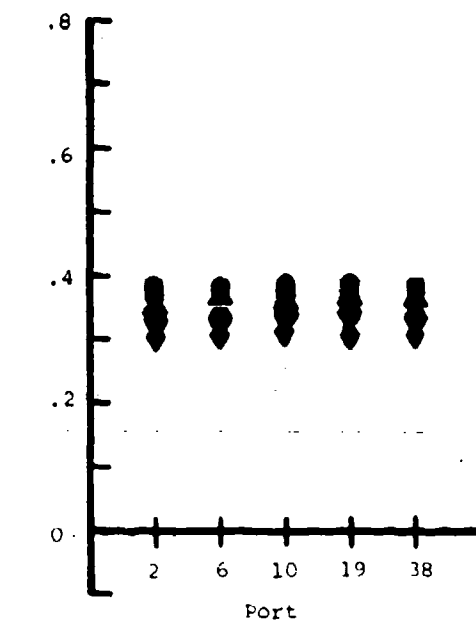
Figure 142. Measured Surface Pressure Coefficient Along Rays Through the Elliptic Cone Vortex (M_∞ =4, = 5, =0.326, =0.156,
, = 0, = 10°, = 15°,)
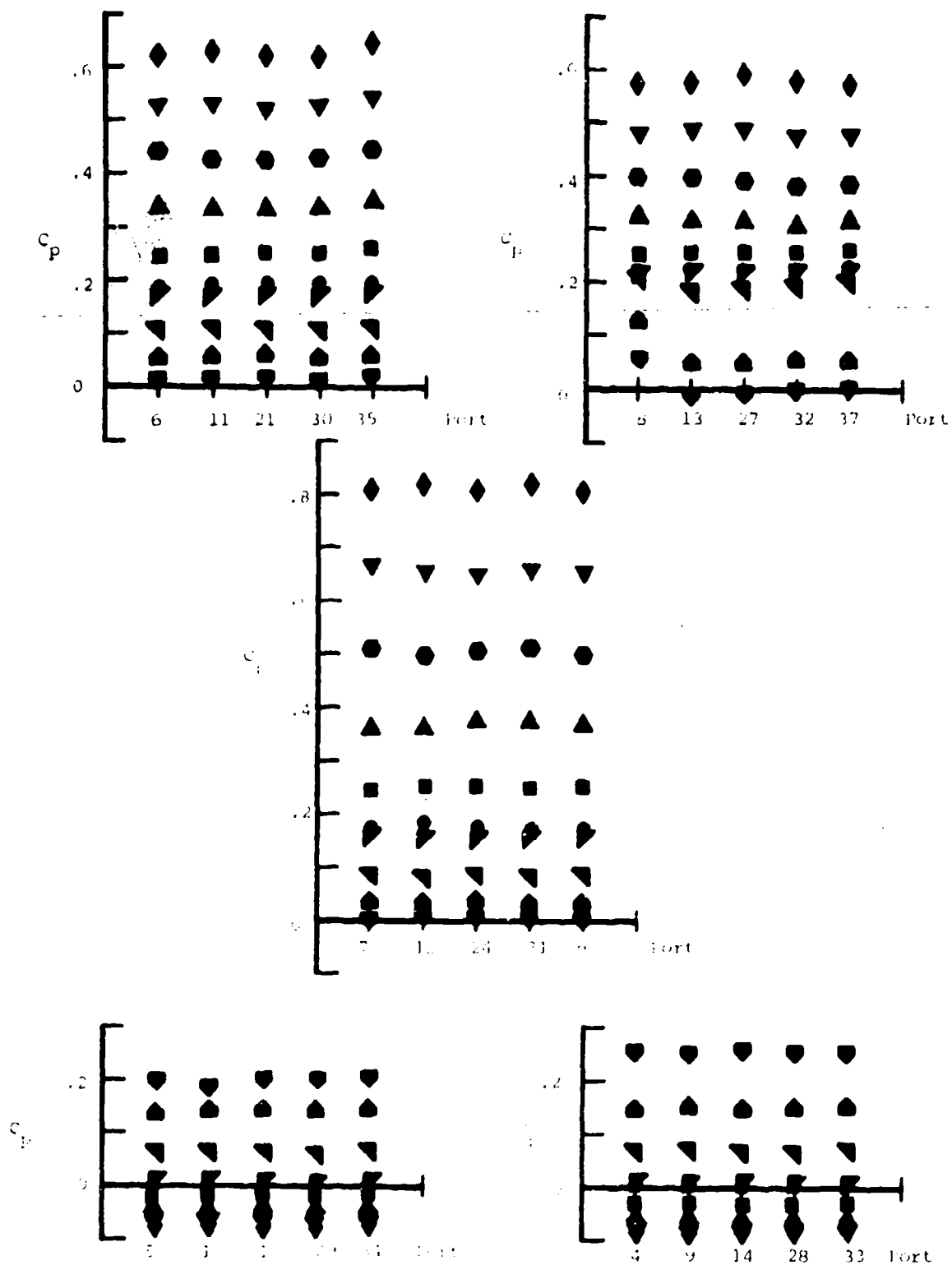
Figure 143. Measured Surface Pressure Coefficient Along Rays Through the Circular Cone with a Right Vortex ($R_\infty = 6$, $M_\infty = .320$, $c_l = .156$, $\alpha = 20°$, ...)
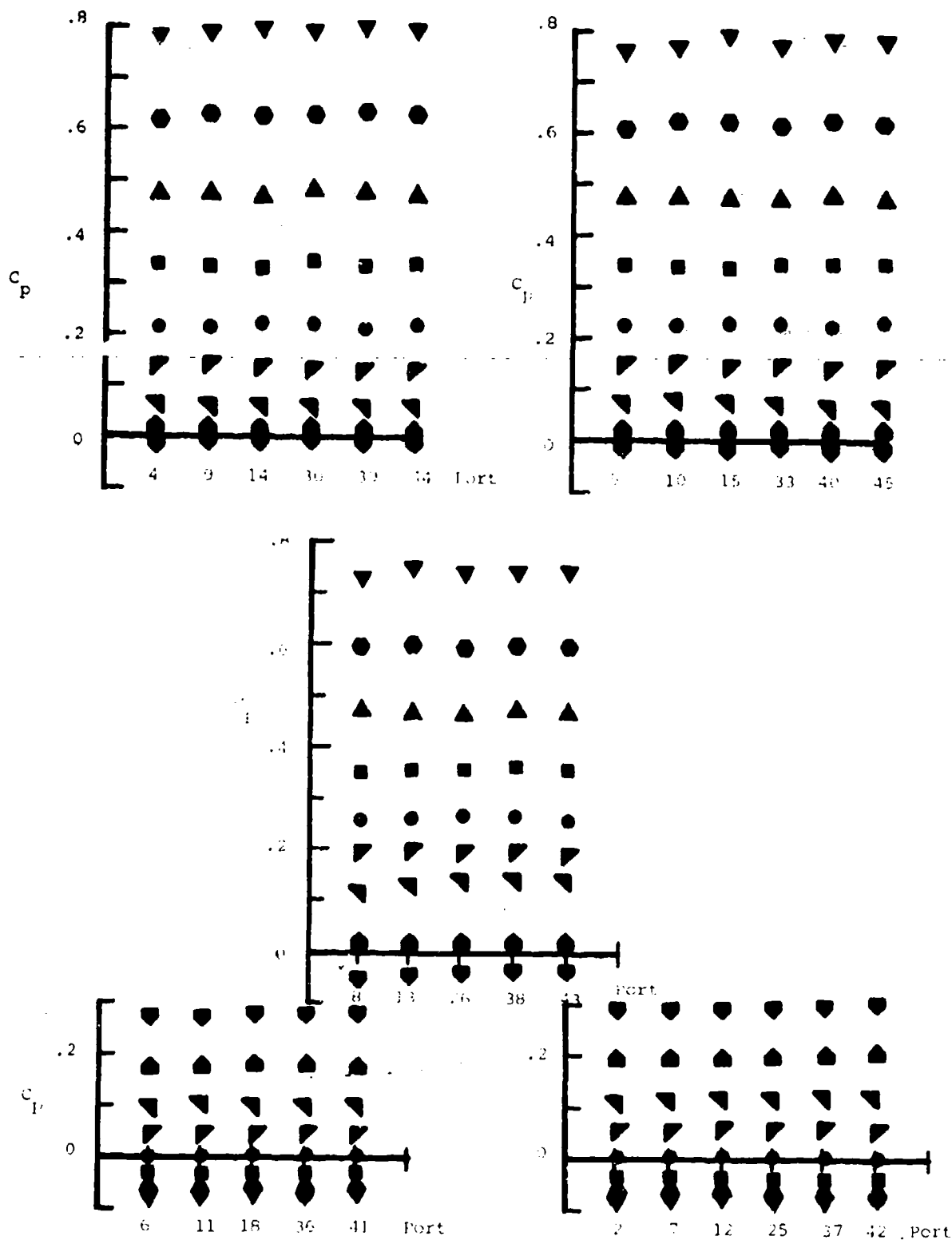
Figure 144. Measured Surface Pressure Coefficient Along Rays Through the Elliptic Cone ...

variation of the surface pressure coefficient along a ray through the vertex of the model. The data given in Figures 142, 143, and 144, as well as other data obtained in the tests but not presented here, show that the conical flow assumption holds quite well.

Figures 145, 146, and 147 compare the measured surface pressures on the -elliptical cone with those computed from the theoretical analysis in Section II. The results of Section II can be written

$$\frac{C_p}{\delta^2} = \frac{cp_0}{\epsilon^2} + \frac{\alpha}{\delta} \frac{C_{p0}}{\delta} \cos \phi + \frac{\epsilon_2}{\delta} \frac{Cp_2}{\delta} \cos 2\phi$$

Here c_{p0}/δ, C_{p0}/δ, and C_{p2}/δ are functions of the hypersonic small disturbance parameter K_δ and the ratio of specific heats γ. With M_∞ given and $\delta = 18.68$ degrees, the hypersonic similarity parameter can be calculated. Also, the eccentricity factor $\epsilon_2/\delta = 0.478$, a value sufficiently large that the perturbation scheme of Section II is likely to yield significant errors.

As the results of Figures 145, 146, and 147 show, the contribution of second-order terms proportional to ϵ_2^2, $\alpha\epsilon_2$, and α^2 are significant and must be included if reasonable agreement is to be achieved between theory and experiment.

Figure 148 compares the measured surface pressure coefficient at $M_\infty = 4$ on the circular cone waverider with the theoretical results obtained using the results given in Section II. Recall that $M_\infty = 4$, the waverider models are on their design conditions. The theoretical results predict the trends observed in the measurements quite well on the compression side of the circular cone waverider. The theoretical result for the upper surface of this waverider, namely zero pressure coefficient also agrees very well with the measurements on that surface.

Figure 149 compares the measured surface pressure coefficient at $M_\infty = 4$ on the elliptic cone waverider with the theoretical results obtained in
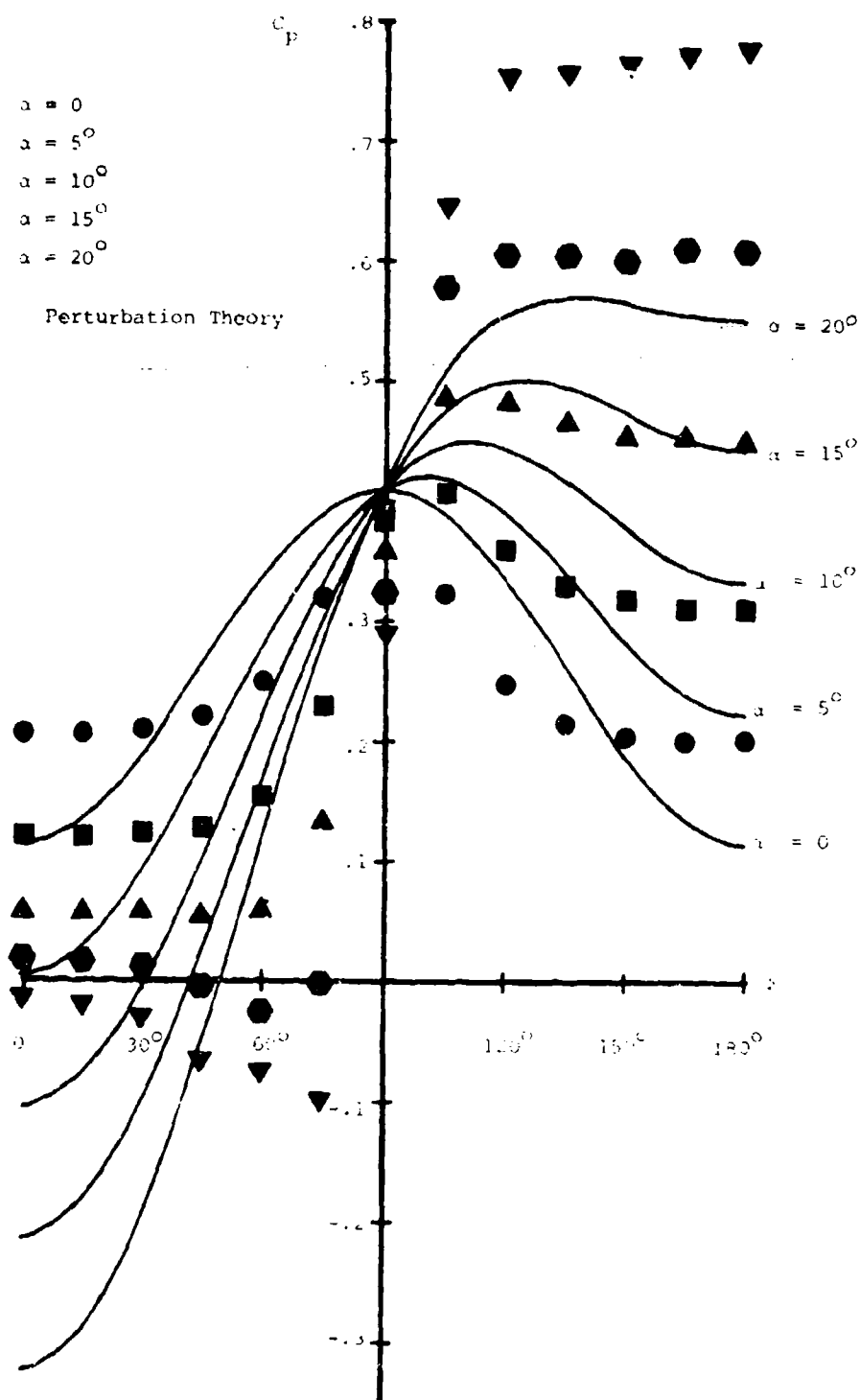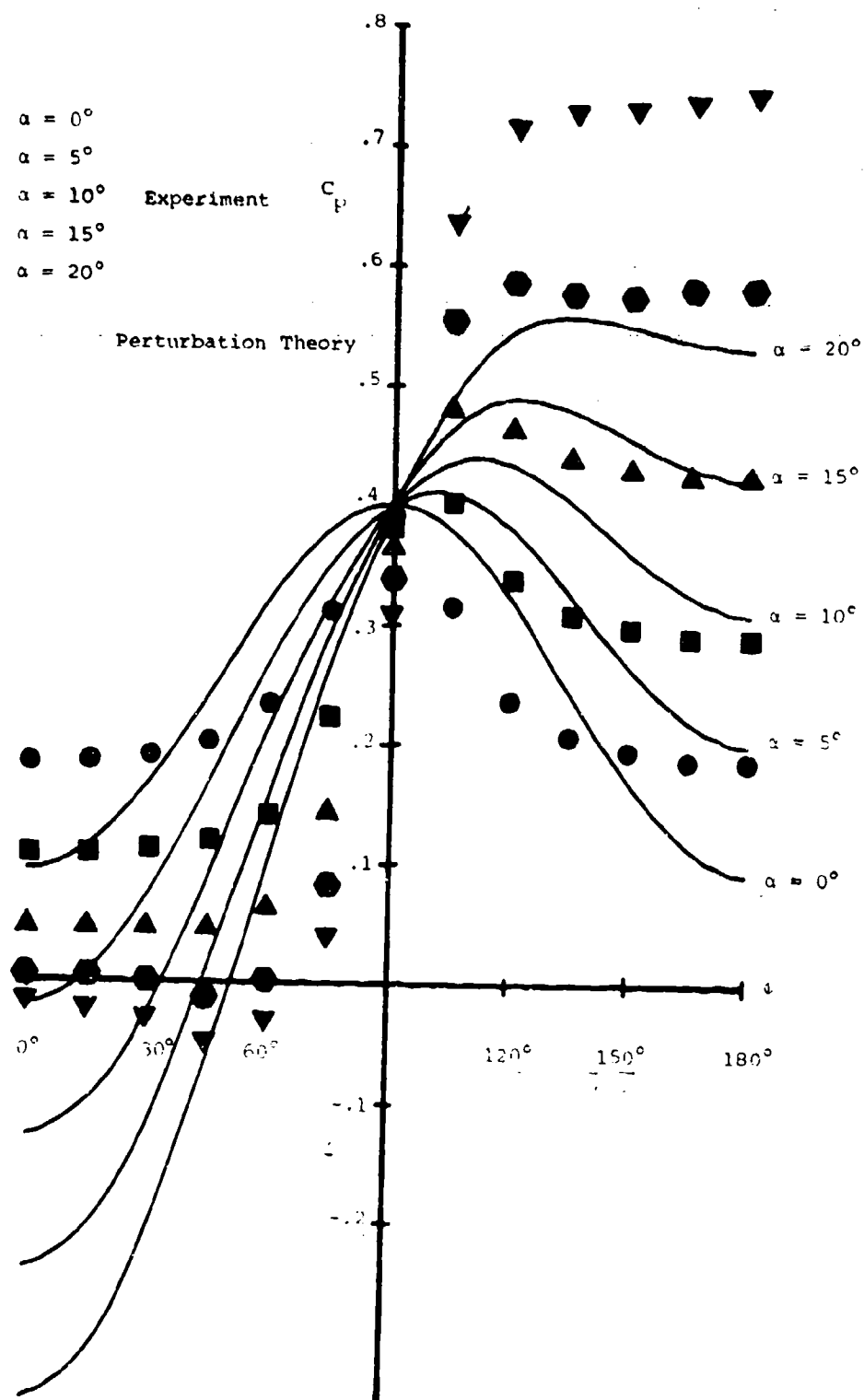
Figure 145. Surface pressure coefficient on Elliptic Cone, Comparison of Perturbation Theory and Experiment (M = 3, ... = 0, ... =0.426, ... =0.15).

Figure 146. Surface Pressure Coefficient on Elliptic Cone, Comparison of Perturbation Theory and Experiment

Experiment
- 0°
= 5°
= 10°
= 15°
= 20°

——— Perturbation Theory
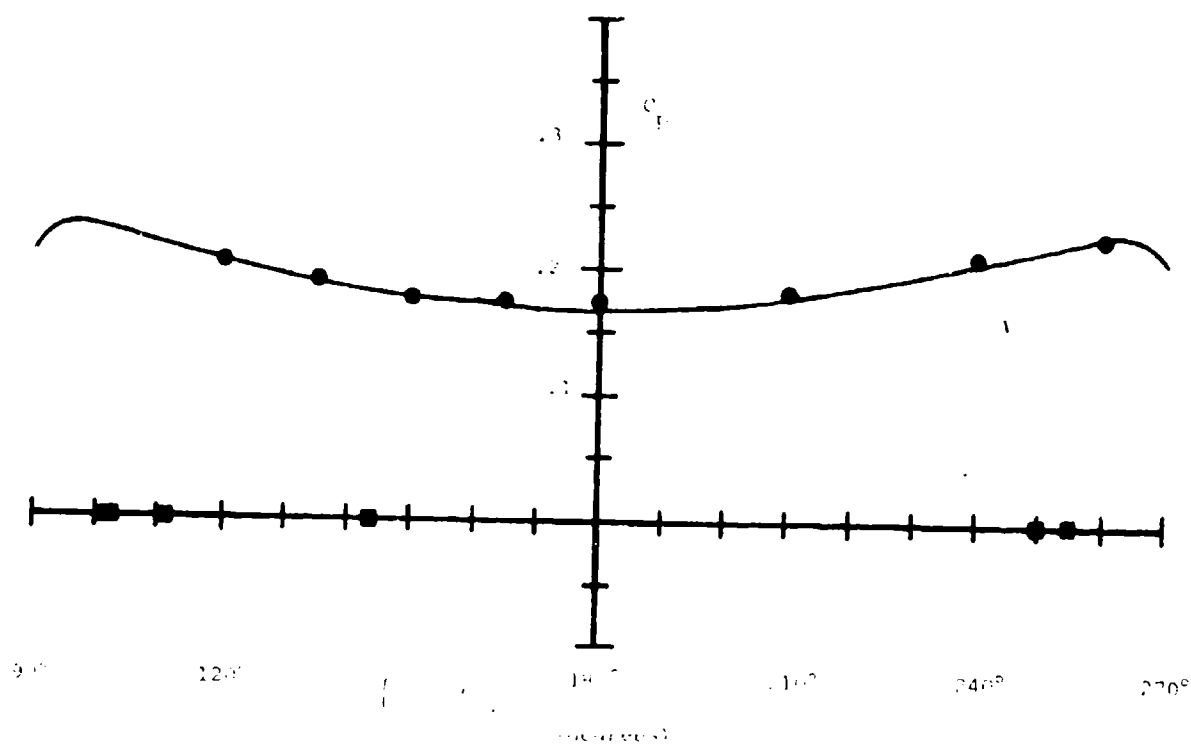
Figure 148. Comparison of theory and experiment for circular cone .... (M = 4.00, α = 3.70, ...)
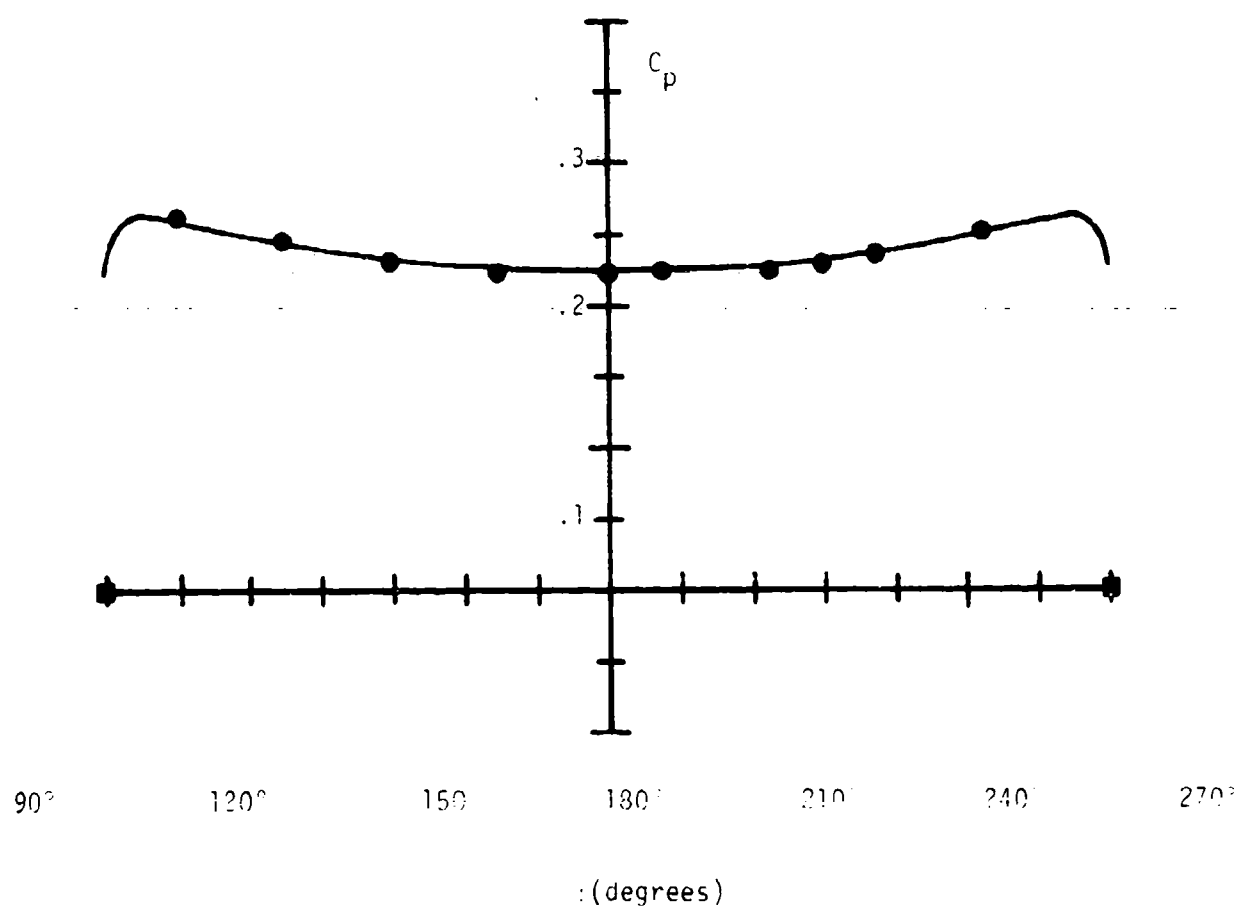
Figure 149. Comparison of Theory and Experiment for Elliptic Cone
             Waverider Surface Pressure Coefficient (M = 4.02,
             ·, lower compression surface, upper surface)

Section II. Again, the observed trends in the experimental data are reproduced by the theory. The measured upper and lower surface pressure coefficients agree quite well with the theoretical estimates.

Figures 150 through 161 present off-design surface pressure coefficient data for the circular cone waverider for freestream Mach numbers of 3, 4, and 5, respectively. The data for $M_\infty = 3.5$, 4.5 do not show any important differences with the data presented here. Figures 150, 154, and 158 give compression surface data for various angles of attack from -20 to +20 degrees at zero sideslip angle. Figures 151, 155, and 159 give the corresponding upper surface data. Data for sideslip angles from 0 to -20 degrees at zero angle of attack are given in Figures 152, 156, and 160 for the compression surface while Figures 153, 157, and 161 give corresponding upper surface results. In all of these figures, the actual data points are plotted as solid symbols. In order to be able to connect the data points with solid lines in a fashion that would preserve the symmetry in the zero sideslip data, these data points were reflected about ϕ = 180 degrees to give the open data points in Figures 151 through 161. Thus the open data points in these figures do not represent actual measurements; they are obtained by assuming symmetry about ϕ = 180 degrees. Examination of Figures 150 through 161 shows that effects of mach number variations from 3 to 5 have little effect on the coefficient distribution, although the maximum pressure coefficient does decrease as M_∞ increases. Also, these data show no evidence of strong secondary shock waves for off-design conditions. As yet there are no theoretical techniques available for calculating the off-design behavior of these waverider configurations. There are no theoretical results in Figures 150 through 161 for comparison.
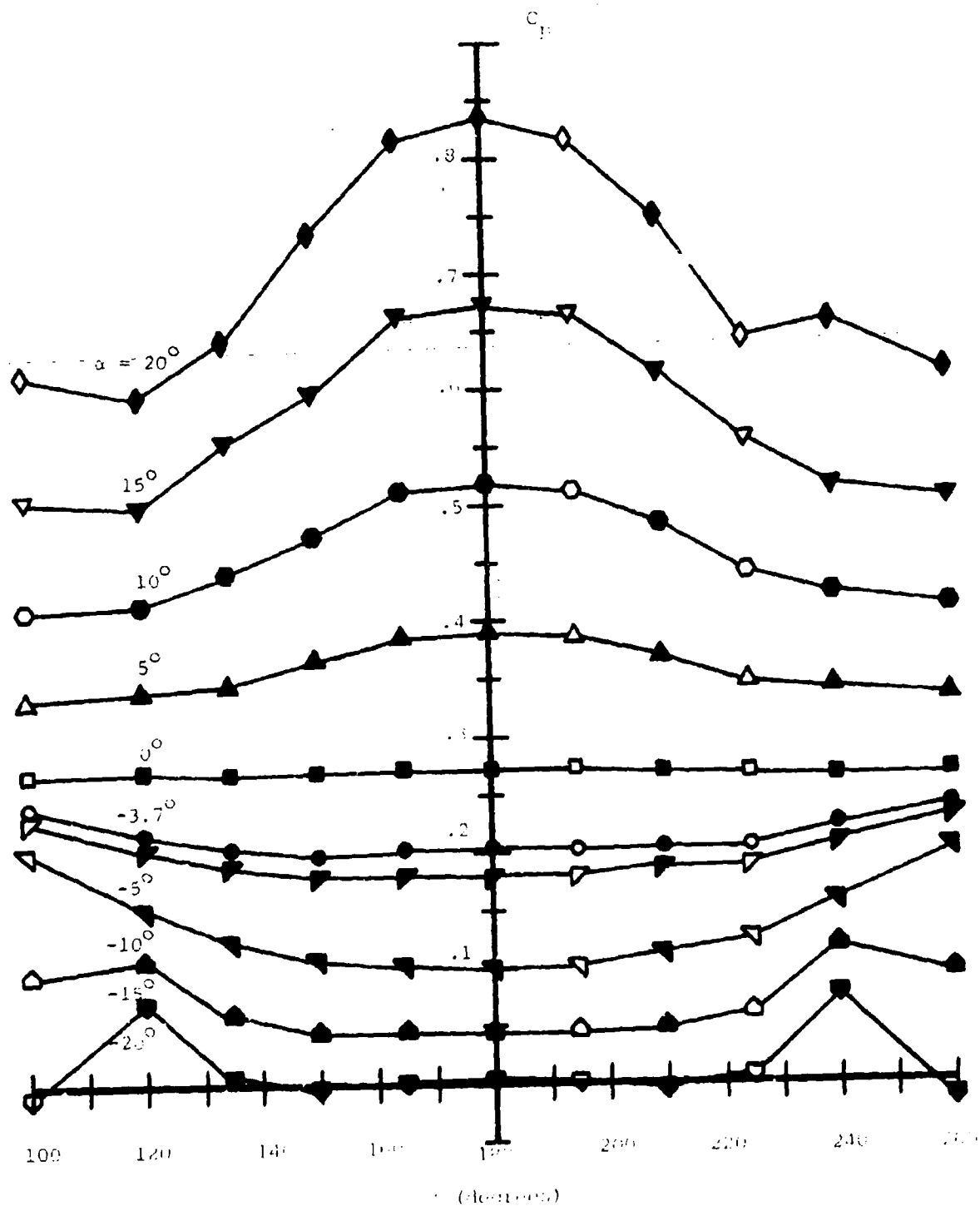
353

Figure 159. [illegible caption text with circular arc blade
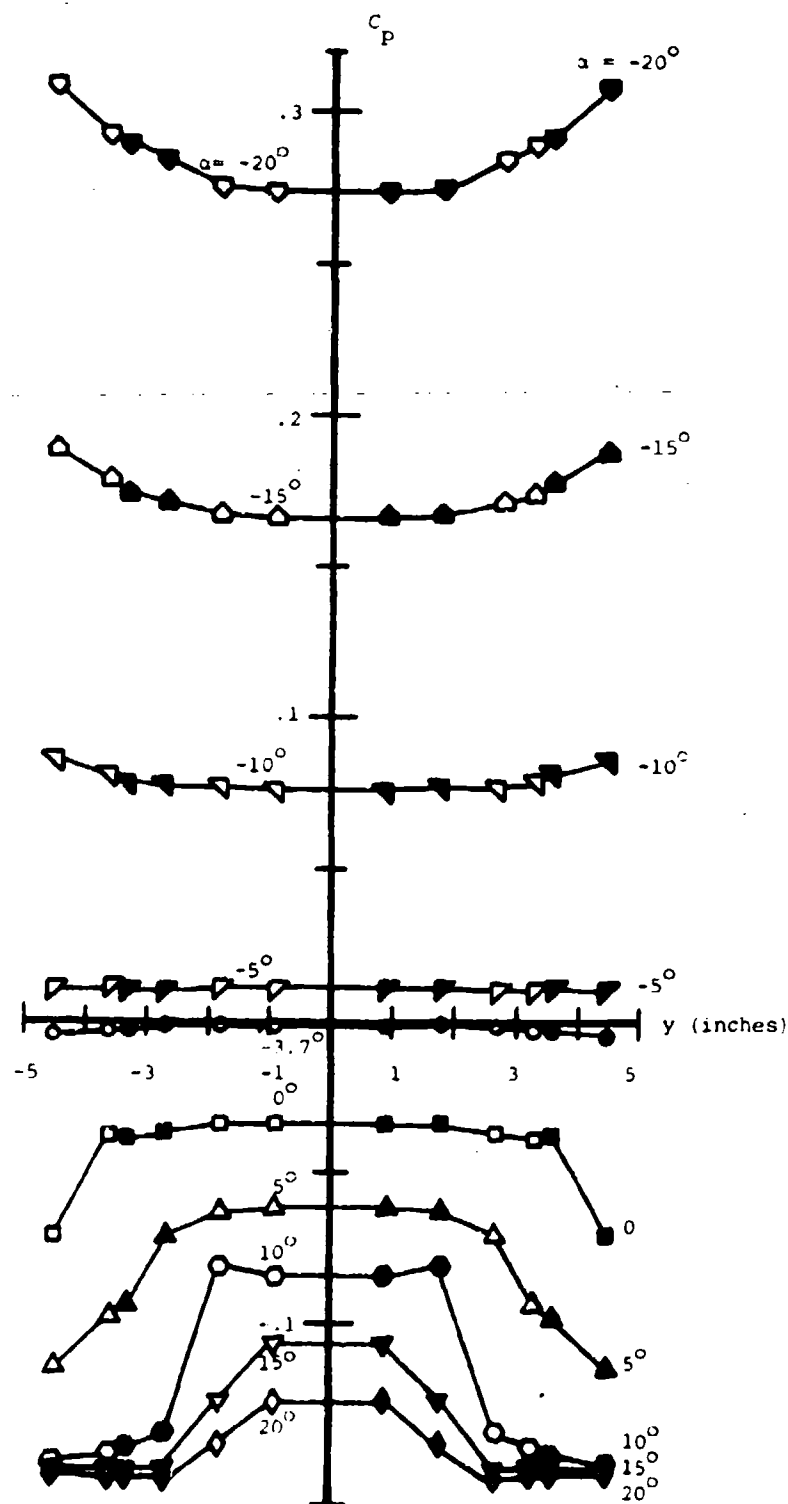Lower Surface ... angle of attack
M = ... (Reynolds ...)]

Figure 151. Measured Surface Pressure Coefficient on Circular Cone Waverider Upper Surface at Various Angles of Attack. (M = 3, β = 0, open symbols indicated for symmetry)
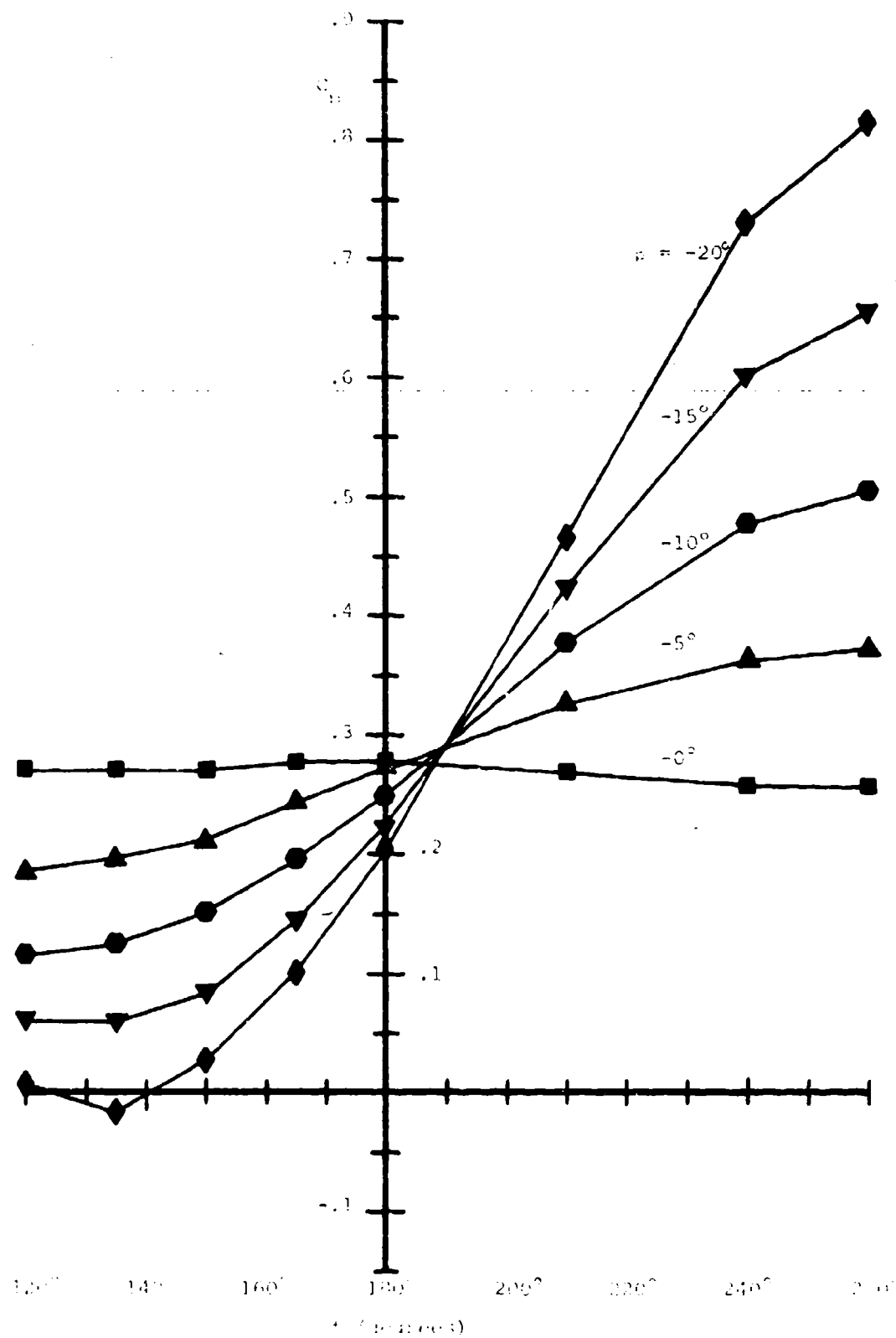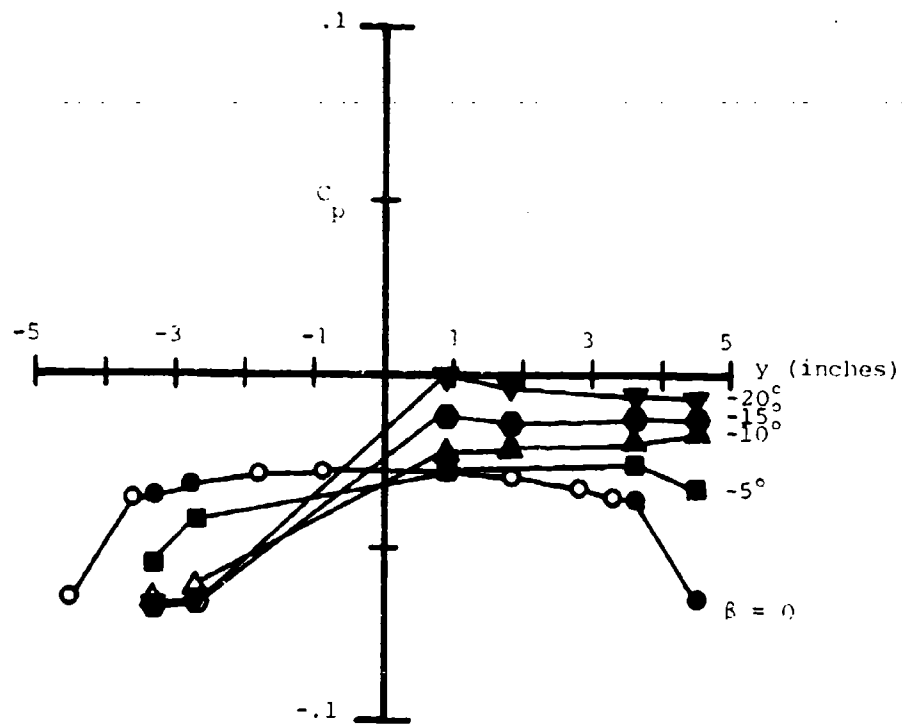
Figure 1.. ...

Figure 153. Measured Surface Pressure Coefficient on Circular Cone
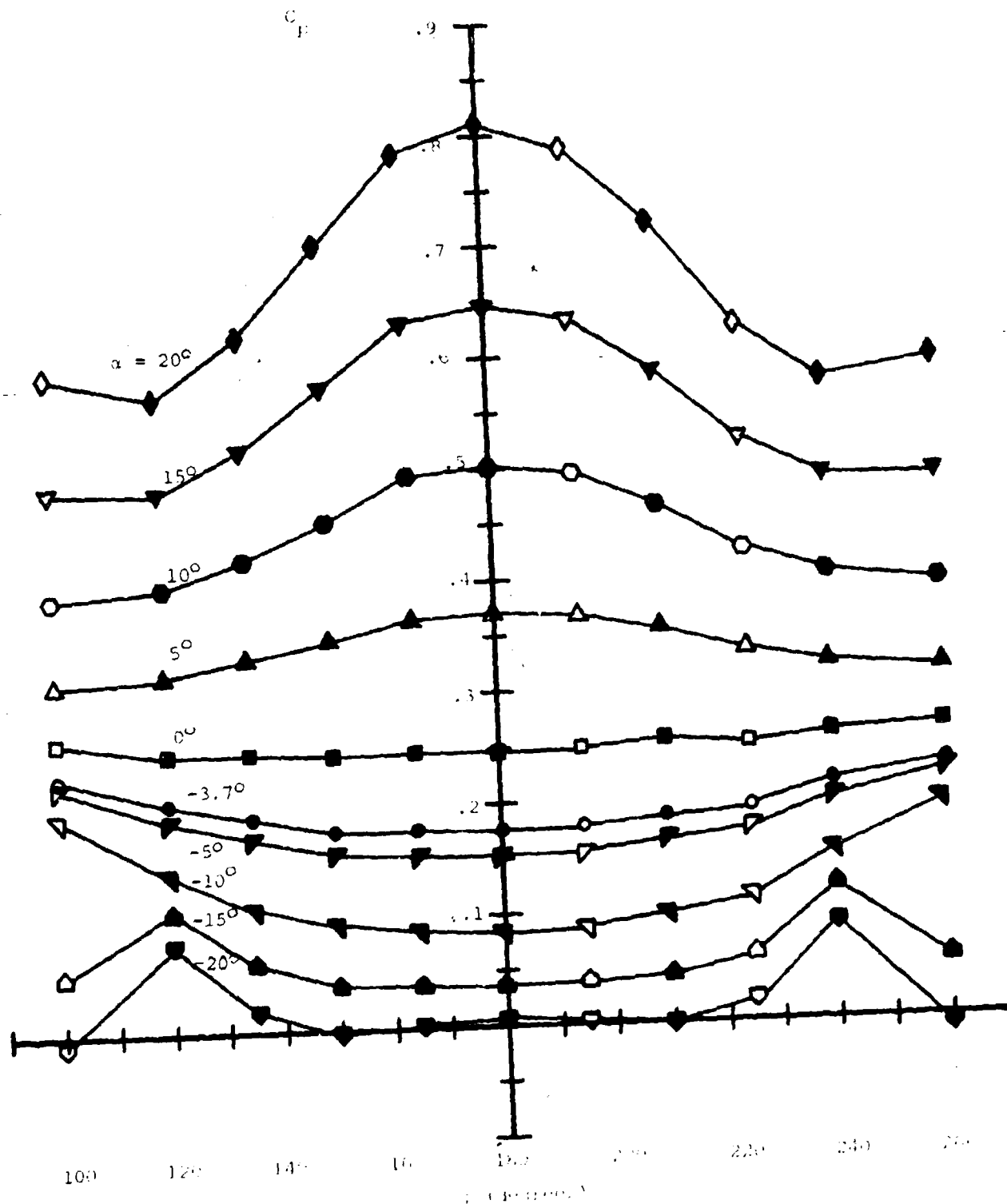Waverider Outer Surface at Various Angles of Yaw
$(M_\infty = 3, \alpha = 0)$

Figure 154. Measured Surface Pressure Coefficient of Circular Cone-Cylinder
(Lower Compression Surface at Various Angles of Attack
(M_∞ = 6; open symbols obtained by symmetry)

Figure. Spanwise distribution of section normal force on a circular wing without tip jet for span stations y = ±4, ±3, etc.; open symbols — circulation data; solid symbols — pressure data.

Figure ... Calculated surface pressure coefficient on circular cone
boundary for various temperature ... surface of variation angle
of attack and ...
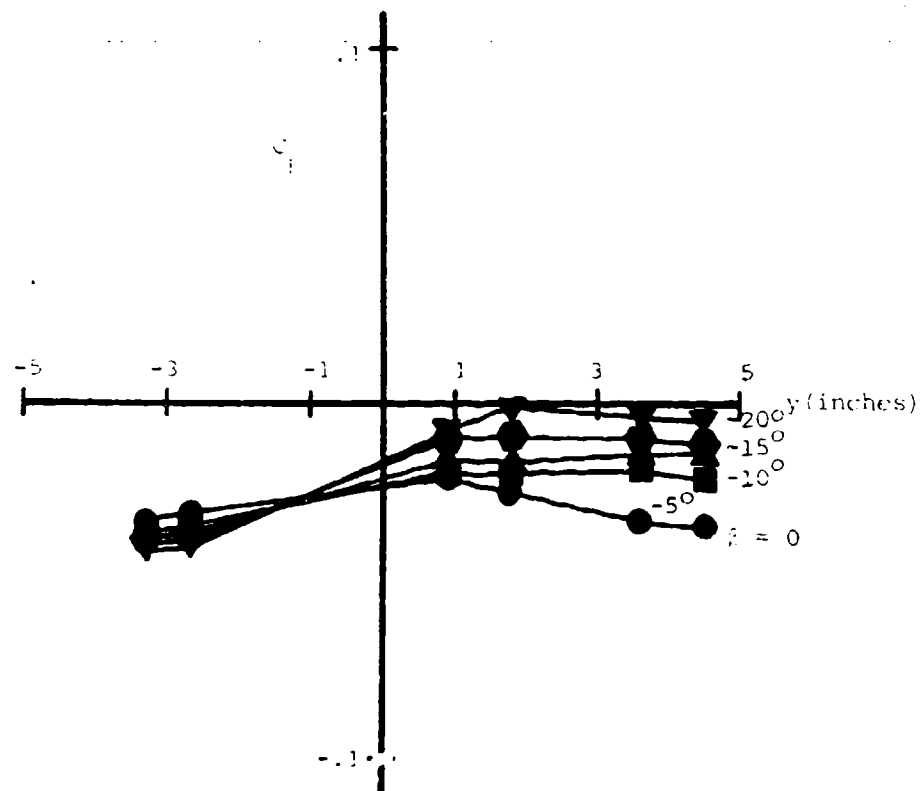
Figure 157 — Measured Surface Pressure Coefficient on Circular Cone Waverider Upper Surface at Various Angles of Yaw ($M_\infty = 4$, ...)

C_p

.8

.7

.6

$\alpha=20°$

15°

.5

10°

.4

5°

.3

0°

-3.7°

.2

-5°

-10°

.1

-15°

-20°

100   120   140   160   180   200   220   240   260

: (degrees)
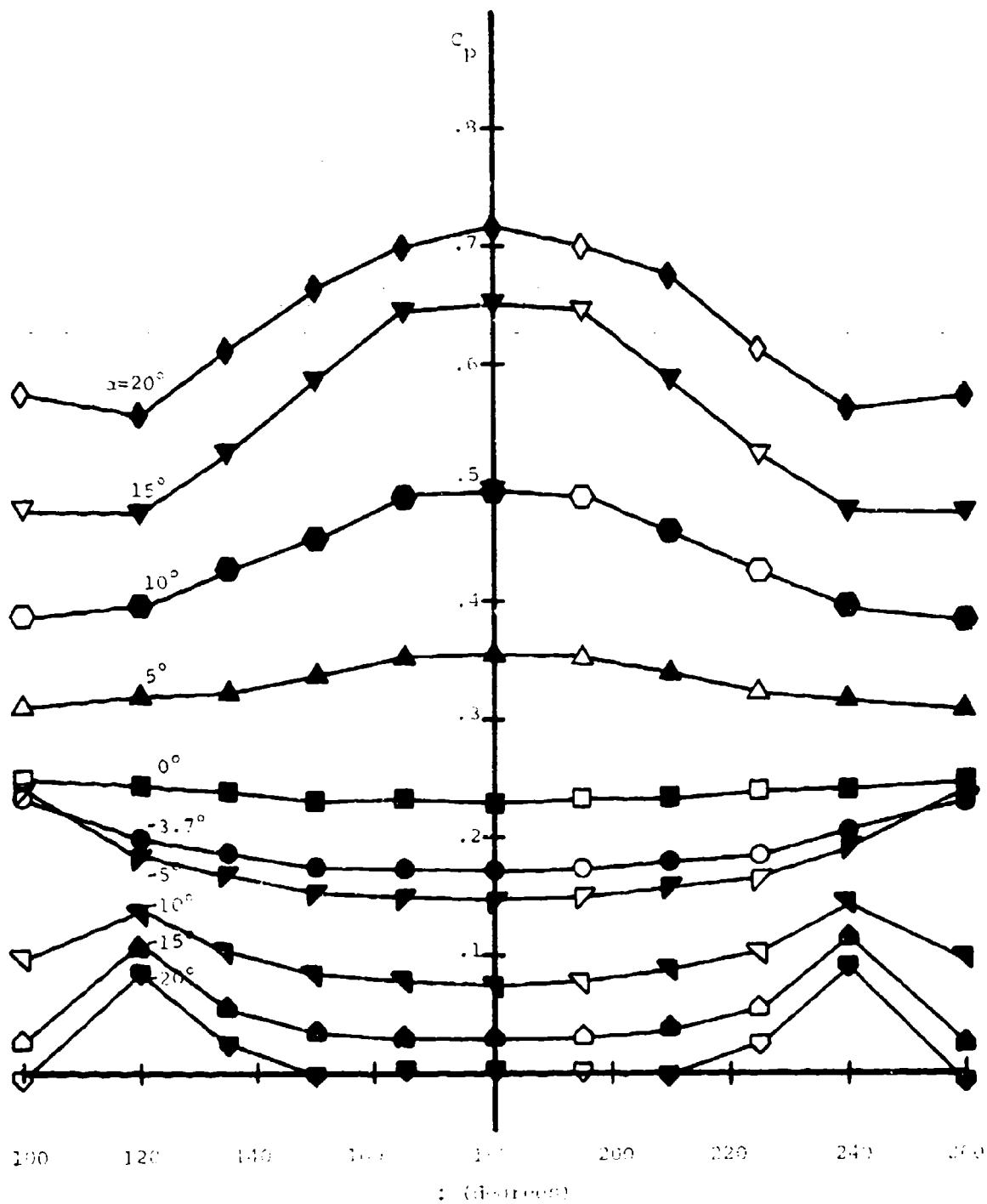
Figure 158. Measured Surface Pressure Distribution on Circular Cone Waverider Lower Compression Surface at Various Angles of Attack ($M_\infty = 6$, $\phi = 0$, other symbols obtained by symmetry)
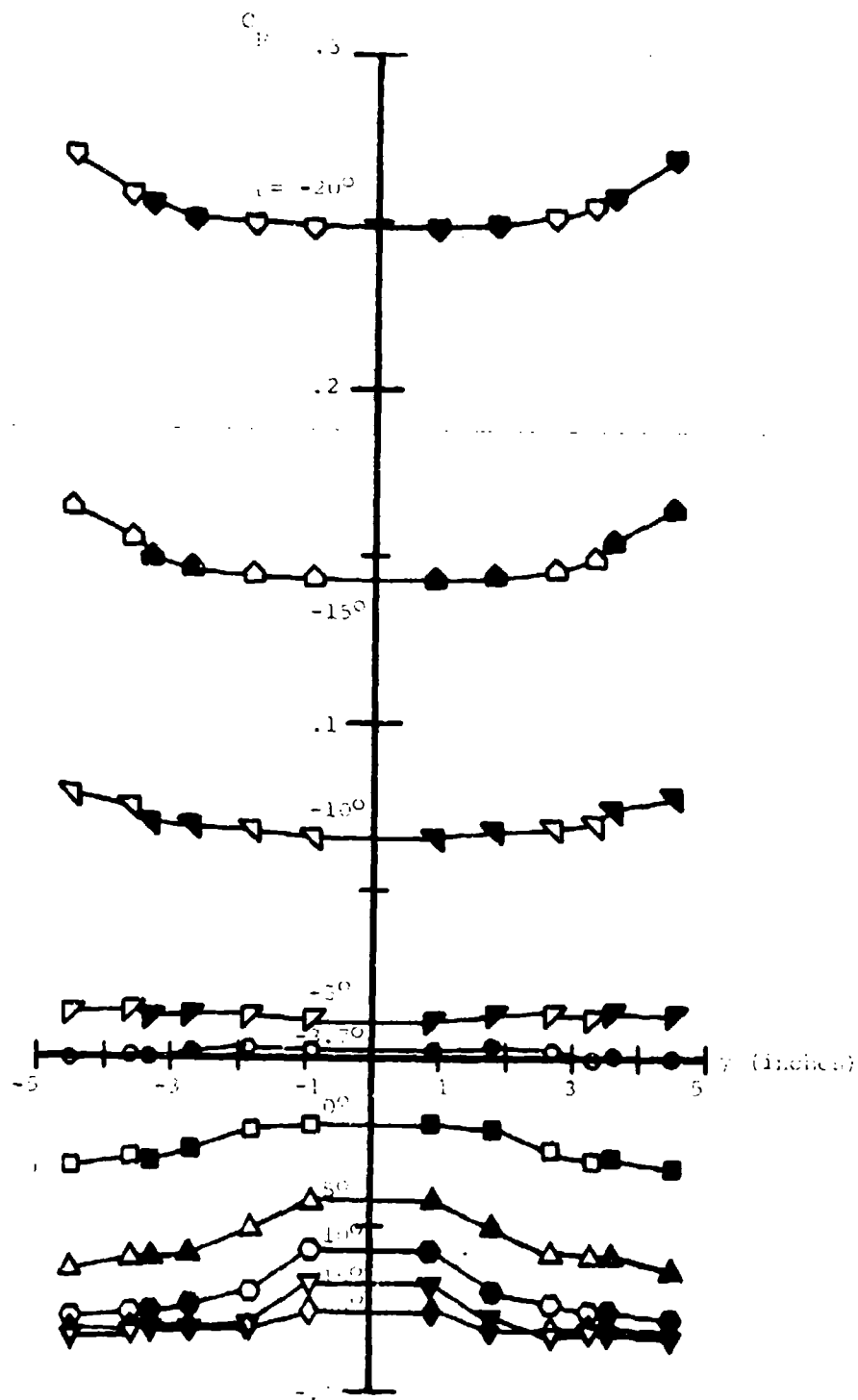
Figure caption (illegible)

Figure 160. Measured Surface Pressure Coefficient on Circular Cone Waverider Lower Compression Surface at Various Angles of Yaw (M = ∞, α = 0)

Figure 161. Measured Surface Pressure Coefficient on Circular Cone Waverider Upper Surface at Various Angles of Yaw

Figures 162 thourgh 173 give analogous results for the surface pressure
coefficient on the elliptic cone waverider. Again, the effects of Mach number
variations in the range 3 to 5 are small. In addition, these data show no
evidence of strong secondary shock waves for off-design conditions.

The data in these figures show that as the angle of attack α is increased
through positive values, the pressure coefficient on the windward symmetry
line increases almost linearly with α while the pressure coefficient on the
leeward surface decreases with α, again almost linearly. Similarly, there is
a nearly linear increase in the maximum surface pressure coefficient as the
sideslip angle β increases.

8. DISCUSSION AND CONCLUSIONS

A comprehensive set of data for the forces, moments, and surface pressure
coefficients on two cone-derived waveriders has been presented together with a
corresponding comparative set for for an elliptic cone. The waverider models
are taken from a fundamental generic class of lifting bodies. The on-design
condition for these bodies is accurately described by the perturbation theory
of Reference 5. The data substantiate the accuracy of the theory for the
on-design conditions and show the deviations resulting from changes in both
orientations and Mach numbers. The waveriders produce significantly larger
lift forces than the comparative elliptic cones. The winglets on the elliptic
cone, which were meant to fashion a pseudo-waverider configuration, produced
only modest improvements in lift over the elliptic cone without the winglets.
The lift over drag ratio representing a measure of aerodynamic efficiency was
2.5 times greater for the on-design elliptic-cone waverider than for the
maximum L/D for the elliptic cone. The forces and moments on the waveriders
decreased as the Mach number increased from 3 to 5. The Schlieren data
together with the surface oil-flow results provided information that the flows

Figure 162. Measured Surface Pressure Coefficient on Elliptic Cone Waverider Lower Compression Surface at Various Angles of Attack ($M_\infty = 3$, ... open symbols obtained by symmetry.)

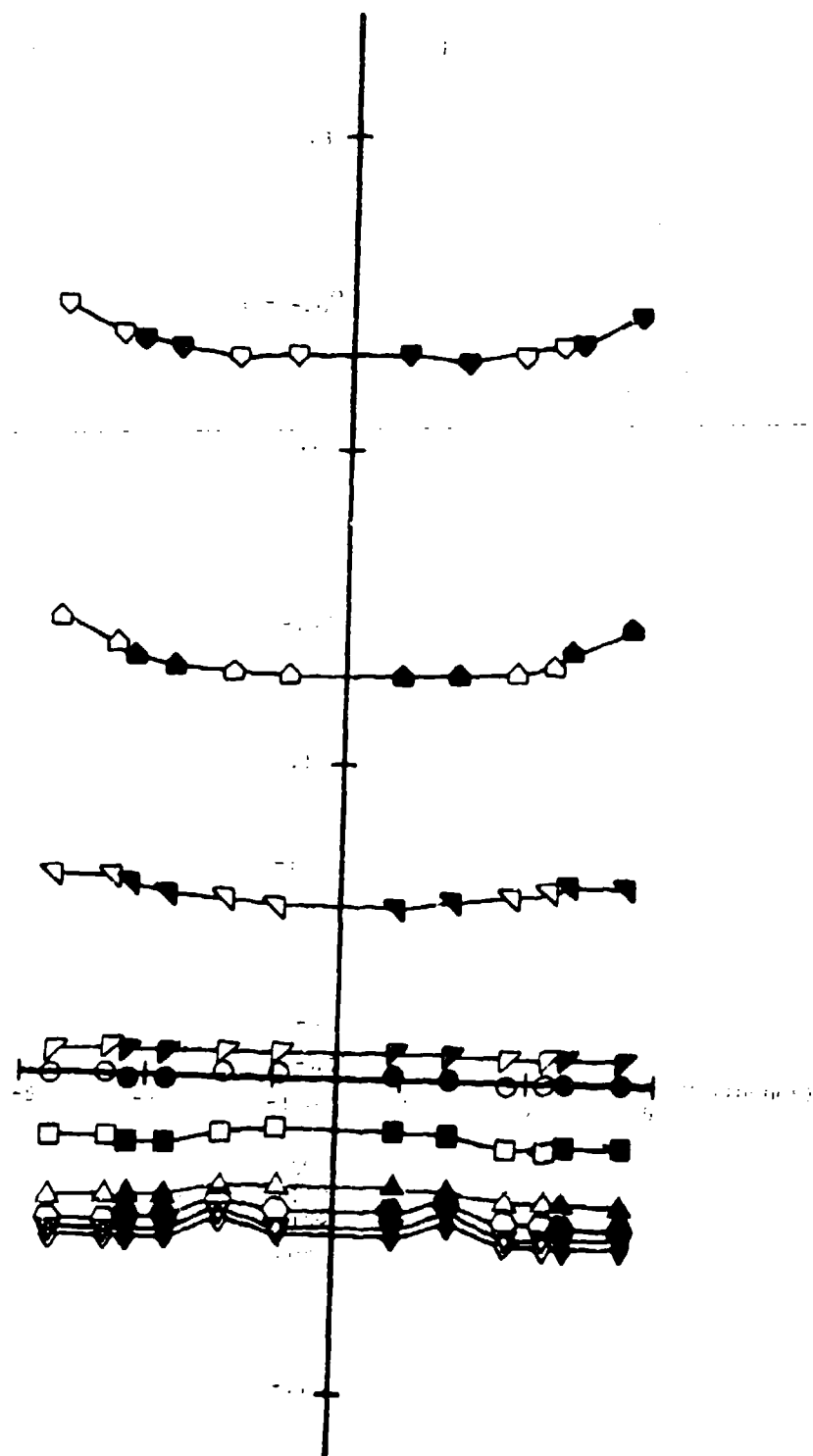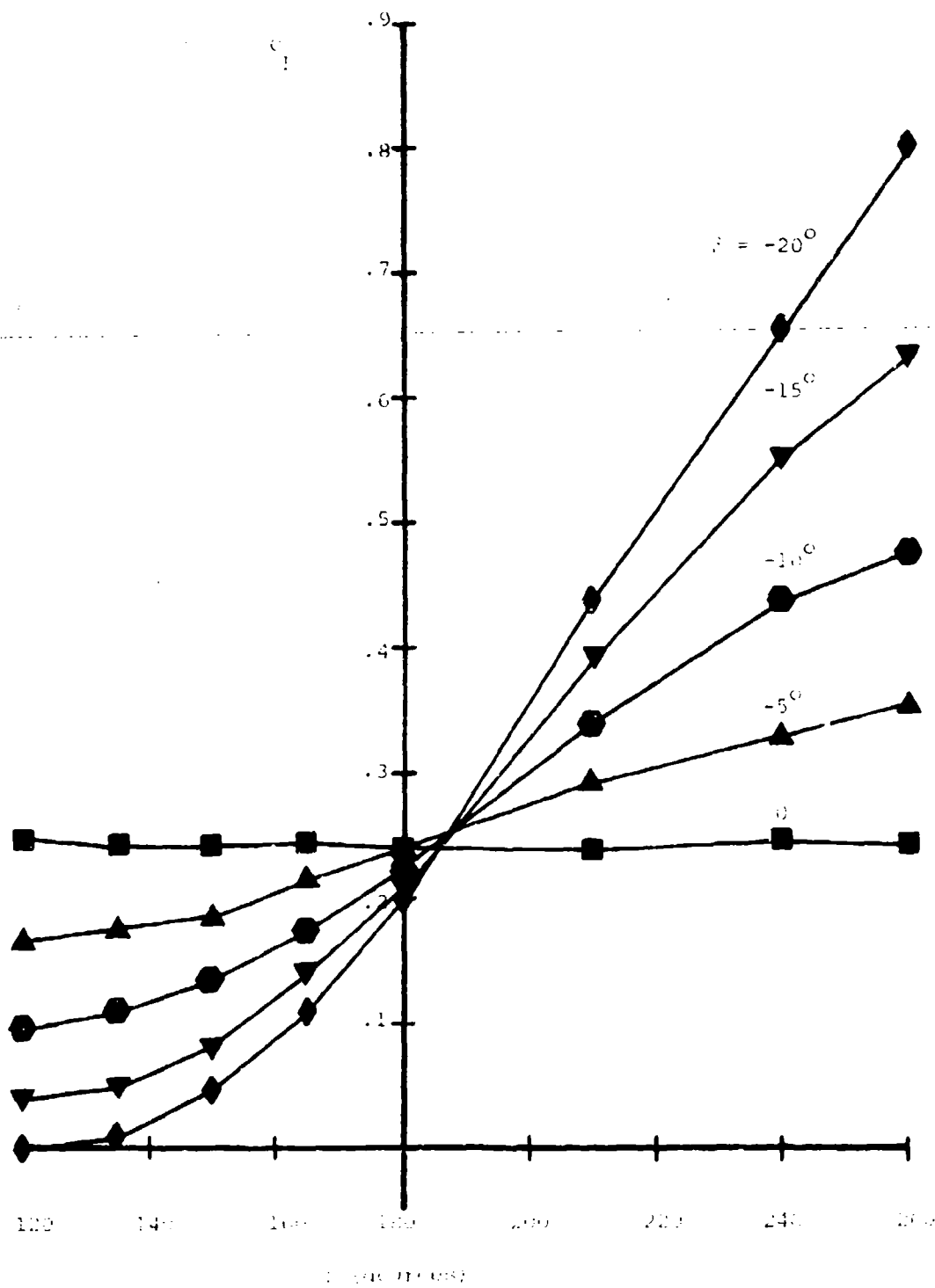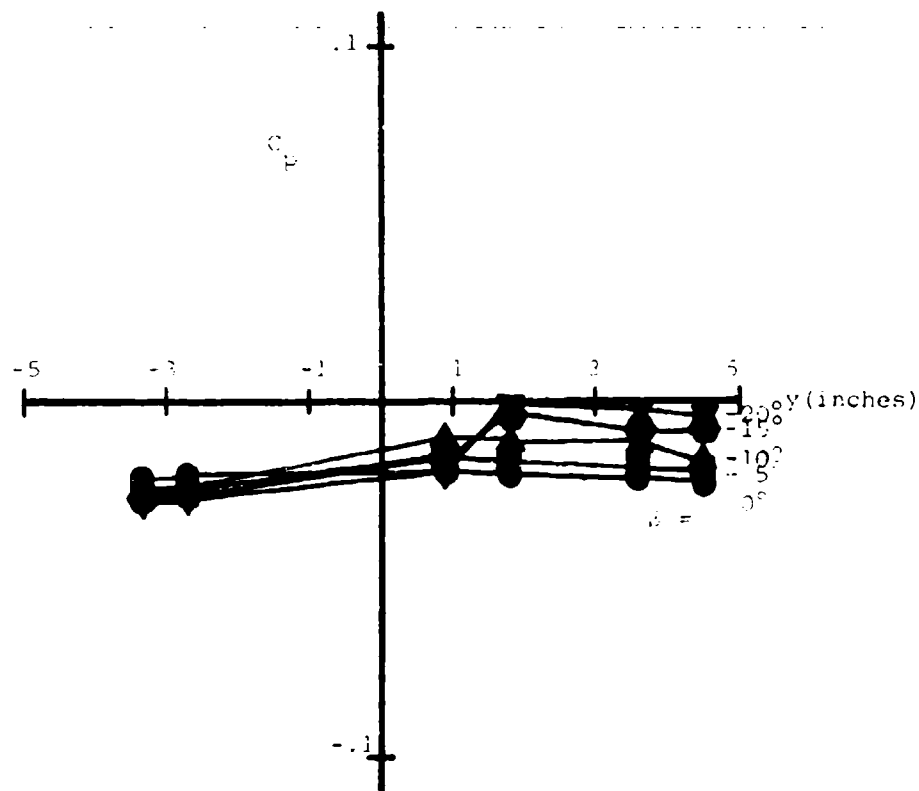Figure 16. Measured Surface Pressure Coefficient on Elliptic Cone Upper and Lower Surface at Various Angles of Attack ($M_\infty = 3$, $\beta = 0$, 0.6 ...)

Figure 164. Measured Surface Pressure Coefficient on Elliptic Cone Waverider Lower Compression Surface at Various Angles of Yaw (M_∞ = 8, α = 0)

Figure 165. Measured Surface Pressure Coefficient on Elliptic Bow Water Jet Upper Surface at Various Angles of Yaw $(U_\infty = 3, \ldots)$

(degrees)
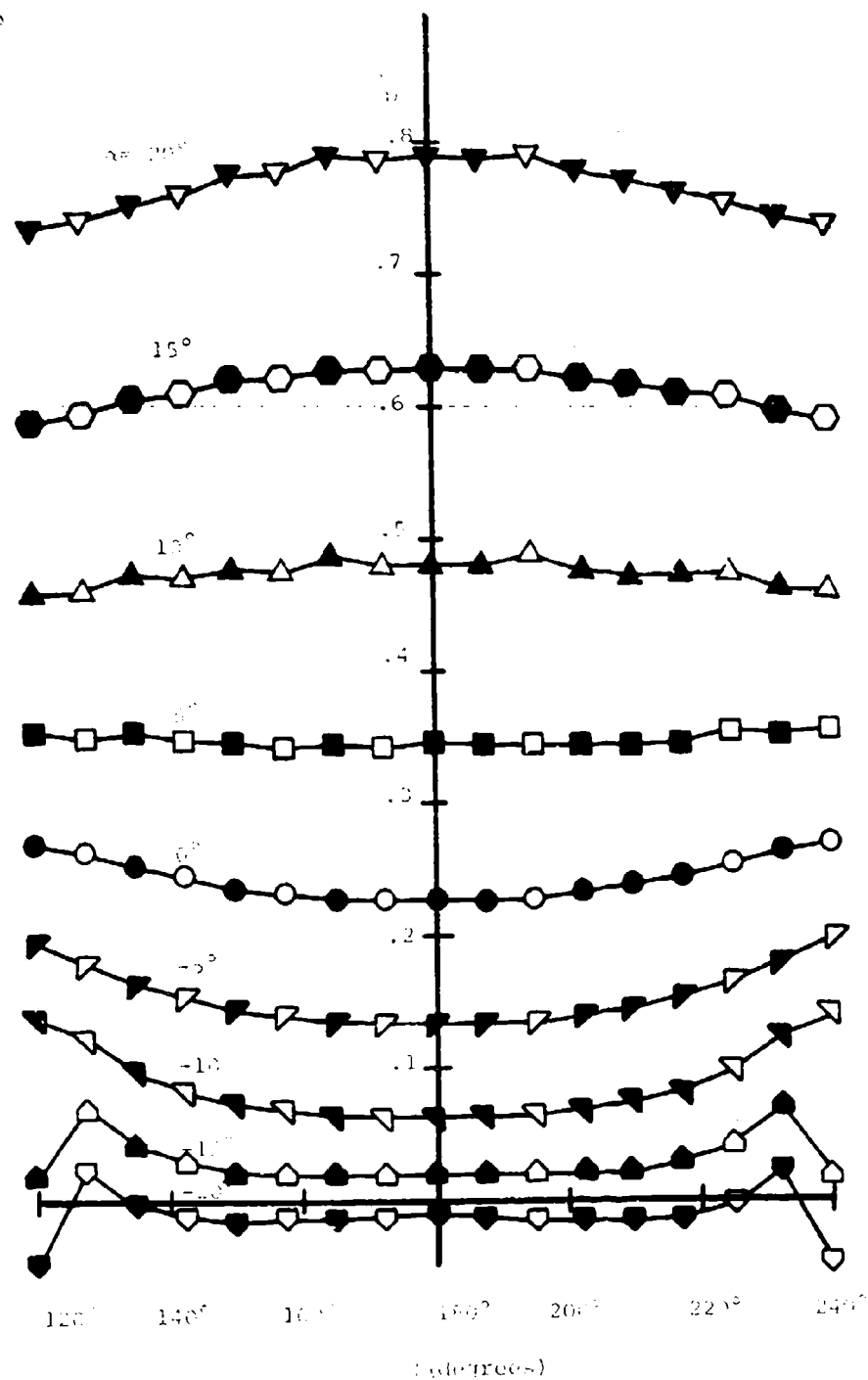
Figure 160. Measured Surface Pressure Coefficient on Elliptic Cone Over-
lying Lower Centerline Surface at Various Angles of Attack
(M_∞=4, open symbols obtained by symmetry.)
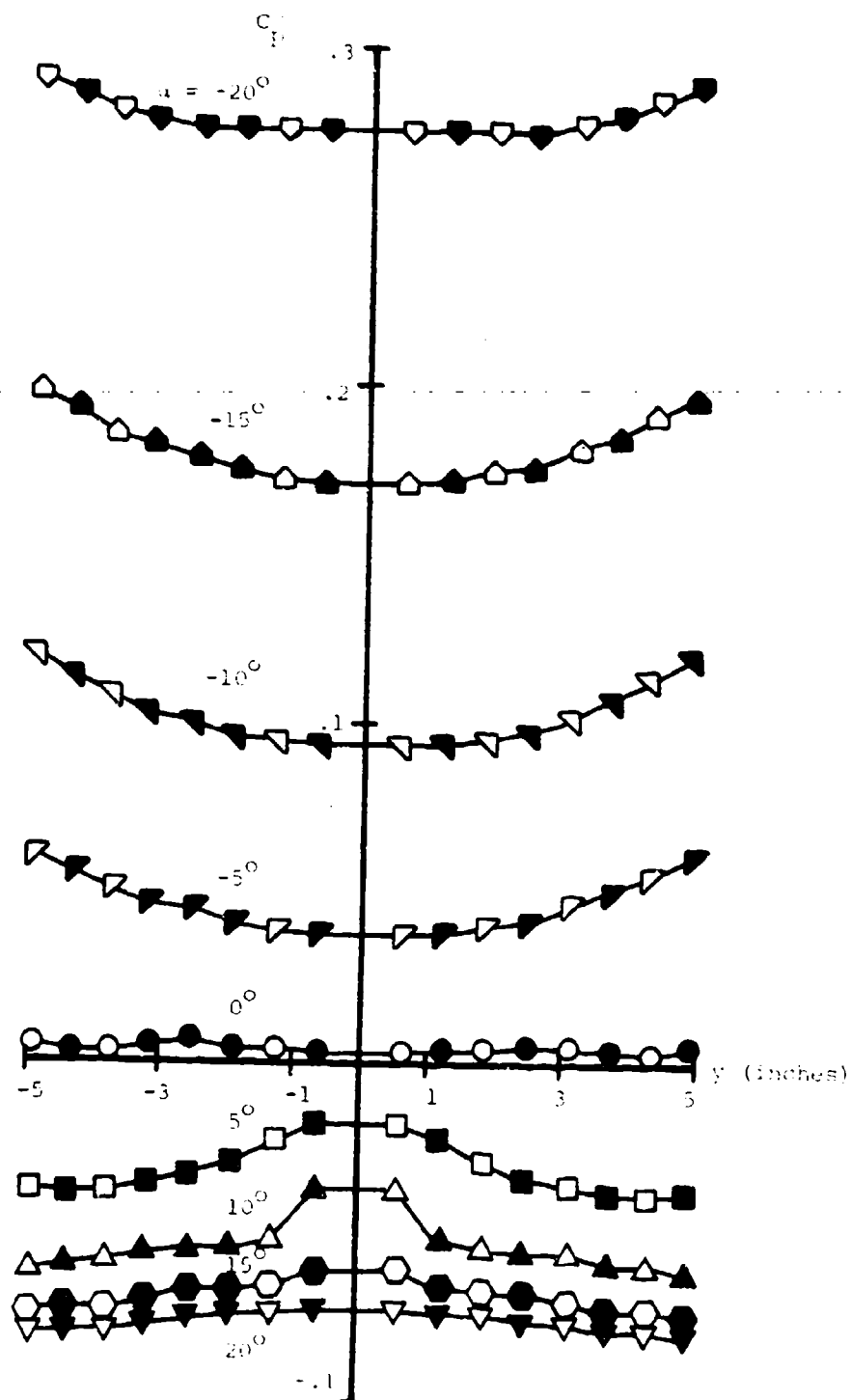
Figure 167. Measured Surface Pressure Coefficient on Elliptic Cone Waverider Upper Surface at Various Angles of Attack ($M_\infty = 4$, $a = 5$, zero yaw symmetry)
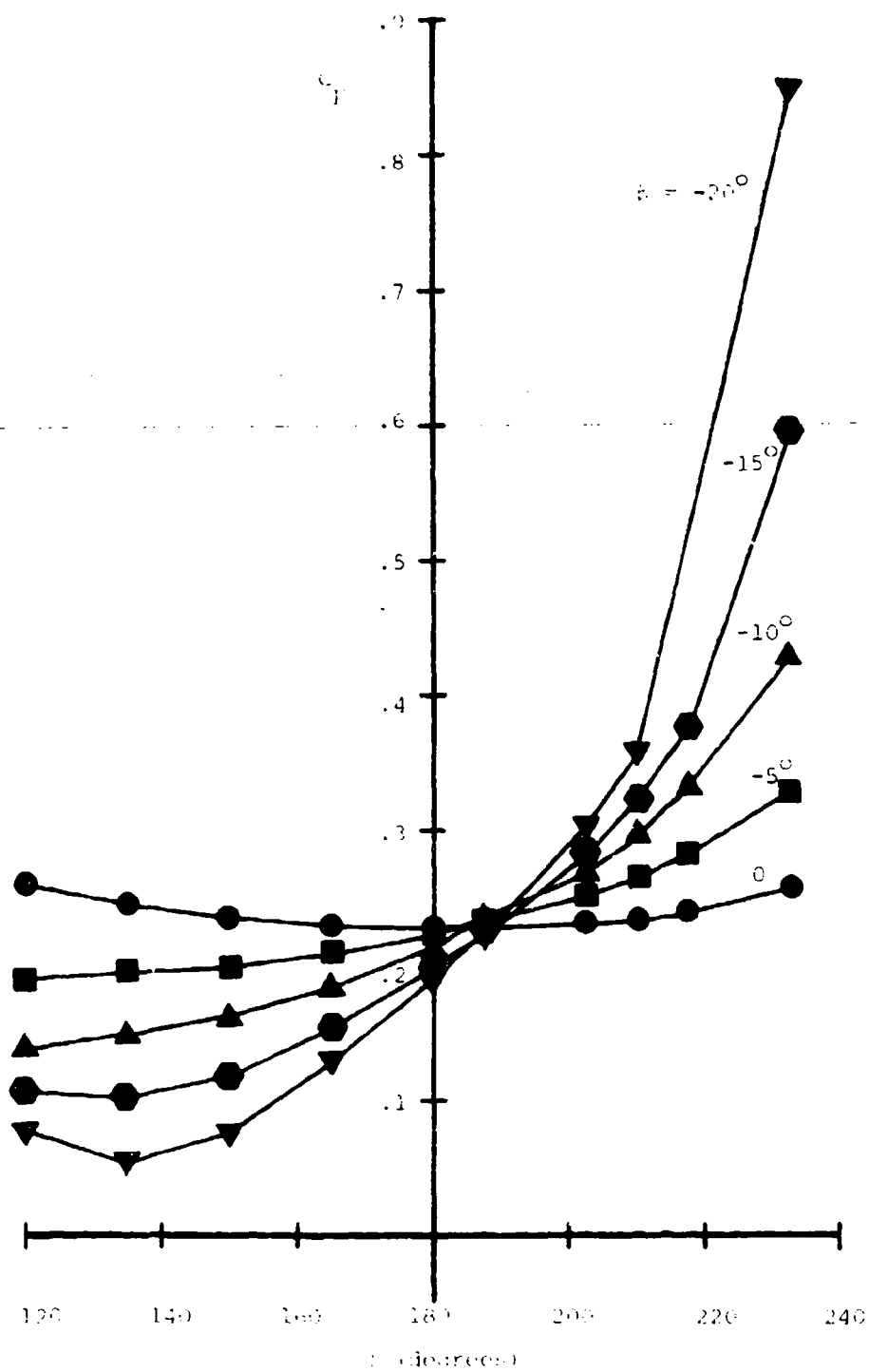
Figure 168   Measured Surface Pressure Coefficient on Elliptic Cone
Waverider Lower Compression Surface at Various Angles of
Yaw ($M_\infty = 4$, $\alpha = 0$)
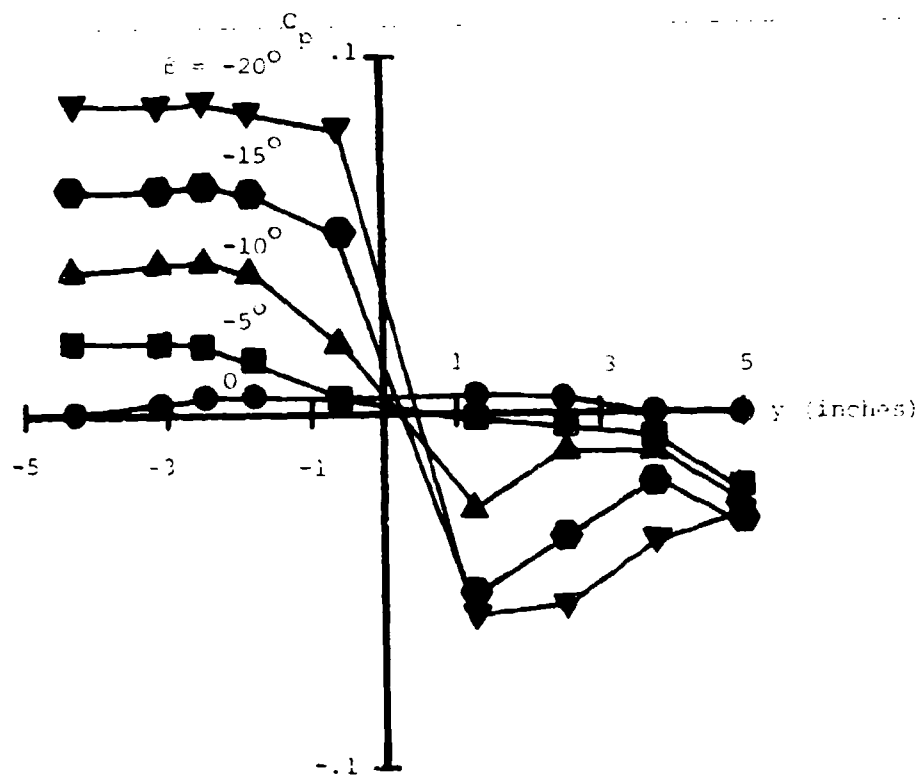
Figure 169. Measured Surface Pressure Coefficient on Elliptic Cone
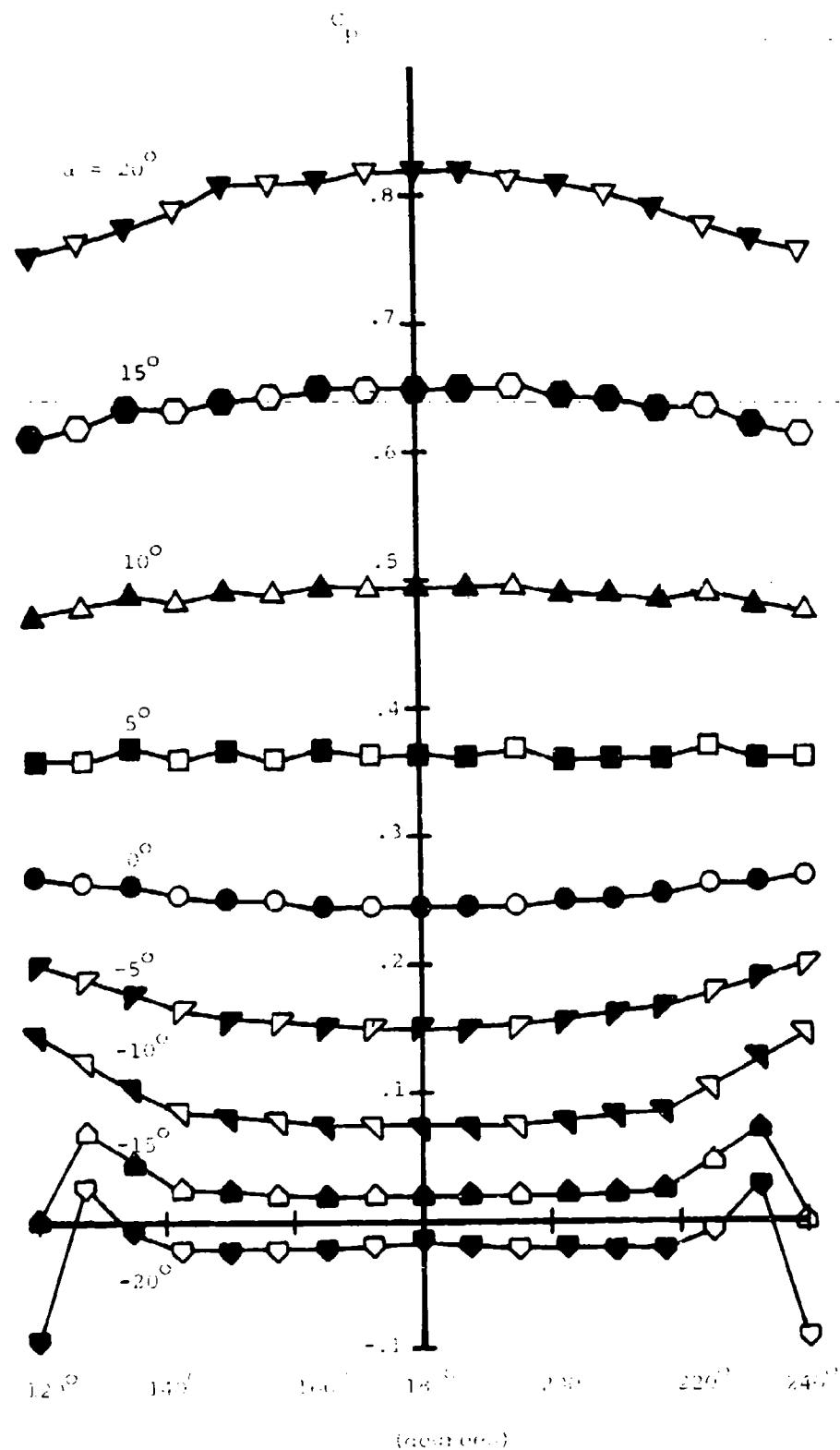Waverider Upper Surface at Various Angles of Yaw
$(M_\infty = 4, \ \alpha = 0)$
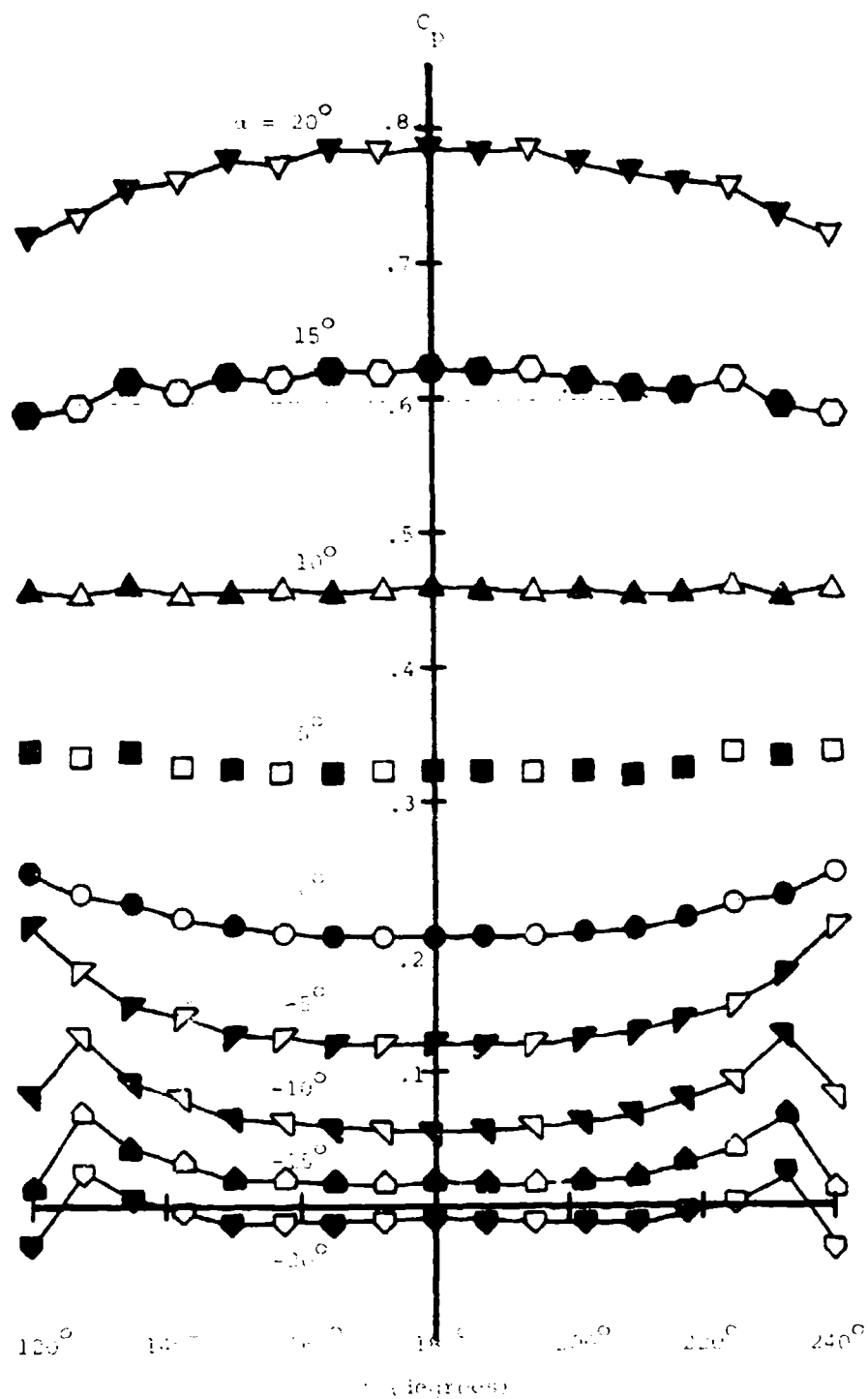
Figure 170. Measured Surface Pressure Coefficient on Elliptic Cone
Waverider Lower Compression Surface at Various Angles of
Attack ($M_\infty = 5$, ..., open symbols obtained by symmetry)
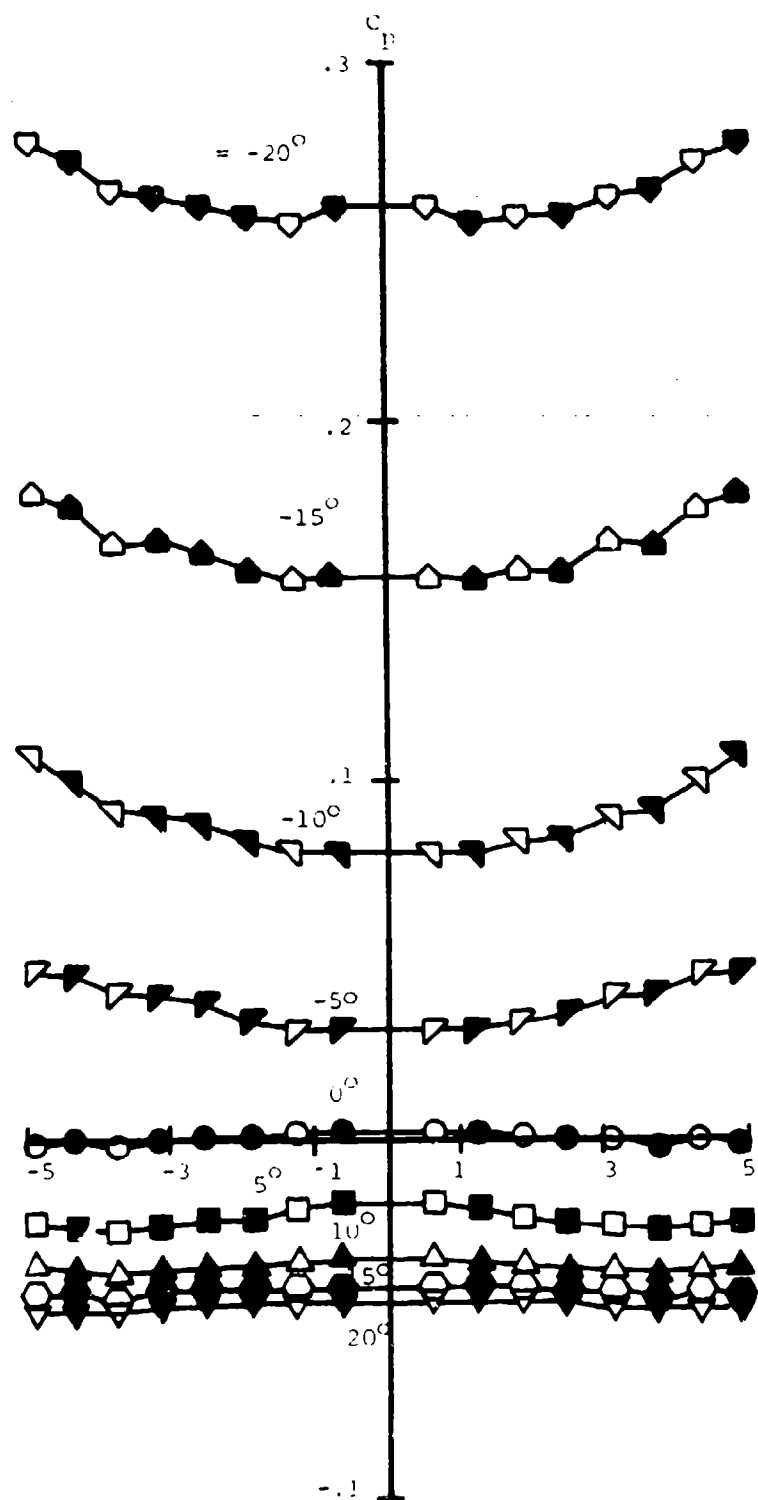
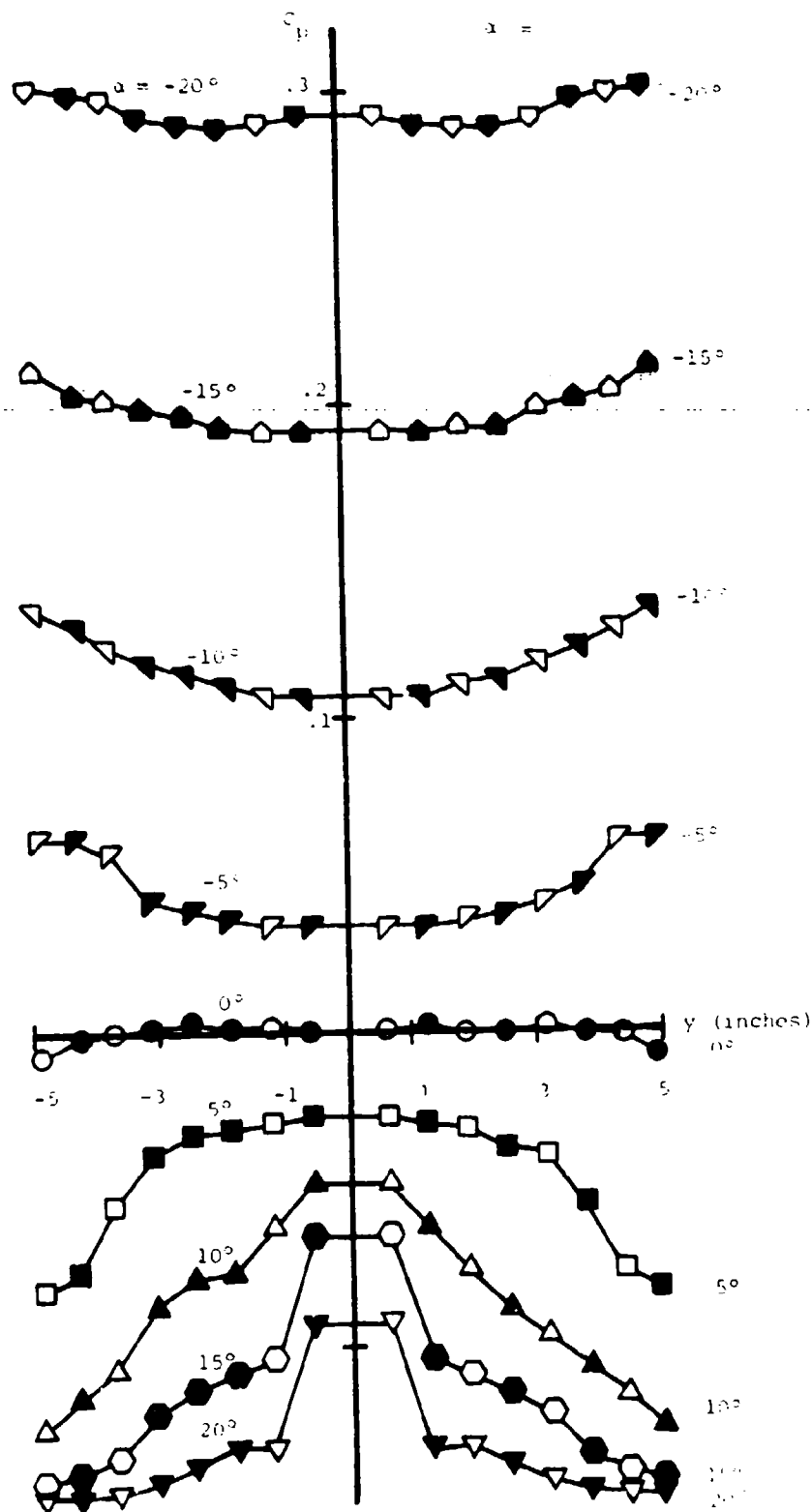Figure 171. Measured Surface Pressure Coefficient on Elliptic Cone Waverider - Upper Surface at Various Angles of Attack ($M_\infty = 5$, $\gamma = 8$, solid symbols obtained by symmetry)
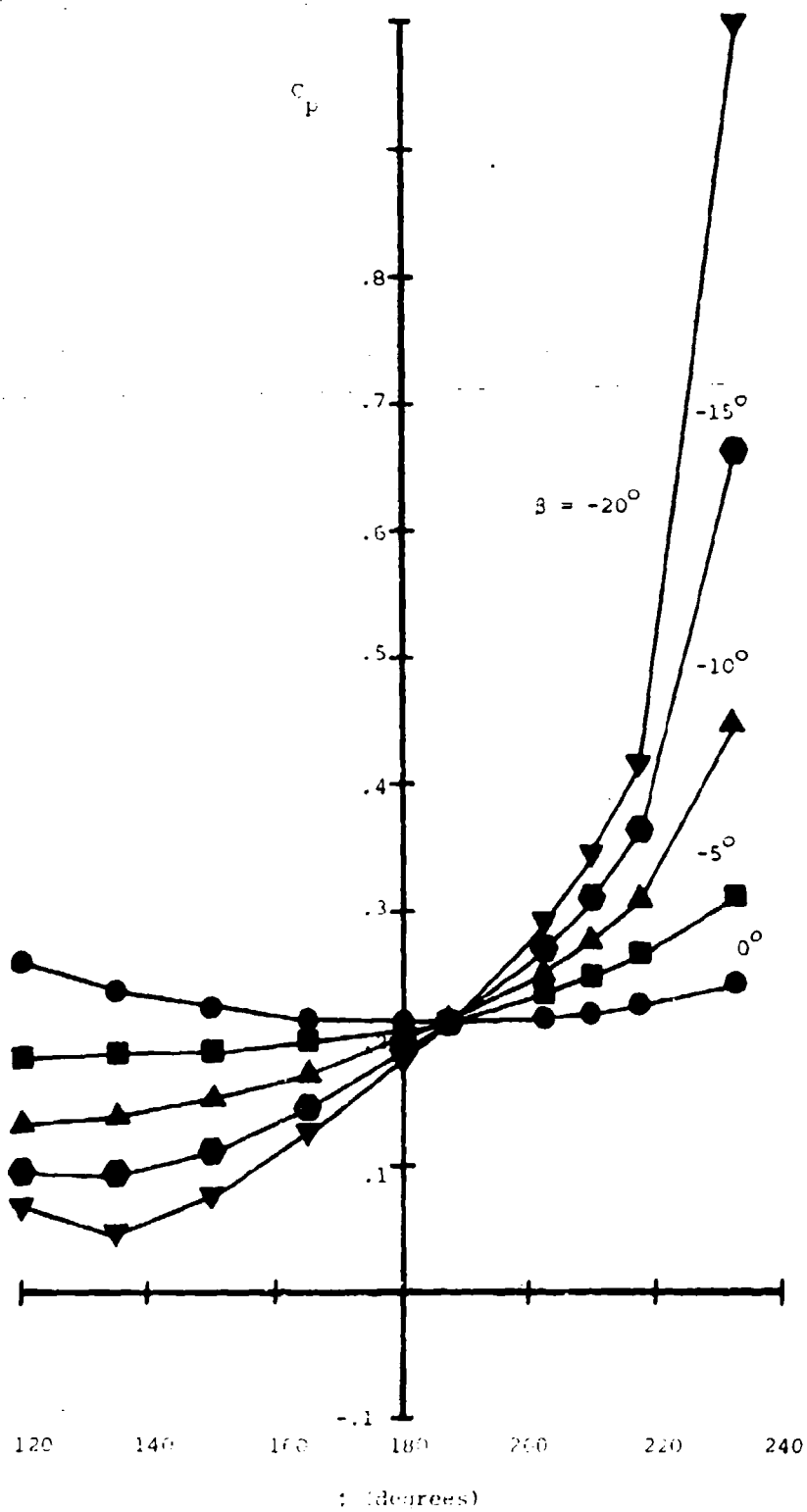
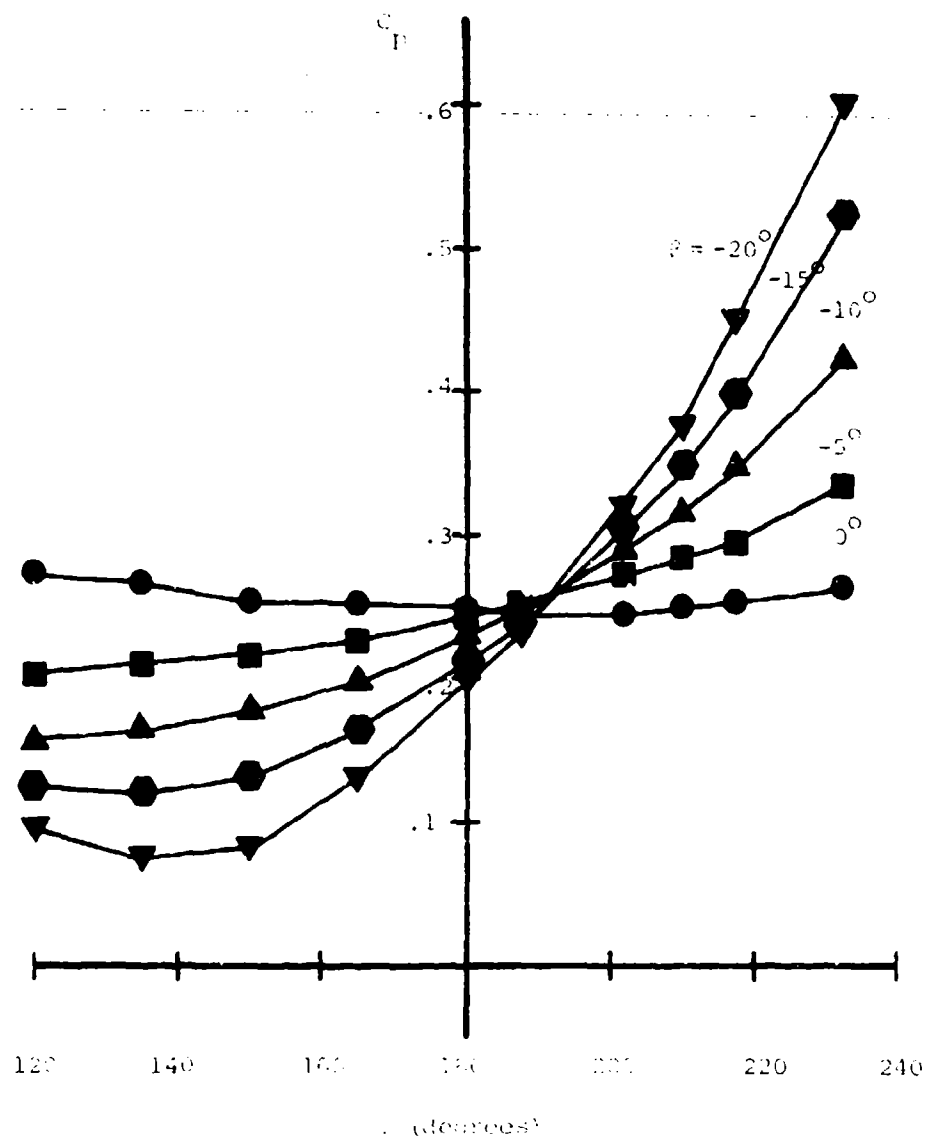Figure 172. Measured Surface Pressure Coefficient on Elliptic Cone Waverider Lower Compression Surface at Various Angles of Yaw ($M_\alpha = 5$, $\iota = 0$)
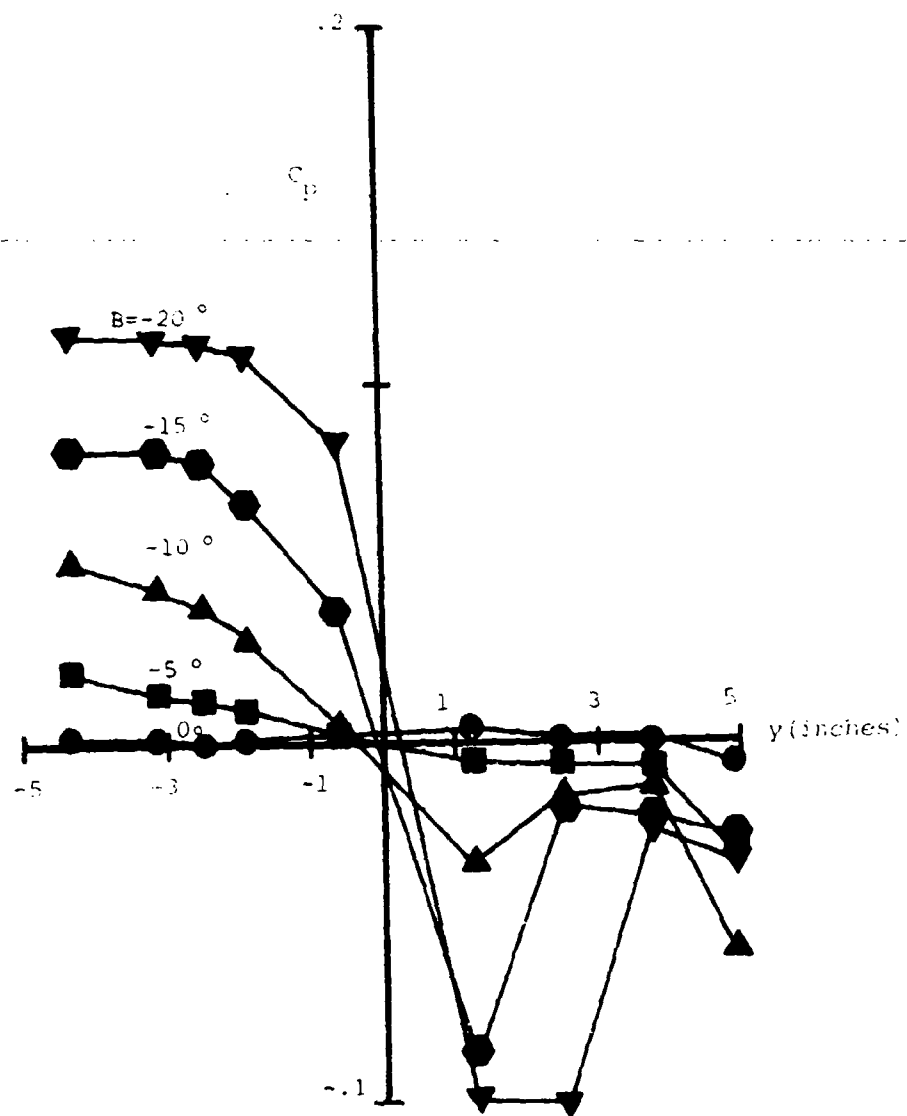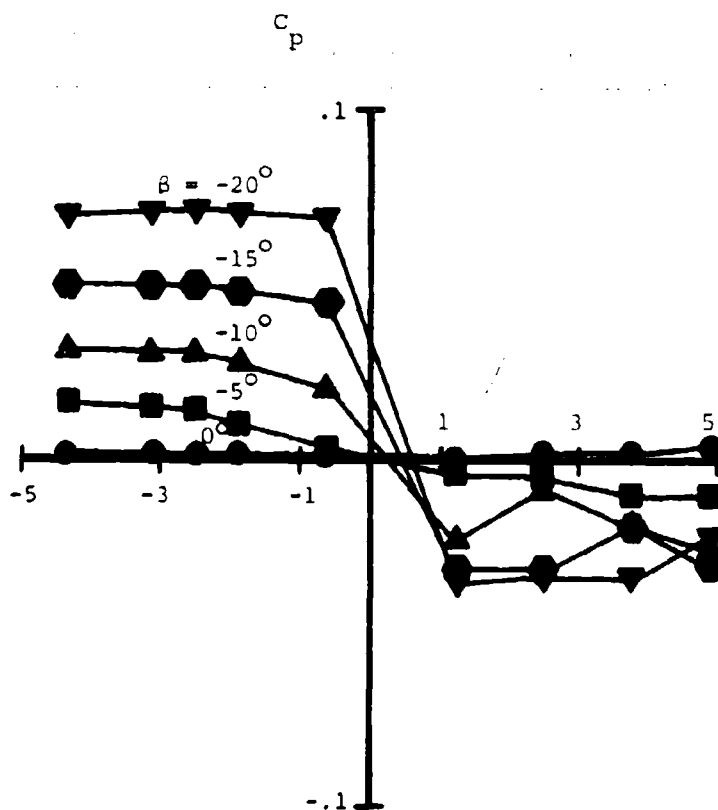
Figure 173 . Measured Surface Pressure Coefficient on Elliptic Cone Waverider
Upper Surface of Various Angles of Yaw ($M_\infty = 5$, $\alpha = 0$)

were always conical and clean, without strong secondary shocks or separations over the entire range of testing conditions. These tests taken with the supporting theoretical background make the cone-derived waveriders very attractive and viable contenders for future hypersonic missile and aircraft configurations.

SECTION V

CONCLUDING REMARKS

The results of a combined theoretical and experimental research program, pertaining to a new class of supersonic lifting bodies, have been presented. The theoretical program is based on a perturbation analysis of the basic axisymmetric steady flow past a cone. Approximate analytic results are obtained and cast within the framework of hypersonic small-disturbance theory. The results are particularly appropriate for parametric studies. The experimental program verified the theoretical analyses of two waverider configurations for the on-design condition. Moreover, it provided information for off-design conditions for which no theoretical method of calculation is presently available. The combined results indicate that the new waverider configurations are strong contenders for modern missile design technology requiring high L/D ratios, good volumetric storage, high maneuverability, and low radar signatures.

The experimental program for the contract period of this report also contained windtunnel tests on the two waverider models at $M_\infty = 8$ for forces and moments, schlieren data, and oil-flow data. The results of these tests were obtained too late to be included in this report, but some of the results are reported elsewhere (Reference 74). The complete results of these tests will be described in the final report for the succeeding contract period of this research program.

Future work pertaining to the aerodynamics of cone-derived waveriders will be undertaken in a follow-on research program. This program will include configuration optimization, blended inlets, boundary-layer development, and static and dynamic stability performance.

REFERENCES

1. Nonweiler, T. R. F., "Delta Wings of Shape Amenable to Exact Shock Wave Theory." J. Royal Aero. Soc., Vol. 67, 1963, p. 39.

2. Kuchemann, D., "Hypersonic Aircraft and Their Aerodynamic Problems." Progress in Aeronautical Sciences, Vol. 6, Edited by D. Kuchemann and L. H. G. Stern, Pergamon Press, London, 1965, p. 271.

3. Kuchemann, D. and Weber, J., "An Analysis of Some Performance Aspects of Various Types of Aircraft Designed to Fly Over Different Ranges at Different Speeds." Progress in Aeronautical Sciences, Vol. 9, Edited by D. Kuchemann, et al, Pergamon Press, London, 1968, p. 329.

4. Jones, J. G., "A Method for Designing Lifting Configurations for High Supersonic Speeds Using the Flow Fields of Non-Lifting Cones." R.A.E. Report No. Aero 2624, A.R.C. 24846, 1963.

5. Rasmussen, M. L., "Lifting-Body Configurations Derived from Supersonic Flows Past Inclined Circular and Elliptic Cones." AIAA Paper 79-1665, August, 1979.

6. Chiang, C. W., and Wagner, R. D., "Analysis of Supersonic Conical Flows." NASA TN D-5884, 1970.

7. Babenko, K. I., Voskresenskii, G. P., Lyubimov, A. N., and Rusanov, V. V., "Three Dimensional Flow of Ideal Gas Past Smooth Bodies." NASA TT F-380, 1966.

8. Kutler, P., Applications of Selected Finite Differences Techniques to the Solution of Conical Flow Problems, Ph.D. Dissertation, Iowa State University, Ames, Iowa, 1969.

9. Klunker, E. B., South, J. C., and Davis, R. M., "Calculation of Nonlinear Conical Flows By the Method of Lines." NASA TR R-374, 1971.

10. South, J. C., "Application of the Method of Integral Relations to Supersonic Nonequilibrium Flow Past Wedges and Cones." NASA TR R-205, 1964.

1 . Van Dyke, M. D., "The Slender Elliptic Cone as a Model for Nonlinear Supersonic Flow Theory." Journal of Fluid Mechanics, Vol. 1, Part 1, 1956, pp. 1-15.

12. Chapkis, R. T., "Hypersonic Flow Over an Elliptic Cone: Theory and Experiment." Journal of the Aeronautical Sciences, Vol. 28, No. 11, 1961, pp. 844-854.

13. Ferri, A., Ness, N., and Kaptita, T., "Supersonic Flow Over Conical Bodies without Axial Symmetry." Journal of the Aeronautical Sciences, Vol. 20, No. 8, 1953, pp. 563-571.

14. Lees, L., "Note on the Hypersonic Similarity Law for an Unyawed Cone." Journal of the Aeronautical Sciences, Vol. 18, No. 9, 1951, pp. 700-702.

15. Mascitti, V. R., "Calculation of Linearized Supersonic Flow Over Slender Cones of Arbitrary Cross Section." NASA TN D-6818, July, 1972.

16. Vaglio-Laurin, R. and Van Dyke, M. D., "A Discussion of Higher-Order Approximations for the Flow Field About a Slender Elliptic Cone." Journal of Fluid Mechanics, Vol. 3, Part 6, 1958, pp. 638-644.

17. Martellucci, A., "An Extension of the Linearized Characterisitcs Method for Calculating the Supersonic Flow Around Elliptic Cones." J. Aero. Sci., Vol. 27, No. 9, 1960, pp. 667-674.

18. Stocker, P. M. and Mauger, F. E., "Supersonic Flows Past Cones of General Cross Section." Journal of Fluid Mechanics, Vol. 13, Part 3, 1962, pp. 383-399.

19. Kaattari, G., "Method for Predicting Pressures on Elliptic Cones at Supersonic Speeds." NASA TN D-5952, August, 1970.

20. Pottseep, L., "Inviscid Hypersonic Flow Over Unyawed Circular Cones." J. Aero. Sci., Vol. 27, No. 7, 1960, p. 558.

21. Rasmussen, M. L., "On Hypersonic Flow Past an Unyawed Cone." AIAA Journal, Vol. 5, No. 8, 1967, pp. 1495-1497.

22. Doty, R. T., "Hypersonic Flow Past an Inclined Cone." M.S. Thesis, Aerospace, Mechanical and Nuclear Engineering, University of Oklahoma, 1972.

23. Doty, R. T. and Rasmussen, M. L., "Approximation for Hypersonic Flow Past an Inclined Cone." AIAA Journal, Vol. 11, No. 9, 1973, pp. 1310-1315.

24. Cheng, H. K., "Hypersonic Flows Past a Yawed Circular Cone and Other Pointed Bodies." Journal of Fluid Mechanics, Vol. 12, 1962, pp. 169-191.

25. Melnik, R. E., "Vortical Singularities in Conical Flow." AIAA Journal, Vol. 5, No. 4, 1967, pp. 631-637.

26. Zakkay, V., and Visich, M., Jr., "Experimental Pressure Distribution on Conical Elliptic bodies at $M_\infty = 3.09$ and 6.0." Polytechnic Institute of Brooklyn, PIBAL Report No. 467, March 1959.

27. Munson, A. G., "The Vortical Layer on an Inclined Cone." Journal of Fluid Mechanics, Vol. 20, 1964, pp. 625-643.

28. Chan, Y. Y., "An Experimental Study of a Yawed Circular Cone in Hypersonic Flow." AIAA Journal, Vol. 7, No. 10, Oct. 1979, pp. 2035-2037.

29. Hayes, W. D., and Probstein, R. F., Hypersonic Flow Theory, Vol. 1, Inviscid Flows, Academic Press, New York, 1966.

30. Epstein, P. S., "On the Air Resistance of Projectiles." Proc. Nat. Acad. Sci. 17, 1931, pp. 532-54".

31. Van Dyke, M. D., "A Study of Hypersonic Small-Disturbance Theory." NACA Report No. 1194, Supersedes Tech. Note No. 3173, 1954.

32. Kranov, N. F., "Aerodynamics of Bodies of Revolution." Elsevier, N.Y., 1970, p. 493.

33. Fisher, L. R., "Equations and Charts for Determining the Hypersonic Stability Derivatives of Combinations of Cone Frustums Computed by Newtonian Impact Theory." NASA TN D-149, November, 1959.

34. Ericsson, L. E., "Generalized Unsteady Embedded Newtonian Flow." Journal of Spacecraft and Rockets, Vol. 12, No. 12, pp. 718-726, December 1975.

35. Mahood, G. E. and Hui, W. H., "Remarks on Unsteady Newtonian Flow Theory," Aeronautical Quarterly, 27, pp. 66-79, 1976.

36. Khalid, M. and East, R. A., "Stability Derivatives of Blunt Slender Cones at High Mach Numbers." Aeronautical Quarterly, pp. 559-589, November, 1979.

37. Khalid, M. and East, R. A., "High Mach Number Dynamic Stability of Pointed Cones at Small Angles of Attack." AIAA Journal, Vol. 18, No. 9, pp. 1263-1265, 1980.

38. McIntosh, S. C, "Hypersonic Flow Over an Oscillating Wedge." AIAA Journal, Vol. 3, No. 3, pp. 433-440, 1965.

39. Barron, R. M., "Oscillating Airfoils: Part I. Wedges of Arbitrary Thickness in Supersonic and Hypersonic Flow." AIAA Journal, Vol. 16, No. 10, pp. 1076-1083, 1978.

40. Barron, R. M., and Mandl, P., "Oscillating Airfoils: Part II. Newtonian Flow Theory and Application to Power-Law Bodies in Hypersonic Flow." AIAA Journal, Vol. 16, No. 11, pp. 1132-1138, 1978.

41. Fleeter, S. and Riffel, R. E., "Time-Variant Aerodynamics of Oscillating Airfoil Surfaces in a Supersonic Flowfield." AIAA Journal, Vol. 17, No. 5, pp. 465-470, 1979.

42. Tobak, M. and Wehrend, W. R., "Stability Derivatives of Cones at Supersonic Speeds." NACA Technical Note 3788, September, 1956.

43. Zartarian, G., Hsu, P. T., and Ashley, H., "Dynamic Airloads and Aeroelastic Problems of Entry Mach Numbers." Journal of Aerospace Sciences, Vol. 28, March, 1961.

44. Kawamura, R. and Tsien, F-H, "Aerodynamic Stability Derivatives of Axisymmetric Bodies Moving at Hypersonic Speeds." Proceedings of the Third International Congress in the Aeronautical Sciences, Spartan-MacMillan, Washington, pp. 827-835, 1964.

45. Brong, E. A., "The Flow Field About a Right Circular Cone in Unsteady Flight." General Electric Company Report FDL-TDR-64-148, 1964.

46. Brong, E. A., "The Flow Field About a Right Circular Cone in Unsteady Supersonic Flight," AIAA Paper 65-398, 1965.

47. Hsu, P. T., "Solution of the Supersonic Flow Field Around an Oscillating Circular Cone." M.I.T. Fluid Dynamics Research Laboratory Report 64-5, Massachusetts Institute of Technology, December, 1964.

48. McIntosh, S. C., "Studies in Hypersonic Flow Theory." Ph.D. Thesis. Department of Aeronautics and Astonautics, Stanford University, 1965.

49. Orlik-Ruckemann, K. J., "Simple Formulas for Unsteady Pressure on Slender Wedges and Cones in Hypersonic Flow." J. of Spacecraft and Rockets, Vol. 6, No. 1, pp. 1209-1211, 1969.

50. Orlik-Ruckemann, K. J., "Oscillating Slender Cone in Viscous Hypersonic Flow." AIAA Journal, Vol. 10, No. 9 pp. 1139-1140, 1972.

51. Rasmussen, M. L., "Lifting-Body Configurations Derived from Supersonic Flows Past Inclined Circular and Elliptic Cones." AIAA Paper 79-1665. Proceedings of AIAA Atmospheric Flight Mechanics Conference for Future Space Systems, pp. 295-305. Boulder, Colorado, August 6-8, 1979.

52. Rasmussen, M. L. and Lee, H. M., "Approximation for Hypersonic Flow Past a Slender Elliptic Cone." AIAA Paper 79-0364. AIAA 17th Aerospace Sciences Meeting, New Orleans, LA, January 15-17, 1979.

53. Jischke, M. C., "Supersonic Flow Past Conical Bodies with Nearly Circular Cross Sections." AIAA Paper 80-0028. AIAA 18th Aerospace Sciences Meeting, Pasadena, CA, January 14-16, 1980.

54. Sims, J. L., "Tables for Supersonic Flows Around Right Circular Cones of Small Angle of Attack." NASA SP-3007, 1964.

55. Giragosian, P. A., "Critical Aerodynamic Technology Issues in Air-to-Air Missile Design." AIAA Paper 79-0089, presented at the AIAA Aerospace Sciences Meeting, New Orleans, LA, January, 1979.

56. Nielsen, J. N., "Missile Aerodynamics - Past, Present, Future." AIAA Paper 79-1819, presented at the AIAA Aircraft Systems and Technology Meeting, New York, NY, August 1979.

57. Rasmussen, M. L., "Lifting-Body Configurations Derived from Supersonic Flows Past Inclined Circular and Elliptic Cones." AIAA Paper 79-1665, presented at the AIAA Atmospheric Flight Mechanics Meeting, Denver, CO, August 1979.

58. Jischke, M. C., "Supersonic Flow Past Conical Bodies with Nearly Circular Cross-Sections." AIAA Paper 80-0028, presented at the AIAA Aerospace Sciences Meeting, Pasadena, CA, January 1980.

59. Sychev, V. V., "On the Theory of Hypersonic Gas Flow with a Power Law Shock Wave." J. Appl. Math. Mech., Vol. 24, pp. 7560765, 1960.

60. Guiraud, J. P., "Asymptotic Theory in Hypersonic Flow." Proc. International Symposium on Fundamental Phenomena in Hypersonic Flow (J. G. Hall, ed.), Cornell Univ. Press, Ithaca, NY, pp. 70-84, 1966.

61. Yakura, J. K., "Theory of Entropy Layers and Nose Bluntness in Hypersonic Flow." Hypersonic Flow Research, Vol. 7 (F. R. Riddell, ed.), Academic Press, New York, pp. 421-470, 1962.

62. Fiorino, T. D., "An Integral Approximation for Shock Shapes Over Slender Bodies in Inviscid Hypersonic Flow." Ph.D. Dissertation, University of Oklahoma, Norman, Oklahoma, 1970.

63. Schneider, W., "A Uniformly Valid Solution for the Hypersonic Flow Past Blunted Bodies." J. Fluid Mech., Vol. 31, pt. 2, pp. 397-415, 1968.

64. Fiorino, T. D. and Rasmussen, M. L., "Integral Approximation for Slender Body Shock Shapes in Hypersonic Flow." AIAA Journal, Vol. 12, pp. 1735-1737, 1974.

65. Hayes, W. D., "On Hypersonic Similitude." Quarterly of Applied Mathematics, Vol. 5, pp. 105-106, 1947.

66. Busemann, A. and Walcher, O., "Profilergenschaften bei ueber schallgeschwindigkeit." Forschung aus dem Gebeit des Ingenieurwewsens, Vol. 4, 1933.

67. Venn, J. and Flower, J. W., "Shock Patterns for Simple Caret Wings." J. Roy. Aero. Soc. 74, 1970, pp. 339-348.

68. Nardo, C. T., "Aerodynamic Characteristics of Two-Dimensional Waverider Configurations." AIAA Journal, Vol. 10, No. 9, 1972, p. 1258.

69. Woods, B. A., "The Construction of a Compression Surface Based on an Axisymmetrical Conical Flow Field." R.A.E. Tech. Note No. Aero 2900, A.R.C. 25087, 1963.

70. Squire, L. C., "The Aerodynamics of Lifting Bodies at High Supersonic Speeds." J. Roy. Aero. Soc. 75, 1971, p. 18.

71. Linnell, R. D., "Two-Dimensional Airfoils in Hypersonic Flows." Journal of Aeronautical Sciences, Vol. 16, 1949, pp. 22-30.

72. Test Facilities Handbook (Eleventh Edition), "Von Karman Gas Dynamics Facility, Vol. 3." Arnold Engineering Development Center, Arnold Air Force Station, Tennessee, June 1979.

73. Lanham, D. L., "Static Force, Pressure, and Oil-Flow Visualization Tests of Supersonic Aerodynamic Lifting Bodies at Mach Numbers 3 to 5." AEDC TSR-80-V12, Arnold Engineering Development Center, Arnold Air Force Station, Tennessee, February 1980.

74. Rasmussen, M. L., Daniel, D. C., and Jischke, M. C., "Supersonic Aerodynamics of a Class of Cone-Derived Waveriders," 12th Navy Symposium on Aeroballistics, David W. Taylor Naval Ship Research and Development Center, May 1981.

APPENDIX A

SIMPLE APPROXIMATIONS FOR THE WAVERIDERS

The pressure coefficient on the shock layer of the on-design waveriders has the form

$$C_p(\theta,\phi) = c_{p0}(\theta) + \alpha\, C_{p0}(\theta) \cos\phi + \epsilon_2 C_{p2}(\theta) \cos 2\phi \qquad (A-1)$$

Where c_{p0} is for the basic circular cone, c_{p0} is the angle-of-attack perturbation of the basic cone and C_{p2} the eccentricity perturbation of the basic cone. Integration of the pressure over the surface leads to the forces and moments on the waveriders, for which no simple general expression can be obtained. A simple approximation, however, can be obtained in the following way.

Consider axisymmetric supersonic flow past a circular cone of semivertex angle δ with a conical shock of semivertex angle β. Any plane passing through the cone axis is a stream surface in the shock layer. Choose any two axial planes oriented with an angle Λ from a horizontal axial plane. Select the portion of these planes between the body and shock as infinitesimal-thickness delta wings, and construct the ideal conical waverider shown in Figure A-1. The angle Λ is called the dihedral angle. The area of the base for slender cones is $A_b = \pi L^2 \delta^2 (1+2\Lambda/\pi)/2$, and the planform area projected on the horizontal plane is $L^2\beta \cos\Lambda$. If the pressure in the shock layer is taken as a constant, then Equations (659) and (660) for the normal-force and axial-force coefficients can be easily derived.

For the circular-cone and elliptic-cone waveriders depicted in Figure 121 an average value of C_p from Equation (A-1) and a suitable modification of the base area and shock angle could be used. The simplest approximation occurs when the basic-cone results are used:
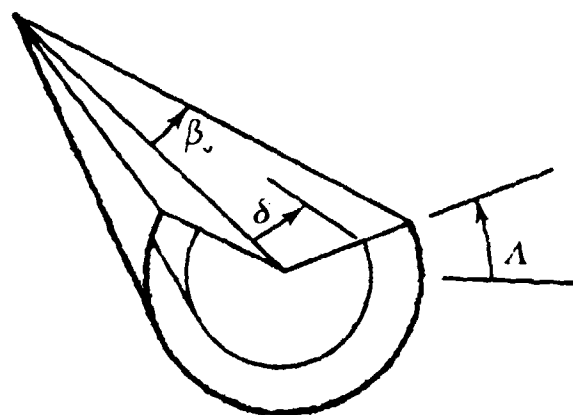
Figure A-1. Idealized Conical Waverider

$$\sigma^2 = \beta^2/\delta^2 = (\gamma+1)/2 + 1/\kappa\delta^2 \quad , \tag{A-2}$$

$$\frac{C_{pp}(\delta)}{\delta^2} = 1 + \frac{\sigma^2 \ln \sigma^2}{\sigma^2-1} \quad , \tag{A-3}$$

INITIAL DISTRIBUTION

DTIC/DCA	2	DR F. R. DEJARNETTE, N.C. STATE UNIV	1
AUL/LSE	1	DR DAVE WHITFIELD, MISS STATE UNIV	1
ASD/ENFEA	1	DR LEWIS SCHIFF NASA AMES RES CTR	1
AFATL/DLODL	2	MR CHARLEY JACKSON NASA LANGLEY RES	
AFATL/CC	1	CENTER	1
HQ USAF/SAMI	1	DR LEON SCHINDEL NSWC	1
OO-ALC/MMWMC	2	MR V. DAHLEM AFWAL/FIM	1
AFIS/INOT	1	HUGHES ACFT CO/MR D. CARLSON	1
ASD/ENESS	1	MCDONNELL DOUGLAS/DR ROBERT KREIGER	1
HQ TAC/DRA	1	NORTHROP CORP/HEINZ GERHARDT	1
HQ USAFE/DOQ	1	VOUGHT CORP/DR C. H. HAIGHT	1
HQ PACAF/DOOQ	2	VOUGHT CORP/J. A. WOLFE	1
HQ TAC/INAT	1	NEAR, INC/DR MICHAEL HEMSCH	1
ASD/XRX	1	AEDC ARNOLD AFS TN/LARRY TRIMMER	1
USA TRADOC SYS ANAL ACT TECH LIB	1	NEAR INC/M.M. BRIGGS	1
COMIPAC/PT-2	1	ADVANCED FLUID MECHANICS/ALAN RATLIFF	1
HQ PACAF/OA	1	GENERAL ELEC CO/DR JAMES DAYWITT	1
SAFALR	1	TECHNOLOGY INC/DALE GEPKIN	1
HQ AFSC/DLW	1	BENDIX CORP/PAUL A MURAD	1
HQ AFSC/IGFW	1	UNIV OF TEXAS/DR JOHN BERTIN	1
HQ AFSC/SDZ	1	AFOSR/NA	1
AFWAL/MLTM	1	GRUMMAN AEROSPACE CORP/G. KUTZ	1
AFWL/NTSA	2	GRUMMAN AEROSPACE CORP/C. DRAGOWITZ	1
REDSTONE SCI INFO CTR DRSMI-RPR	2	GENERAL DYNAMICS CORP/JOE LORIA	2
NAV RESEARCH LAB CODE 2627	1	MARTIN MARIETTA AEROSPACE/J. WILLIAMS	3
NAV SYS CMD AIR VEHICLE DIV	1	BOEING CORP/NICHOLAS MALAMBI	1
NAV SYS CMD TECH LIB	1	UNIV OF OKLAHOMA/DR MARTIN JISCHKE	2
NAV SURF WPN CTR CODE X211	1		
USNC CODE 3431	1		
SANDIA NATIONAL LABS TECH LIB	1		
RAND CORPORATION LIBRARY D	1		
BATTELLE COLUMBUS LAB TACTEC RED CTR	1		
NAV WPNS EVAL FAC CODE 80	1		
USNWC CODE 3163	1		
AFATL/DLY	1		
AFATL/DLJC	3		
DR RASMUSSEN, UNIV OF OKLAHOMA	15		
USA MTL CMD DRSMI-RDK	1		
AFATL/DLA	1		
AFATL/DLMA	1		
AFATL/DLDL	1		
AD/XRC	1		
AD/SDE	1		
AD/SD4	1		
AD/SD102	1		
AD/YMC	1		
3246 TESTW/T7	1		
AD/CZ	1		
DR MARK CLARKSON UNIV OF FL	1		
R. C. NELSON, UNIV OF NOTRE DAME	1		

SUPPLEMENTARY

INFORMATION

ERRATA

AFATL-TR-81-19

AERODYNAMICS OF SUPERSONIC LIFTING BODIES

AIR FORCE ARMAMENT LABORATORY

ARMAMENT DIVISION

EGLIN AIR FORCE BASE, FLORIDA 32542

Remove cover, Form 1473, and preface and insert attached pages.
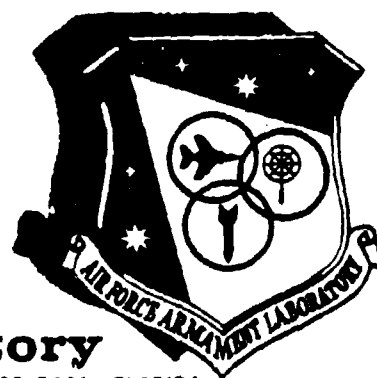
AFATL-TR-81-19

Aerody‑‑‑‑‑s Of Supersonic Lifting ‑oo‑es

M C Jischke
M L Rasmussen

UNIVERSITY OF OKLAHOMA
SCHOOL OF AEROSPACE
MECHANICAL AND ENGINEERING
NORMAN, OKLAHOMA 73019

FEBRUARY 1981

FINAL REPORT FOR PERIOD OCTOBER 1977-SEPTEMBER 1980

Air Force Armament Laboratory
AIR FORCE SYSTEMS COMMAND ★ UNITED STATES AIR FORCE ★ EGLIN AIR FORCE BASE, FLORIDA

NOTICE

Please do not request copies of this report from the Air Force Armament Laboratory. Additional copies may be purchased from:

National Technical Information Service
5285 Port Royal Road
Springfield, Virginia 22161

Federal Government agencies and their contractors registered with Defense Technical Information Center should direct requests for copies of this report to:

Defense Technical Information Center
Cameron Station
Alexandria, Virginia 22314

REPORT DOCUMENTATION PAGE		READ INSTRUCTIONS BEFORE COMPLETING FORM
1. REPORT NUMBER AFATL-TR-81-19	2. GOVT ACCESSION NO.	3. RECIPIENT'S CATALOG NUMBER
4. TITLE (and Subtitle) Aerodynamics of Supersonic Lifting Bodies		5. TYPE OF REPORT & PERIOD COVERED Final Report October 1977 to September1980
		6. PERFORMING ORG. REPORT NUMBER
7. AUTHOR(s) M. C. Jischke M. L. Rasmussen		8. CONTRACT OR GRANT NUMBER(s) AFOSR-77-3468 F08635-79-C-0017
9. PERFORMING ORGANIZATION NAME AND ADDRESS University of Oklahoma School of Aerospace, Mechanical and Nuclear Engineering Norman, Oklahoma 73019		10. PROGRAM ELEMENT, PROJECT, TASK AREA & WORK UNIT NUMBERS PE: 61102F JON: 2307E105
11. CONTROLLING OFFICE NAME AND ADDRESS Air Force Armament Laboratory Armament Division Eglin Air Force Base, Florida 32542		12. REPORT DATE February 1981
		13. NUMBER OF PAGES 407
14. MONITORING AGENCY NAME & ADDRESS(if different from Controlling Office)		15. SECURITY CLASS. (of this report) UNCLASSIFIED
		15a. DECLASSIFICATION/DOWNGRADING SCHEDULE
16. DISTRIBUTION STATEMENT (of this Report) Approved for public release; Distribution Unlimited		
17. DISTRIBUTION STATEMENT (of the abstract entered in Block 20, if different from Report)		
18. SUPPLEMENTARY NOTES Availability of this report is specified on verso of front cover.		
19. KEY WORDS (Continue on reverse side if necessary and identify by block number) Theoretical Aerodynamics Lifting Bodies Wind Tunnel Tests Boundary Layer Analysis		

20. ABSTRACT (Continue on reverse side if necessary and identify by block number)
This report describes a combined theoretical and experimental program of
research in the aerodynamics of supersonic lifting bodies. Analytical
perturbation techniques are used to study the supersonic flow past slightly
elliptical cones, cones whose cross-sections deviate slightly but
arbitrarily from that of a right circular cone, cones of small longitudinal
curvature, and right circular cones undergoing small harmonic pitching and/
or plunging motions. These studies all involve perturbations of the well-known
(continued on reverse)

DD FORM 1473 EDITION OF 1 NOV 65 IS OBSOLETE

20. Continued

solution for supersonic flow past a right circular cone. Closed-form
analytical results are achieved through the use of an approximation
that accurately predicts results over the entire range of the hypersonic
similarity parameter. These results give hypersonic limiting solutions that
agree well with other independent analyses and, at the same time, agree
exactly with linearized theory in the linear theory limit. Comparisons with
experiment, where possible, also show good agreement.

PREFACE

This work was conducted by the University of Oklahoma, Norman, Oklahoma, and was sponsored by the Air Force Armament Laboratory (AFATL) under Air Force Contract No. F08635-79-C-0017. The contract monitor for AFATL was Dr. Donald C. Daniel. The experiments were conducted at the Arnold Engineering Development Center (AEDC), Arnold Air Force Station, Tennessee. The experimental results were obtained by ARO, Inc. (a subsidiary of Sverdrup and Parcel and Associates, Inc.), contract operator of AEDC. The experiments were conducted in the Von Karman Gasdynamics Facility of AEDC from 22 October 1979 to 26 October 1979 and 14 December 1979 to 19 December 1979. The entire period covered by this report is October 1977 to September 1980.

Dr. Donald C. Daniel was Research Manager for the Air Force Armament Laboratory, and Mr. Jerry Hahn and Mr. Davis Lanham, ARO, Inc., AEDC, served as Project Engineers for the wind tunnel work. Important contributions were also made by Mr. Hsiung Ming Lee, Mr. Beom-Soo Kim, Mr. Martin Weeks, and Mr. Henry Kan.

The Public Affairs Office has reviewed this report, and it is releasable to the National Technical Information Service (NTIS), where it will be available to the general public, including foreign nationals.

This technical report has been reviewed and is approved for publication.

FOR THE COMMANDER

CARL A. FORBRICH, JR., Lt Col, USAF
Chief, Munitions Division

(The reverse of this page is blank)